AFRL-ML-WP-TR-1998-4134

PROCEEDINGS OF THE 1997 USAF AIRCRAFT STRUCTURAL INTEGRITY PROGRAM CONFERENCE

VOLUME II

ASIP

Gary K. Waggoner
AFRL/Materials and
Manufacturing Directorate
Wright-Patterson AFB, Ohio

John W. Lincoln
ASC/Deputy for Engineering
Wright-Patterson AFB, Ohio

James L. Rudd
AFRL/Air Vehicles Directorate
Wright-Patterson AFB, Ohio

USAF Aircraft Structural Integrity Program Conference
Hyatt Regency San Antonio
San Antonio, Texas

AUGUST 1998

FINAL REPORT FOR PERIOD 2-4 DECEMBER 1997

Approved for public release; distribution unlimited

MATERIALS AND MANUFACTURING DIRECTORATE
AIR FORCE RESEARCH LABORATORY
AIR FORCE MATERIEL COMMAND
WRIGHT-PATTERSON AFB OH 45433-7734

NOTICE

This technical report has been reviewed and is approved for publication.

Gary K. Waggoner

GARY K. WAGGONER
Chief
Systems Support Division

REPORT DOCUMENTATION PAGE

Form Approved
OMB No. 0704-0188

1. AGENCY USE ONLY *(Leave blank)*	2. REPORT DATE	3. REPORT TYPE AND DATES COVERED
	August 1998	Final, 2-4 December 1997

4. TITLE AND SUBTITLE
Proceedings of the 1997 USAF Aircraft Structural Integrity Program Conference, Volume II

5. FUNDING NUMBERS
PE 62102F
PR 4349
TA TE
WU CA

6. AUTHOR(S)
1-Gary K. Waggoner, AFRL/MLS, Compiler & Editor; 2-John W. Lincoln, ASC/ENF; and 3-James L. Rudd, AFRL/VAS, Editors

7. PERFORMING ORGANIZATION NAME(S) AND ADDRESS(ES)
1-Materials & Manufacturing Directorate and 3-Air Vehicles Directorate, Air Force Research Laboratory; 2-Aeronautical Systems Center, Deputy for Engineering, all three of the Air Force Materiel Command, Wright-Patterson AFB OH 45433

8. PERFORMING ORGANIZATION REPORT NUMBER

9. SPONSORING/MONITORING AGENCY NAME(S) AND ADDRESS(ES)
Materials & Manufacturing Directorate
Air Force Research Laboratory
Air Force Materiel Command
Wright-Patterson Air Force Base, OH 45433-7734
POC: Gary K. Waggoner, AFRL/MLS, 937-255-2282

10. SPONSORING/MONITORING AGENCY REPORT NUMBER
AFRL-ML-WP-TR-1998-4134

11. SUPPLEMENTARY NOTES
See AFRL-ML-WP-TR-1998-4133 for Volume I

12a. DISTRIBUTION AVAILABILITY STATEMENT
Approved for public release; distribution is unlimited.

12b. DISTRIBUTION CODE

13. ABSTRACT *(Maximum 200 words)*
This report contains the proceedings of the 1997 USAF Structural Integrity Program Conference held at the Hyatt Regency Hotel in San Antonio, Texas, from 2-4 December 1997. The conference, which was sponsored by the Aeronautical Systems Center's Engineering Directorate and the Air Force Research Laboratory's Air Vehicles and Materials and Manufacturing Directorates, was hosted by the San Antonio Air Logistics Center Aircraft Directorate, Aircraft Structural Integrity Branch (SA-ALC/LADD). This conference, as in previous years, was held to permit experts in the field of structural integrity to communicate with each other and to exchange views on how to improve the structural integrity of military weapon systems. Sessions were primarily focused on analysis and testing, engine structural integrity, structural materials and inspections, structural repair, and force management. This year, as in previous years, our friends from outside the U.S. borders provided the audience with outstanding presentations on activities within their countries. It is anticipated this conference will include their contributions in the agenda of future meetings.

14. SUBJECT TERMS

15. NUMBER OF PAGES

16. PRICE CODE

17. SECURITY CLASSIFICATION OF REPORT	18. SECURITY CLASSIFICATION OF THIS PAGE	19. SECURITY CLASSIFICATION OF ABSTRACT	20. LIMITATION OF ABSTRACT
UNCLASSIFIED	UNCLASSIFIED	UNCLASSIFIED	SAR

VOLUME II

SESSION VII

FATIGUE AND CRACK GROWTH

Chairman - *J. Gallagher*
Air Force Research Laboratory

ALCOA

Damage Tolerance Characterization of Thick, Wrought Aluminum Products with and without Stress Relief:

Focus on Toughness and Crack Growth Characteristics to Capture Advances in Forging Stress Relief Technology

R. J. Bucci[1], R. W. Bush[1] and G. W. Kuhlman[2]
Aluminum Company of America
(1) Alcoa Technical Center, Alcoa Center, PA 15069
(2) Alcoa Forging Division, Cleveland, OH 44105

The 1997 USAF Aircraft Structural Integrity Program Conference
San Antonio, TX
December 2-4, 1997

ALCOA

Abstract

Heat treated, high strength aluminum alloy die-forgings have traditionally been a preferred starting stock material for many airframe structural components embodying a heavy/thin cross-section mix. In recent efforts to lower their costs, manufacturers have become increasingly critical of forging's sometimes excessive machining warpage/distortion behavior in contrast to that of machined plate. This, coupled with an almost universal perception that forgings are less predictable than plate in their performance, prompted development of new Alcoa quench technology, that when effectively combined with cold compressive stress relief, yields much improved forging machining performance with residual stress levels on par with those of stretched plate. The resulting forging stress relief improvement offers significant cost saving potential in both manufacturing (fewer machining steps, less shimming, reduced flow times) and operation (root cause fix to unanticipated stress corrosion problems).

Residual stress, when present, increases data scatter and, as extensively illustrated in this work, can also erroneously skew experimental toughness and crack growth property measurements. Evidence is presented that deep-slotted fracture mechanics type specimens, excised from forgings without stress relief, commonly display non-conservative property inflation. Consequently, advance of promising new forging stress relief technology has been impeded by the illusion that stress relieved forging toughness and crack growth properties are inferior to the erroneously skewed property values historically associated with non-stress relieved forgings.

The paper describes cause, distribution and effects of quenching induced residual stress on damage tolerance assessment of safe-crack growth forged parts. Guidelines to minimize property test/evaluation problems are presented with validation examples. A recommended method to remove residual stress bias from forging fracture property characterization is also presented so that advances in forging residual stress relief technology can be more routinely qualified and exploited. The effect of residual stress on transfer between coupon and full component test results is also discussed.

Material selections are being increasingly driven by manufacturing cost considerations.

ALCOA

- Forgings have long been used in structural airframe parts with heavy/thin cross-section mix.
  - Advantage of net shape parts (minimal machining, favorable buy to fly ratio)
  - Thoroughly wrought microstructure (imparts superior fatigue resistance)
  - Multi-directional mechanical work (improves property balance - all directions)
  - Contour-following grain flow (improves corrosion and crack growth resistance)
- Manufacturers are increasingly challenging forging use.
  - Adverse machining cost impact of residual stress induced warpage problem
  - Recent advances in thick plate quality/performance offer attractive alternative
  - Almost universal perception that forgings are less predictable than plate
- Forgings have not stood idle.
  - Advances in lead/flow times
  - Breakthrough developments in residual stress relieval
  - Concurrent engineering methods
- Residual stress complexities in DADT characterization are presently impeding advanced forging technology approval.

Thermal quench residual stresses are typically compressive at the surface and tension in the interior.

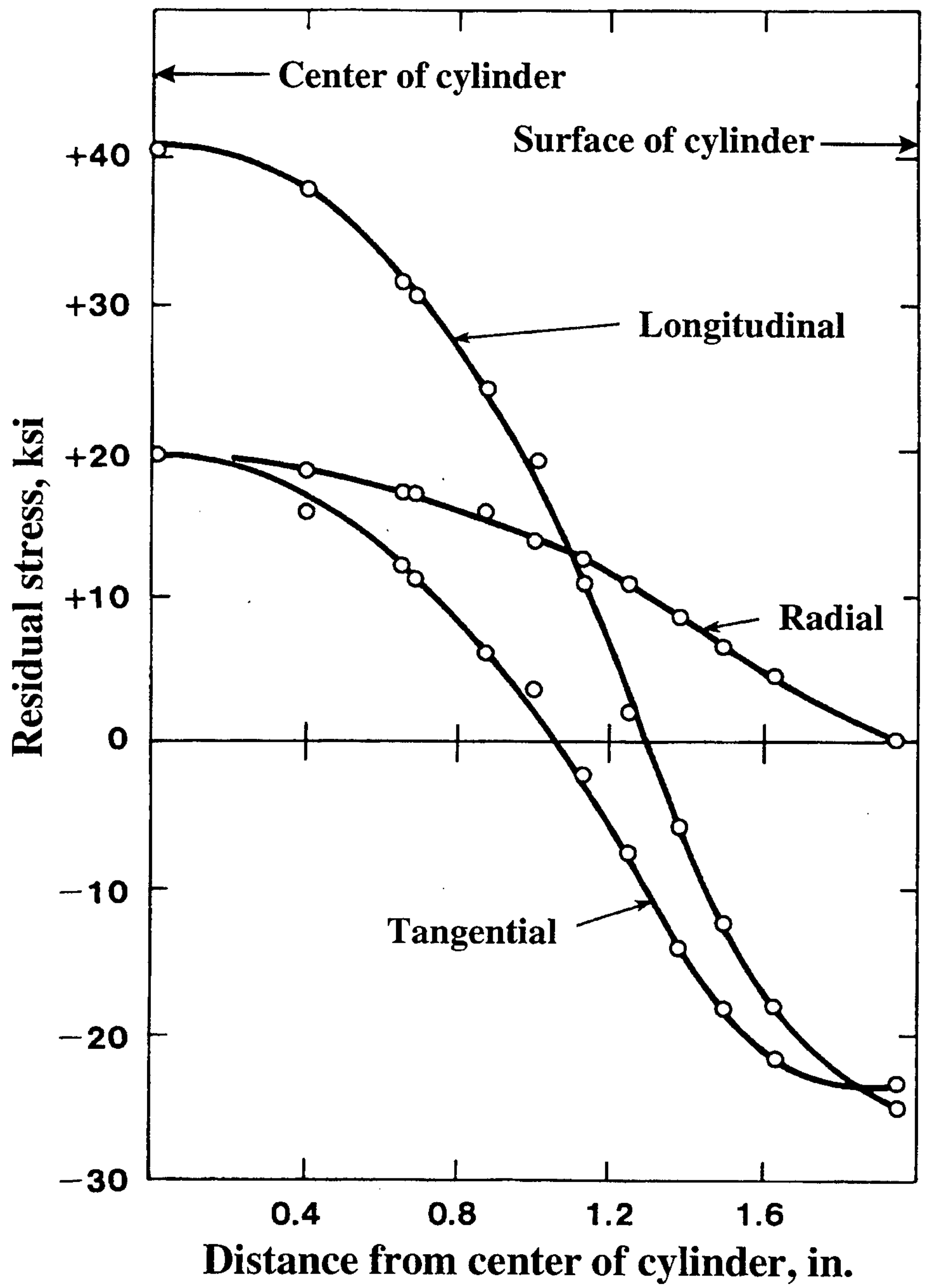

Residual stress distribution of Al 7075 cylinder quenched in cold water spray

Quench rate can appreciably impact residual stress magnitude and range.

In general, the faster the quench, the greater the residual stress.

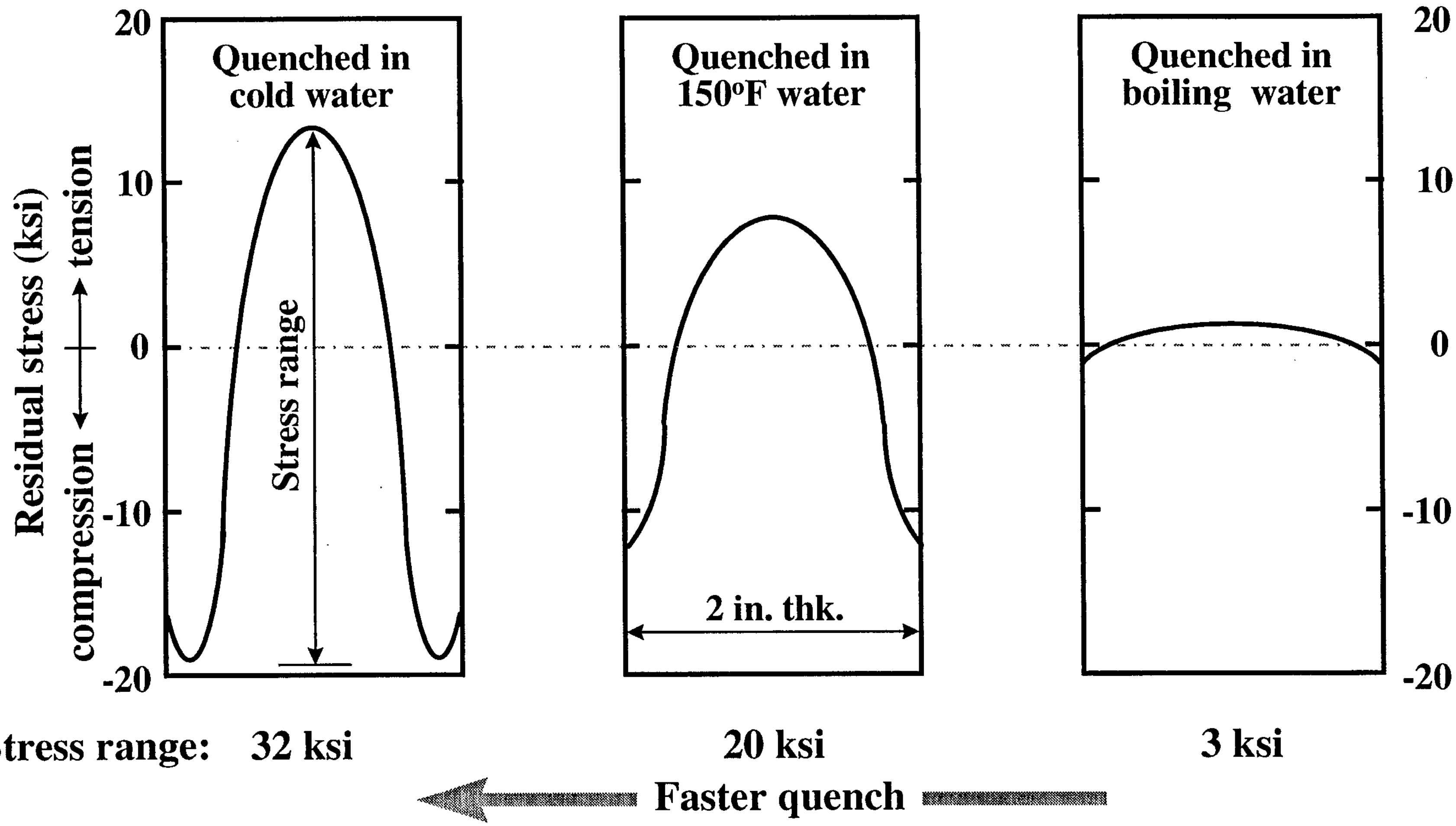

Effect of quench water temperature on 7XXX Al forging residual stress

Advanced stress relief technology is now commercialized to alleviate forging machining distortion and fit-up related SCC problems.

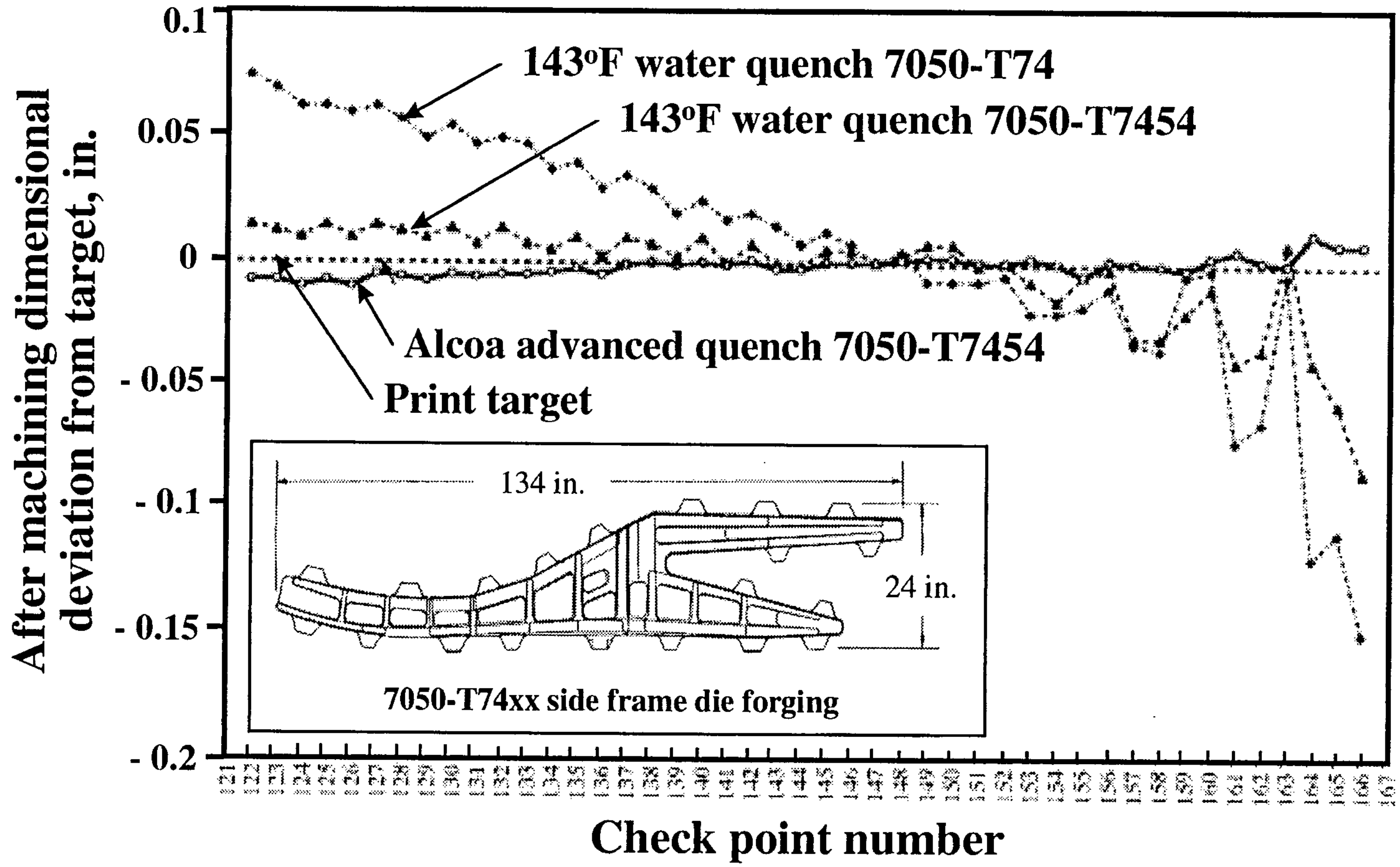

Contrast in machining performance of aluminum 7050-T74xx die-forging Alcoa quench, water quench, compressive stress relief in finish dies

ALCOA

Coupling new Alcoa quench technology with cold compression stress relief has demonstrated aluminum forging residual stress levels on par with those of stretched plate.

Compression Stress Relief (2 methods)

- **Restrike in cold finish die (-Txx54)**
  - **Involves nominal 1% mechanical stretch with no reshaping process**
  - **Avoids additional die cost**

- **Cold work with separate die (-Txx52)**
  - **Involves compression and some reshaping to achieve 1 to 5% permanent set**
  - **Achieves tighter dimensional tolerance**
  - **Allows tailored/more complete stress relief**

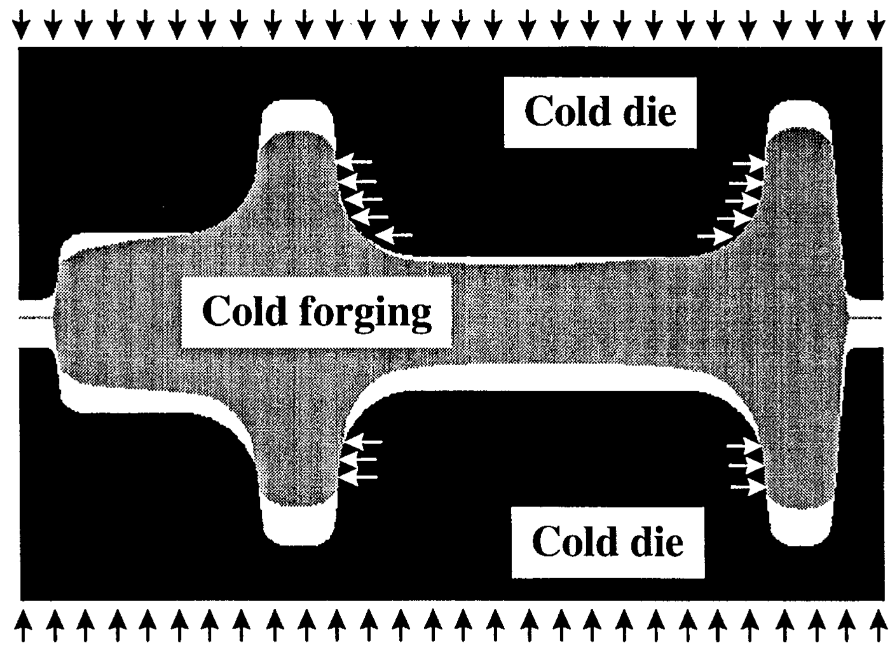

Illustration of mechanical stretch associated with cold restrike

Thick/shaped product evaluations demand caution to when residual stresses are involved.

ALCOA

- Test coupons removed from unfully stress relieved parts contain residual stress.
  - Coupon isolation partially relieves the original stress, and redistributes the profile of that remaining.
  - While residual stress magnitude within the excised coupon is smaller than that of its host, the potential for testing error can still be significant.
- Residual stress induced testing bias confounds material comparison.
  - When bias occurs, the test result is often inflated (i.e., exaggerates material capability).
  - Statistical data pooling, however, may yield overly conservative property allowables because of the scatter effect.
  - Review of the literature reveals the problem is widespread.
- The problem has far-reaching implications on DADT approvals for a number of promising cost-saving technologies.
  - New stress relief tempers (e.g., -T7454 & -T7452).
  - Net & near net shapes (e.g., forgings, extrusions, castings, spray form).
  - Monolithic structure (next generation air vehicles).
  - Forging retrofit in older aircraft (e.g., replace 7075 & 7079-T6 with new 7xxx-T7x).

ALCOA

Residual stress induced bias in damage tolerance property testing has been a recurrent problem for years.

- Inaccurate R&D conclusions (lost time & resources).
  - Failed scale-up efforts (unfulfilled promise of initial coupon results).
  - Wasted time and effort in certification and process surveillance testing.
  - Inconsistencies that kill promising technologies at early stage.
- Corrupted data bases (potential for non-conservatism).
- Current industry test standards/specifications do not adequately address the effect.
  - Compact specimens generally exhibit the greatest problem, though other specimen types are not immune.
- Sensitivity to the problem will grow in the drive for increasingly integral structure.

Residual stress bias can be masked as a geometry effect.

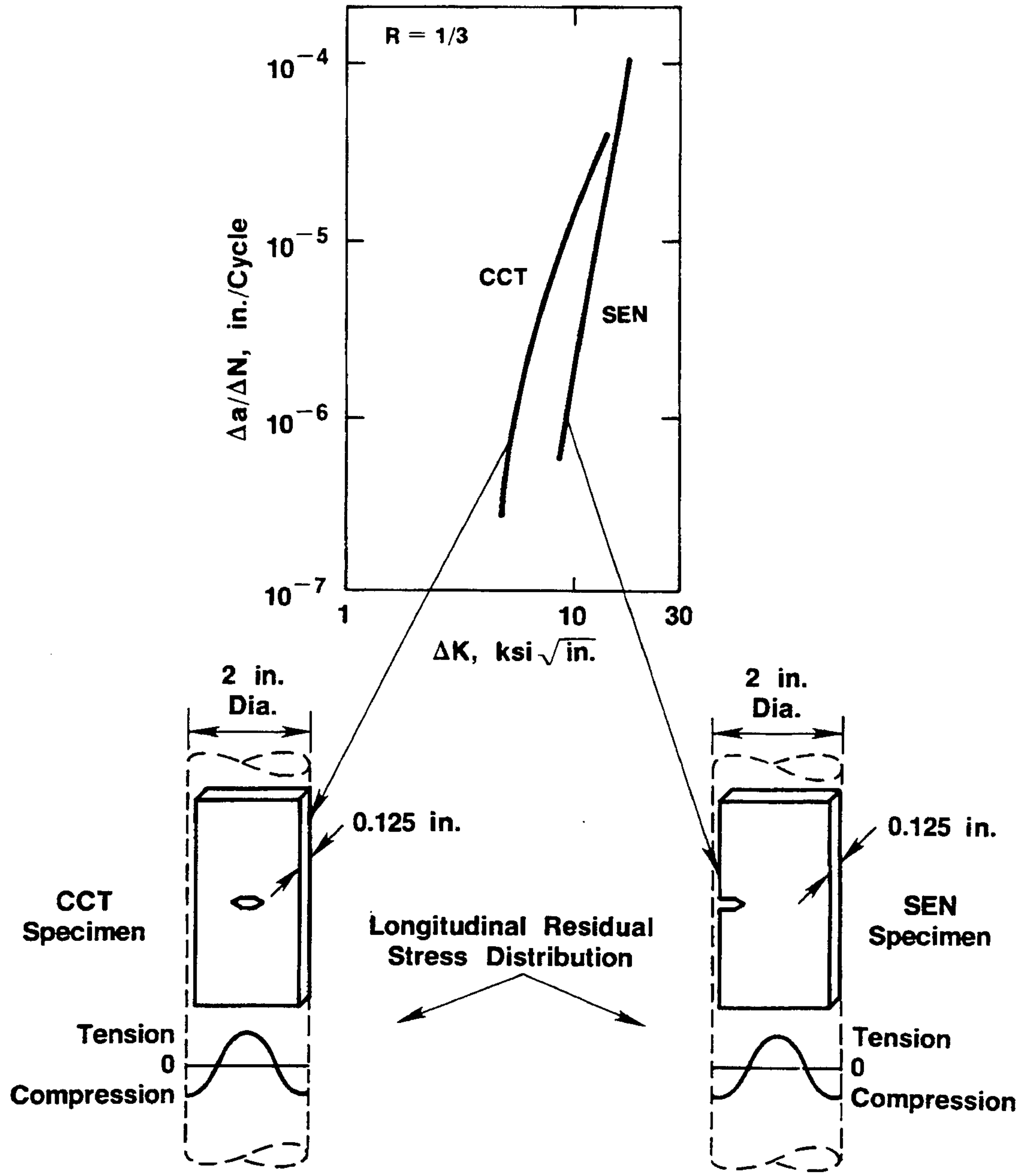

Crack initiates where stress normal to crack plane is tensile (high FCGR)

Crack initiates where stress normal to crack plane is compressive (slow FCGR)

Effect of specimen type on FCGR measurement from non-stress relieved 7xxx Al extruded rod.

Fracture toughness test results from partially stress relieved product can be misleading without proper interpretation.

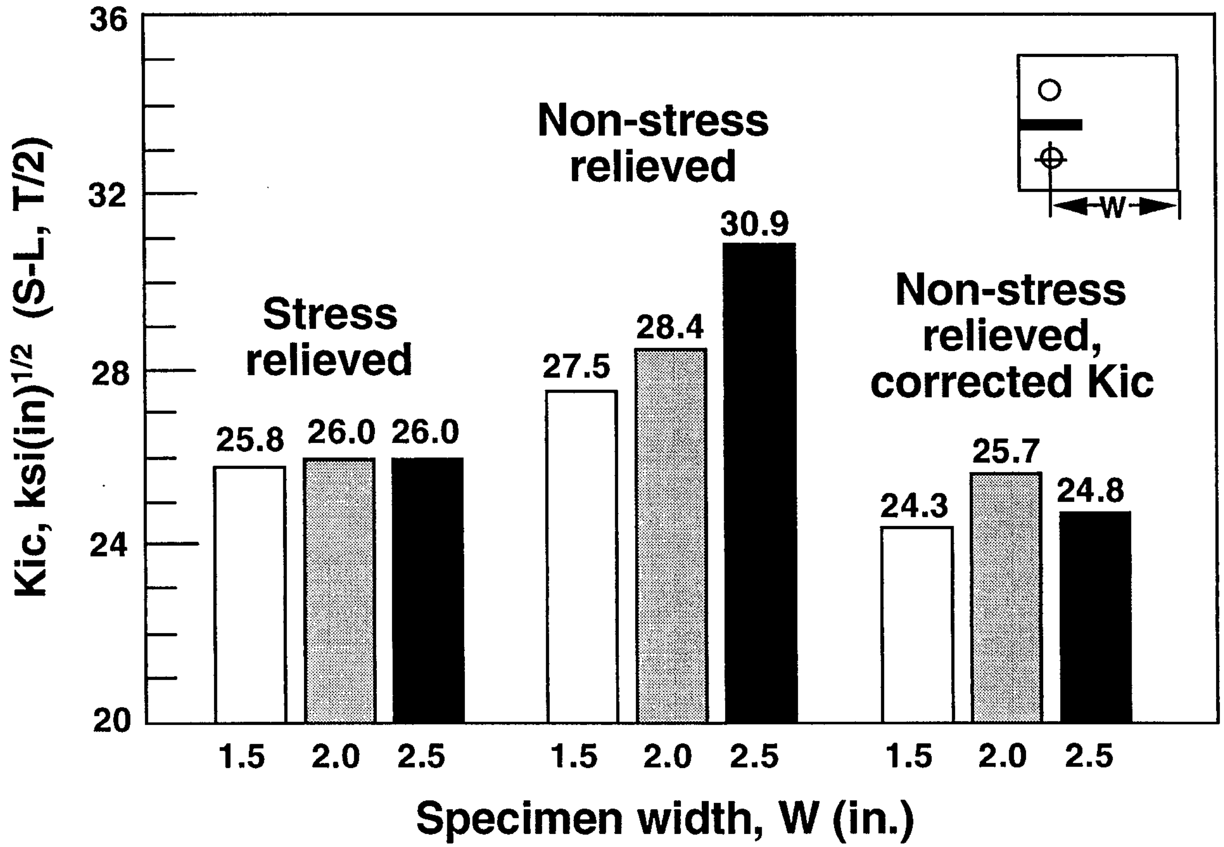

Interaction of internal stress state and specimen size on fracture toughness measurements from comparable 4-in. thick 7050-T74 hand forged billets, one stress relieved and the other not.

Typical quench residual stress profile for a rectangular section

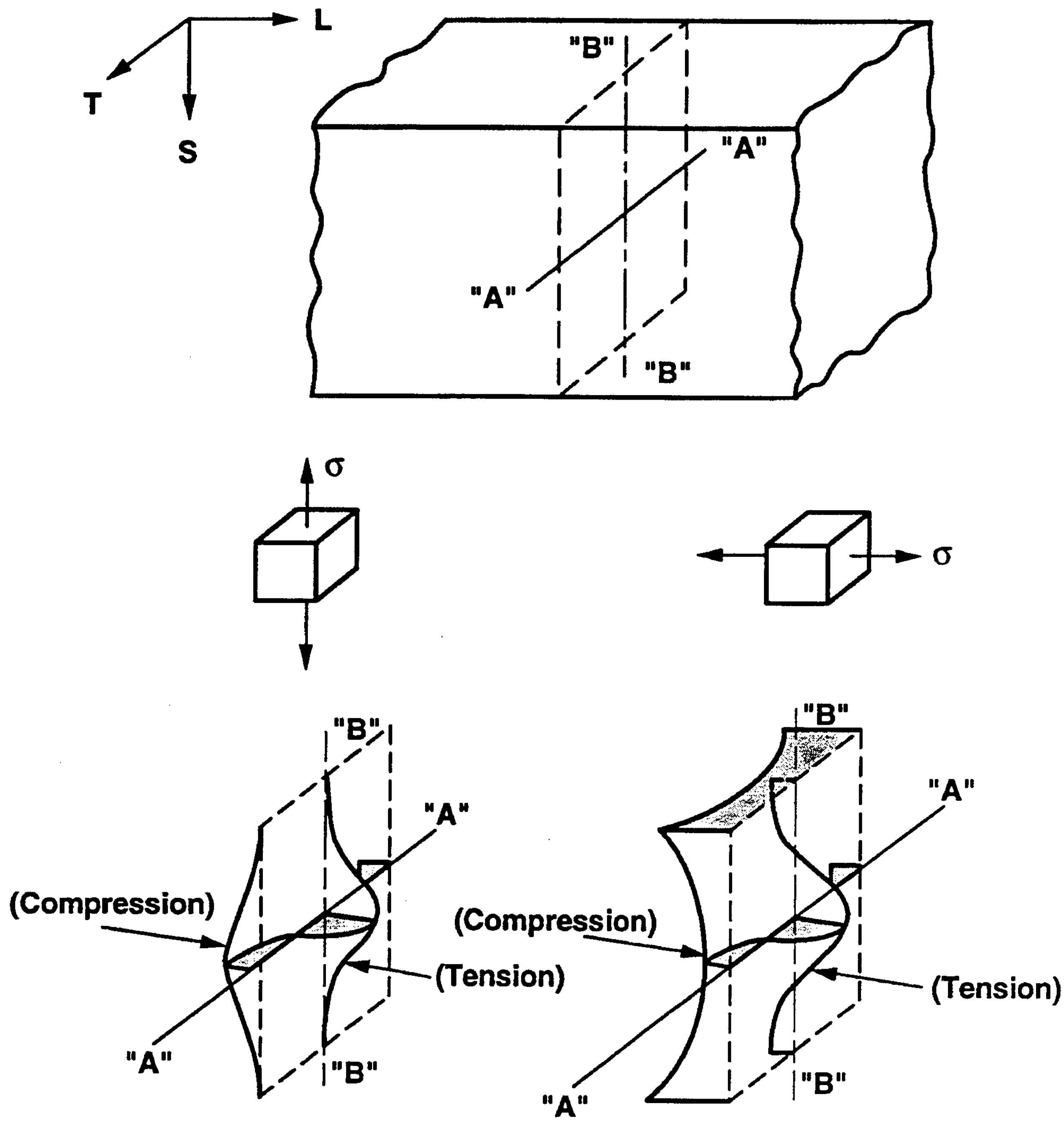

Excessive crack front curvature is often a cue that residual stress bias is present.

Broken fracture toughness specimen halves

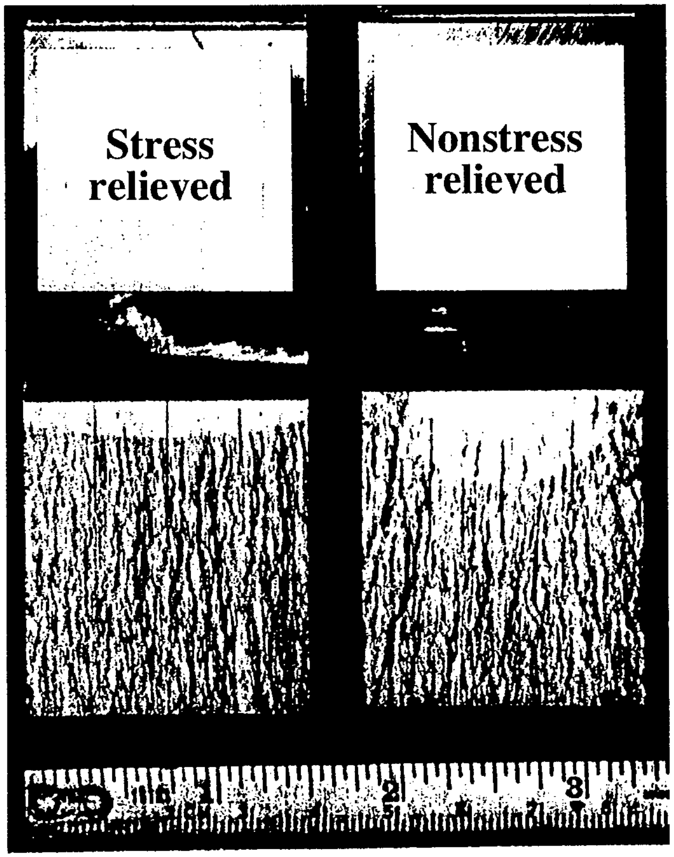

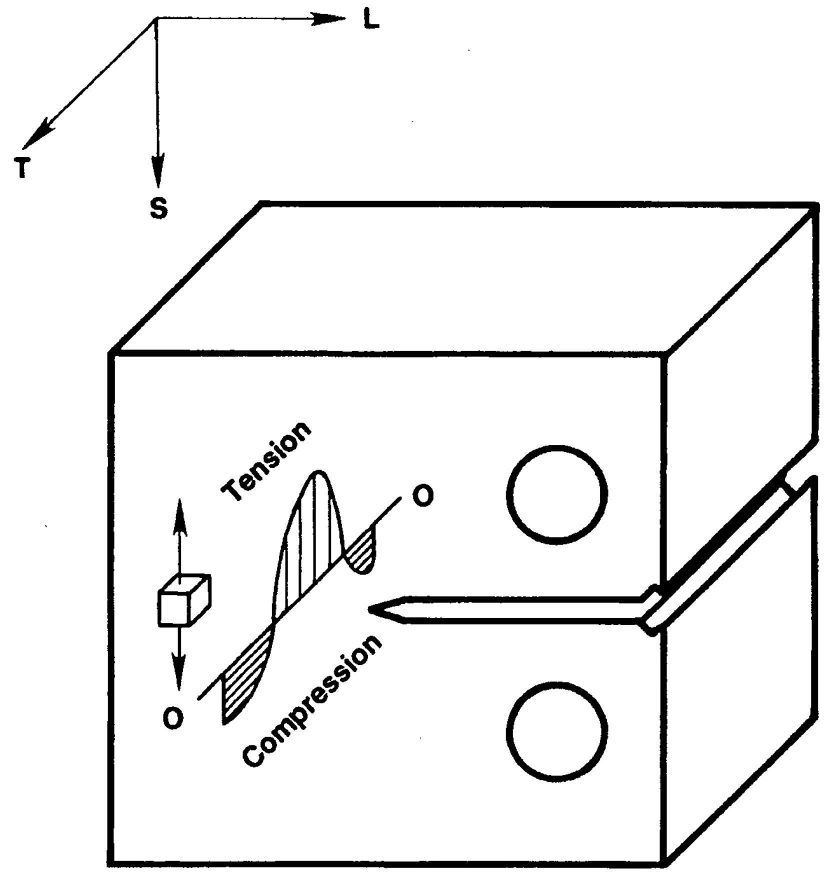

Effect of through-thickness internal stress distribution (normal to the notch plane) on fracture toughness specimen precrack shape.

Residual stress induced-bending can measurably impact crack tip stress intensity factor.

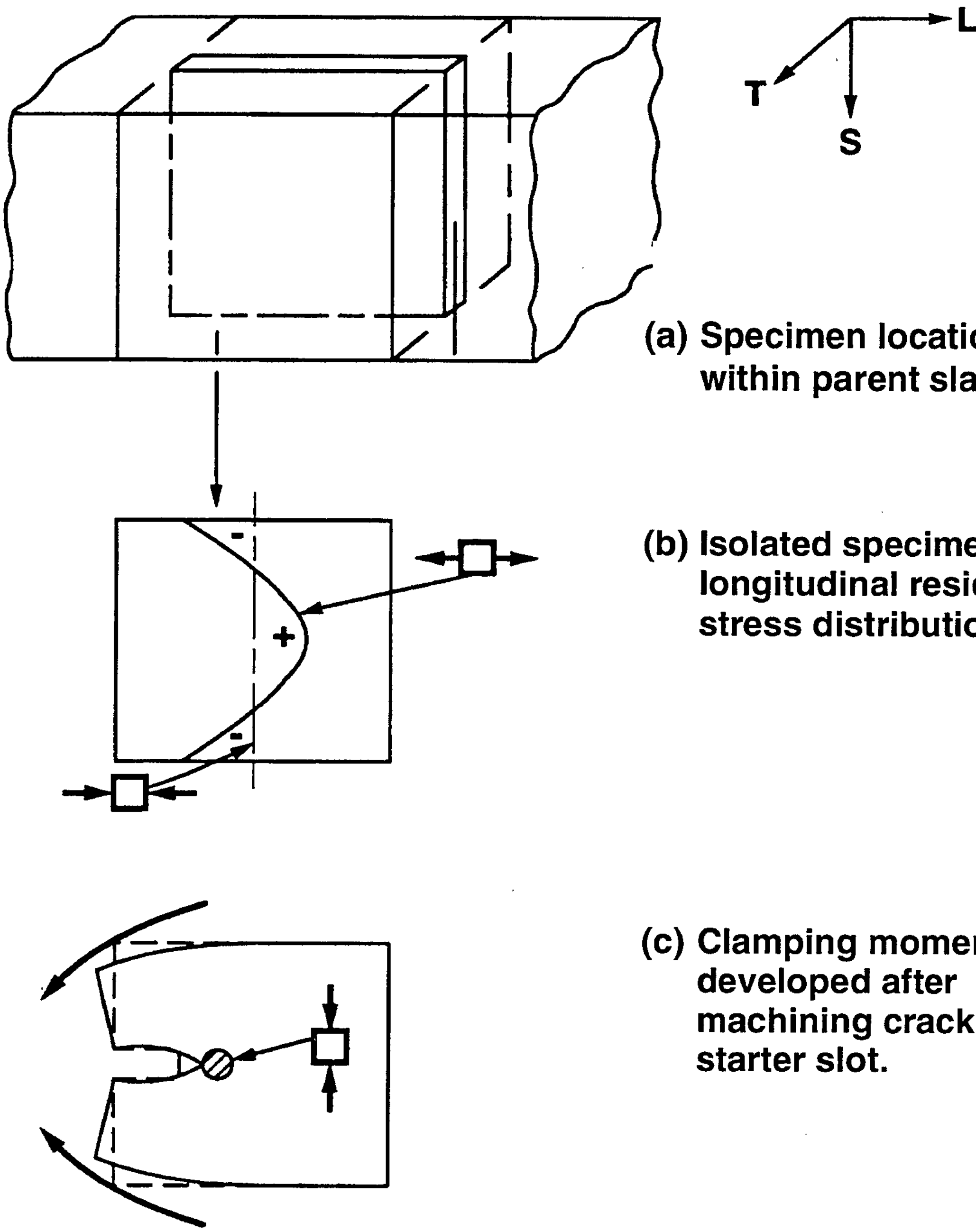

(a) Specimen location within parent slab.

(b) Isolated specimen longitudinal residual stress distribution.

(c) Clamping moment developed after machining crack starter slot.

Portrayal of crack tip clamping associated with residual stress distribution aligned parallel to a compact specimen notch plane.

Classical LEFM similitude breaks down when residual stress is appreciable & ignored.

Part / **Coupon**

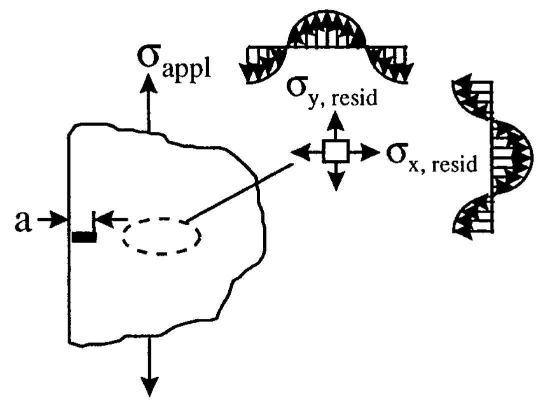

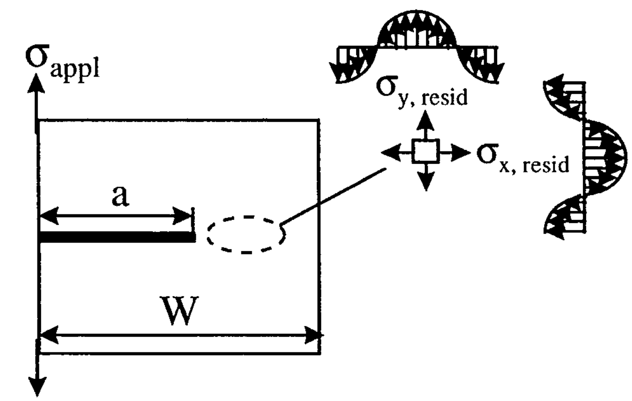

$$\mathbf{K = \sigma_{appl}(\pi a)^{1/2}\, Y(a/W) + \sigma_{resid}\, f(a, a/W)}$$

Y, f = geometric functions, W = part, specimen size

	Part	Coupon
σ_{appl}	large	small
a	small	large
$\sigma_{resid}/\sigma_{appl}$	small	large

Residual stress induced bias is magnified in the coupon test.

The potential for residual stress bias is detectable from warning signs.

ALCOA

- Fracture toughness
  - Machining distortion in specimen preparation.
  - Excessive crack front curvature.
  - Unusually high loads or number of cycles required for precracking.
  - Nonlinear load-COD trace (elastic portion of test record).
  - Property shift with change in specimen configuration.
- Fatigue crack growth
  - Similar to fracture toughness test, but more subtle.
  - Small thickness to width ratios may negate crack curvature, giving the test a valid appearance.
  - Significant crack closure effect.
  - Because the applied stress magnitudes are typically less, potential for artifactual data are greater in FCG testing than in toughness testing.

A simplified correction practice has been devised for Kic testing.

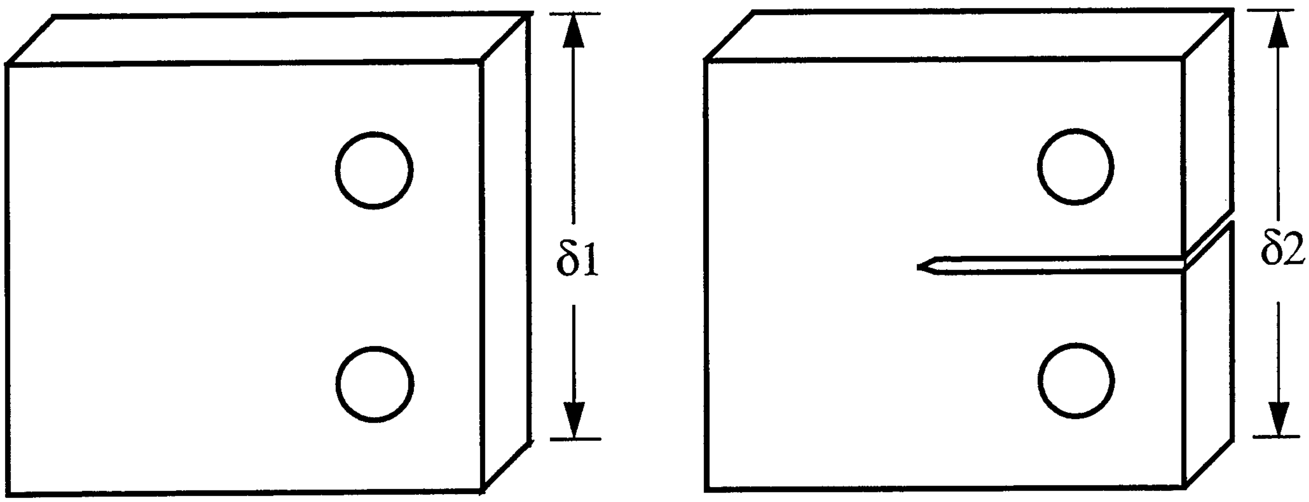

$$\Delta\delta = \delta 1 - \delta 2$$

Measure the specimen height before and after machining the crack starter notch.

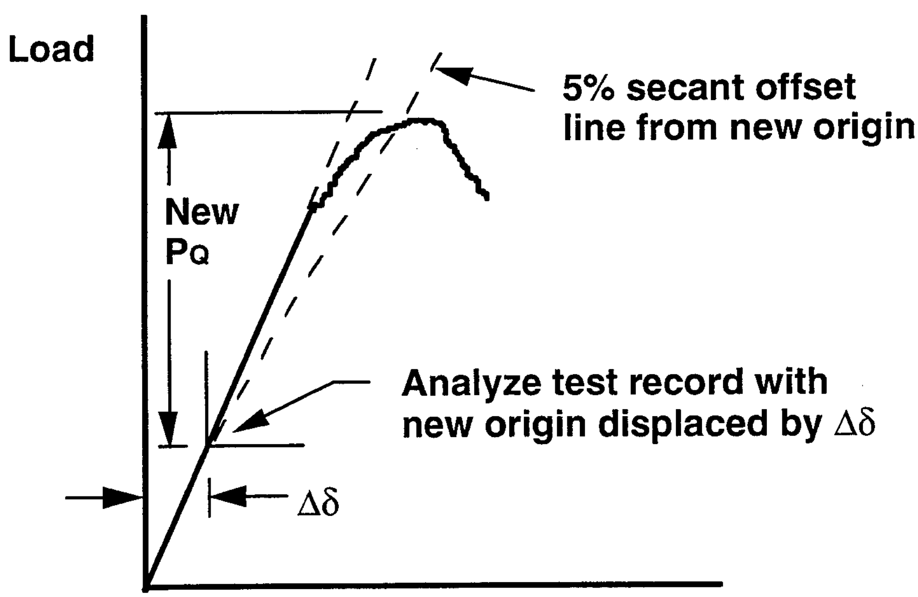

Kic test residual stress correction schematic

After correction, 7050-T74 hand forging K_Q values show little effect of quench history.

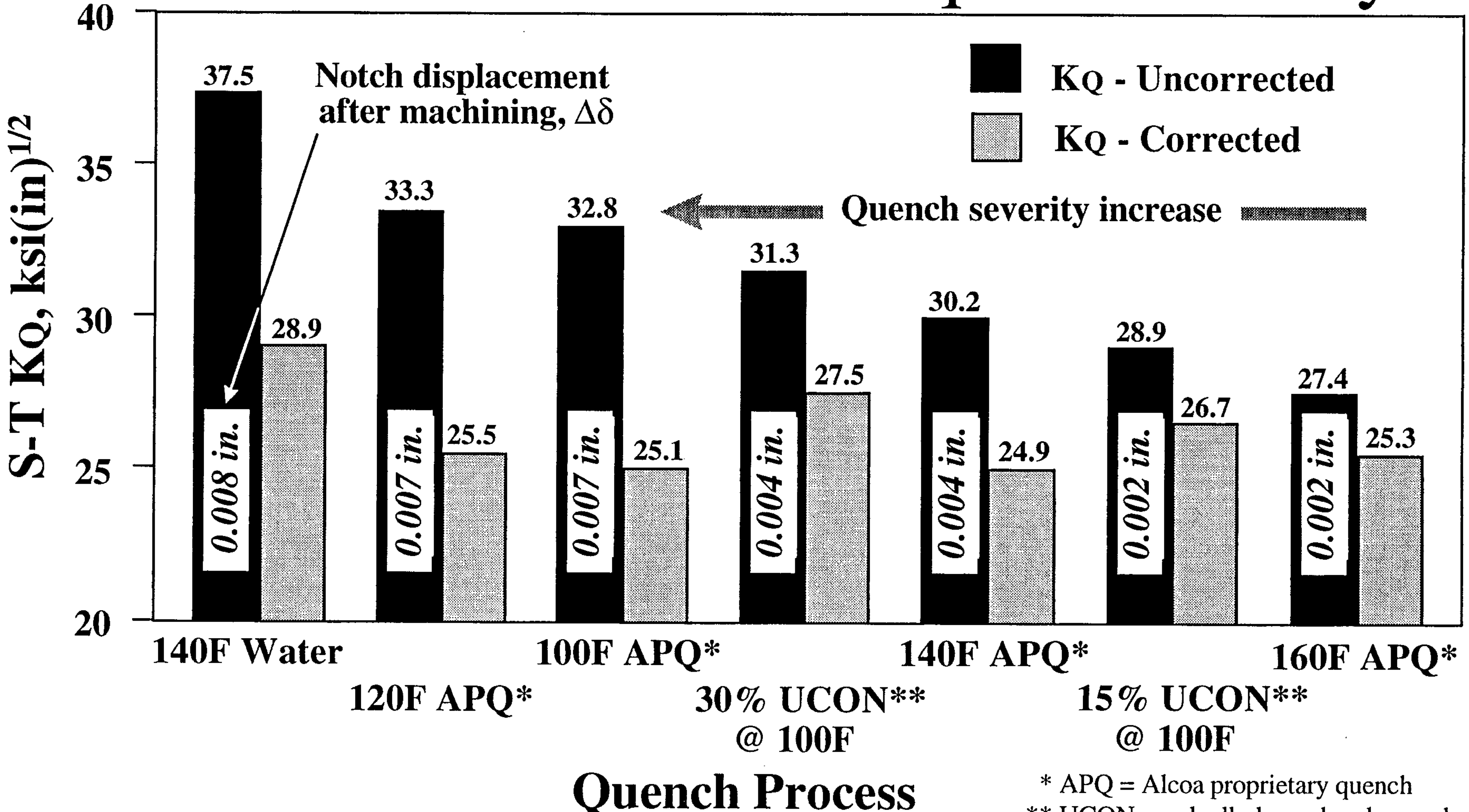

* APQ = Alcoa proprietary quench
** UCON = polyalkylene glycol quench

Effect of quench process on 7050-T74 hand forging (1.5") fracture toughness measurements with and without correction for residual stress bias

New quench technology and better test methods are available to reduce the residual stress effect.

- *Contrast of 7050-T74 hand forging corrected and uncorrected K_Q values show that new Alcoa proprietary quench (APQ) reduces residual stress bias in raw test result.*
- *After correction, the 7050-T74 toughness (K_Q) values agree with valid Kic values obtained from compression stress relieved 7050-T7452 product.*

Effect of temper and test method on S-L fracture toughness of 7050-T74X hand forging

	7050-T74*		7050-T7452**
Quench media	K_Q uncorrected (ksi$\sqrt{in}$)	K_Q corrected (ksi$\sqrt{in}$)	Kic valid (ksi$\sqrt{in}$)
140F water	37.5	28.9	25.6
140F APQ	30.2	24.9	25.5
160F APQ	27.4	25.3	25.5

* Quench & age, ** Quench, compression stress relieve & age

A protocol to purge residual stress bias from FCGR data has been established.

(Bucci, ASTM STP 743, 1981 & Bush et. al., ASTM STP 1189, 1993)

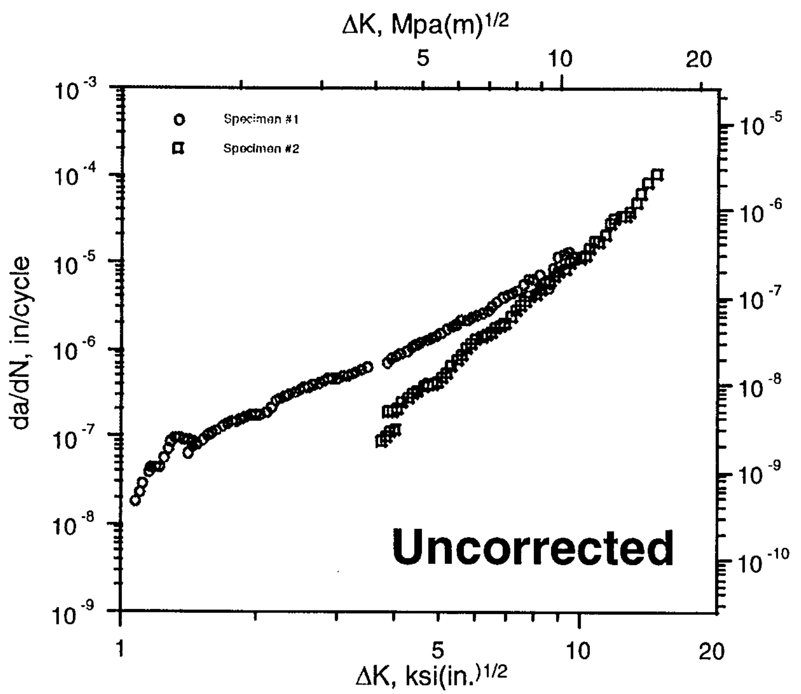

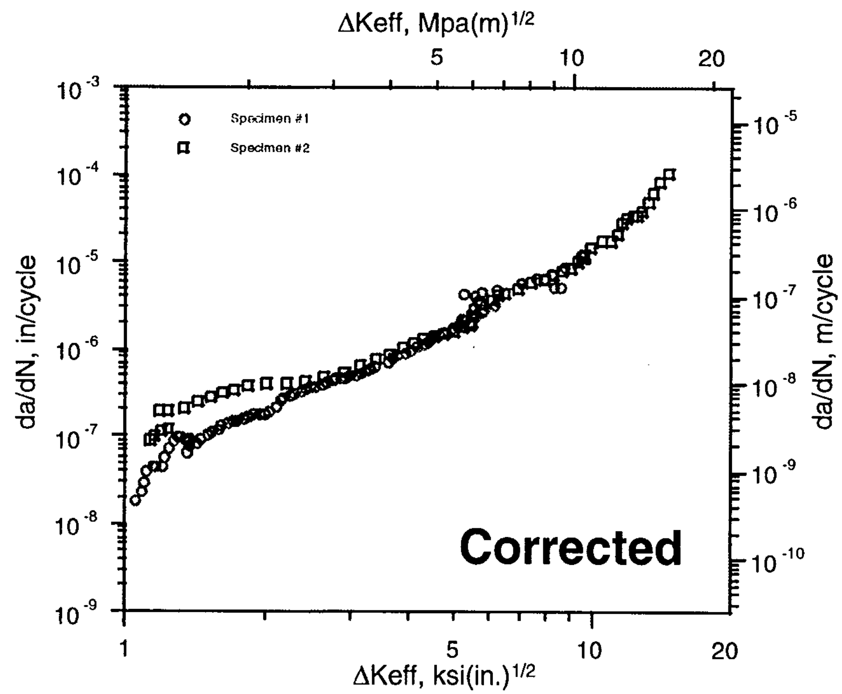

FCGR data from two incompletely stress relieved 7050-T7452 forgings
(S-L orientation, R = 0.33, high humidity air)

Closure-based correction of suspect FCGR data is derivable from the raw load-COD traces.

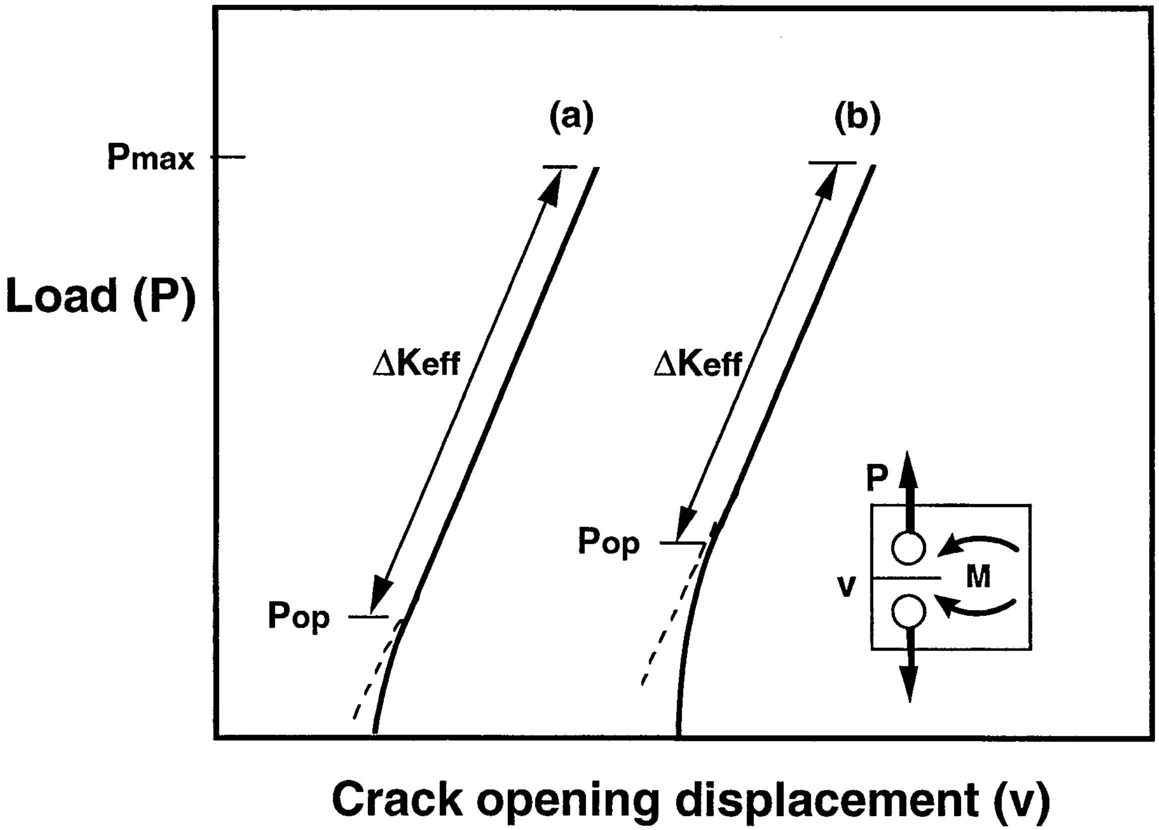

Pop = crack opening load attributed to crack closure effect (Elber).

FCG occurs for $P \geq Pop$

(a) Residual stress free (M = 0).

(b) Pop increase with residual stress induced clamping moment, M.

Effect of residual stress on load-COD trace

Residual stress bias can be deduced from decay in closure load with crack advance.

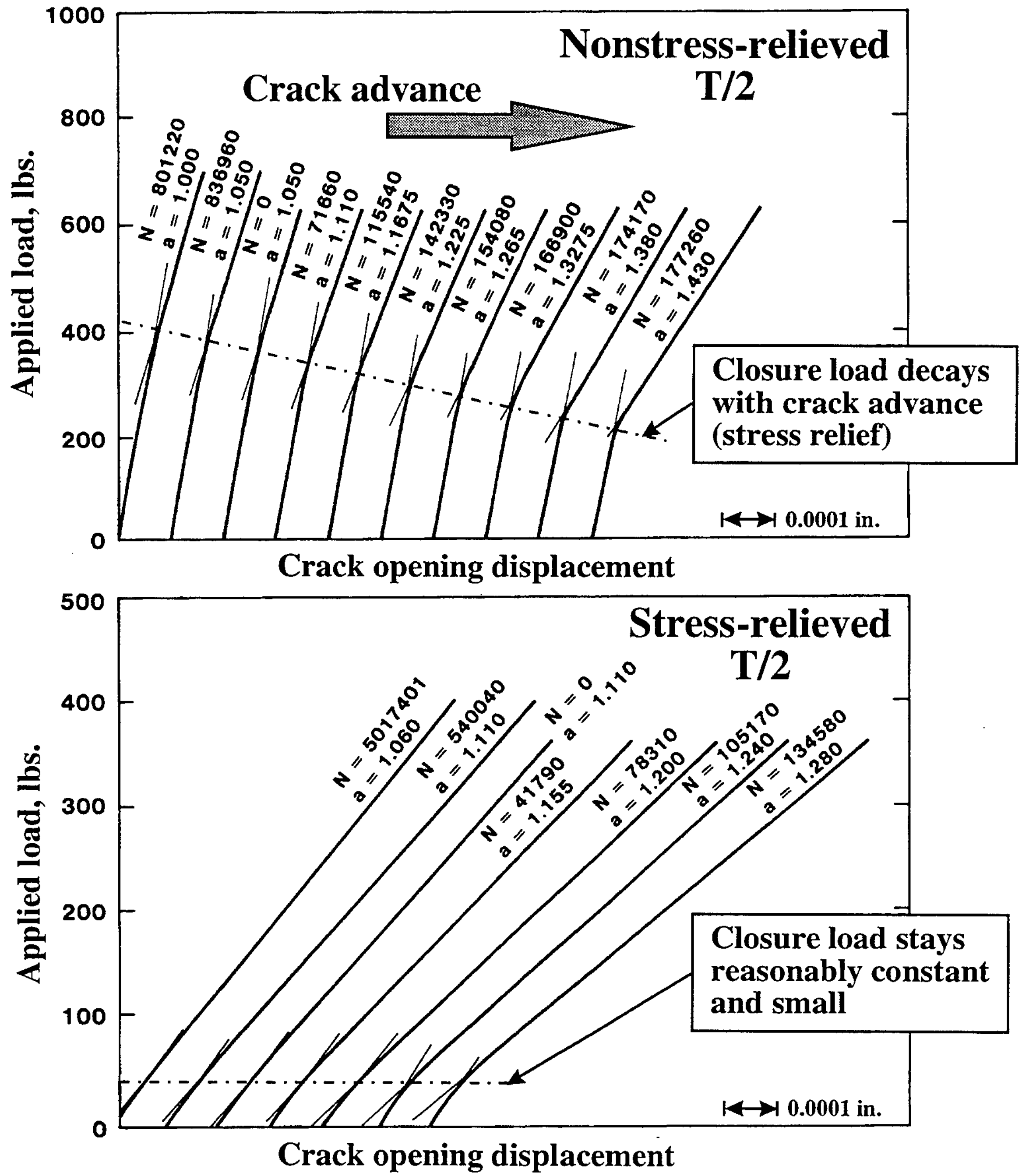

Load-COD traces from FCG tests of high strength Al product evaluated in a non-stress relieved (top) and stress relieved (bottom) condition.

ALCOA

Alloy 7050 plate and forging display similar FCGR behaviors when the residual stress effect is purged.

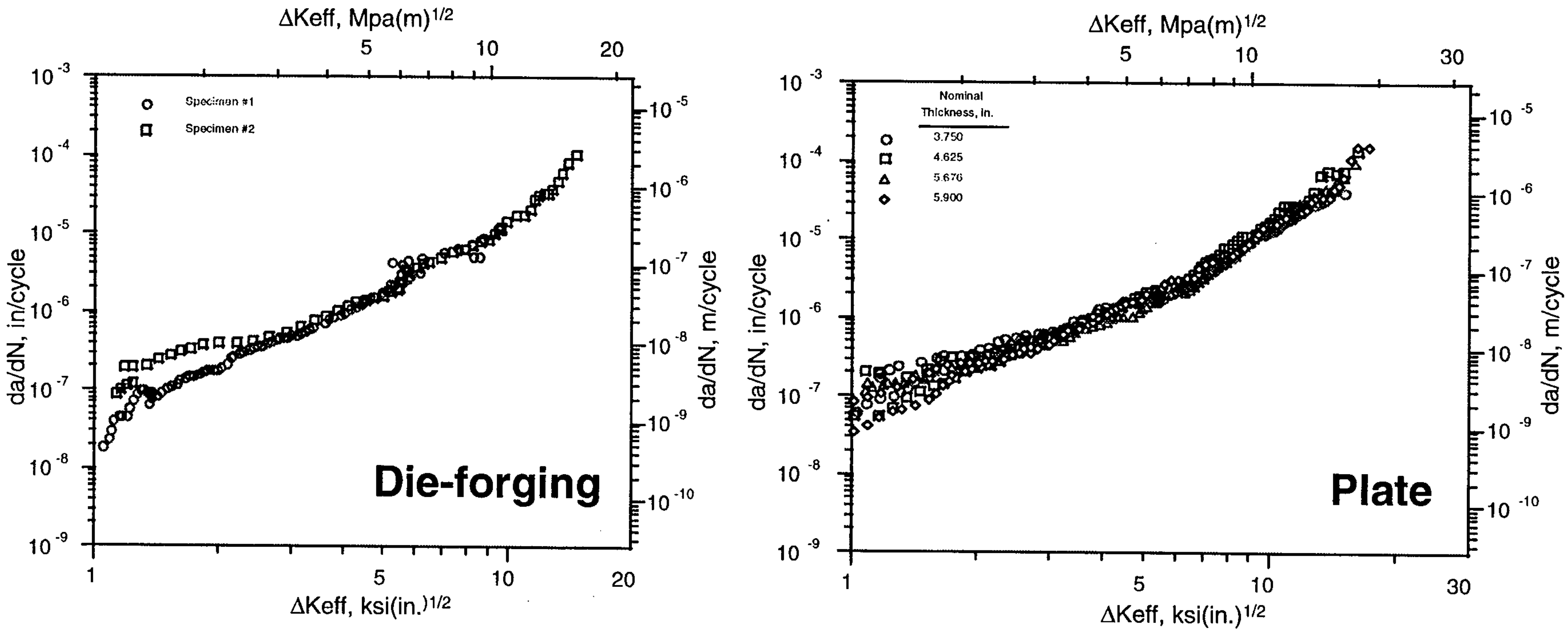

Closure corrected FCGR data for 7050-T745X plate and non-stress relieved forgings

(S-L orientation, R = 0.33, high humidity air)

Suspect FCGR data on varied products is readily found in the open literature.

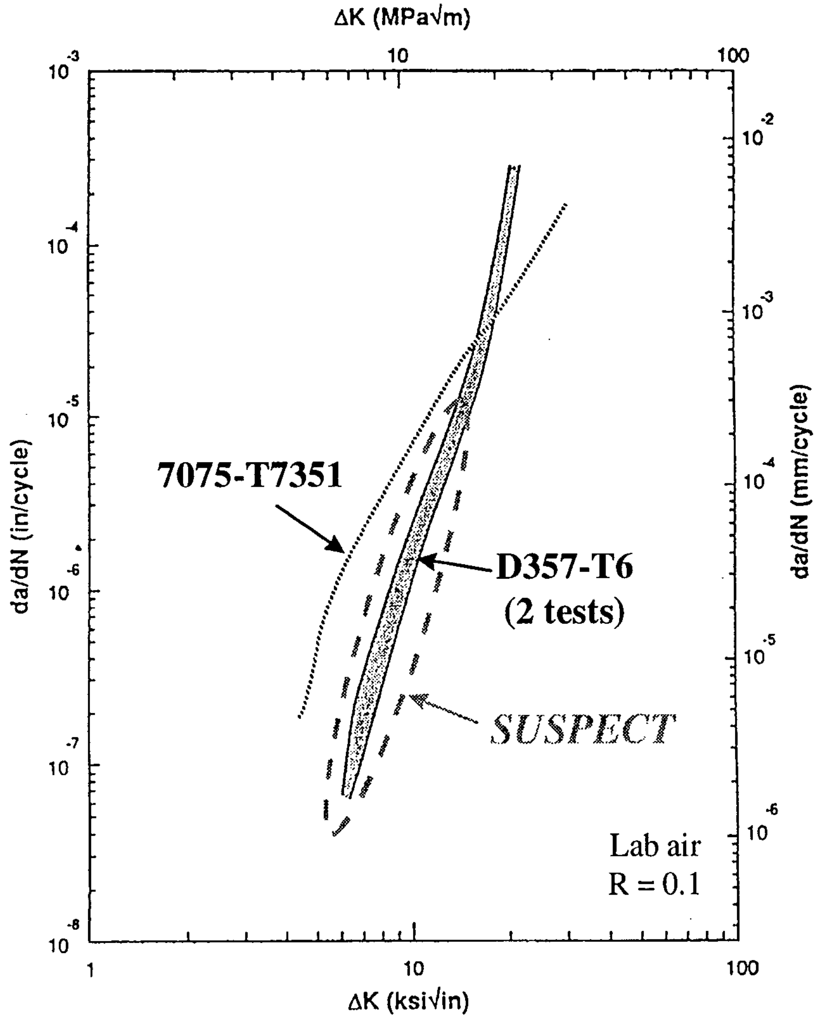

Grade A/B D357-T6 Casting

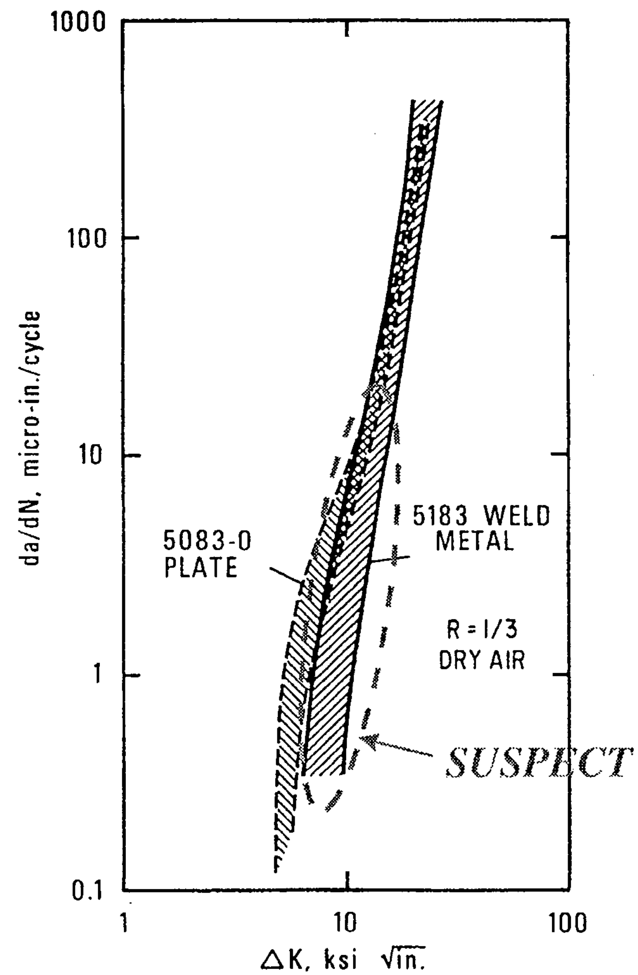

5xxx Al Alloy Butt Weld Joint

Conclusions/recommendations

ALCOA

- Understanding of heat treat induced residual stress cause/effects on toughness & crack growth characterizations has been presented so advances in aluminum forging & residual stress relief technology can be more routinely applied.
- The lessons learned have broader implications.
  - A variety of aluminum product technologies can be affected (e.g., forgings, castings, extrusions, rapid solidification (powder metal) products, MMCs, weldments, …).
  - Individual test values can be inflated, historical data sets skewed, and scatter increased.
  - The problem is widespread, but largely underappreciated.
- Guidelines have been presented to minimize the testing problems.
  - Warning signs and validity checks for residual stress bias.
  - Residual stress bias correction practices.
  - Compact specimens exacerbate the problem; when in doubt, use center crack specimens.
- The intensified drive for parts consolidation warrants insertion into industry design and product specification practices.
  - Stronger advocacy for standards upgrading & component validations.
  - Purge/replace contaminated data sets (various industry design handbooks).
  - Treat with sense of urgency to improve quality of decisions and reduce waste.

The Effect of Prior Corrosion Damage on the Short Crack Growth Rates of Two Aluminum Alloys

Ms. Amy M.H. Taylor*
TexSEM Laboratories, Inc.
392 East 12300 South, Suite H
Draper, Utah 84020

Dr. David W. Hoeppner, P.E.
Department of Mechanical Engineering
University of Utah
Salt Lake City, Utah 84112

Abstract

A study was performed using two aluminum alloys, 2024-T351 and 7075-T651, subjected to prior corrosion and then fatigue. The resulting crack nucleation and the "short" fatigue crack growth were observed using an "in-situ" scanning electron microscope. This unique machine allowed visual observation of a crack on the surface of the material during fatigue cycling at high magnifications. Baseline tests without corrosion were conducted to compare the "short" fatigue crack growth rates with those of prior corroded specimens.

Four tests were conducted. One specimen was subjected to corrosion prior to fatigue and one specimen was run as a baseline fatigue test for each of the two aluminum alloys. Specimens were pitted in 3.5% salt water for 28 hours. It was hypothesized that the prior corrosion would accelerate the fatigue crack growth rate in the "short" crack region and that cracks would form from discontinuities on the surface, such as corrosion pits.

Based on the results, it was found that prior corrosion does influence the fatigue crack growth rate and that the two materials exhibit different crack growth behavior. The specimens subjected to prior corrosion exhibited accelerated crack growth rates compared to the baseline tests.

The 7075 specimens had faster crack growth rates than the 2024 specimens. The baseline tests and the prior corroded 2024 specimen displayed crack growth rates that increased, then decreased, then increased again as ΔK increased. The 7075 specimens did not show a dramatic drop-off in crack growth rate as seen in the 2024 tests.

This work is unique in that combining prior corrosion and short crack behavior has not been greatly researched. These are relatively new fields of research but they are important because they model real-world behavior of materials. Further work should be conducted in this area to statistically substantiate the results presented here.

Introduction

Research at Battelle has found that corrosion costs the United States 300 billion dollars annually, one third of which is avoidable [1]. Corrosion acting with fatigue is a major maintenance concern in the aircraft industry. As the aircraft fleet ages, these time dependent failure modes are becoming even greater concerns. In a recent survey performed by the authors and their colleagues, corrosion and/or fretting were found to be a contributing factor in at least 687 incidents and accidents from 1974 to 1994 in military and commercial aircraft in the United States [2].

Often aircraft are left to sit while not in service at which time corrosion may occur. Because inspections are currently based on flight hours and not calendar hours, the corrosion may not be discovered until the aircraft has been put into service. During this time, however, cracks may have nucleated from the corrosion damage, which can grow during subsequent flight of the aircraft. These cracks are cause for alarm as they may not be discovered before they have become critical.

Because of this, prior corrosion damage, such as pitting damage, is cause for concern in aviation safety.

"Short" fatigue crack growth added to prior corrosion damage may lead to reduced component lifetime. It has been shown in the past two decades that "short" crack growth rates vary from long crack growth rates in that "short" cracks grow faster below the threshold stress intensity value. Therefore, life predictions according to long crack growth data may be unconservative when a crack is in the "short" crack region. Because of this the effort in "short" crack research has been increased but little has been done concerning prior corrosion damage in the "short" crack regime. Coupled together, prior corrosion and "short" crack growth may reduce the expected lifetime or time/cycles between inspection intervals of an aircraft significantly.

Prior Corrosion

Much research has been done on simultaneous corrosion and fatigue damage and it has been found that corrosion accelerates the rate of fatigue and failure. However, often the corrosion and fatigue act sequentially. When an aircraft is in flight it experiences cyclic loading. When it is on the ground, moisture builds up on the aircraft. As an aircraft sits (and when it is in the air), the corrosion process takes place. Thus, the sequential action of these time dependent failure modes may produce different results than the simultaneous action.

It has been found that pit characteristics vary according to loading, environment, and material [3]. When comparing the sizes and shapes of pits formed in 7075-T6 from zero load, sustained load, and fatigue load, Lorie Grimes

found that the corrosion pits formed by the fatigue load were larger than the others and that they were more spread across the surface. Therefore, it can be seen that the expected fatigue lives due to each will vary from each other.

Du, Chiang, Kagwade, and Clayton found that when aluminum alloy 2024-T3 was fatigued and then exposed to a corrosive solution and then fatigued again that the fatigue life was greater than had the material been corroded and then fatigued [4].

Short Cracks

The idea that the behavior of "short" cracks varies from long cracks did not occur until the mid 1970s. All work on crack growth was done assuming long crack behavior. Scientists discovered that in the short crack region a crack exhibits characteristics which are not valid using linear elastic fracture mechanics (LEFM). Over the past decade it has been realized that short crack growth may change the estimated life of a component. Short cracks may make the estimated life non-conservative. Therefore, it is necessary to analyze the behavior of short cracks in order to learn their effects on crack propagation rates and how to take these potential effects into account.

To distinguish between a long and short crack would perhaps simply be to say where LEFM is valid and where it is not, respectively. R.O. Ritchie and S. Suresh have discussed the types of short cracks and what mechanisms lead to accelerated short crack growth [5]. They relate crack driving force, local plasticity, microstructure, crack shape, crack extension, premature crack closure, and local crack tip environment to the differences between long and short crack growth. A

crack may be short or small on several bases but there is no quantitative value that is yet agreed upon to say when a crack is short and when it is long. According to Ritchie and Suresh, a crack may be short with respect to the microstructure, the section size (physically short), or the scale of local plasticity [6]. Physically short cracks were observed in this study where the difference in minimum and maximum stress intensity factors below the threshold value.

The Combination of Aluminum, Prior Corrosion, and Short Crack Growth

A crack spends much of its life in the nucleation and formation stages where crack growth begins in the short crack region. To understand crack behavior, short crack studies need to be performed to prevent unexpected failure. It is obvious that much more study needs to be done involving the synergistic effects of corrosion and crack formation and propagation on common aircraft materials, such as 2024-T3 and 7075-T6 aluminum alloys.

Test Methodology

Test Apparatus

The fatigue tests were conducted in an electro-hydraulic servo-controlled 25 kN "in-situ" fatigue machine coupled with MTS components. This machine is unique in that the specimen is attached in the grips inside a scanning electron microscope (SEM). Thus, the specimen may be monitored at high magnifications while the fatigue load is applied and cracks may be identified as they form and grow.

Specimen Description

Because of their widespread use in aircraft, which are susceptible to both fatigue loading and corrosion pitting, 2024-T3 and 7075-T6 aluminum alloys were studied. The material was obtained in rod form (0.500 in OD) from Affiliated Metals. A groove was machined into the rectangular cross-section of the specimens to act as a point of stress concentration. This was done to ensure crack growth on the side of the specimen facing the SEM column. It was found that the stress concentration factor in the groove was 1.409 according to [7]. Two baseline specimens, one of each material, were tested without the prior corrosion. These tests were compared with the two specimens run with the prior corrosion to determine if there was a change in short crack growth rate due to the prior corrosion.

Pits were introduced to the surface prior to the fatigue loading. This was done to model prior corrosion damage on structures. The specimens were covered with paraffin wax all over to protect the metal except for the small region of the machined groove where the pitting would take place. The specimens were pitted in a 2 liter bath of 3.5% NaCl and distilled water at 25°C for 28 hours. The specimens were rinsed with distilled water and acetone and tested immediately after being corroded.

Test Conditions

Fatigue tests were conducted at a frequency of 10 Hz. The R value (P_{min}/P_{max}) used was 0.3. Using a spreadsheet and an initial crack length of 0.01

mm, the load was calculated iteratively to obtain a value of ΔK around 1.0. The solution of ΔK, the change in stress intensity factor, was derived for a part-circular crack in a simple stress field on the surface of the material. From A.C. Pickard's solution for a part-circular crack, for this experiment ΔK becomes:

$$\Delta K = M_G M_B M_S \frac{2}{\pi} \Delta\sigma \sqrt{\pi c}$$

where:
K = stress intensity,
M_G = general correction factor,
M_B = back-face correction factor,
M_S = side-face correction factor,
$\Delta\sigma$ = change in stress,
c = 1/2 crack length.

The experimental matrix is shown in the following table.

Table 1. Experimental Matrix and Testing Loads

Specimen	Pre-crack Load, kN ($\%S_{ty}$)	Test Load, kN ($\%S_{ty}$)
X1-2024	2.90 (85%)	2.90 (85%)
P4-2024	2.39 (70%)	2.39 (70%)
P2-7075	3.84 (75%)	3.07 (60%)
P3-7075	3.07 (60%)	3.07 (60%)

A.K. Vasudevan and S. Suresh found the value of ΔK_{th} for alloys 2024-T3 and 7075-T6 exposed to a corrosive environment [85]. For 2024-T3, $\Delta K_{th} = 3.2$ MPa$\sqrt{m}$ and for 7075-T6, $\Delta K_{th} = 2.1$ MPa$\sqrt{m}$.

Crack Growth Readings

Crack growth was measured using photographs taken with the SEM. A micron marker is given on a photograph. This allows the length of a crack to be found by measuring the crack at a known magnification and multiplying it by the micron marker value. For example, at 1000x magnification, 1 cm equals 10 mm. A crack that measured 3 cm on a photograph would actually be 30 μm long.

To find a crack initially, the surface was monitored every 5,000 cycles. Once a crack had formed and was detected, measurements were taken when crack growth was visible on the SEM. The specimen was loaded as crack readings were taken so that the crack would be visible. Crack readings were taken until a crack length of 1-2 mm was measured at which point long crack growth behavior would take over.

Discussion of Results

Baseline Test Results

The first test was specimen X1-2024. Many crack-like features were visible on the surface of this specimen but were aligned in the direction of loading and after numerous cycles did not appear to be growing. The first crack detected was 48 μm long. Six more cracks were found and data were also taken on those.

The second test was P2-7075. The surface of this specimen contained more discontinuities than the 2024 specimen. It had a cleaner surface in that it was freer

of polishing residue. The first crack was detected at a length of 27 μm. Eight more cracks were discovered and all but one propagated.

For each of the specimens, the multiple cracks formed at constituent particles (inclusions and intrinsic discontinuities) on the surface that appeared to have been filled with polishing compound that did not rinse off in the acetone bath. The cracks grew from one constituent particle to another. The line of the crack growth was not always normal to the direction of loading.

These two specimens displayed similar fatigue crack growth data. The crack growth rate increased, decreased, and then tended to increase again. This is common behavior for short crack data. Crack #1 on specimen X1-2024 displays typical crack growth data for this specimen, shown in the da/dN versus ΔK plot in Figure 1. The initial ΔK was 2.64 MPa$\sqrt{m}$. The data are bunched around a crack growth rate of 1.00E-13. It sharply decreases and then sharply increases.

Figure 2 shows a low initial ΔK of 2.01 MPa$\sqrt{m}$ of crack #2 on specimen P2-7075. The decrease in crack growth rate is not as dramatic on the 7075 specimen as on the 2024 specimen. But P2-7075 does display the same increase, decrease, and slight increase again.

The crack growth rates of the two baseline tests were similar. It appears as though the 7075 specimen had a marginally increased crack growth rate compared to the 2024. The values of ΔK were lower on P2-7075 as would be expected because the ΔK_{th} value of 7075 is lower than 2024.

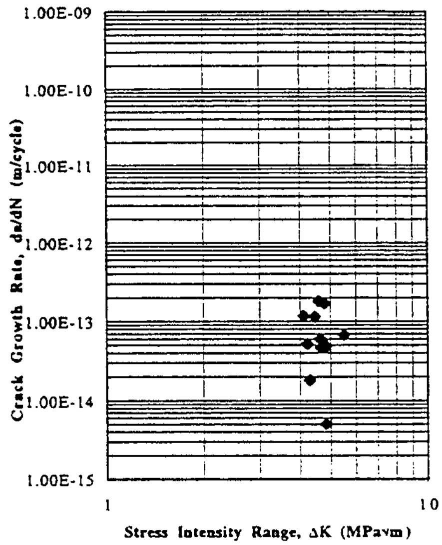

Figure 1. da/dN versus ΔK for X1-2024, Crack #1.

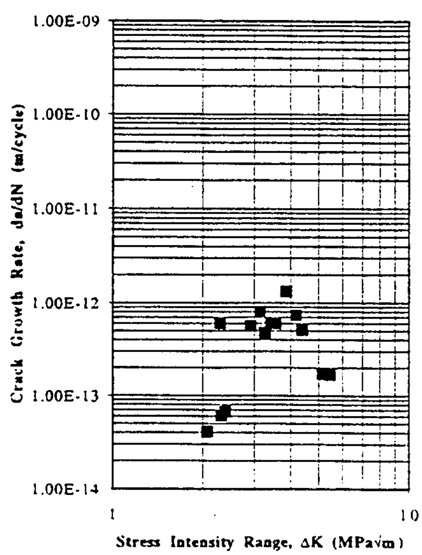

Figure 2. da/dN versus ΔK for P2-7075, Crack #2.

Prior Corroded Test Results

The prior corroded surfaces of the two aluminum alloys showed damage in the form of pits with some exfoliation of the surface before testing began. Figure 3 shows the damage on the surface of specimen P3-7075. Two specimens, one of each material, were tested with the prior corrosion damage.

A crack of 62 μm was first detected on specimen P4-2024. Four additional cracks were monitored on the surface. This specimen was highly damaged due to corrosion, more so than the 7075 specimen. Multiple pits were bunched together and large areas of exfoliation were present.

The last specimen, P3-7075, was tested at loads that were too high to keep the ΔK low enough to remain in the short crack region. The first crack detected on this specimen was 160 μm long at a ΔK of 7.40 MPa$\sqrt{m}$. A shorter crack was found that was 64 μm and a ΔK of 4.61 MPa$\sqrt{m}$. Five cracks were monitored on this specimen.

The surfaces of the prior corroded specimens were more difficult to scan because of the corrosion induced damage on them. While scanning the surface it was difficult to determine exactly what was a crack. Mudcracking was visible on both specimens. This made it difficult to know if a crack was growing through the material or whether it was a layer of material peeled from the surface that was cracked.

Specimen P4-2024 displayed similar crack growth behavior as the two baseline tests but with an increased crack growth rate. The increase, decrease, and

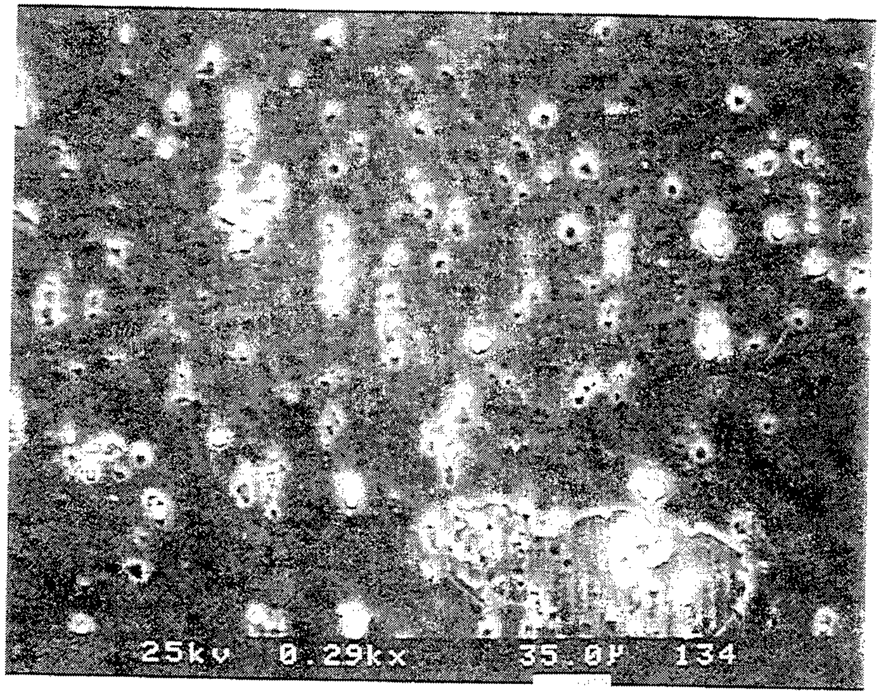

Figure 3. Damage on the surface of specimen P3-7075
before fatigue load was applied.

then increase was present in the crack growth data. The da/dN versus ΔK plot for crack #1 is shown in Figure 4. The initial ΔK was 2.48 $MPa\sqrt{m}$.

The data for crack #1 on specimen P3-7075 are given in Figure 5. This plot shows how the crack growth rate for the cracks on this specimen increased but did not decrease as seen in the other tests. The crack growth rates for this specimen were faster than the baseline tests and the prior corroded P4-2024 test. This may be caused by the increased initial value of ΔK.

Overall, the 7075 specimens had a faster short crack growth rate than the 2024 specimens. The prior corrosion did increase the fatigue crack growth rate in comparison to the baseline tests. The damage from the prior corrosion provided areas of higher stress concentration and reduced area from which cracks formed. It was more difficult to examine the surfaces of these specimens due to the damage as would be the case in the field when inspecting components subjected to corrosive conditions.

Fractography

Visual examination of the fracture surfaces showed that crack growth took place only on the top face of the specimen as was desired. The shape of the fatigue region of the crack was not truly half-penny shaped. This may have an effect on the validity of the stress intensity factor solution.

A fractographic analysis verified that crack nucleation occurred at constituent particles on the base specimens and from pits on the prior corroded specimens. This is most likely due to the increased stress concentration factor at

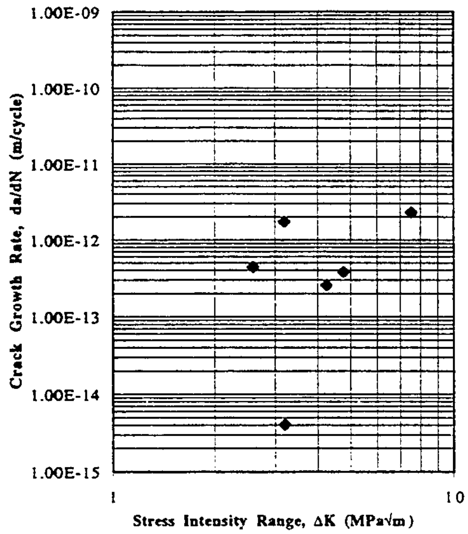

Figure 4. da/dN versus ΔK for P4-2024, Crack #1.

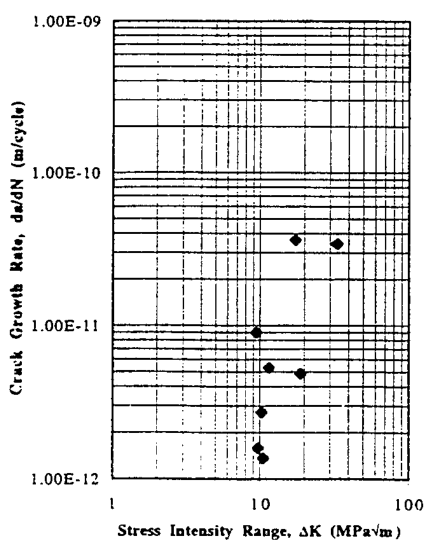

Figure 5. da/dN versus ΔK for P3-7075, Crack #1.

these points and, on the pitted specimens, the reduction in area may also be a factor. Figure 6 shows a crack nucleation site on specimen P4-2024. The radial marks point back to the point of origin of the crack. Other cracks on the surface are also visible on the surface which did not cause failure.

Figure 7 shows striation-like markings on specimen X1-2024. Striation marks were difficult to find on these specimens because of the small fatigue region. However, they were present on both types of aluminum. A secondary crack is visible in Figure 8 from specimen P3-7075. Cleavage characteristics in the fatigue region are also shown on this figure. The fast fracture region shows ductile dimples.

Because testing was conducted inside of an SEM considerable fractographic characteristics were observed during testing. Fractography of the fracture surface did confirm the sites of crack nucleation at pits and constituent particles and showed the shape of the fatigue region.

Conclusions

Based on the results presented, the following conclusions were drawn:

1. The prior corrosion did have an effect on the short crack fatigue crack growth rate. It was increased from the base tests.
2. The 7075 specimens had faster crack growth rates than the 2024 specimens. The baseline tests and the prior corroded 2024 specimen displayed crack growth rates that increased, then decreased, then increased again as ΔK

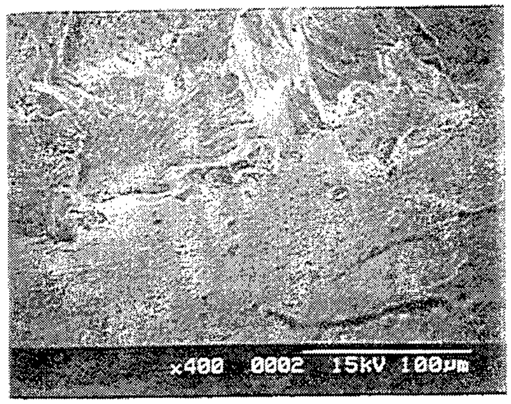

Figure 6. Nucleation site and surface damage and cracks in specimen P4-2024.

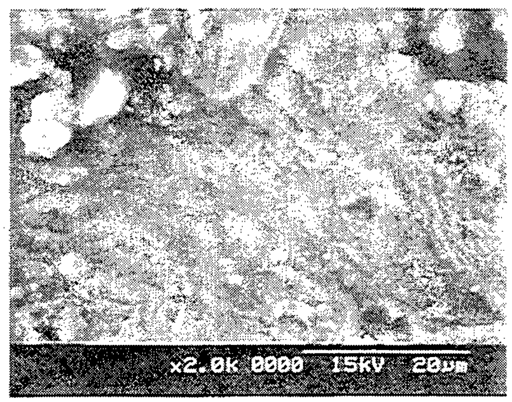

Figure 7. Possible striation marks in specimen X1-2024.

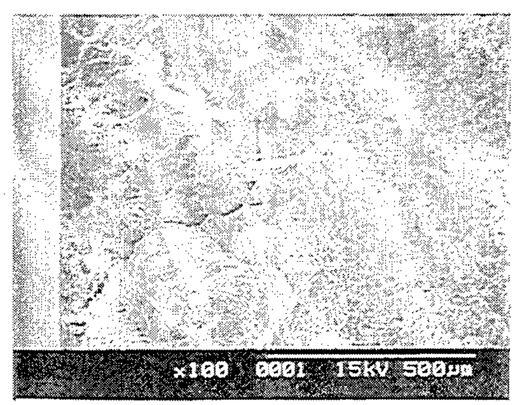

Figure 8. Secondary crack and ductile dimples on the fracture surface of specimen P3-7075.

increased. The base test of 7075 material did not show as dramatic a drop-off in crack growth rate as the 2024 tests. The prior corroded 7075 specimen data increased but did not decrease as the other specimen did.

3. The damage on the surface of the prior corroded specimens was in the form of corrosion pits and exfoliation. This made it more difficult to scan the surface of the material. The pitting and exfoliation made it harder to distinguish cracks from mudcracking.

4. Results from one test at each test condition are not conclusive statistically. They give an idea of the behavior but should be backed up by subsequent tests that are statistically planned.

5. The method of crack measuring provided a good estimate of what was taking place.

Acknowledgments

The authors wish to thank all of the past and present members of the Quality and Integrity Design Engineering Center at the University of Utah for their assistance and ideas.

References

[1] Battelle, "Economic Effects of Metallic Corrosion in the United States: A 1995 Update," (1995), p.3.

[2] D.W. Hoeppner, Lorie Grimes, Amy Hoeppner, Jim Ledesma, Tom Mills, and Akbar Shah, "Corrosion and Fretting as Critical Aviation Safety Issues: Case Studies, Facts, and Figures from US Aircraft Accidents and Incidents," ICAF 95: Estimation Enhancement and Control of Aircraft Fatigue Performance, vol. 1 (West Midlands: EMAS, 1995), pg.87-109.

[3] Lorie R. Grimes, "A Comparative Study of Corrosion Pit Morphology in 7075-T6 Aluminum Alloy" (Masters thesis, University of Utah, 1995), p.87.

[4] M.L. Du, F.P. Chiang, S.V. Kagwade, and C.R. Clayton, "Synergism between Corrosion and Fatigue of AL2024-T3 Alloy," Structural Integrity in Aging Aircraft, vol. 47 (1995), p.1.

[5] R.O. Ritchie and S. Suresh, "Mechanics and Physics of the Growth of Short Cracks," Behavior of Short Cracks in Airframe Components (Toronto: AGARD, 1983), p.1-1.

[6] Ibid., p.1-1.

[7] Warren C. Young, Roark's Formulas for Stress and Strain (New York: McGraw Hill, Inc., 1989), p.730.

[8] A.K. Vasudevan and S. Suresh, "Influence of Corrosion Deposits on Near-Threshold Fatigue Crack Growth in 2XXX and 7XXX Series Aluminum Alloys," Metallurgical Transactions A, vol. 13A (December, 1982), pg.2271-2280.

SHORT & LONG FATIGUE CRACKS:
Analysis and Implications to Life Prediction

A. K. Vasudévan
Materials Division, ONR-332
Office of Naval Research
Arlington, Virginia

K. Sadananda
Materials Technology, Code-6323
Naval Research Labs, Washington, D. C.

USAF ASIP Conference
San Antonio, Texas
3 Dec 1997

Outline

- Background
- TWO Parametric description of Damage
  - Examples
- Extension of the Concepts
  - Short Cracks
  - Overloads
  - Role of K_{max}
- Implications
  - Sensors
  - Life Prediction

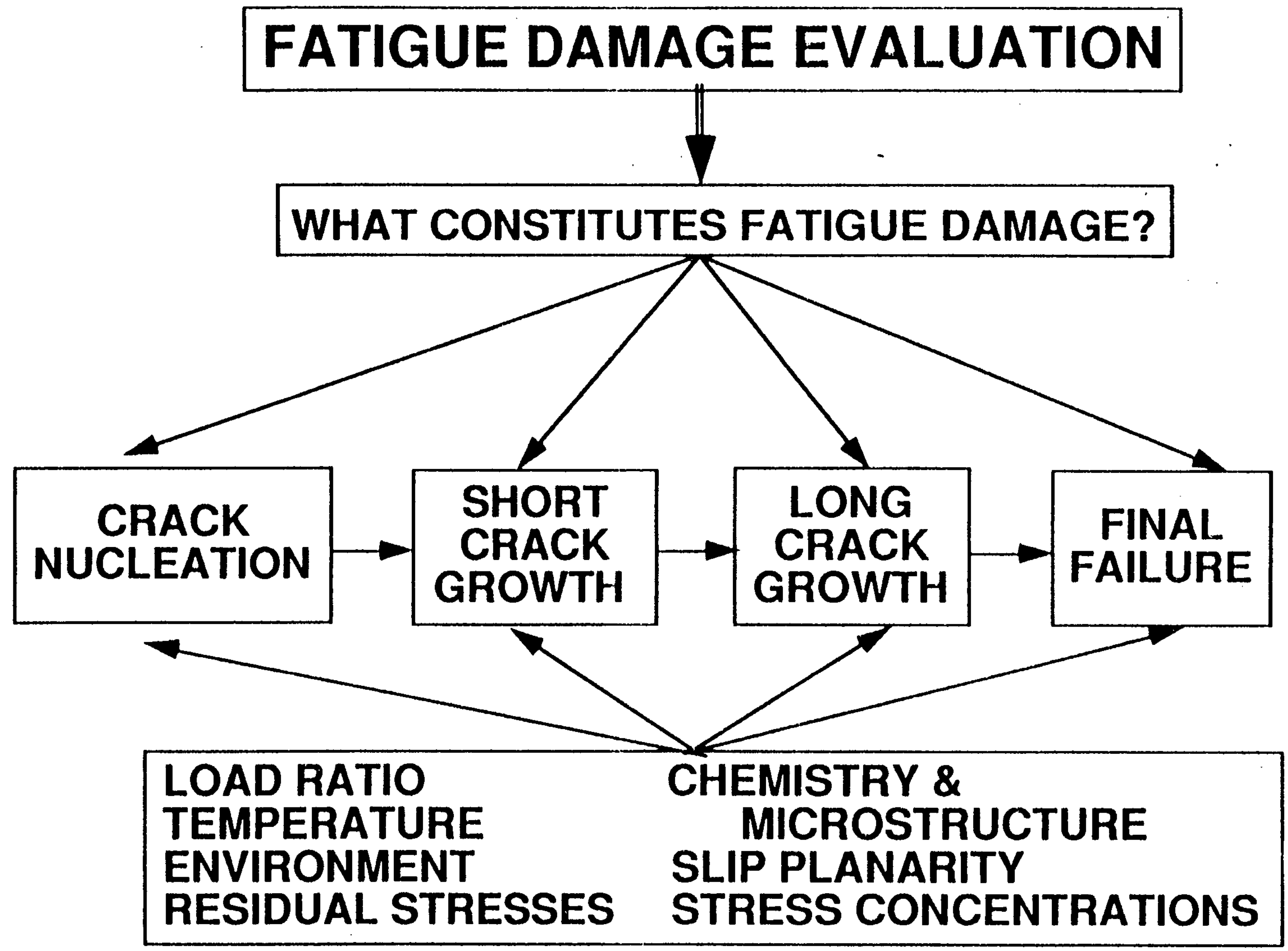
FATIGUE DAMAGE EVALUATION
WHAT CONSTITUTES FATIGUE DAMAGE?
CRACK NUCLEATION
SHORT CRACK GROWTH
LONG CRACK GROWTH
FINAL FAILURE
LOAD RATIO
TEMPERATURE
ENVIRONMENT
RESIDUAL STRESSES
CHEMISTRY & MICROSTRUCTURE
SLIP PLANARITY
STRESS CONCENTRATIONS

Beevers et al (1973, 1979)

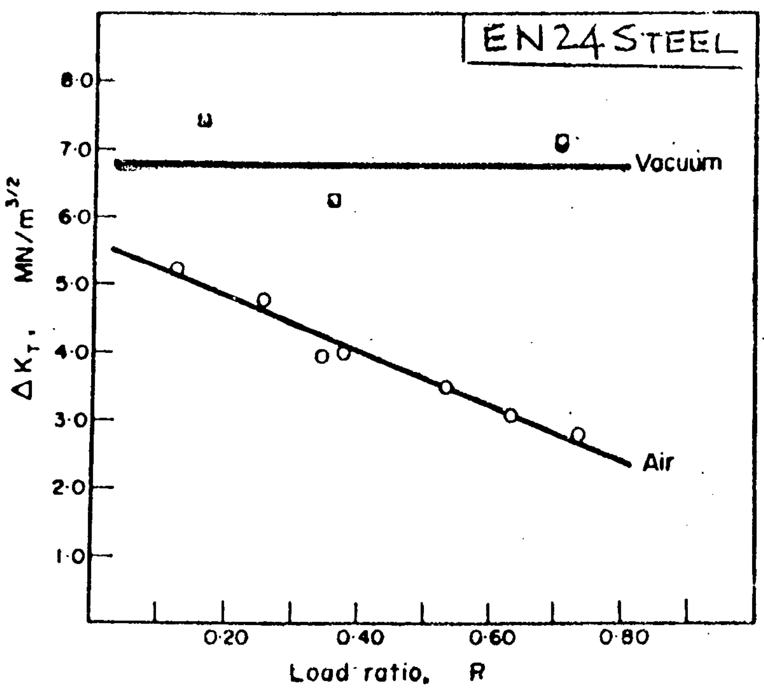

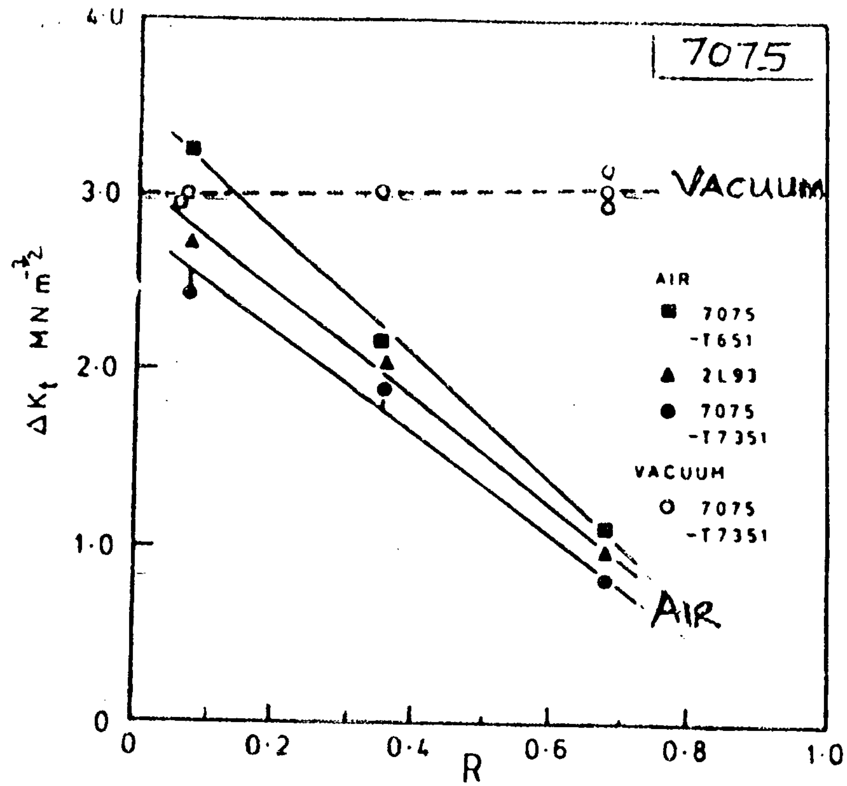

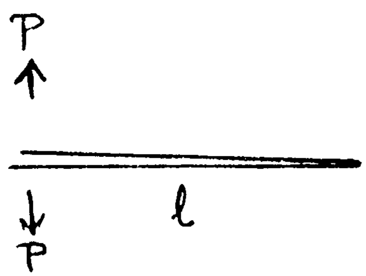

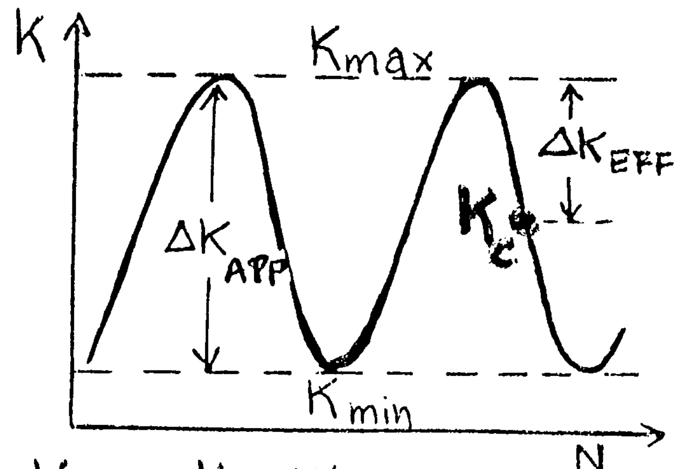

CLOSURE FROM:–

- PLASTICITY
- **ASPERITY:**
  - OXIDE
  - ROUGHNESS
  - CORROSION DEBRIS

$$\Delta K_{EFF} = K_{MAX} - K_c < \Delta K_{APP} \text{ for } K_c > K_{min} \quad (\text{low } R)$$
$$= \Delta K_{APP} = K_{MAX} - K_{min} \text{ for } K_c \leq K_{min} \quad (\text{high } R)$$

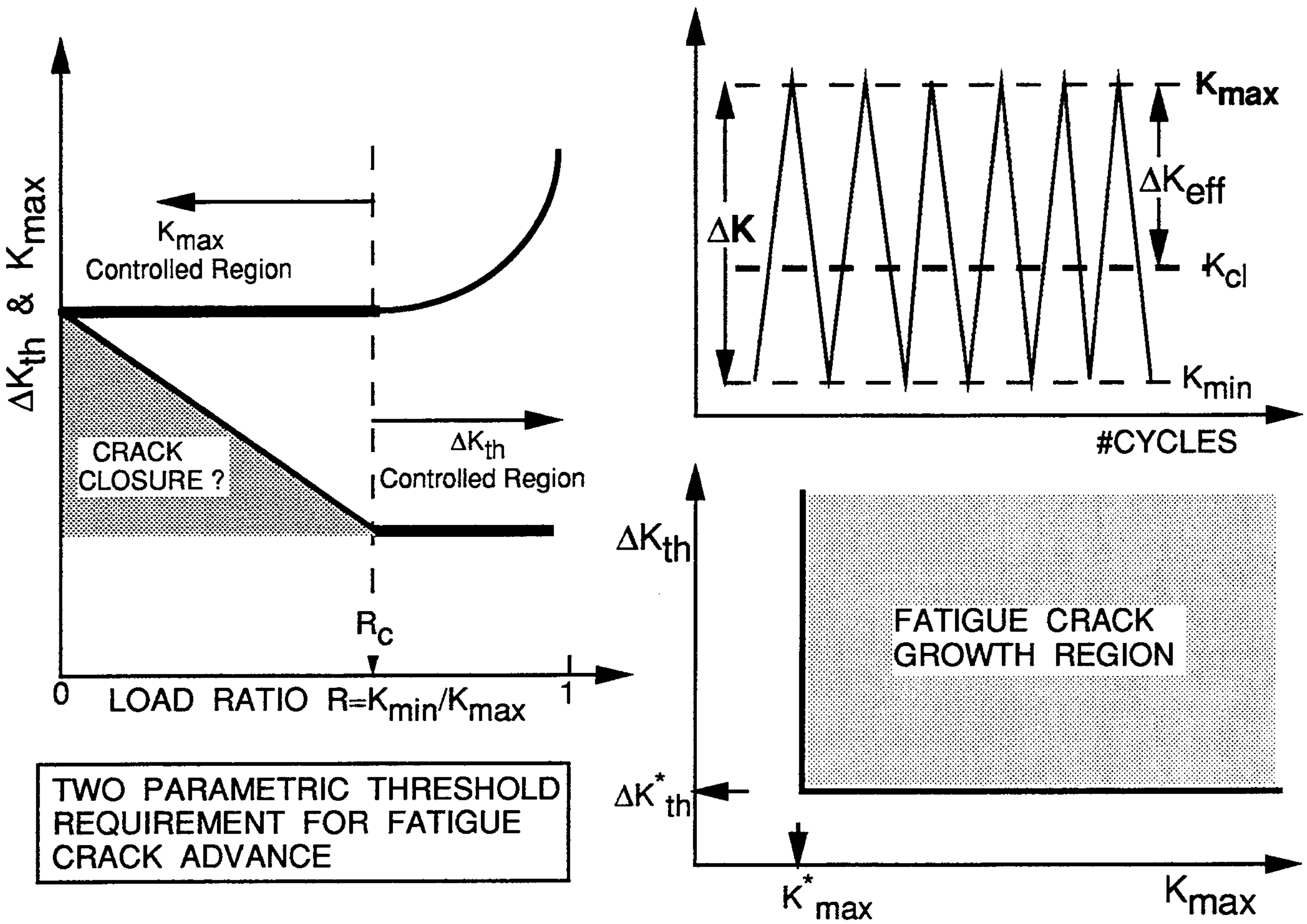
ΔKth & Kmax
Kmax
Controlled Region
CRACK
CLOSURE ?
ΔKth
Controlled Region
Rc
0
LOAD RATIO R=Kmin/Kmax
1
TWO PARAMETRIC THRESHOLD REQUIREMENT FOR FATIGUE CRACK ADVANCE
Kmax
ΔK
ΔKeff
Kcl
Kmin
#CYCLES
ΔKth
FATIGUE CRACK GROWTH REGION
ΔK*th
K*max
Kmax

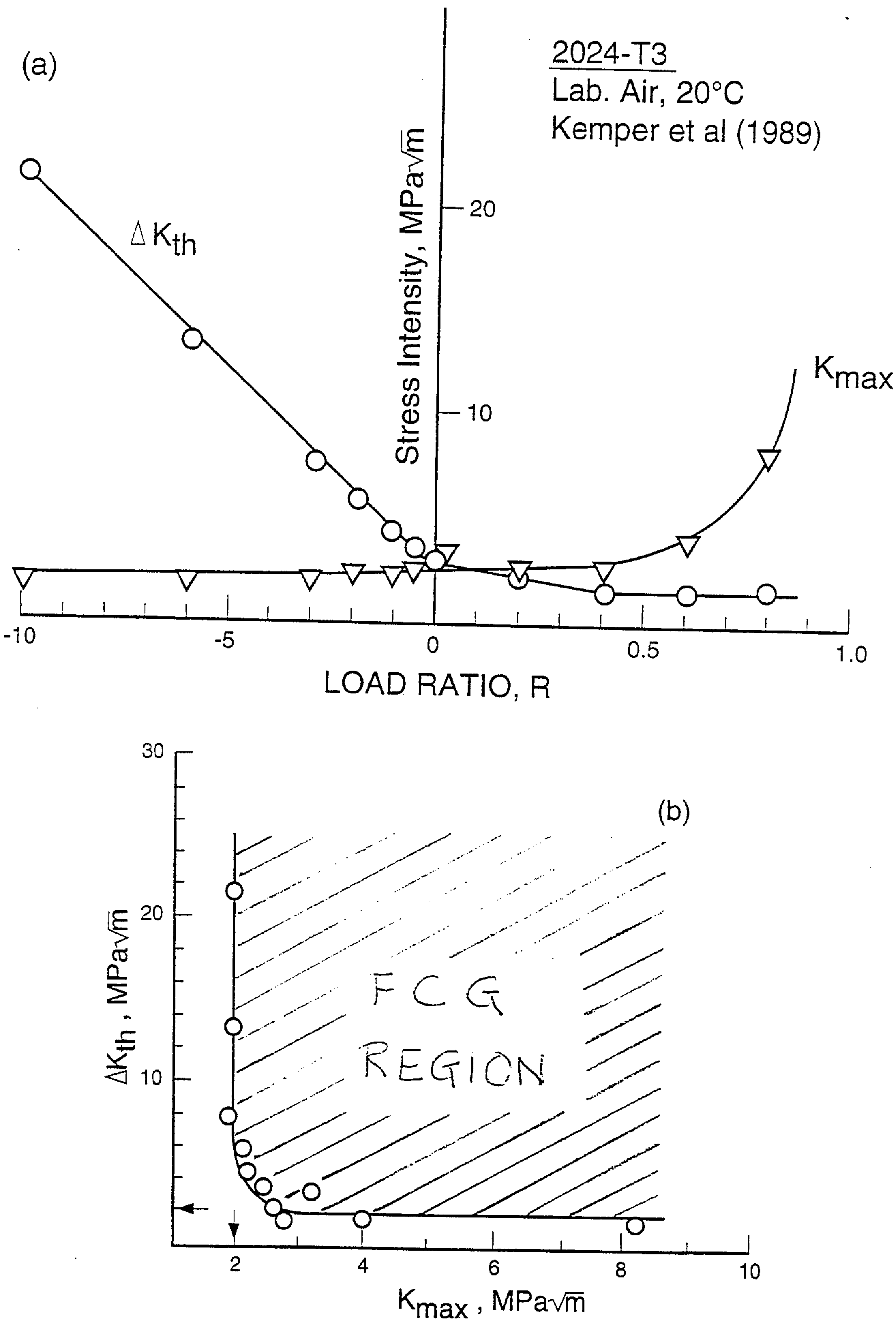

(a)
2024-T3
Lab. Air, 20°C
Kemper et al (1989)
Stress Intensity, MPa√m
20
10
Δ Kth
Kmax
-10
-5
0
0.5
1.0
LOAD RATIO, R
(b)
30
20
10
ΔKth , MPa√m
FCG
REGION
2
4
6
8
10
Kmax , MPa√m

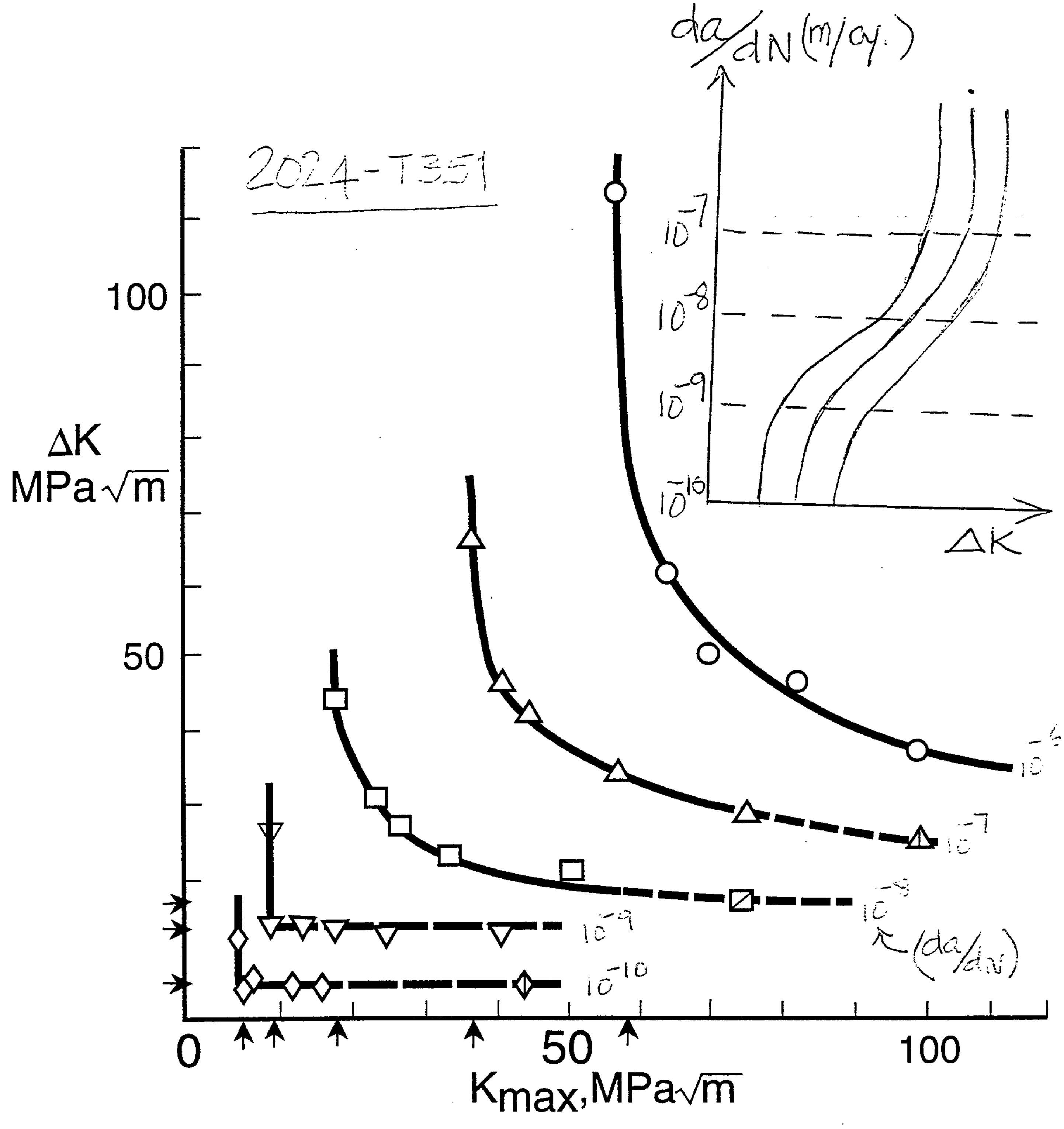
2024-T351
da/dN (m/cy.)
10^{-7}
10^{-8}
10^{-9}
10^{-10}
ΔK
100
50
ΔK MPa√m
10^{-6}
10^{-7}
10^{-8}
(da/dN)
10^{-9}
10^{-10}
0
50
100
Kmax, MPa√m

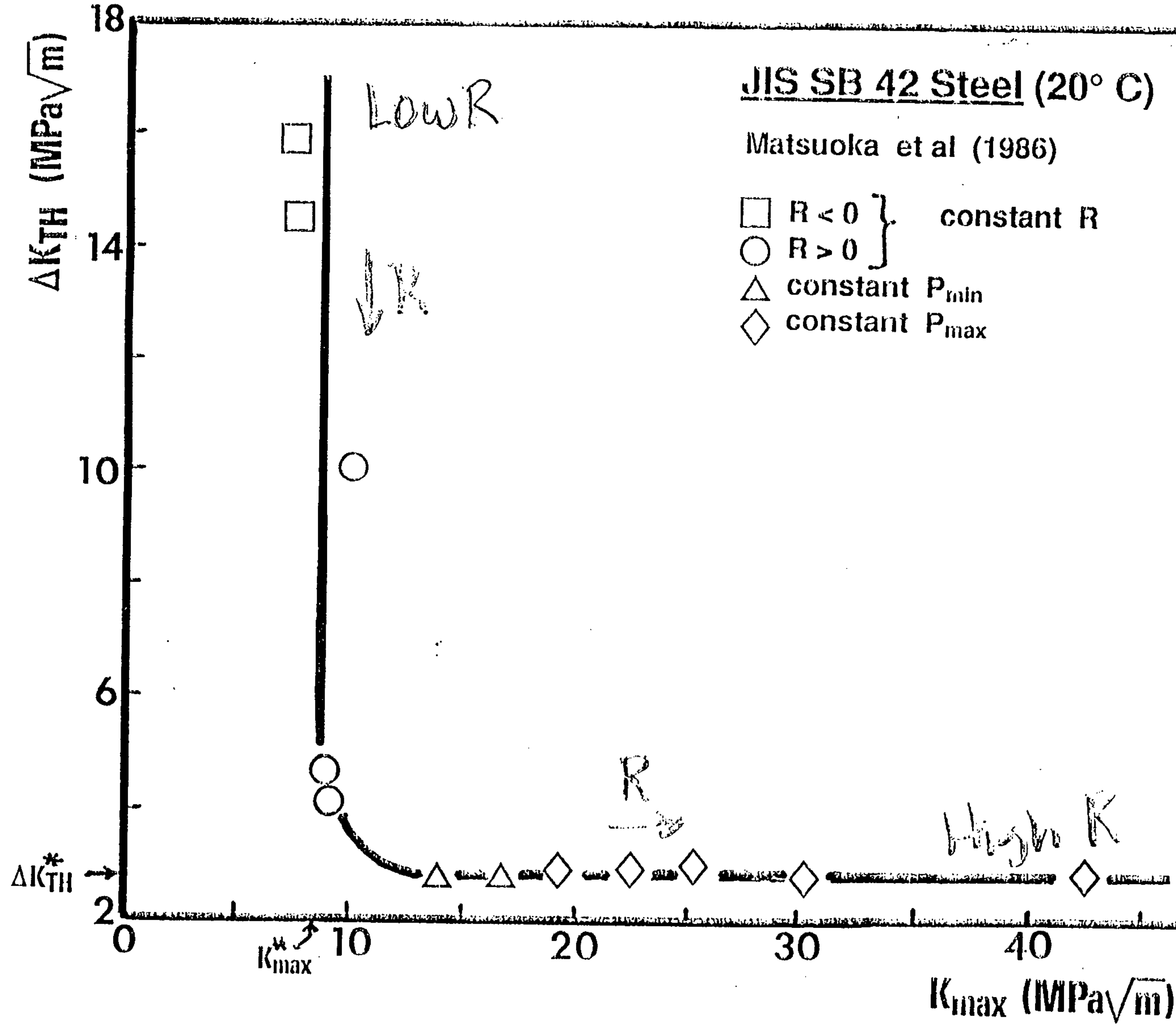
JIS SB 42 Steel (20° C)
Matsuoka et al (1986)
R < 0
R > 0
constant R
constant P_{min}
constant P_{max}
Low R
R
R
High R
ΔK_{TH} (MPa$\sqrt{m}$)
ΔK^*_{TH}
K^*_{max}
K_{max} (MPa$\sqrt{m}$)
18
14
10
6
2
0
10
20
30
40

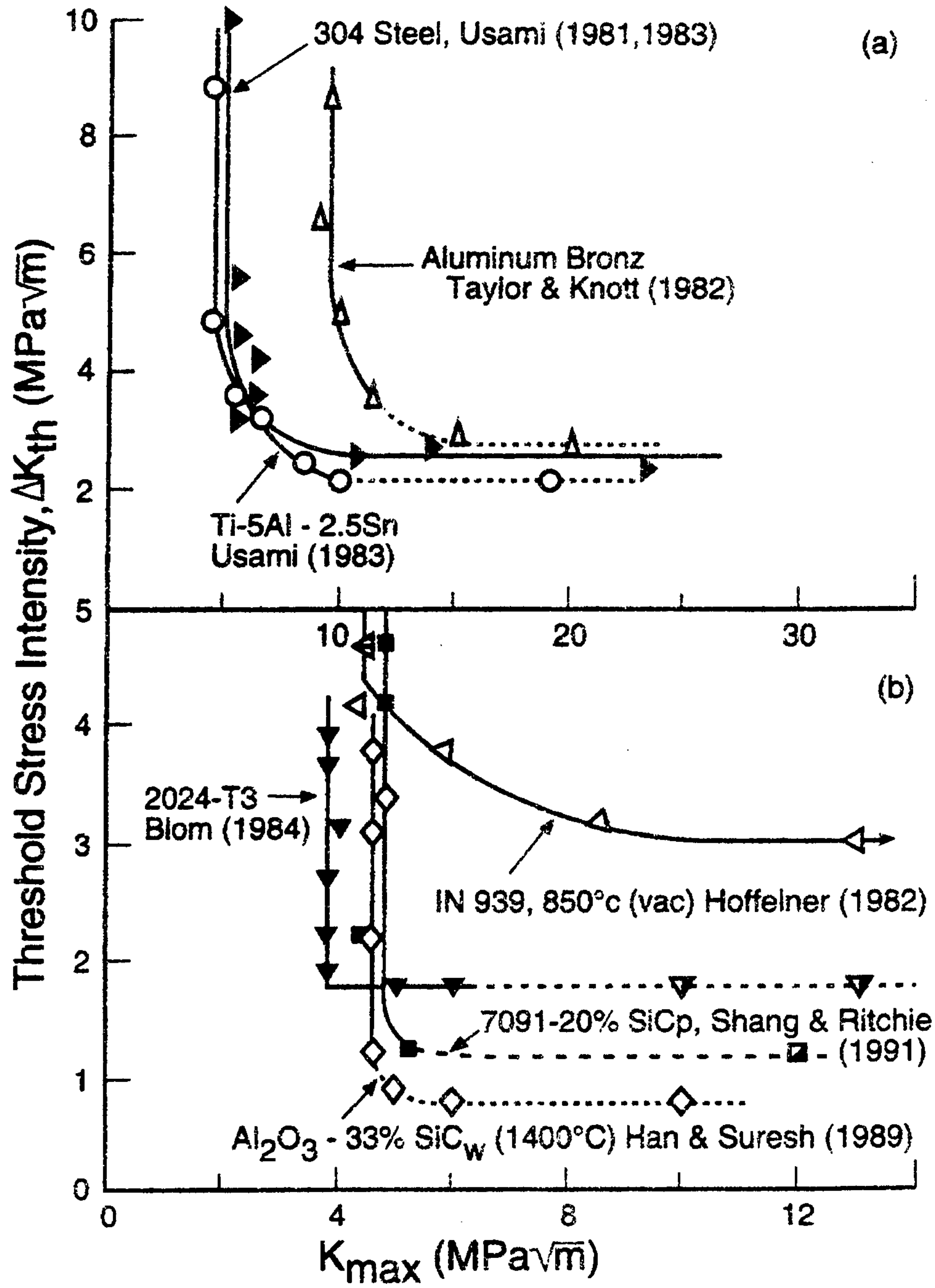

304 Steel, Usami (1981,1983)
(a)
Aluminum Bronz
Taylor & Knott (1982)
Ti-5Al - 2.5Sn
Usami (1983)
(b)
2024-T3
Blom (1984)
IN 939, 850°c (vac) Hoffelner (1982)
7091-20% SiCp, Shang & Ritchie
(1991)
Al2O3 - 33% SiCw (1400°C) Han & Suresh (1989)
Threshold Stress Intensity, ΔKth (MPa√m)
Kmax (MPa√m)

Crack Growth Rate Equation with Two Parameters

$$da/dn = (\Delta K - \Delta K^*_{th})^n \cdot (K_{max} - K^*_{max})^m \quad — (1)$$

For constant crack growth rate, C, in terms of ΔK vs. Kmax
The equation reduces to:

$$da/dn = C = (\Delta K - \Delta K^*_{th})^n \cdot (K_{max} - K^*_{max})^m \quad — (2)$$

Which reduces to:

$$\Delta K = \Delta K_{th} + \{C/(K_{max} - K^*_{max})^m\}^{1/n} \quad — (3)$$

For simplicity, taking C in the range of (0.25-1) and $n \approx 1$, the above equation reduces to:

$$\Delta K = \Delta K^*_{th} + \{C/(K_{max} - K^*_{max})^m\} \quad — (4)$$

as K_{max} approaches infinity, ΔK approaches ΔK^*_{th}
as K_{max} approaches K^*_{max}, ΔK approaches infinity

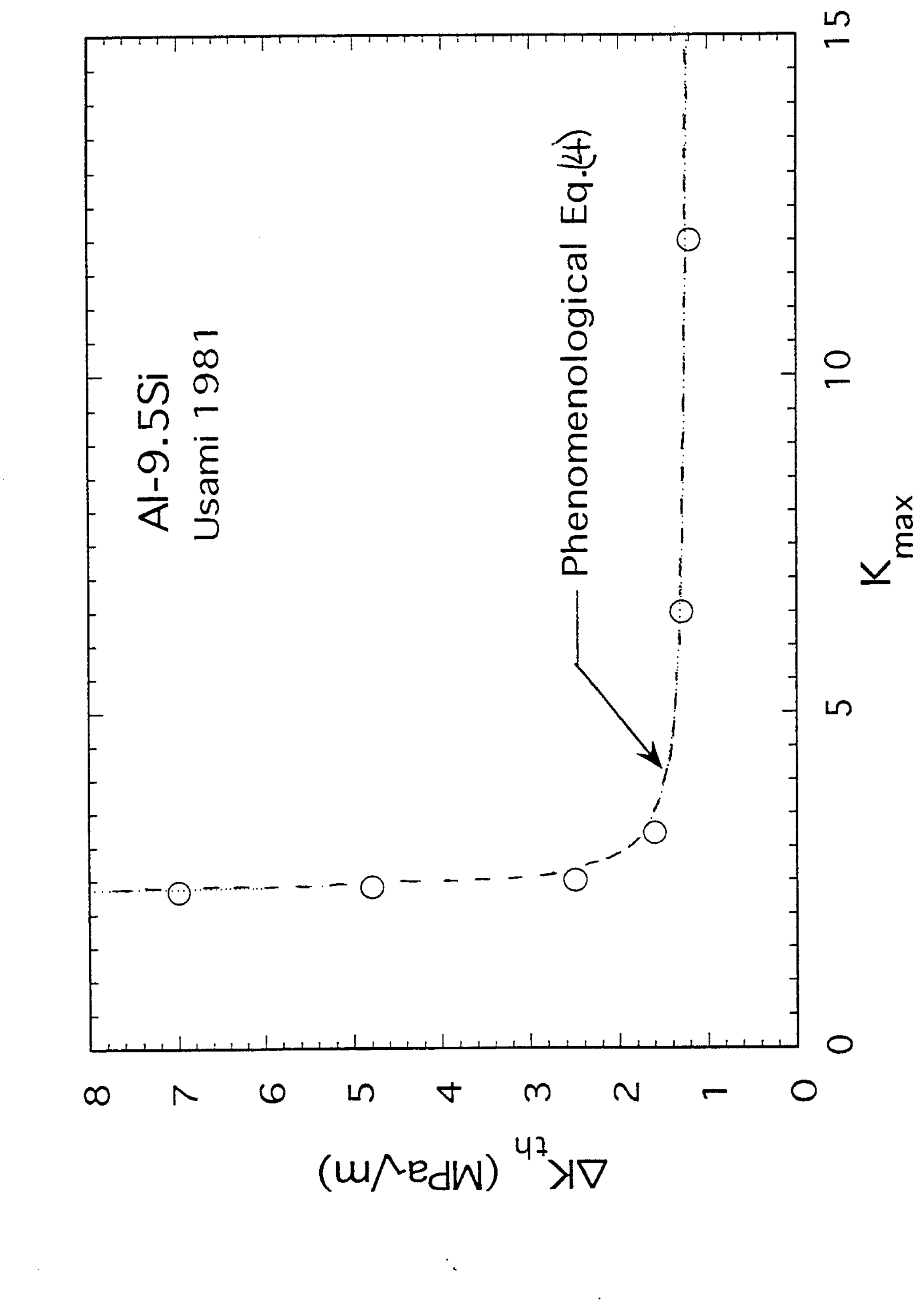

Al-9.5Si
Usami 1981
Phenomenological Eq.(4)
K_{max}
ΔK_{th} (MPa√m)
0
5
10
15
0
1
2
3
4
5
6
7
8

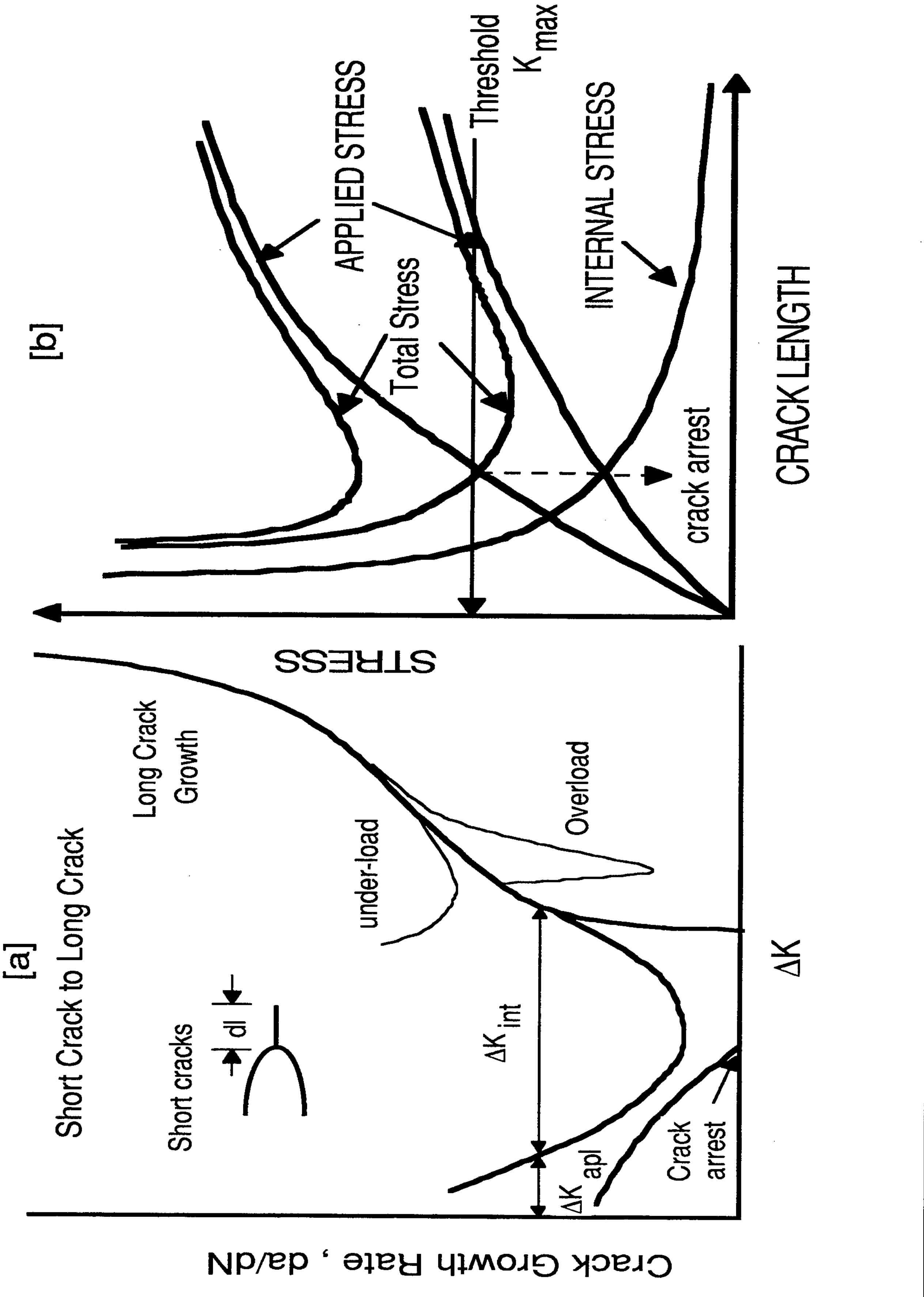
[a]
Short Crack to Long Crack
Short cracks
dl
Long Crack Growth
under-load
Overload
ΔK_{int}
ΔK_{apl}
Crack arrest
Crack Growth Rate , da/dN
ΔK
[b]
APPLIED STRESS
Threshold K_{max}
INTERNAL STRESS
Total Stress
crack arrest
STRESS
CRACK LENGTH

SHORT CRACK GROWTH IN 7075 ALLOY

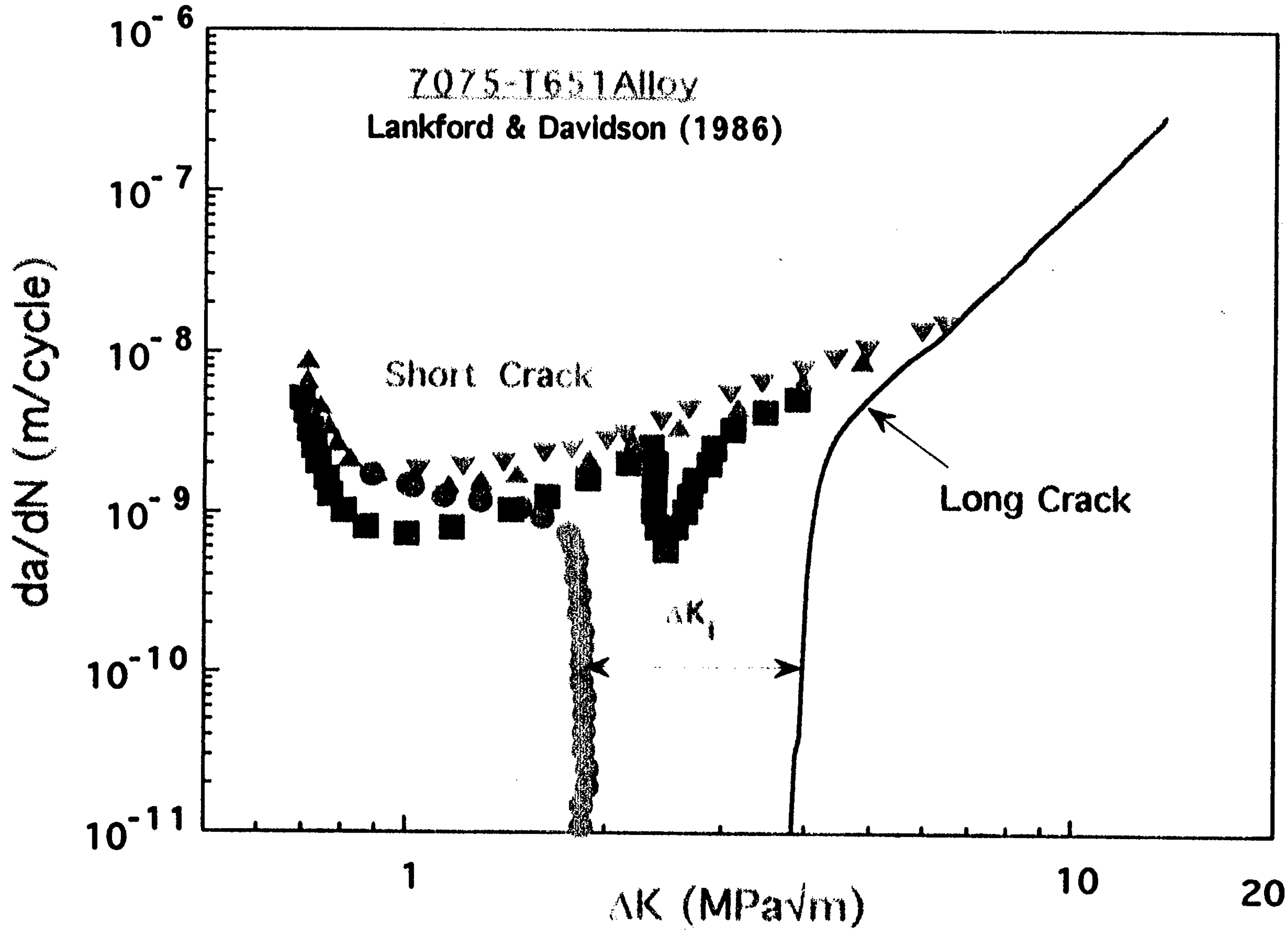

Variation of Internal Stress with Distance

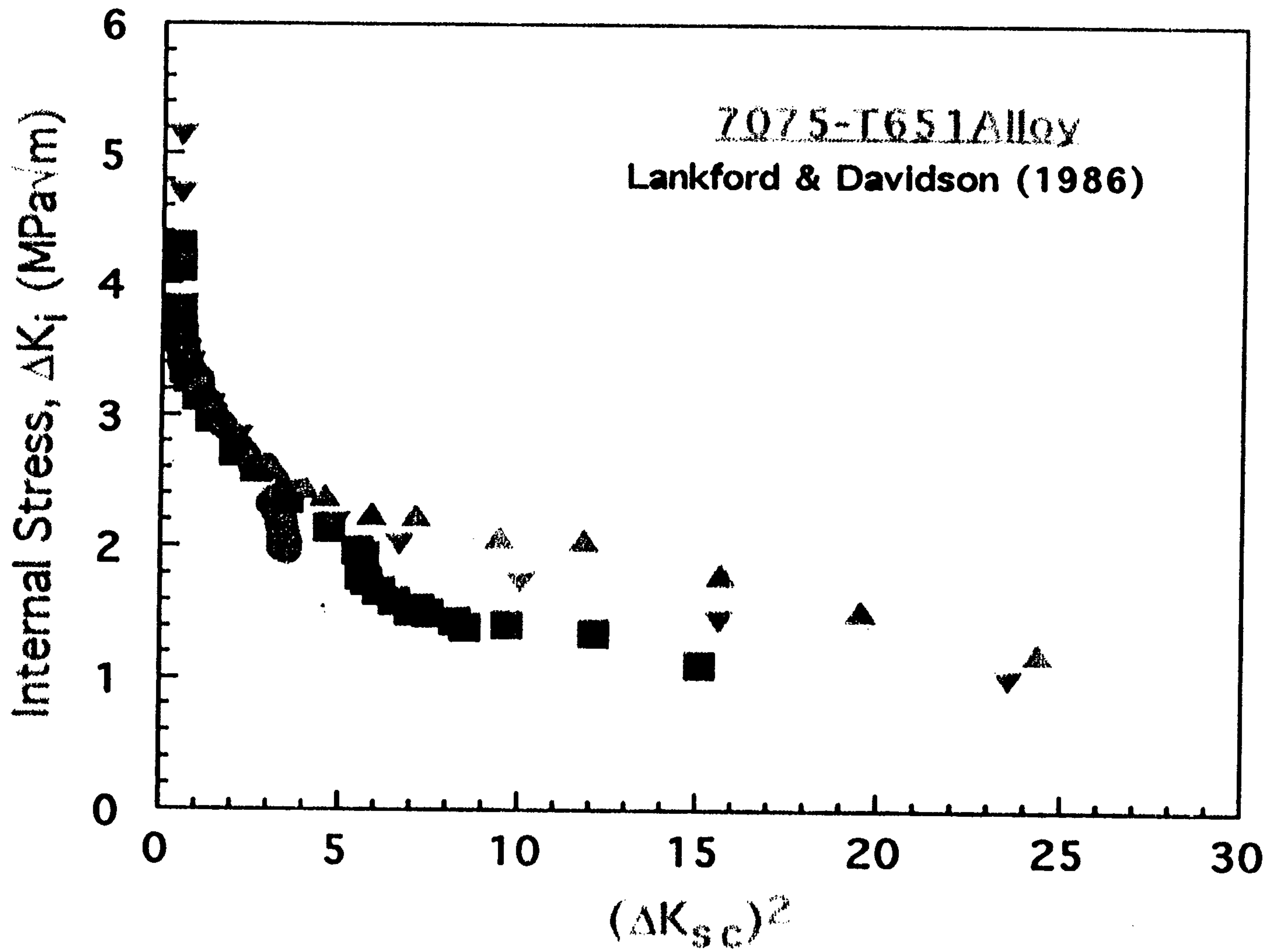

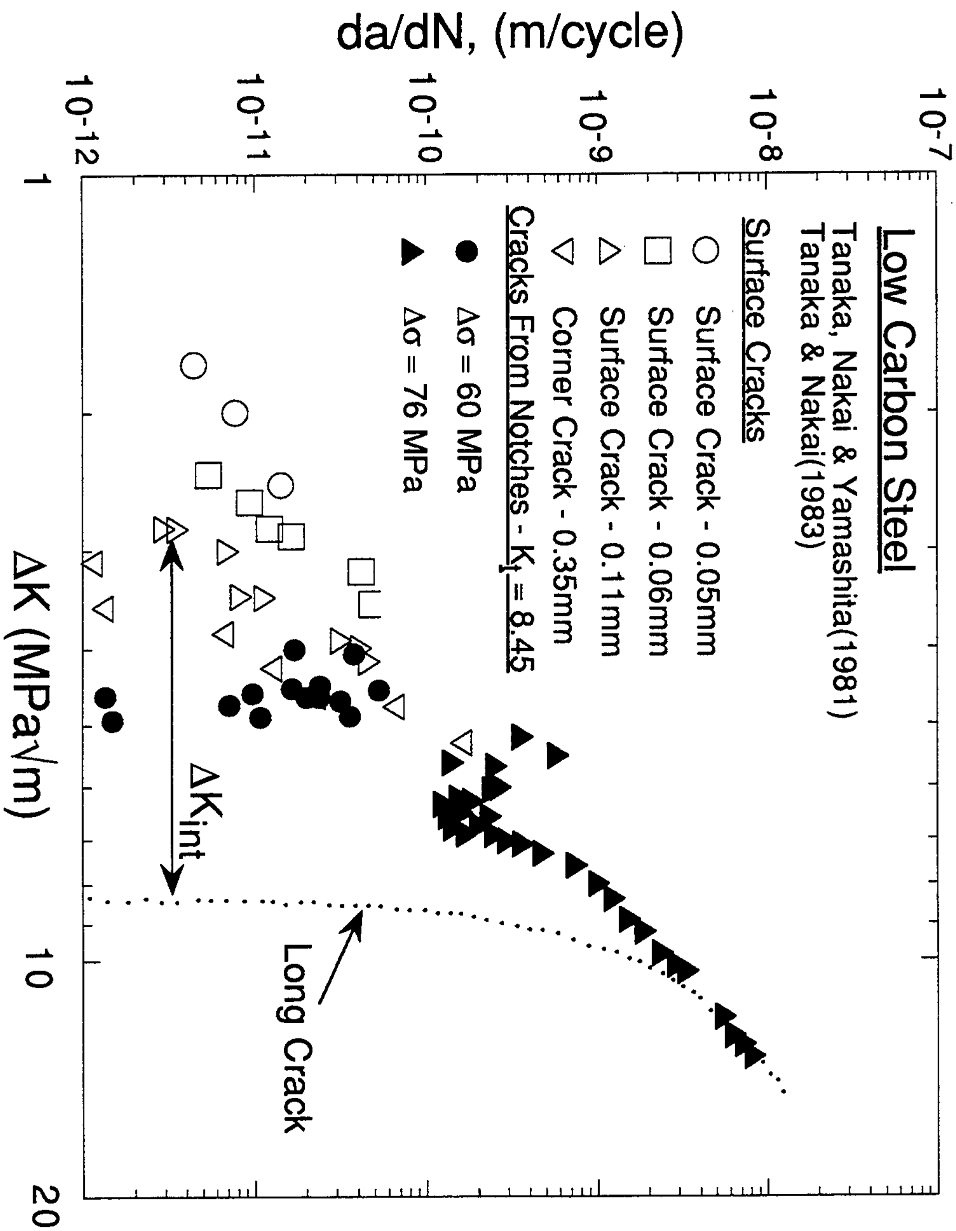

da/dN, (m/cycle)
10-7
10-8
10-9
10-10
10-11
10-12
1
10
20
ΔK (MPa√m)
Low Carbon Steel
Tanaka, Nakai & Yamashita(1981)
Tanaka & Nakai(1983)
Surface Cracks
Surface Crack - 0.05mm
Surface Crack - 0.06mm
Surface Crack - 0.11mm
Corner Crack - 0.35mm
Cracks From Notches - Kt = 8.45
Δσ = 60 MPa
Δσ = 76 MPa
ΔKint
Long Crack

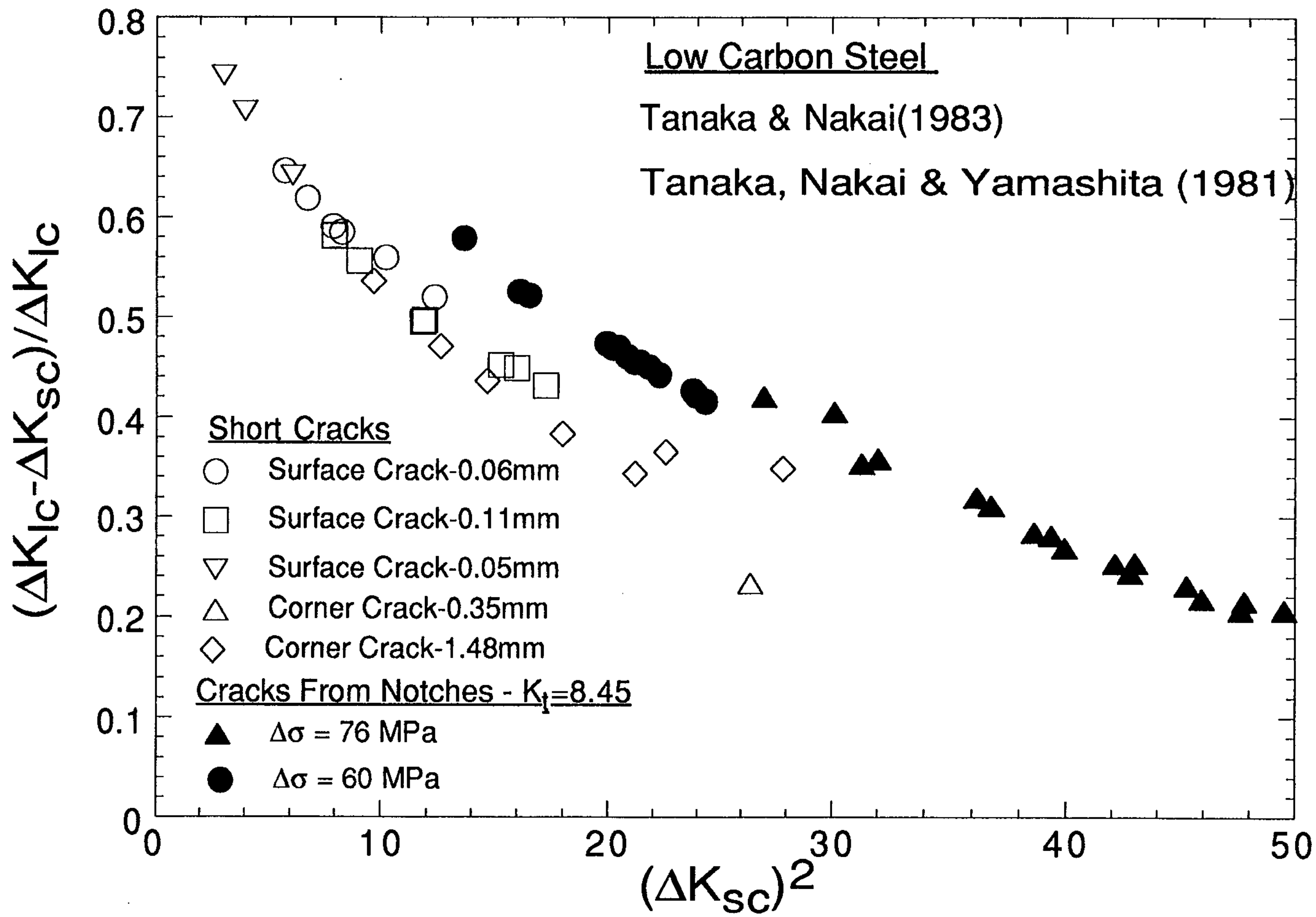
Low Carbon Steel
Tanaka & Nakai(1983)
Tanaka, Nakai & Yamashita (1981)
Short Cracks
Surface Crack-0.06mm
Surface Crack-0.11mm
Surface Crack-0.05mm
Corner Crack-0.35mm
Corner Crack-1.48mm
Cracks From Notches - K_t=8.45
$\Delta\sigma$ = 76 MPa
$\Delta\sigma$ = 60 MPa
$(\Delta K_{Ic}-\Delta K_{sc})/\Delta K_{Ic}$
$(\Delta K_{sc})^2$
0
0.1
0.2
0.3
0.4
0.5
0.6
0.7
0.8
0
10
20
30
40
50

Nucleation to short to long crack

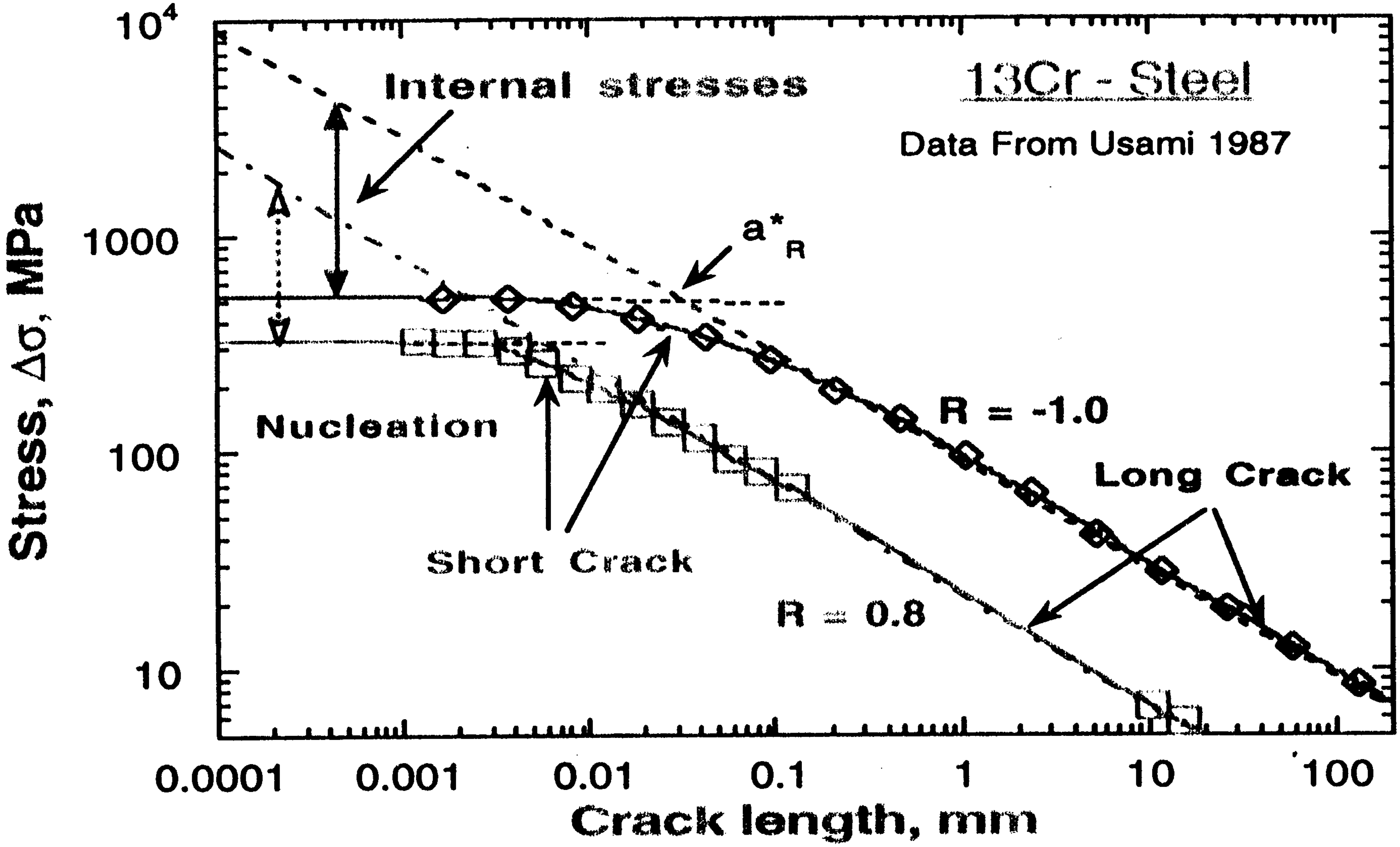

DAMAGE SPECTRUM : CRACK NUCLEATION TO CRACK GROWTH

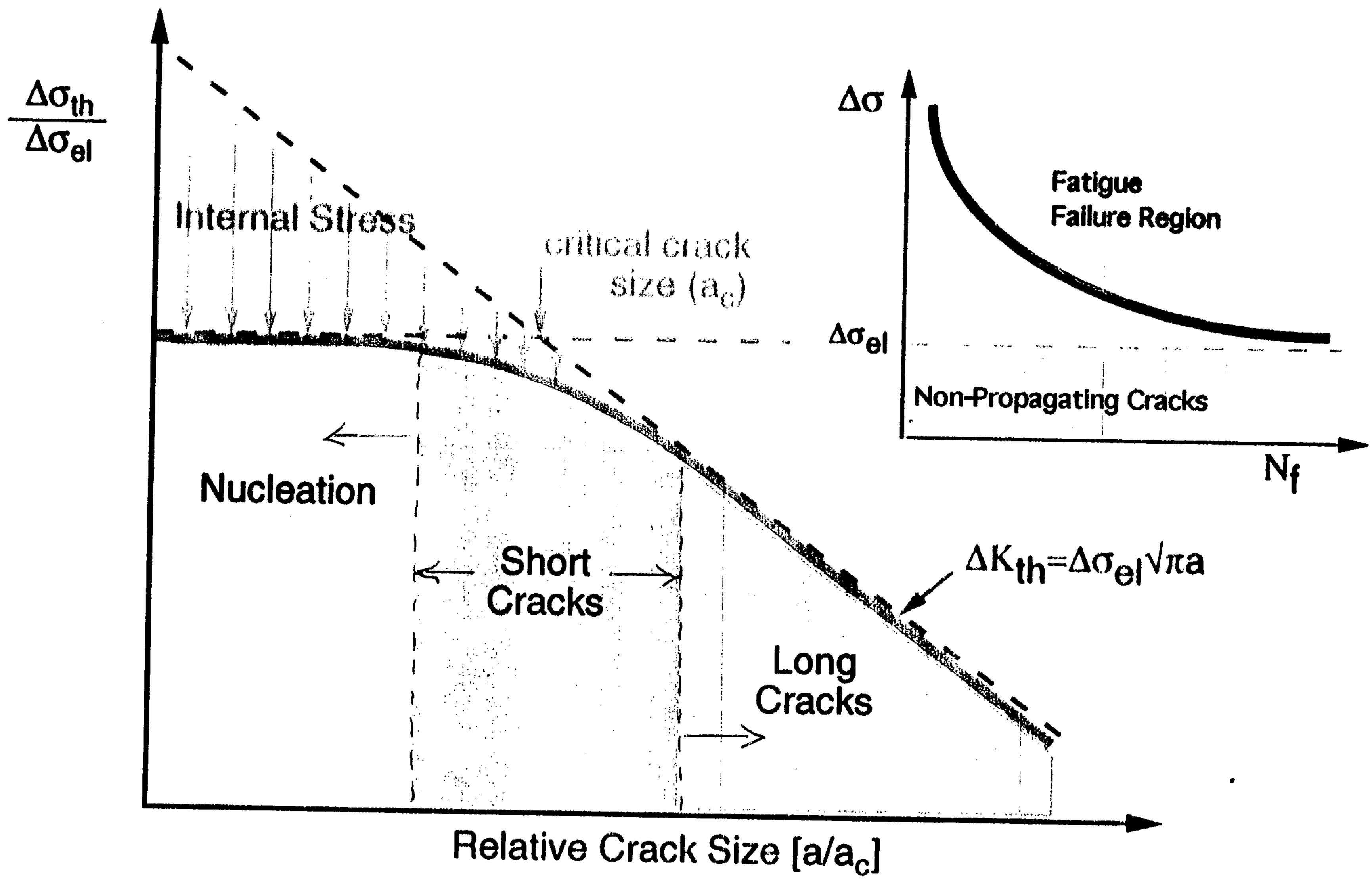

EXAMPLES OF *INTERNAL STRESSES* THAT AFFECT FATIGUE LIFE

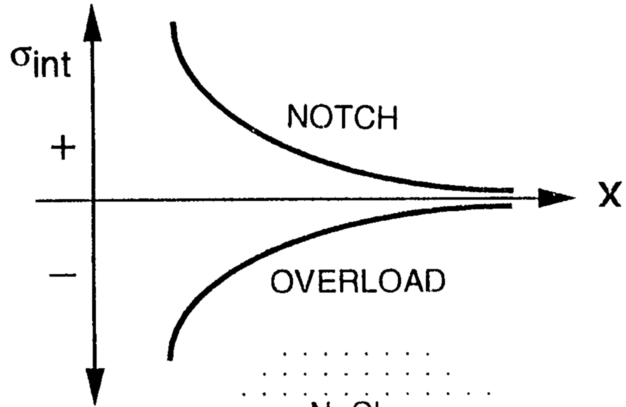

- $K_{int} = f[\sigma_{int} \sqrt{l}]$
- $K_{max}^{TOTAL} = K_{max}^{APP} \pm K_{int}$
- ΔK is normally less affected by σ_{int}

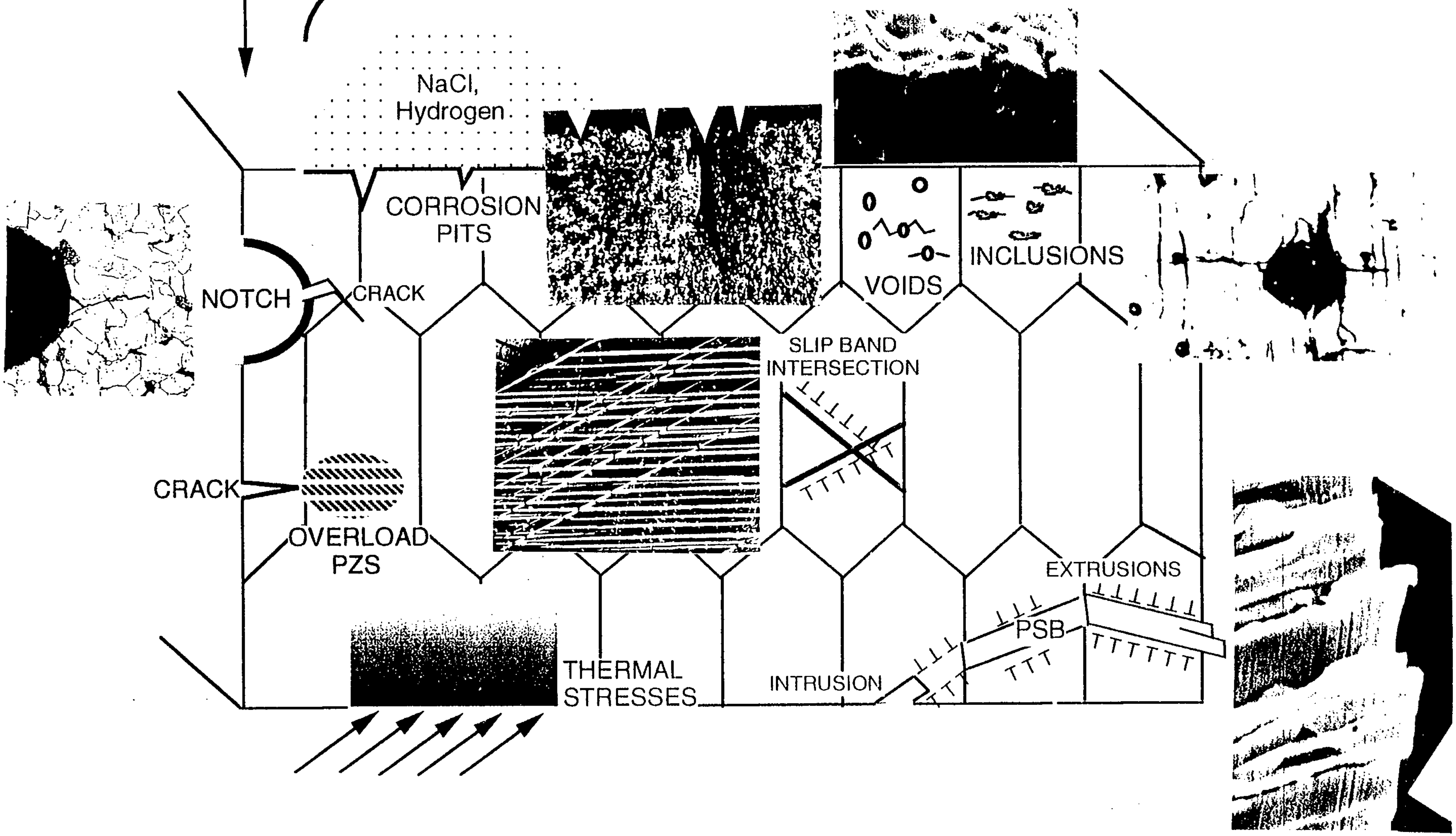

TWO METHODS OF ESTIMATING *INTERNAL STRESSES*

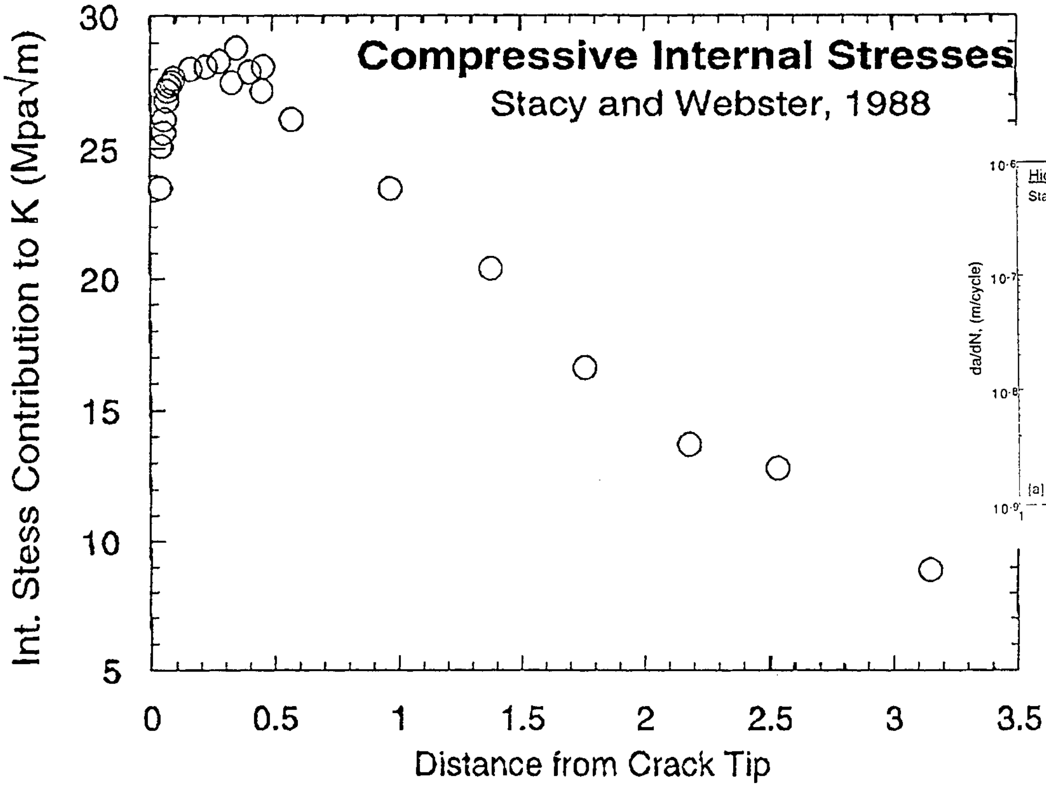

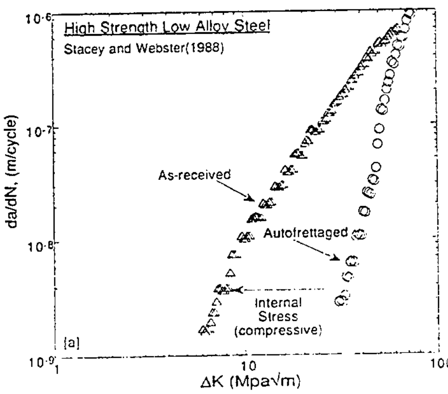

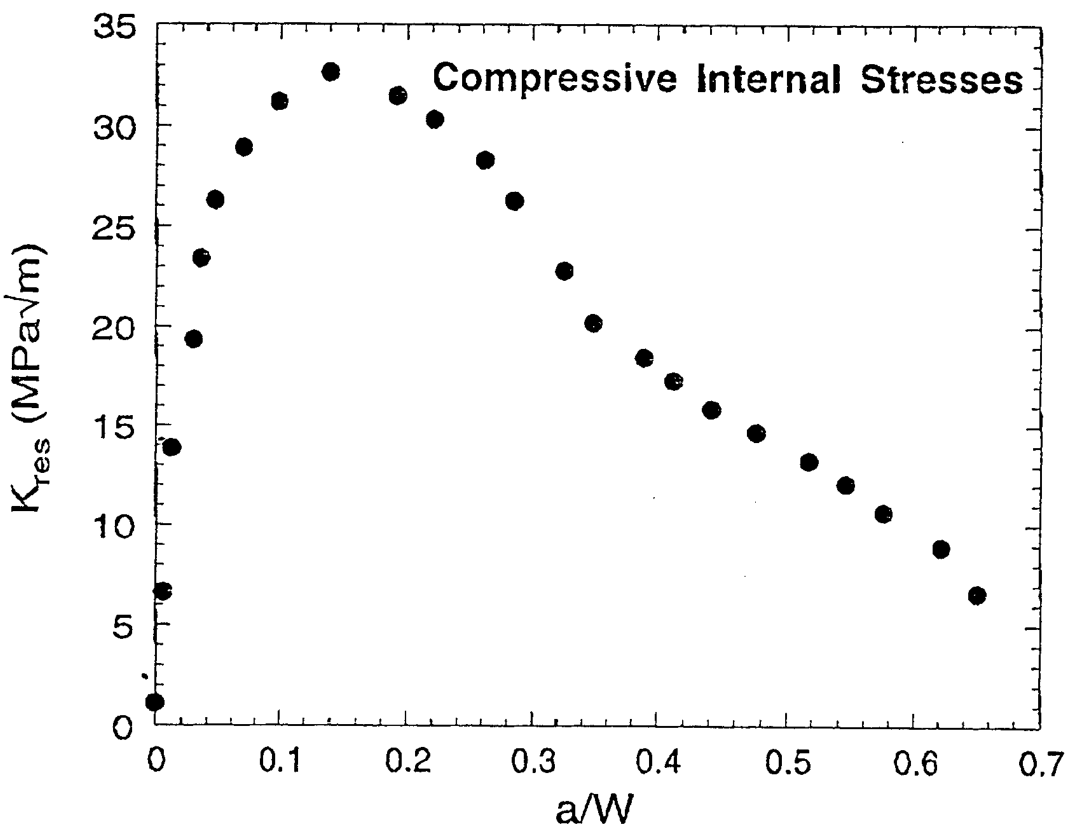

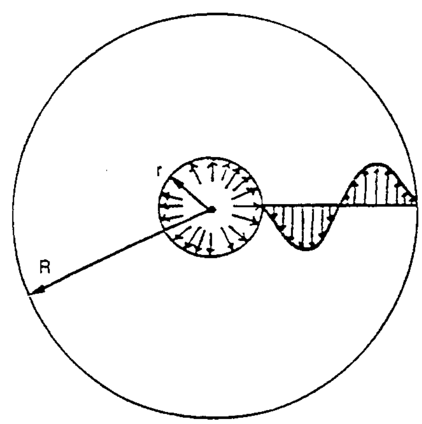

Hoop stresses in a auto frettaged tube

ROLE OF K_{max} IN OVERLOAD RETARDATION

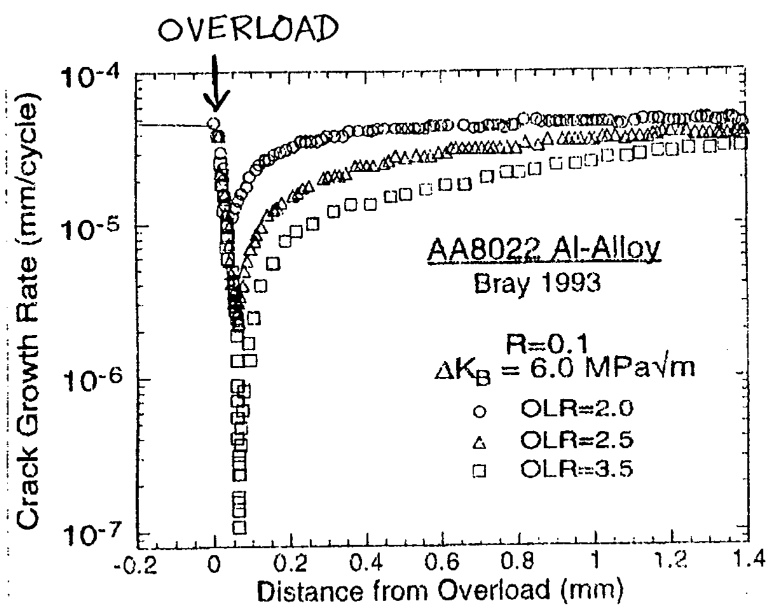

Fig. 4. Crack growth rate after overload in 8022 Al-alloy

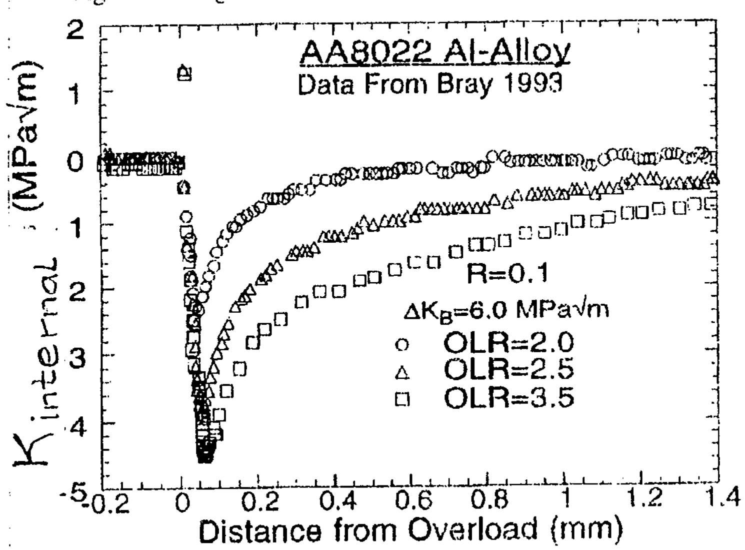

Fig. 5. Internal stress contribution from overload on crack growth

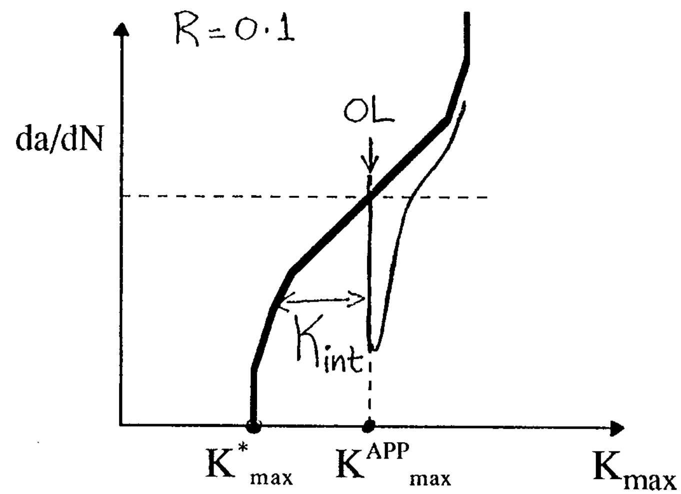

K^*_{max} **~ 1.7 Mpa√m**

$K^{TOTAL}_{max} = K^{APP}_{max} - K_{internal} = 6.6 - 4.8 =$ **1.8 Mpa√m**

At OLR > 4.0 → CRACK ARRESTS

SUMMARY-1

- Analytical framework presented for short & long fatigue cracks using the two-parameter approach
- Long crack growth represents the *fundamental* material behavior : ΔK^*th and K^*max
- Short crack behavior arises due to the presence of the *internal stresses:* notch-tip stresses, residual stresses etc
  - crack arrests when $Ktotal < K^*max$ and growth occurs when $Ktotal > K^*max$
  - short crack anamoly arises due to : not including the two thresholds & relevant internal stresses
- Overload retardations are due to the *perturbations* in the Kmax due to *internal stresses*
- Considerations of Kmax as a driving force parameter is essenstial to the description of fatigue damage

FATIGUE DAMAGE ANALYSIS

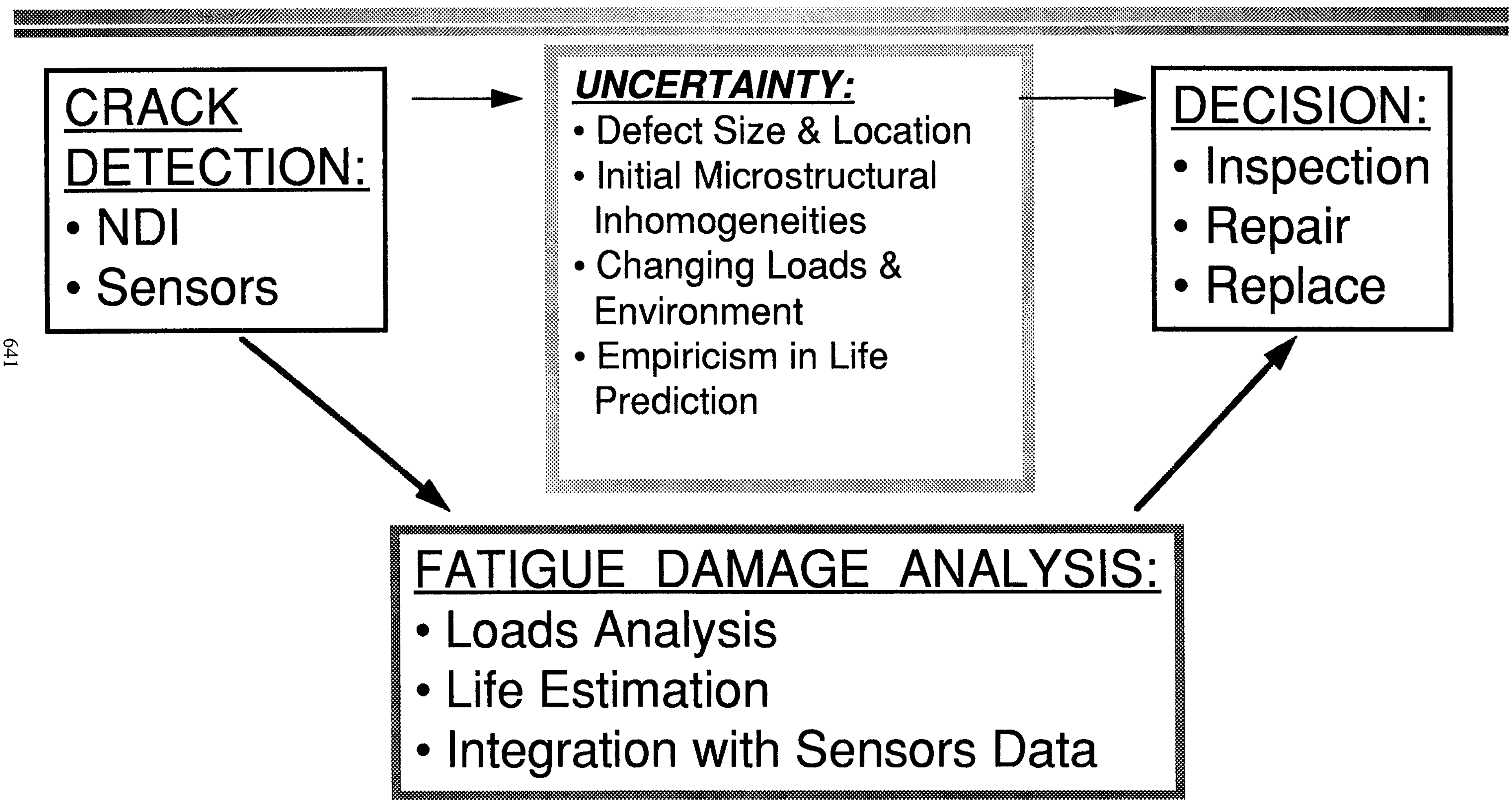

ISSUES

- How to relate the sensor's information to fatigue life prediction ?
- Challenges:
  - where to put the sensors? location? hidden parts?
  - calibration with simulated cracks?
  - need *unambiguous* interpretation of sensor signals in service operations
  - how to convert sensor's data to damage *without* much *ambiguity*

Conclusions

- Analytical methods to predict fatigue life must include: ΔK, K_{max} and K_{int} parameters
- *All* deviations from steady state crack growth can be accounted by the presence of the *internal stresses* intruduced during service
- Understanding and quantifying the role of internal stresses is fundamental to the development of a reliable LPM
- Integrated models for fatigue damage connecting:

Crack Nucleation--->Short Crack--->Long Crack--->Final Failure

Fatigue Articles by A. K. Vasudevan & K Sadananda (1992-present)

1. Reconsideration of Fatigue Crack Closure, A. K. Vasudevan, K. Sadananda & N. Louat, Scripta Metall. et Mater., vol. 27, 1673, 1992.
2. A Theoretical Analysis of Fatigue Crack Closure, N. Louat, K. Sadananda, M. S. Duesbery & A. K. Vasudevan, Metall. Trans., vol 24A, 2225,1993.
3. Two Critical Stress Intensities for Threshold Fatigue Crack Propagation, A. K. Vasudevan, K. Sadananda & N. Louat, Scripta Metall. et Mater., vol. 28, 65,1993.
4. Fatigue Crack Growth in Metal Matrix Composites, A. K. Vasudevan & K. Sadananda, Scripta Metall. et Mater., vol.28, 837, 1993.
5. Critical Evaluation of Crack Closure and Related Phenomena : I Background and Experimental Results, A. K. Vasudevan, K. Sadananda & N. Louat, in Fatigue '93 , Eds. J. P. Bailon & J. I . Dickson, Montreal, Canada, vol.I, p. 565, 1993.
6. Critical Evaluation of Crack Closure and Related Phenomena : II Theoretical Evaluation, K. Sadananda , N. Louat & A. K. Vasudevan, in Fatigue '93 , Eds. J. P. Bailon & J. I . Dickson, Montreal, Canada, vol. I, p.571, 1993.
7. Development of New Concepts for Fatigue Crack Thresholds, K. Sadananda & A. K. Vasudevan, NRL Review '93., p.161, 1993.
8. Critical Evaluation of Crack Closure and The Driving Force for High Temperature Fatigue Crack Growth, K. Sadananda & A. K. Vasudevan, in Aspects of High Temeprature Deformation & Fracture of Crystalline Materials, JIMIS-7 Proc., Eds. Y. Hasoi et al, Nagoya, Japan, p. 551, 1993,
9. A Study of Crack Closure, Fatigue Crack Threshold & Related Phenomena, A. K. Vasudevan, K. Sadananda & N. Louat, Matls. Sc & Engg., vol.A188, p.1, 1994.(invited review)
10. A new Interpretation for Fatigue Crack Propagation, A. K. Vasudevan & K. Sadananda, in Strutural Integrity :Experiments-Models-Applications, ECF-10, Eds. K-H. Schwalbe & C. Berger, EMAS Publs., vol.2, p.1461, 1994.
11. Canonical Theory of Fatigue Crack Growth, K. Sadananda & A. K. Vasudevan, in Strutural Integrity : Experiments-Models-Applications, ECF-10, Eds. K-H. Schwalbe & C. Berger, EMAS Publs., vol.2, p.1309, 1994.

Fatigue Articles (contd)

12. Fatigue Crack Growth in Aluminum-Base Alloys,A. K. Vasudevan & K. Sadananda, in 4th International Conference on Aluminum Alloys, Eds. T. H. Sanders, Jr & E. A. Starke, Jr, vol.3, p.227, 1994, (invited review).
13. Analysis of Fatigue Crack Closure & Thresholds, K. Sadananda & A. K. Vasudevan, ASTM Fracture Mechanics 25th volume, ASTM STP - 1220, p.484, 1995.
14. Classification of Fatigue Crack Growth Behavior, A. K. Vasudevan & K. Sadananda, Metallurgical . & Materials. Transaction. vol.26A, p.1221,1995.
15. Fatigue Crack Growth in Ceramics & Composites, K. Sadananda & A. K. Vasudevan, 19th Annual Conf. on Advanced Ceramic Materials, & Structures, ACS Proc., p. 181,1995.
16. New Concepts Applied to Fatigue Crack Growth in Composites, K. Sadananda & A. K. Vasudevan, COMPOSITES '95: Recent Advances in Japan & USA, CCM-VII, p. 569,1995.
17. Fatigue Crack Growth Bevavior in Titanium Aluminides, K. Sadananda & A. K. Vasudevan, Materials Science & Engg., vol. A192/193, p.490,1995.
18. Fatigue Crack Growth Behavior of Composites, A. K. Vasudevan & K. Sadananda, Metallurgical & Materials Transactions.A, vol. 26A, p. 3199, 1995.
19. The Controlling Parameters of Fatigue Crack Growth Behavior in Al-Li 8090 Alloy, C. A. Green, T. L. Holtz, K. Sadananda & A. K. Vasudevan, Micromechanics of Advanced Materials, Edtrs. S. N. G. Chu et al., p.127, 1995.
20. Dislocation-Crack Interactions & their Relevance to Fatigue Crack Growth, K. Sadananda, A. K. Vasudevan & N. Louat, Micromechanics of Advanced Materials, Edtrs. S. N. G. Chu et al., p.147, 1995.
21. A Unified Framework for Fatigue Crack Growth, K. Sadananda & A. K. Vasudevan, FATIGUE '96 Conference, Berlin, Eds. G. Lutjering & N. Nowack, Vol. 1, p. 375, 1996.
22. Fatigue Crack Growth in Advanced Materials, A. K. Vasudevan & K. Sadananda, FATIGUE '96 Conference, Berlin, Eds. G. Lutjering & N. Nowack, Vol. 1, p. 473, 1996.

Fatigue Articles (contd.)

22. Fatigue Crack Growth in Advanced Materials, A. K. Vasudevan & K. Sadananda, FATIGUE '96 Conference, Berlin, Eds. G. Lutjering & N. Nowack, Vol. 1, p. 473, 1996.
23. Short Fatigue Crack Growth Behavior, K. Sadananda, & A. K. Vasudevan, ASTM-STP 27th Symposium on Fatigue & Fracture Mechanics, 1997, in press.
24. High Temperature Fatigue Crack Growth, K. Sadananda & A. K. Vasudevan, Int. Journal of Fatigue, 1997, in press.
25. Short Fatigue Cracks - Implications & Applications, K. Sadananda & A. K. Vasudevan, Int. Journal of Fatigue, 1997, in press.
26. Role of Grain size & Precipitates on Long Fatigue Cracks, A. K. Vasudevan & K. Sadananda, Int. Journal of Fatigue, 1997, in press.
27. Short Fatigue Crack Growth Phenomena, International Materials Review [invted review], 1997, in preparation
28. Role of Environment on Fatigue Crack Propagation, A. K. Vasudevan & K. Sadananda, TriCity Corrosion Conference Proceedings, in press, 1998.
29. Role of K_{max} on Fatigue Crack Growth, K. Sadanandan, A. K. Vasudevan, S. Biner & K. Jata; Paul Paris Symposium TMS Proceedings, in press, 1998.

<u>NOTE</u>: The proceedings of the First International Fatigue Conference held at Cape Cod, in Sept. 1997 will be published in the International Journal of Fatigue, to be published by Elsevier, London, Dec 1997-Jan1998.

Second International Conference on
FATIGUE DAMAGE IN STRUCTURAL MATERIALS

Organized by

A. K. Vasudevan, Office of Naval Research

J. T. Cammett, Naval Aviation Depot

T. Nicholas, Airforce Labs.

K. Jata, Airforce Labs.

- Topics: Crack Initiation & Crack Growth
  - microstructure & environmental effects
  - variable amplitude/service loading
  - mechanisms, models & applications
- Date & Place: August 31-September 4, 1998 ← (Abstracts due by Jan 15, 1998)
  Hyannis, Cape Cod, Mass., USA
- For details contact: Ms. Barbara Hickernell, Engineering Foundation, New York:212-705-7836(phone); 212-705-7441(FAX); engfnd@aol.com; & www. engfnd.org

SESSION VIII

FATIGUE CRACK AND GROWTH

Chairman - *E. Davidson*
Aeronautical Systems Center

Fretting As a Fatigue Crack Nucleation Mechanism A Close-up View

Dr. Charles B. Elliott III*, P.E.
Dr. David W. Hoeppner, P.E.
Quality and Integrity Design Engineering Center
Department of Mechanical Engineering
University of Utah
Salt Lake City, Utah 84112-9208

Abstract

Personnel in the Quality and Integrity Design Engineering Center (QIDEC) at the University of Utah, investigated the fatigue characteristics of 8090 T7 and 7075 T7351 aluminum alloys under fretting conditions in air and vacuum environments. The purpose of this investigation was to provide insights into the effects of corrosion, specifically oxidation in air, on the fretting fatigue process. As a result of this investigation, it is concluded that crack nucleation and early propagation are influenced by material, environment, and local conditions in the area of relatively great damage where the crack is formed. It is recommended that where the effects of fretting fatigue are an issue, the local conditions that influence the fretting fatigue process should be investigated. Understanding these conditions for the materials being investigated may help in developing procedures for alleviating the effects of fretting fatigue.

Introduction

Life reduction due to fretting is having significant impact on Air Force systems. It is a major factor causing the high cycle fatigue problems currently being investigated by the Air Force. This paper discusses some of the factors that influence fretting and the fretting fatigue process.

ASTM defines fretting as "a wear phenomenon occurring between two surfaces having oscillatory relative motion of small amplitude."[1] In air the process includes oxidation of the wear debris which is trapped between the two surfaces. When fatigue loading is present the combined fretting fatigue process can result in a reduction in fatigue life of more than an order of magnitude compared to fatigue without fretting.

The fretting fatigue test system used in this experimentation was developed within QIDEC to enable testing either in air or a scanning electron microscope (SEM) vacuum environment. This allows investigation of fretted surfaces of specimens tested in the SEM without the SEM vacuum being broken. Therefore, fretting fatigue damage of specimens tested in the SEM can be considered as resulting from wear only, whereas damage from tests in air results from the concurrent wear and oxidation mechanisms. A top-view picture of the fretting fatigue load frame is shown in Figure 1, and the load frame mounted in the SEM is shown in Figure 2. Additional information concerning the test system is in references 2 and 3.

The experimentation was conducted to develop cycles-to-failure fretting fatigue data for the 8090 T7 and 7075 T7351 aluminum alloys under various conditions in air and vacuum environments and to gain insights into the effects of corrosion on the fretting fatigue process. To address the second objective, that of gaining insights, fractographic investigations were conducted of specimens that had failed during testing. Additionally, tests of eighteen specimens were stopped prior to failure so that the fretted surfaces could be investigated in the SEM and the specimens could be sectioned for metallographic investigation to gain insights into the crack nucleation process. This paper focuses on the SEM, metallographic, and fractographic investigations. The cycles-to-failure data are summarized in this

paper to enable the reader to put the pictographic results in perspective. They are reported in reference 2 and in the paper submitted for publication as noted in references 4.

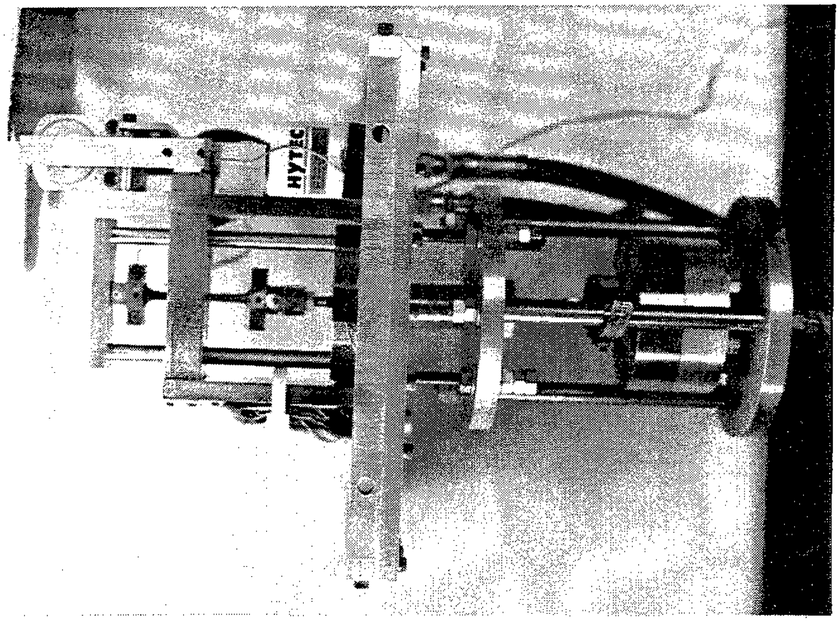

Figure 1. A top-view picture of the fretting fatigue load frame. The vertical plate in the center acts as the SEM lid. The part to the left of this plate fits into the SEM.

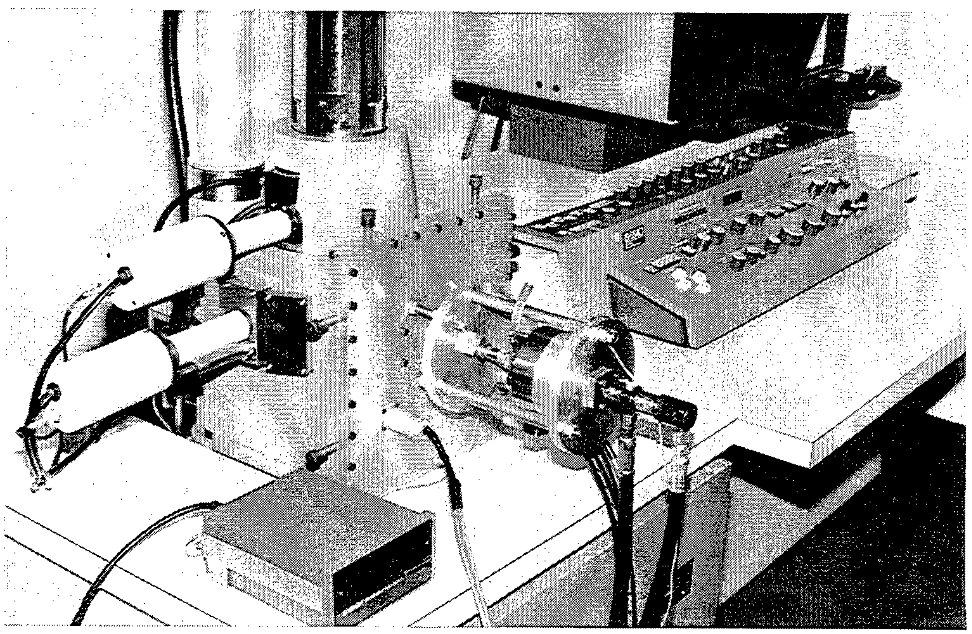

Figure 2. The fretting fatigue load frame mounted in the SEM.

Results of the Investigation

The cycles-to-failure data from this program are summarized in Table 1 for each material. As expected, cycles-to-failure decrease when the wear mechanism of fretting in a vacuum is added to fatigue, with a further decrease when the testing is conducted in air so that oxidation also is a factor. Note the influence of the materials. For the 8090-T7 alloy the wear mechanism is relatively important compared to the corrosion mechanism. However, for the 7075-T7351 alloy the corrosion mechanism is dominant in reducing cycles-to-failure and the overall reduction is greater.

Table 1. Material Average Cycles-to-failure Date

Conditions of testing	8090-T7	7075-T7351
Fatigue without fretting	1,759,527	2,537,695
Fretting fatigue in a vacuum (assumed wear only)	403,223	2,377,757
Fretting fatigue in air (oxidation and wear)	341,980	106,706

An example of the fretted surface of a specimen tested in air is shown in Figure 3. Prior to testing, the surfaces of this and all other specimens were sanded and polished with the final polish being 1 micron diamond compound. The direction of the fatigue loading in all SEM pictures of fretted surfaces is towards the upper right corner of the picture. The fretting fatigue cracks run generally perpendicular to the direction of fatigue loading from upper left to lower right in SEM pictures of fretted surfaces. This fretted surface is characteristic of the surfaces of all specimens tested. Numerous areas where relatively great damage has occurred can be seen in the upper right portion of the fretting pattern. These are the areas where cracks tended to nucleate. Most of the fretted surface pictures which follow will be of such areas of relatively great damage.

Figure 4 shows a crack that has nucleated in and propagated through the fretted surface of a specimen. Although generally perpendicular to the direction of

fatigue loading, locally the crack propagated along the contour of the heavy fretting so that at each point along its path it tended to circle the dominant local area of relatively great damage. The influence of local fretting conditions on crack nucleation and early propagation was apparent throughout the investigation.

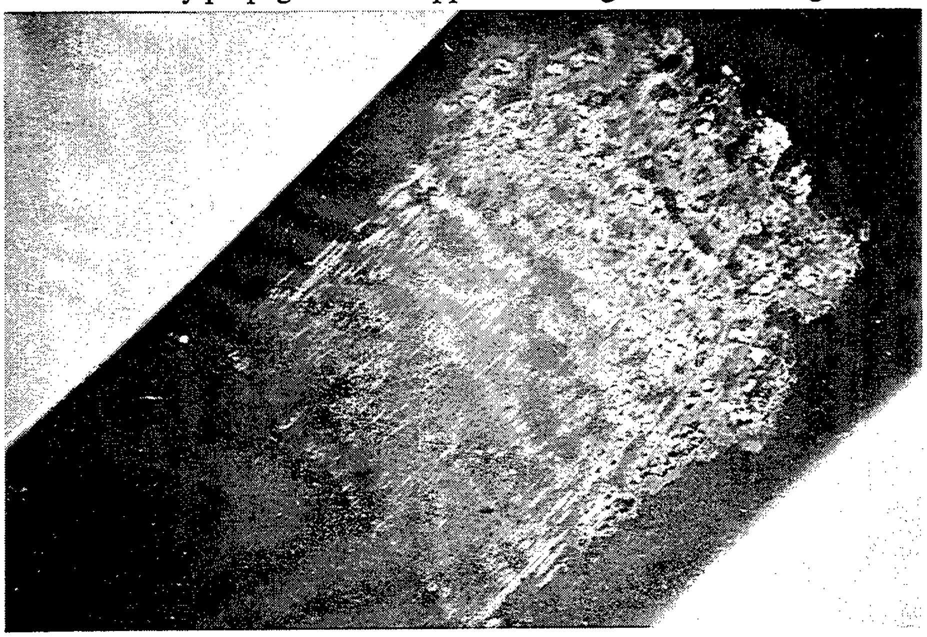

Figure 3. An example of the surface of a specimen tested in air. The fretted area is shown in the center of the picture. The direction of fatigue loading is towards the upper right corner of the picture. (17x magnification)

Figures 5 and 6 show two 8090 specimens tested under identical conditions and for the same number of cycles except that the specimen in Figure 5 was tested in the SEM vacuum and the specimen in Figure 6 was tested in air. The effects of adhesive wear and smearing are apparent for the specimen in Figure 5, but the damage is less severe than that of the specimen in Figure 6. The smearing was a characteristic of specimens tested in the SEM for both materials. The more severe damage was characteristic of specimens tested in air for both materials. A crack is propagating through the damaged area on the surface of the specimen in Figure 6. Figure 7 shows a cross section through this area with the specimen material on the bottom of the picture. Cracks to the left and right are growing towards each other and might be expected to enlarge the pit as opposed to

propagating to failure. One branch of a crack on the left side of the picture appears to have started to grow into the material.

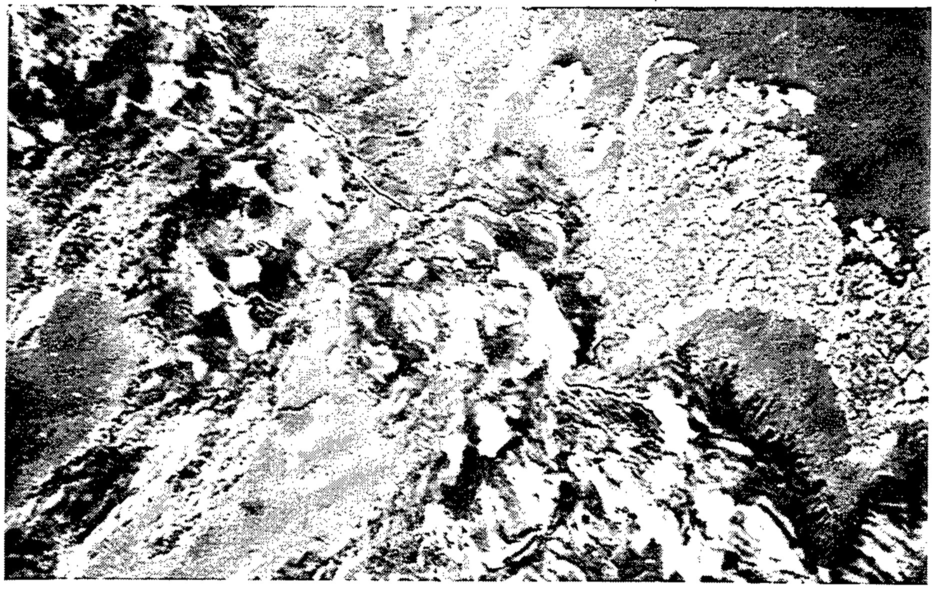

Figure 4. The fretted surface of a specimen showing a meandering crack that at any point is generally circling the dominant local area of relatively great damage. (150x magnification)

Figure 5. The fretted surface of an 8090 specimen which was tested in a vacuum. The effects of adhesive wear and smearing are apparent, but the damage is less severe than that seen on specimens tested in air such as the specimen in Figure 6. (150x magnification)

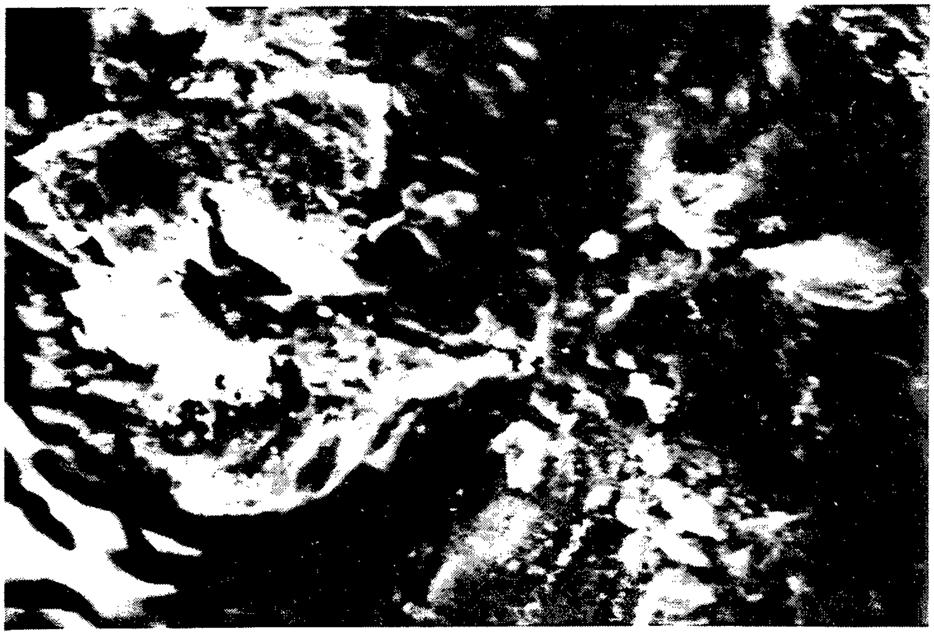

Figure 6. A crack propagating from a pit on the surface of an 8090 specimen which was tested in air. A cross section through this area of damage is shown in Figure 7. (470x magnification)

Figure 7. A cross section through the damaged area shown in Figure 6. Cracks to the left and right are growing towards each other. One branch of a crack on the left side appears to have started to grow into the material. (490x magnification)

Figure 8 shows the fretted surface of a 7075 specimen tested in air. Cracking can be seen in each of the more severe areas of damage in this picture. In each case the cracking is oriented towards the center of the localized damage. Figure 9 shows a cross section through an area of damage on this specimen. As with the 8090, specimen, cracks to the left and right are growing towards each other and might be expected to enlarge the pits. However, for the 7075 material the cracking is closer to the surface of the specimen.

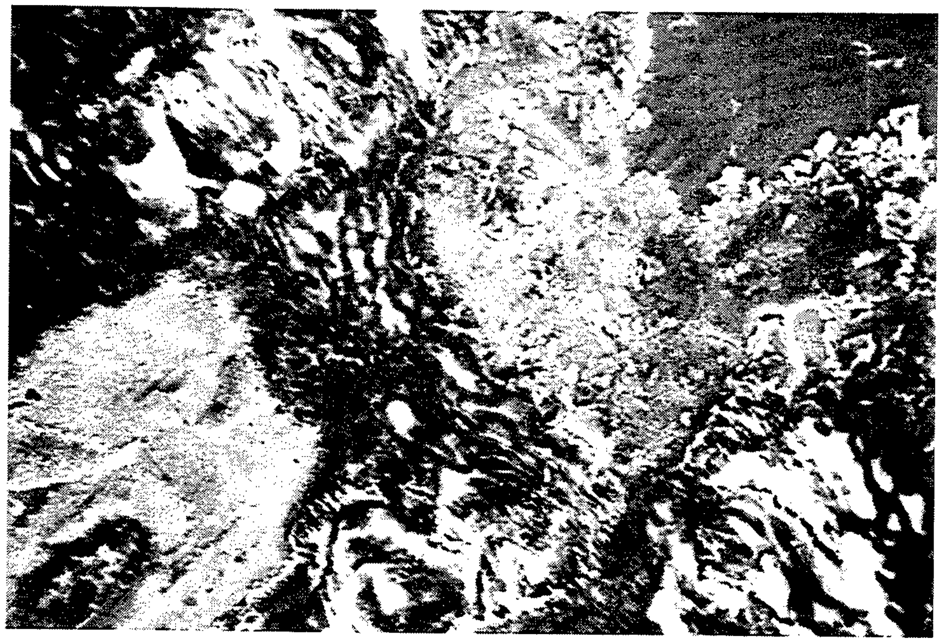

Figure 8. The fretted surface of a 7075 specimen. Three regions of localized damage can be seen. Each has cracks that are oriented towards the center of the localized damage. (270x magnification)

Figures 10 and 11 show cross sections of the fretted surfaces of an 8090 and a 7075 specimen respectively. These specimens were cut so that their long axes were across the thickness of the rolled plates of material. This meant that the fatigue loading would tend to cause crack propagation along the grain direction near the center axis of the plate of material. The tendency for the cracks to connect causing pits or troughs is evident for the 8090 material in Figure 10 as it was for both materials in the previous figures where specimens were cut with long axes parallel to the surfaces of the plates of material. However the crack in the 7075

material is oriented along the grain direction and propagating directly into the material. That this would cause more rapid propagation to failure in the 7075 material was reflected in the test parameters. During the pretest it was determined that the 7075 specimen life at the planned fatigue loading would not provide sufficient cycles-to-failure to allow meaningful test results. Therefore the fatigue loading on the through-the-thickness 7075 specimens was reduced.

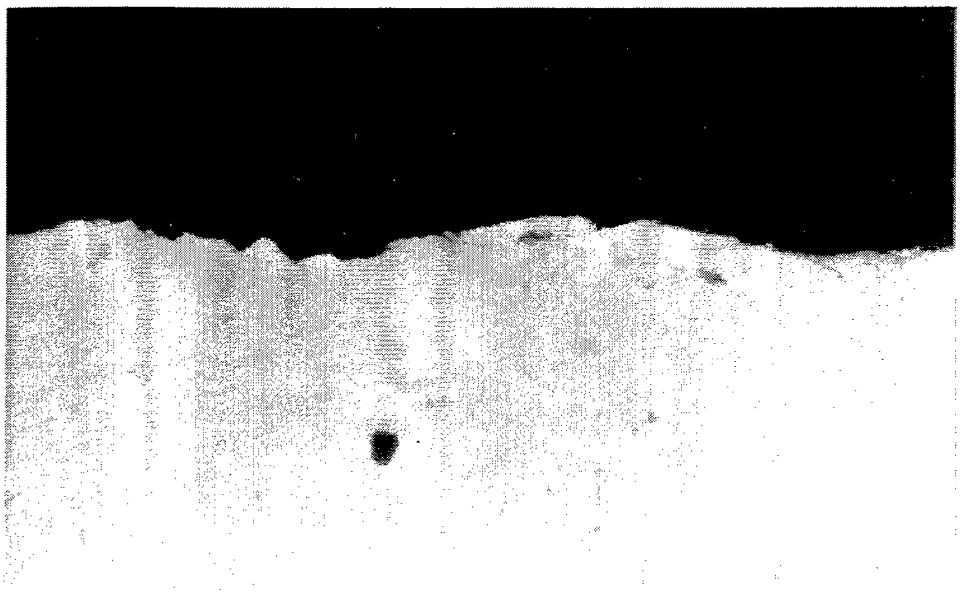

Figure 9. A cross section through a damaged area shown in Figure 8. Cracks from the surface tend to join, but in regions closer to the surface than was observed with 8090 specimens such as shown in Figure 7. (990x magnification)

The bottom half of Figure 12 shows the fracture surface of an 8090 specimen tested in air. A nucleation site and several levels of cracks can be seen at the center of the picture. These are further from the viewer than the features at the very bottom of the picture. It is as if the viewer is looking at the nucleation site from the top of a cliff. The fracture surface of the 7075 specimen shown in the bottom half of Figure 13 has more features but less relief and fewer facets than the 8090 specimen in Figure 12. Again, this would indicate that different localized mechanisms of crack nucleation and early propagation are involved for different materials.

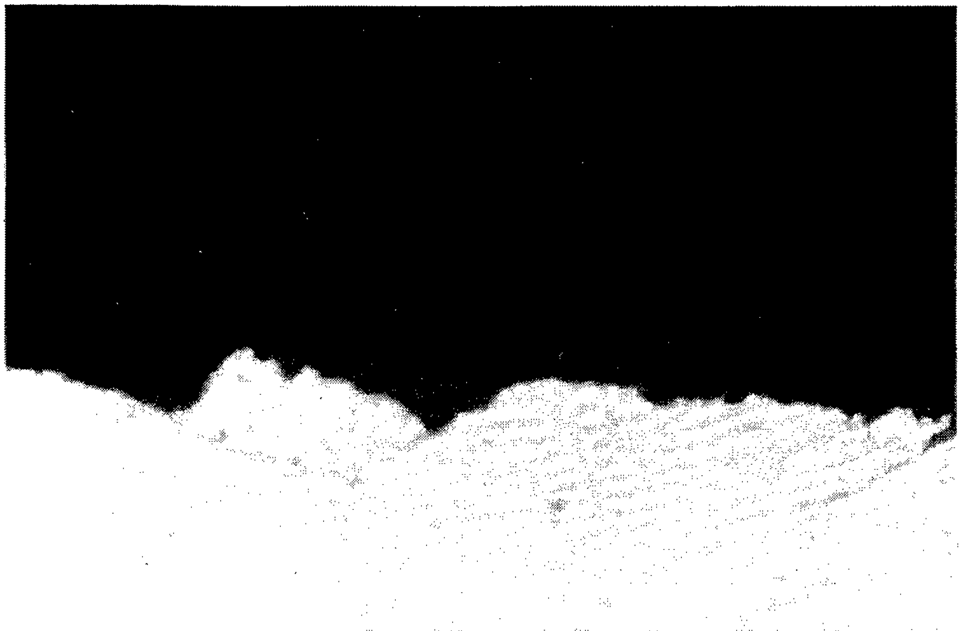

Figure 10. Cross section through a damaged area on the surface of a through-the-thickness 8090 specimen. The tendency of cracks to connect causing pits or troughs is evident. (990x magnification)

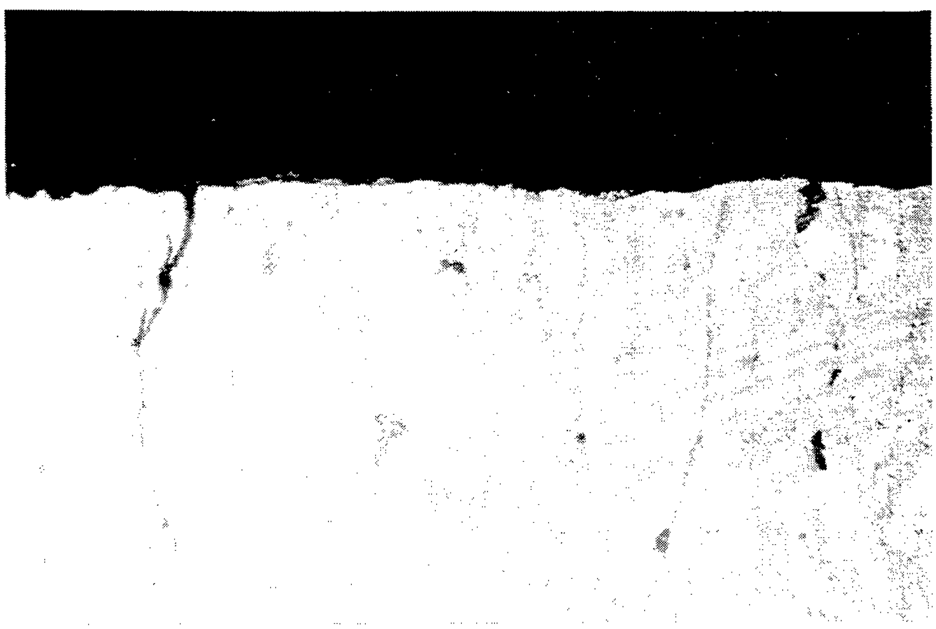

Figure 11. Cross section through a damaged area on the surface of a through-the-thickness 7075 specimen. The tendency of cracks to connect causing pits or troughs is <u>not</u> evident. Instead, the crack is oriented to the grain direction and propagating directly into the material. (470x magnification)

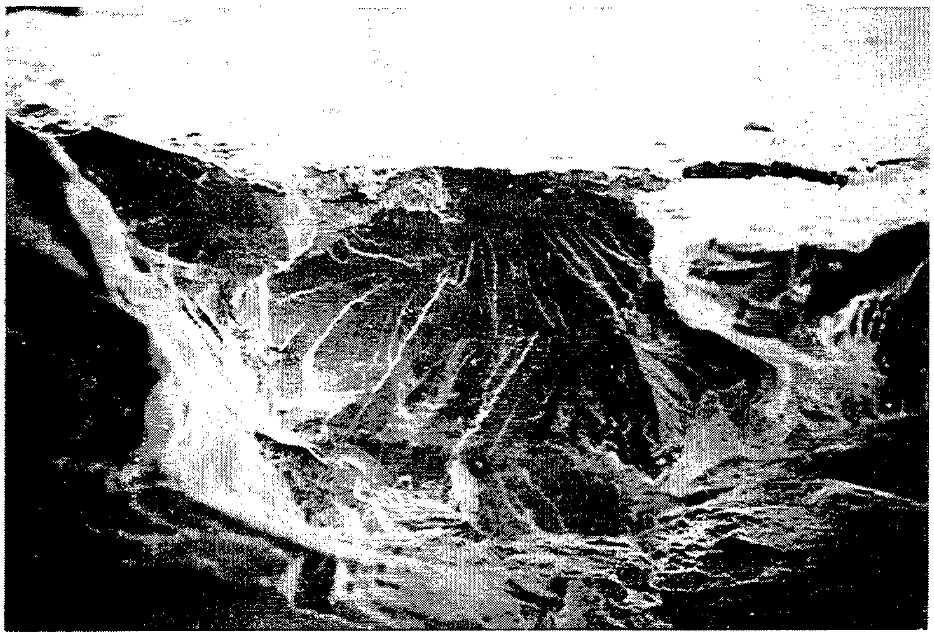

Figure 12. The fracture surface of an 8090 specimen showing a nucleation site and several levels of cracking. These are further from the viewer than the features at the bottom of the picture. It is as if the viewer is looking at the nucleation site from the top of a cliff. (71x magnification)

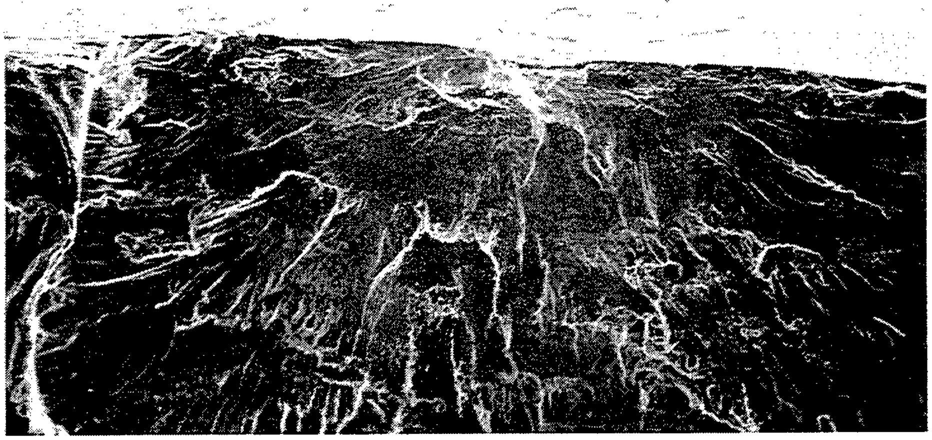

Figure 13. A partial pit can be seen on the fracture surface of a 7075 specimen which has more features, but less relief and fewer facets than the fracture surface of 8090 specimens such as that in Figure 12. (78x magnification)

Conclusions

Based on the fretting surface, metallographic, and fractographic investigations conducted in this research program, it is concluded that:

- Areas of relatively great damage on a fretted surface can be caused by adhesive wear.
- These areas have more severe damage if corrosive mechanisms also are active.
- Cracks nucleate at or near surfaces of areas of relatively great damage and propagate within and from these areas.
- For specimens tested in air, these cracks can join other cracks or return to the surface, forming pits or troughs and debris, or propagate into the material.
- Cracks also propagate into the material from the bottoms of the pits and troughs.
- Crack nucleation and early propagation are influenced by material, environment, and local conditions in the area of relatively great damage where the crack is formed.

Recommendations

Where the effects of fretting fatigue are an issue, the local conditions that influence the fretting fatigue process should be investigated. Understanding these conditions for the materials being investigated may help in developing procedures for alleviating the effects of fretting fatigue.

Acknowledgment

The author's are grateful to Alcoa for providing the 8090 alloy used in this research.

References

1. *Compilation of ASTM Standard Definitions*, 6th Edition, ASTM, Philadelphia, PA, 1986.

2. Elliott, C. B. III, *Fretting of 8090 and 7075 Aluminum Alloys under Interrupted Fatigue Loading Conditions in Air and Vacuum Environments,* dissertation, University of Utah, 1993.

3. Elliott, C. B. III and Hoeppner, D. W., "A Fretting Fatigue System Useable in a Scanning Electron Microscope," *Fretting Fatigue*, ESIS 18 (edited by R. B. Waterhouse and T. C. Lindley) 1994, Mechanical Engineering Publications, London, pp. 211-217.

4. Elliott, C. B. III and Hoeppner, D. W., The Importance of Wear and Corrosion Failure Mechanisms on the Fretting Fatigue Behavior of Two Aluminum Alloys," Submitted for publication to *Wear*.

An Evaluation of Empirical and Analytical Models for Predicting Fatigue Crack Propagation Load Interaction Effects

by

K. Walker
(Senior Professional Officer)

DSTO, AERONAUTICAL AND MARITIME RESEARCH LABORATORY
Airframes and Engines Division
506 Lorimer St, Fishermens Bend, Victoria, Australia, 3207.
Ph: (61 3) 9626 7961 Fax: (61 3) 9626 7089
email: Kevin.Walker@dsto.defence.gov.au

1. INTRODUCTION

The development and evaluation of models to predict fatigue crack growth in metallic structures under spectrum loading is a topic which has received a great deal of attention in the last 20 years. References 1 to 9 detail some of the studies which have been undertaken. There are a large number of computer programs incorporating various models for predicting fatigue crack growth. The author is aware of at least 12 (Broek, Cracks, Cracks IV, Cracks 84, MODGROW, AFGROW, CORPUS, ONERA, PREFFAS, FASTRAN, STRIPY, CG90). The various programs and models fall into one of two categories as follows:

a. Empirical. Empirical models employ various techniques for modelling the baseline constant amplitude crack growth rate data (eg tabular inputs which are then subject to interpolation/extrapolation, and equations such as Forman or Walker which fit a curve to the measured data). Empirical load interaction models with "calibration" constants are then used to account for effects such as retardation and therefore match a prediction with observed or measured behaviour.

b. Analytical. Some models utilise the crack closure theory to explain the R-ratio and load interaction effects and apply this to the prediction. A certain degree of empiricism still exists, however the method by which the R-ratio and load interaction effects are accounted for is based on a more scientific theory than simply curve fitting observed behaviour or incorporating an otherwise meaningless constant which can be adjusted to give a desired result.

The aim of the work presented in this paper was to assess the performance of the empirical models compared with the analytical closure model approach. Test data was available for relatively simple centre crack specimens machined from 7075-T651 Aluminium Alloy plate material (Reference 10). The specimens were pre-cracked and then subjected to a simplified variable amplitude fighter aircraft load spectrum. The peak load in the baseline spectrum (equal to a cg acceleration of N_z = 7.5 g) was approximately 28% of the yield stress of the material. The spectrum was altered to simulate placard flight restrictions which may be imposed to conserve the fatigue life

of an aircraft. The restrictions (at 6.5 g and 5 g, see Figures 2 and 3) and an artificial peak load increase (to 8.5 g, see Figure 3) resulted in significant changes to the crack growth life which would not be predicted by a model which does not account for load interaction effects.

2. SPECIMEN TESTING

The specimen test results used in this work were obtained from Reference 10. The specimens were machined from 7075-T651 Aluminium Alloy. The geometry used was a fixed end, centre crack specimen as shown in Figure 1 below.

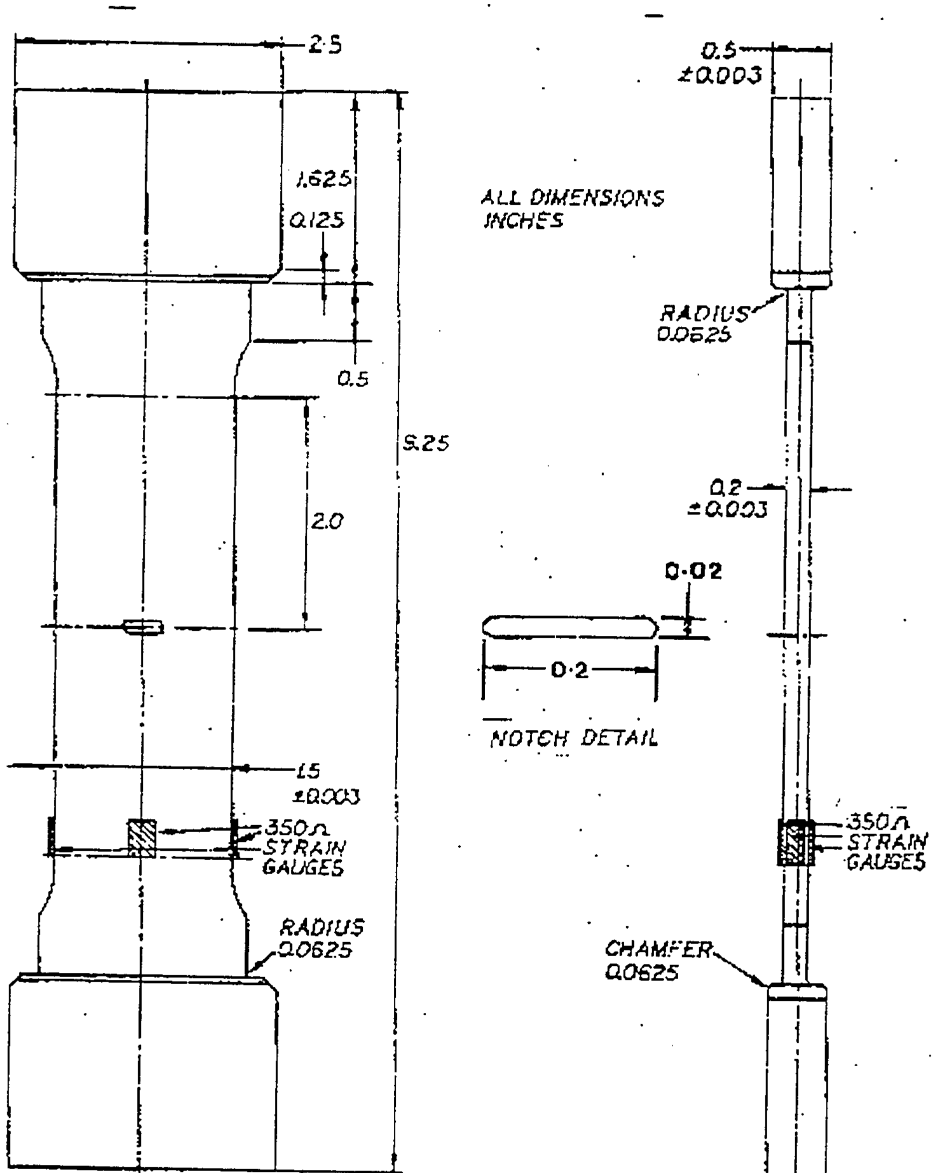

Figure 1. Fixed End Centre Crack 7075-T651 Specimen

A central slot was machined into the specimens using Electrical Discharge Machining (EDM) and they were then subjected to constant amplitude pre-cracking until a crack length of 0.15 inch (a=0.15 inch, 2a=0.30 inch) was reached. The final maximum load during pre-cracking was 3,000 pounds. The spectrum loading applied later was such that this load level was exceeded in the first 10 cycles. Residual effects from pre-cracking were therefore not anticipated.

The specimens were subjected to four variations of a simplified Mirage fighter aircraft spectrum;

(i) the unmodified Mirage spectrum,

(ii) clipped at 6.5 g,

(iii) clipped at 5 g, and

(iv) with the 7.5 g peak (which occurs once in a 100 flight, 66.6 hour block) increased to 8.5 g.

All loading variables other than the spectrum itself were kept constant throughout the tests in order to isolate the effect of spectrum modification. A scaling factor of remote stress per g of 2.5 ksi per g was used. The spectrum is detailed in Figure 2 and 3, and Tables 1 and 2 below.

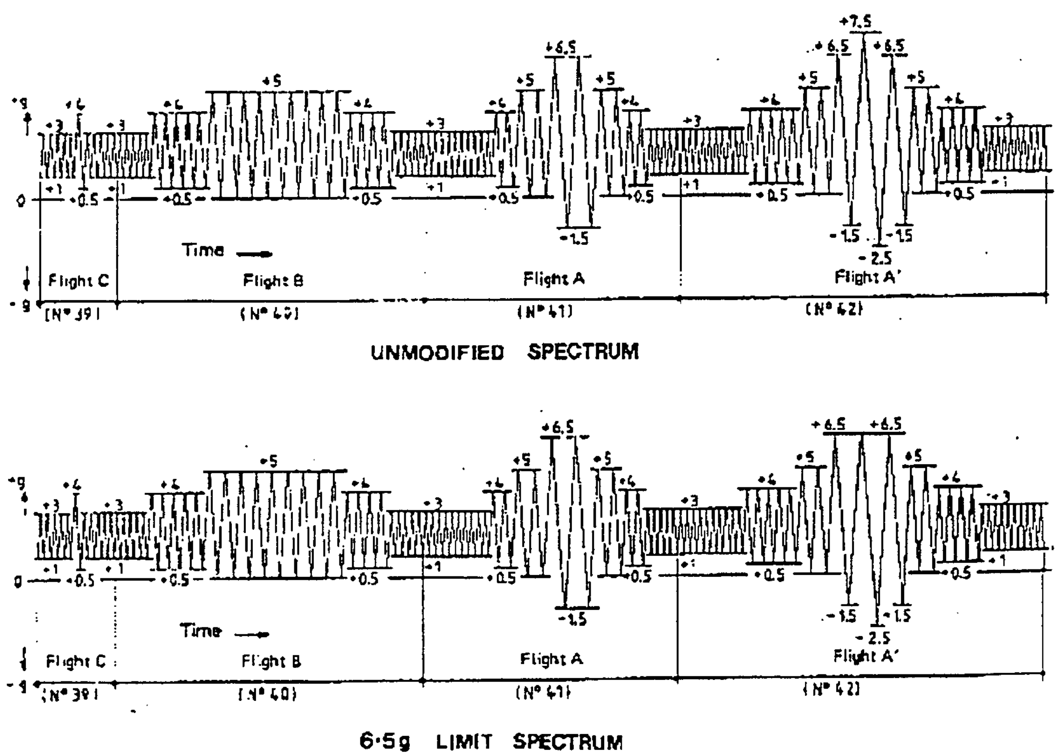

Figure 2. Representative Segments From the Unmodified and 6.5 g Limit Spectra

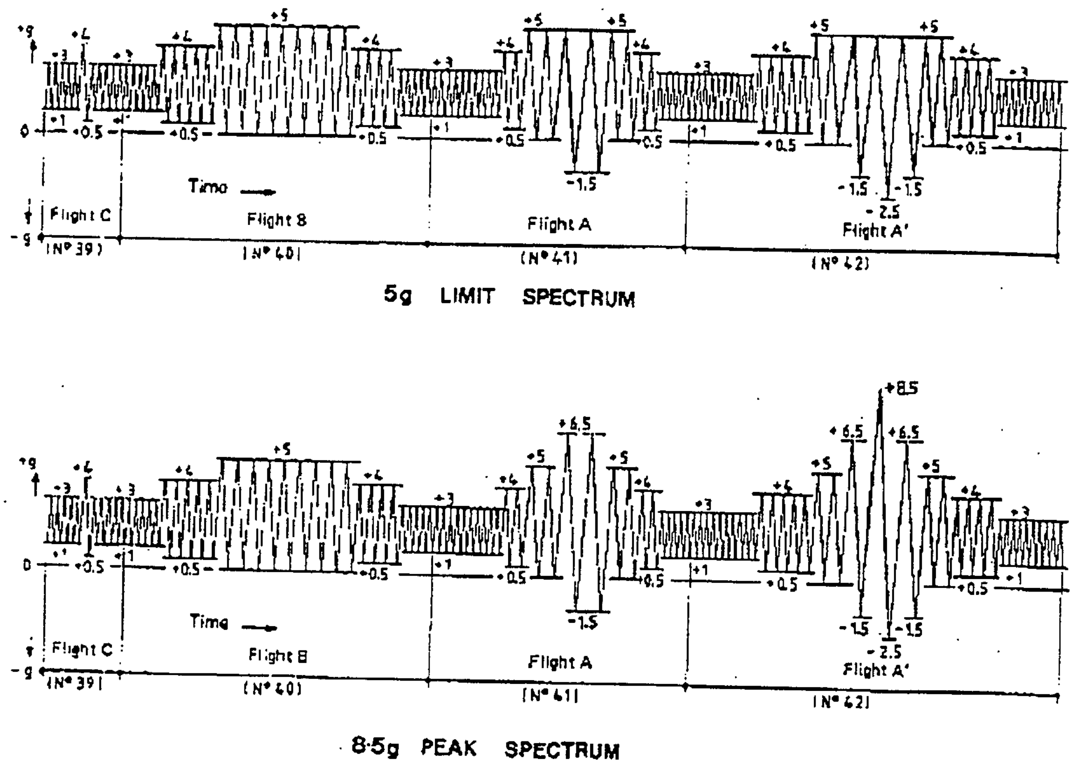

Figure 3. Representative Segments From the 5 g Limit and 8.5g Peak Spectra

		STEP								
Flight	Spectra	1	2	3	4	5	6	7	8	9
A'	Unmodified	10 cycles +3/+1	5 cycles +4/+0.5	2 cycles +5/0	1 cycle +6.5/-1.5	1 cycle +7.5 /-2.5	1 cycle +6.5/-1.5	2 cycles +5/0	4 cycles +4/+0.5	10 cycles +3/+1
A'	6.5 g Limit	10 cycles +3/+1	5 cycles +4/+0.5	2 cycles +5/0	1 cycle +6.5/-1.5	1 cycle +6.5 /-2.5	1 cycle +6.5/-1.5	2 cycles +5/0	4 cycles +4/+0.5	10 cycles +3/+1
A'	5 g Limit	10 cycles +3/+1	5 cycles +4/+0.5	2 cycles +5/0	1 cycle +5/-1.5	1 cycle +5 /-2.5	1 cycle +5/-1.5	2 cycles +5/0	4 cycles +4/+0.5	10 cycles +3/+1
A'	8.5 g Peak	10 cycles +3/+1	5 cycles -4/+0.5	2 cycles +5/0	1 cycle +6.5/-1.5	1 cycle +8.5 /-2.5	1 cycle +6.5/-1.5	2 cycles +5/0	4 cycles +4/+0.5	10 cycles -3/+1
A	Unmodified 6.5 g Limit 8.5 g Peak	10 cycles +3/+1	5 cycles +4/+0.5	2 cycles +5/0	2 cycles +6.5/-1.5	2 cycles +5/0	2 cycles +4/0.5	5 cycles +3/+1	-	-
A	5 g Limit	10 cycles +3/+1	5 cycles +4/+0.5	2 cycles +5/0	2 cycles +5/-1.5	2 cycles +5/0	2 cycles +4/0.5	5 cycles +3/+1	-	-
B	ALL	5 cycles +3/+1	5 cycles +4/+0.5	9 cycles +5/0	4 cycles +4/+0.5	5 cycles +3/+1	-	-	-	-
C	ALL	5 cycles +3/+1	1 cycle +4/+0.5	5 cycles +3/+1	-	-	-	-	-	-

Table 1. Flight Segment Spectra

1	2	3	4	5	6	7	8	9	10	11	12	13	14	15
B	C	C	B	C	C	C	A	C	C	B	B	A	C	C
16	17	18	19	20	21	22	23	24	25	26	27	28	29	30
C	B	A	C	B	B	B	A	C	C	C	A	A	C	C
31	32	33	34	35	36	37	38	39	40	41	42	43	44	45
B	B	B	C	B	A	B	C	C	B	A	A’	B	C	C
46	47	48	49	50	51	52	53	54	55	56	57	58	59	60
A	A	B	B	C	C	B	C	C	B	C	B	B	C	C
61	62	63	64	65	66	67	68	69	70	71	72	73	74	75
C	A	B	A	C	C	C	B	A	B	B	B	C	B	C
76	77	78	79	80	81	82	83	84	85	86	87	88	89	90
C	A	B	C	B	A	B	C	C	B	A	A	B	C	C
91	92	93	94	95	96	97	98	99	100					
B	C	C	B	B	C	B	C	A	C	-	-	-	-	-

Table 2. Sequence of Flight Segments in a Block Representing 100 Flights, 66.6 Hours (1989 cycles)

Three specimens were subjected to the unmodified spectrum, two specimens to the 6.5 g limit spectrum, three specimens to the 5 g limit spectrum and one specimen to the 8.5 g limit spectrum. All specimens were tested to failure which occurred at a half crack length a of between 0.5 and 0.6 inch. The crack growth curves are plotted in Figure 4 below. There is very little scatter in the results where several tests were performed under the same spectrum. It is therefore considered reasonable to conclude that the differences in crack growth rate can be attributed solely to the differences in the load spectra.

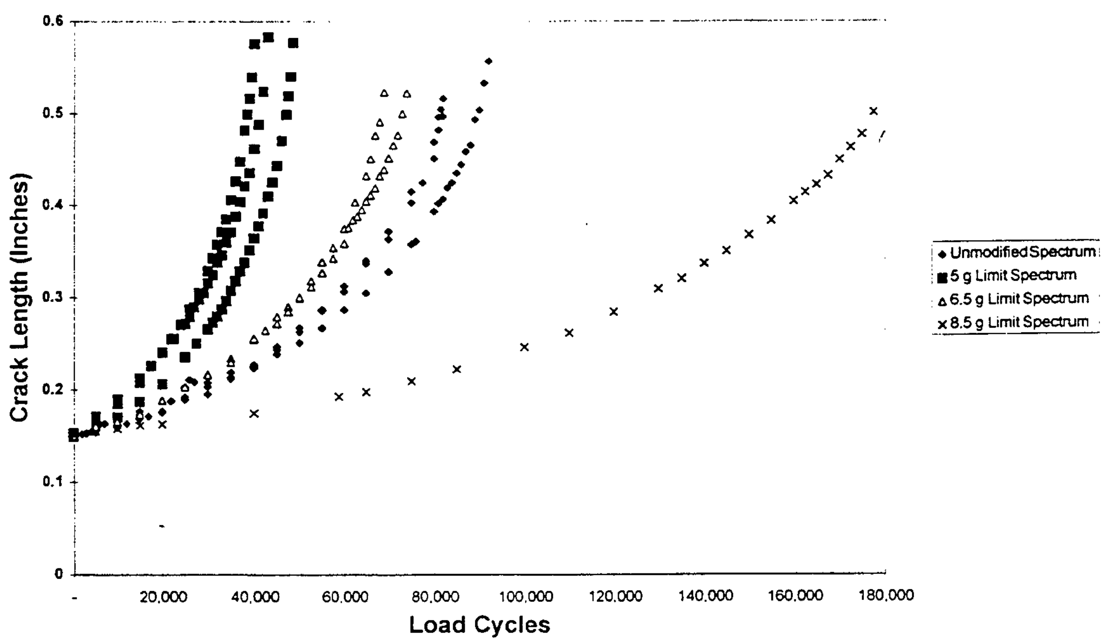

Figure 4. Experimental Crack Growth Results for Four Mirage Spectra Variations (Reference 10)

The crack growth results clearly demonstrated the load interaction effects expected under spectrum loading. When the peak load was clipped at 6.5 g, there was a loss of retardation effect and the crack growth life was shorter. Clipping at 5 g led to an even shorter life. Increasing the peak load from 7.5 to 8.5 g (a load which occurs once per block of 1989 cycles) doubled the life. These results were therefore able to be used to assess the adequacy of the various models to predict the load interaction effects.

3. PREDICTIVE MODELS

The predictive models examined here can be classified either as empirical (CRACKS84, Broek, AFGROW) or based on the analytical closure model (FASTRAN II). A description of the significant features of each is presented in this section.

3.1 CRACKS84

A program called CRACKS84 was used in the Reference 10 work. The results are reproduced here for comparison purposes. CRACKS84 was based on a program called CRACKGRO and was obtained from the USAF and modified to run on a Gould 9080 computer running a UNIX operating system. CRACKS84 is based on the standard Linear Elastic Fracture Mechanics (LEFM) approach to fatigue crack propagation. The code includes stress intensity factor solutions for various geometries, several different crack growth rate models and several load interaction effect models. Reference 10 gives full details on the program and how it was applied in this case. The load interaction models used were none, Basic Willenborg, Generalised Willenborg and Willenborg/Chang.

3.2 Broek

A suite of software has been developed by Dr D. Broek from FractuREsearch Inc in the USA (Reference 11). The software also utilises the LEFM approach. The retardation models examined were none, Willenborg, Calibrated Wheeler and Calibrated Broek. The software is windows based and runs on a PC.

3.3 AFGROW

AFGROW is a fatigue crack growth software package developed by the US Air Force at Wright Patterson Air Force Base, OHIO, USA (Reference 12). AFGROW is a workstation based, graphically interactive computer program for simulation of fatigue crack growth in common structural geometries subject to spectrum loading. It is designed to run either on a PC under Windows 95, or under a UNIX operating system. For the current work the PC Windows 95 version was used. The program uses the LEFM approach and the retardation models examined were none, Willenborg, Wheeler and Closure.

3.4 FASTRAN II

FASTRAN II is a PC based life prediction code based on the crack closure concept and is used to predict crack length against cycles from a specified initial crack size to failure for many common crack configurations found in structural components. The model is based on plasticity induced fatigue crack closure and is used to calculate the stress level at which the crack tip becomes fully open during cyclic loading (Reference 13), leading to the concept of an effective applied stress intensity range (ΔKeff). The model is expected to provide a more accurate measure of the crack growth rate for a spectrum loading situation.

4. INPUT DATA

4.1 Common Inputs

The inputs which were common to all programs were as follows:

a. Specimen Width = 1.5 inch

b. Specimen Thickness = 0.2 inch

c. Initial Crack Length, a_i = 0.15 inch

d. Final Crack Length, a_f = 0.60 inch

e. Specimen Geometry: Finite width centre crack sheet

f. Material: 7075-T651 Aluminium Alloy

g. Loading: Uniaxial Tension

h. Spectra: Expressed in terms of "g" with a scale of 2.5 ksi per g

i. Material Yield Strength, σ_{ys} = 67 ksi

j. Plane Strain Fracture Toughness, $K_{IC} = 35 ksi\sqrt{inch}$

4.2 CRACKS 84

4.2.1 Crack Growth Rate Data

As detailed in Reference 10, the crack growth rate data was modelled using the Walker equation as follows:

$$\frac{da}{dN} = C_a\left[\left(1-R\right)^{m-1} \Delta K\right]^n \text{ for } R \geq 0.0$$

$$\frac{da}{dN} = C_a[(1+R^2)^q K_{\max}]^n \text{ for } R \prec 0.0$$

Where:

$\frac{da}{dN}$ = Crack growth rate

ΔK = Stress intensity factor range

$K_{\max}$ = Maximum stress intensity in the cycle

C_a, m, n, q = material constants

As detailed in Reference 10, the available material data (Reference 15) was modelled with three straight line segments with C_a and n values as follows (inch and ksi units):

$C_{a1} = 4.9329 \times 10^{-10}$

$n_1 = 4.4533$

$C_{a2} = 2.4379 \times 10^{-8}$

$n_2 = 2.60$

$C_{a3} = 7.3126 \times 10^{-12}$

$n_3 = 5.1766$

A value of $m = 0.6$ was determined.

A "typical" value of $q = 1.0$ was used.

A value of threshold stress intensity range, ΔK_{TH}, of $2.5 ksi\sqrt{inch}$ was used. CRACKS 84 included an option to allow ΔK_{TH} to change as a function of stress ratio, R. This option was not used, ie ΔK_{TH} was kept constant. This had no impact on the prediction in any case since the smallest ΔK cycles even at the starting crack length exceeded $2.5 ksi\sqrt{inch}$.

Positive and negative stress ratio limits, ie values of R above and below which stress ratio is presumed not to have an effect on crack growth rate were required to be input. "Typical values" of +0.75 and -0.99 were used.

4.2.2 Load Interaction Model Input Data

The load interaction models used in CRACKS 84 (Basic Willenborg, Generalised Willenborg and Willenborg/Chang) are all influenced by the size of the plastic zone which is calculated as follows:

$$r_y = \frac{1}{\gamma\pi}\left[\frac{K_{max}}{\sigma_{ys}}\right]^2$$

Where:

r_y = radius of plastic zone

K_{max} = maximum stress intensity due to the current load

σ_{ys} = material yield stress

γ = 2 for plane stress, 6 for plane strain

For a through crack case, CRACKS 84 assumes plane stress conditions.

The Generalised Willenborg model introduced another parameter known as the overload shut-off ratio, R_{so}. A typical value of 2.3 was used.

4.3 BROEK

4.3.1 Crack Growth Rate Data

The Broek software includes a Walker equation option for modelling the crack growth rate data, but it does not allow the user to input the equation in several "regions" each with a different slope (n) and intercept (C) value. It also does not incorporate a threshold in the equation. There is, however, the option of a tabular input where the crack growth rate for a range of R ratios is input as a function of ΔK. The Mirage spectra consisted of sub blocks of constant amplitude cycles which covered a limited range of R ratios. There were eight R ratios in total, ie R = -0.500, -0.385, -0.333, -0.300, -0.294, 0, 0.125 and 0.333. The Broek software could only accommodate a maximum of six R ratios in the table, so the data at R = -0.333 and R = -0.294 were left out. It was considered that the results would not be significantly affected since there was data at fairly close R ratios in the table. The table was adjusted so that an extremely small crack growth rate corresponded to ΔK levels below the threshold

value of $2.5 ksi\sqrt{inch}$, thus modelling the threshold behaviour in a similar fashion to CRACKS 84. The Walker equation representation of the crack growth rate relation is shown for selected R ratios in Figure 5.

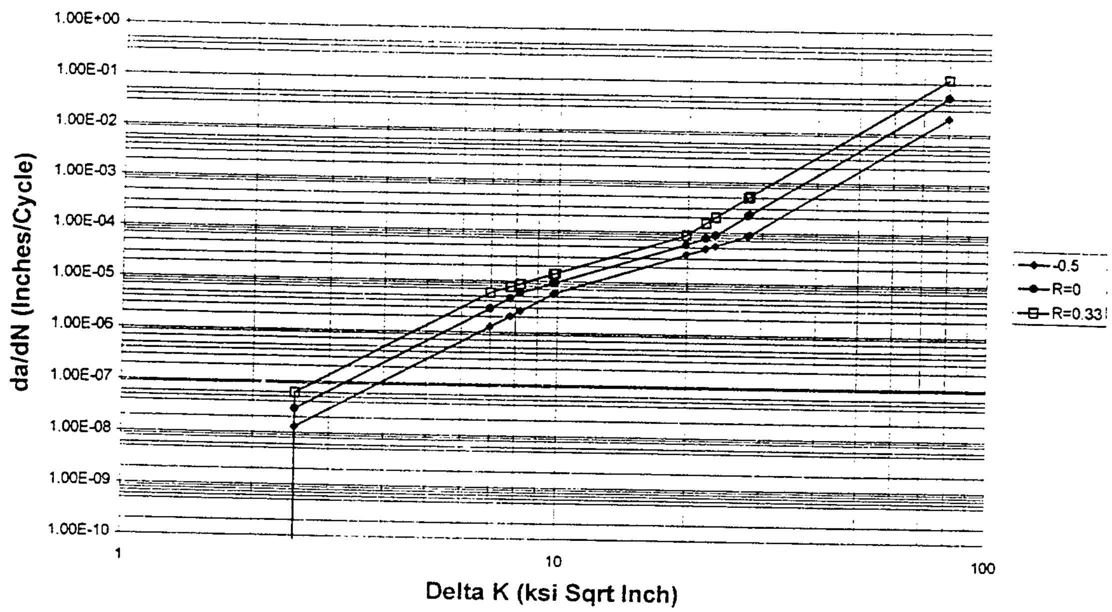

Figure 5. Walker Equation Model of Crack Growth Rate Data for 7075-T651

4.4 AFGROW

4.4.1 Crack Growth Rate Data

AFGROW was able to accept up to 5 straight line segments for the Walker equation, so the three sets of slope and intercept (n and C) as per CRACKS 84 were used. AFGROW does not request a value of the parameter "q" (see Section 4.2.1). The program deals with negative R ratio data by using the "Harter T Method" (Reference 12). It does prompt for positive and negative stress ratio limits. Although +0.75 and -0.99 were used with CRACKS 84, AFGROW only allows up to +1.0 and -0.5 on the negative side. Because the lowest R ratio in the Mirage spectra was -0.5, it was considered reasonable to set the negative limit at -0.5 and this should give a consistent result with the CRACKS 84 predictions. The positive limit was set at 0.75 as per CRACKS 84.

4.5 FASTRAN II

4.5.1 Crack Growth Rate Data

The FASTRAN II approach requires that you obtain the effective stress intensity range, ΔK_{eff}, as a function of crack growth rate for the material of interest. Newman (Reference 13) has developed a computer program to process raw data using a given constraint factor, α, to produce the ΔK_{eff} data. Data was available from Reference

14 for 7075-T6 material. This data is plotted along with the Walker equation data at R=0 and R=0.75 in Figure 6 below. The Newman data was considered to be consistent with the other data and was used to perform the predictive runs with FASTRAN II. Some modification was made to the constraint factor, α , and this is discussed in Section 5.6.

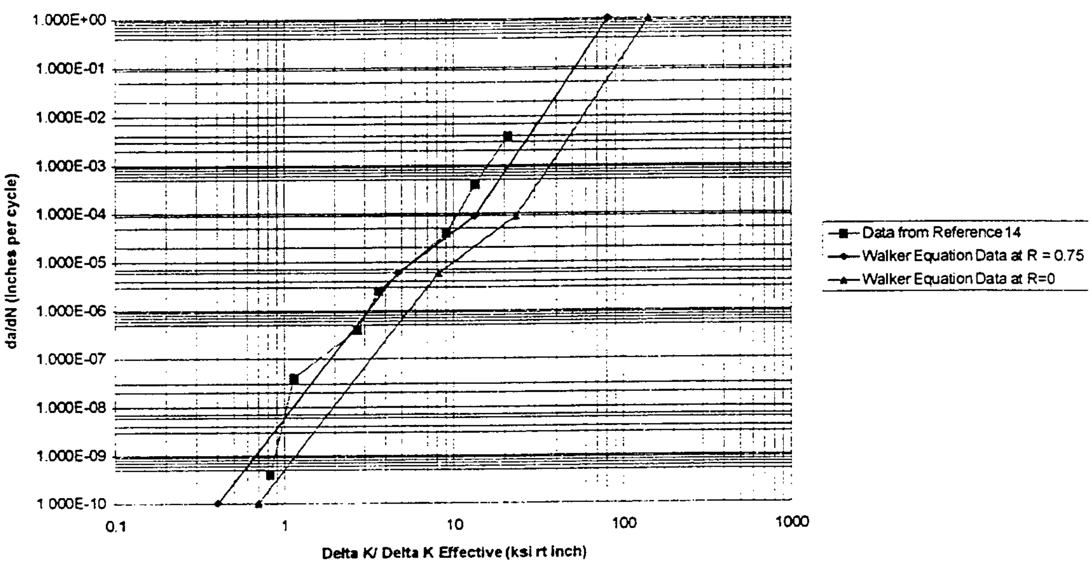

Figure 6. Comparison of Newman's 7075-T6 data with Walker Equation Data

5. RESULTS

5.1 No Retardation

The first case to be considered was a prediction without any retardation effects being considered. This does not apply to FASTRAN II because it can only be run with load interaction effects being considered. The results are summarised in Table 3 below:

Spectrum	Experimental Result	Predictive Model		
		CRACKS 84	BROEK	AFGROW
Unmodified	85,630	48,552	49,422	48,746
6.5 g	71,714	48,945	49,473	48,887
5.0 g	44,006	52,402	52,426	52,431
8.5 g	178,965	46,567	49,365	48,592

Table 3. Comparison of Experimental and Predicted Crack Growth Lives (in cycles) from $a_i = 0.15$ inch to Failure (approximately a = 0.6 inch) with No Retardation Modelling.

These results are considered to be reasonably consistent. They have been obtained by essentially using the same material data, albeit converted into a different format to suit each particular program. In each model, the predicted life is increased slightly for the 6.5 g and 5.0 g spectra, and reduced for the 8.5 g spectrum (compared to the unmodified spectrum). This is expected because the retardation effects are not predicted.

5.2 Willenborg Retardation Model

The results when the Willenborg retardation model was selected are shown in Table 4 below. In the case of CRACKS 84 there are three variations of the Willenborg model.

Spectrum	Experimental Result	CRACKS 84			Broek	AFGROW
		Basic Willenborg	Generalised Willenborg	Willenborg / Chang		
Unmodified	85,630	90,323	66,457	64,334	99,969	75,329
6.5 g	71,714	80,377	63,876	64,335	100,242	75,655
5.0 g	44,006	64,715	56,482	57,855	114,721	58,832
8.5 g	178,965	122,144	76,400	66,450	99,885	76,402

Table 4. Comparison of Experimental and Predicted Crack Growth Lives (Cycles) from $a_i = 0.15$ inch to Failure (approximately a = 0.6 inch) Using the Willenborg Retardation Model

5.2.1 CRACKS 84, Basic Willenborg

For the unmodified spectrum, the prediction with this retardation model (90,323 cycles) has increased significantly from the no retardation case (48,552 cycles) to be much closer to the experimental result (85,630 cycles). Relative to that result, the model predicts a shorter life for the 6.5 g spectrum and a shorter life again for the 5 g spectrum. A longer life is predicted for the 8.5 g spectrum. The absolute values of the predictions are not accurate, but the trend follows the same pattern as the experimental results.

5.2.2 CRACKS 84, Generalised Willenborg

The trends here are similar to the Basic Willenborg model.

5.2.3 CRACKS 84, Willenborg / Chang

Once again, the trends are in the expected direction but the absolute values of the predictions vary. The Basic Willenborg model appears to have given a better result in this case than either the Generalised Willenborg or the Willenborg/Chang model.

5.2.4 Broek, Willenborg

As per the CRACKS 84 predictions, the unmodified spectrum result has increased significantly (49,422 to 99,969 cycles). Relative to this, the predicted lives at 6.5 g and 5 g have <u>increased</u> which is opposite to the experimental results and contradicts the trends observed with CRACKS 84. The predicted life at 8.5 g has <u>decreased</u> which is also the opposite of what would be expected. The author has raised concerns about these results with Dr Broek at FractuREsearch Inc in the USA.

5.2.5 AFGROW, Willenborg

As per the previous observations, the unmodified spectrum result has increased significantly (from 48,746 to 75,329 cycles). Relative to this, the 6.5 g spectrum result is a slightly longer life which is <u>not</u> in the expected direction. The 5 g result is shorter than the unmodified spectrum and the 8.5 g result is longer. Both of these have moved in the expected direction.

5.3 Wheeler Retardation Model

The results for the Wheeler retardation model are shown in Table 5 below:

Spectrum	Experimental Result	Wheeler Model	
		Broek m = 0.835	AFGROW m = 0.86
Unmodified	85.630	85,546	85,274
6.5 g	71.714	80.789	80,313
5 g	44.006	61,043	61,477
8.5 g	178,965	104,193	105,436

Table 5. Comparison of Experimental and Predicted Crack Growth Lives (Cycles) from $a_i = 0.15$ inch to Failure (approximately a = 0.6 inch) Using the Wheeler Retardation Model

In this case the trends are in the expected direction for both sets of software and the results are consistent with each other. The calibration parameters of m = 0.835 and 0.86 for Broek and AFGROW respectively were obtained by getting a "match" for the unmodified spectrum.

5.4 Broek Retardation Model

The Broek retardation model was calibrated to the Unmodified Spectrum results and the predictions are shown in Table 6 below:

Spectrum	Experimental Result	Broek Model Factor = 1.3
Unmodified	85,630	87,860
6.5 g	71,714	79,257
5 g	44,006	50,432
8.5 g	178,965	206,477

Table 6. Comparison of Experimental and Predicted Crack Growth Lives (Cycles) from $a_i = 0.15$ inch to Failure (approximately a = 0.6 inch) Using the Broek Retardation Model

A full plot of these crack growth predictions compared with the experimental data are shown in Figures 7 to 10 below.

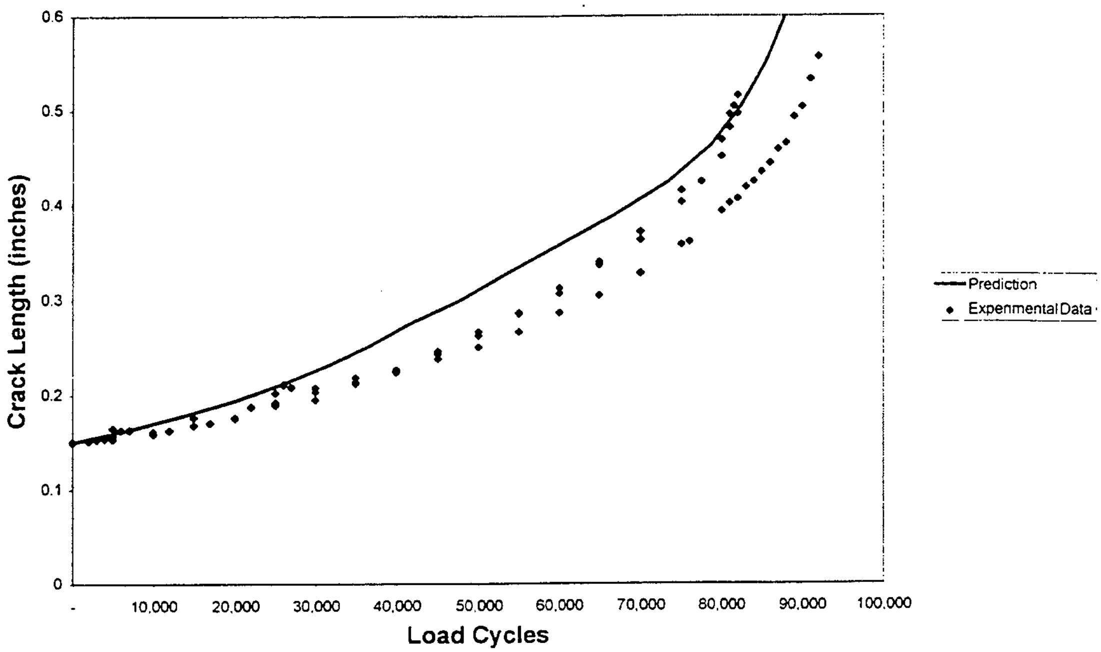

Figure 7. Unmodified Spectrum, Broek Retardation Model (Calibration Factor = 1.3), Experimental Data and Prediction

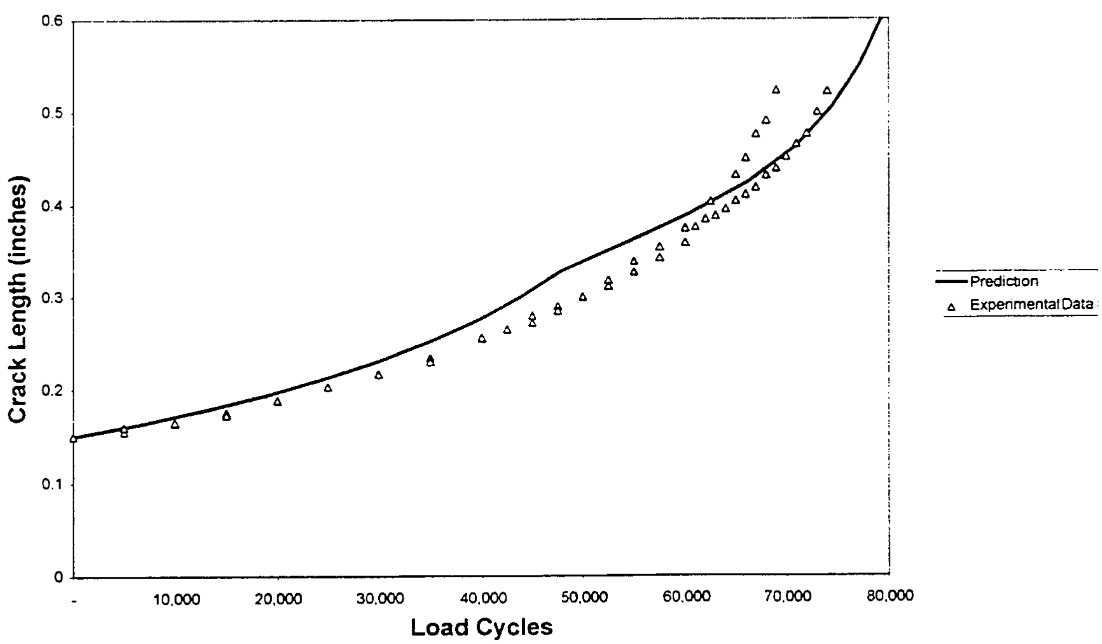

Figure 8. 6.5 g Limit Spectrum, Broek Retardation Model (Calibration Factor = 1.3), Experimental Data and Prediction

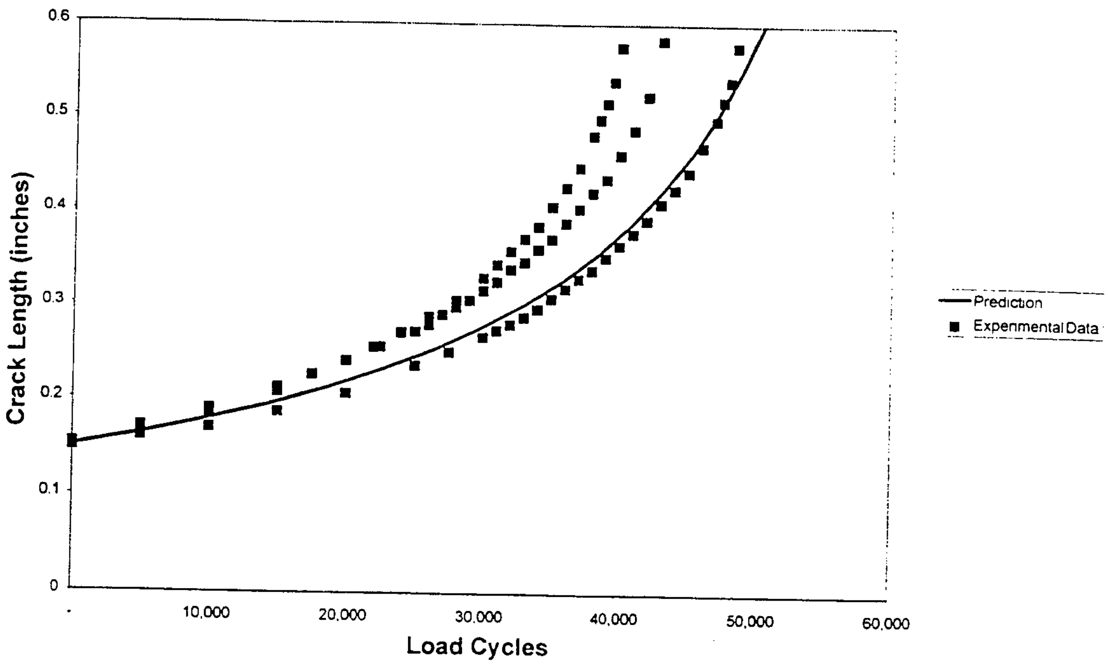

Figure 9. 5 g Limit Spectrum, Broek Retardation Model (Calibration Factor = 1.3), Experimental Data and Prediction

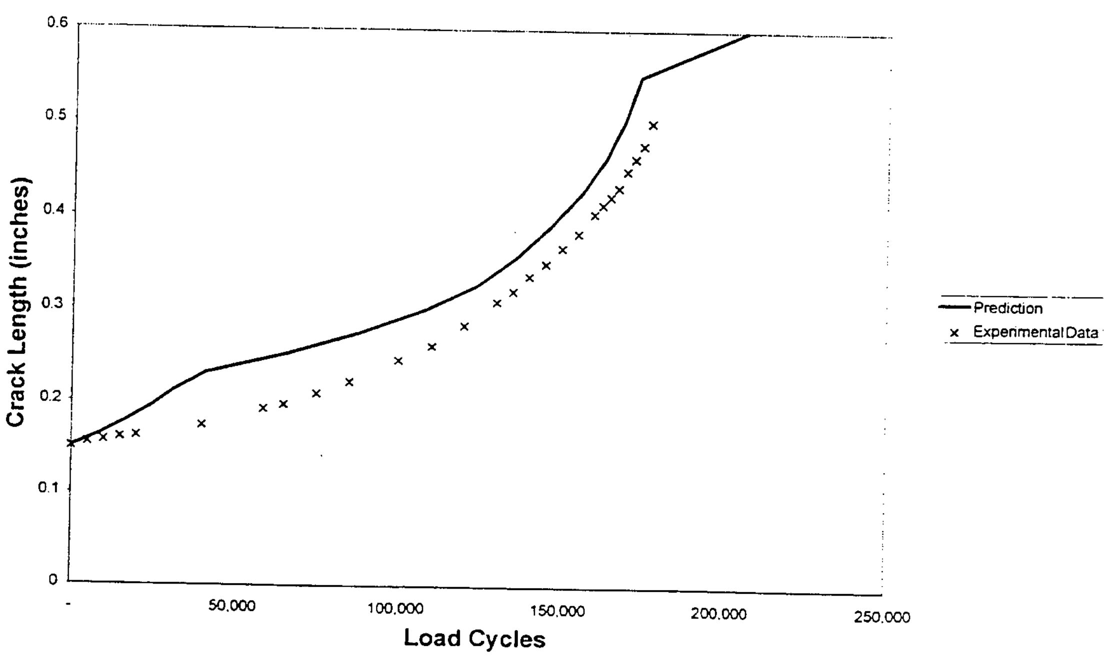

Figure 10. 8.5 g Limit Spectrum, Broek Retardation Model (Calibration Factor = 1.3), Experimental Data and Prediction

5.5 Closure Model (AFGROW)

AFGROW included a "Closure Retardation Model" option, but it appears to be significantly different to the analytical model used in FASTRAN II. The model relies on the user inputting the Crack Opening Load Ratio (OLR) at R = 0. For the results

presented here the default value of OLR = 0.15 was used. The results are shown in Table 7 below:

Spectrum	**Experimental Result**	**AFGROW Closure Model OLR (R=0) = 0.15**
Unmodified	85,630	45,792
6.5 g	71,714	45,342
5 g	44,006	46,508
8.5 g	178,965	47,716

Table 7. Comparison of Experimental and Predicted Crack Growth Lives (Cycles) from a_i = 0.15 inch to Failure (approximately a = 0.6 inch) Using the AFGROW Closure Retardation Model

5.6 FASTRAN II

The crack growth rate data used with the FASTRAN II program (see Sect 4.5.1) was obtained from centre crack specimens of 2.3 mm thickness. The specimens tested under the Mirage spectra were 5 mm thick and this would have a significant effect on the constraint factor, α. The constraint factor in the "constraint loss" regime (Reference 14) was adjusted until FASTRAN II gave the correct prediction for the unmodified spectrum. This was essentially a "calibration" of the da/dN vs ΔK_{eff} data. The "calibrated" data was then used to predict the crack growth under the other spectra. The α conditions necessary were as follows:

da/dN < 2.76 x 10^{-5} inches per cycle, α = 1.8

da/dN > 2.76 x 10^{-4} inches per cycle, α = 1.57

For intermediate rates, α was varied linearly with the logarithm of crack growth rate (Reference 13).

The crack growth predictions obtained are shown in Table 8 below:

Spectrum	Experimental Result	FASTRAN II Prediction
Unmodified	85,630	85,080
6.5 g	71,714	73,182
5 g	44,006	46,276
8.5 g	178,965	201,092

Table 8. Comparison of Experimental and Predicted Crack Growth Lives (Cycles) from $a_i = 0.15$ inch to Failure (approximately a = 0.6 inch) Using FASTRAN II with $\alpha = 1.57$ in the constraint loss regime

The full plot of the crack growth predictions for FASTRAN II compared with the experimental data are shown in Figures 11 to 14 below.

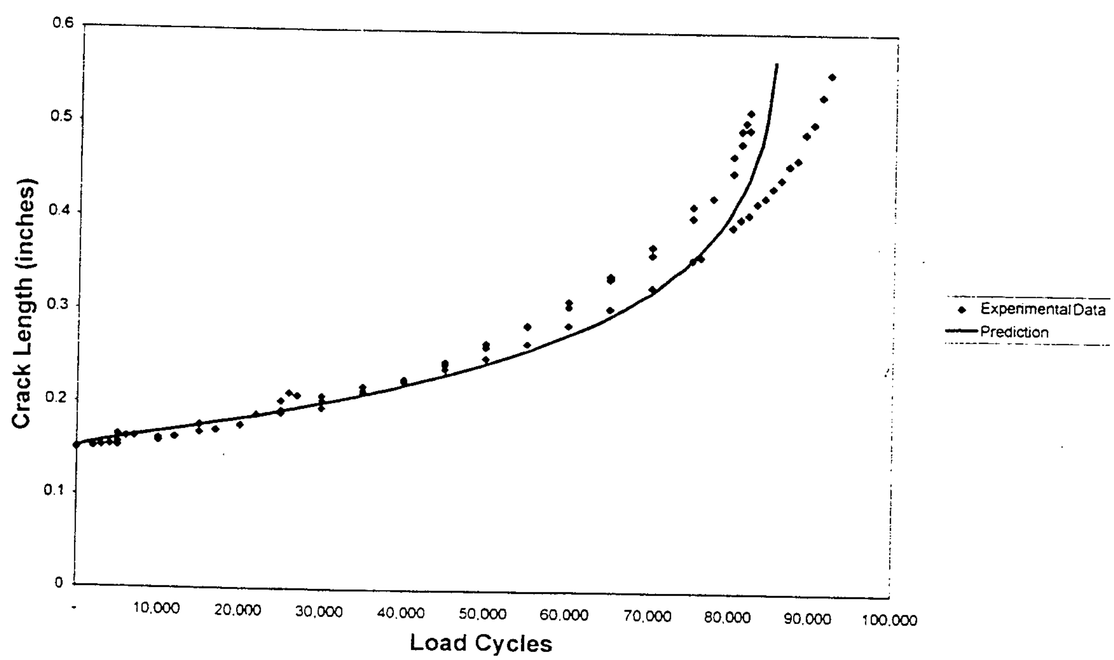

Figure 11. Unmodified Spectrum, FASTRAN II, Experimental Data and Prediction

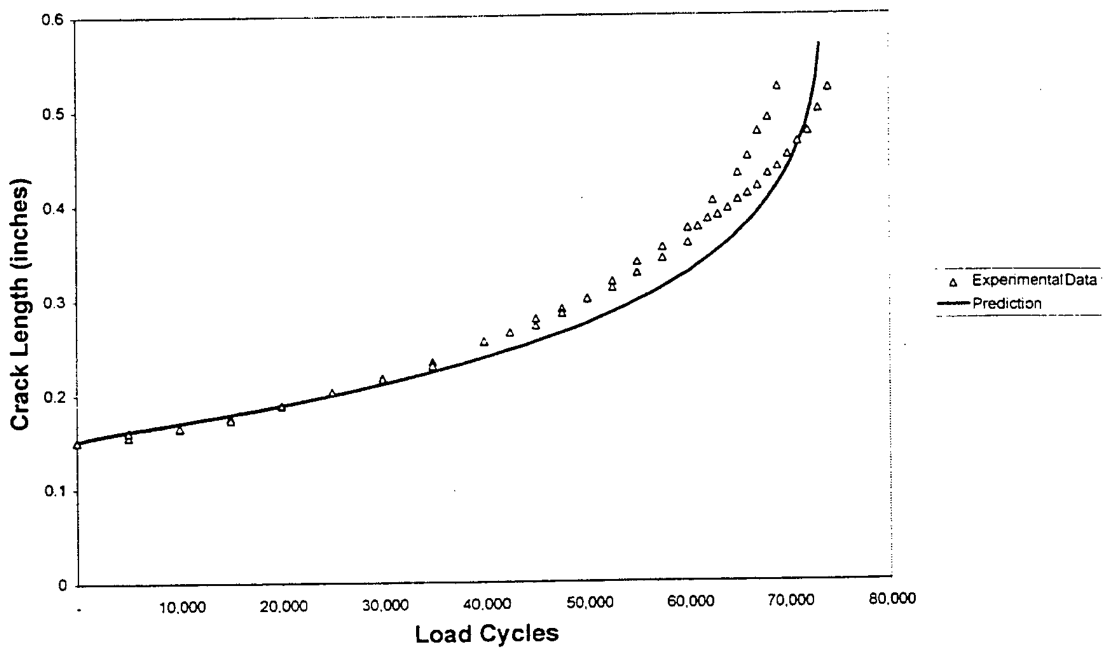

Figure 12. 6.5 g Limit Spectrum, FASTRAN II, Experimental Data and Prediction

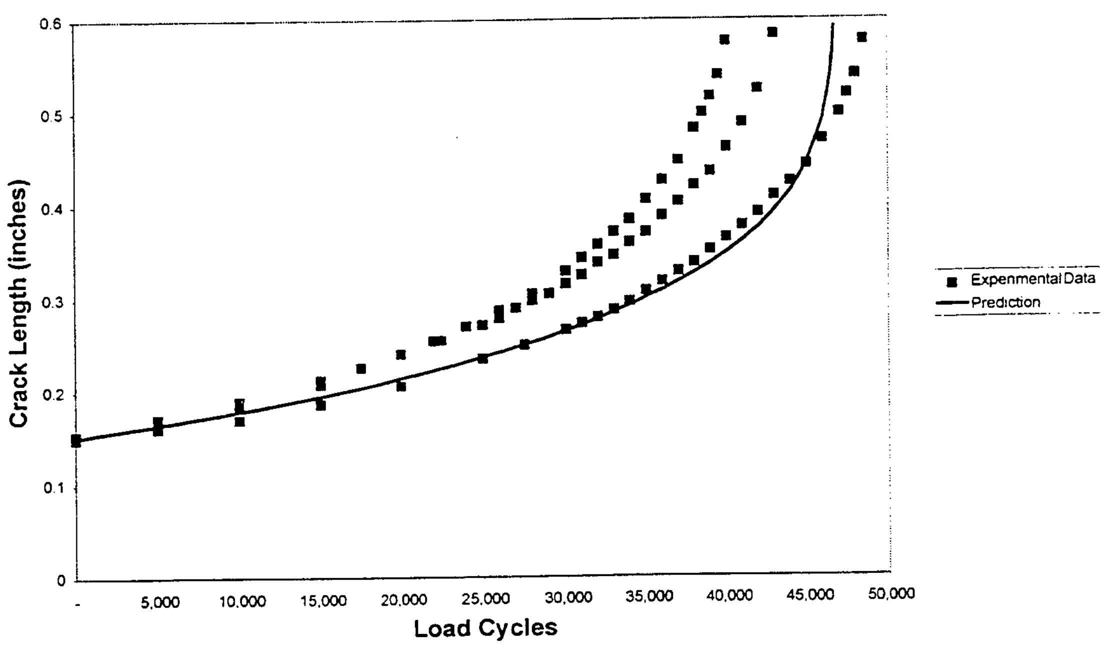

Figure 13. 5 g Limit Spectrum, FASTRAN II, Experimental Data and Prediction

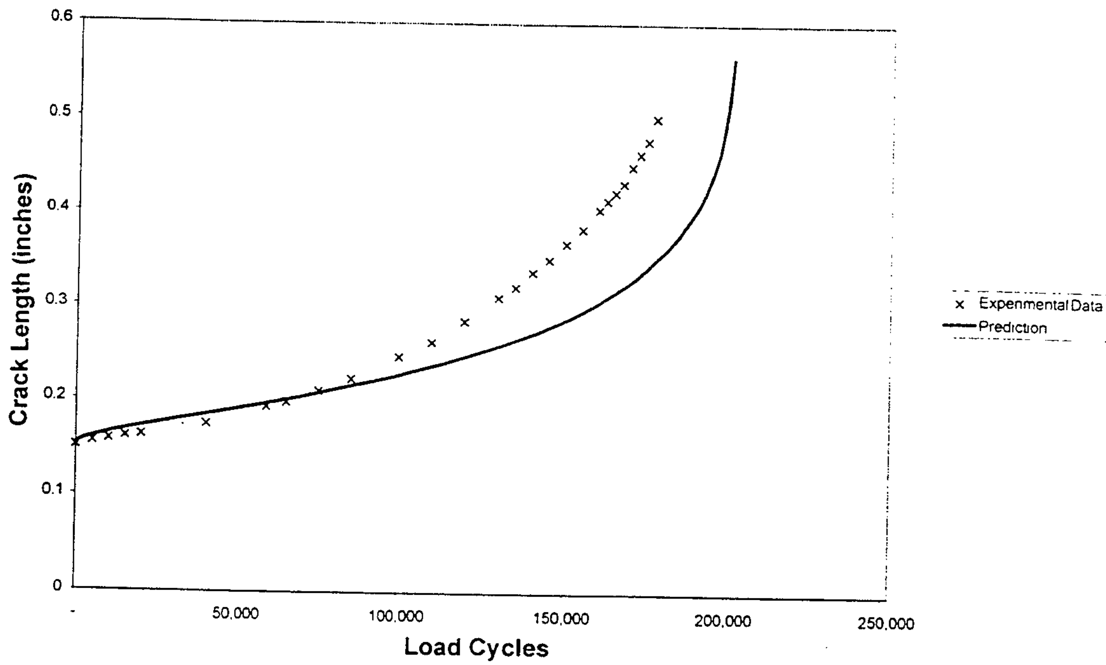

Figure 14. 8.5 g Limit Spectrum, FASTRAN II, Experimental Data and Prediction

6. DISCUSSION AND CONCLUSIONS

A range of fatigue crack growth prediction models and a range of software packages have been evaluated for their ability to deal with load sequence effects for long fatigue crack test data. The test data utilised clearly demonstrated a load sequence interaction effect. Observations/ comments are as follows:

a. The empirical models all gave similar results for the no retardation case. As expected, the spectrum changes did not alter the predictions greatly.

b. The Willenborg model produced inconsistent and illogical results in the Broek and AFGROW packages, and more sensible results with CRACKS 84. There appear to be many variations with the Willenborg model, and the reason for the inconsistencies could only be ascertained by examining the source code for the various programs. The result of this study will be conveyed to the authors of the Broek software and AFGROW because these programs are currently in use. CRACKS 84 is obsolete, and it is not (to the author's knowledge) being actively used.

c. AFGROW and Broek gave reasonably consistent results for the Wheeler retardation model. The model correctly predicted the direction in which the crack growth would change with a spectrum change, but the ratio of predicted lives was not well predicted.

d. The calibrated Broek retardation model gave good results when you examine the final life tables (Table 6). However the plots (Figures 7 to 10) show that the total curve is not always well modelled. The prediction for the 8.5 g peak load case

(Figure 10) in particular exhibits some unusual bumps. These bumps appear to be more pronounced when the spectrum contains higher peak loads. The prediction for the 5 g case is a smooth curve with little indication of bumps. The bumps are not a phenomenon which occur in the experimental results.

e. The AFGROW closure model did not give good results. The 5 g result goes against the expected trend, and the magnitude of the variation in growth life compared with the unmodified spectrum is significantly less than observed in all cases. Further investigation is required.

f. FASTRAN II produced the best predictions (see Figures 11 to 14). An encouraging aspect to this is that there is a physical explanation to the "calibration" process which took place. The baseline crack growth data had been obtained from thinner (2.3 mm) specimens. The thicker specimens used in the Mirage spectrum testing would be expected to have a higher constraint level. Having calibrated the model to the unmodified spectrum, very good predictions were obtained for the other spectra.

The results of this exercise demonstrate the superior performance of Newman's analytical crack closure model for predicting fatigue crack growth under spectrum loading. This is consistent with the findings in References 5 and 6. The empirical nature of the other models leads to inconsistent and illogical results. These results are for a relatively simple 2-D crack configuration and the models would not be expected to perform any better for a more complex geometry or more complicated loading. There also appears to be inconsistency in how the models have been coded into the software, particularly for the Willenborg retardation model.

The disadvantage with the FASTRAN II approach is the issue of the baseline crack growth rate data. However, this exercise has shown that as observed by Newman (References 13 and 14), data from high R-ratios can be used to approximate the da/dN vs ΔK_{eff} relation (see Figure 6). The constraint factor, α , can be used as a calibration factor. It is not, however, simply an empirical or arbitrary calibration. The constraint factor needs to be adjusted to reflect the level of constraint present in the particular case being analysed when compared to the constant amplitude test data. There will always be some degree of compromise inherent in this because the constraint varies along any crack front (ie whether it is a through crack or a part through crack). The analytical crack closure model is considered to be the best option for predicting fatigue crack growth under spectrum loading.

7. ACKNOWLEDGEMENTS

The author wishes to thank Mr Brendan Murtagh from AMRL for his assistance throughout this work, and Messers Jim Newman and Dave Dawicke at NASA Langley for advice and assistance with running the FASTRAN II program. Thanks also to Dr Francis Rose and Dr Chun Wang from AMRL for their technical advice, assistance and review.

REFERENCES

1. Finney, J. M. and Machin, A.S., "A Test of Some Fatigue Crack Growth Prediction Models"

2. Schijve, Jaap, "Prediction Methods for Fatigue Crack Growth in Aircraft Material", Fracture Mechanics : Twelfth Conference, ASTM STP 700, American Society for Testing and Materials, 1980, pp 3-34.

3. Chang, J.B., and Engle, R.M., "Improved Damage Tolerance Analysis Methodology", Journal of Aircraft, Vol 21, No 9, September 1984, pp 722-730.

4. Newman, J. C., "A Crack Closure Model for Predicting Fatigue Crack Growth Under Aircraft Spectrum Loading", ASTM STP 748, American Society for Testing and Materials, 1981.

5. Salvetti, A., Lazzeri, L., and Pieracci, A., "An Assessment of Fatigue Crack Growth Prediction Models for Aerospace Structures", AGARD Report 797, Sept 1993.

6. Lazzeri, L., Pieracci, A. and Salvetti, A., "An evaluation of Fatigue Crack Growth Prediction Methods Used in Aircraft Design", Proceedings of the 18 th ICAF Symposium, pp 615-645 EMAS publ. 1995.

7. Wang, G.S., and Blom, A.F., "A Strip Model for Fatigue Crack Growth Predictions Under General Load Conditions", Engineering Fracture Mechanics, Vol 40, No 3, pp 507-533, 1991.

8. Ball, D.L., "Non-Linear Fatigue Crack Growth Analysis for Problems with Small Scale Yielding", presented at 1993 USAF Structural Integrity Program Conference, San Antonio TX, 30 November 1993.

9. Ball, D.L., "Proposed Integration of Notch-Strain and Fatigue Crack Growth Analyses", Journal of Aircraft, Vol 27, No 3, April 1990, pages 358-367.

10. Walker, K., "The Effect on Fatigue Crack Growth Under Spectrum Loading of an Imposed Placard "G" Limit", Masters Thesis, Purdue University, December 1987.

11. Broek, D., "Software for Practical Fracture Mechanics and Damage Tolerance Analysis", Windows Version, 1995

12. Kirshnan, S., Boyd, K.L. and Harter, J.A., "Structural Integrity Analysis and Verification of Aircraft Structures", AFGROW Users Manual, Version 3.0.4, August 1995.

13. Newman, J. C., "FASTRAN II - A Fatigue Crack Growth Structural Analysis Program", NASA Technical Memorandum 104159, February 1992.

14. Newman, J., Phillips, E., and Swain, M.H., "Fatigue Life prediction Methodology Using Small Crack Theory", NASA Technical Memorandum 110307, January 1997.

15. " Damage Tolerant Design Handbook - A Compilation of Fracture and Crack Growth Rate Data for High Strength Alloys", MCIC-HB-01R, University of Dayton Research Institute, and Materials Laboratory, Air Force Wright Aeronautical Laboratories, Wright Patterson Air Force Base, December 1983.

Metals
Ceramics &
N.D.E. Division

Air Force Research Laboratory - Materials and
Manufacturing Directorate

A New Concept to Describe Load Interaction Effects in Fatigue Crack Propagation

M. Lang

Air Force Research Laboratory (AFRL/MLLN),

Wright-Patterson AFB, OH 45433-7817

NRC -associate

The 1997 USAF Aircraft Structural Integrity Program Conference,

2-4 Dec. 1997, San Antonio, Texas.

The ΔK_{eff}-Concept

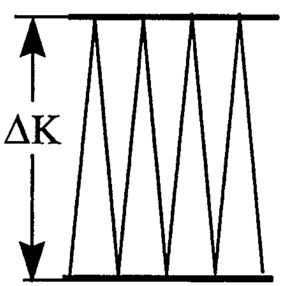

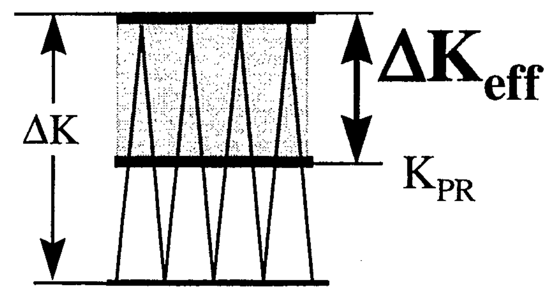

$$\boxed{\Delta K_{eff} = K_{\max} - K_{PR} - \Delta K_T}$$

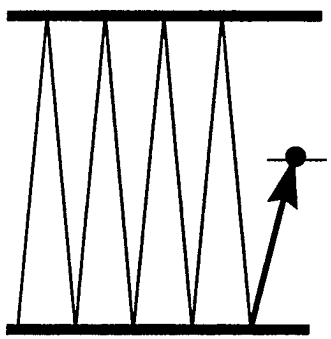

crack
propagates
above K_{PR}

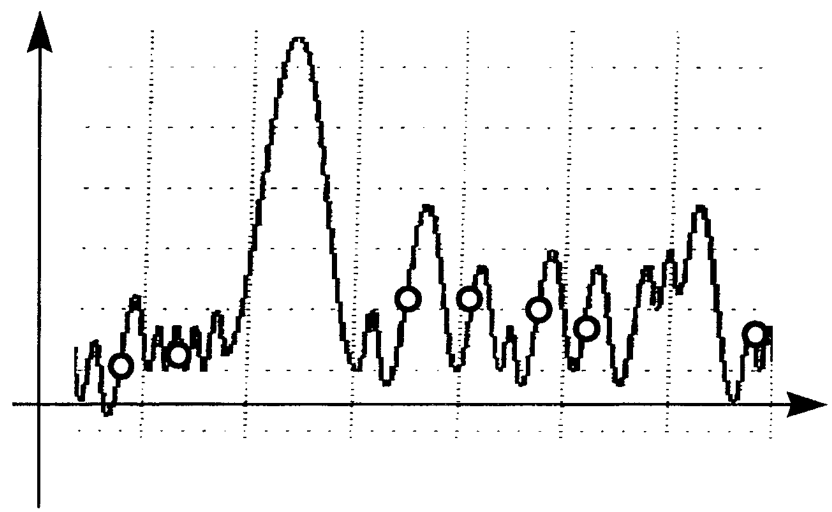

Crack Propagation Load Measurement Method (CPLM)

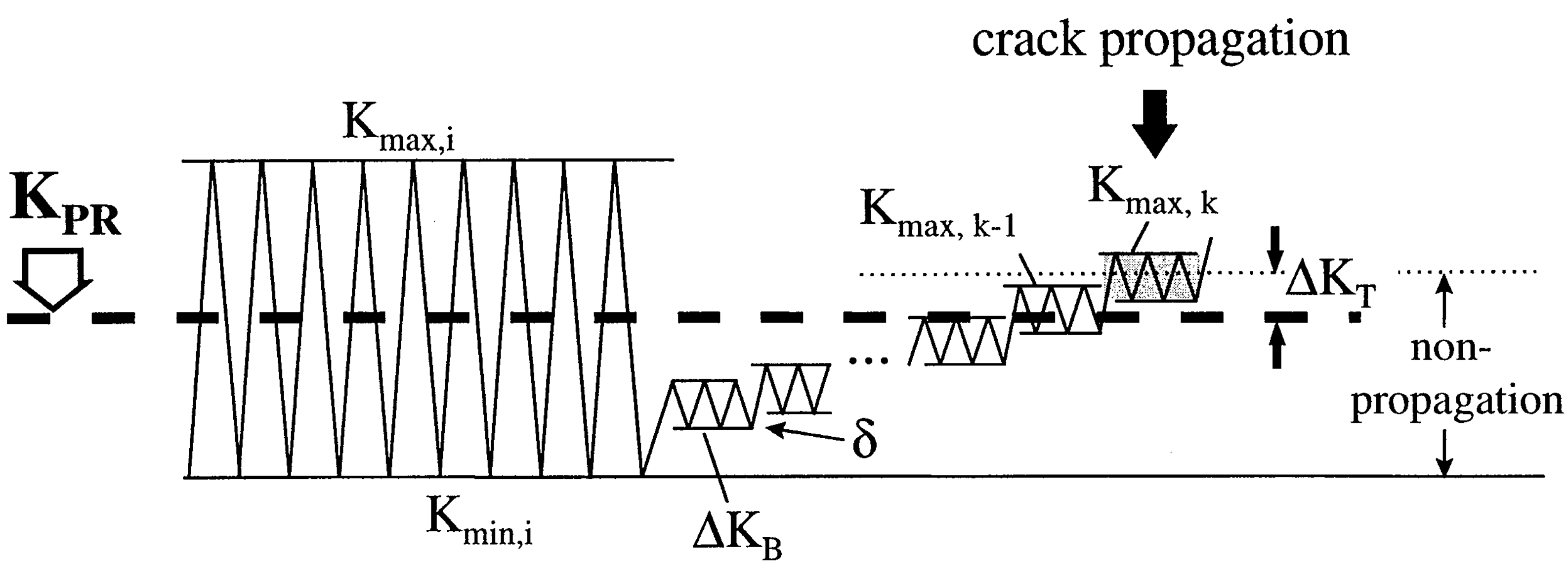

$$K_{PR} = \frac{\left(K_{\max,k} + K_{\max,k-1}\right)}{2} - \Delta K_T$$

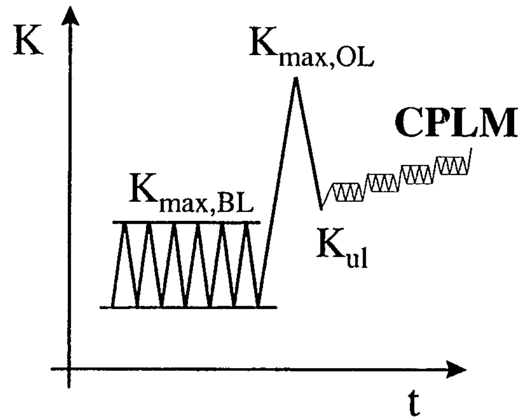

R_{BL}	$K_{max,OL}$ [MPa√m]	K_{ul} [MPa√m]
0.1	19 23 28	1; 4; 5 1; 4.5 1; 5
0.33	22.8 27.6	0.5; 2; 4; 8 1; 4; 10
0.47	24 31.5	1; 2.5; 7; 11 1; 7; 13
0.68	24.7 32.3	2.5; 13; 16 1; 13; 21
0.8	27 32	16 1.5; 16; 24

CT-specimens,
W=50mm, B=10mm

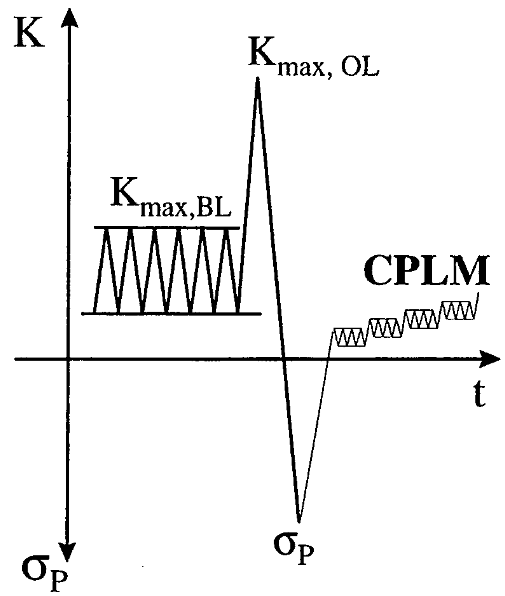

R_{BL}	$K_{max,OL}$ [MPa√m]	σ_P [MPa]
0.1	19	0; -92.5, -185; -231, -277; -314
	23	0, -92.5, -185 -231, -277
	28	-25; -80; -130, -185 -231, -277
	32	6.5; -92.5; -185;-277
0.33	27.6	-92.5, -231
0.47	31.5	-92.5, -231
0.68	32.3	-92.5, -231
0.8	32	-92.5 -231

CCT-specimens,
W=160mm, B=8mm

Al 7475-T7351

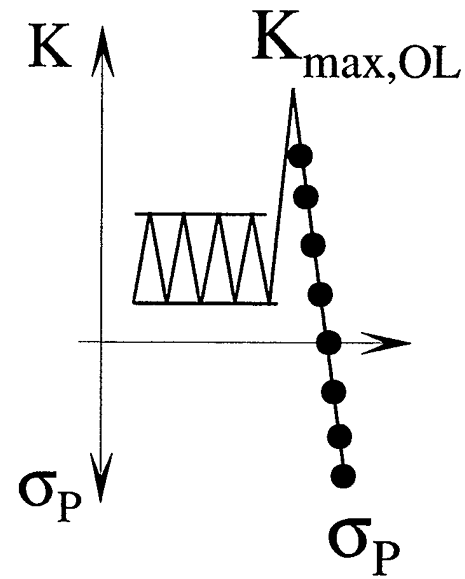

Al 7475-T7351

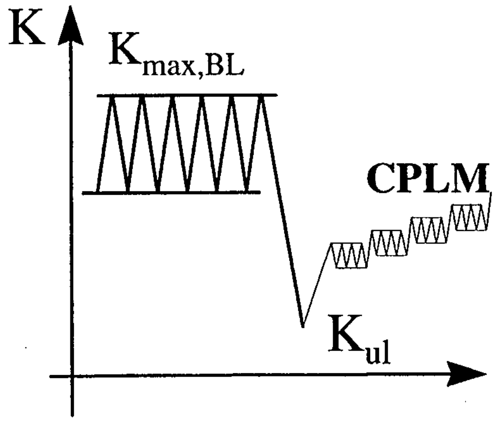

R_{BL}	K_{ul} [MPa√m]
0.33	1
0.47	2
0.68	0.6, 7
0.8	1, 6

CT-specimens,
W=50mm, B=10mm

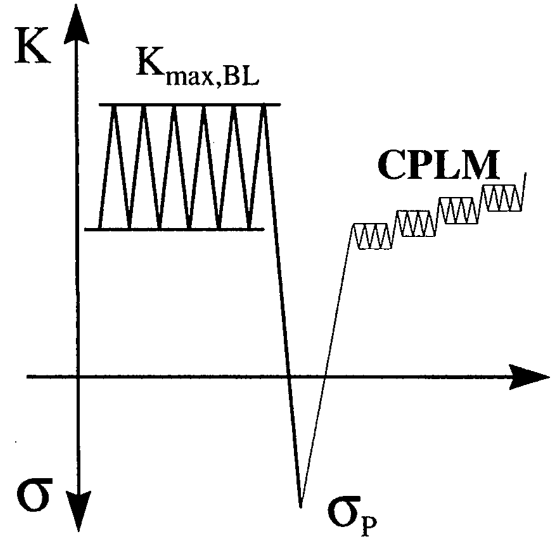

R_{BL}	σ_P [MPa]
0.1	-46; -92.5; -277
	-92.5; -185; -277
	-92.5; -185
	-185; -277
	-92.5; -185
0.33	-139
0.47	-139
0.68	-139
0.8	-139

CCT-specimens,
W=160mm, B=8mm

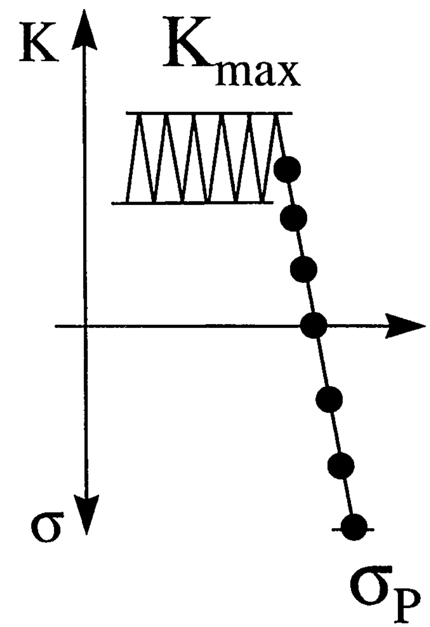

CA- tension/compression

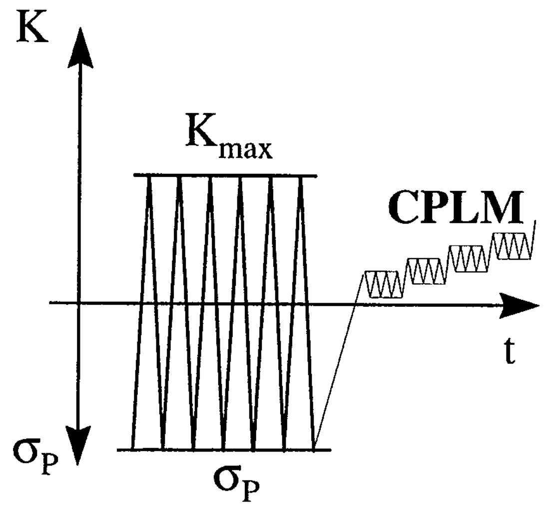

K_{max} [MPa√m]	σ_P [MPa]
10	-92.5 -139 -185
15	-46 -139
19	-92.5 -139 -185
23	-92.5
28	-46 -139

Al 7475-T7351

CCT-specimens,
W=160mm,
B=8mm

Multiple OL/CL

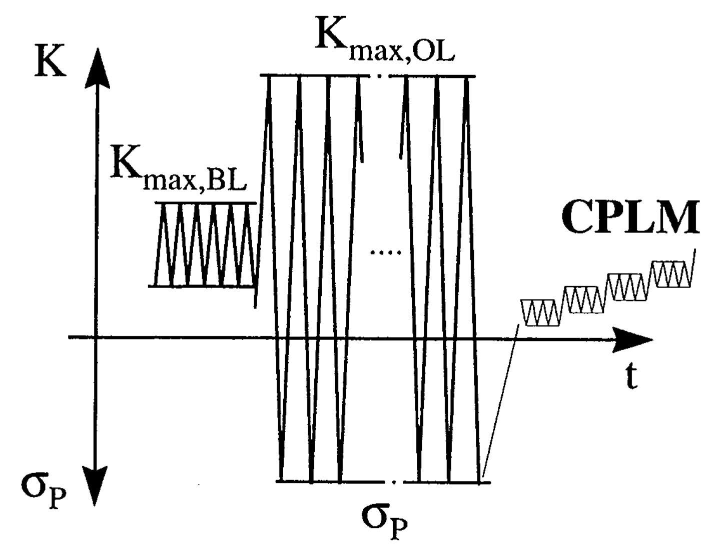

R_{BL}	$K_{max, OL}$ [MPa√m]	σ_D [MPa]	OL/CL -cycles, [N_{OC}]
0.1	23	-92.5	3; 5; 10; 20; 100
0.33	27.6	-92.5	3; 5; 10; 20; 100
0.47	31.5	-92.5	3; 5; 10; 20; 100
0.68	32.3	-92.5	3; 5; 10; 20; 100

Al 7475-T7351

CCT-specimens,
W=160mm, B=8mm

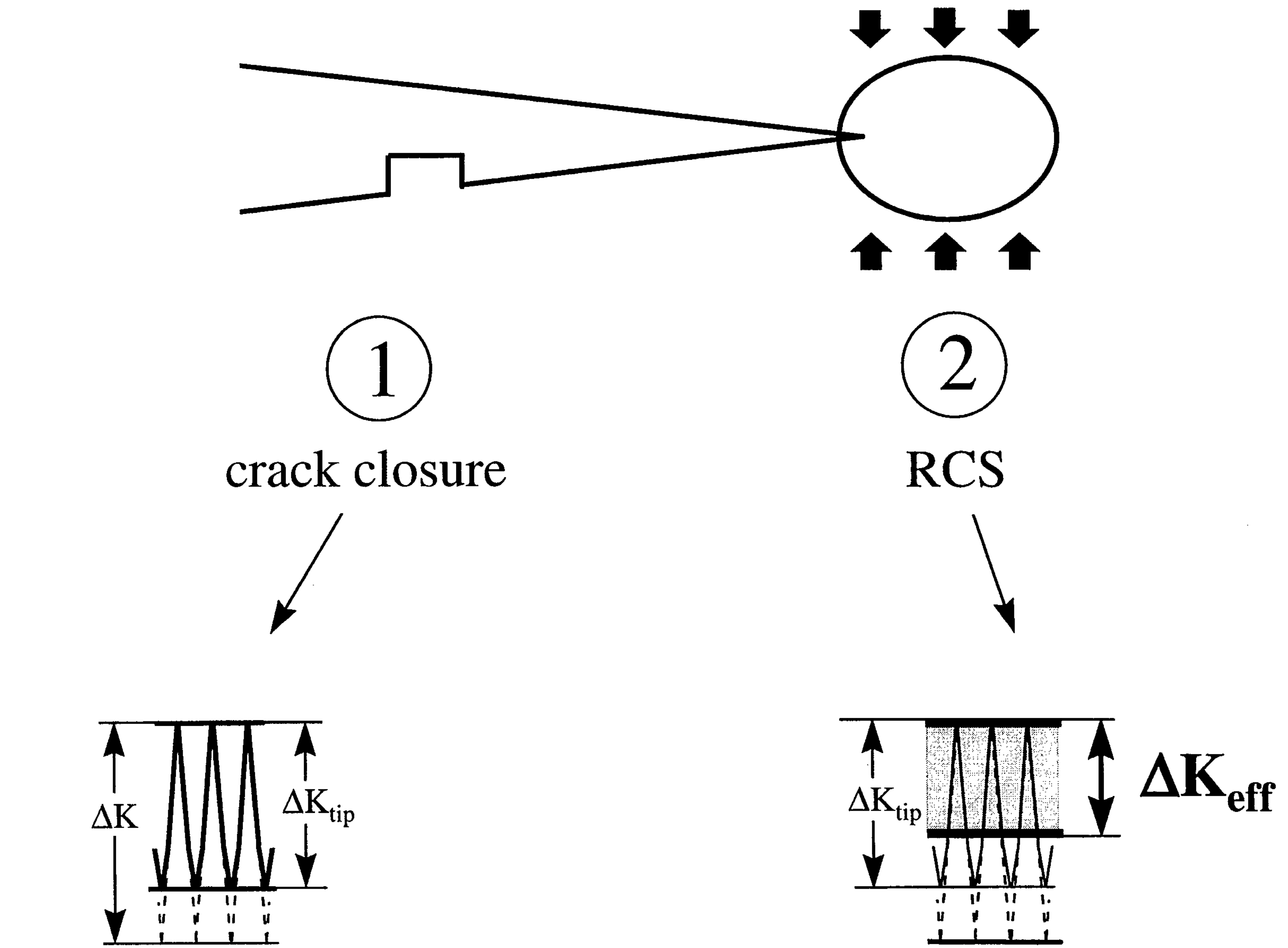

$$\Delta K_{tip} = K_{\max} - K_W$$

$$\boxed{\Delta K_{eff} = K_{\max} - K_{PR} - \Delta K_T}$$

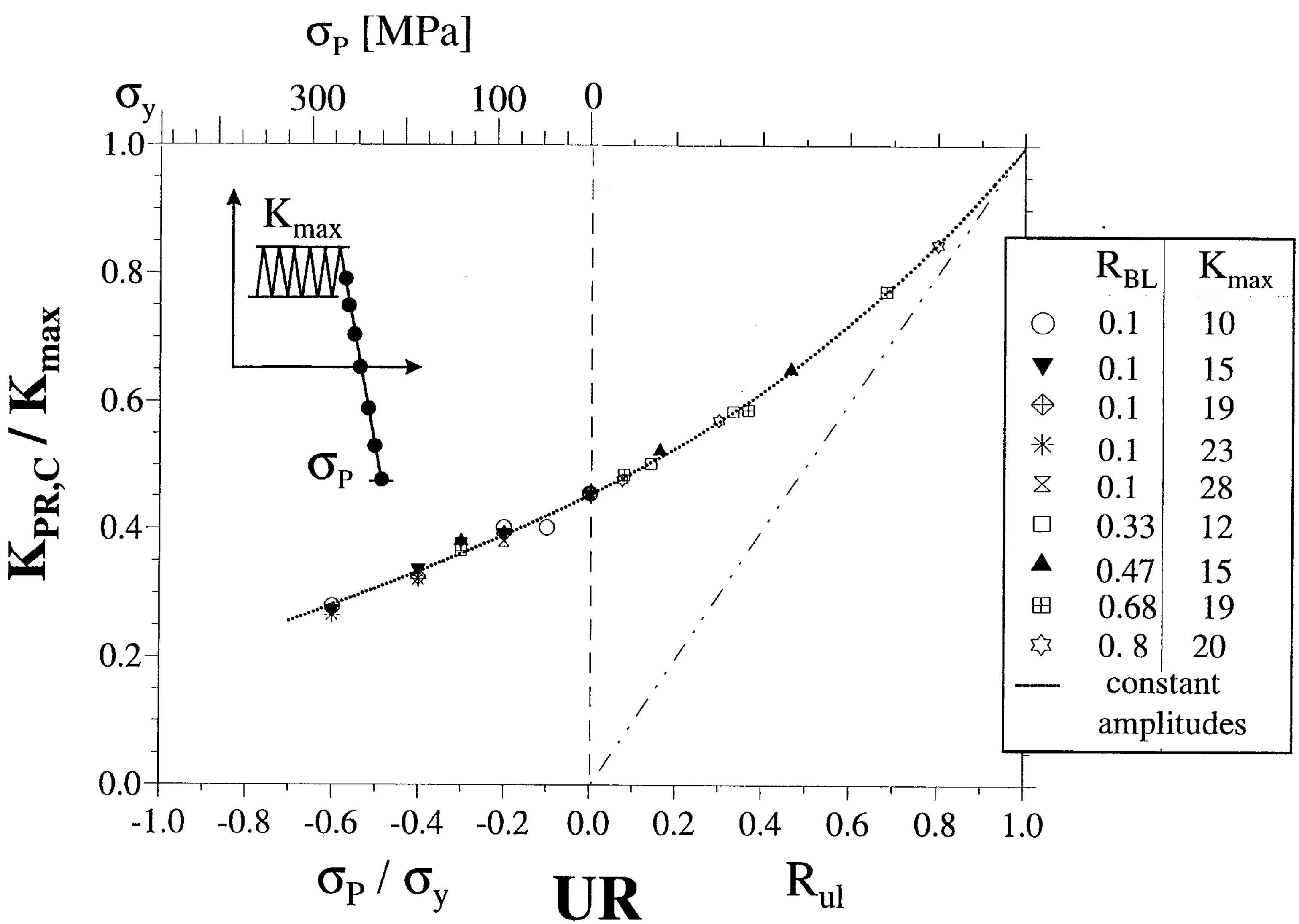

$$K_{PR,C} = \left(0.453 + 0.34 \cdot UR + 0.134 \cdot UR^2 + 0.07 \cdot UR^3\right) \cdot K_{max}$$

$$\boxed{K_{PR,C} = g\left(UR\right) \cdot K_{max}}$$

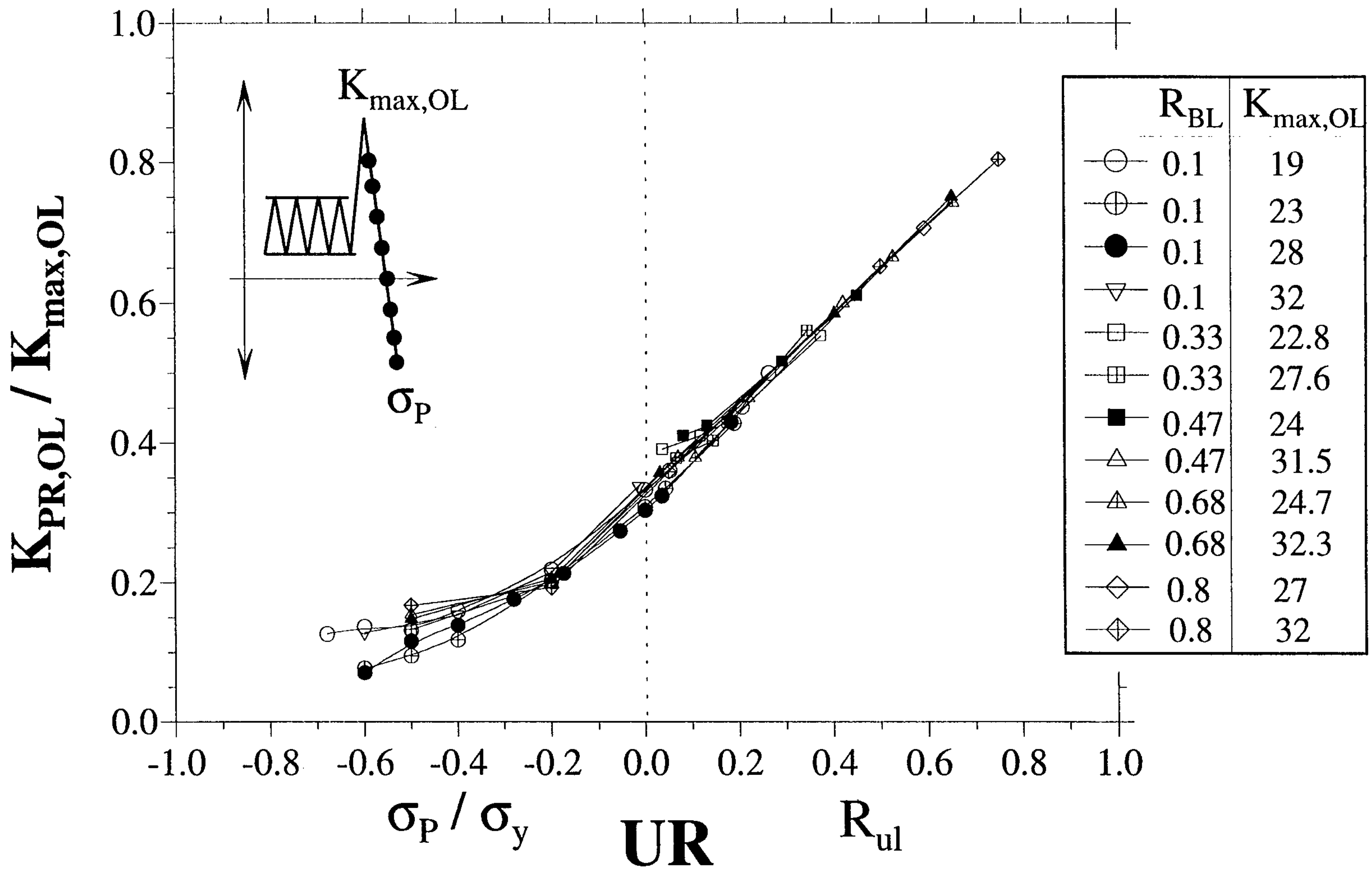

$$K_{PR,OL} = \left(0.322 + 0.58 \cdot UR + 0.241 \cdot UR^2 - 0.18 \cdot UR^3\right) \cdot K_{\max,OL} \quad [-0.7 < \mathrm{UR} < 1]$$

$$\boxed{K_{PR,OL} = h(UR) \cdot K_{\max,OL}}$$

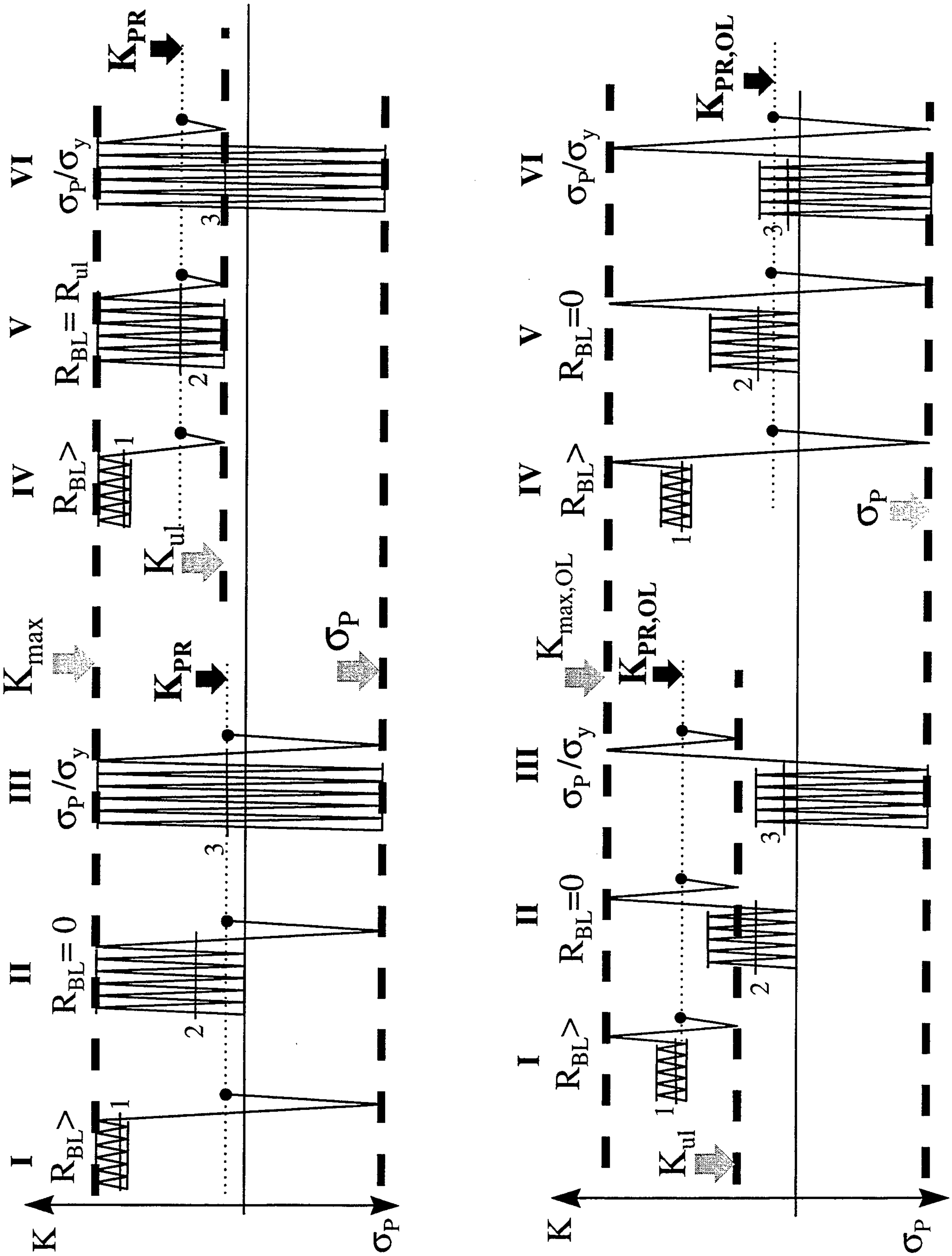
I
II
III
IV
V
VI
$R_{BL}>$
$R_{BL}=0$
σ_P/σ_y
$R_{BL}>$
$R_{BL}=R_{ul}$
σ_P/σ_y
K
σ_P
K_{max}
K_{PR}
σ_P
K_{ul}
K_{PR}
1
2
3
I
II
III
IV
V
VI
$R_{BL}>$
$R_{BL}=0$
σ_P/σ_y
$R_{BL}>$
$R_{BL}=0$
σ_P/σ_y
K
σ_P
K_{ul}
$K_{max,OL}$
$K_{PR,OL}$
σ_P
$K_{PR,OL}$

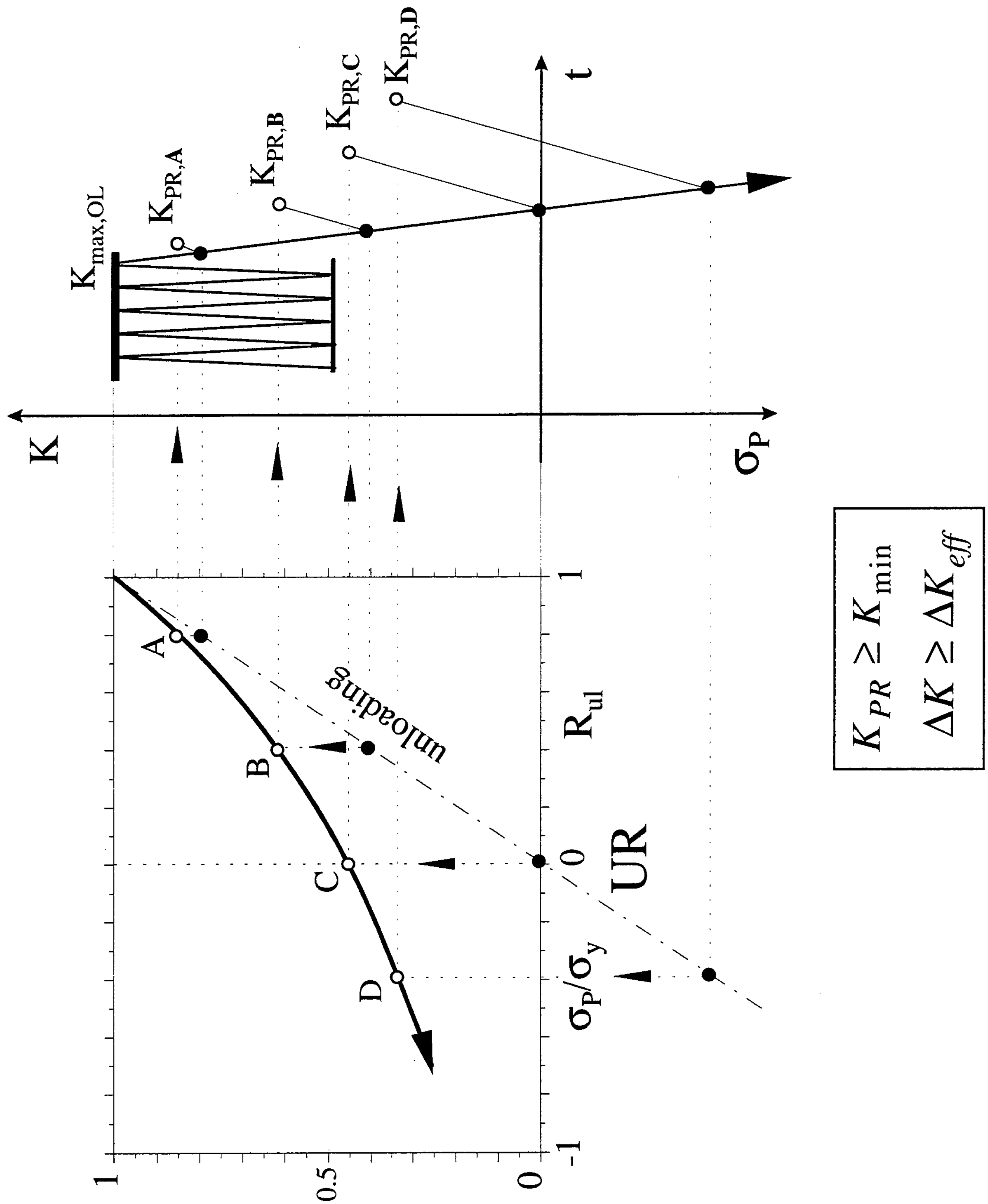

$K_{max,OL}$
$K_{PR,A}$
$K_{PR,B}$
$K_{PR,C}$
$K_{PR,D}$
K
t
σ_P
$K_{PR,C} / K_{max}$
1
0.5
0
-1
R_{ul}
σ_P/σ_y
UR
A
B
C
D
unloading
$K_{PR} \geq K_{min}$
$\Delta K \geq \Delta K_{eff}$

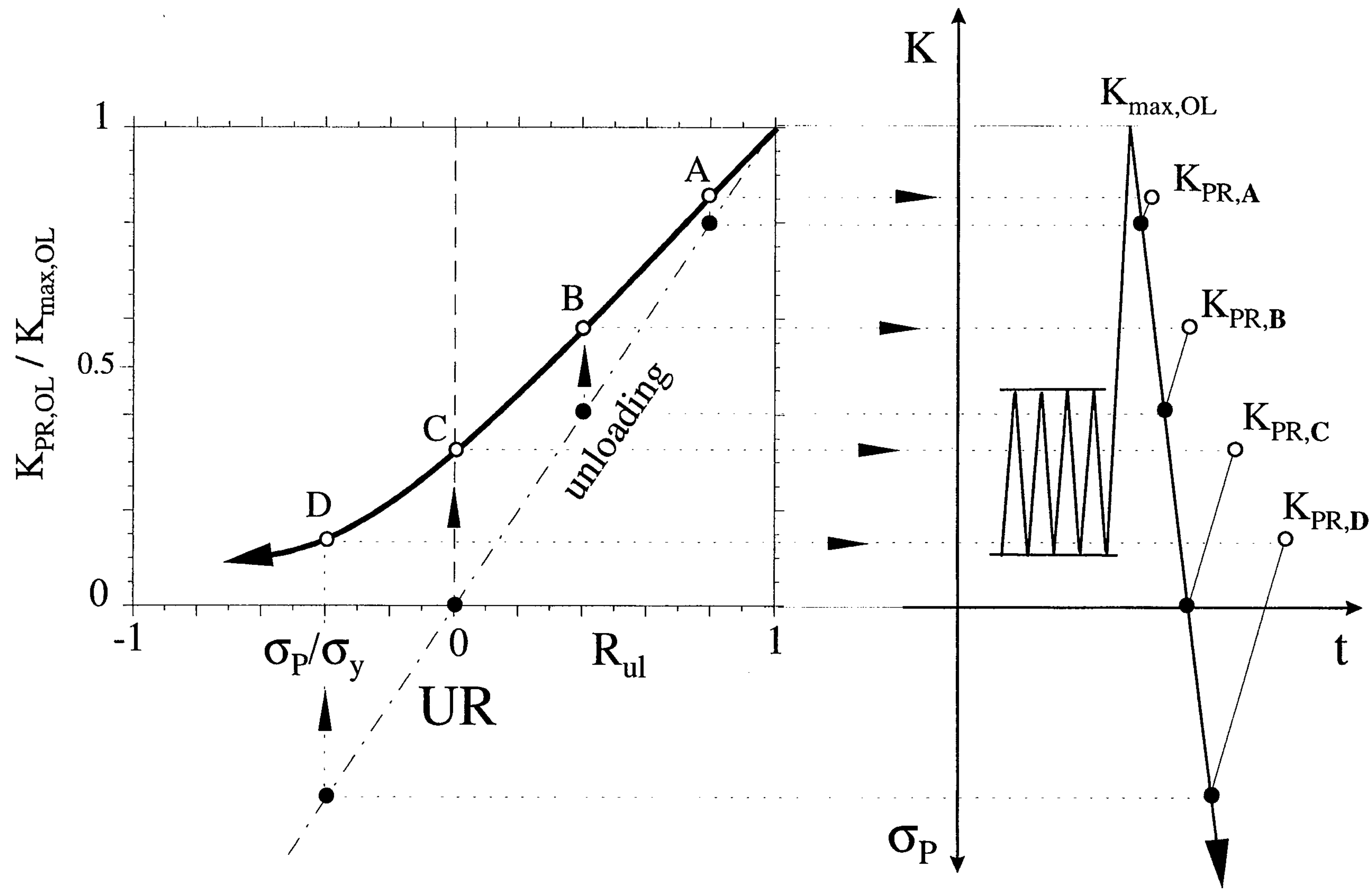

$$K_{PR} \geq K_{\min}$$
$$\Delta K \geq \Delta K_{eff}$$

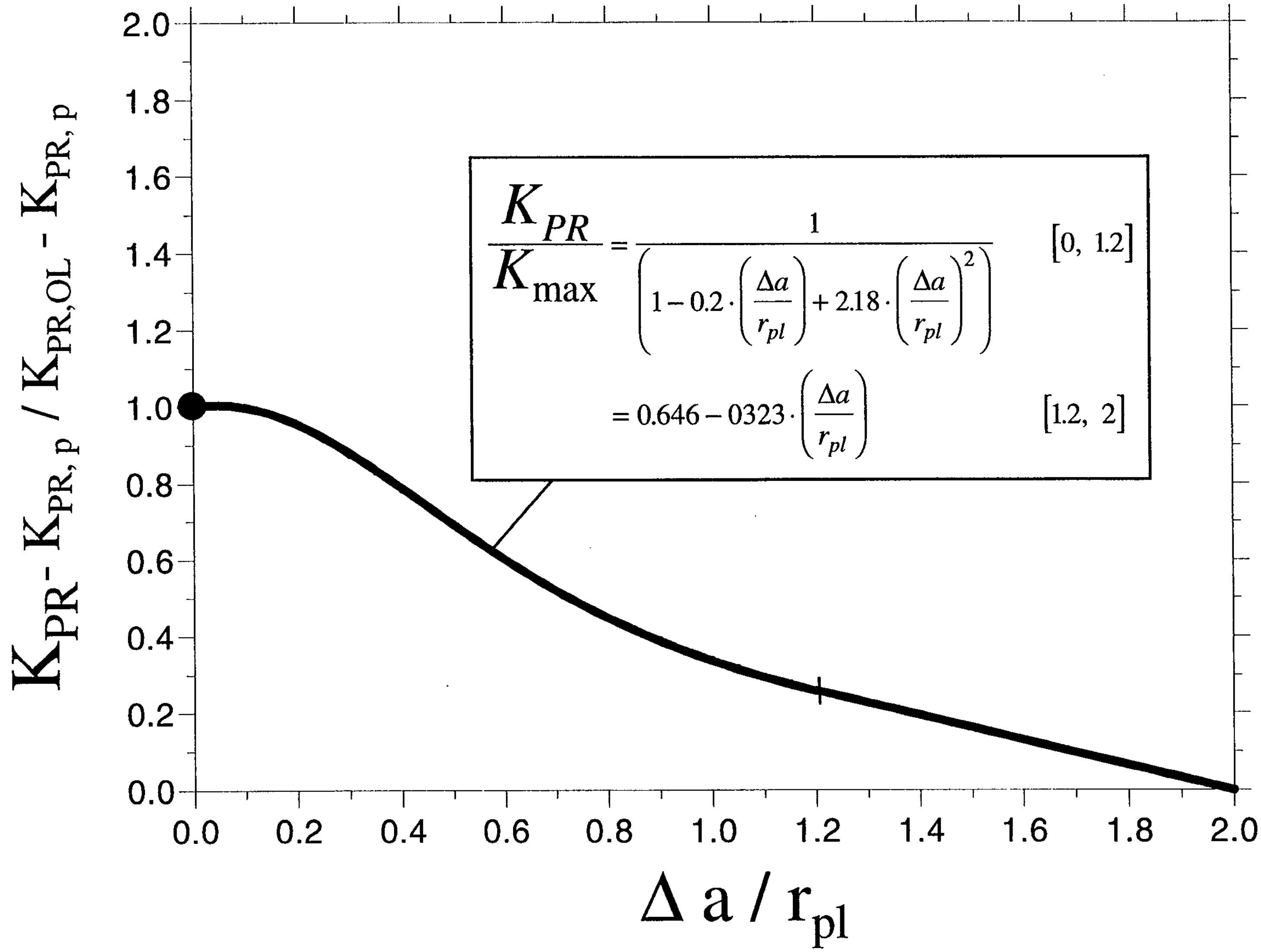

$$\frac{K_{PR}}{K_{max}} = \frac{1}{\left(1 - 0.2 \cdot \left(\frac{\Delta a}{r_{pl}}\right) + 2.18 \cdot \left(\frac{\Delta a}{r_{pl}}\right)^2\right)} \quad [0,\ 1.2]$$
$$= 0.646 - 0323 \cdot \left(\frac{\Delta a}{r_{pl}}\right) \quad [1.2,\ 2]$$
$K_{PR} - K_{PR,\,p} \,/\, K_{PR,OL} - K_{PR,\,p}$
$\Delta a \,/\, r_{pl}$
0.0
0.2
0.4
0.6
0.8
1.0
1.2
1.4
1.6
1.8
2.0

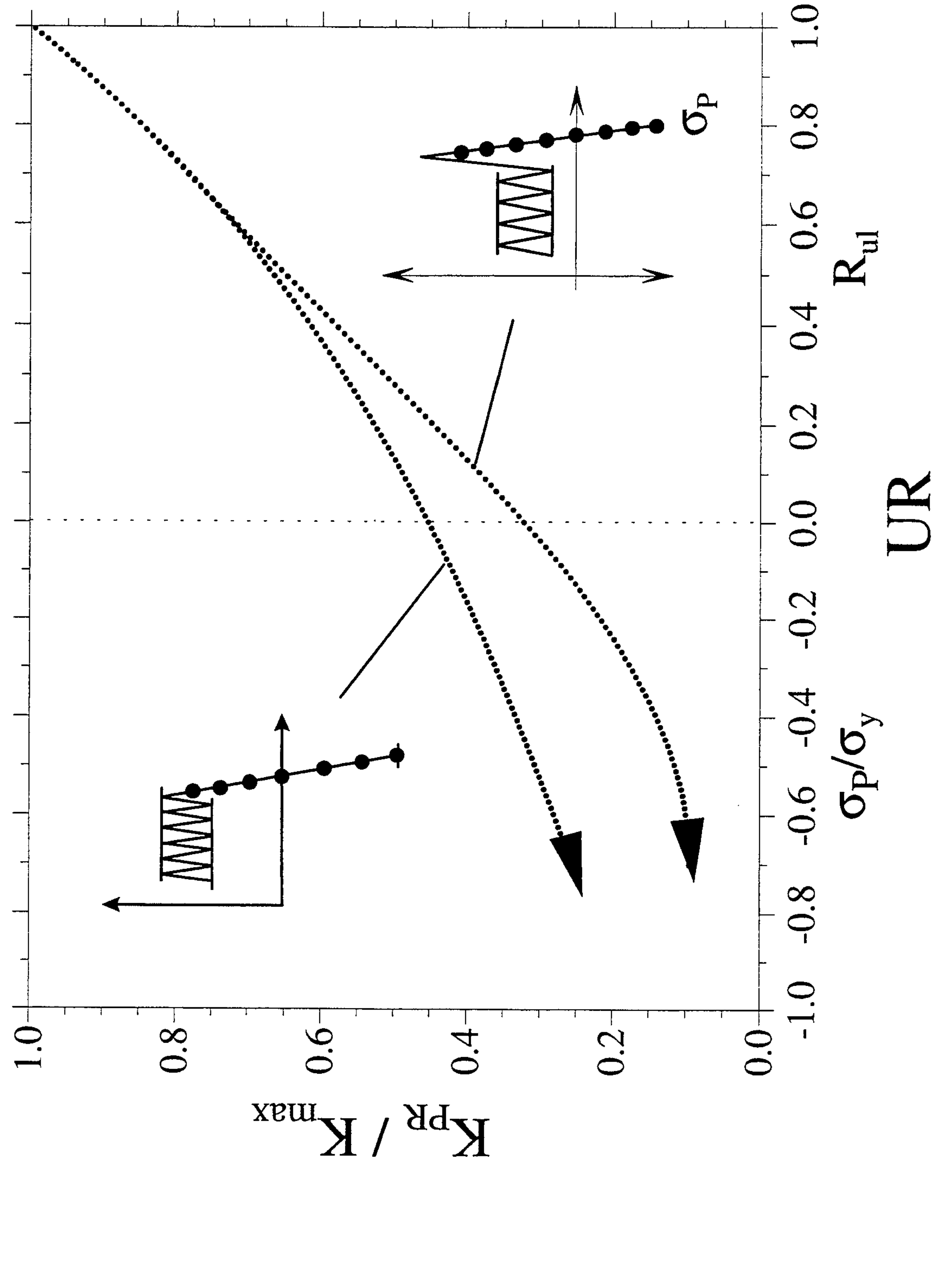

K$_{PR}$ / K$_{max}$
1.0
0.8
0.6
0.4
0.2
0.0
-1.0
-0.8
-0.6
-0.4
-0.2
0.0
0.2
0.4
0.6
0.8
1.0
σ$_P$/σ$_y$
R$_{ul}$
σ$_P$
UR

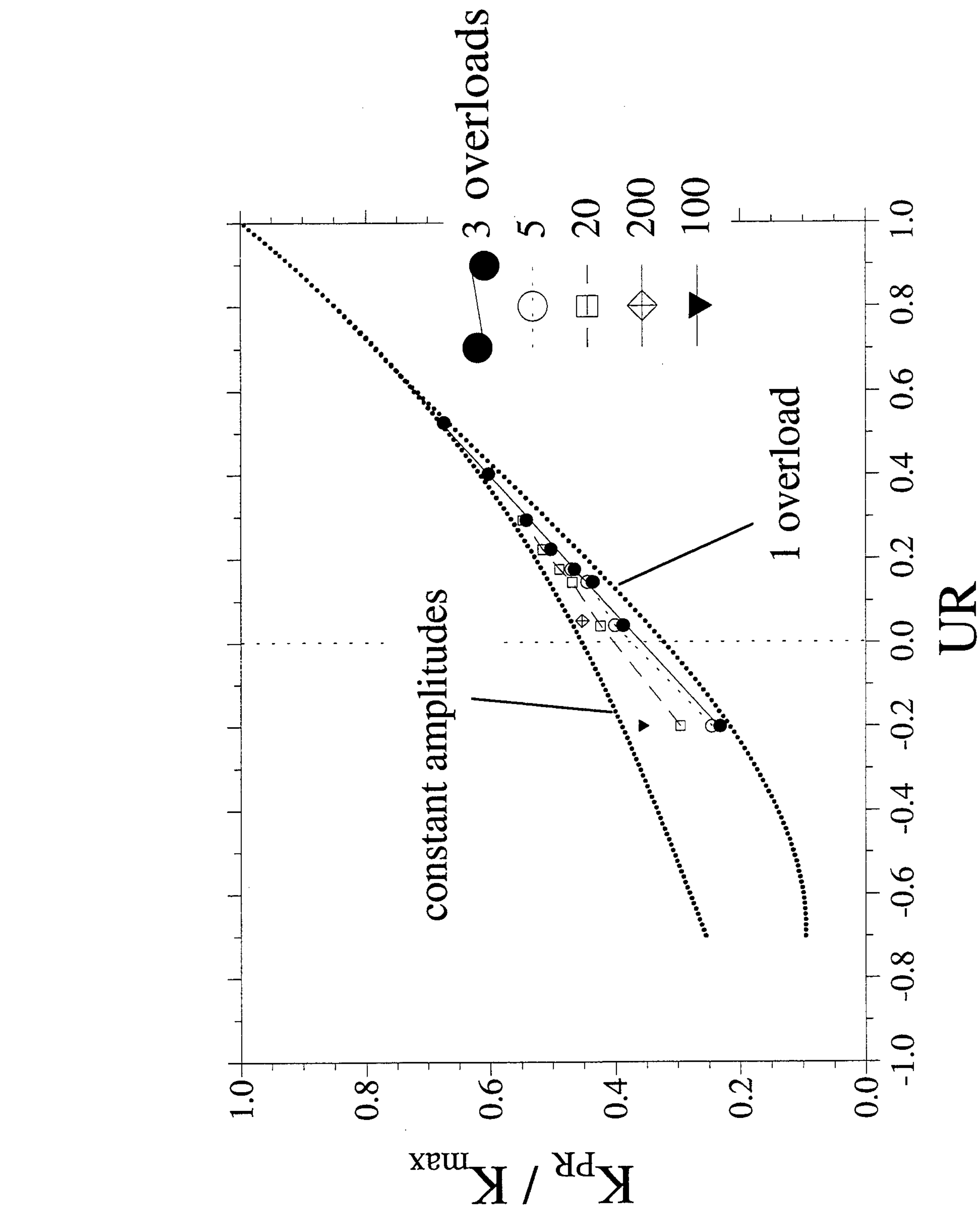

3 overloads
5
20
200
100
1 overload
constant amplitudes
UR
K_{PR} / K_{max}
1.0
0.8
0.6
0.4
0.2
0.0
-0.2
-0.4
-0.6
-0.8
-1.0

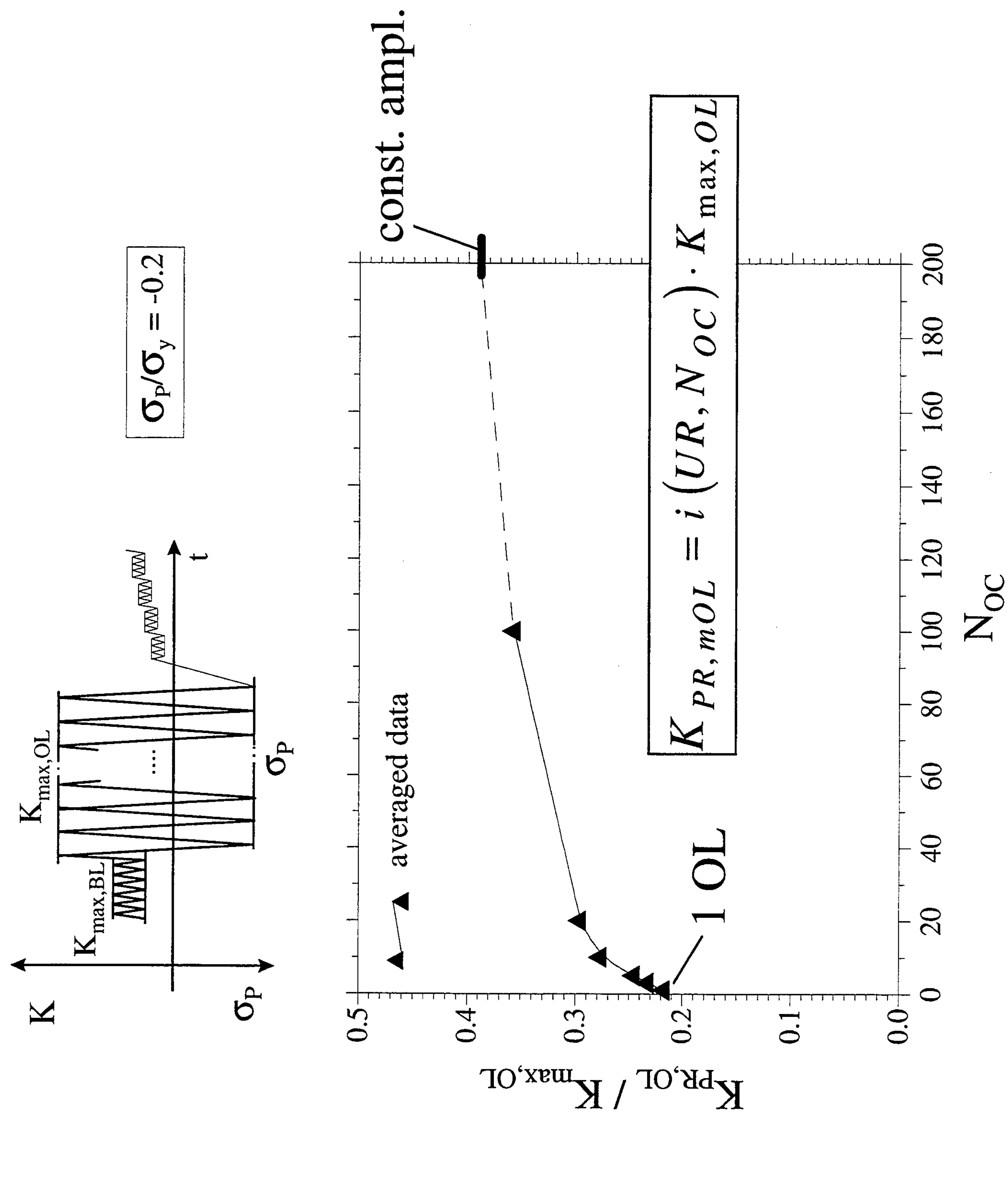

K
σ_P
$K_{max,BL}$
$K_{max,OL}$
σ_P
t
$\sigma_P/\sigma_y = -0.2$
const. ampl.
averaged data
1 OL
$K_{PR,mOL} = i\left(UR, N_{OC}\right) \cdot K_{max,OL}$
$K_{PR,OL} / K_{max,OL}$
N_{OC}
0.5
0.4
0.3
0.2
0.1
0.0
0
20
40
60
80
100
120
140
160
180
200

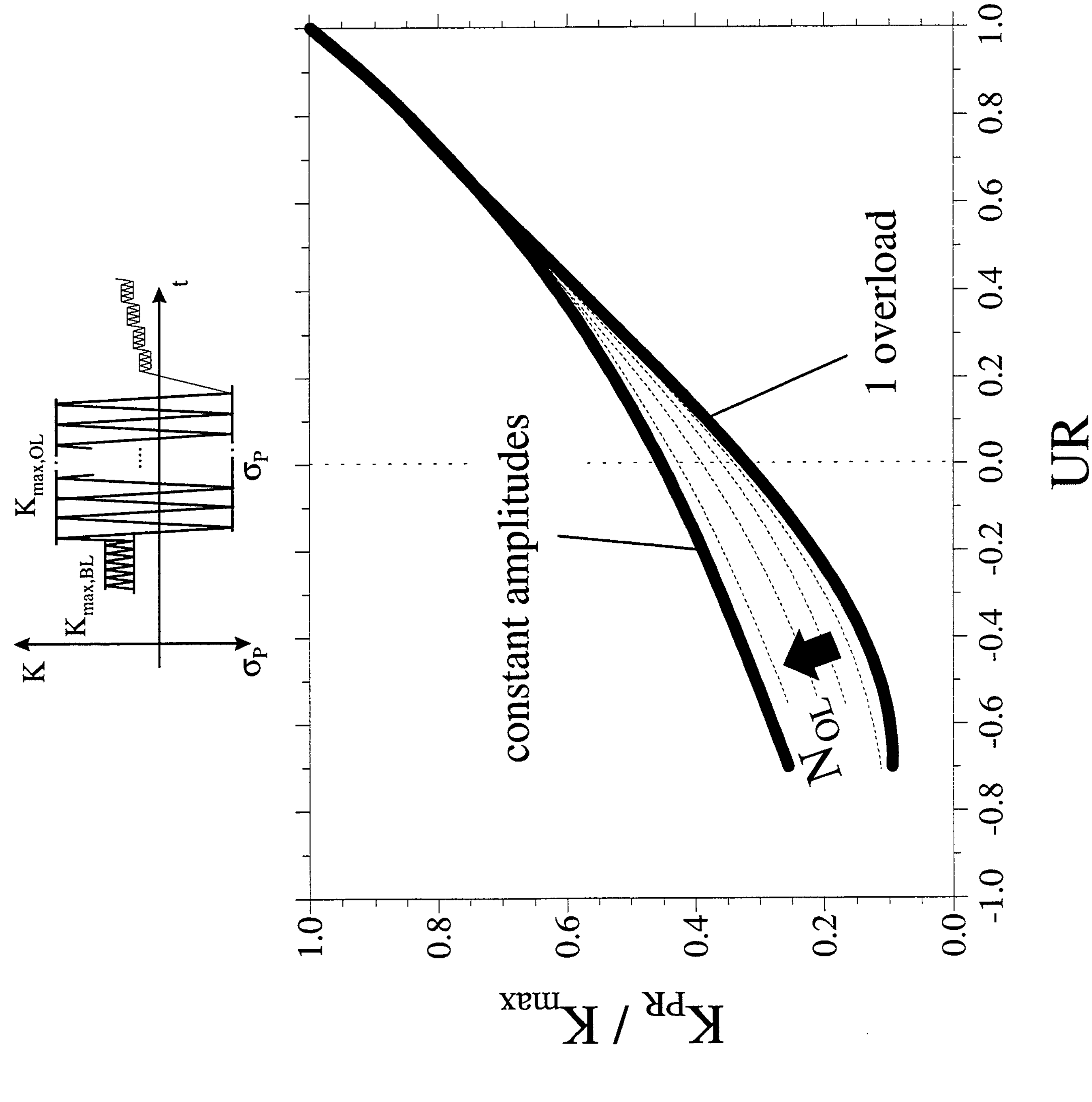

K
$K_{max,BL}$
$K_{max,OL}$
σ_P
t
constant amplitudes
1 overload
N_{OL}
K_{PR} / K_{max}
UR

The Three Possible Types of Cycles

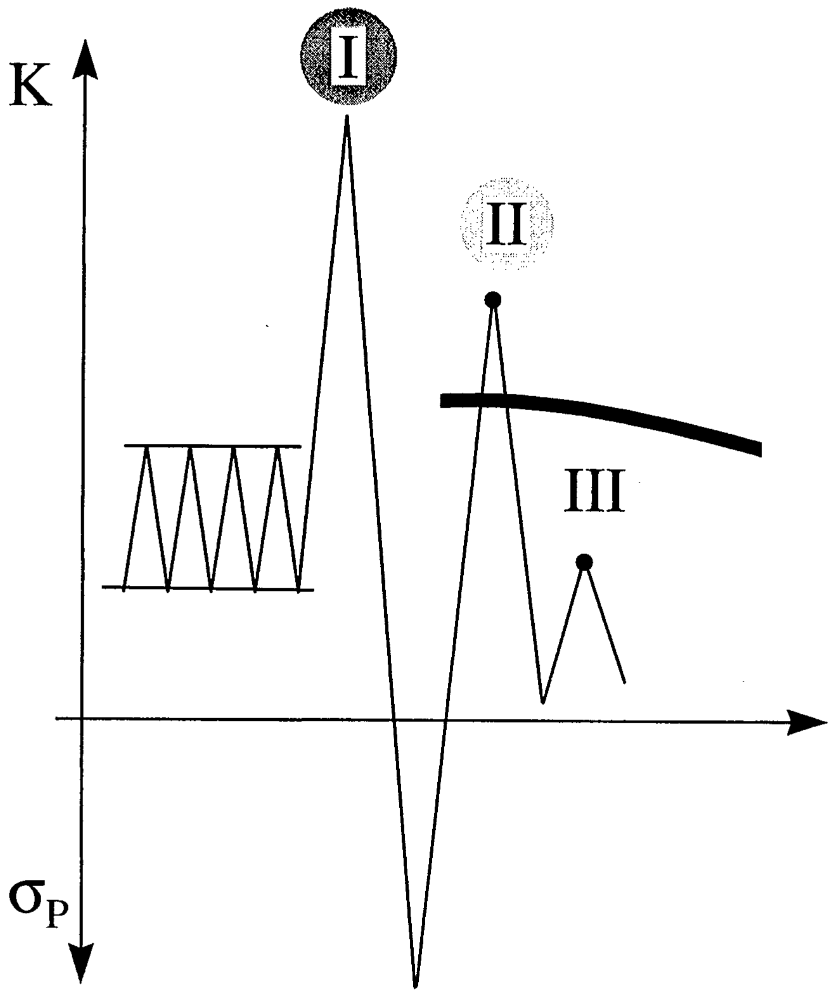

I $K_{PR,OL} \le (K_{PR} / K_{max})_I \le K_{PR,C}$

II $K_{PR,C} \le (K_{PR} / K_{max})_{II} \le 1$

III $(K_{PR} / K_{max})_{III} > 1$

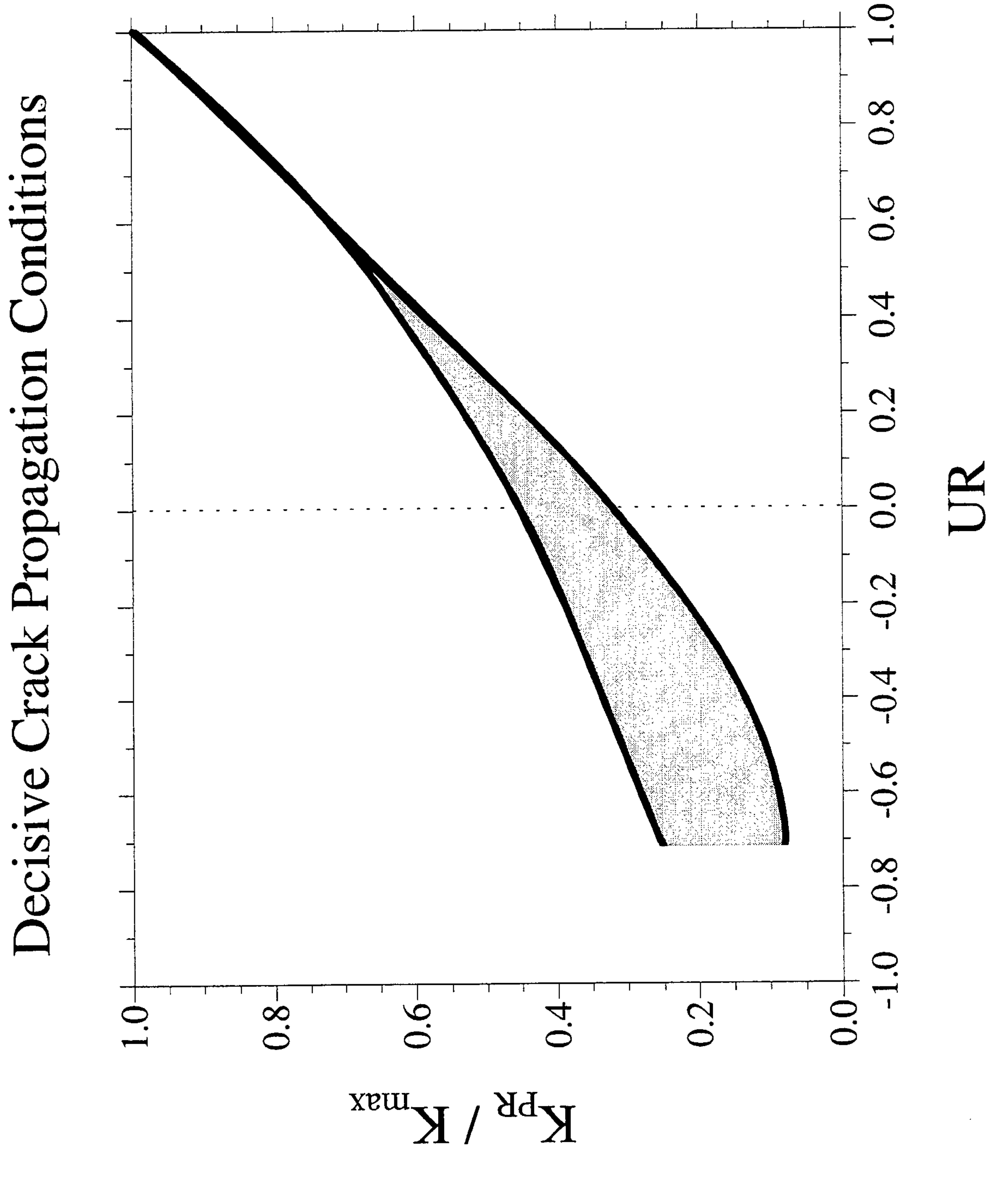

Decisive Crack Propagation Conditions
1.0
0.8
0.6
0.4
0.2
0.0
-0.2
-0.4
-0.6
-0.8
-1.0
UR
K_{PR} / K_{max}

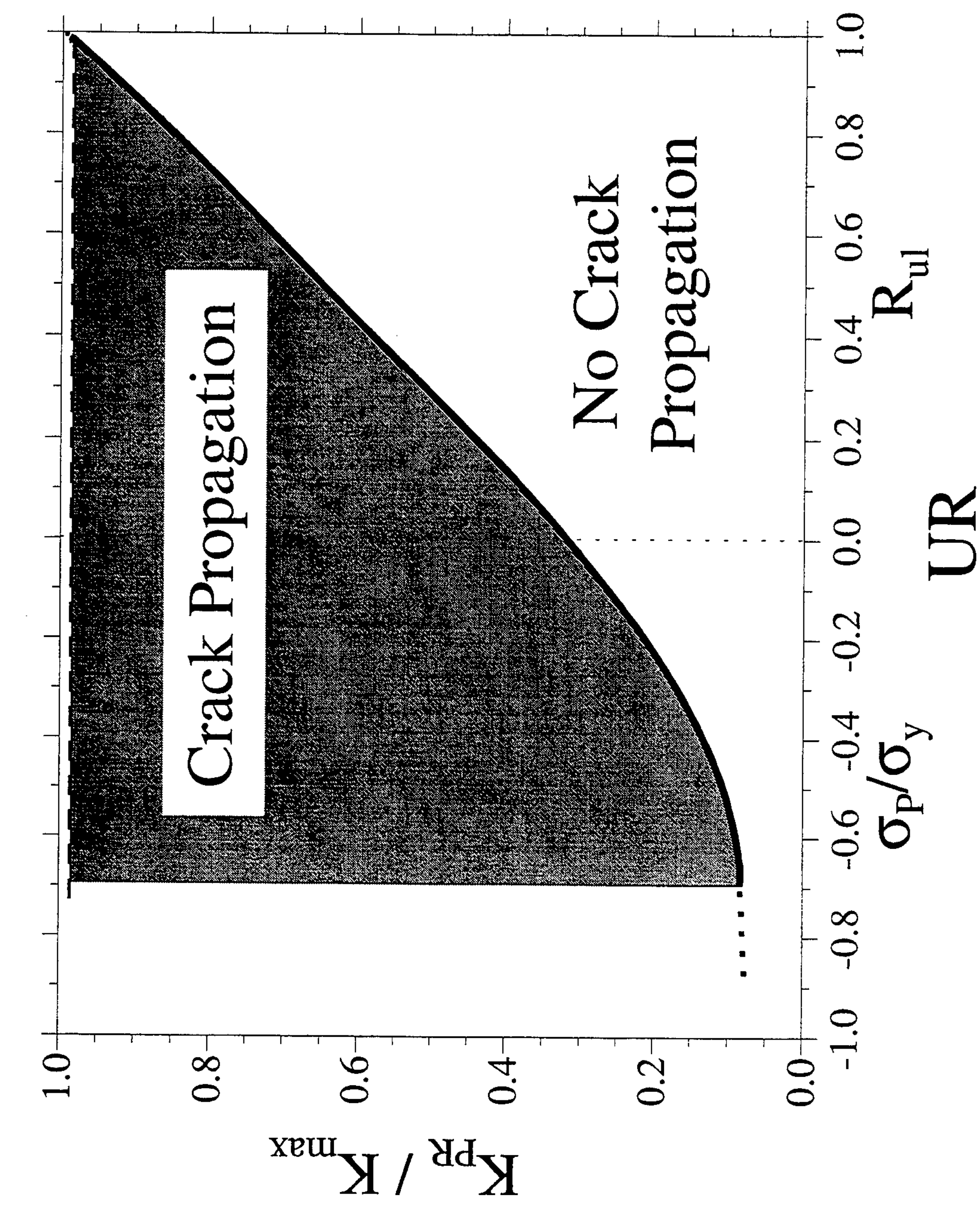
Crack Propagation
No Crack
Propagation
K_{PR} / K_{max}
σ_P/σ_y
R_{ul}
UR
1.0
0.8
0.6
0.4
0.2
0.0
-1.0
-0.8
-0.6
-0.4
-0.2
0.0
0.2
0.4
0.6
0.8
1.0

Map of Possible Crack Propagation Conditions

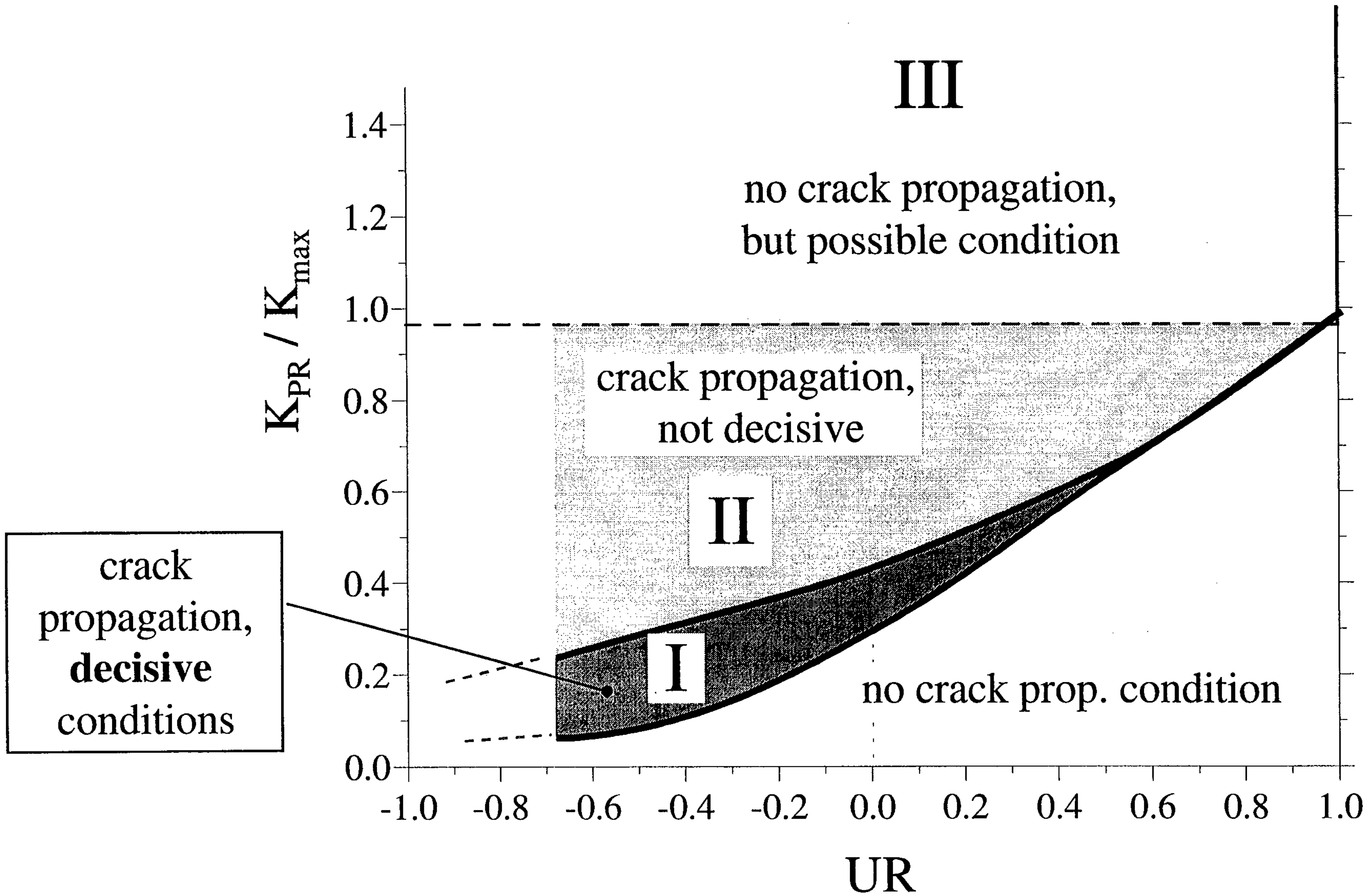

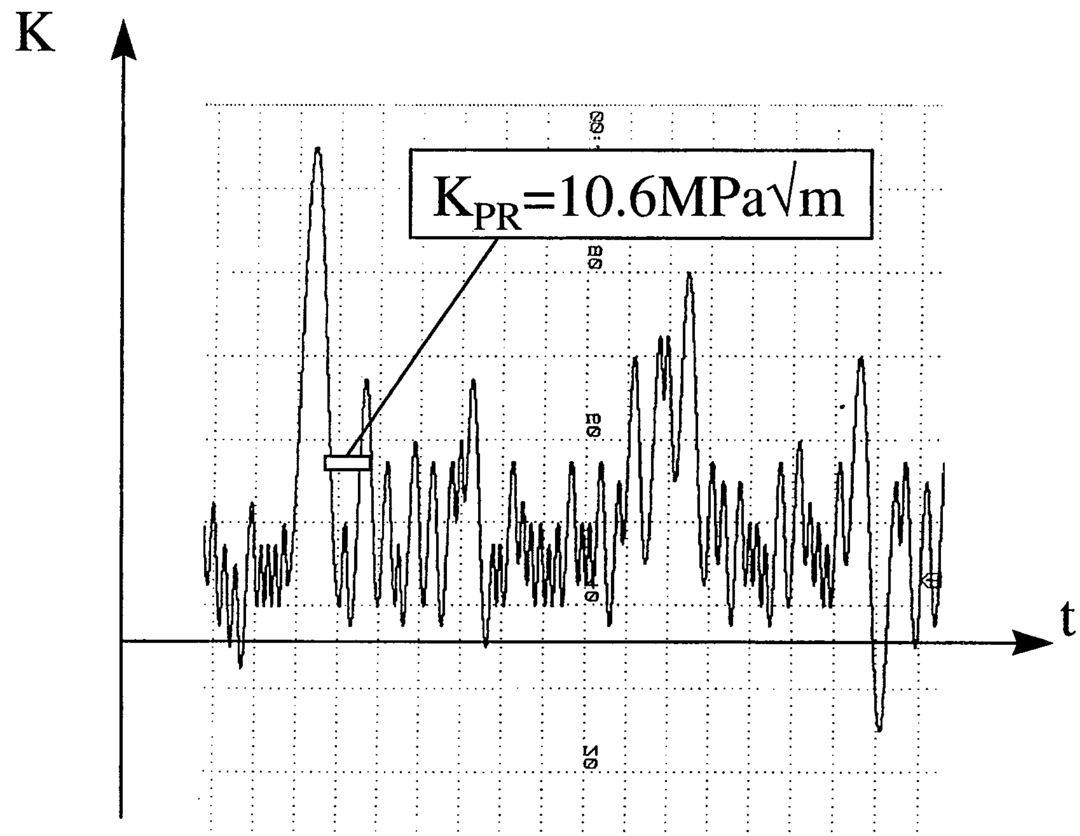

K_w=2.8MPa√m

R_{tip}=0.1045

K_{PR}/ $K_{max, OL}$= 0.385

K_{PR} =<u>10.3 MPa√m</u>

Multiple Overloads $R_{BL}=0.1$

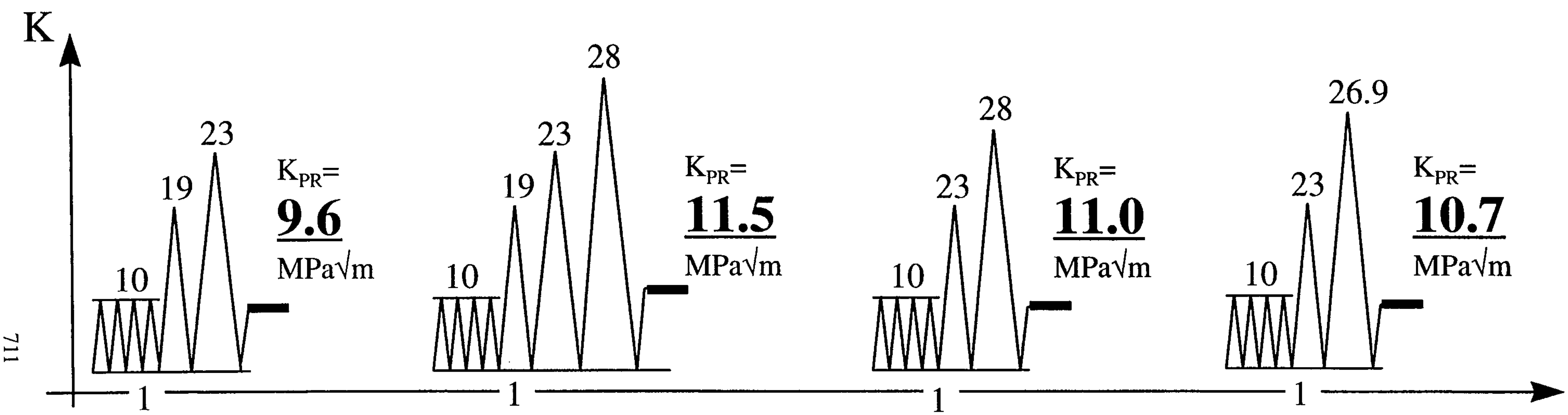

PRED: $K_{PR}=$ **9.3** MPa√m

PRED: $K_{PR}=$ **11.6** MPa√m

PRED: $K_{PR}=$ **11.0** MPa√m

PRED: $K_{PR}=$ **10.5** MPa√m

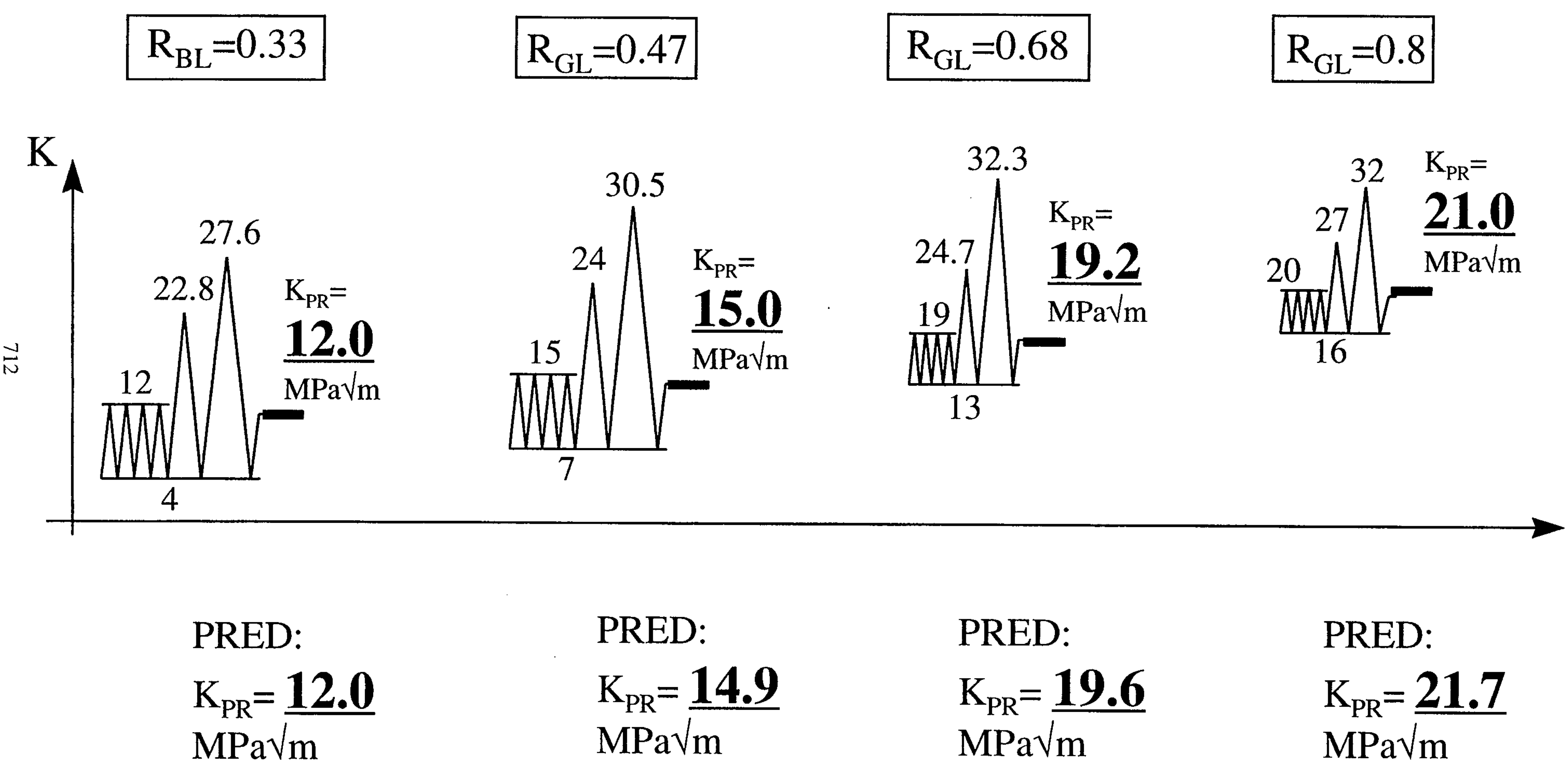

R_{BL}=0.33
R_{GL}=0.47
R_{GL}=0.68
R_{GL}=0.8
K
12
22.8
27.6
4
K_{PR}= **12.0** MPa√m
15
24
30.5
7
K_{PR}= **15.0** MPa√m
19
24.7
32.3
13
K_{PR}= **19.2** MPa√m
20
27
32
16
K_{PR}= **21.0** MPa√m
PRED: K_{PR}= **12.0** MPa√m
PRED: K_{PR}= **14.9** MPa√m
PRED: K_{PR}= **19.6** MPa√m
PRED: K_{PR}= **21.7** MPa√m

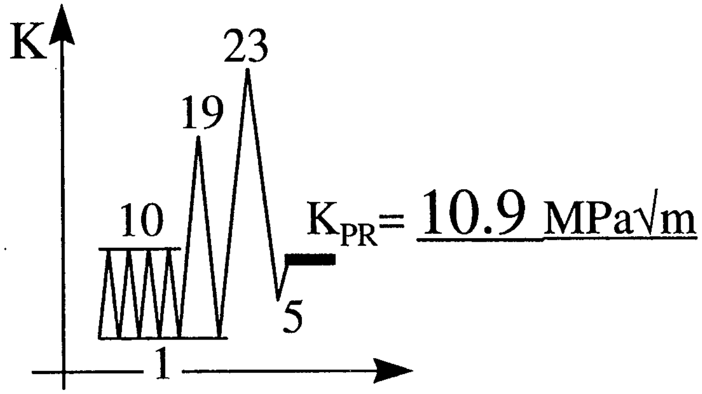

PRED: K_{PR}=11.0 MPa√m

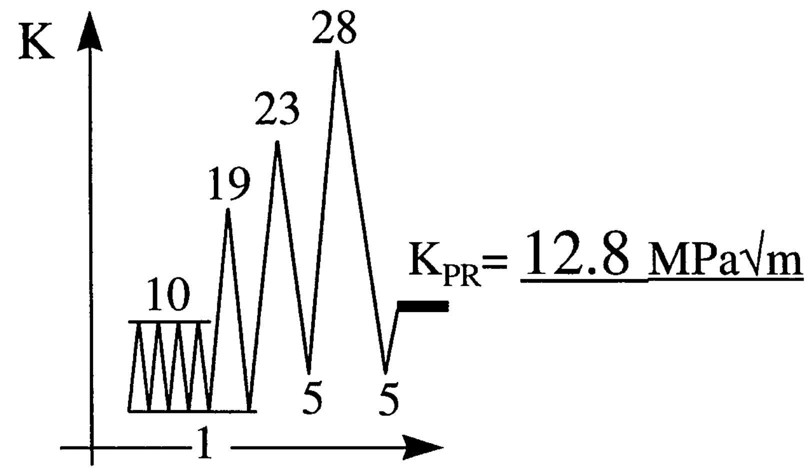

PRED: K_{PR}= 13.3 MPa√m

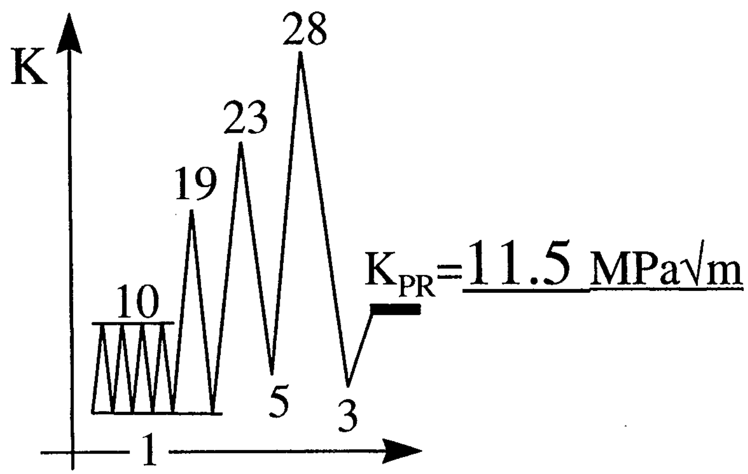

PRED: K_{PR}= 12.0 MPa√m

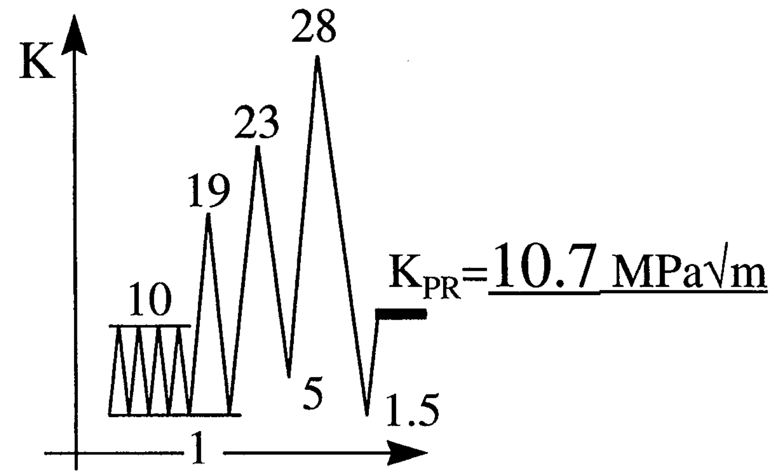

PRED: K_{PR}=11.1 MPa√m

SUMMARY

- The bases of a FCG- model were presented which is the result of an experimental study using Al 7475-T7351.

- The critical parameter, the crack propagation stress intensity factor, K_{PR}, was determined after different loading sequences using the CPLM - method (ΔK_{eff}). The experimental results were described by basically three equations.

1) $K_{PR,C} = g(UR) \cdot K_{\max}$

2) $K_{PR,OL} = h(UR) \cdot K_{\max,OL}$

3) $K_{PR,\,mOL} = i(UR, N_{OL}) \cdot K_{\max,OL}$

- A twofold concept is used where the influence of crack closure and residual compressive stresses in front of the crack tip are treated separately.

- The FCG-model is based on the map of the three possible crack propagation conditions. An arbitrary loading spectrum consists only those three types of cycles. The model determines K_{PR} and the respective crack growth increment cycle by cycle for arbitrary loading sequences.

DETERMINING FLIGHT LOADS AND CRACK GROWTH RATES FROM FAILED AIRCRAFT STRUCTURAL COMPONENTS

Dr. Donald A. Shockey
Takao Kobayashi, Charles G. Schmidt, and Richard W. Klopp
SRI International, Menlo Park, CA 94025
and
Dr. Thomas H. Flournoy
Federal Aviation Administration Technical Center
Atlantic City, NJ 08405

Poulter Laboratory

DAS/12-4-97

DETERMINING FLIGHT LOADS AND CRACK GROWTH RATES FROM FAILED AIRCRAFT STRUCTURAL COMPONENTS

Donald A. Shockey, Takao Kobayashi,
Charles G. Schmidt, and Richard W. Klopp
SRI International, Menlo Park, CA 94025
and
Thomas H. Flournoy
Federal Aviation Administration
Technical Center, Atlantic City, NJ 08405

SUMMARY—The possibility of deducing load spectrum parameters from fatigue failure surfaces is explored by applying innovative, three-dimensional topographic characterization and analysis techniques to failure surfaces in aluminum sheet. Precise, high-resolution elevation maps of fracture surfaces were obtained using confocal optics scanning laser microscopy. Elevation power spectral density curves resulting from a fast Fourier transform of the elevation data appear sensitive to stress intensity range and environment. A conjugate fracture surface matching procedure, FRASTA, can detect and may provide a way to quantify overloads.

Poulter Laboratory

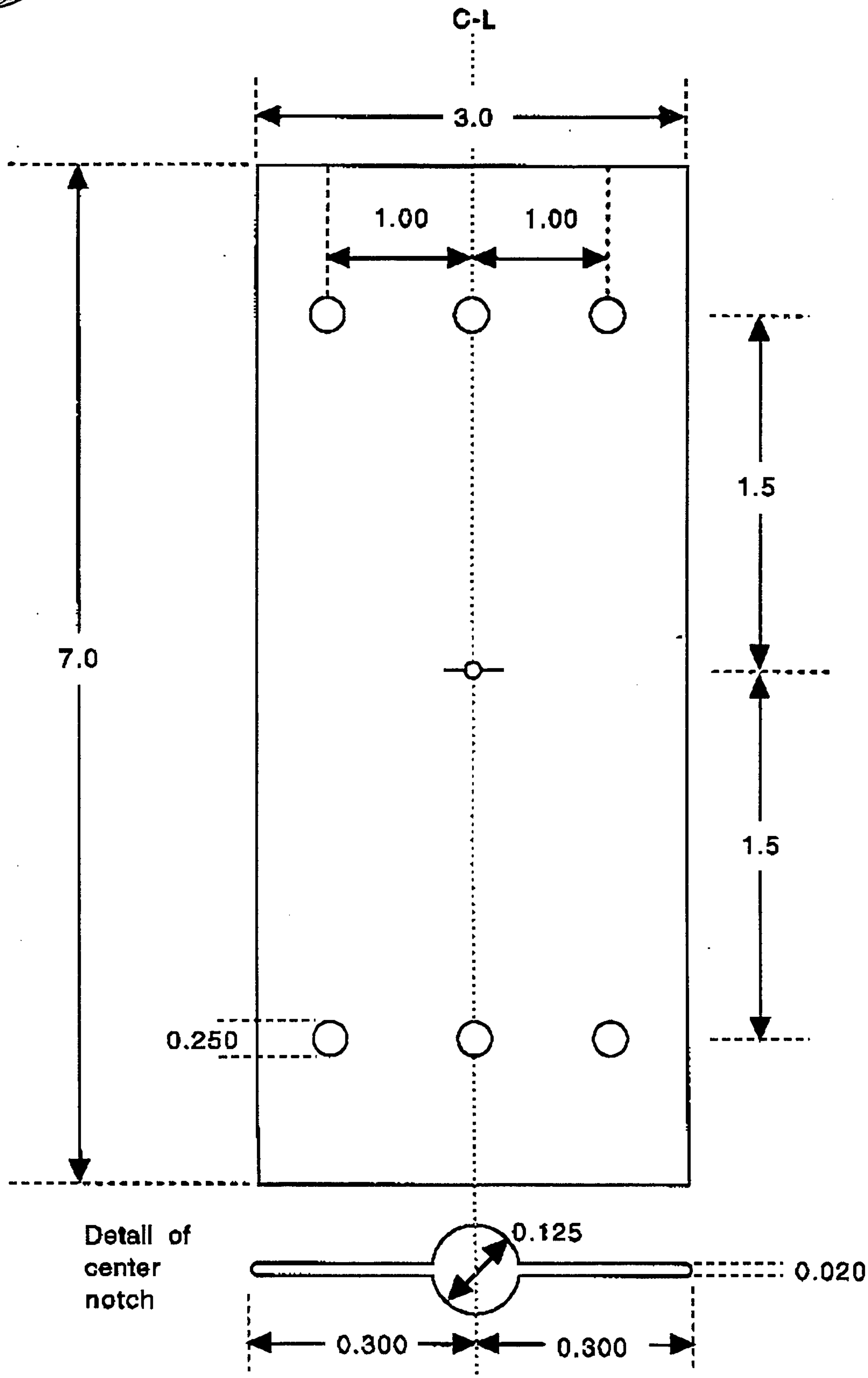

thickness =
0.0395

all
dimensions
in inches

Gray-scale Images and Perspective Views of Topography of Conjugate Fracture Surfaces Produced Under Low and High ΔK Fatigue Conditions

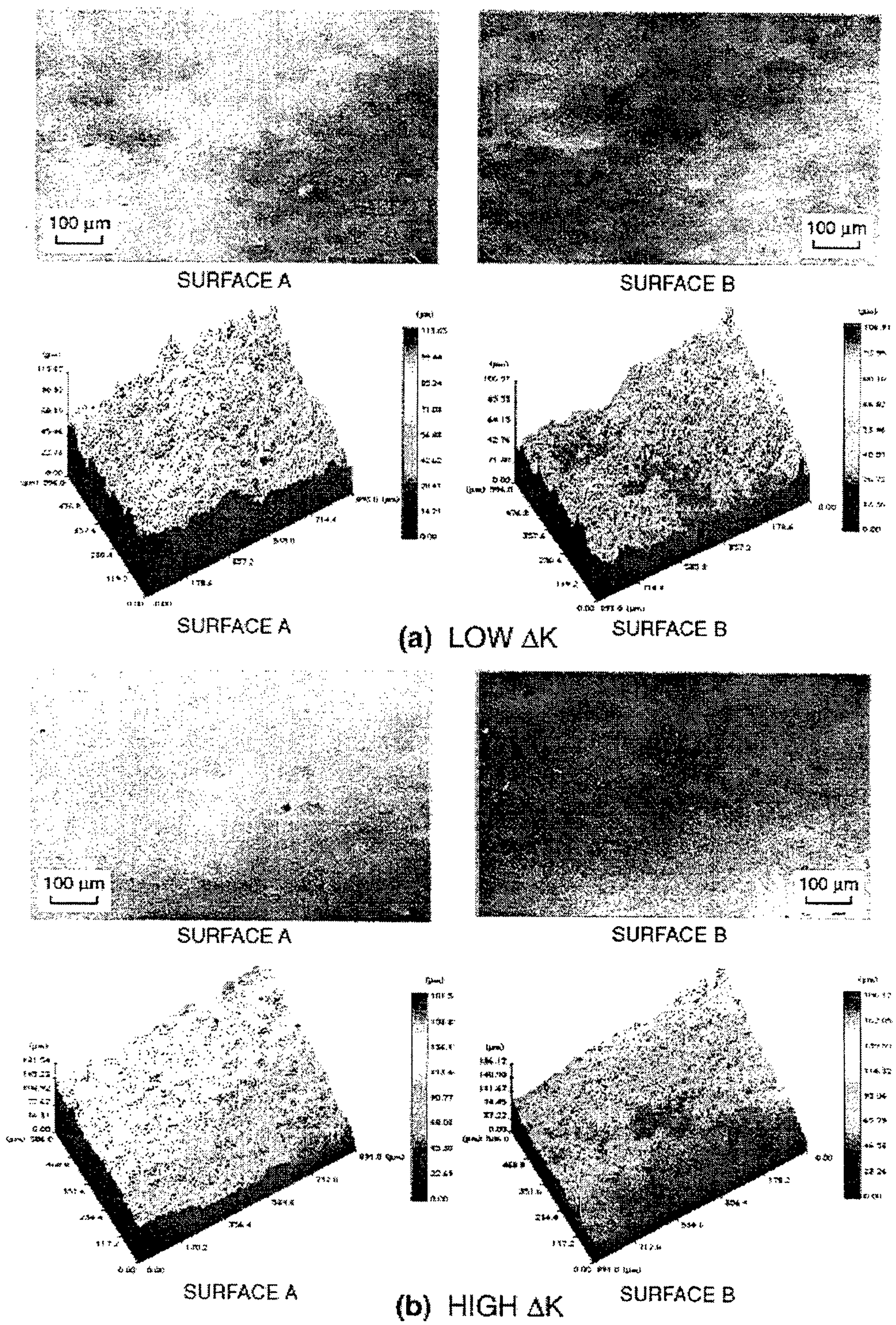

CPM-5082-78

Fast Fourier Transform Power Spectra for Conjugate Fatigue Failure Surfaces Produced Under High and Low ΔK Loading Conditions

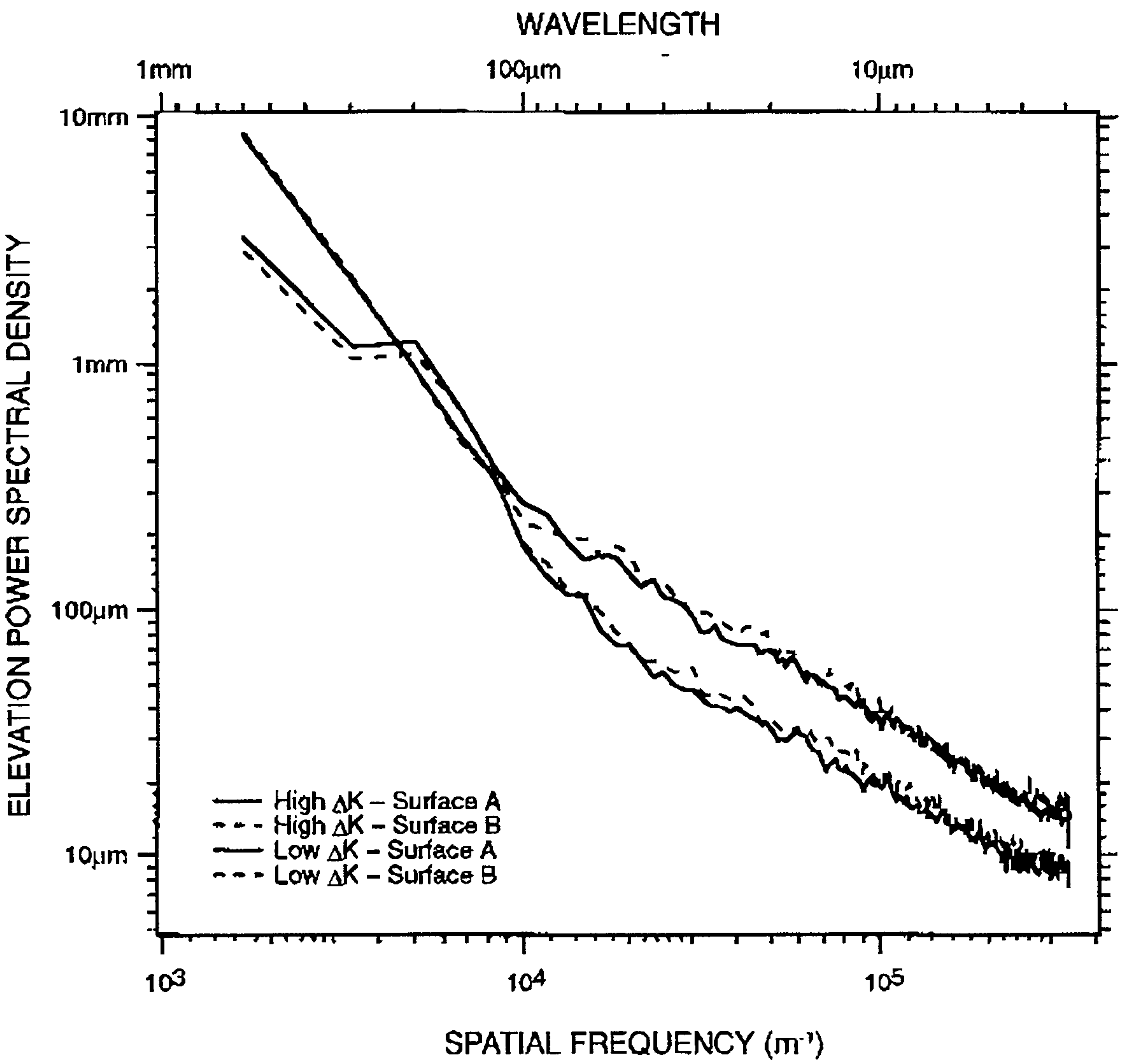

CAM-5082-81

Poulter Laboratory

EPSD Curves for Two Specimens Tested Under Identical Conditions

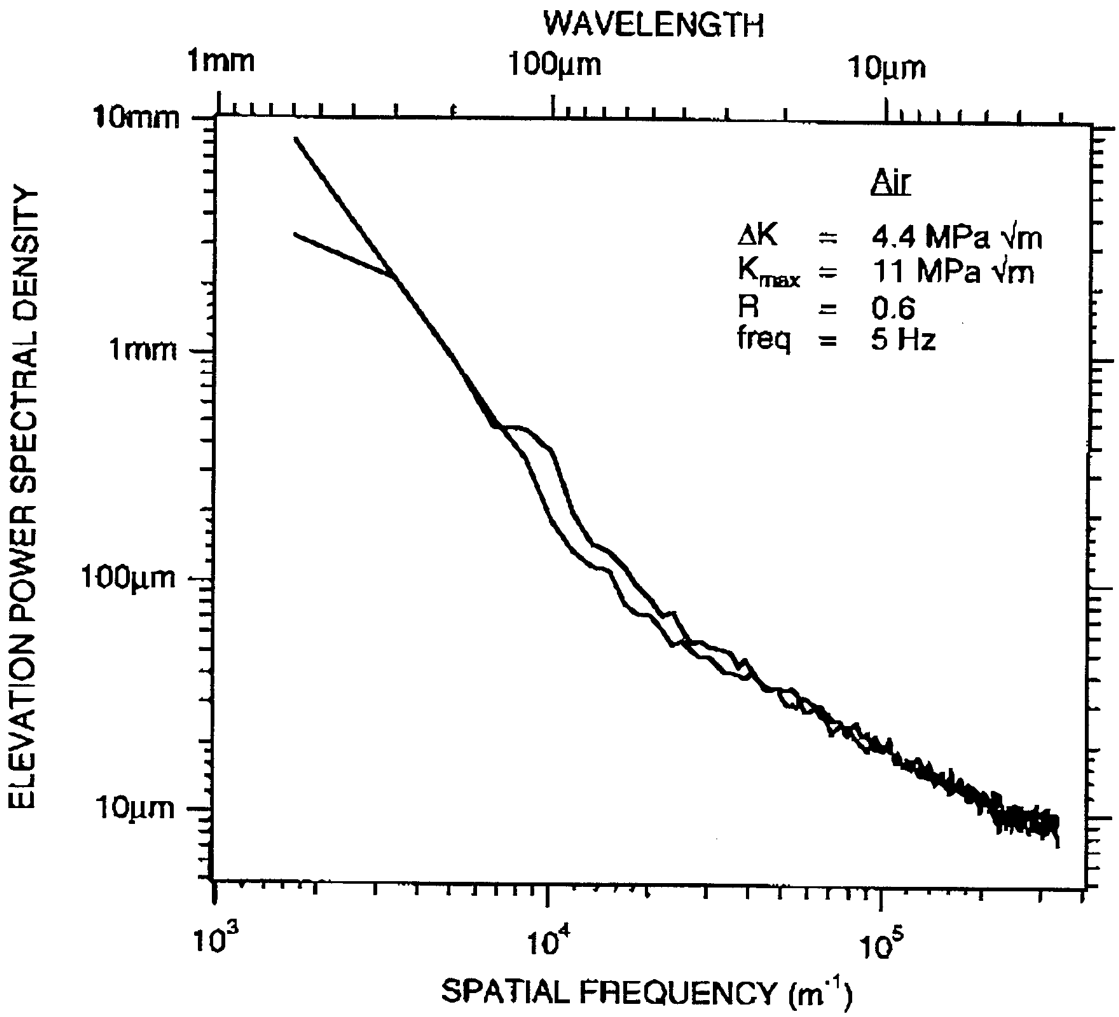

Power Curves for Fatigue Surfaces Produced in Air and Vacuum

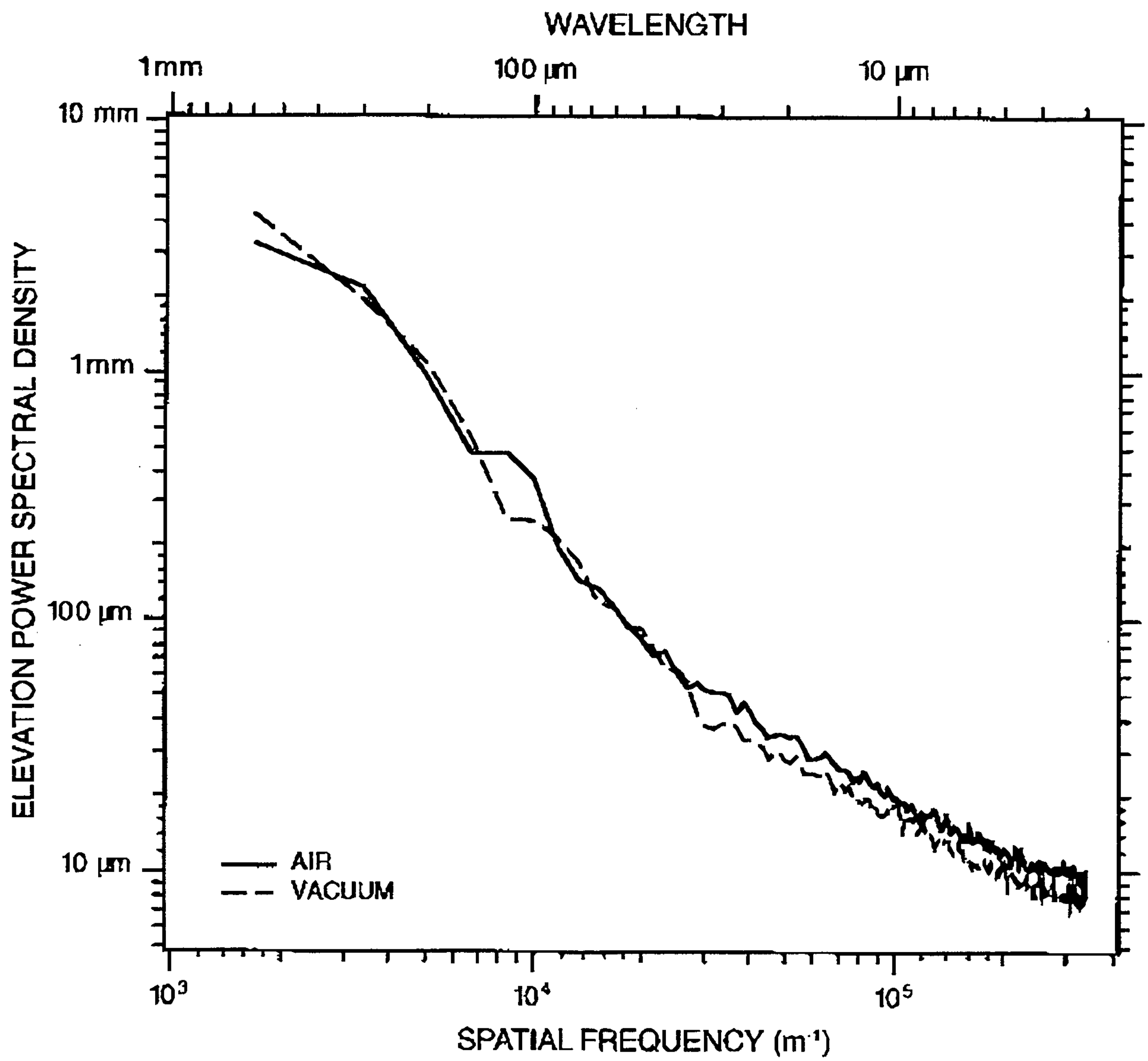

CAM-5082-82

Poulter Laboratory

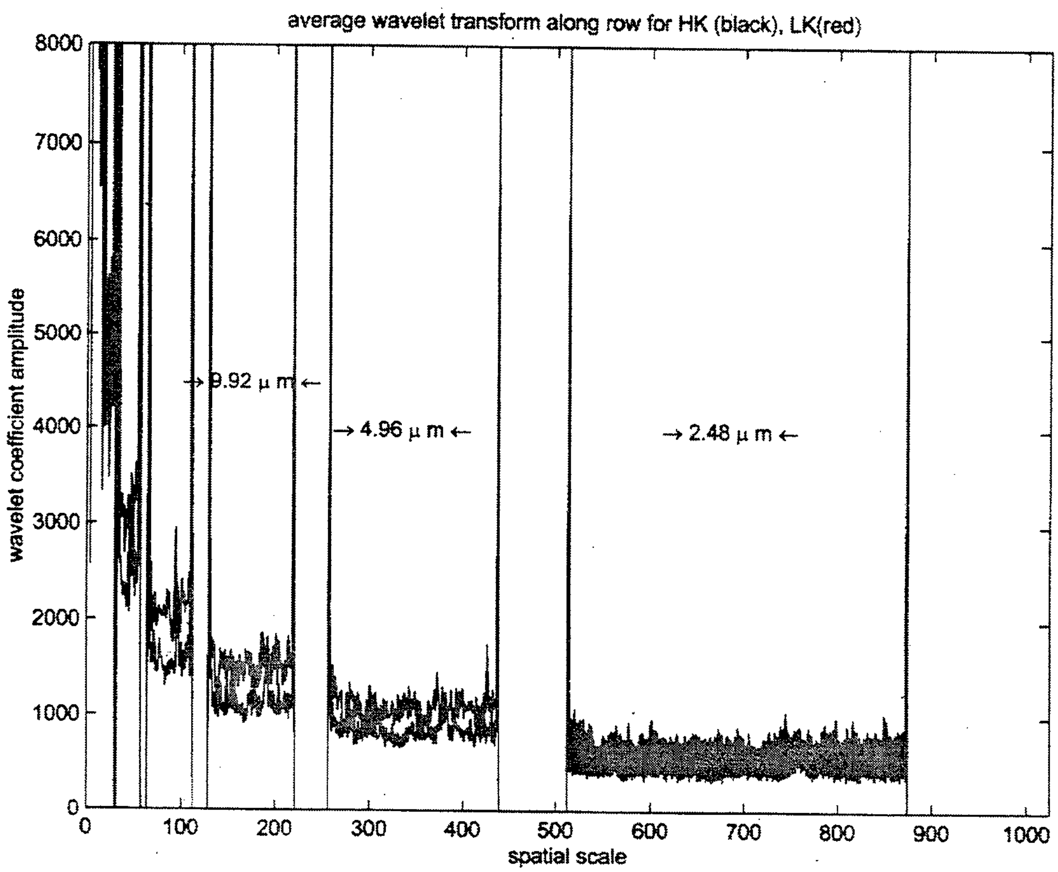
average wavelet transform along row for HK (black), LK(red)
wavelet coefficient amplitude
spatial scale
→ 9.92 μ m ←
→ 4.96 μ m ←
→ 2.48 μ m ←
0
1000
2000
3000
4000
5000
6000
7000
8000
100
200
300
400
500
600
700
800
900
1000

Peak Stress Intensity Versus Crack Length for Fatigue Experiment Showing Overloads

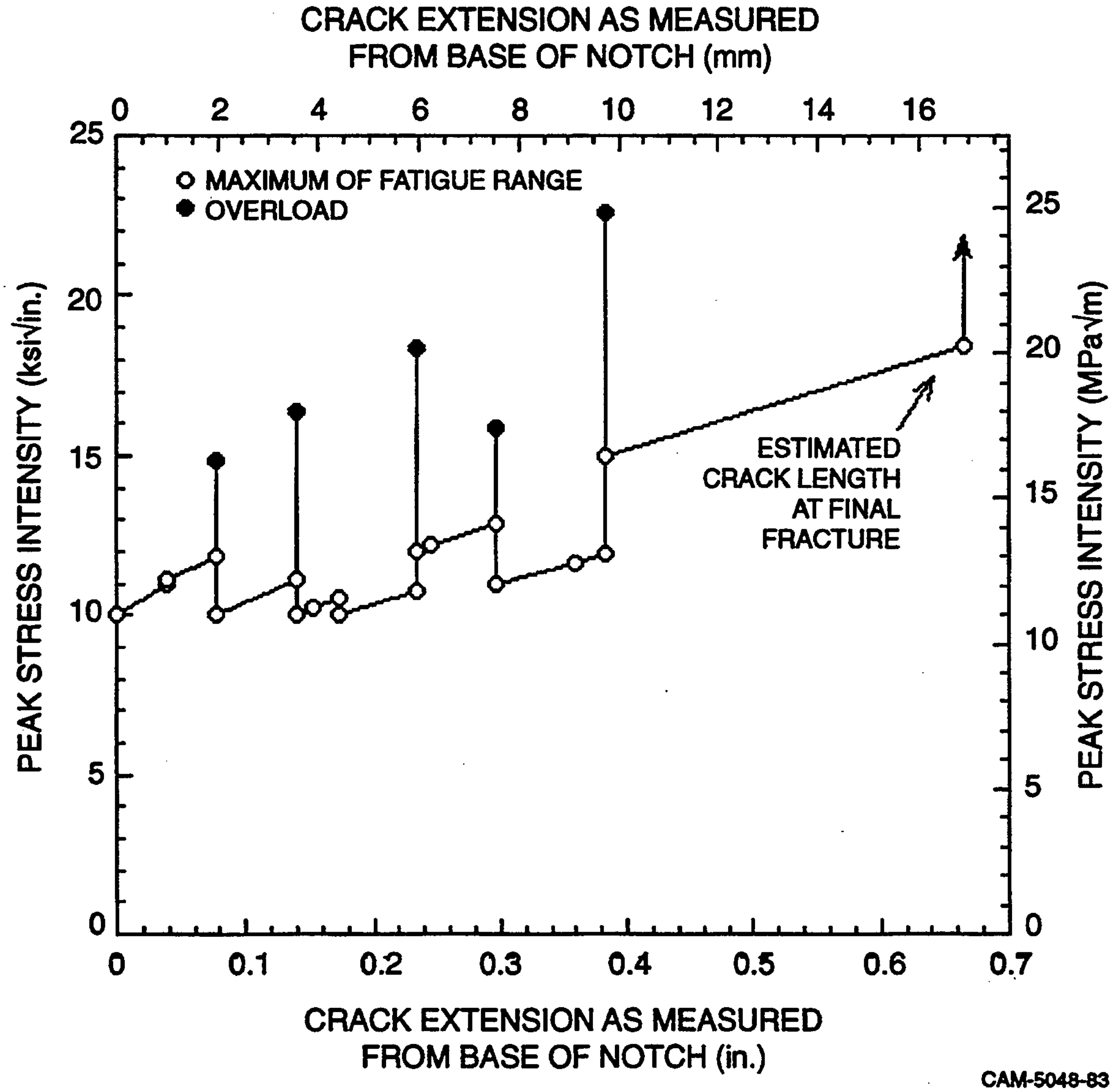

Poulter Laboratory

A Series of Plan Views of a Crack Front at Increasing Topograph Displacements

(White areas indicate separated material; black areas indicate intact material)

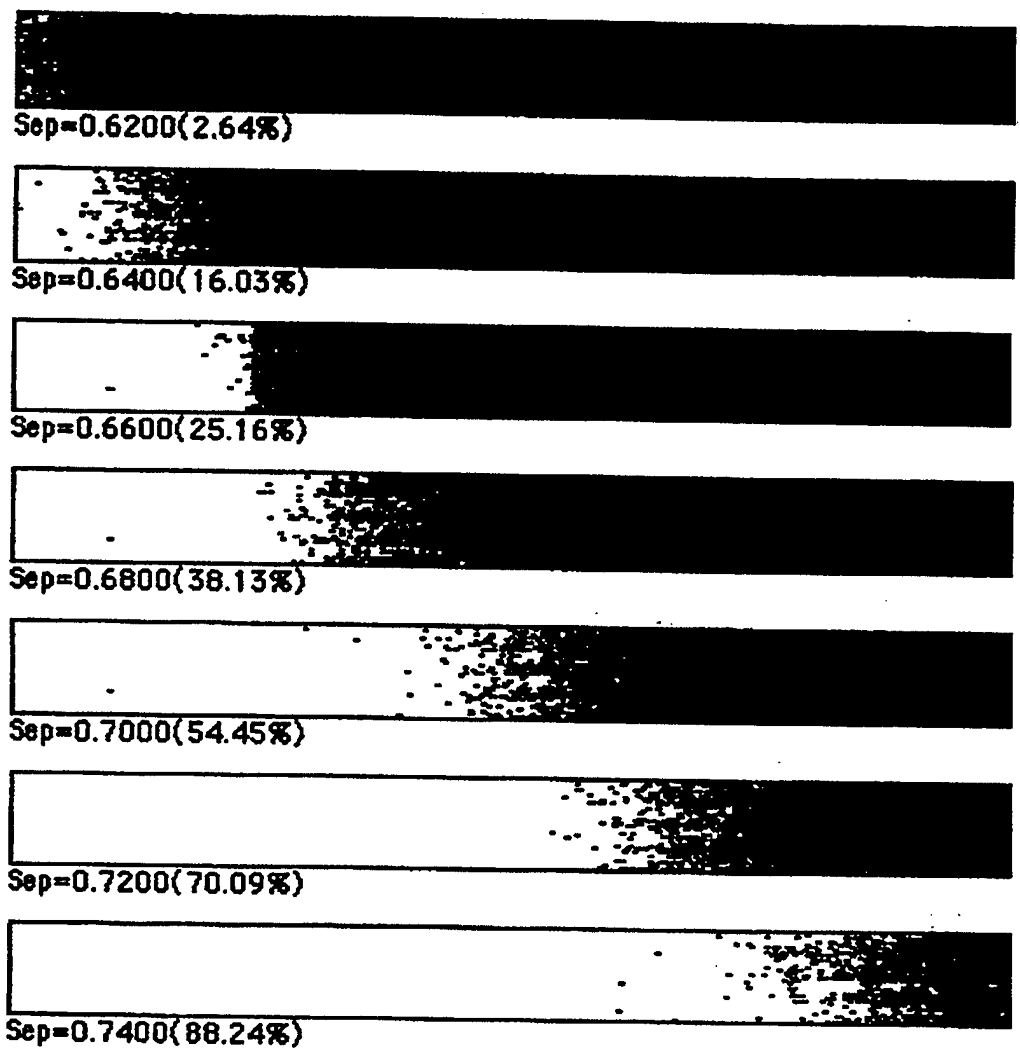

CAM-5048-84

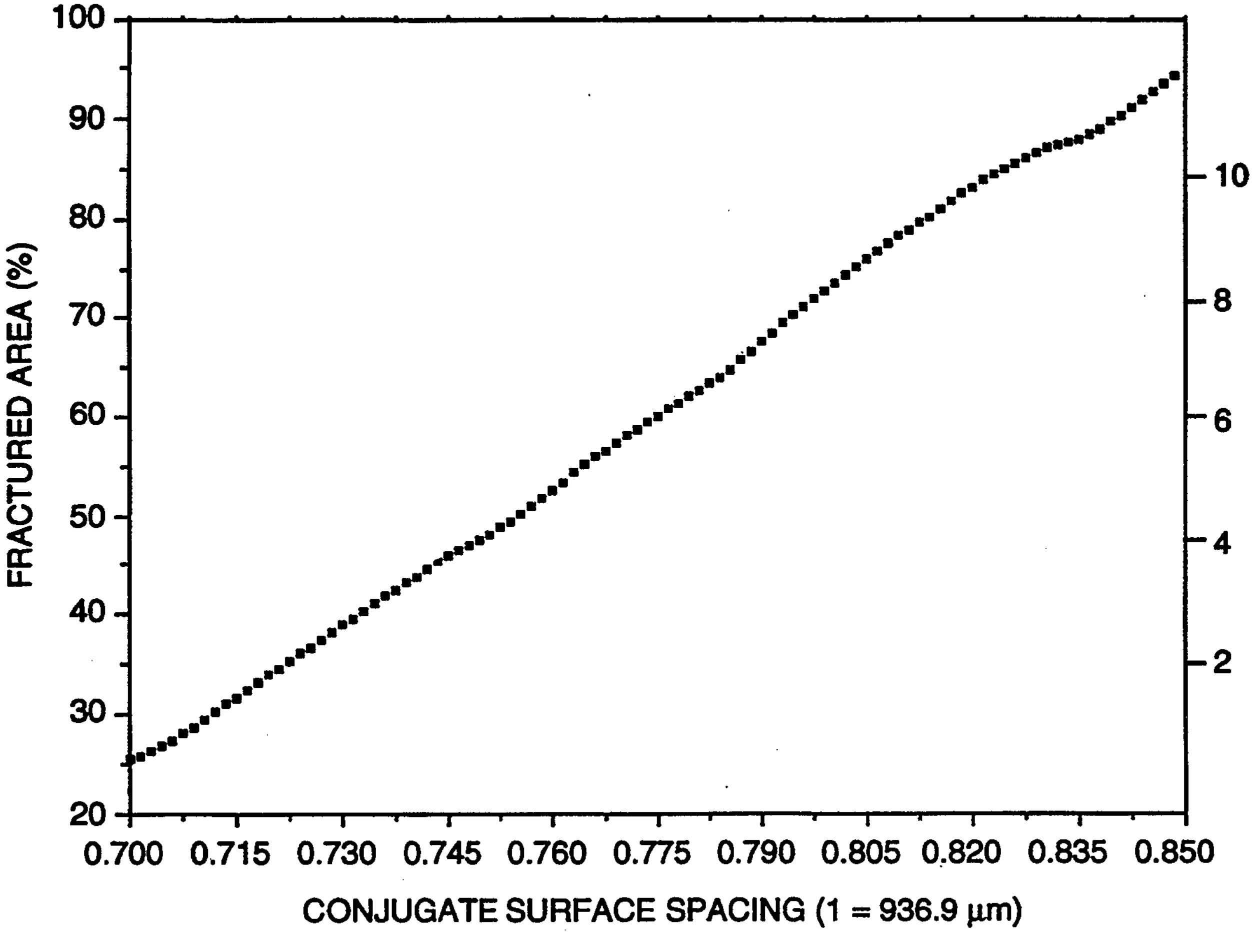
100
90
80
70
60
50
40
30
20
FRACTURED AREA (%)
10
8
6
4
2
CRACK EXTENSION (mm)
0.700 0.715 0.730 0.745 0.760 0.775 0.790 0.805 0.820 0.835 0.850
CONJUGATE SURFACE SPACING (1 = 936.9 μm)

CAM-5048-87

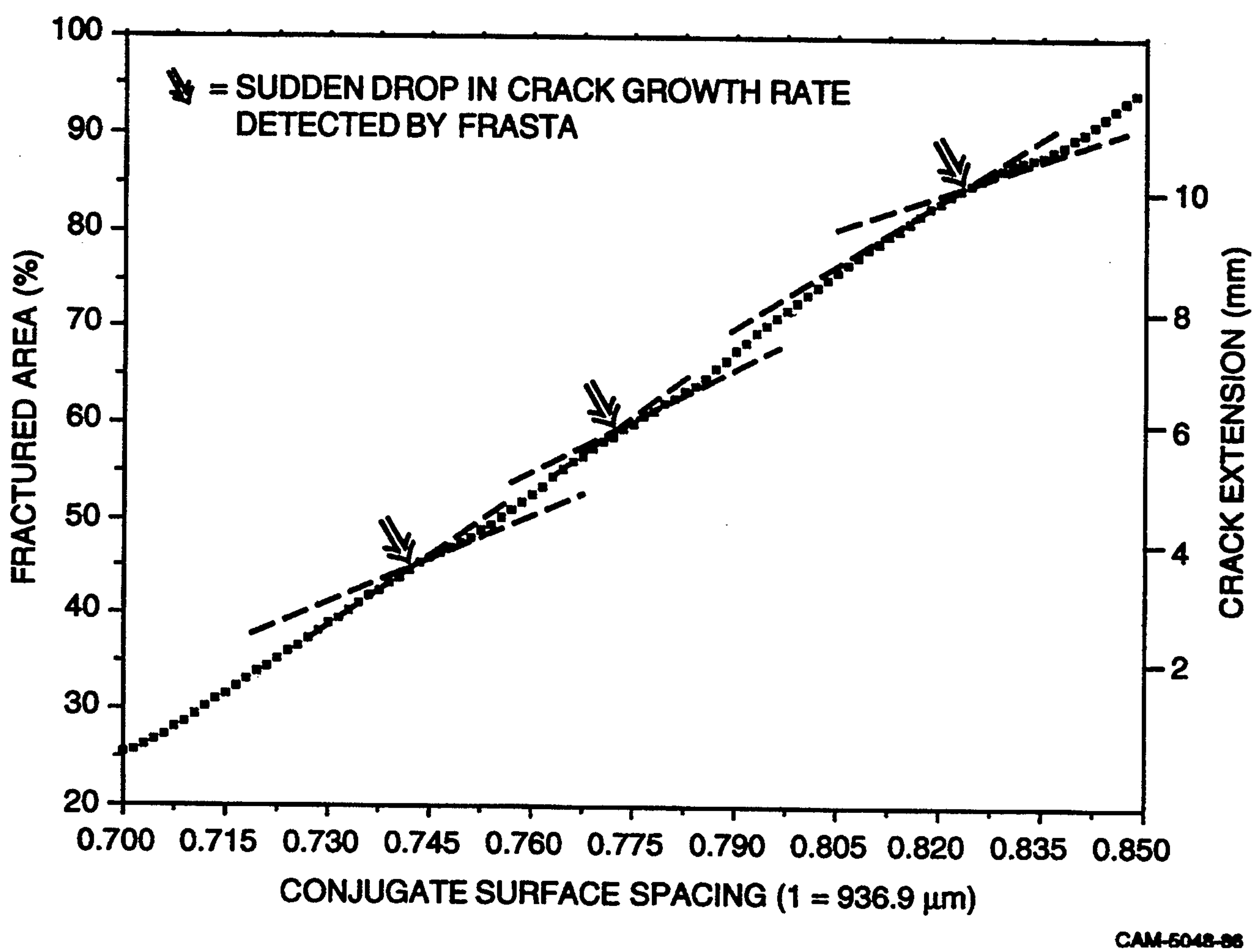

= SUDDEN DROP IN CRACK GROWTH RATE DETECTED BY FRASTA
FRACTURED AREA (%)
CRACK EXTENSION (mm)
CONJUGATE SURFACE SPACING (1 = 936.9 µm)
100
90
80
70
60
50
40
30
20
10
8
6
4
2
0.700
0.715
0.730
0.745
0.760
0.775
0.790
0.805
0.820
0.835
0.850
CAM-5048-86

Fracture Progression Curve Relation to Overloads Shown

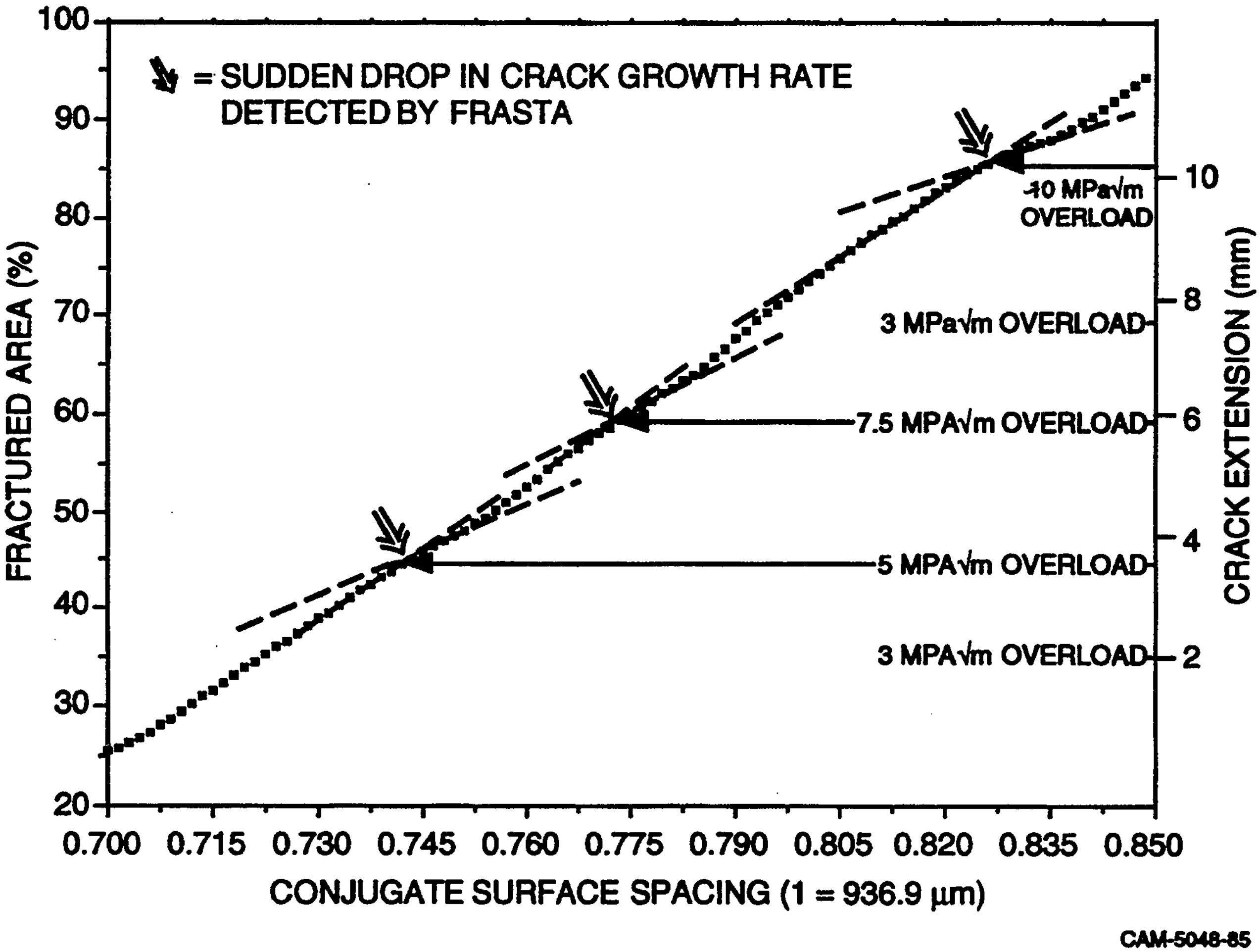

CAM-5048-85

Poulter Laboratory

CONCLUSIONS

- Important but previously unobtainable information regarding the conditions that produced fatigue failures can likely be obtained from fracture surfaces.

- Keys to extracting this information are a fast and accurate method for characterizing fracture surface topography and a three-dimensional analysis of the data.

- Fourier analyses to fracture surfaces may provide the basis for a library of reference curves useful in determining the load spectrum and environment conditions that caused a service failure.

CONCLUSIONS (concluded)

- Comparison of conjugate fracture surface topographs may indicate and quantify details of the overload spectrum experienced by a component that failed in fatigue.

- Shapes of striations may be quantifiable by stereoscopy or COSLM and provide a means to determine maximum and minimum values of the cyclic load spectrum.

- These expectations should be explored to seek advances in failure analysis technology.

Full-Scale Testing of Fuselage Panels Obtained from Retired Aircraft

D.Y. Jeong,[1*] S.J. Kokkins,[2*] T.H. Flournoy,[3] J.V. Canha,[1]
G.W. Neat,[1] and D.E. Nieser[4]

[1] U.S. Department of Transportation
Research and Special Programs Administration
John A. Volpe National Transportation Systems Center
Cambridge, MA 02142

[2] Foster-Miller, Inc.
Waltham, MA 02154

[3] U.S. Department of Transportation
Federal Aviation Administration
William J. Hughes Technical Center
Atlantic City, NJ 08405

[4] U.S. Air Force
OC-ALC/LACRA
Tinker AFB, OK 73145

ABSTRACT. Under the joint sponsorship of the U.S. Department of Transportation and the U.S. Air Force, Foster-Miller, Inc. is carrying out a research program to conduct fatigue and residual strength testing of full-scale, curved, stiffened, fuselage sections from retired Boeing 707 and C/KC-135 aircraft. This program also includes non-destructive inspection to detect the presence of any cracking or corrosion damage prior to panel testing. The specific objectives of this program are: (1) to demonstrate the feasibility of performing realistic cyclic testing of fuselage structures removed from actual aircraft; and (2) to perform full-scale tests to determine fatigue and residual strength of fuselage panels with lap splices. This paper will report on the status of the work-in-progress.

1.0 BACKGROUND

In support of the Federal Aviation Administration William J. Hughes Technical Center's (FAA/WJHTC) National Aging Aircraft Program, a facility to test full-scale fuselage panels was designed and built by Foster-Miller, Inc. (FMI) in the late 1980s [1] under contract to the John A. Volpe National Transportation Systems

* Presenters at the 1997 USAF Aircraft Structural Integrity Program (ASIP) Conference.

Center (Volpe Center). This facility, referred to as the FAA Aging Aircraft Test Fixture (Figure 1), has been used to examine the fatigue and residual strength of fuselage panels containing widespread fatigue damage (WFD) in lap splices [2]. A unique feature of this fixture is that it employs water rather than air as a pressurization medium to create biaxial loading. Whiffle-tree systems are used to distribute force uniformly across the ends of the test panel. Hydraulic cylinders at one end of the panel provide this pulling force. A series of turnbuckles anchor the panel on the sides which incorporate specially-designed elastic restraints to provide proper loading of both skins and circumferential frames. An inflatable seal closes the gap between the panel and the tub to prevent leakage.

Figure 1. FAA Aging Aircraft Test Fixture.

Prior to 1997, only laboratory panels with structural details resembling a Boeing 737 (B-737) airplane had been used at the Aging Aircraft Test Facility. Validation of the laboratory panels was achieved when strain data collected from the panels agreed reasonably well with strain data collected during a ground-pressurization test of an actual B-737 airplane [3].

The U.S. Department of Transportation (U.S. DOT) and the U.S. Air Force (USAF) are now collaborating on a joint research program to examine the fatigue and static strength of fuselage panels obtained from disassembly of retired aircraft. Specifically, panels have been obtained from retired Boeing 707 (B-707) and

C/KC-135 aircraft. In other words, panels from actual aircraft are being used in this on-going program which comprises two parts. The first part involves non-destructive inspection (NDI) characterization of the panels to detect any type of damage (i.e., fatigue cracking and/or corrosion) prior to testing. The second part entails a testing program to evaluate the fatigue and residual strength of the panels.

This paper will describe the work in-progress on this research program. To date, NDI evaluations have been completed on four aircraft panels (two B-707 panels and two C/KC-135 panels), and testing has been completed on two B-707 panels.

2.0 DESCRIPTION AND USAGE HISTORY OF AIRCRAFT PANELS

The FAA Aging Aircraft Test Facility accommodates panels that are 120 inches in length and 68 inches along the circumference with a constant radius of curvature of 75 inches. This radius may vary over a limited range, but due to the modular design of the fixture, substitution of certain components can be made to accommodate a wide range of radii from commuter to wide-body types of aircraft. In the current test program, panels with limited structural interaction with windows, doors, and other design details were preferred. Because of these restrictions, fuselage panels were taken from the crown area of various retired airplanes. Table 1 gives a brief description of the fuselage panels collected for the present test program to date. Structural variations among the panels are noted in the table as well.

Table 1. Summary of Panel Descriptions.

Panel No.	USAF ID No.	Type A/C	Stringer Pitch	Body Stations	Stringer-Skin Connection	Skin Thickness	Remarks
1	CZ186	B-707	9.5 in.	BS540 to BS600 Port Side	Spot welds and rivets at frames	0.046 in. to 0.047 in.	Tear strap width is 3 in. Stringer-frame ties at all stringers.
2	CZ186	B-707	9.5 in.	BS1080 to BS1240 Port Side	Continuous rivets only	0.062 in. to 0.064 in.	Tear strap width is 3 in. Less than half of stringer-frames crossings had ties, but were removed before testing.
3	CA029	C-135	9.0 in.	BS980 to BS1140 Port Side	Spot welds and rivets at frames	0.068 in. to 0.070 in.	No tear straps. No stringer-frame ties.
4	CA029	C-135	9.0 in.	BS440 to BS680 Port Side	Spot welds and rivets at frames	0.048 in. to 0.049 in.	No tear straps. No stringer-frame ties.

NOTE: The fuselage radius is 74 inches for both the B-707 and C/KC-135 aircraft.

Two panels were obtained from a B-707 airplane that had accumulated 22,071 flight cycles during 77,742 flight hours of in-service usage between January 1967 and October 1990. Although both panels were taken from the same airplane, the skin thicknesses were nominally different. A panel taken from the crown area forward of the wing between Body Stations BS540 and BS600 had a skin thickness of 0.046 to 0.047 inch, including coatings. A panel taken from the crown area aft of the wing between Body Stations BS1080 and BS1240 had a skin thickness between 0.062 and 0.064 inch. Other structural differences were observed in these two fuselage sections in addition to the difference in skin thickness. For example, in the forward section of the fuselage, the stringers were attached to the skins via spot welds. In the aft section, the stringers were attached to the skin by riveting. Crossings of the frames and the stringers were reinforced with tie clips in the forward-section panel. In the aft section, ties were located at less than half of the stringer-frames crossings when the panel was delivered to the test facility. Before testing, however, the stringer-frame ties were removed from the aft-section panel to ensure uniform load transfer. Also, variations in stringer cross-section are evident, even within the same runs in a given panel.

Two panels were obtained from a C/KC-135 airplane that accumulated 2,792 flight cycles during 14,267 flight hours between February 1958 and July 1992. As in the case of the B-707 airplane, the two panels from the same C/KC-135 airplane had different skin thicknesses. A panel taken forward of the wing between Body Stations BS440 and BS680 had a nominal skin thickness of 0.048 and 0.049 inch. A panel taken aft of the wing between Body Stations BS940 and BS1140 had a nominal skin thickness of 0.068 and 0.070 inch. Riveting of the lap joints in the C/KC-135 fuselage panels did not employ the commercial-type machined countersink on the skin (as used in the B-707 lap joints). Rather, after positioning and drilling of the rivet holes, the two skins were dimpled together in a countersink die, producing a cone-shaped engagement at every rivet hole, after which a flush-head rivet was installed.

3.0 PANEL PREPARATION

The aircraft sections removed from the retired airplanes required some modifications to accommodate the test fixture. These modifications included:

- sizing the test area of the panel to ensure a longitudinal lap joint near the center
- cleaning and degreasing the panels
- stripping paint at the lap joints and edges for instrumentation
- removing stringers at locations where the panel is attached to the fixture

- cutting skin edges and frame ends to final size
- installing doubler strips on each side of the panel (three layers per side)
- removing of stringer-frame ties (in the second B-707 panel only)
- reinforcing the frame ends
- drilling loading holes

During the panel preparations it was discovered that the longitudinal lap splices were not bonded with an adhesive. However, it was found that a zinc chromate primer was applied to both faying surfaces, and was probably wet when the panel skins were joined. This primer dried in place, and in many, but not all, places connected the upper and lower skins in the overlap.

4.0 NON-DESTRUCTIVE INSPECTION (NDI) OF FUSELAGE PANELS

The B-707 and C/KC-135 panels were inspected with five different NDI techniques to detect for prior damage:[1]

- Thermal Wave Imaging (Wayne State University)
- Magneto-Optic Imaging (PRI Instrumentation)
- D-Sight (National Research Council Canada)
- Pulsed Eddy Current (Iowa State University)
- Ultrasound via "dripless bubbler" technique[2] (Iowa State University)

A description of these various NDI techniques is beyond the scope of this paper, but specific details of these methods can be found in the open literature [4-8].

No evidence of fatigue cracking was found in any of the fuselage panels. In most areas, the NDI surveys found little, if any corrosion in these panels (which, as noted previously, were taken from aircraft over 30 years old). However, in Panel #2 (the thicker of the two B-707 panels which was taken from an aft crown section), a few areas of hidden lap joint corrosion in the range of 10 to 20% thickness loss were suggested by two NDI methods: pulsed eddy current and ultrasound. The effects of this will be determined during the testing of the panel. Also, in all cases, post-test dismantling of the joints will provide direct viewing of these internal joint surfaces.

---

1 Affiliations of the technical staff performing the various NDI techniques are listed in parentheses.

2 "Dripless bubbler" essentially refers to a captured water column that incorporates a water vacuum return system.

5.0 CORRELATION OF STRAIN GAGE DATA WITH ANALYSIS

Strain gage measurements were taken at various locations on a B-707 panel to ensure proper loading. Figure 2 shows a schematic of the strain gage layout for the instrumented B-707 panel. The panel was instrumented with ten gages, located mostly along the vertical centerline (midway) between frames. All but two gages were oriented to measure strains in the circumferential (hoop) direction. The other two gages measured strains in the longitudinal (axial) direction.

Finite element (FE) analyses based on large deformation theory were conducted by the Volpe Center as part of the present research program. The development of the finite element model for the B-707 fuselage panel was facilitated based upon previous experience in analyzing strain fields in a B-737 fuselage [3]. Moreover, the FE model developed for the B-737 fuselage panel was modified to examine the B-707 panels in the present study.

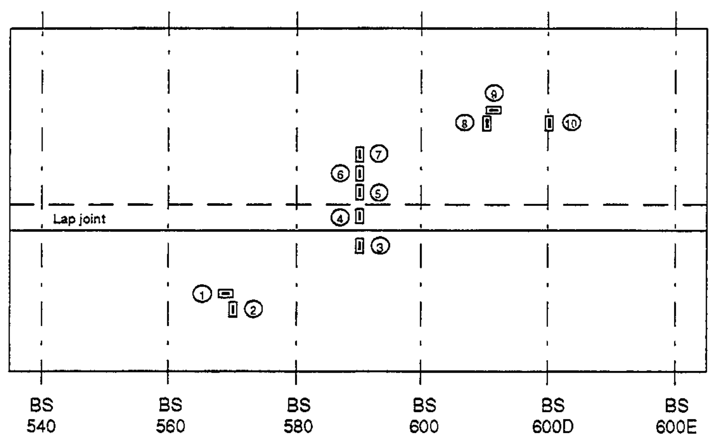

Figure 2. Schematic of strain gage layout for B-707 test panel.

The actual strains measured from the B-707 panel at an internal pressure of 9.5 psi are compared with the strains calculated from the finite element model at the same pressure level in Table 2. The strain level in the lap joint area could not be calculated accurately with the present model without mesh refinement. Otherwise, the calculated strains are within 20% of the actual strains.

Table 3 lists hoop and longitudinal stresses calculated at the gage locations by the FE model. From elementary strength of materials considerations of a pressurized thin-walled cylinder, the theoretical ratio between the longitudinal stress and the hoop stress is equal to one-half. In Table 3, the ratio is slightly less than the

theoretical value, but the FE results are reasonable because the fuselage structure is stiffened. Also, in the previous study for the B-737 aircraft [3], the FE analysis calculated longitudinal-to-hoop stress ratios between 0.475 and 0.503. The theoretical hoop stress for a thin-walled cylinder with radius (74 inches) and skin thickness (0.040 inch) equal to that of a B-707 pressurized to 9.5 psi is equal to 17.6 ksi. The FE results for hoop and longitudinal stresses at the midbay locations in the B-707 panel are about 77% and 72% of the thin-walled cylinder approximation, respectively.

Table 2. Measured and Calculated Strains in B-707 Panel at 9.5 psi.

Gage No.	Strains			Gage Location (a)
	Actual	FE	% diff.	
1(b)	157	224	-42.7%	15
2	1404	1119	20.3%	15.5
3	956	1102	15.3%	2.5
4	1533	(c)	-	0
5	1161	1082	6.8%	2
6	1281	1113	13.1%	4
7	1297	1114	14.1%	6
8	1176	1118	4.8%	13.5
9 (b)	195	224	-14.9%	14
10 (d)	893	940	-5.3%	13.5

NOTES:
(a) All gage locations are in inches relative to gage number 4 which was placed 1.5 inches from the bottom edge of the lap splice. All but one gage is mounted midway between frames.
(b) This gage measures strain in the longitudinal (or axial) direction. All but two gages are oriented to measure hoop (or circumferential) strains.
(c) The present finite element model requires mesh refinement to calculate accurate strains in the lap joint area.
(d) This gage is mounted above a frame. All other gages are mounted midway between frames.

Table 3. Calculated Stresses in B-707 Panel at 9.5 psi.

Gage No. (a)	FE Calculations for Stresses		
	σ_ξ (ksi)	σ_θ (ksi)	σ_ξ/σ_θ
1	6.46	13.7	0.472
2	6.47	13.7	0.473
3	6.50	13.6	0.481
4	(b)	-	-
5	6.24	13.2	0.472
6	6.40	13.6	0.470
7	6.43	13.6	0.472
8	6.49	13.7	0.472
9	6.45	13.7	0.472
10	4.97	11.4	0.437

NOTES:
(a) Refer to Table 2 for specific location of strain gages.
(b) The present finite element model requires mesh refinement to calculate accurate strains in the lap joint area.

6.0 FATIGUE AND RESIDUAL STRENGTH TESTING OF B-707 PANELS

To date, testing has been completed on two B-707 panels. During the fatigue tests on both panels, the pressure was cycled between 1 and 9.5 psi[3] at a rate of 720 cycles per hour. Fatigue crack growth was monitored with a 10x microscope at roughly 1,000-cycle intervals after initial cracking was observed. This visual method had been performed in previous fatigue tests conducted by FMI. Moreover, MSD-type cracks emanating 0.050 inch from the rivet head have been successfully detected using this method in laboratory panels which were made from bare, smooth aluminum. In the actual B-707 aircraft, multiple layers of paint made visual detection of initial cracking difficult[4]. Visual detection of cracking was enhanced when the panel was slightly pressurized which opened the cracks. Furthermore, the panel pressurization was considered safe since water was used for the internal loading. Initially, the panel paint surface had been left intact on the panel, but after the first visible sign of cracking, the surface of the panel was stripped and cleaned to increase the likelihood of finding additional cracks.

6.1 Panel #1

The first B-707 panel was taken from the crown area, forward of the wing between Body Stations BS540 and BS600E.

6.1.1 Fatigue Test

The significant events in the fatigue test conducted on the first B-707 panel are summarized as follows:

- The first visible sign of fatigue cracking was observed after 36,000 cycles in the fixture[5].
- First linkup of adjacent MSD-type[6] cracks occurred after 47,500 cycles in the fixture.

---

[3] The use of water as a pressurization medium requires tension-to-tension cycling. The corresponding pressure range in the fatigue test was 8.5 psi which is approximately equal to the nominal operating pressure of 8.6 psi for the B707 aircraft.

[4] Eddy current-based NDI methods can be used for crack detection if the exact point of crack formation is desired during such testing.

[5] The cycle counts reported in this section are the number of cycles accumulated in the test fixture. A representative value for the fatigue life of the panel can be obtained by adding the number of cycles accumulated during in-service usage to the number of cycles accumulated in the fixture. The B-707 panels accumulated 22,071 cycles during in-service usage.

- All cracking occurred in the upper row of rivets in a bay characterized as having "light" corrosion by D-sight.
- Fatigue cycling was stopped after 48,616 cycles in the fixture, at which time successive linkup of MSD cracks[7] had created a single isolated crack with an overall length of 14.5 inches.

Figure 3 shows the crack growth data obtained from the first B-707 panel test. The visible crack length is the distance measured from the edge of the rivet hole to the crack tip. The number of cycles are those accumulated while the panel was in the test fixture. Rivets were numbered consecutively across the panel. The letters "L" and "R" refer to the left and right sides of the rivets. The figure indicates that initial cracking occurred at Rivets 14 and 15 which are roughly midbay between frames (rivet spacing in this row was 1 inch with frames at 20-inch intervals).

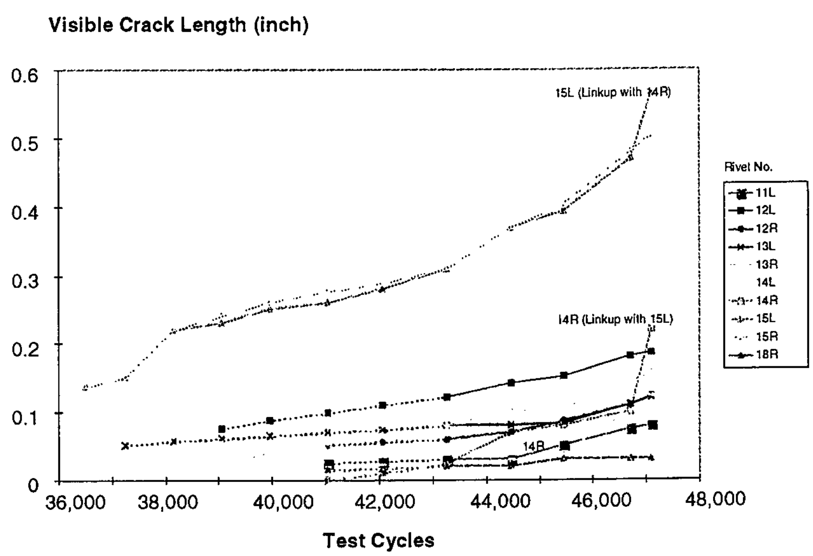

Figure 3. Crack growth in upper rivet row of B-707 panel.

---

[6] MSD is an acronym for multiple-site damage, and is a source of widespread fatigue damage (WFD) characterized by the simultaneous presence of fatigue cracks in the same structural element.

[7] It was possible for cycling to take place even with relative long cracks because the panel was sealed internally with a soft rubber dam to minimize leakage without artificially restraining the edges of the skin.

6.1.2 Residual Strength Test

A 14.5-inch lead crack with MSD-type cracks was created as a result of the fatigue testing (Figure 4). When the panel was pressurized to 0.5 psi, the crack surfaces were separated by about 0.25 inches due to bulging in the lap skins. With a starting pressure of 0.5 psi, the pressure was slowly increased at a rate of 0.2 psi per second until panel failure[8] occurred at 13.0 psi. At the failure pressure, the crack tip closest to the aft end turned along the tear strap. The other crack tip apparently began to curve along the tear strap. Moreover, the failure resulting from this test would have been considered a "controlled" depressurization in an actual aircraft.

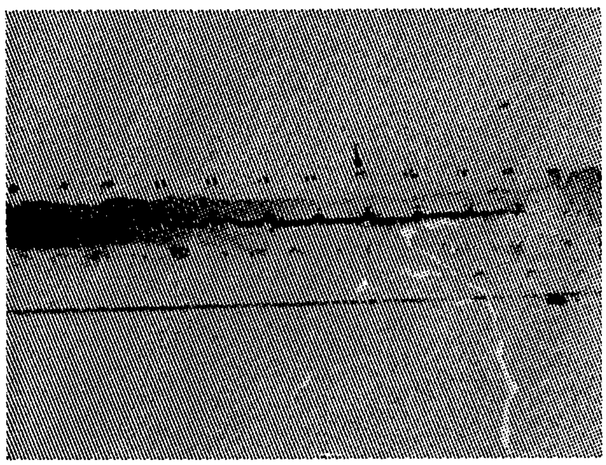

Figure 4. One-bay crack created by successive linkups of MSD cracks.

6.2 Panel #2

The second B-707 panel (Panel #2) was taken from the same airplane as Panel #1. Panel #2 was cut out of a section aft of the wing, and had a greater skin thickness than Panel #1. The structural differences between the two panels were described previously in Section 2.0.

6.2.1 Fatigue Test

Fatigue testing is now continuing past 100,000 cycles with no visible signs of fatigue damage.

---

[8] In this context, "failure" means that the damage (i.e., cracking) in the panel was such that hydraulic pressure could not be maintained to continue testing.

6.2.2 Residual Strength Test

Depending on the results of the fatigue testing, a residual strength test may be conducted on this thicker panel.

7.0 ESTIMATION OF WFD THRESHOLD FOR B-707 PANELS

The onset of widespread fatigue damage (WFD) was estimated for the B-707 aircraft by applying a methodology developed during previous research in the Aging Aircraft Research Program [9]. This methodology requires an analysis tool to determine the residual strength of the fuselage structure with WFD and fatigue crack growth data from tests.

In the present study, the residual strength of B-707 panels was examined using a compatibility displacement (CD) analysis. Plastic collapse of ligaments between adjacent cracks was assumed as a failure criterion for linkup of MSD-type cracks. The CD analysis, however, relies on the knowledge of a bulging factor to predict the residual strength in a curved stiffened panel. A bulging factor for a one-bay crack in a B-707 panel was back-calculated from the results of the residual strength test. The bulging factor for the one-bay crack was then modified to account for a two-bay crack in the WFD threshold estimates. The CD analysis also relies on the knowledge of rivet flexibility. Two values for the rivet flexibility were assumed in the CD analysis to estimate upper and lower bounds of residual strength. The lower bound estimate represents a panel without adhesive bonding. The upper bound estimate represents a panel with infinitely stiff rivets. Based on the CD analysis, the corresponding critical MSD-crack lengths were found to be 0.09 and 0.15 inch.

The most rapid crack growth rate observed in the fatigue test was used to estimate the number of cycles for an MSD-type crack to grow to the critical length. Based on the data shown in Figure 3, the MSD-crack lengths of 0.09 and 0.15 inch correspond to 31,400 and 37,600 cycles in the test fixture, respectively. Adjusting these values to account for the difference in the stress ratio[9], the number of cycles to reach 0.09 and 0.15 inch are 35,100 cycles and 42,000 cycles. Adding the number of cycles from in-service usage, the WFD threshold is estimated to be between 57,800 and 64,100 cycles.

[9] The test fixture applies stress cycles with non-zero minimum stress. The ratio of minimum stress to maximum stress is roughly equal to 0.1. In an actual aircraft, the minimum stress, and therefore the stress ratio, is zero.

When this methodology was previously applied for the B-737, the WFD threshold was estimated to be between 32,300 to 43,500 cycles [9]. These estimates, however, were based upon fatigue testing on a completely debonded lap-splice panel which may have resulted in conservative estimates of the WFD threshold. The main structural difference between the B-707 and the B-737 aircraft is the skin thickness (thinner thickness in the B-737, 0.036 versus 0.040 inch).

8.0 CONCLUSIONS AND FUTURE WORK

Although the joint FAA/USAF research program is on-going, the following conclusions can be stated:

- Fatigue and residual strength testing of two fuselage panels from actual aircraft have been successfully completed using the FAA Aging Aircraft Test Fixture.

- Based on testing and analysis, the onset of widespread fatigue damage (WFD) in a B-707 panel with 0.040 inch skin thickness is estimated to be between 58,000 and 64,000 cycles.

Future work in this program will include the following:

- Fatigue and residual strength tests will be performed on panels obtained from retired C/KC-135 airplanes. Such tests would be the first to be performed on panels with the dimpled lap joint construction at the Aging Aircraft Test Facility. In terms of fatigue and static strength, the dimpled joint is expected to be stronger than the conventionally-riveted joint without bonding because the rivets and the engaged skins should act together without any relative motion between them. It is expected that the strength of the dimpled joint would be comparable to that of a conventionally-riveted and well-bonded joint. However, the formation of WFD in the dimpled joint is expected to be different due to the lack of a knife edge from the machined countersink and the presence of a turned-down lip at the hole from the dimple.

- The lap splices in the test panels will be disassembled after residual strength testing to verify the NDI measurements.

This research program is expected to be completed by December 1998, at which time additional results will be reported to the research community.

REFERENCES

[1] Samavedam, G., and D. Hoadley: 1994. "Fracture and Fatigue Strength Evaluation of Multiple Site Damaged Aircraft Fuselages-Curved Panel Testing and Analysis." Final Report: DOT/FAA/CT-94/10.

[2] Samavedam, G., D. Hoadley, and D. Thomson: 1993. "Full-Scale Testing and Analysis of Curved Aircraft Fuselage Panels." Final Report: DOT/FAA/CT-93/78.

[3] Jeong, D.Y., D.P. Roach, J.V. Canha, J.C. Brewer, and T.H. Flournoy: 1995. "Strain Fields in Boeing 737 Fuselage Lap Splices: Field and Laboratory Measurements with Analytical Correlations." Final Report: DOT/FAA/CT-95/25.

[4] Favro, L.D., T. Ahmed, X. Han, L. Wang, X. Wang, P.K. Kuo, and R.L. Thomas: 1996. "Thermal wave imaging of disbonding and corrosion on aircraft." *Review of Progress in Quantitative Nondestructive Evaluation, Vol. 15.* Edited by: D.O. Thompson and D.E. Chimenti. New York: Plenum Press, pp. 1747-1753.

[5] Fitzpatrick, G.L., D.K. Thome, R.L. Skaugset, and W.C.L. Shih: 1996. "Magneto-optic eddy current imaging of subsurface corrosion and fatigue cracks in aging aircraft." *Review of Progress in Quantitative Nondestructive Evaluation, Vol. 15.* Edited by: D.O. Thompson and D.E. Chimenti. New York: Plenum Press, pp. 1159-1166.

[6] Komorowski, J.P., S. Krishnakumar, R.W. Gould, N.C. Bellinger, F. Karpala, and O.L. Hageniers: 1996. "Double pass retroreflection for corrosion detection in aircraft structures," *Material Evaluation 54,* pp. 80-86.

[7] Bieber, J.A., S.K. Shaligram, J.H. Rose, and J.C. Moulder: 1997. "Time-gating of pulsed eddy current signals for defect characterization and discrimination in aircraft lap-joints," *Review of Progress in Quantitative Nondestructive Evaluation, Vol. 16.* Edited by: D.O. Thompson and D.E. Chimenti. New York: Plenum Press, pp. 1915-1921.

[8] Patton, T.C. and D.K. Hsu: 1995. "Field demonstration of the dripless bubbler ultrasonic scanner," *Review of Progress in Quantitative Nondestructive*

Evaluation, Vol. 14. Edited by: D.O. Thompson and D.E. Chimenti. New York: Plenum Press, pp. 2269-2276.

[9] Jeong, D.Y. and P. Tong: 1997. "The onset of multiple site damage and widespread fatigue damage in aging airplanes," *Proceedings of the 1996 USAF Structural Integrity Program Conference, Vol. II,* USAF Report No. WL-TR-4055, pp.729-749.

SESSION IX

ANALYTICAL METHODS

Chairman - *C. Harris*
NASA Langley

Evaluation of Progressive Fracture in Woven and Non-woven Composite Panels

Levon Minnetyan and Ryan A. Lund
Clarkson University, Potsdam, New York 13699-5710

Christos C. Chamis and Pascal K. Gotsis
National Aeronautics and Space Administration
Lewis Research Center, Cleveland, Ohio 44135

Presented at the 1997 USAF Aircraft Structural Integrity
Program Conference
San Antonio, Texas, December 2-4, 1997

OUTLINE

- Background
- Computational simulation method
- Damage evolution and damage energy
- Graphite/epoxy woven and non-woven composites
- Damage progression under tension and compression
- Effect of in-plane shear on damage progression
- Response to short beam flexure
- Conclusions

OBJECTIVES:

- **Review briefly progressive fracture concepts and respective computer code - CODSTRAN.**
- **Describe its application to woven fabric composites.**
- **Present typical results with comparisons from non-woven composites.**

CODSTRAN SIMULATION CYCLE

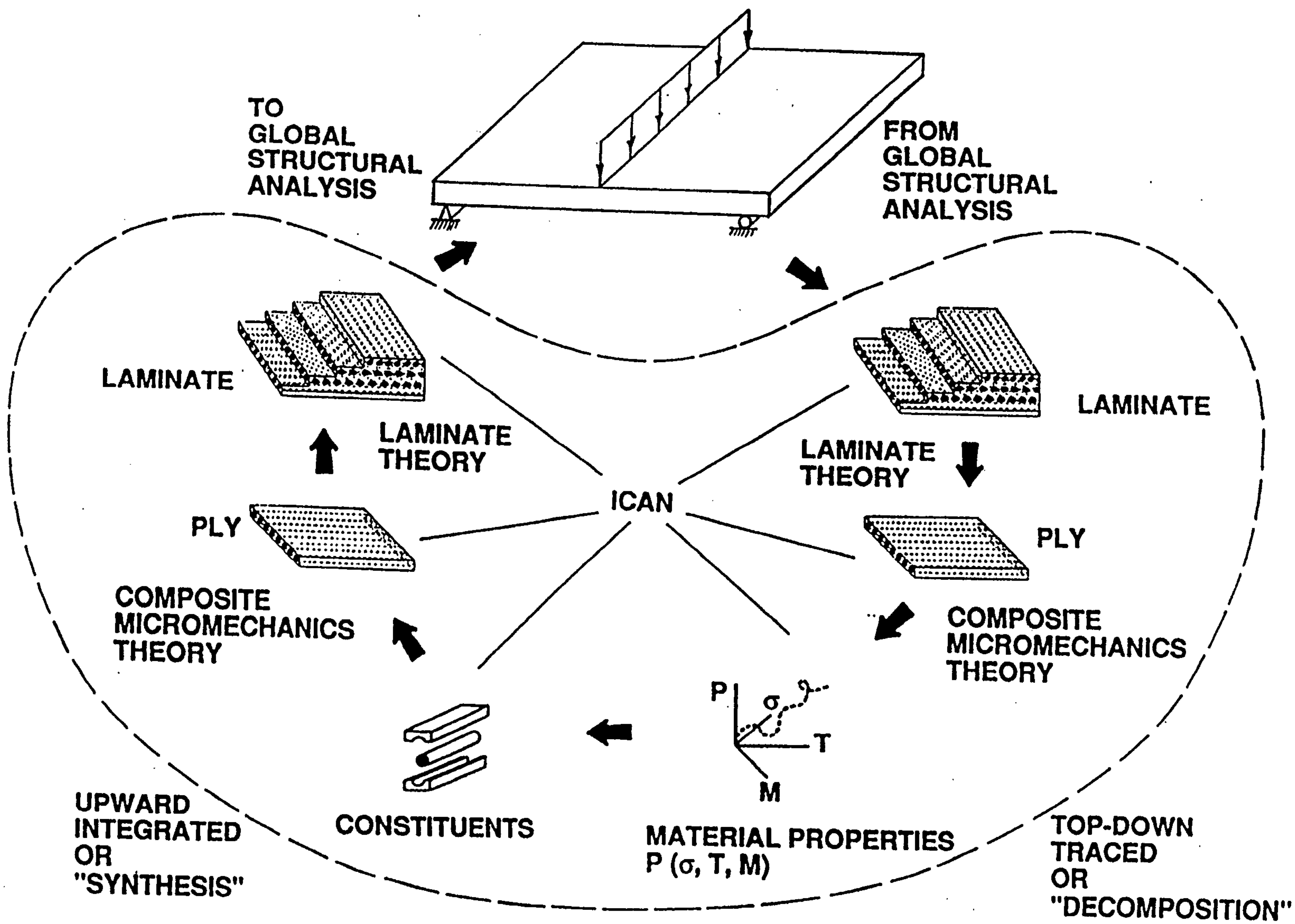

PLY MICROSTRESSES THROUGH COMPOSITE STRESS PROGRESSIVE DECOMPOSITION

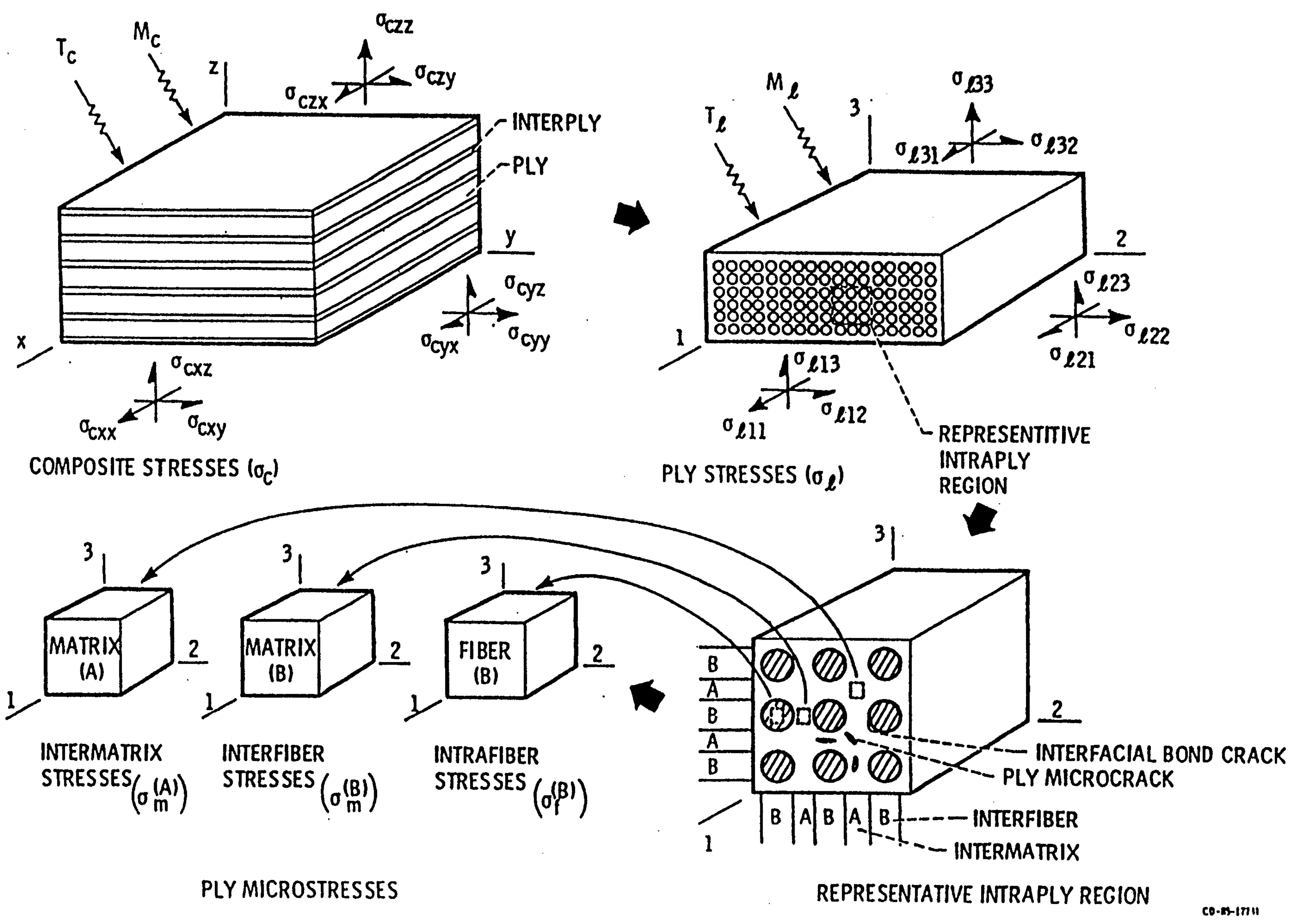

Ply (Lamina) Fracture Modes Tracked by CODSTRAN

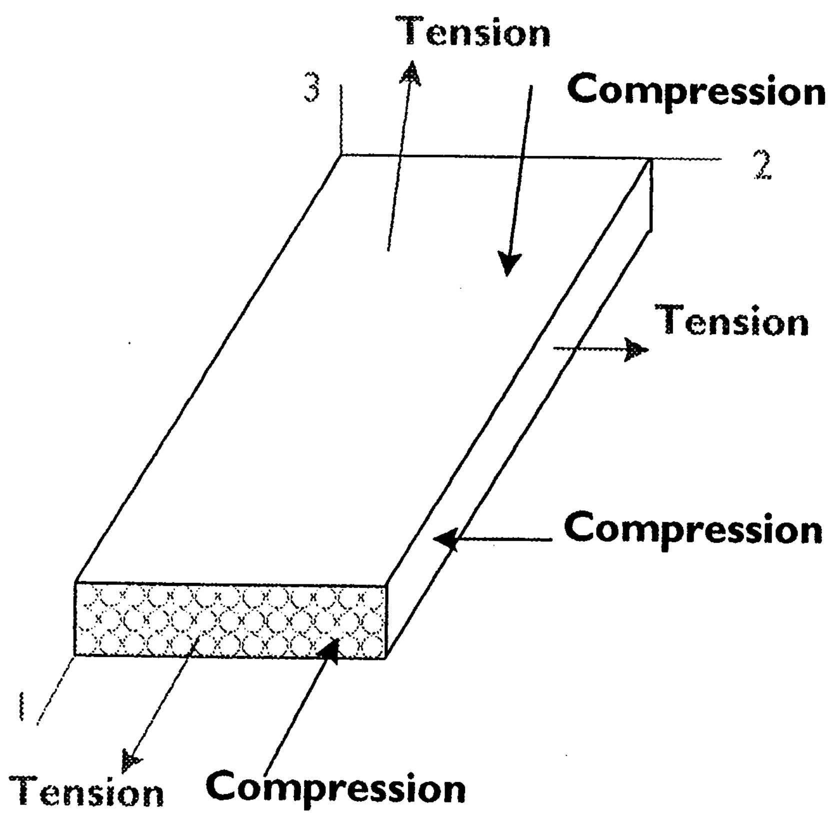

Normal

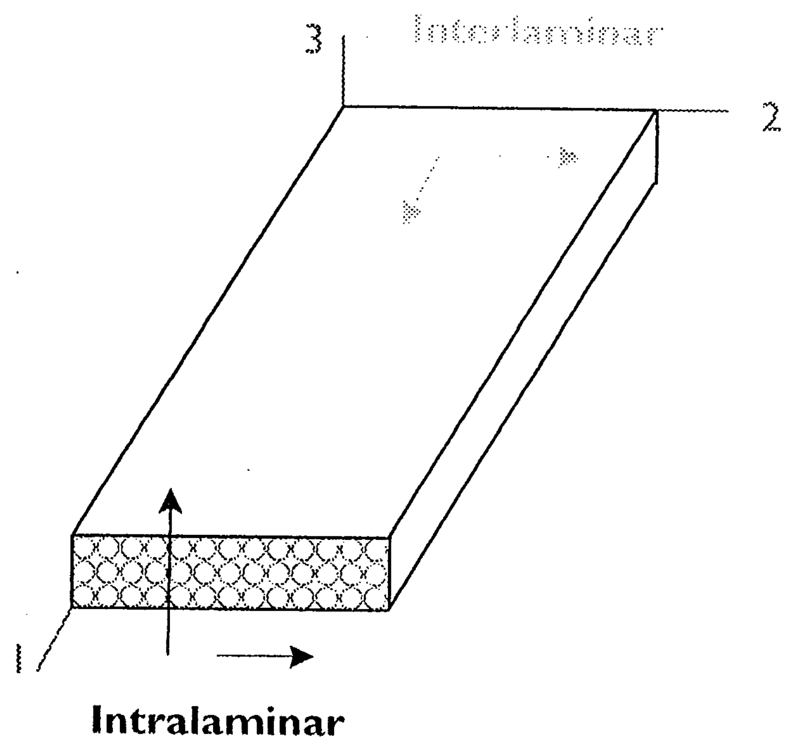

Shear

Intra and Inter Ply

Interply Layer (Matrix) Fracture Modes Tracked by CODSTRAN

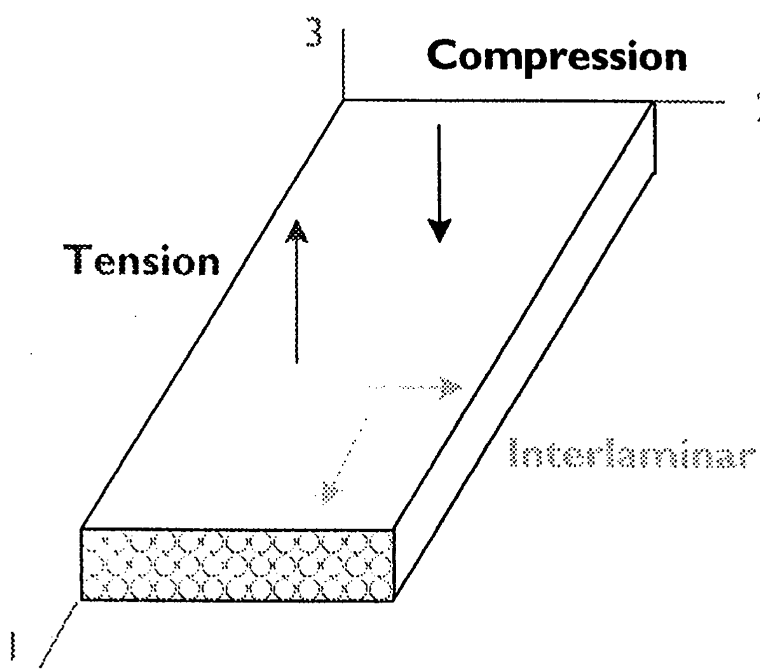

Normal and Shear

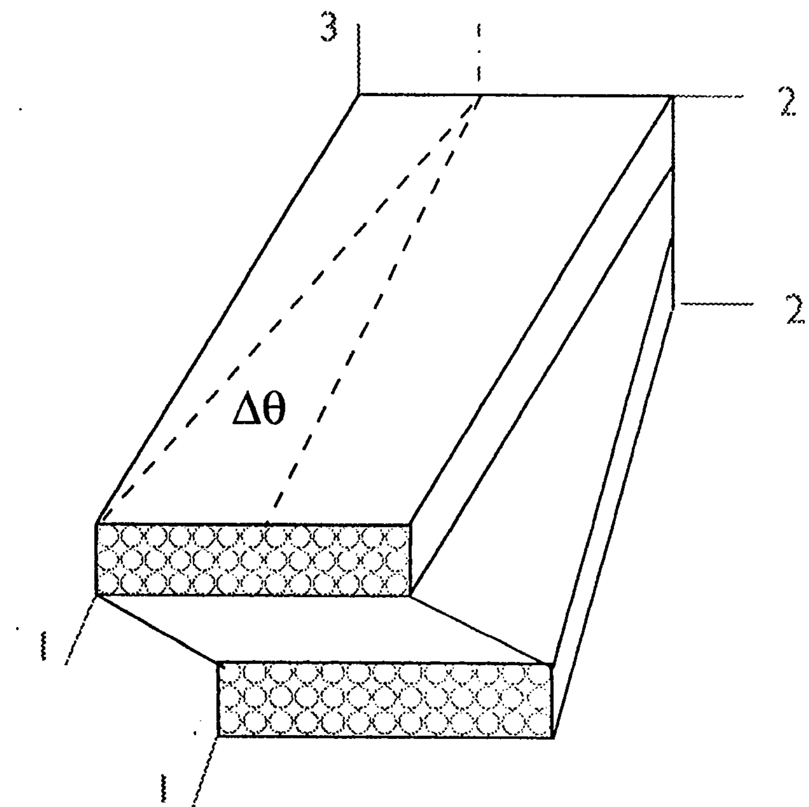

Interply Relative Rotation (Δθ)
Scissoring Effect

CODSTRAN LOAD INCREMENTATION

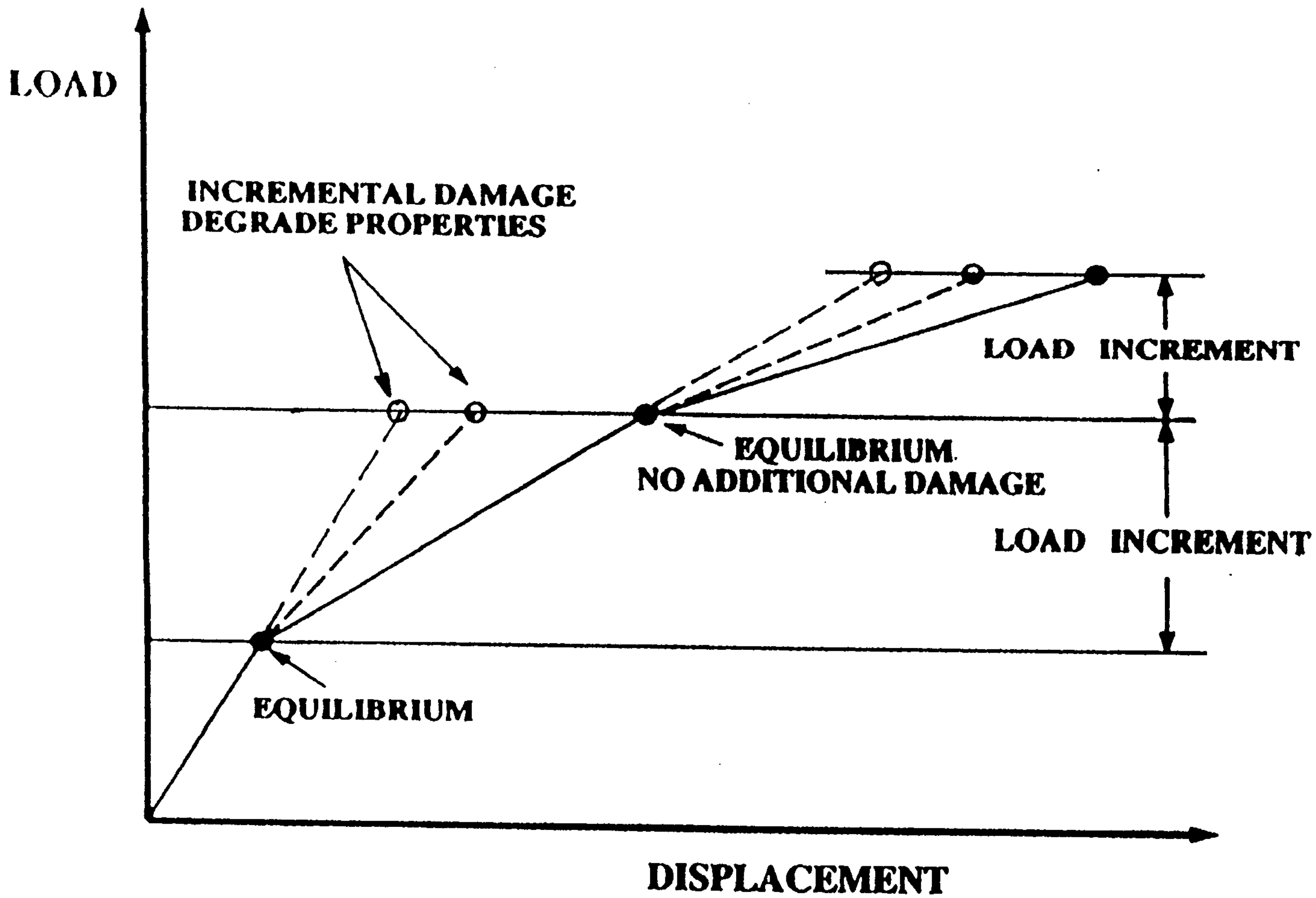

DAMAGE ENERGY COMPUTATION

- Damage energy is the sum of discharged strain energies computed on the basis of the exhausted composite failure modes.
- If a failure mode is associated with the stress component σ_i, and the strain energy density associated with σ_i is $(\sigma_i)^2/(2E_i)$, the damage energy contribution of that failure mode is $V_d(\sigma_i)^2/(2E_i)$,

  where σ_i is the failure stress, E_i is the elastic modulus, and V_d is the local damage volume that is computed as the tributary area of the damaged node multiplied by the thickness of the damaged ply.
- The summation of all local damage energies is the damage energy of the structure.
- A sudden increase of the structural damage energy with a small increase in loading indicates that a damage propagation stage has been entered.
- The sum of all local damage volumes V_d is recorded as the total damage volume. The structural damage volume also increases at the damage propagation stage.

AS-4 Graphite Fiber Properties:

Number of fibers per end = 10000
Fiber diameter = 0.3 mills
Fiber density = 0.063lb/in^3
Longitudinal normal modulus = 33 MSI
Transverse normal modulus = 2.0 MSI
Poisson's ratio (ν_{12}) = 0.20
Poisson's ratio (ν_{23}) = 0.25
Shear modulus (G_{12}) = 2.0 MSI
Shear modulus (G_{23}) = 1.0 MSI

Longitudinal thermal expansion coefficient = -5.5 μin/in/°F
Transverse thermal expansion coefficient = -0.56 μin/in/°F
Longitudinal heat conductivity = 580 BTU-in/hr/in^2/°F
Transverse heat conductivity = 58 BTU-in/hr/in^2/°F
Heat capacity = 0.17 BTU/lb/°F
Tensile strength = 540ksi
Compressive strength = 486 ksi

HMHS Epoxy Matrix Properties:

Matrix density = 0.0457 lb/in^3
Normal modulus = 0.62 MSI
Poisson's ratio = 0.34
Coefficient of thermal expansion = 40 μin/in/°F
Heat conductivity = 1.25 BTU-in/hr/in^2/°F
Heat capacity = 0.25 BTU/lb/°F
Tensile strength = 12.3 ksi
Compressive strength = 61.3 ksi
Shear strength = 21.4 ksi
Allowable tensile strain = 0.02
Allowable compressive strain = 0.05
Allowable shear strain = 0.04
Allowable torsional strain = 0.04
Void conductivity = 0.225 BTU-in/hr/in^2/°F
Glass transition temperature = 420°F

STRESS-STRAIN RELATIONS AND DAMAGE PROGRESSION FOR WOVEN AND NON-WOVEN COMPOSITES SUBJECTED TO TENSION AND SHEAR (N_x/N_{xy}=20)

AS-4/3501-6 Graphite/Epoxy; V_f=0.64

Composite thickness=0.2 in.

Woven: 16 layers of plain-weave preforms

Non-woven: 32 plies $[0/90]_{16s}$

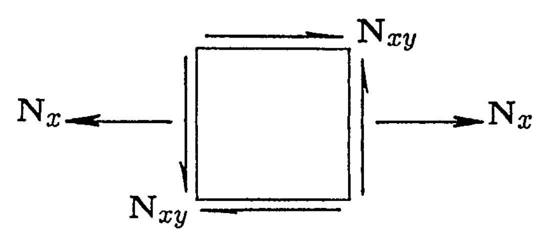

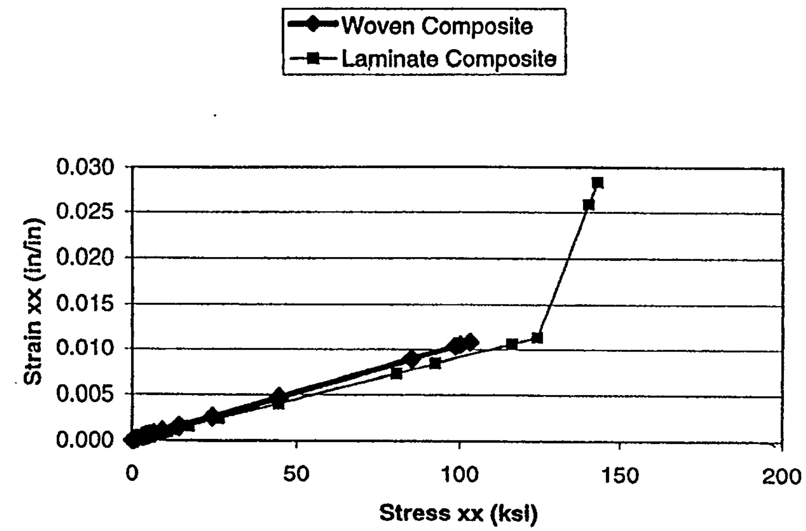

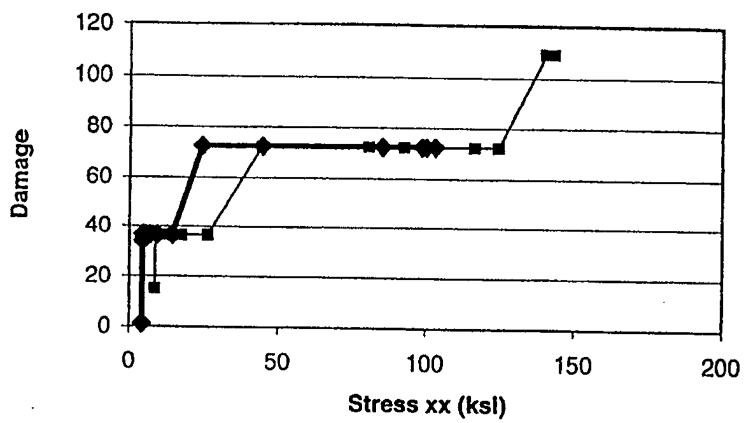

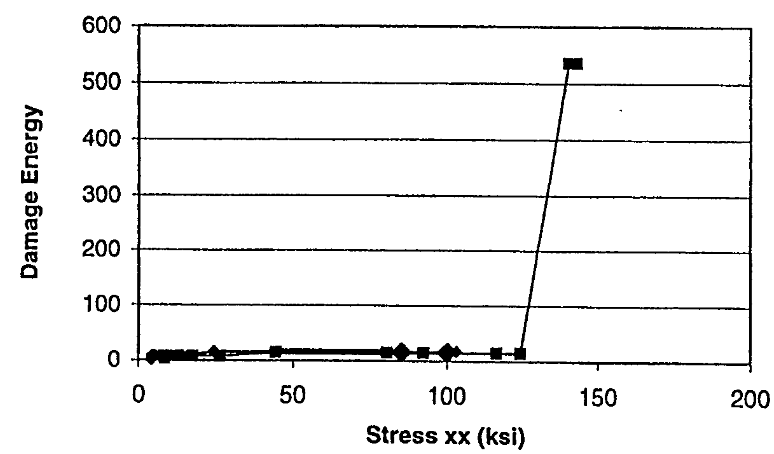

STRESS-STRAIN RELATIONS AND DAMAGE PROGRESSION FOR WOVEN AND NON-WOVEN COMPOSITES SUBJECTED TO TENSION AND SHEAR (N_x/N_{xy}=10)

AS-4/3501-6 Graphite/Epoxy; V_f=0.64
Composite thickness=0.2 in.
Woven: 16 layers of plain-weave preforms
Non-woven: 32 plies $[0/90]_{16s}$

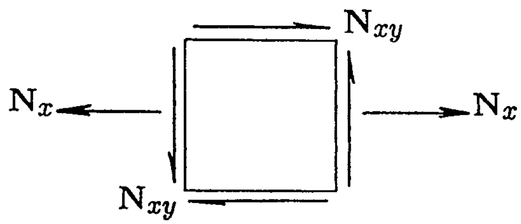

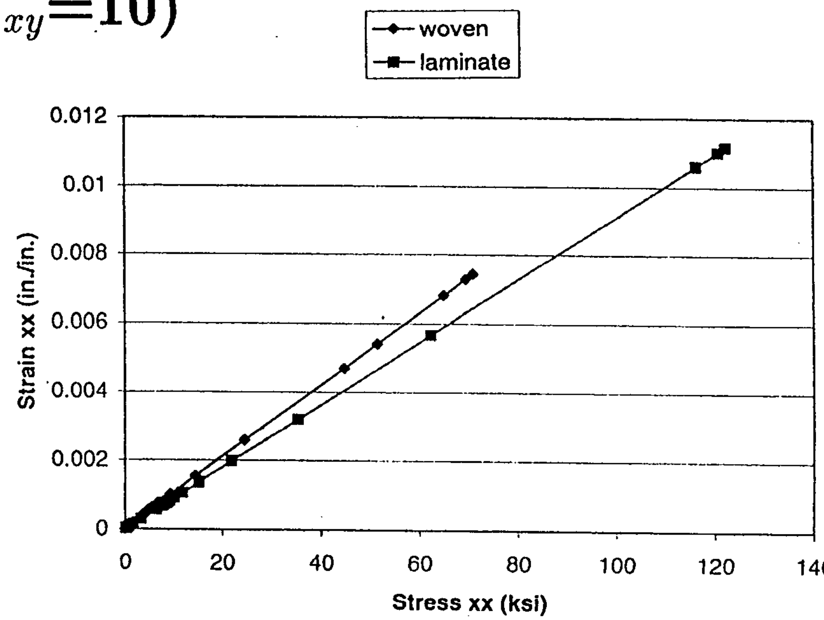

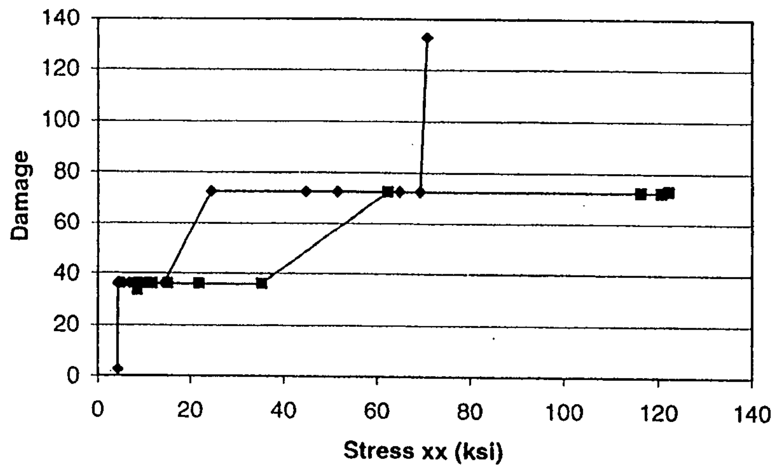

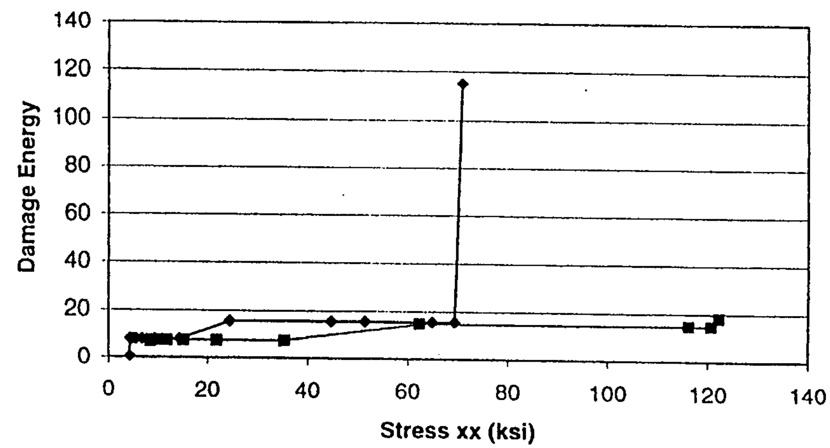

STRESS-STRAIN RELATIONS AND DAMAGE PROGRESSION FOR WOVEN AND NON-WOVEN COMPOSITES SUBJECTED TO TENSION AND SHEAR ($N_x/N_{xy}=5$)

AS-4/3501-6 Graphite/Epoxy; $V_f=0.64$
Composite thickness=0.2 in.
Woven: 16 layers of plain-weave preforms
Non-woven: 32 plies $[0/90]_{16s}$

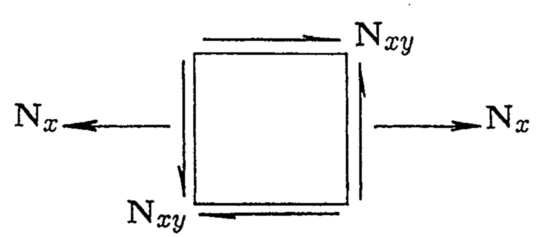

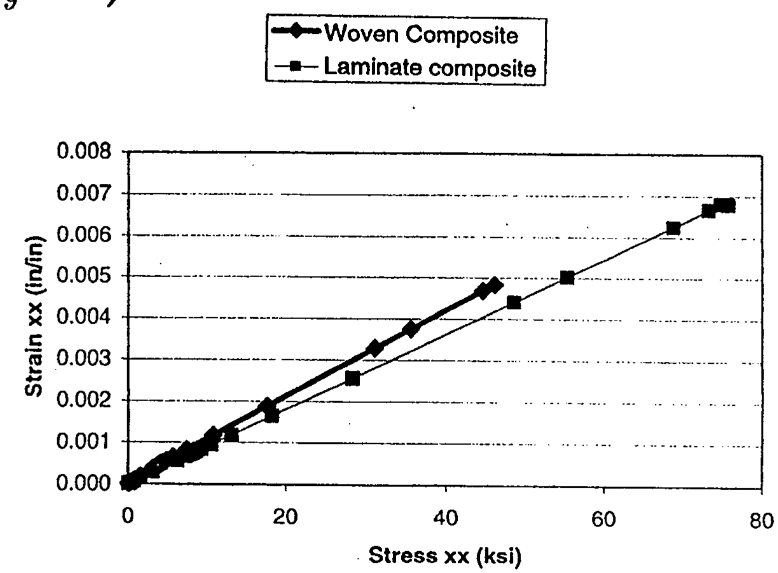

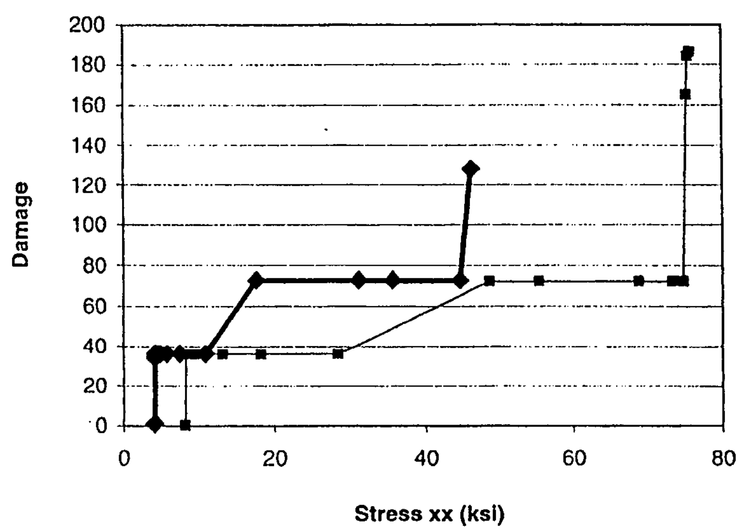

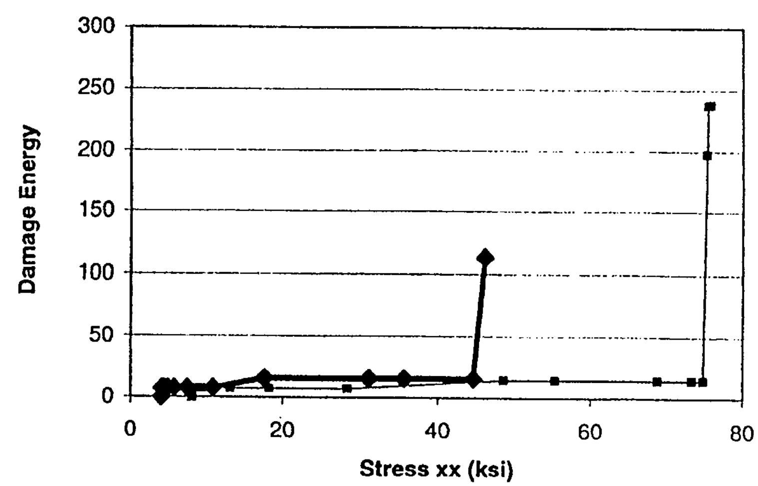

TENSION WITH SHEAR LOADING

Structural fracture of woven an non-woven composite panels subjected to tension and shear were evaluated:

- The average tensile strength of woven composites is 37 percent lower than that of non-woven composites.
- The stiffness of woven composites is 14 percent lower than that of non-woven composites.
- Damage initiation, growth, and propagation stages are commenced at lower loads for woven composites.
- Structural fracture occurs suddenly with the failure of 0° fibers for both woven and non-woven composites.
- As the shear component of the load is increased the ultimate strength is decreased for both woven and non-woven composites.

STRESS-STRAIN RELATIONS AND DAMAGE PROGRESSION FOR WOVEN AND NON-WOVEN COMPOSITES SUBJECTED TO COMPRESSION AND SHEAR ($N_x/N_{xy}=10$)

AS-4/3501-6 Graphite/Epoxy; $V_f=0.64$
Composite thickness=0.2 in.
Woven: 16 layers of plain-weave preforms
Non-woven: 32 plies $[0/90]_{16s}$

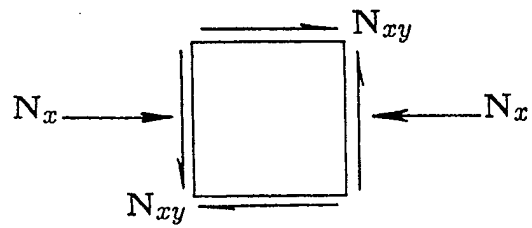

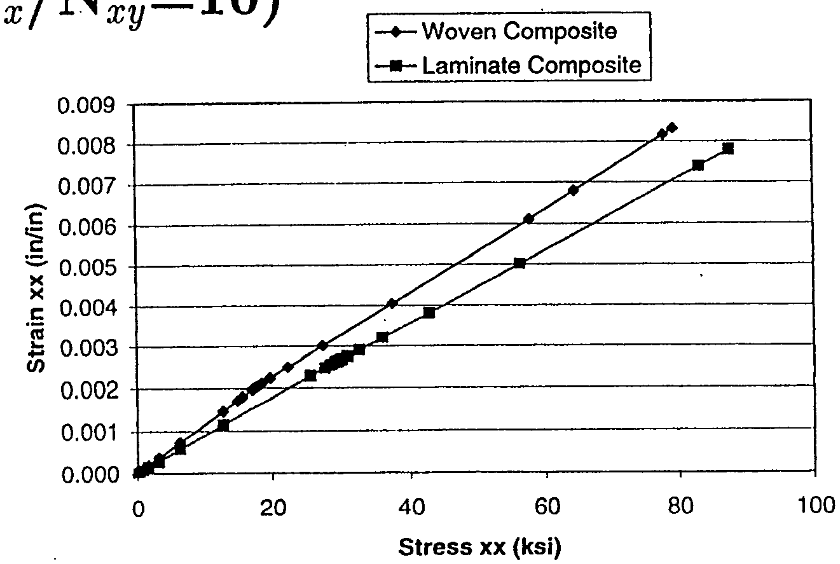

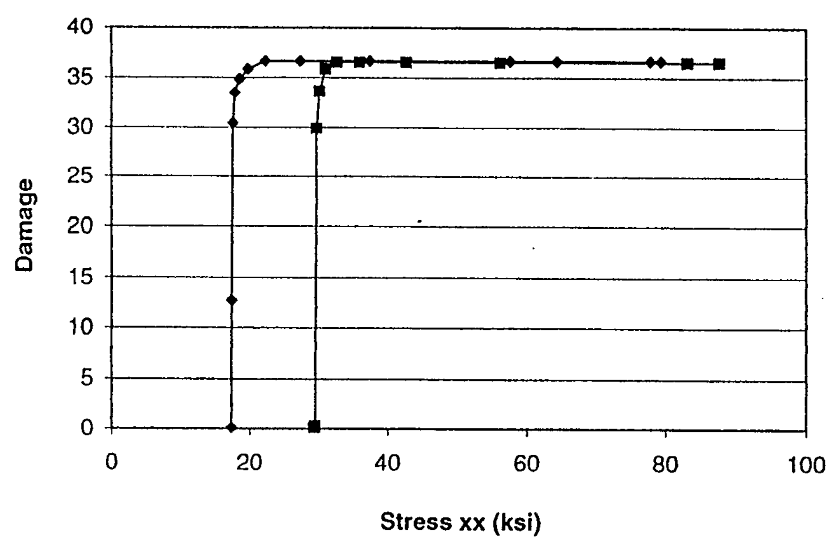

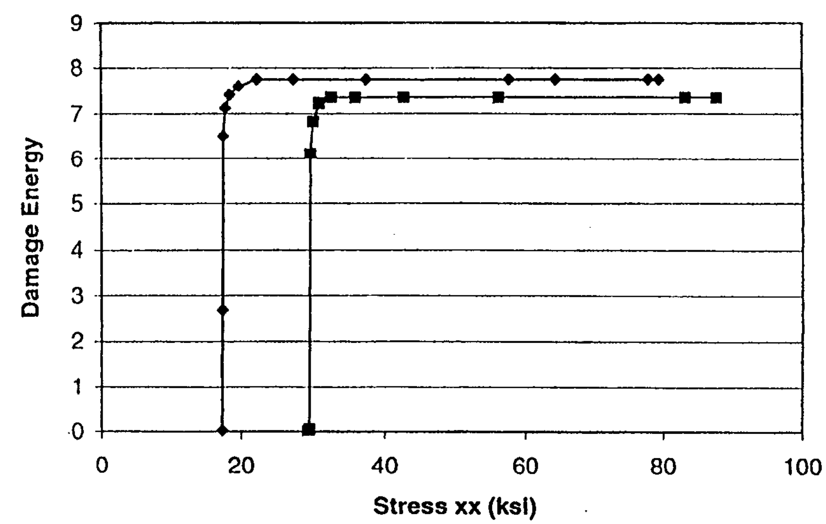

STRESS-STRAIN RELATIONS AND DAMAGE PROGRESSION FOR WOVEN AND NON-WOVEN COMPOSITES SUBJECTED TO COMPRESSION AND SHEAR ($N_x/N_{xy}=5$)

AS-4/3501-6 Graphite/Epoxy; $V_f=0.64$
Composite thickness=0.2 in.
Woven: 16 layers of plain-weave preforms
Non-woven: 32 plies $[0/90]_{16s}$

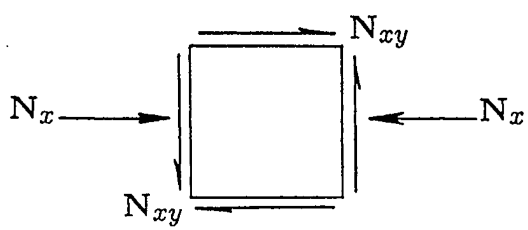

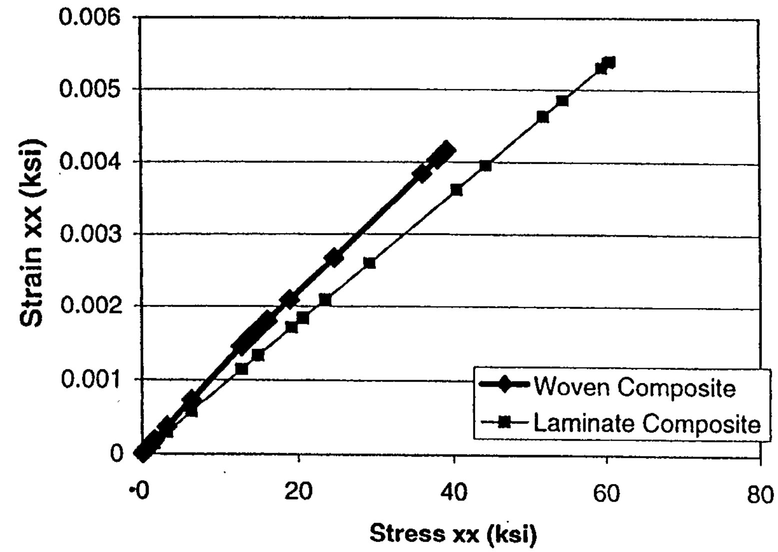

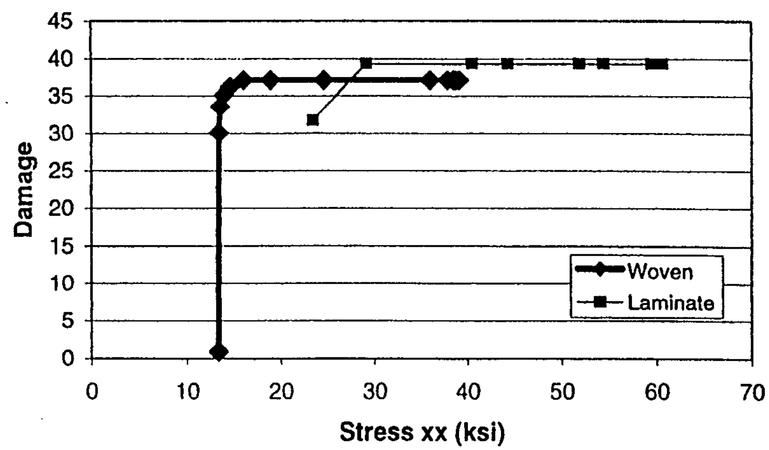

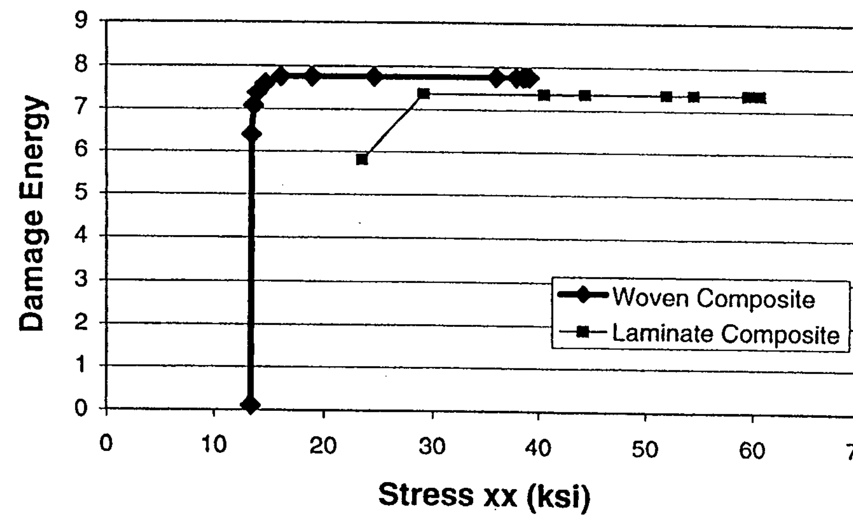

COMPRESSION WITH SHEAR LOADING

Structural fracture of woven an non-woven composite panels subjected to compression and shear were evaluated:

- The average compressive strength of woven composites was 22 percent lower than that of non-woven composites.
- The stiffness of woven composites was 16 percent lower than that of non-woven composites.
- The damage initiation stage was initiated at a lower load for woven composites.
- After damage initiation was completed there was no damage growth stage. Structural fracture occurred suddenly with the compressive failure of 0° plies for both woven and non-woven composites.
- As the shear component of the load was increased the ultimate strength was decreased for both woven and non-woven composites.
- Increasing the shear component of loading increased the difference between the strengths of woven and non-woven composites.

EFFECT OF SHEAR ON THE TENSILE AND COMPRESSIVE STRENGTHS OF WOVEN AND NON-WOVEN COMPOSITES

AS-4/3501-6 Graphite/Epoxy; $V_f=0.64$
Composite thickness=0.2 in.
Woven: 16 layers of plain-weave preforms
Non-woven: 32 plies $[0/90]_{16s}$

———— Woven
- - - - - - Non-woven

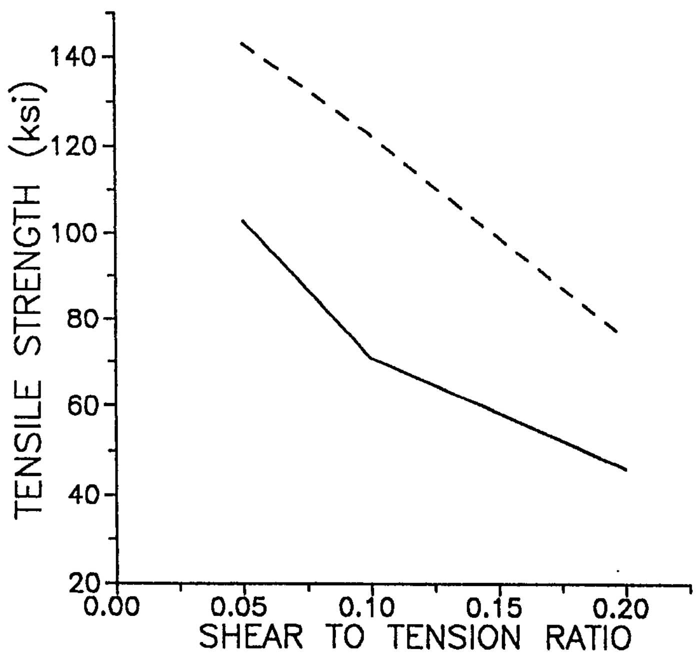

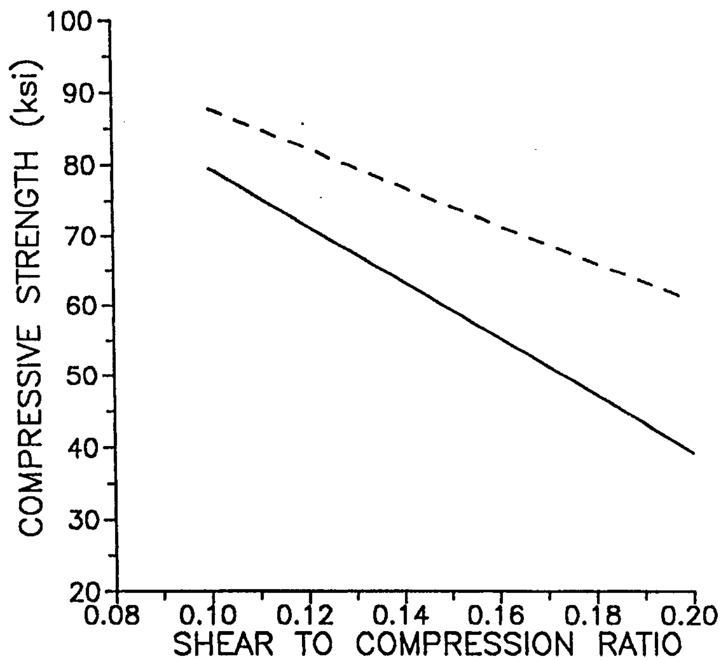

SHORT SPAN FLEXURAL LOADING OF WOVEN AND NON-WOVEN COMPOSITES

- A short simply supported and centrally loaded beam with 1.5 in. span, and 1.25 in. width was investigated.
- Non-woven and layer-to-layer angle interlock woven composite beams were simulated.

AS-4/3501-6 Graphite/Epoxy; V_f=0.64
Composite thickness=0.2 in.
Woven: 3-D angle interlock preform
Non-woven: 32 plies $[0/90]_{16s}$

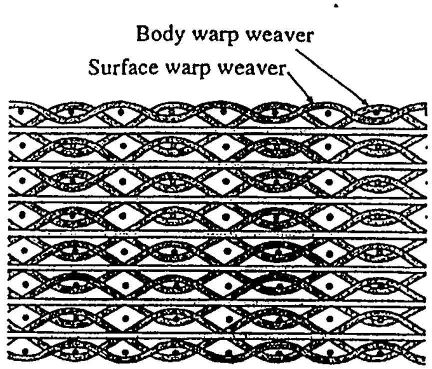

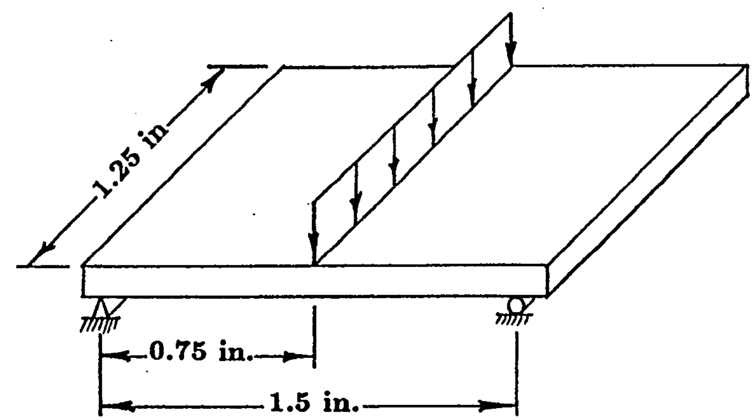

SHORT SPAN FLEXURAL RESPONSE OF WOVEN AND NON-WOVEN COMPOSITES

AS-4/3501-6 Graphite/Epoxy; $V_f=0.64$
Composite thickness=0.2 in.
Woven: 3-D angle interlock preform
Non-woven: 32 plies $[0/90]_{16s}$

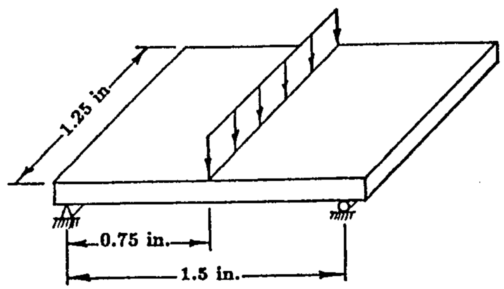

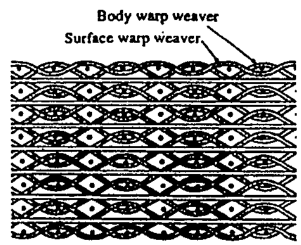

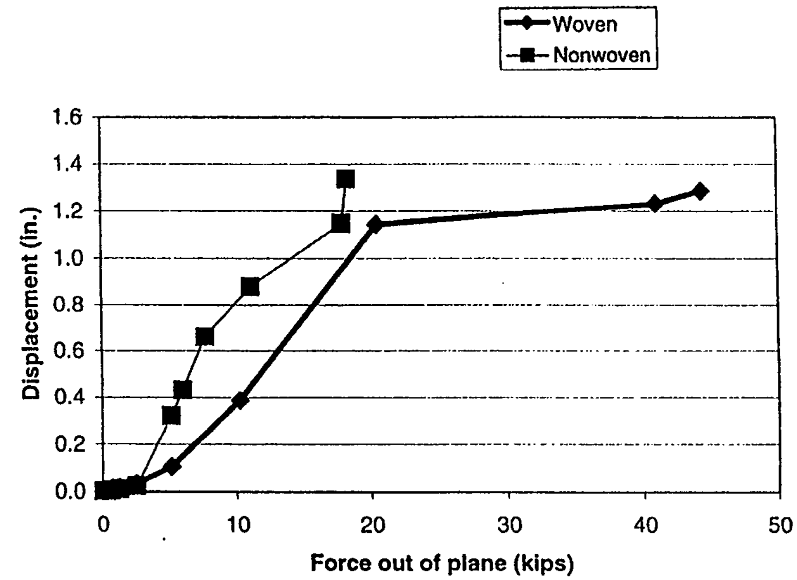

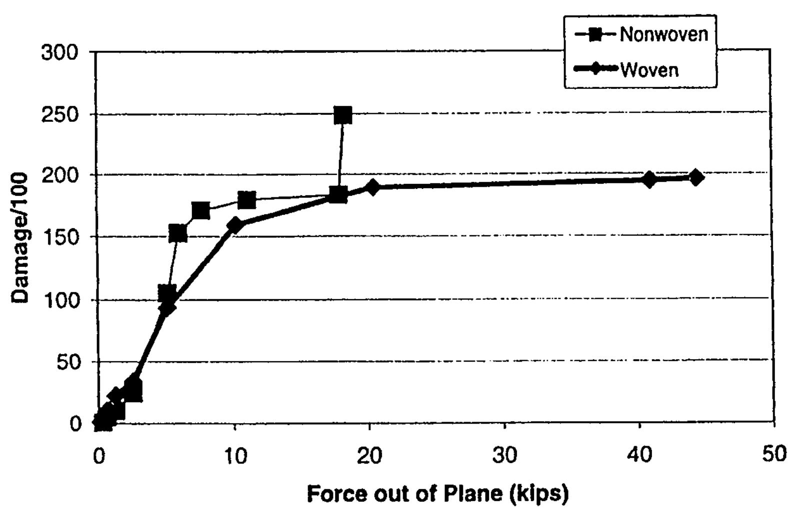

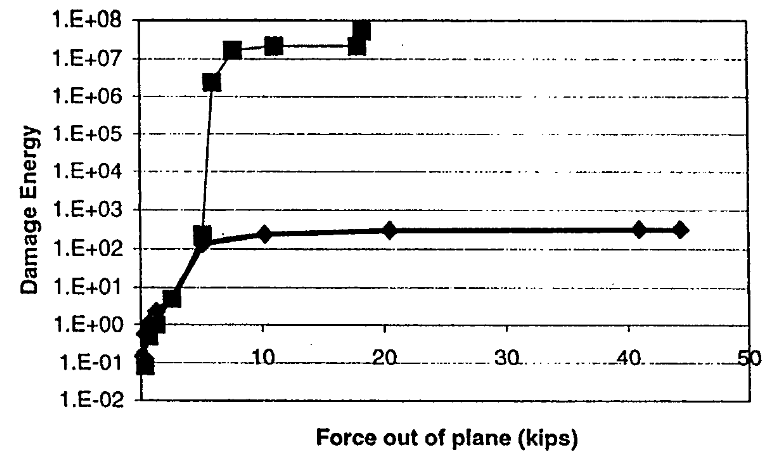

TRANSVERSE LOADING OF BEAM

Structural fracture of woven an non-woven composite simply supported beams subjected to central loading was investigated:

- The flexural strength of the woven composite was approximately twice the flexural strength of the non-woven composite.
- Both woven and non-woven composites began damage initiation by transverse tensile fractures of the 90° plies under the same loading. However, damage growth was more pronounced and abrupt for the non-woven composite.
- After damage initiation, the apparent stiffness of the woven composite was significantly higher than the stiffness of the non-woven composite.
- Deflections at failure were approximately the same for both woven and non-woven composites.
- The damage energy increased much more rapidly for the non-woven composite.

CONCLUSIONS

1. Progressive damage and fracture of woven and non-woven composites has been simulated under tensile and compressive loads with the presence of shear.
2. Non-woven composite panels are stronger than woven composite panels when subjected to tension or compression with shear.
3. Non-woven composite panels are stiffer than woven composite panels when subjected to tension or compression with shear.
4. Both woven and non-woven cross-ply composites are sensitive to the presence and magnitude of in-plane shear stresses.

CONCLUSIONS (CONTINUED)

5. Under compressive loading, the magnitude of in-plane shear stresses affects the woven composites more significantly compared to the effects on non-woven composites.
6. Non-woven composite panels are weaker than 3-D woven composite panels when subjected to short beam flexure.
7. Non-woven composite panels are less stiff than 3-D woven composite panels when subjected to short beam flexure.

Next Generation Design and Analysis Procedures for Bonded Composite Repairs

HIROSHI KAWAI
KEVIN G. O'SULLIVAN
PADRAIC E. O'DONOGHUE
D. SCOTT PIPKINS
Knowledge Systems, Inc., 81 East Main Street, Forsyth, GA 31029-1828, e-mail: ksi@mylink.net

J.H. PARK
SATYA N. ATLURI
Georgia Institute of Technology, Computational Modeling Center, Rm. 225 French Bldg., Atlanta, GA 30332-0356

Abstract: An efficient and accurate computational methodology and associated software (PC-Rep) for the analysis and design of bonded composite repairs is described. PC-Rep runs on personal computers including laptops and features a convenient graphical user interface. The software can be used to compute a variety of parameters important in repair design such as patched stress intensity factors and crack growth life. These parameters can be used to determine residual strength, inspection intervals and remaining structural life. Comparisons with standard reference solutions are carried out to validate the software. Parametric studies typical of repair design are presented.

1. INTRODUCTION

Infrastructure the world over is aging. This infrastructure includes buildings, bridges, roads, pipelines, and aircraft. As it ages there is growing concern about the structural integrity of much of this infrastructure. Economic and market forces have forced industry and government agencies to utilize many of the structures which make up the infrastructure well beyond their original design lives. For example, in 1988, 22% of Boeing 727's were operating beyond their original design life. This percentage has continued to increase since that time.

There are essentially two ways of dealing with the aging infrastructure problem. The first is to retire existing infrastructure and replace it. The second is to repair the existing infrastructure. While the first solution is perhaps more desirable, it is not always viable from an economic perspective. Thus, it is imperative that strategies to repair aging infrastructure be developed. By doing so, the service lives of the infrastructure can be extended beyond that for which it was originally designed.

A promising infrastructure repair technique is the use of adhesively bonded composite repairs. Bonded composite repairs offer an economical means of repairing cracked or damaged structure which does not drastically increase the weight of the structure. Adhesively bonded composite repairs have many advantages over mechanically fastened repairs such as: (i) new stress concentrations are not introduced into the repaired structure due to rivet holes; (ii) the repair patches are readily formed into complex

shapes; (iii) high stiffness to weight and strength to weight ratios of the patch; and (iv) high corrosion and fatigue resistance of the composite. This repair technique has been primarily used in the area of military aviation. However, it is equally well suited for use in commercial aviation as well as the repair of civil infrastructure such as buildings and bridges.

In order to properly design an adhesively bonded composite repair of a structure, many factors must be considered. These include:

- global stiffening of the structure due to the high stiffness of the composite patch;
- the effect of size, shape, thickness (including taper) and material properties of the composite patch on the crack-tip stress intensity factors, skin and patch stresses, adhesive shear strain, and peel stresses;
- the effect of the material properties of the adhesive on the crack-tip stress intensity factors, skin and patch stresses, adhesive shear strain, and peel stresses;
- the effect of thermal cycling on the composite repair; and
- the effect of disbonds on the performance of the composite repair.

This paper describes an efficient and accurate computational methodology and associated software (PC-Rep) for the analysis and design of bonded composite repairs. It builds on the work of Park, Ogiso and Atluri (1992); and Nagaswamy, Pipkins and Atluri (1996). PC-Rep runs on personal computers including laptops and features a convenient graphical user interface. The software can be used to compute a variety of parameters important in repair design such as patched stress intensity factors and crack growth life. These parameters can be used to determine residual strength, inspection intervals and remaining structural life.

2. ANALYSIS OF REPAIRS

There are several methods for the analysis of patched cracks. They can be broadly classified as either analytical or numerical. A review of these methods can be found in Nagaswamy, Pipkins and Atluri (1996). In this paper the focus will be on the usability of these methods in a maintenance environment. The repair design requirements in this environment are conflicting; fast turnaround (minutes) yet accurate. From the structural design point of view, accuracy usually means utilizing a numerical method such as the finite element method. However, finite element analyses (FEA) may not always be done quickly in a maintenance environment for several reasons. These include: lack of personnel knowledgeable in FEA; the unavailability of FEA software (pre and post processors and solver) due to cost; and the unavailability of computer hardware needed for FEA. As a result of one or more of these reasons, traditional FEA software is not typically of great interest to maintenance organizations.

In recognition of this fact, several pieces of software featuring easy to use graphical user interfaces (GUI), fast solution times, and minimal hardware requirements have come into use in recent years. These include CalcuRep, RAPID and PC-Rep. CalcuRep and PC-Rep are applicable to bonded composite repairs while RAPID is for mechanical doubler

type repairs. CalcuRep [Fredell (1994)] is based on the analytical approach of Rose (1981). RAPID, developed by the Federal Aviation Administration (FAA), is also based on an analytical approach wherein displacement compatibility is enforced between the repair, structure and mechanical fasteners. PC-Rep, developed by Knowledge Systems, Inc., has an outstanding feature which distinguishes it from these two codes. The analysis performed by PC-Rep is based upon the finite element method. However, PC-Rep relieves the user of the tedium often associated with finite element analysis. This is so because of the automated state-of-the-art meshing and computational fracture mechanics algorithms that have been implemented in PC-Rep. Thus, the user can enjoy the benefits of finite elements (i.e. arbitrary geometries and unsurpassed accuracy, etc.) without having to worry about any details of finite element analysis.

The analysis carried out by PC-Rep is based on the Finite Element Alternating Method (FEAM) [Atluri(1997)]. Because the repaired structure is not homogeneous, the FEAM must be used in a two stage analysis [Nagaswamy, Pipkins and Atluri (1996)]. The stages are as follows.

1. Evaluation of the stresses exerted by the adhesive and patch on the base sheet, using a coarse mesh.
2. The stresses obtained from stage 1 are applied as body forces on the base sheet, and the Finite Element Alternating Method is used to find the stress intensity factor.

In stage 1, a traditional finite element methodology is used to deduce the stresses exerted by the patch. As the crack tip is not meshed for the singularity, a coarse mesh is sufficient for this purpose. The sheet and the patch are modeled with eight noded 2D elements. The adhesive is modeled by shear elements as in Jones and Callinan (1981).

Stage 2 consists of an analysis using the 2D Finite Element Alternating Method [Atluri (1997)]. The FEAM is based upon superposition as illustrated in Figure 2.1. In the FEAM, the stresses in the uncracked body are first analyzed, by a traditional finite element method, for the given system of external loading. To model the crack, the tractions at the locations of the crack in an otherwise uncracked body must be erased. To erase the crack face stresses, the tractions found by the finite element solution are reversed. As is often the case, analytical solutions exist for cracks subjected to arbitrary crack face stresses but for infinite bodies. In the present 2D problem a solution is used in which the crack face tractions are given in terms of Chebyschev polynomials. Therefore, if these solutions are to be used for erasing crack face stresses, the residual stresses at the finite body extent in the infinite body have to be erased. This is done by reversing the residual stresses applied to the finite uncracked body. This results in residual tractions on the crack face. To erase these, the analytical solution is used again. This is repeated until convergence is achieved. Convergence is achieved when the stress intensity factors for each analytical iteration become small. The final stress intensity factor is the sum of all the stress intensity factors.

Summarizing, the steps in the 2D Finite Element Alternating Method are:

1. Solve for the uncracked finite body under given loads by traditional finite element method.
2. Compute the stresses at the crack location from step 1.
3. To reverse the above found stresses, use a least-squares approximation to fit the stresses to Chebyschev polynomials.
4. Use the above solution and find the stresses at the boundaries of the finite body.
5. Sum the Chebyschev coefficients to find the stress intensity factors for this iteration.
6. If the stress intensity factor for this iteration is small, then convergence is obtained.
7. If convergence is not obtained, apply the reversed residual stresses on the finite body boundaries and use the traditional finite element method to solve for the displacements and go to step 2.

The solution of the finite size body with a crack is then obtained by summing the results (i.e. displacements, stress intensity factors, etc.) from all iterations.

3. PC-REP

The finite element based analysis technology described in the previous section has been combined with a graphical, menu driven front end and an automatic mesh generator and ported onto a personal computer. This computer package, referred to as PC-Rep, is extremely robust and is capable of fast and accurate calculation of various parameters relating to bonded patch repair. A schematic of a typical patched crack configuration is illustrated in Figure 3.1

3.1. Features

At present this robust package has many attractive features including:

- Convenient Graphical User Interface (GUI)
- Physically Based Inputs
- Automated Analysis and Mesh Generation
- Finite Element Kernel
- Rectangular Metal Skins
- Adhesively Bonded Metal or Composite Patches; Centrally Located on Skin
- One Straight Crack Centrally Located under the Patch
- Remote Uniform Loading Normal to Crack
- Partial Disbond/No Disbond
- Stress Intensity Factor Calculation
- Fatigue Lifetime Determinations
- Adhesive Shear Stress Computation
- Material Property Database
- Patch Shape; Rectangular, Octagonal, Elliptical
- Patch Taper

- Crack Size; Can Extend Beyond Patch
- Stiffeners; Broken, Unbroken
- Residual Stresses from Curing
- Thermal Cycling due to Temperature Differential Between Ground and Cruise

Perhaps the most significant feature of PC-Rep is that all inputs to the program are actual physical quantities as distinct from finite element related data. Based on these physical data, such as patch size, stiffener dimensions, adhesive properties, a pre-processor will automatically generate the optimum finite element mesh and the relevant boundary conditions. This greatly simplifies the usage of PC-Rep.

Another major advantage of PC-Rep is that it allows the user a considerable level of complexity with respect to the design and analysis of bonded patches. Despite this complexity, PC-Rep executes extremely quickly on a personal computer; a matter of minutes. This efficiency is achieved through the use of the finite element alternating method. Some of these features are very important when it comes to the design of patches for aircraft components. Broken/unbroken stiffeners can interact significantly with the crack growth process. Residual stresses and thermal stresses play an important role in the growth of a crack. Patch taper, along with disbond must always be considered. All of these features are captured within a standard PC-Rep analysis. Many of these will be illustrated in Section 4.

3.2. Graphical User Interface

The PC-Rep package consists of three parts; (a) a GUI, (b) a finite element kernel and (c) an automatic mesh generator. The GUI is written in tcl/tk while the mesh generator and the kernel are written in FORTRAN. All user interaction takes place through the GUI. The user does not have to be concerned with the mesh generation or other finite element related details.

The GUI uses a convenient point and click system that allows the user to select various options such as patch configuration, stiffener type, etc. and to specify the appropriate inputs. Figure 3.2 illustrates a typical screen that the user can generate. The right hand side contains buttons that can be used to activate the different options. The left hand side of Figure 3.2 contains a schematic diagram of the patch configuration that is being prepared for analysis. This allows the user to view each update that is made to the analysis model.

When the user selects a particular option from the buttons on the right hand side, a new screen appears that allows the user to input, in a tabular manner, various quantities relevant to that option. For example, Figure 3.3 illustrates the table that appears when the *Patch* option is selected. The user can select from a range of different patch materials, including composites and metals, or else can input the material properties directly. The user can also select the patch shape (rectangular, tapered, octagonal or elliptical) along with the patch dimensions using this screen.

Using the *Analysis Control* option, the user can select the type of analysis that is desired. This can be the direct calculation of the stress intensity factors for the patched crack or else it can be the calculation of the fatigue life of the component, based on the Forman fatigue relationship. Once the analysis is complete, the user can utilize the post-processing options to view the most significant results. These include plots of the stress intensity factor or the fatigue life (number of load cycles) versus the crack length. The user can also examine important quantities such as the maximum shear stress in the adhesive for different patch configurations.

4. ANALYSIS AND RESULTS

The PC-Rep code is used here to analyze a wide variety of patched aircraft configurations.

4.1. Validation Problems

To validate the PC-Rep analyses, comparisons were made with three results from the literature.

4.1.1. Rose's Solution

A number of comparisons were made with the solutions developed by Rose (1982). Here, a rectangular patch was placed over a rectangular plate and a crack is centrally located underneath the patch. The relevant geometrical and material property data are given in Table 4.1. In this table, t_s is the skin thickness, E_s is the elastic modulus of the skin, ν_s is the Poisson ratio of the skin, E_x is the stiffness of the patch parallel to the crack (x direction), E_y is the stiffness of the patch perpendicular to the crack (y direction), G_{xy} is the shear modulus of the patch, ν_{yx} is the Poisson ratio of the patch, G_a is the shear modulus of the adhesive and t_a is the thickness of the adhesive.

For the Rose solution, the plate and patch are infinitely wide but the width of the plate and the patch are taken as 200 mm in the PC-Rep calculation. A uniform unit normal traction (1 MPa) is applied to the base plate in the direction normal to the crack. There are no stiffeners or disbonds included in this calculation. The computed stress intensity factors are presented in Table 4.2 for a range of different values of the patch thickness. It can be seen that there is excellent agreement between the two sets of results.

While the results in Table 4.2 are in very good agreement, it is important to point out a number of differences that exist between the two approaches.

(a) The Rose (1982) solution is applicable when the patched plate is of infinite width but PC-Rep considers the case of a finite plate. When the patch width is less than the plate width, the PC-Rep results will, not surprisingly, be higher than the Rose solution.

To minimize this effect, the width of the plate is selected to be much larger than the length of the crack

(b) The Rose solution assumes the flexibility of the adhesive layer to be

$$F = \frac{t_a}{G_a} \tag{6.1}$$

However, PC-Rep uses the Jones and Callinan (1981) approach where the adhesive layer flexibility is modified by considering the effects of shear deformation of the patch and the base plate. In this case,

$$F = \frac{t_a}{G_a} + \frac{3}{8}\frac{t_s}{G_s} + \frac{3}{8}\frac{t_p}{G_p} \tag{6.2}$$

This effect is more pronounced as the thickness of the patch increases and is also significant when the width of the patch is less than the width of the plate.

4.1.2. Experimental Data

Comparisons were also made with the experimental data of Denney (1995). Table 4.3 contains the appropriate material property and geometrical data and in this instance, the width of the patch is considerably less than the width of the plate (t_p is the thickness of the patch). The maximum and minimum remote uniform stresses are σ_{max} and σ_{min} respectively. The shear modulus of the adhesive was taken as 21.5 MPa for the purpose of these calculations [Chow and Atluri (1997)]. This shear modulus is consistent with the operating stress in the adhesive rather than the initial elastic value of 405MPa. The results, showing crack length as a function of the number of load cycles, are presented in Figure 4.1 and the excellent agreement between the experimental and computed results is obvious.

4.1.3. Other Comparisons

Comparisons have also been made with the results obtained by Park, Ogiso and Atluri (1992). The configuration analyzed in this reference is given in Table 4.4 and the comparison of computed stress intensity factor are given in Table 4.5. The lower results in [Park, Ogiso and Atluri (1992)] are likely due to the fact that the patch is of infinite width.

4.2. Stress Intensity Factor Variation

For the parameters in Table 4.4, a typical plot of the stress intensity factor as a function of crack length is given in Figure 4.2. The patch thickness is taken as 0.6 mm and the applied load is 100 MPa. As can be seen, the stress intensity tends to level off as the crack length approaches the edge of the patch. After the crack extends beyond the patch, the stress intensity factor increases dramatically. These trends are typical of the stress intensity factor behavior that is observed for patched cracks.

4.3. Effect of Stiffeners on Crack Growth

PC-Rep can also be used to consider the influence of stiffeners on crack growth. In the first example, two horizontal and two vertical stiffeners are included. This configuration is illustrated schematically in Figure 4.3 and the stiffeners are symmetrical with respect to the crack. The skin, patch and adhesive geometric and material properties are the same as in Table 4.3. All stiffeners are identical and have a cross section area of 80 mm^2. The horizontal stiffeners are 75 mm from the crack and the vertical stiffeners are 50 mm from the crack center. Figure 4.4 illustrates the computed fatigue lifetimes in the presence of stiffeners. It can be seen that this lifetime is much greater than the case where there are no stiffeners. The effect of the vertical stiffeners is to retard the stress intensity factor increase as the crack approaches the stiffener.

The second example illustrates the effect of a broken stiffener. Here a single vertical stiffener bisects the crack and in one instance the stiffener is broken and in the second it is unbroken. These results are shown in Figure 4.5. As expected, the computed lifetime is much greater when the stiffener is unbroken. These examples illustrate how easy it is to include the important effects of stiffeners in a bonded patch analysis.

4.4. Effects of Patch Size and Shape

Given the flexibility of PC-Rep, it is relatively easy to conduct several parametric studies relating to the size, shape and properties of bonded composite patches. A selection of these results now follows. In each case, the base problem is that described in Table 4.3. There are no stiffeners or disbond and the effect of thermal stresses has been ignored.

4.4.1. Patch Shape

Three different patch shapes are considered; rectangular, octagonal and elliptical. The overall width and height of each patch is the same. For the octagonal patch, the corner cut-outs are all 10 mm in height and 10 mm in width. The fatigue lifetimes are presented in Figure 4.6 and it can be seen that there is not a great deal of difference in the results. The maximum adhesive stresses were also relatively similar in each case.

4.4.2. *Patch Thickness*

The patch thickness is varied to investigate the effect on both the stress intensity factor and also the maximum adhesive shear stress. As expected, the stress intensity factor shows a steady decrease as the thickness is increased and this is illustrated in Figure 4.7. Interestingly, the adhesive stress exhibits a minimum with the stresses rising for very thick patches and also very thin patches. This result is shown in Figure 4.8.

4.4.3. *Taper*

The effect of tapering is very important as it can help to reduce the magnitude of the maximum adhesive shear stress. In this example, the taper width, W_t, and height, H_t, are taken as 5 mm and 8 mm respectively and the thickness of the patch at the edge of the taper is 0.15 mm. Figure 4.9 compares the computed maximum adhesive shear stress with and without taper. The taper has the effect of reducing this maximum stress by up to 15%. However, for very thin patches, the maximum stress does not reduce dramatically. This suggests that the maximum stress in this instance is at the edge of the crack. It was also observed that the stress intensity factors were also not dramatically affected by the taper.

4.4.4. *Vertical Height of Patch*

Figure 4.10 shows the variation in the stress intensity factor as the patch height is increased. The general trend is for the stress intensity factor to decrease moderately with height. The maximum adhesive shear stress also exhibits a moderate increase with increasing patch height.

4.4.5. *Horizontal Width of Patch*

As expected, the stress intensity factor increases as the patch width decreases. This result is illustrated in Figure 4.11. The maximum adhesive shear stress demonstrates a similar trend.

4.5. Residual Stresses and Temperature

As discussed earlier, it is very important to consider the effects of temperature when designing a bonded composite patch due to the residual stresses set up during the curing process and due the thermal stresses set up during the ground-air-ground cycle because of the thermal property mismatch. In this example, the curing temperature is taken as 120°C, the room temperature as 20°C, the maximum ground temperature as 50°C and the minimum ground temperature as -50°C. All other parameters are as in Table 4.3 with the addition of horizontal and vertical stiffeners that are 75 mm and 50 mm from the crack center respectively (cross-section area 80 mm^2) and with the adhesive stiffness at 21.5 MPa.

The effect of these thermal stresses is to increase the stress intensity factor. This is reflected in reduced fatigue lifetimes. This is illustrated in Figure 4.12 where four separate results are presented:

- no residual or thermal stresses
- residual stresses only
- thermal stresses only
- residual and thermal stresses

This result shows the relative importance of including each of these effects.

5. DISCUSSION

This paper clearly demonstrates the importance of new generation software tools that utilize enhanced automation to obtain accurate solutions to highly complex problems. PC-Rep is distinguished from PC based repair codes as the analysis is performed by software that is based upon the finite element method. However, PC-Rep relieves the user of the tedium often associated with finite element analysis. This is so because of the automated state-of-the-art meshing and computational fracture mechanics algorithms that have been implemented in PC-Rep. Thus, it is possible to enjoy the benefits of finite elements (i.e. arbitrary geometries and unsurpassed accuracy, etc.) without having to worry about any details of finite element analysis.

The examples presented in this paper illustrate the feasibility of a personal computer based design procedure for bonded composite repair of aircraft structures. It was easy to consider many significant features such as residual curing stresses, disbond, taper and stiffeners. PC-Rep can be viewed as the new generation design/analysis tool that merges an easy to use GUI with a powerful, yet efficient computational kernel.

REFERENCES

Atluri, S.N., 1997, *Structural Integrity and Durability*, Tech Science Press, Forsyth.

Chow, W.T. and Atluri, S.N., 1997, "Composite patch repairs of cracked metal structures: effects of adhesive nonlinearity, thermal cycling and debonding," accepted for publication in *AIAA Journal.*

Denney, J., 1995, *Fatigue Response of Cracked Aluminum Panel with Partially Bonded Composite Patch*, Masters Thesis, Air Force Institute of Technology.

Fredell, R.S., 1994, *Damage Tolerant Repair Techniques for Pressurized Aircraft Fuselages*, Ph.D. Dissertation, Delft University of Technology.

Jones, R. and Callinan, R.J., 1981, "A design study in crack patching," *Fibre Science and Technology* **14**, 99-111.

Nagaswamy, V., Pipkins, D.S., and Atluri, S.N., 1996, "A FEAM based methodology for analyzing composite patch repairs of metallic structures," *Computer Modeling and Simulation in Engineering* **1**, 263-288.

Park, J.H., Ogiso, T., and Atluri, S.N., 1992, "Analysis of cracks in aging aircraft structures with and without composite patch repairs," *Computational Mechanics* **10**, 169-201.

Rose, L.R.F., 1981, "An application of the inclusion analogy for bonded reinforcements," *International J. of Solids and Structures* **17**, 127-171.
Rose, L.R.F., 1982, "A cracked plate repaired by bonded reinforcements," *International Journal of Fracture* **18**, 135-144.

Tables

$2W_s = 200$ mm; $2H_s = 635$ mm; $t_s = 2.9$ mm
$2W_p = 200$ mm; $2H_p = 152$ mm
$E_s = 73{,}000$ MPa; $\nu_s = 0.33$
$E_x = 25{,}400$ MPa; $E_y = 208{,}000$ MPa; $G_{xy} = 7{,}240$ MPa; $\nu_{yx} = 0.168$
$G_a = 965$ MPa; $t_a = 0.102$ mm
$2a = 38.1$ mm

Table 4.1 Geometrical and Material Property Data used in Comparison with Rose (1982)

Patch Thickness (mm)	PC-Rep Stress Intensity Factor (MPa mm$^{1/2}$)	Rose Stress Intensity Factor (MPa mm$^{1/2}$)
0.1	3.04	3.16
0.2	2.40	2.46
0.3	2.03	2.07
0.4	1.78	1.80
0.5	1.59	1.61
0.6	1.45	1.45
0.7	1.33	1.33
0.8	1.23	1.22
0.9	1.14	1.13
1.0	1.07	1.06

Table 4.2 Computed Stress Intensity Factor Variation with Patch Thickness

$2W_s = 152$ mm; $2H_s = 508$ mm; $t_s = 1.0$ mm
$2W_p = 50$ mm; $2H_p = 56$ mm; $t_p = 0.381$ mm
$E_s = 72{,}400$ MPa; $\nu_s = 0.33$
$E_x = 25{,}000$ MPa; $E_y = 210{,}000$ MPa; $G_{xy} = 20{,}500$ MPa; $\nu_{yx} = 0.168$
$G_a = 405$ MPa; $t_a = 0.127$ mm
$\sigma_{max} = 120$ MPa; $\sigma_{min} = 12$ MPa; $R = 0.1$

Table 4.3 Geometrical and Material Property Data used in Comparison with Denney (1995)

$2W_s = 152$ mm; $2H_s = 508$ mm; $t_s = 2.0$ mm
$2W_p = 50$ mm; $2H_p = 80$ mm
$E_s = 72{,}400$ MPa; $\nu_s = 0.32$
$E_x = 26{,}250$ MPa; $E_y = 210{,}000$ MPa; $G_{xy} = 75{,}000$ MPa; $\nu_{yx} = 0.16$
$G_a = 965$ MPa; $t_a = 0.102$ mm
$\sigma = 1$ MPa
$2a = 20$ mm

Table 4.4 Geometrical and Material Property Data used in Comparison with Park, Ogiso and Atluri (1992)

Patch Thickness (mm)	PC-Rep Stress Intensity Factor (MPa mm$^{1/2}$)	Park et al. Stress Intensity Factor (MPa mm$^{1/2}$)
0.1	2.88	2.80
0.2	2.39	2.19
0.4	1.89	1.68
0.6	1.60	1.35
0.8	1.40	1.18
1.0	1.25	1.01

Table 4.5 Computed Stress Intensity Factor Variation with Patch Thickness

Figures

List of Figure Captions

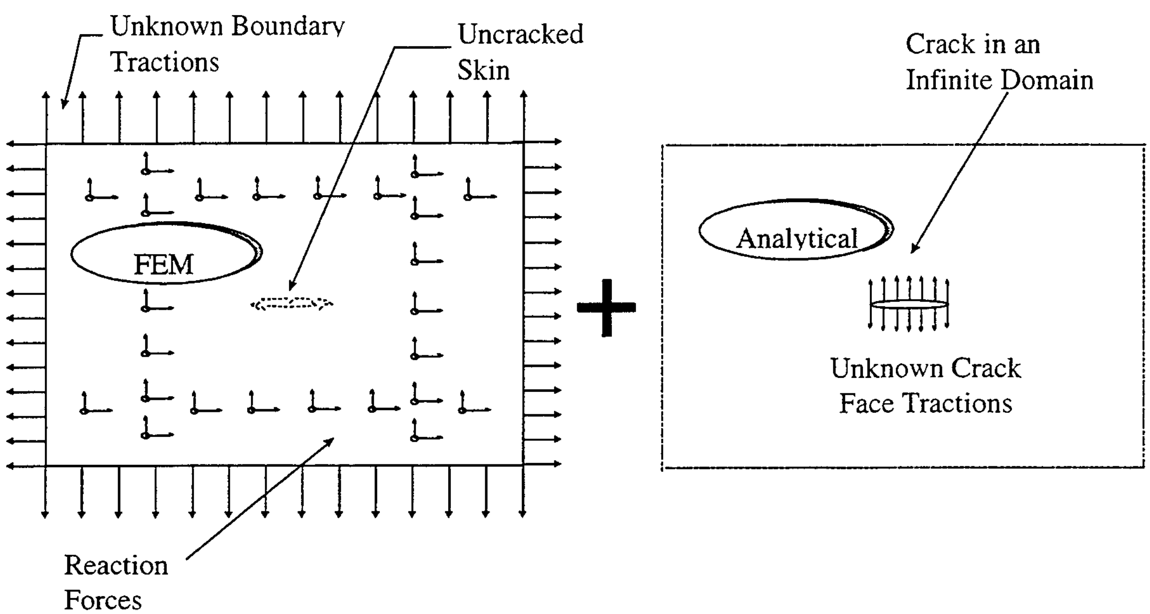
Unknown Boundary
Tractions
Uncracked
Skin
FEM
Reaction
Forces
Crack in an
Infinite Domain
Analytical
Unknown Crack
Face Tractions

Figure 2.1

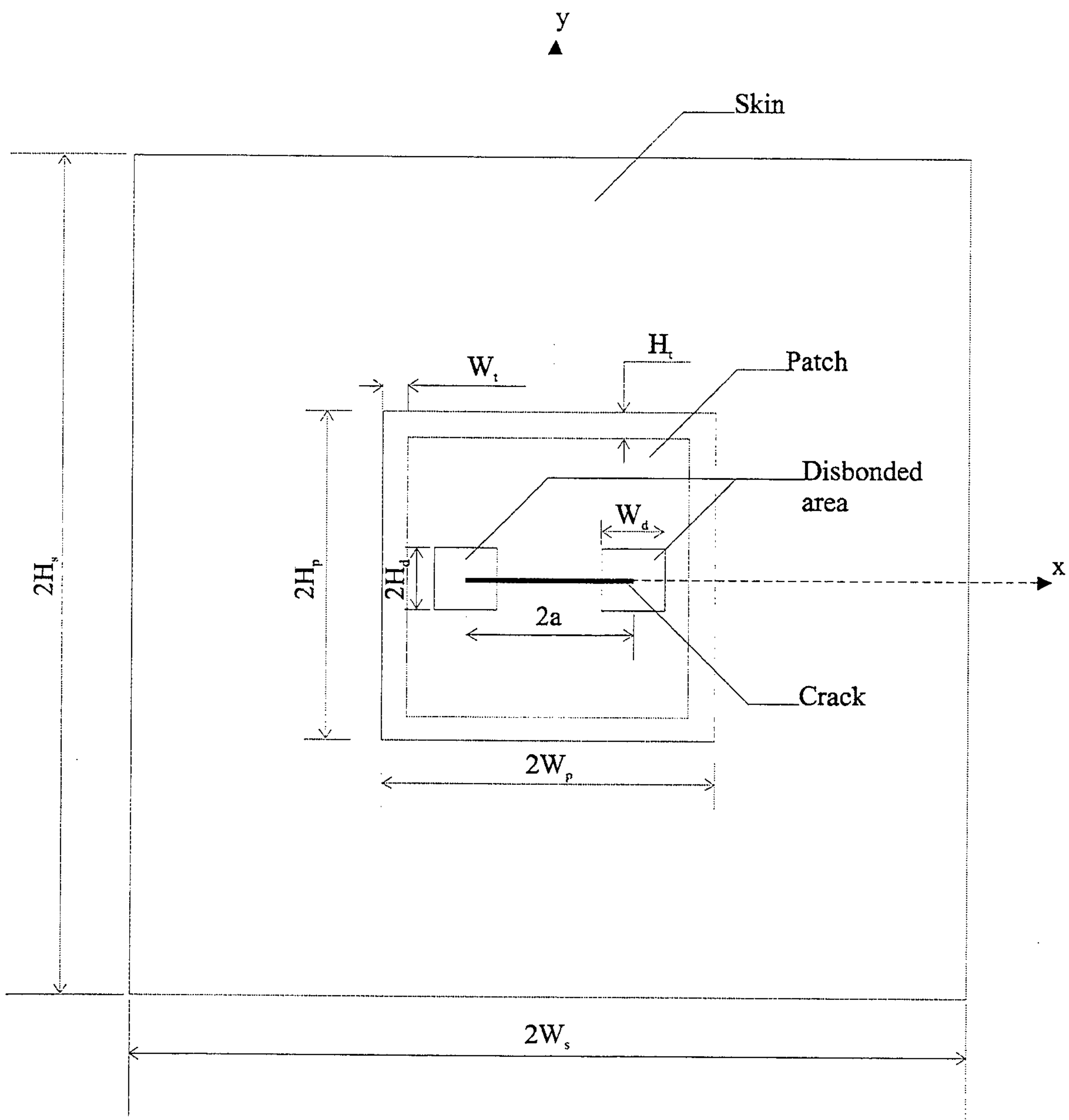
y
Skin
W_t
H_t
Patch
Disbonded area
W_d
$2H_s$
$2H_p$
$2H_d$
x
2a
Crack
$2W_p$
$2W_s$

Figure 3.1

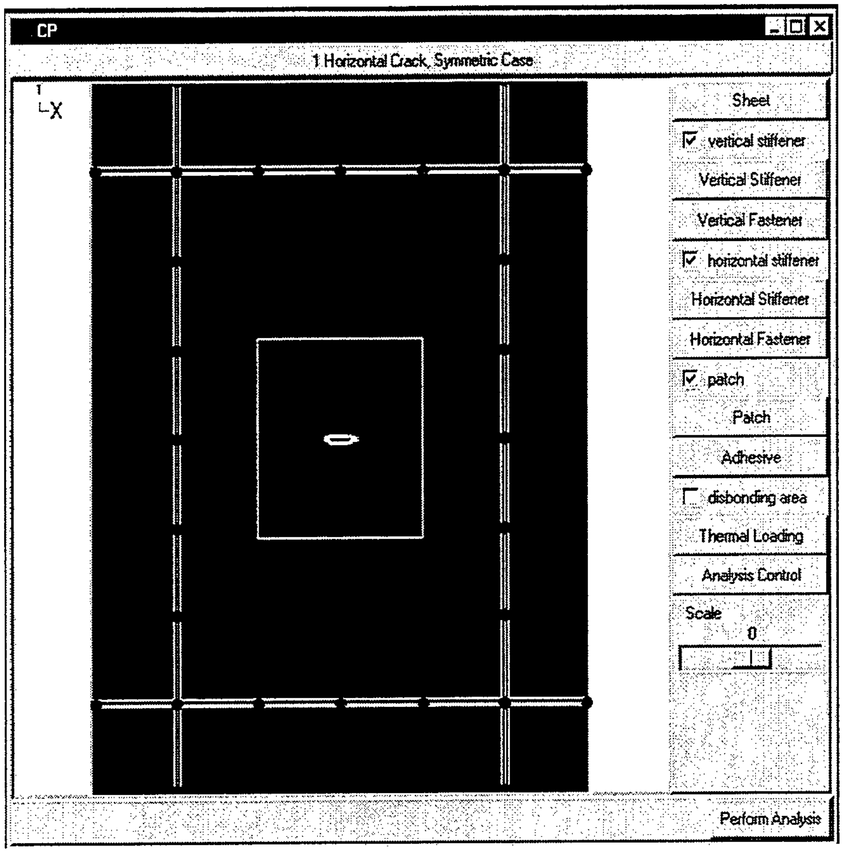
CP
1 Horizontal Crack, Symmetric Case
X
Sheet
vertical stiffener
Vertical Stiffener
Vertical Fastener
horizontal stiffener
Horizontal Stiffener
Horizontal Fastener
patch
Patch
Adhesive
disbonding area
Thermal Loading
Analysis Control
Scale
0
Perform Analysis

Figure 3.2

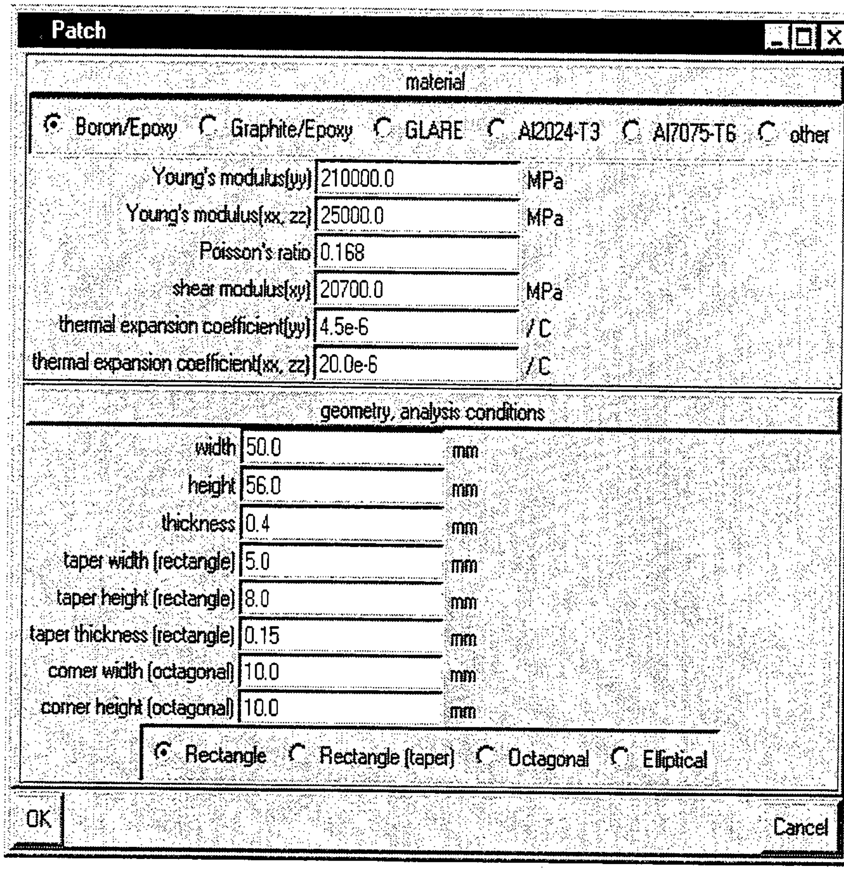
Patch
material
Boron/Epoxy
Graphite/Epoxy
GLARE
Al2024-T3
Al7075-T6
other
Young's modulus(yy) 210000.0 MPa
Young's modulus(xx, zz) 25000.0 MPa
Poisson's ratio 0.168
shear modulus(xy) 20700.0 MPa
thermal expansion coefficient(yy) 4.5e-6 /C
thermal expansion coefficient(xx, zz) 20.0e-6 /C
geometry, analysis conditions
width 50.0 mm
height 56.0 mm
thickness 0.4 mm
taper width (rectangle) 5.0 mm
taper height (rectangle) 8.0 mm
taper thickness (rectangle) 0.15 mm
corner width (octagonal) 10.0 mm
corner height (octagonal) 10.0 mm
Rectangle
Rectangle (taper)
Octagonal
Elliptical
OK
Cancel

Figure 3.3

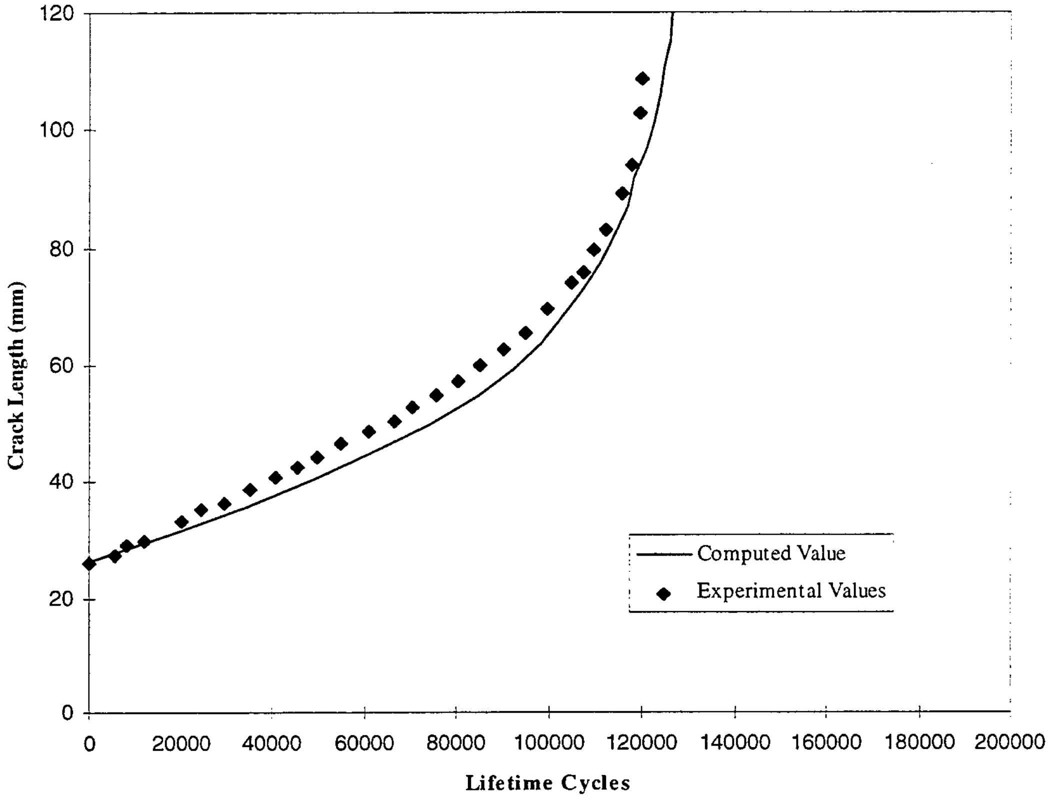
120
100
80
60
40
20
0
Crack Length (mm)
0
20000
40000
60000
80000
100000
120000
140000
160000
180000
200000
Lifetime Cycles
Computed Value
Experimental Values

Figure 4.1

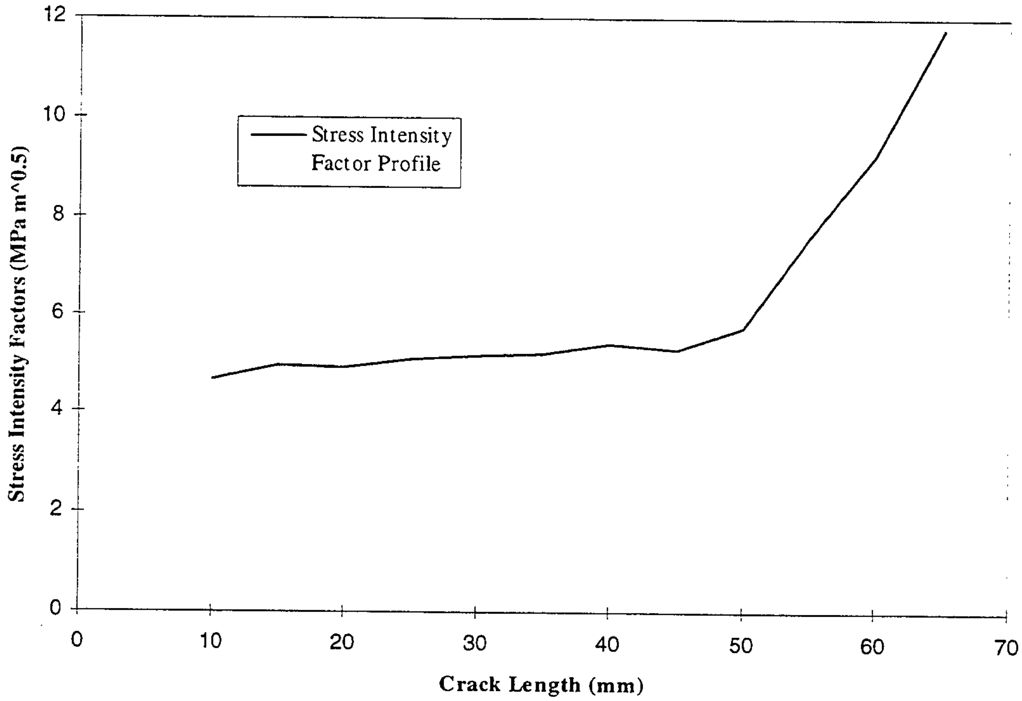
12
10
8
6
4
2
0
0
10
20
30
40
50
60
70
Stress Intensity Factor Profile
Stress Intensity Factors (MPa m^0.5)
Crack Length (mm)

Figure 4.2

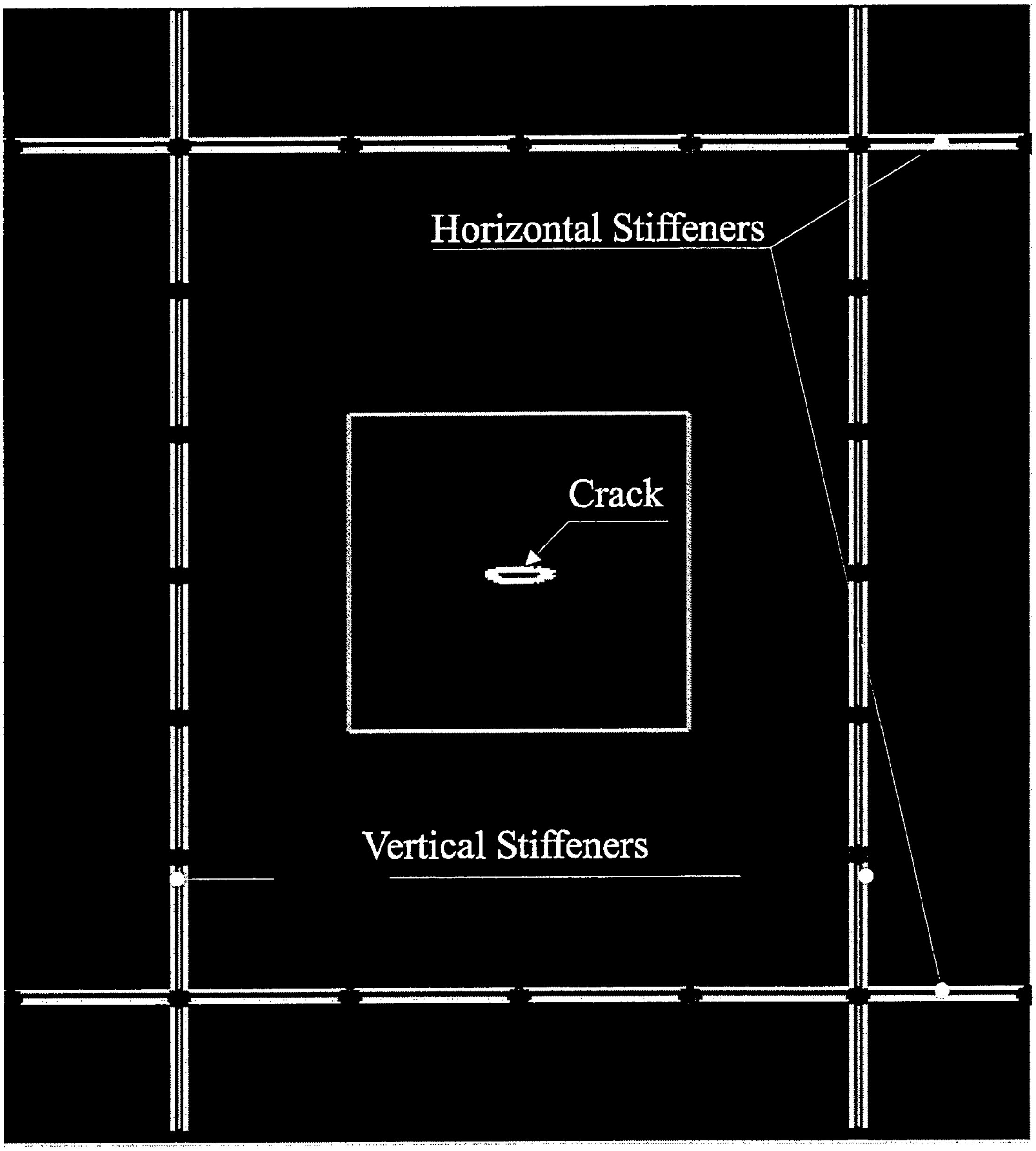

Figure 4.3

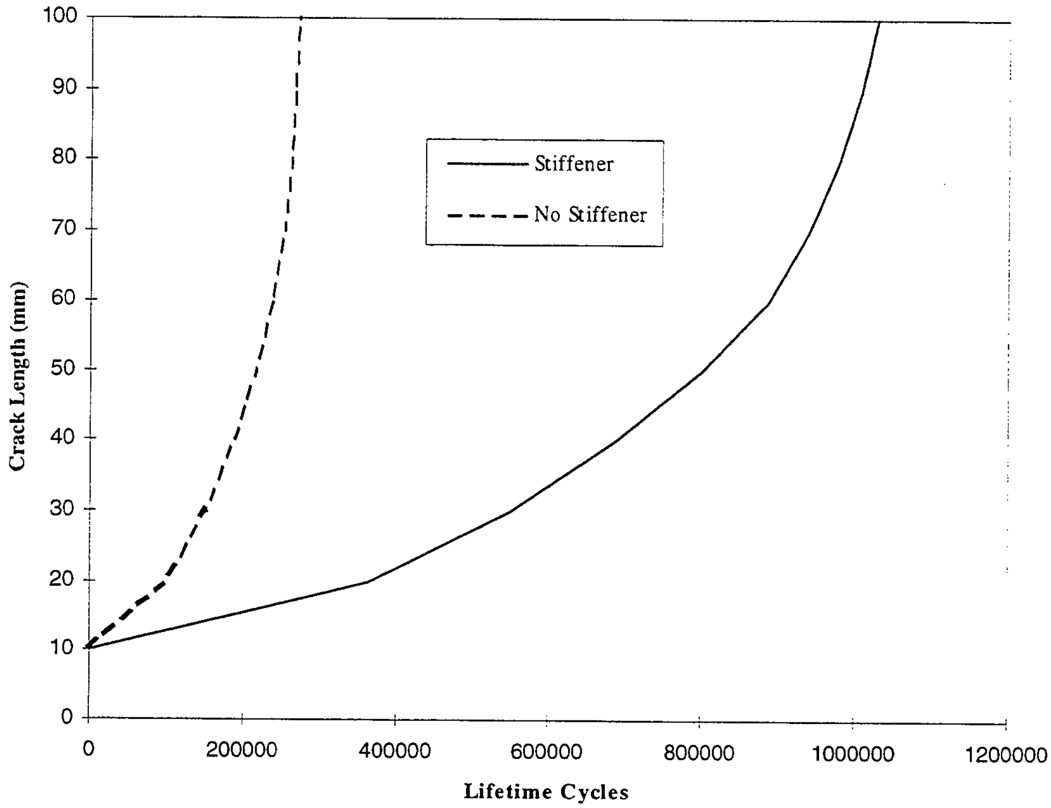

100
90
80
70
60
50
40
30
20
10
0
Crack Length (mm)
Stiffener
No Stiffener
0
200000
400000
600000
800000
1000000
1200000
Lifetime Cycles

Figure 4.4

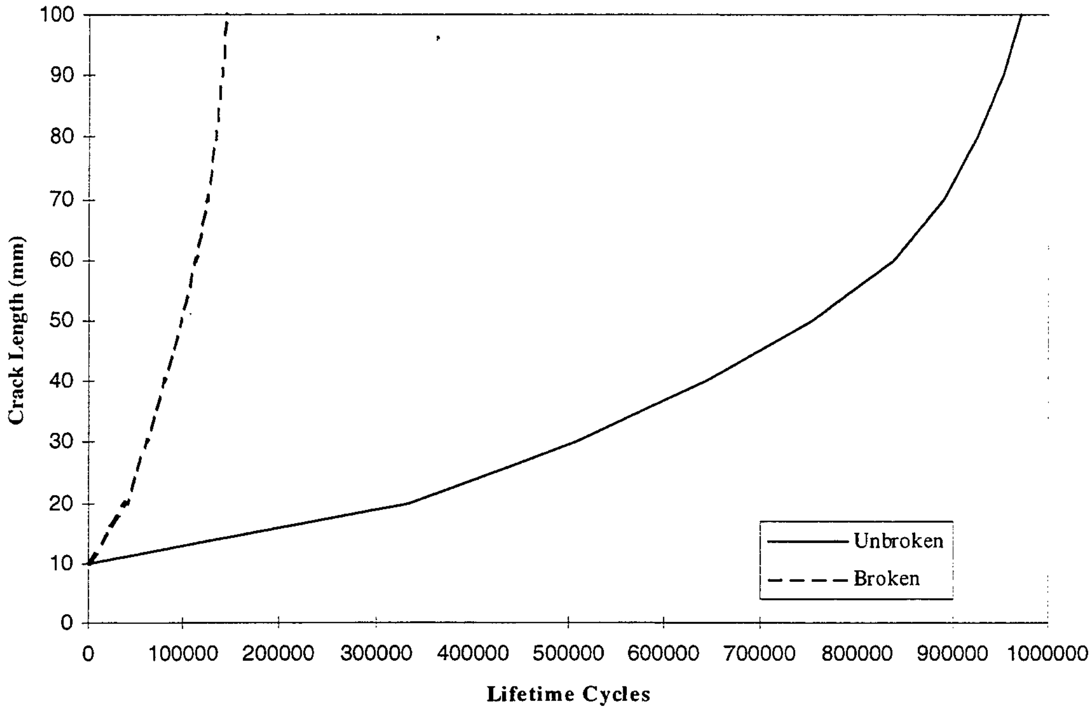

100
90
80
70
60
50
40
30
20
10
0
Crack Length (mm)
0
100000
200000
300000
400000
500000
600000
700000
800000
900000
1000000
Lifetime Cycles
Unbroken
Broken

Figure 4.5

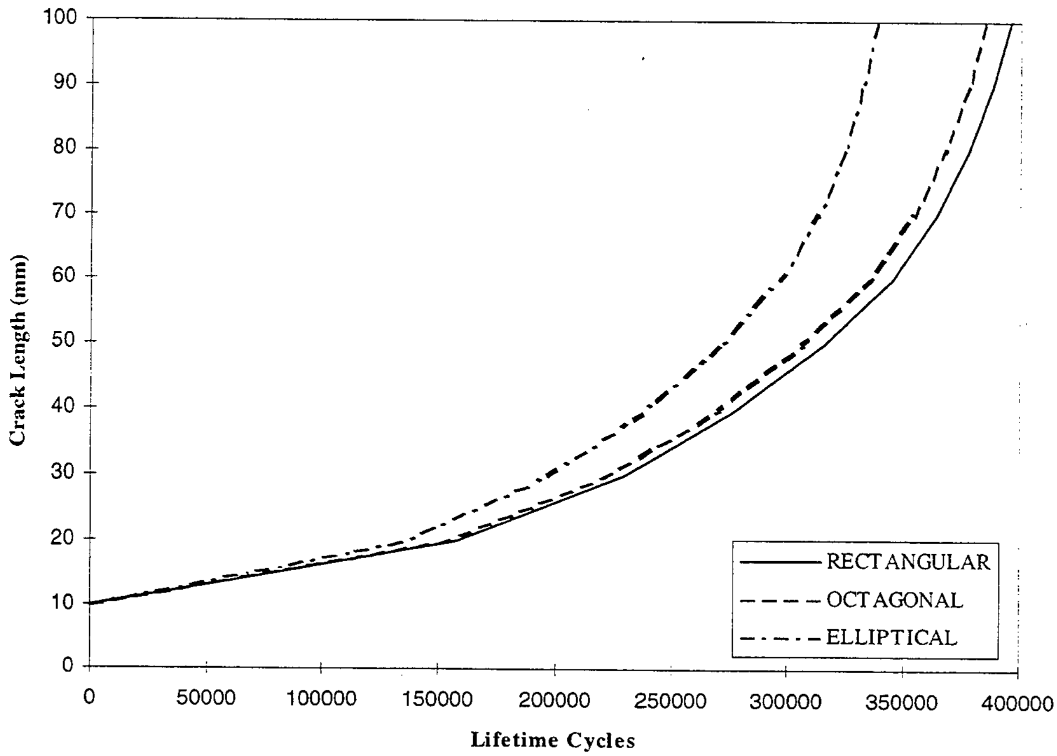

100
90
80
70
60
50
40
30
20
10
0
Crack Length (mm)
0
50000
100000
150000
200000
250000
300000
350000
400000
Lifetime Cycles
RECTANGULAR
OCTAGONAL
ELLIPTICAL

Figure 4.6

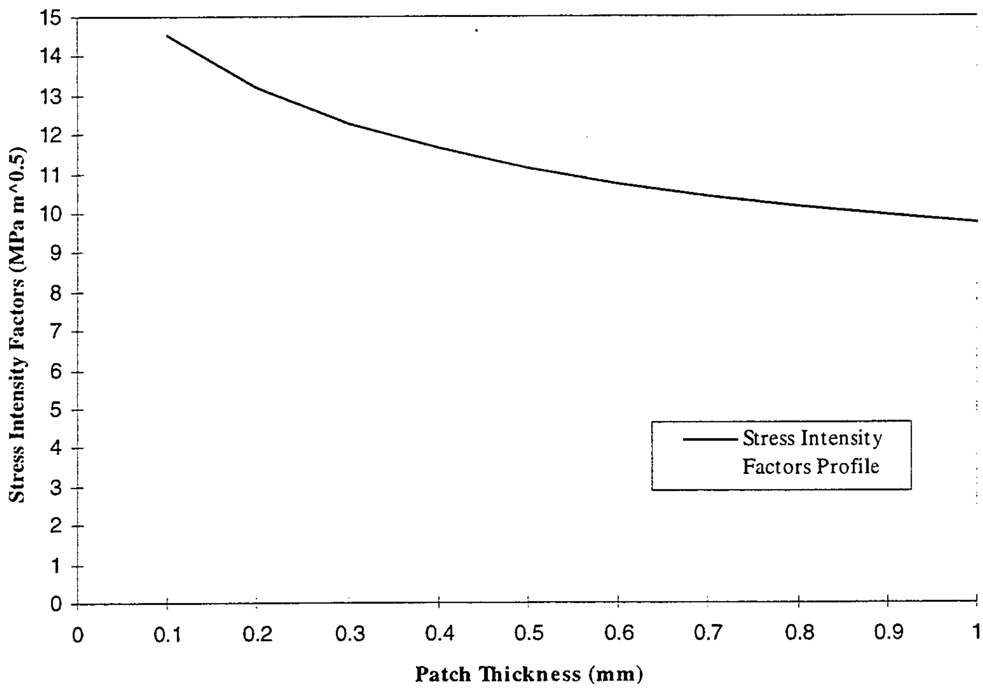

Stress Intensity Factors (MPa m^0.5)
15
14
13
12
11
10
9
8
7
6
5
4
3
2
1
0
0
0.1
0.2
0.3
0.4
0.5
0.6
0.7
0.8
0.9
1
Patch Thickness (mm)
Stress Intensity Factors Profile

Figure 4.7

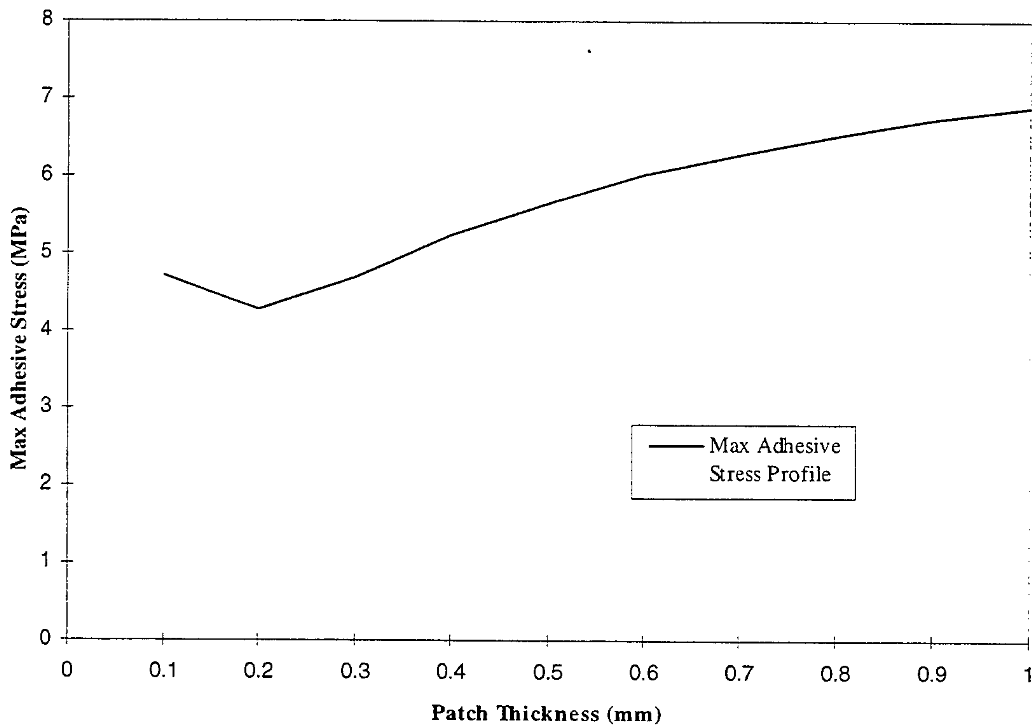

Max Adhesive Stress (MPa)
8
7
6
5
4
3
2
1
0
0
0.1
0.2
0.3
0.4
0.5
0.6
0.7
0.8
0.9
1
Patch Thickness (mm)
Max Adhesive Stress Profile

Figure 4.8

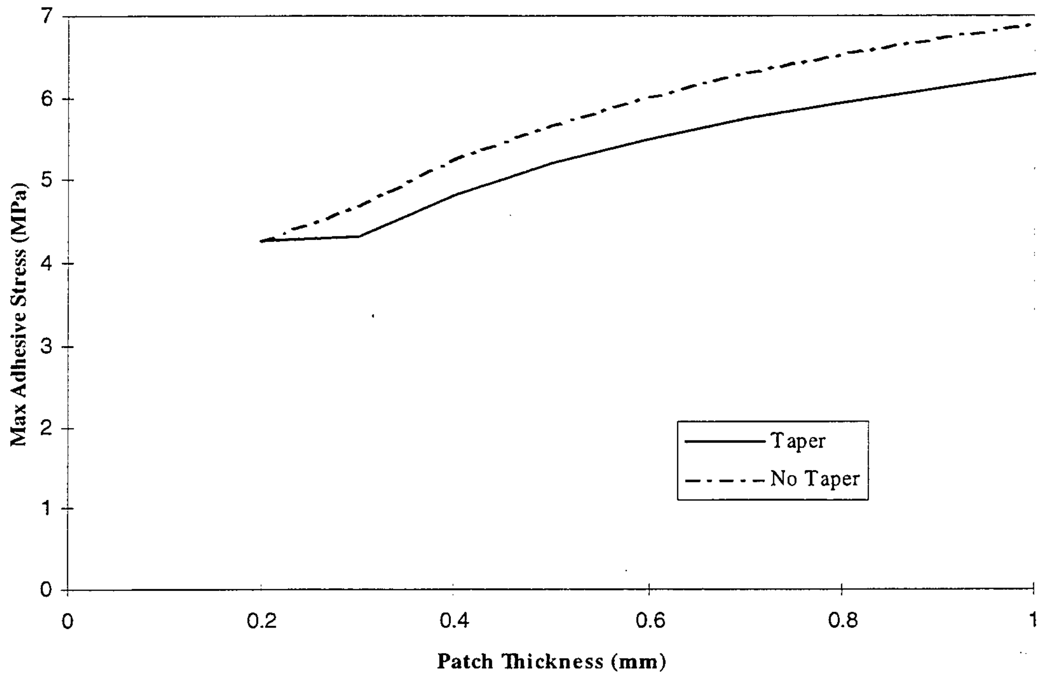

7
6
5
4
3
2
1
0
Max Adhesive Stress (MPa)
Taper
No Taper
0
0.2
0.4
0.6
0.8
1
Patch Thickness (mm)

Figure 4.9

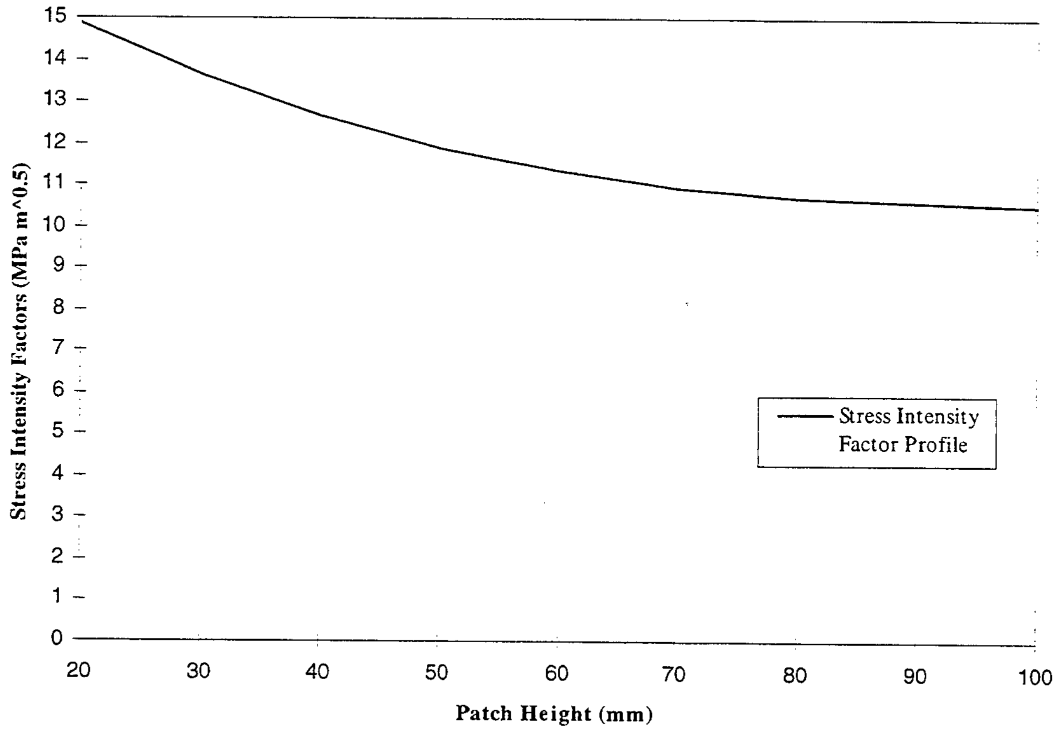
15
14
13
12
11
10
9
8
7
6
5
4
3
2
1
0
Stress Intensity Factors (MPa m^0.5)
20
30
40
50
60
70
80
90
100
Patch Height (mm)
Stress Intensity
Factor Profile

Figure 4.10

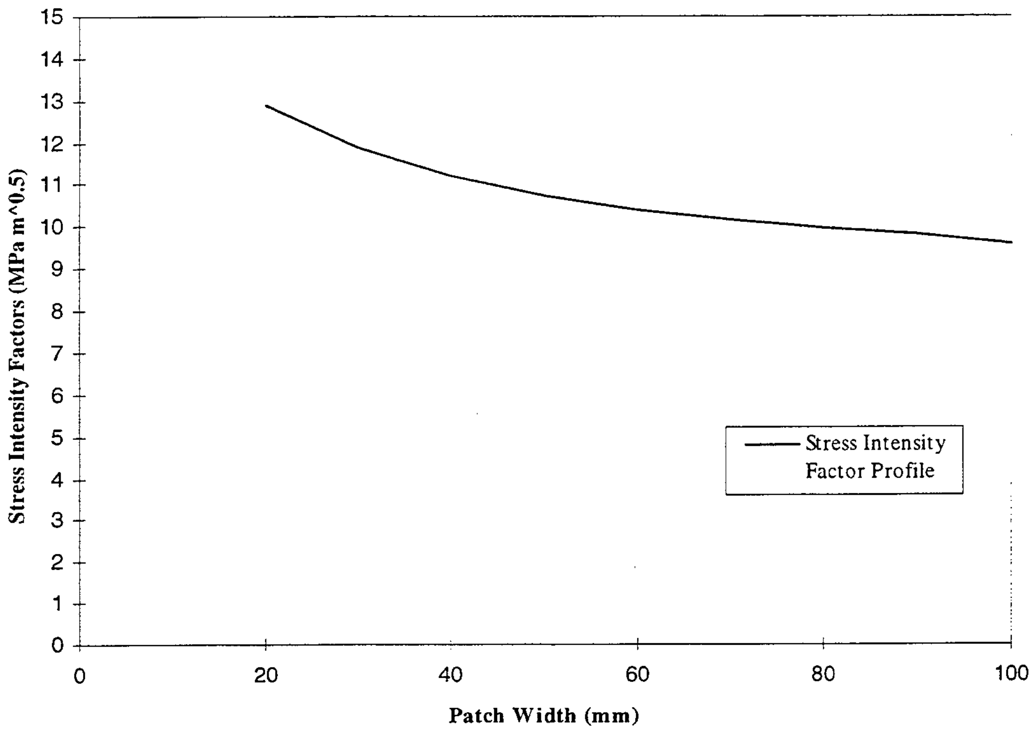

Stress Intensity Factors (MPa m^0.5)
15
14
13
12
11
10
9
8
7
6
5
4
3
2
1
0
0
20
40
60
80
100
Patch Width (mm)
Stress Intensity Factor Profile

Figure 4.11

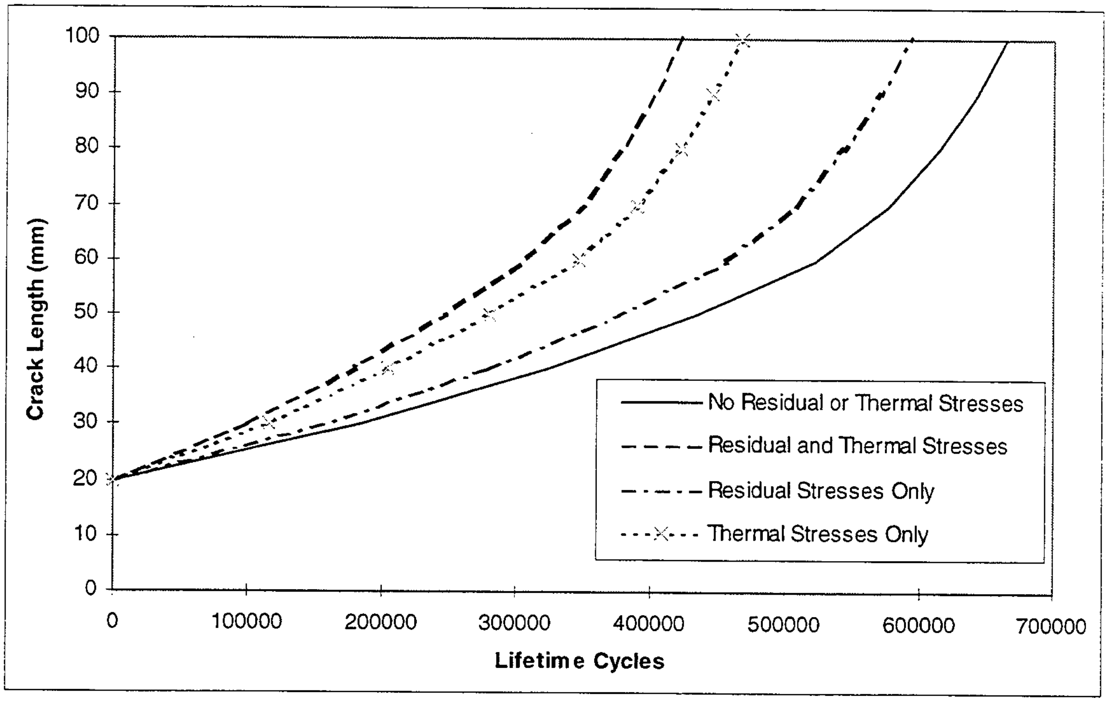

Crack Length (mm)
0
10
20
30
40
50
60
70
80
90
100
Lifetime Cycles
0
100000
200000
300000
400000
500000
600000
700000
No Residual or Thermal Stresses
Residual and Thermal Stresses
Residual Stresses Only
Thermal Stresses Only

Figure 4.12

Assessment of Analysis Methodologies For Predicting Fatigue Crack Growth And Residual Strength of Aging Aircraft

F. W. Brust, R. E. Kurth (Battelle)

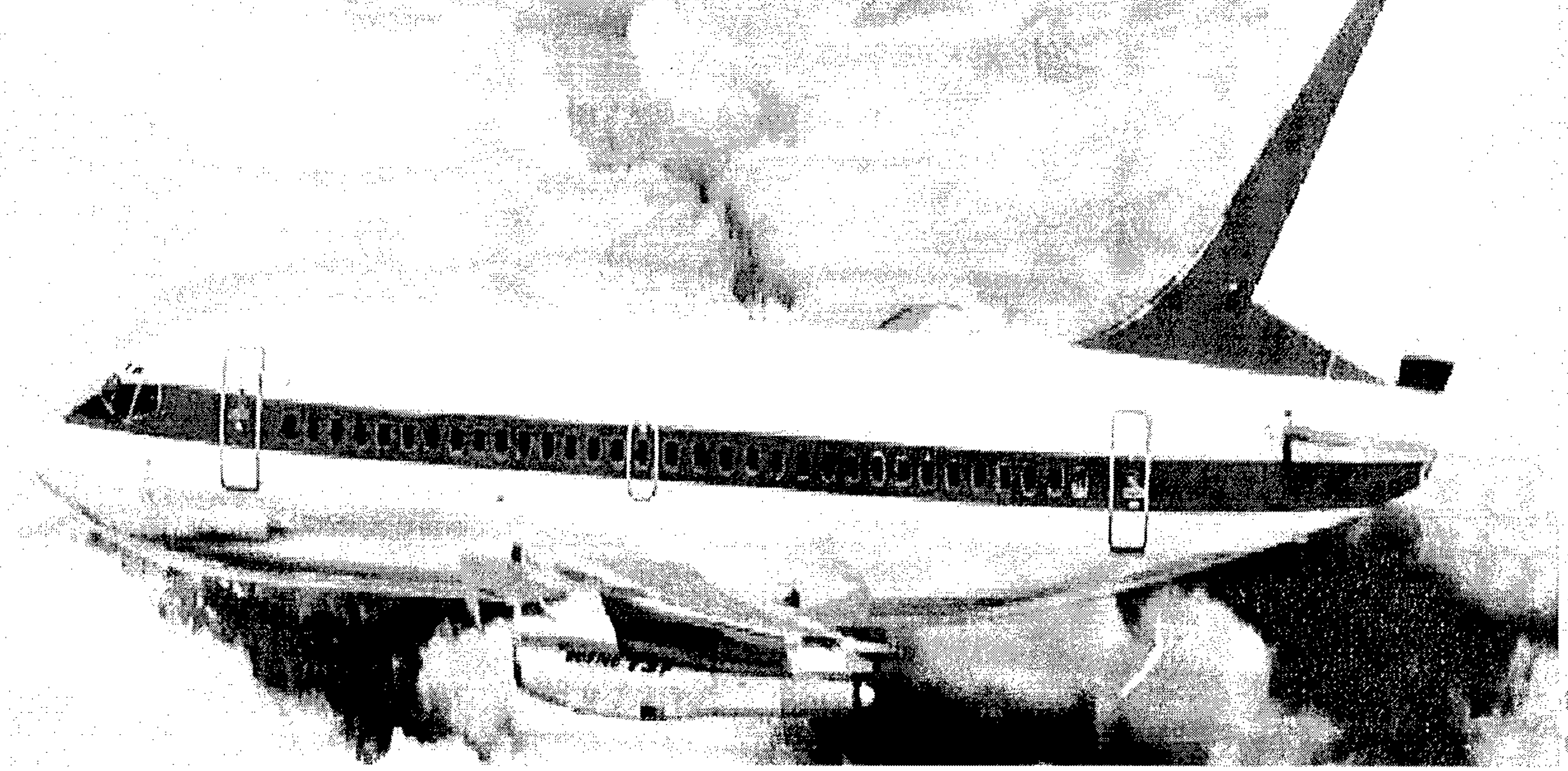

Presentation Outline

- Brief Summary of PWFD Program
  - FAA/Air Force Program (Battelle PM R. Kurth/FAA Program Directors C. Bigelow/J. Bakuckas)
- Deterministic Enabling Methodologies
- AGILE/STAGS/FEAM Overview
  - AGILE/STAGS Definition
  - FEAM - What is it?
- Validation (ABAQUS/ANSYS)
- Program Status
- Current & Future Efforts

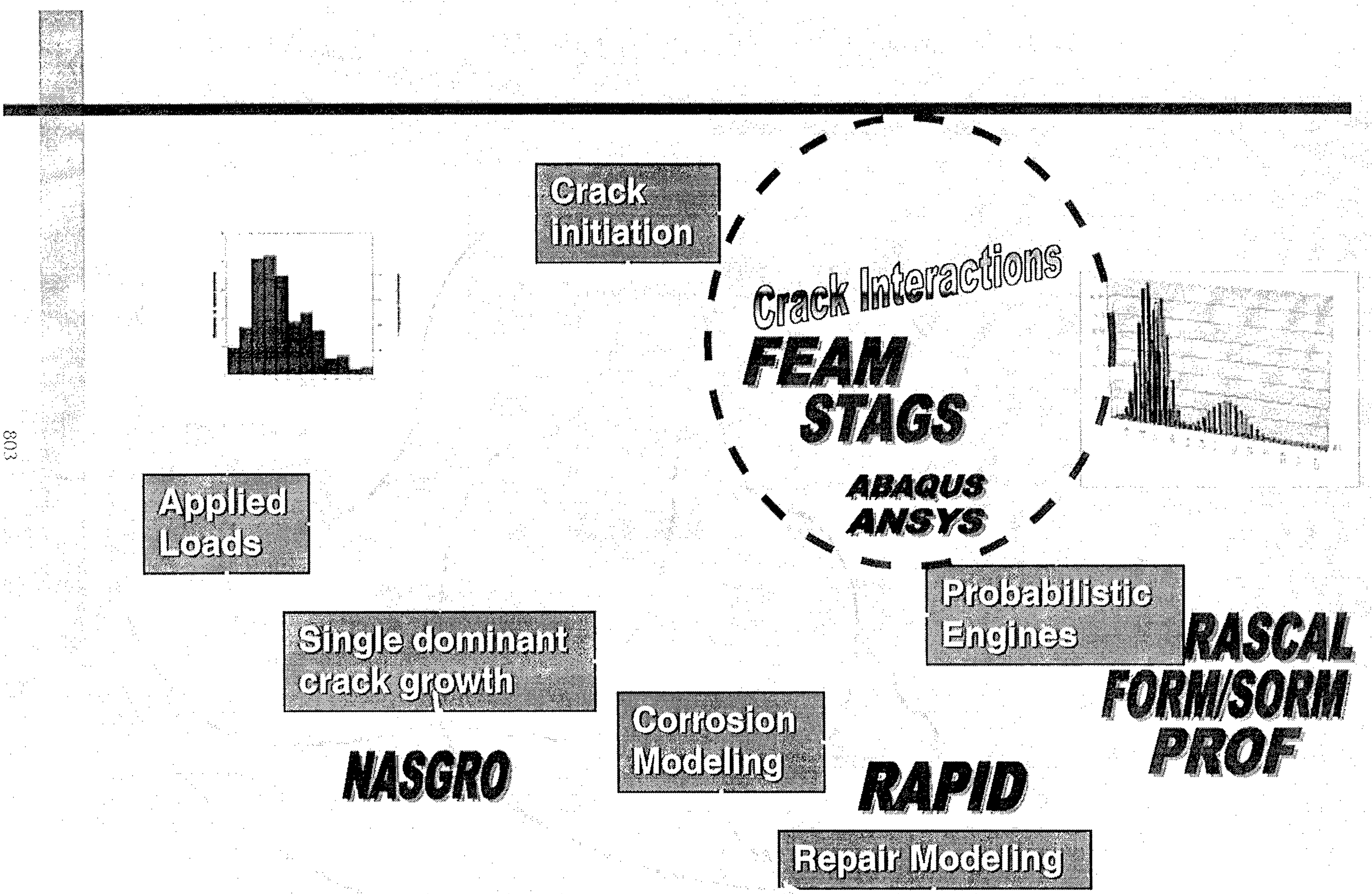
Crack
initiation
Crack Interactions
FEAM
STAGS
ABAQUS
ANSYS
Applied
Loads
Single dominant
crack growth
NASGRO
Corrosion
Modeling
Probabilistic
Engines
RASCAL
FORM/SORM
PROF
RAPID
Repair Modeling

Automated Global-Intermediate-Local Evaluation (AGILE) - STAGS - FEAM

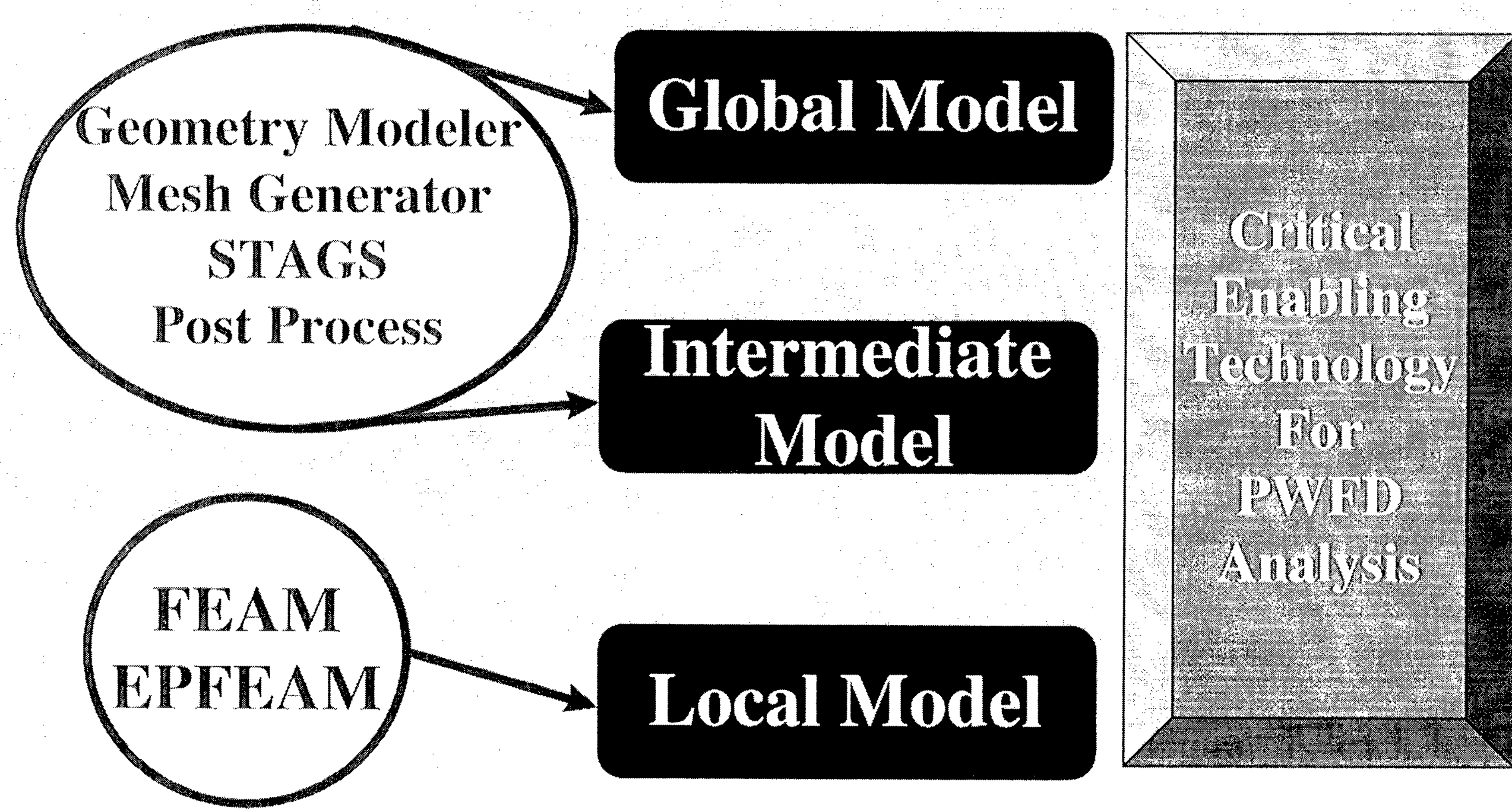

Analysis Procedure

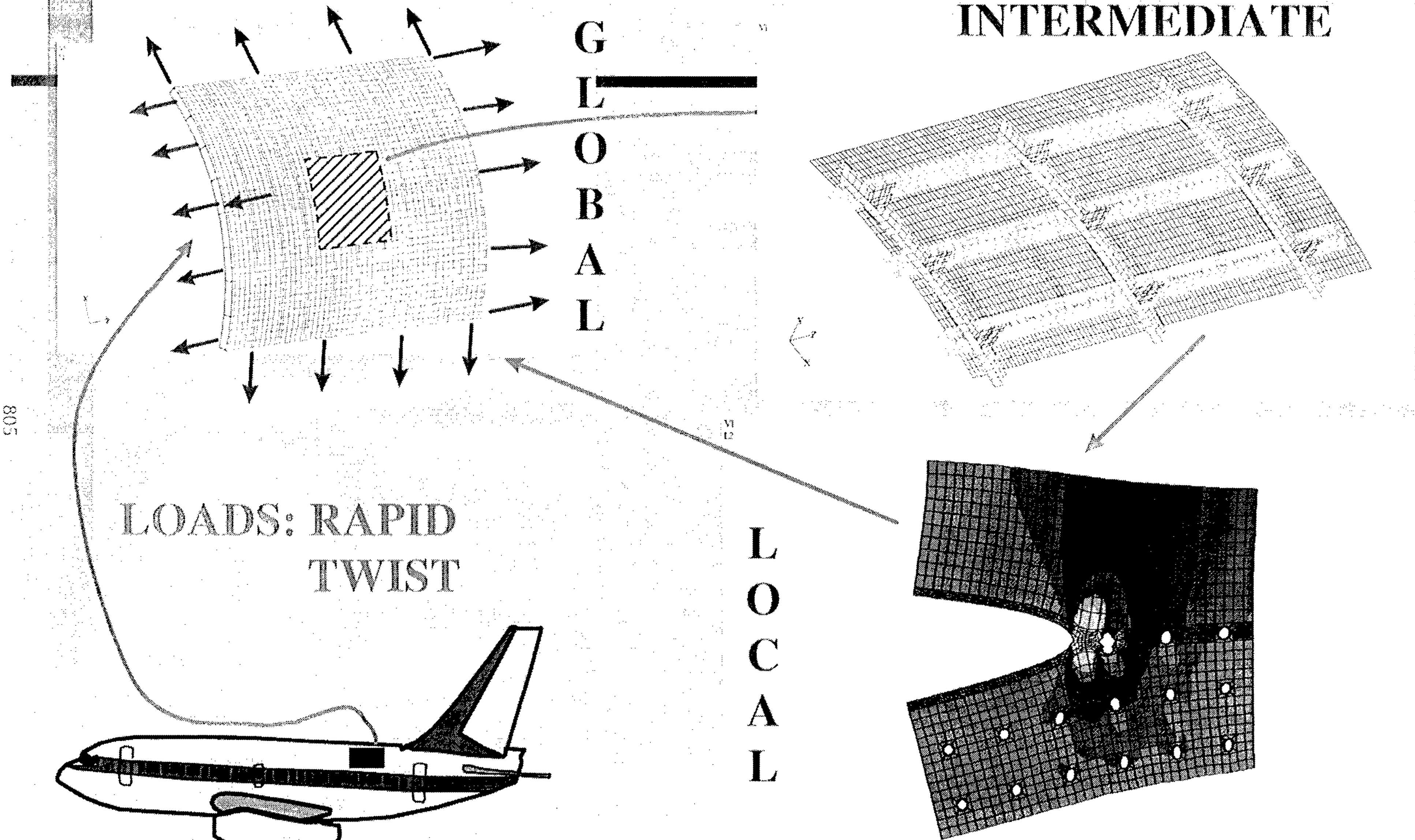

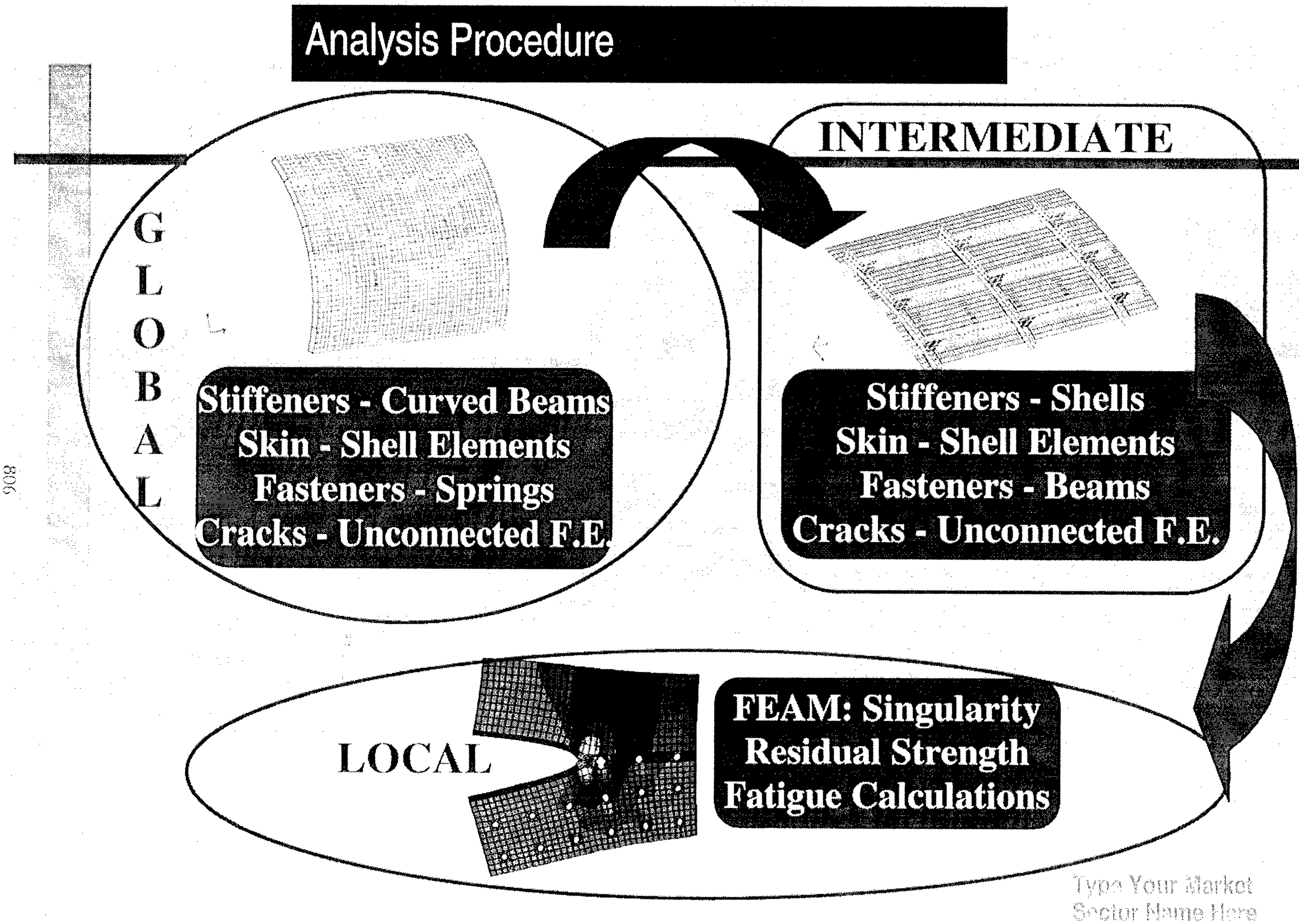
Analysis Procedure
GLOBAL
Stiffeners - Curved Beams
Skin - Shell Elements
Fasteners - Springs
Cracks - Unconnected F.E.
INTERMEDIATE
Stiffeners - Shells
Skin - Shell Elements
Fasteners - Beams
Cracks - Unconnected F.E.
LOCAL
FEAM: Singularity
Residual Strength
Fatigue Calculations
Type Your Market
Sector Name Here

Typical Input AGILE(Fuselage Lap Joint)

```
FS_nFRIntervals     5       # Number Of Frame Intervals
FS_nSTIntervals     8       # Number Of Stringer Intervals
FS_radius           75.0    # Fuselage Radius
...........
FR_E                1.05E7  # Frame Material Young's Modulus
FR_my               0.32    # Frame Material Poisson's Ratio
........
ST_t                0.04    # Stringer Thickness
ST_r0               1.5     # Stringer Height
.........
TS_t                0.04    # Tear Strap Thickness
.........
SC_r0               1.0     # Shear Clip Outside Offset from Frame-Stringer Line
.........
CR_minZ             26.0    # Crack Location (Minimum Z)
CR_maxZ             46.0    # Crack Location (Maximum Z)
.........
IM_maxElementSize 1.0       # Intermediate Model Maximum Element Size
.........
.........
```

Type Your Market
Sector Name Here

Variable Lap Joint Parameters

- Number of Frames/Stringers
- Loading
- Material Properties
- Thickness
- Spacing
- Width of Joint
- Rivet Spacing
- Rivet Diameter
- Model Sizes
- Radius
- Crack Sizes, Numbers,
  And Location

About 30 Lines Of Input

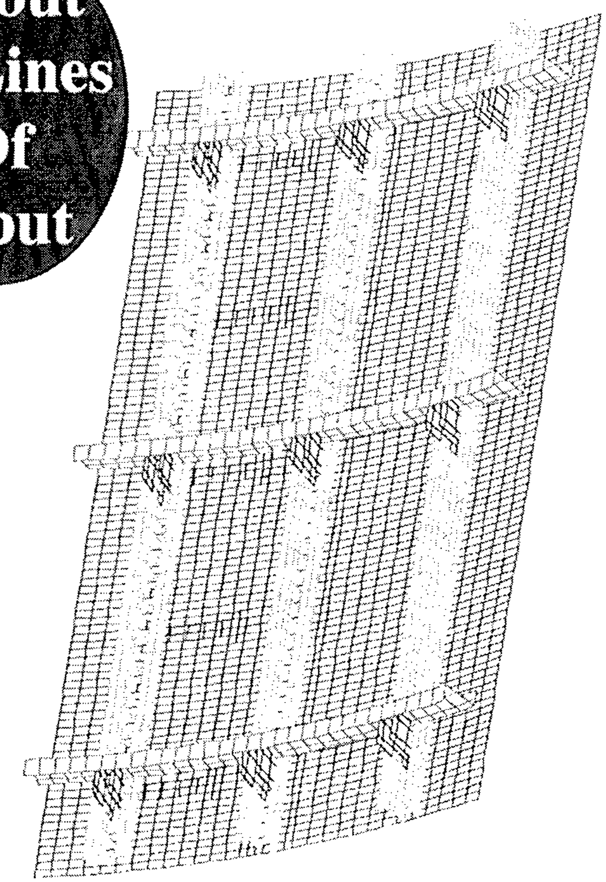

The Method Is Very Old:

- Original Work By Smith, Kobayashi, et al, More Than 20 Years Ago
- Great Improvements Recently With An Improved Analytical Solution (VNA - Solution) and Numerical Methods
- The Method May Now Be Used In the Non-Linear Regime

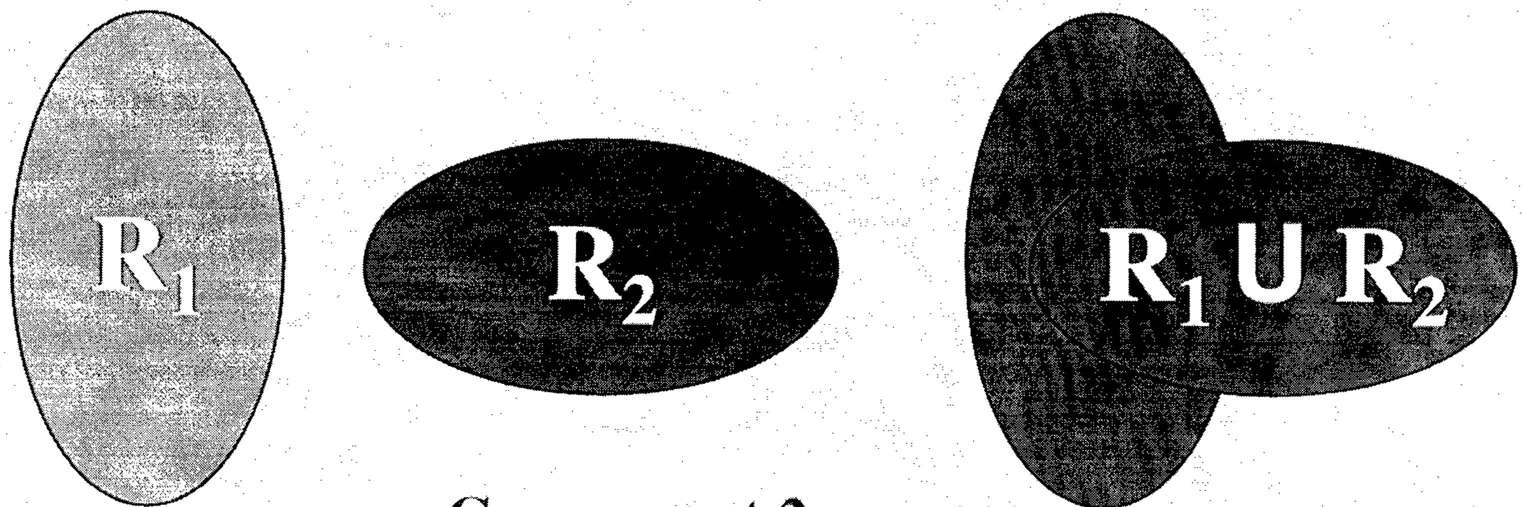

Component 1 Solution Region

Component 2 Solution Region

Schwartz's Solution Region

Sokolnikoff (1956)
Kantorovich and Krylov (1964)

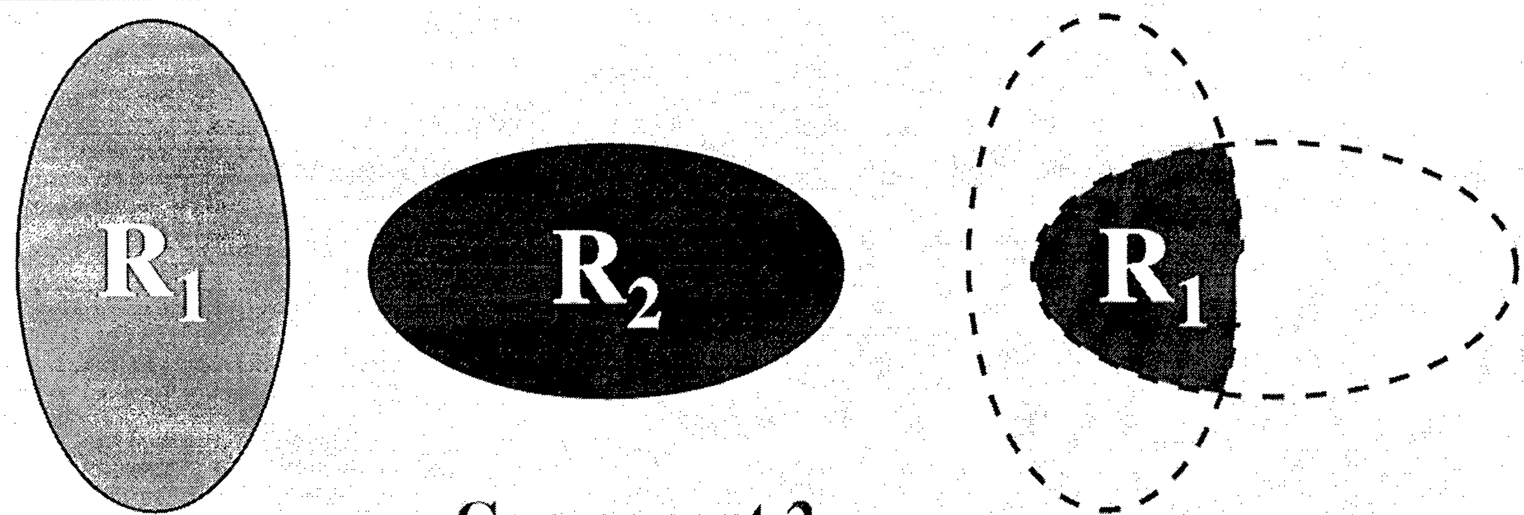

Component 1 Solution Region | Component 2 Solution Region | Neumann's Solution Region

R_1 Infinite Body Solution
R_2 Finite Body (Finite Element Region)

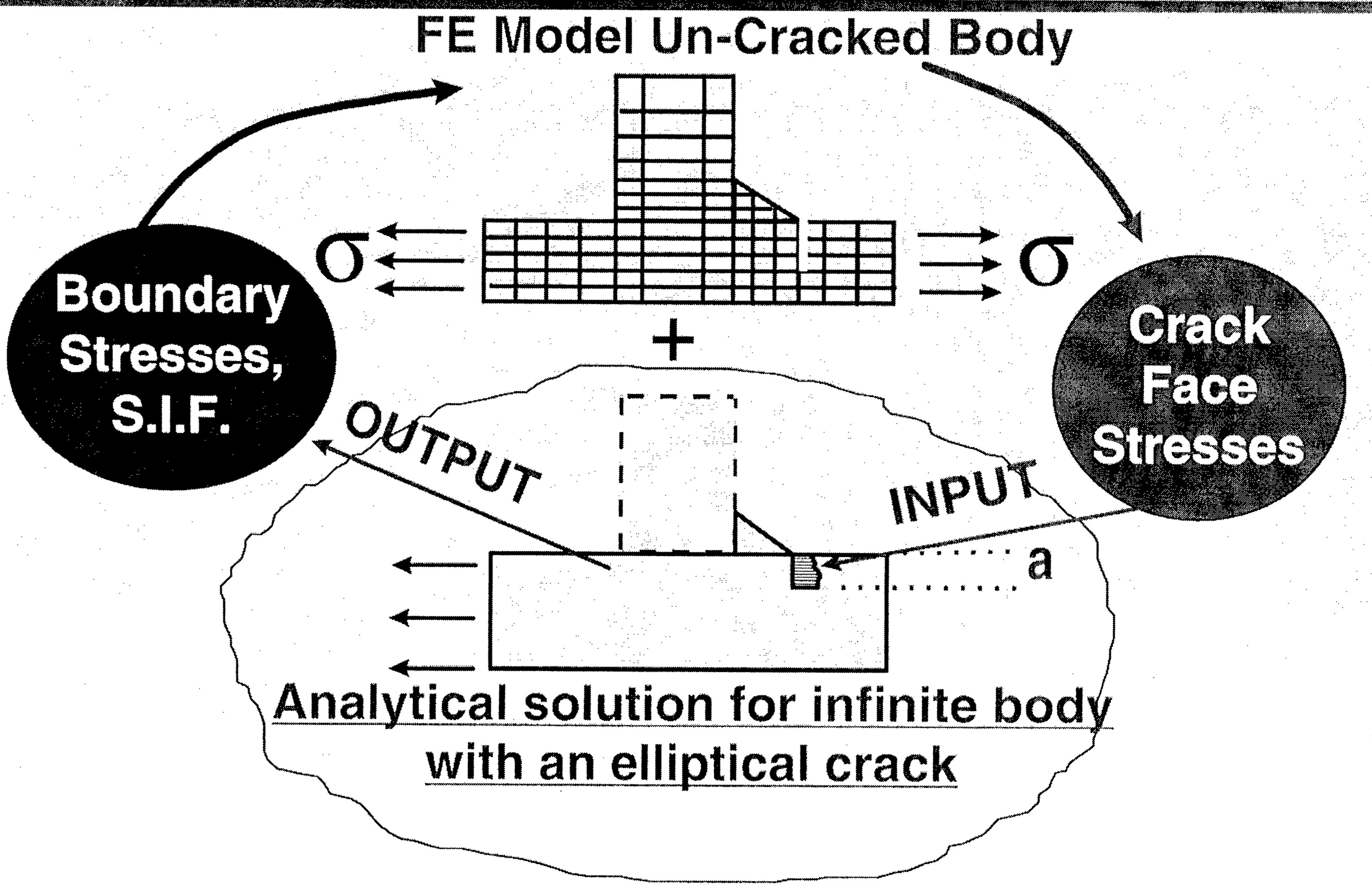
FE Model Un-Cracked Body
σ
σ
+
Boundary Stresses, S.I.F.
Crack Face Stresses
OUTPUT
INPUT
a
Analytical solution for infinite body with an elliptical crack

Finite Element Alternating Method

Today's State-of-the-Art Numerical Fracture Analysis Tool

Crack Mesh Needed for Each Crack and Location
Stiffness Matrix Reduced Each Time
Mesh Development Complicated)

Conventional FEM

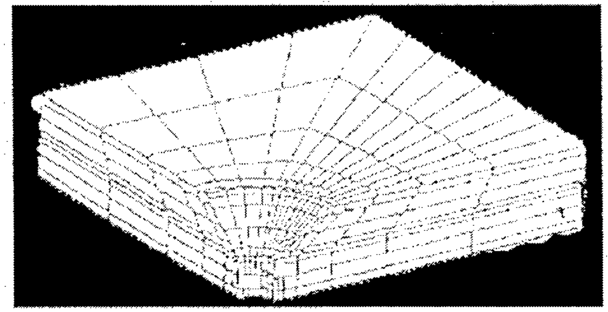

1430 Elements: 6828 Nodes

Countersunk Rivet Hole SIF Calculation

FEAM Alternating Method

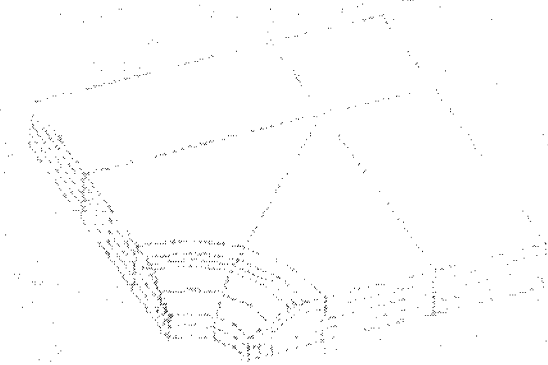

44 Elements: 330 Nodes

- Mesh of Un-cracked Geometry
- Stiffness Matrix Reduced ONCE - Cracks Placed Anywhere
- Mesh Development From Any CAD Package (No Special Crack Tip Meshing Needed)

Type Your Market Sector Name Here

Elastic Problems

- Kobayashi et al (circa 1970)
- Vijayakumar and Atluri (1981)
- Nishioka and Atluri (1983)
- Atluri (1986)
- Rajiyah and Atluri (1989)
- Chen and Atluri (1990)
- Etc.

Battelle Experience

Stonesifer, Brust, and Leis (1992 - Large OD Cylinders)
Brust and Leis (1992 - Creep)
Stonesifer, Brust, and Leis (1993 - Interacting Mixed Mode Cracks)

Aircraft Structures

Nishioka and Atluri (1983b)
Atluri and Tong (1991)
Park and Atluri (1992, 1993)
Park, Sing, Pyo, and Atluri (1993)
Etc.

2D Elastic-Plastic Case

Nikishkov and Atluri (1993)
Park, Sing, Pyo, and Atluri (1993)
Wang, Brust, and Atluri (1997 - Series of Three Papers)

NIST MSD-4 Elastic Analysis Comparison

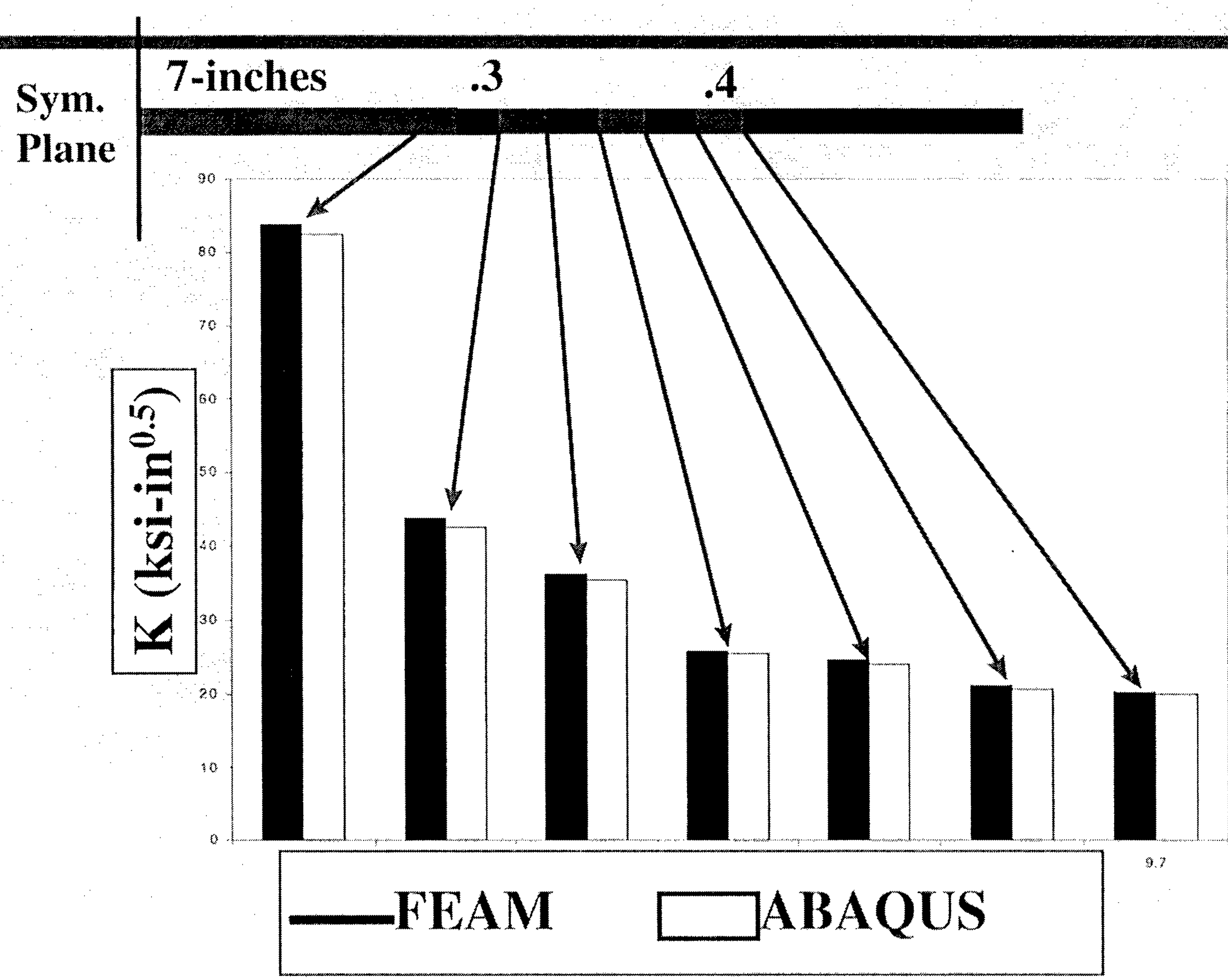

Static Crack Elastic-Plastic Comparison for MSD-4

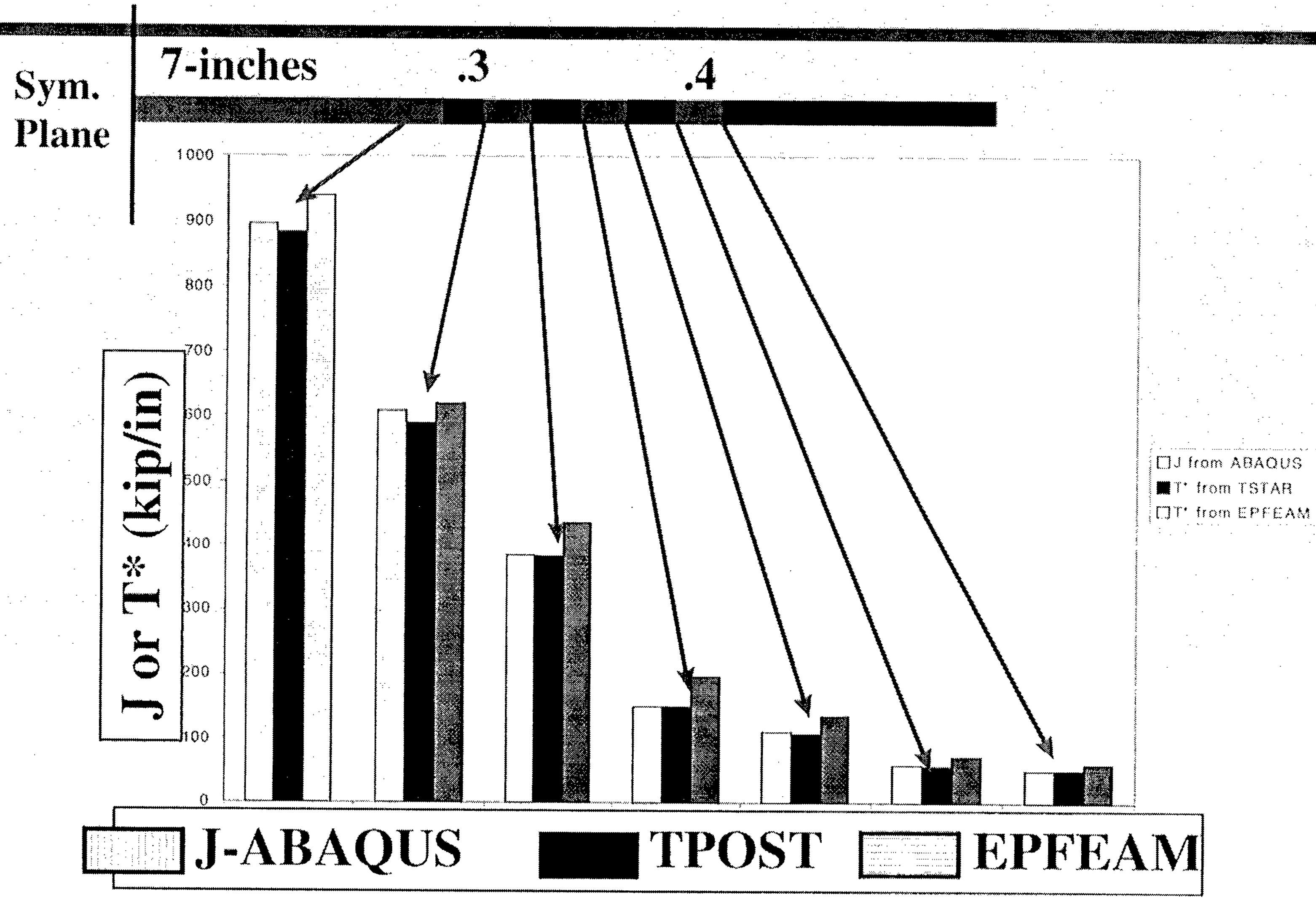

Residual Strength Predictions - EPFEAM

Options: K (Plastic Zone Correction), J, T*, CTOA
Need : R-Curve

NIST Test Comparisons: 10 MSD Tests

Documentation: "The Elastic-Plastic Finite Element Alternating Method (EPFEAM) and the Prediction of Fracture Under WFD Conditions in Aircraft Structures: Parts I, II, III" by L. Wang, F. W. Brust, S. N. Atluri FAA Report Series (Also Published in Computational Mechanics)

CTOA Documented in NASA Langley Reports (Newman)

MSD-4 - FAA report

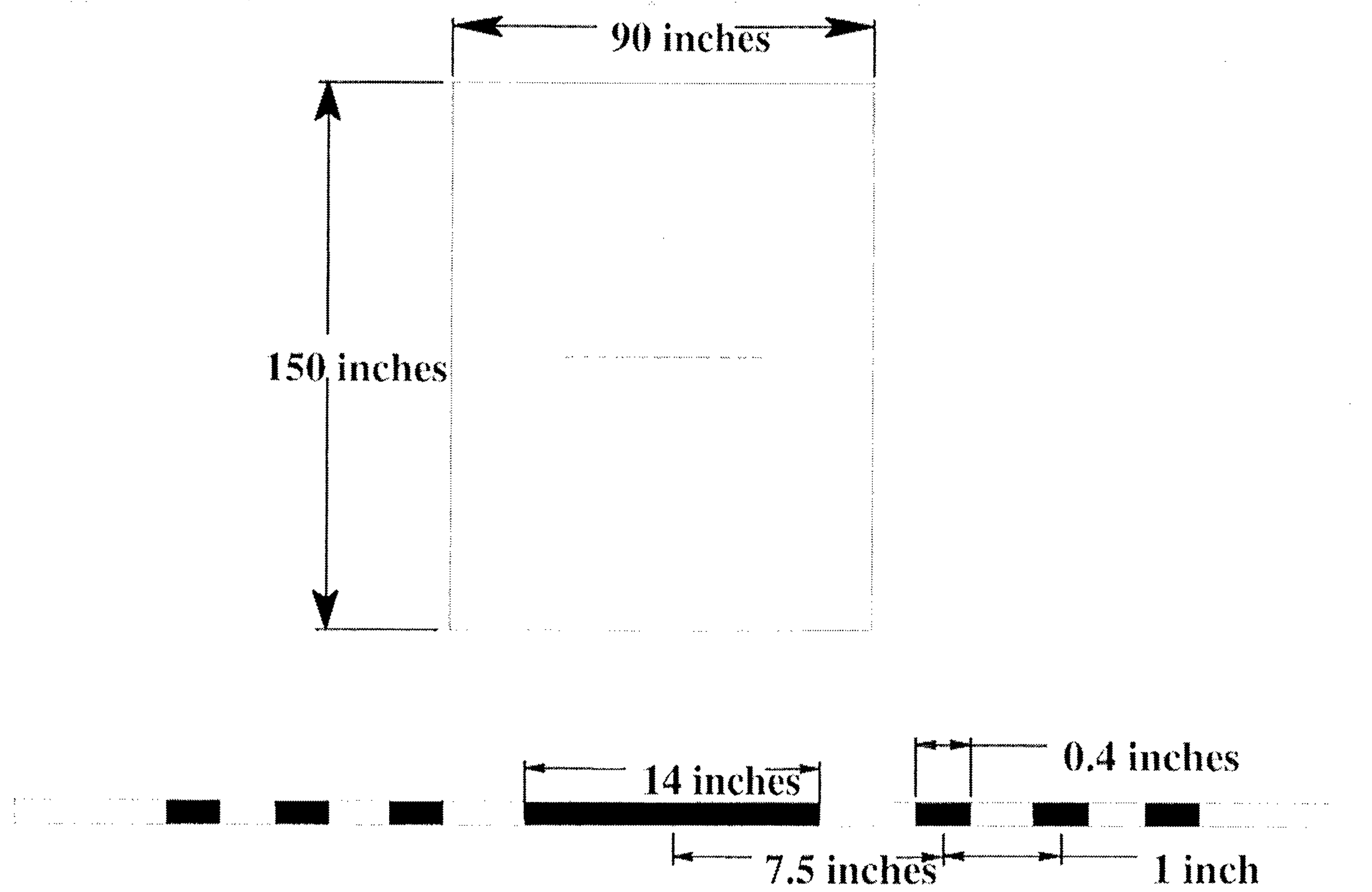

Derivation of epsilon for MSD-4 analysis

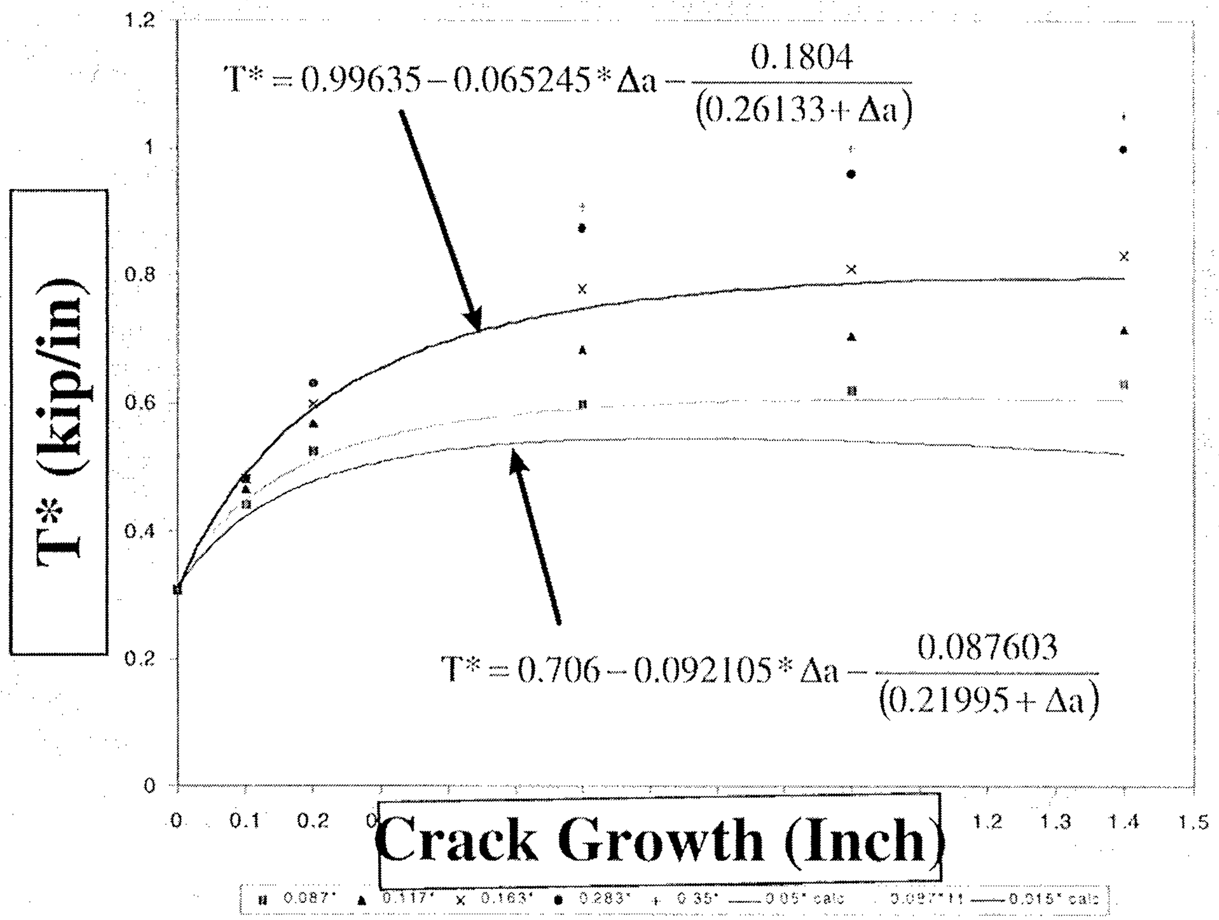

MSD-4 Load Predictions

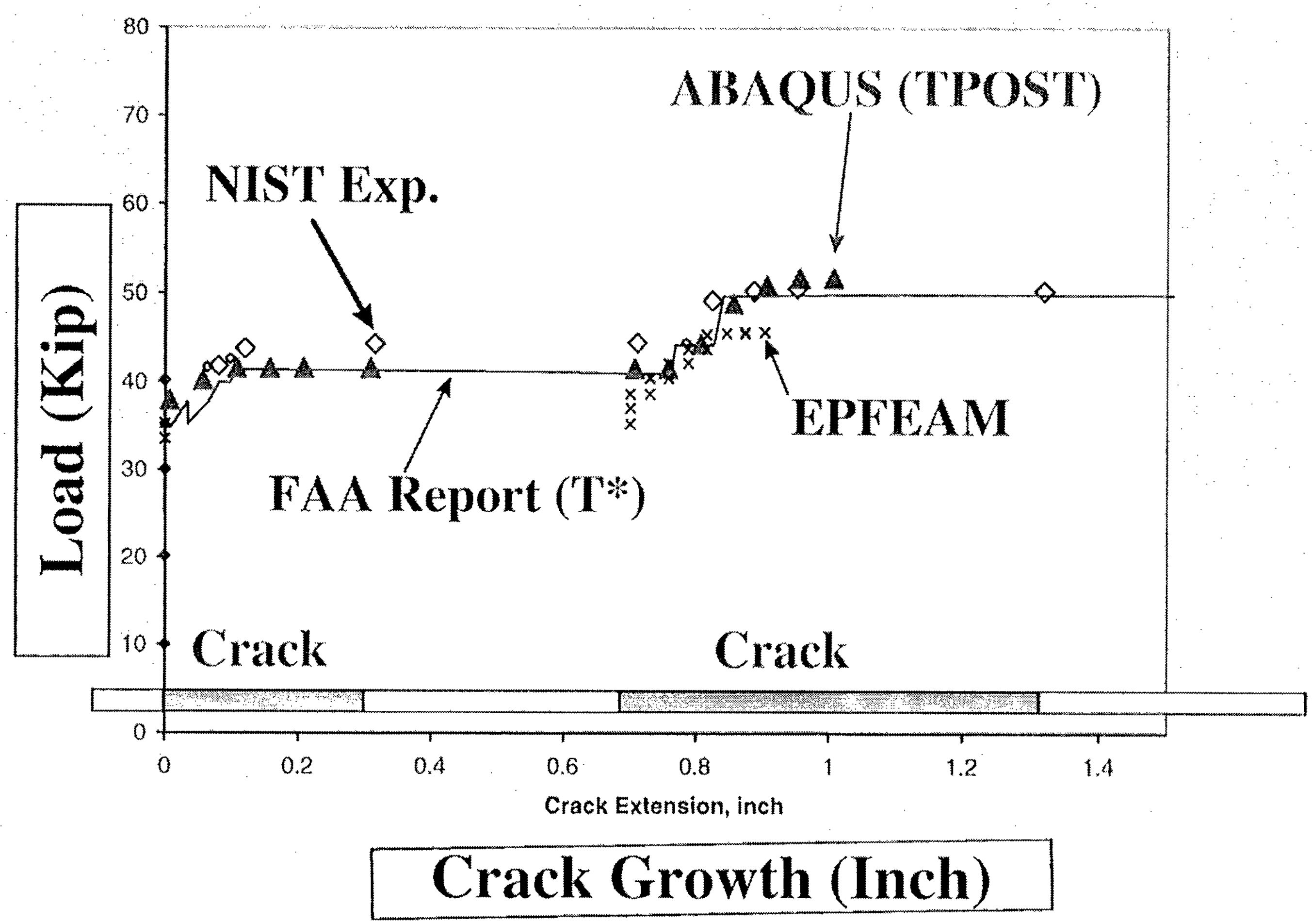

MSD-4 Load Predictions - with CTOA

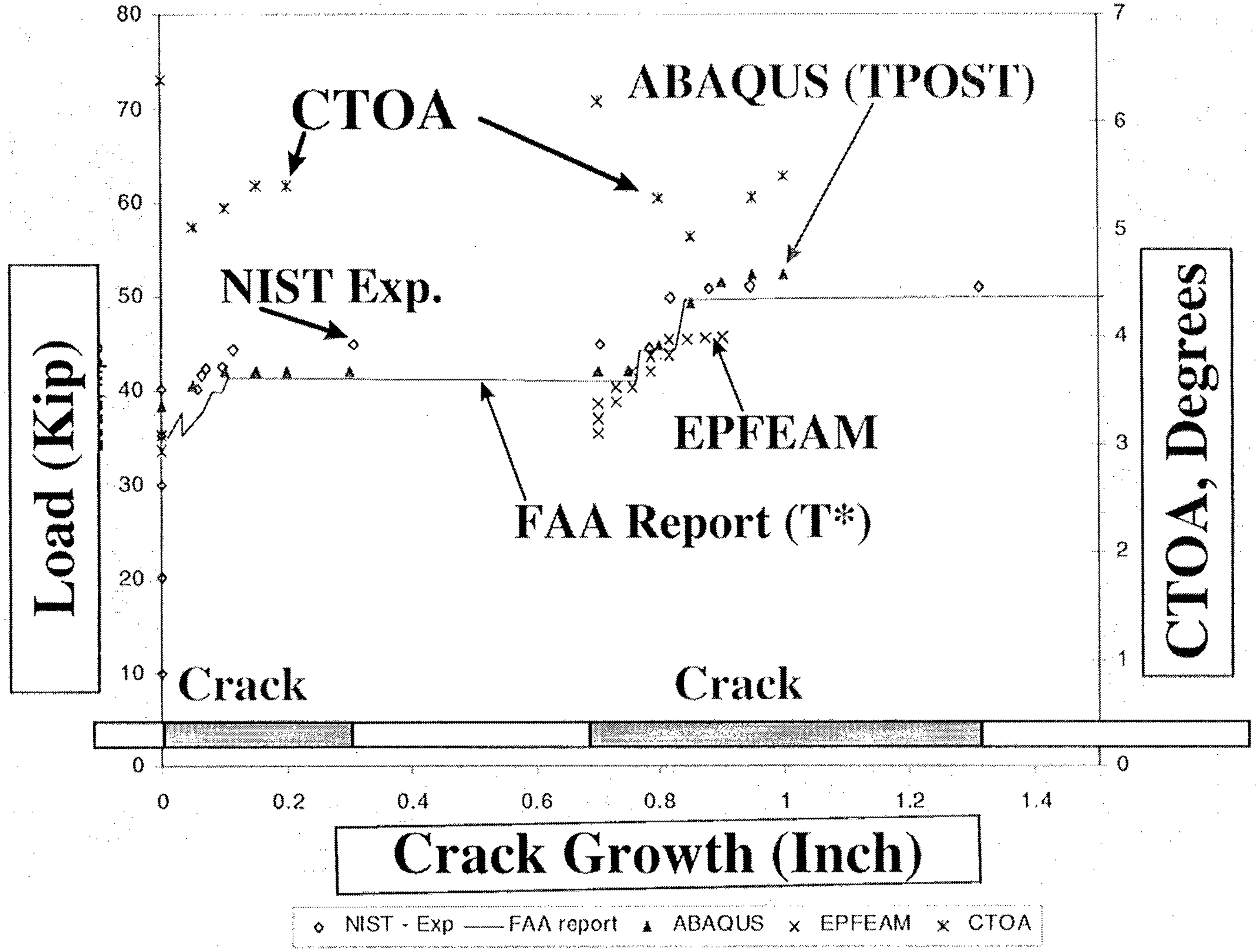

Plastic zone size at a=8.0" - ABAQUS

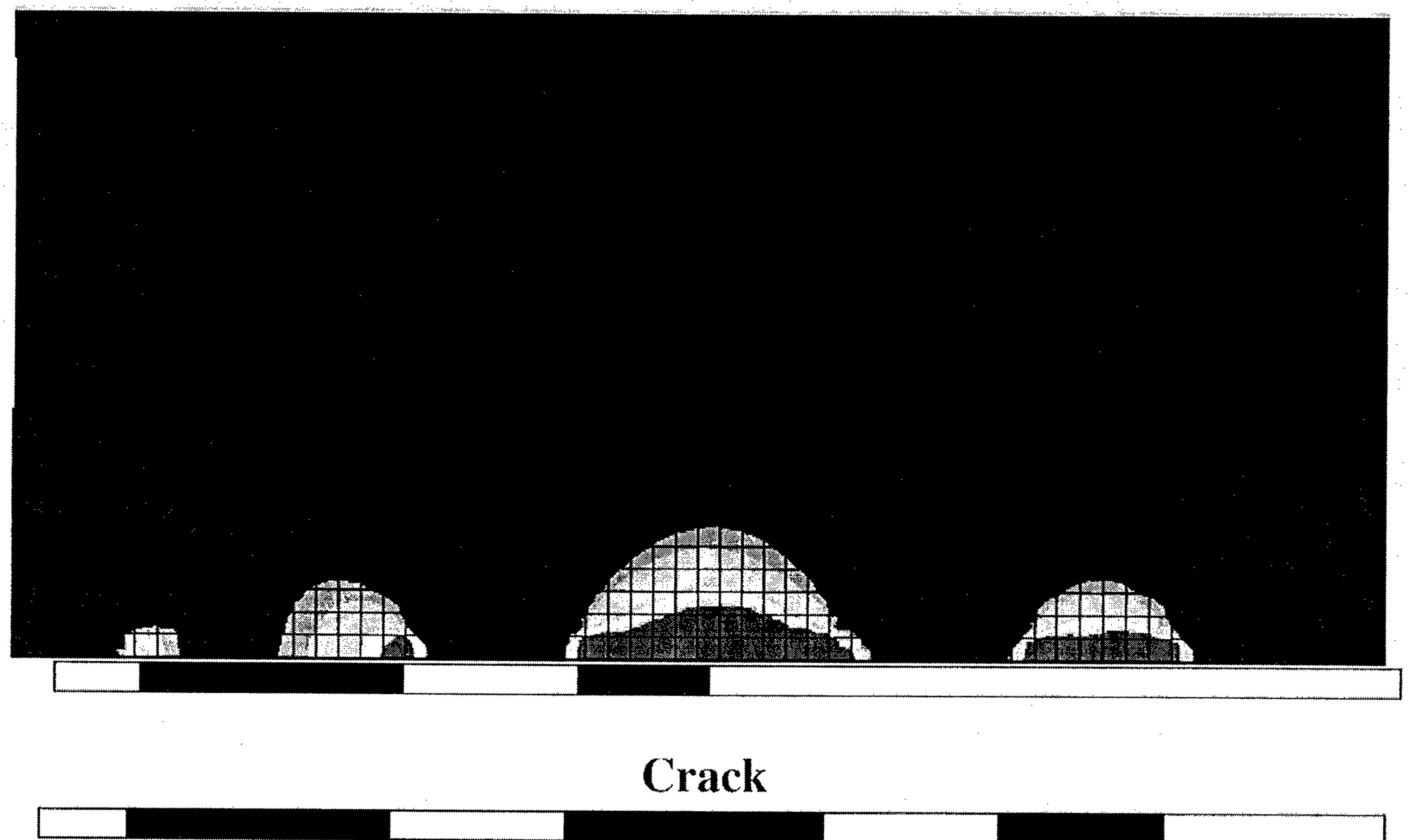

Plastic zone size - EPFEAM

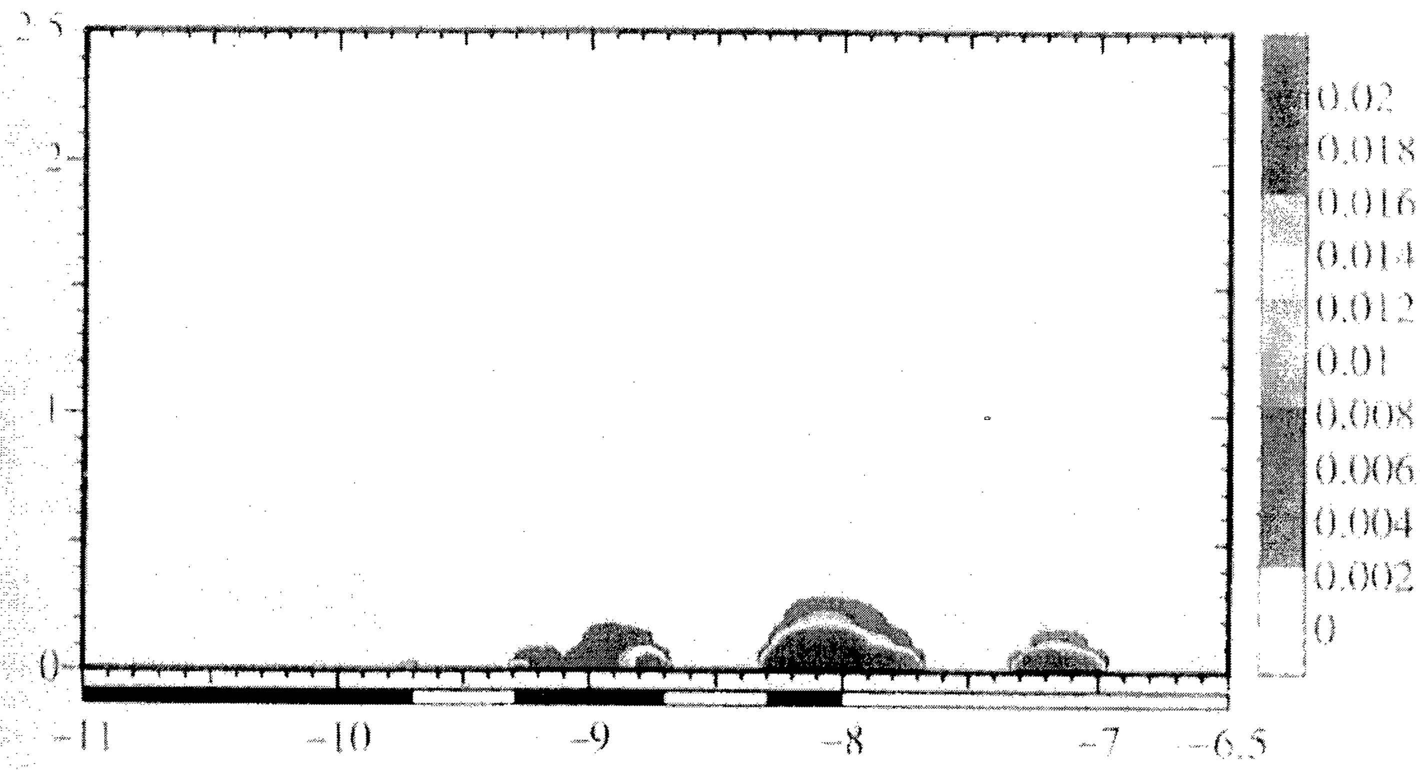

(b) $a = 8.0$ in

SF3D Verification

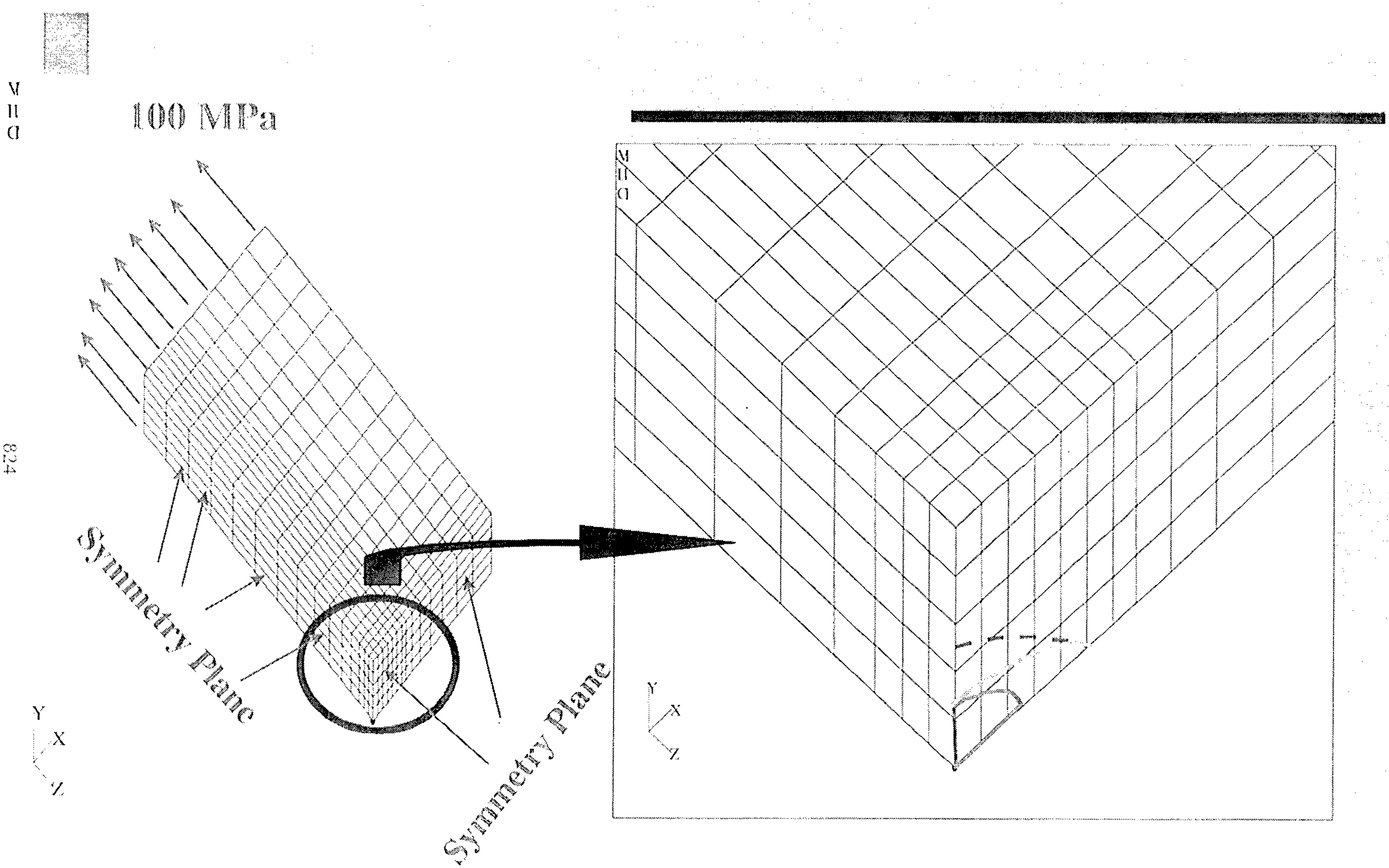

3D FEAM Validation

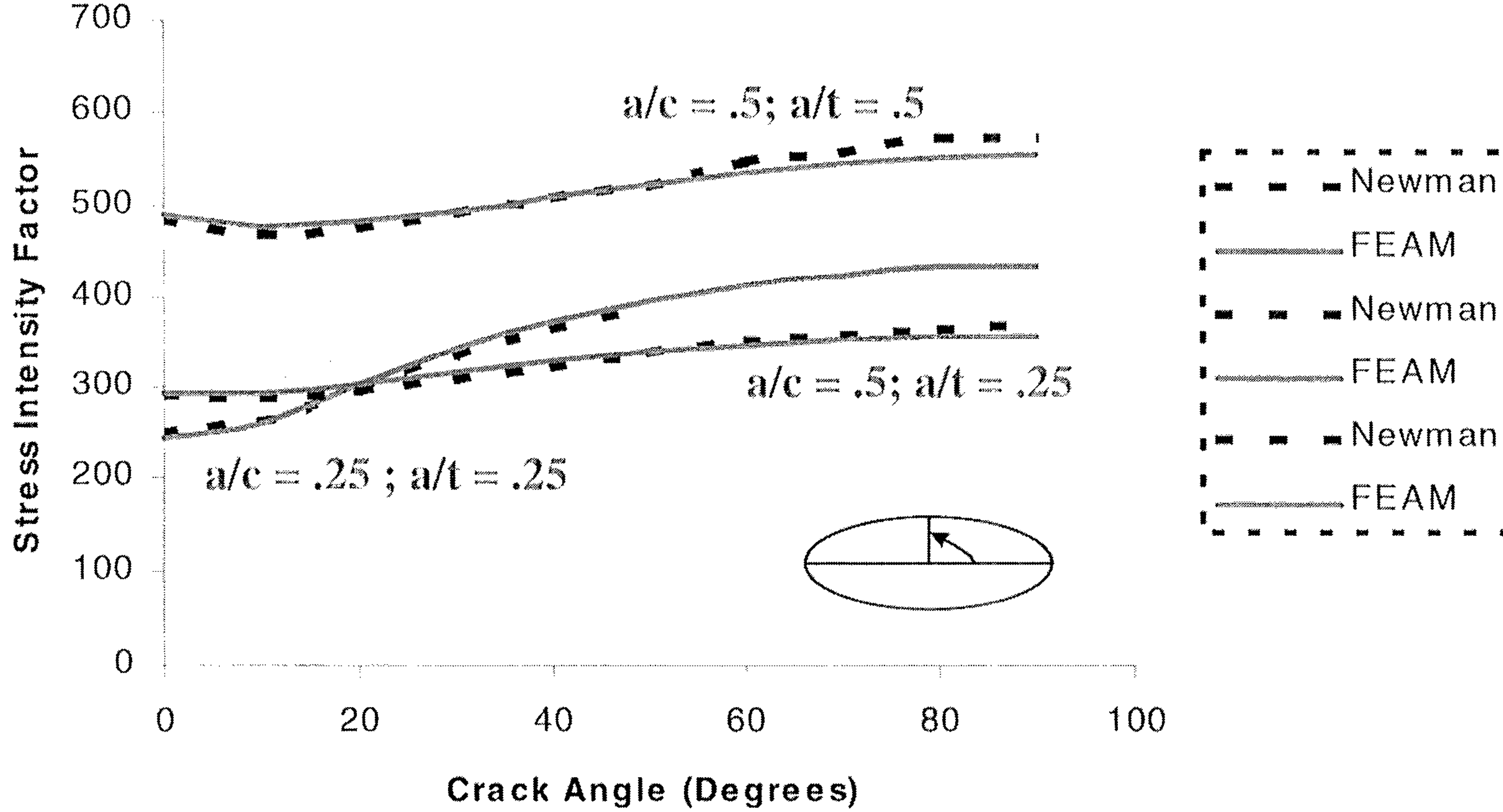

Type Your Market Sector Name Here

Deterministic Assessment/Validation

- Seven example problems Validated To Date
- Lap Splice Case - Partial Two-Bay Crack With MSD
- Ran comparison between AGILE (STAGS,FEAM) and ABAQUS
- Validation With ANSYS and ABAQUS With Battelle T* USER Routines

Deterministic Assessment/Validation

Example 3

- Fuselage Radius = 75 in
- 5 frame intervals at 20 inch spacing
- 8 stringer intervals at 10 inch spacing
- half width of lap joint = 1.5 inches
- 20 inch lead crack with two MSD cracks at the rivet hole ahead of the crack
- Pressure = 8.5 psi

Global Model - Example 3

Loads From Rapid or User Input

AGILE/STAGS

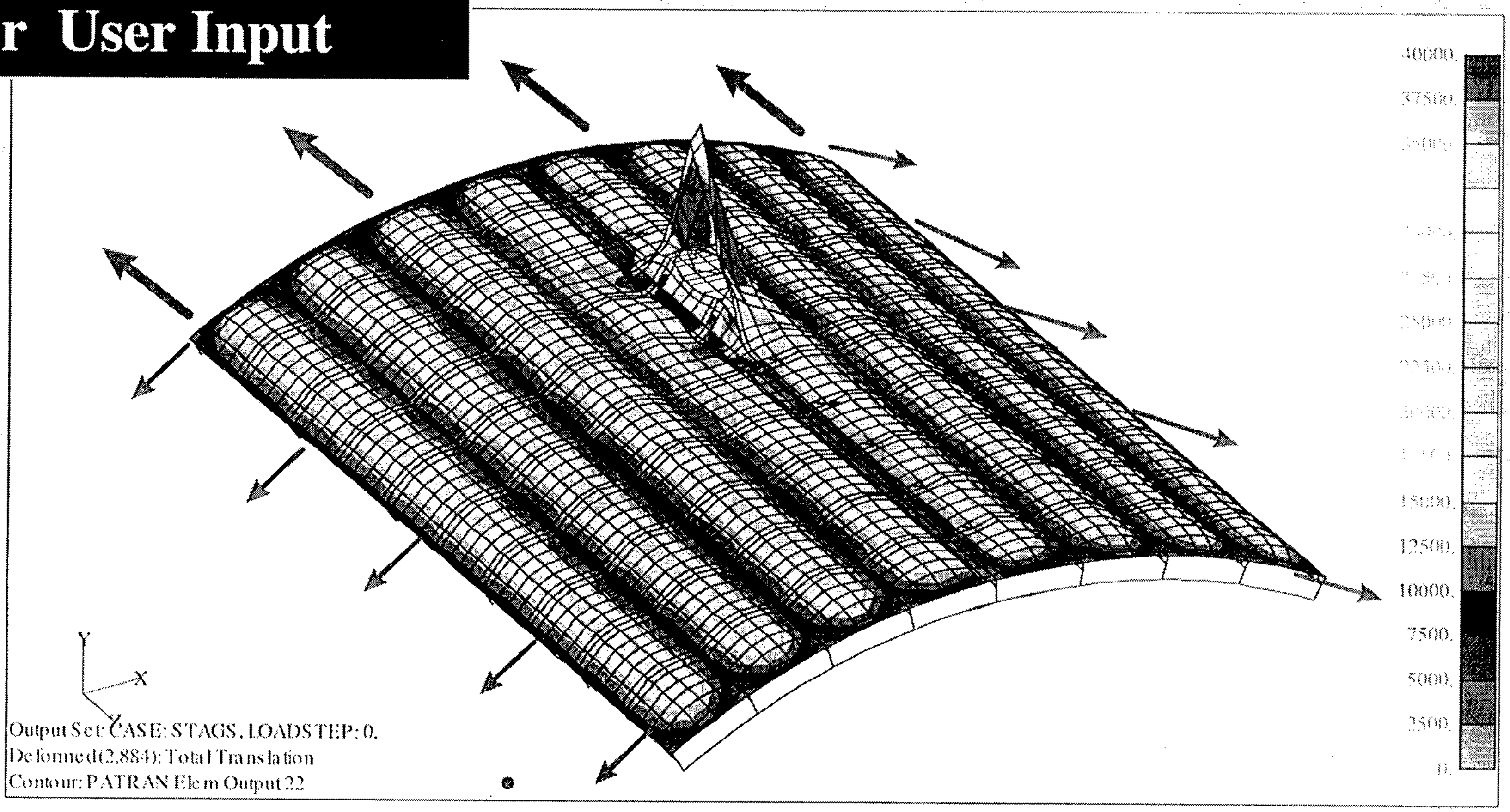

Intermediate Model - Example 3

Understructure

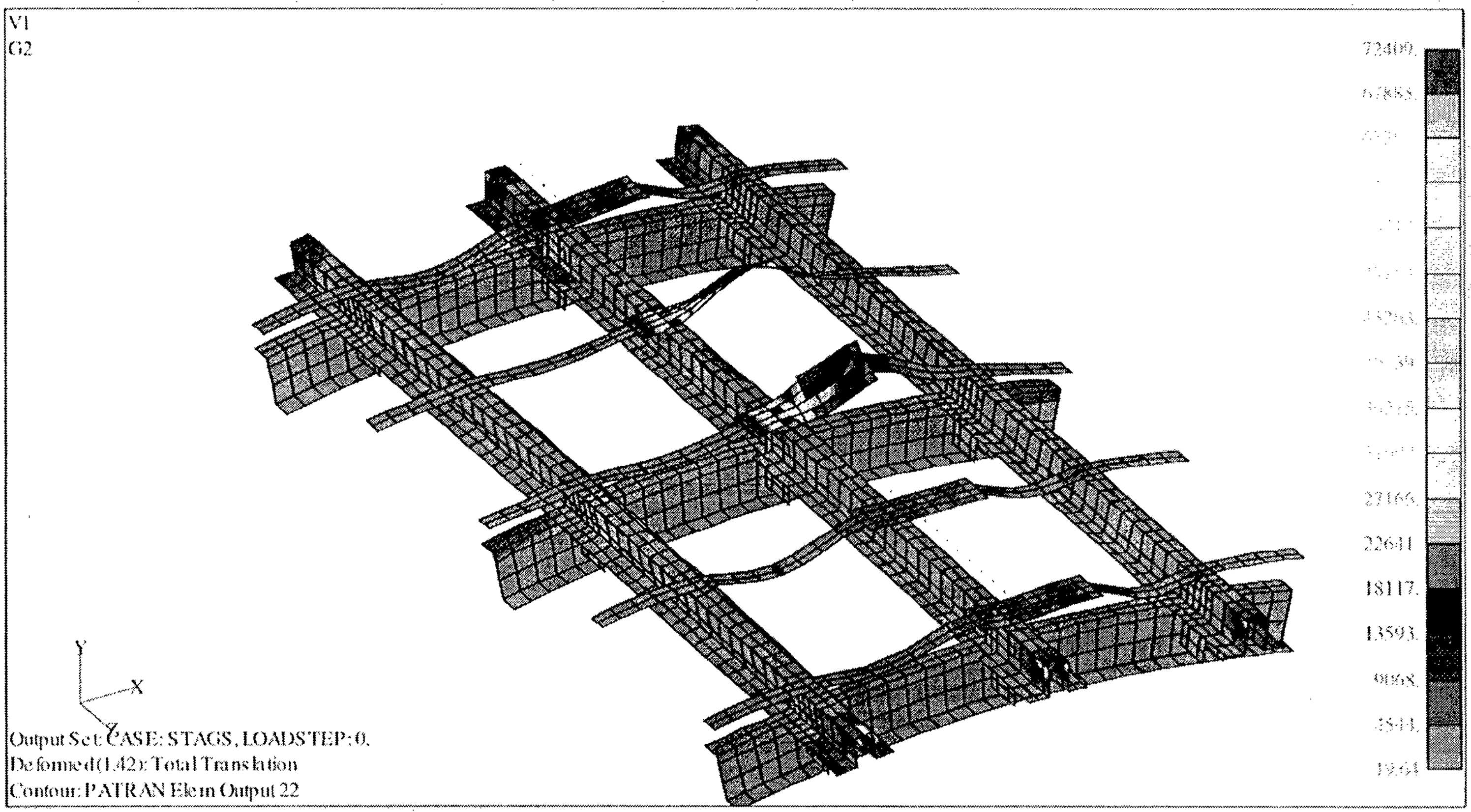

Deterministic Assessment/Validation

Equivalent Von-Mises Stress

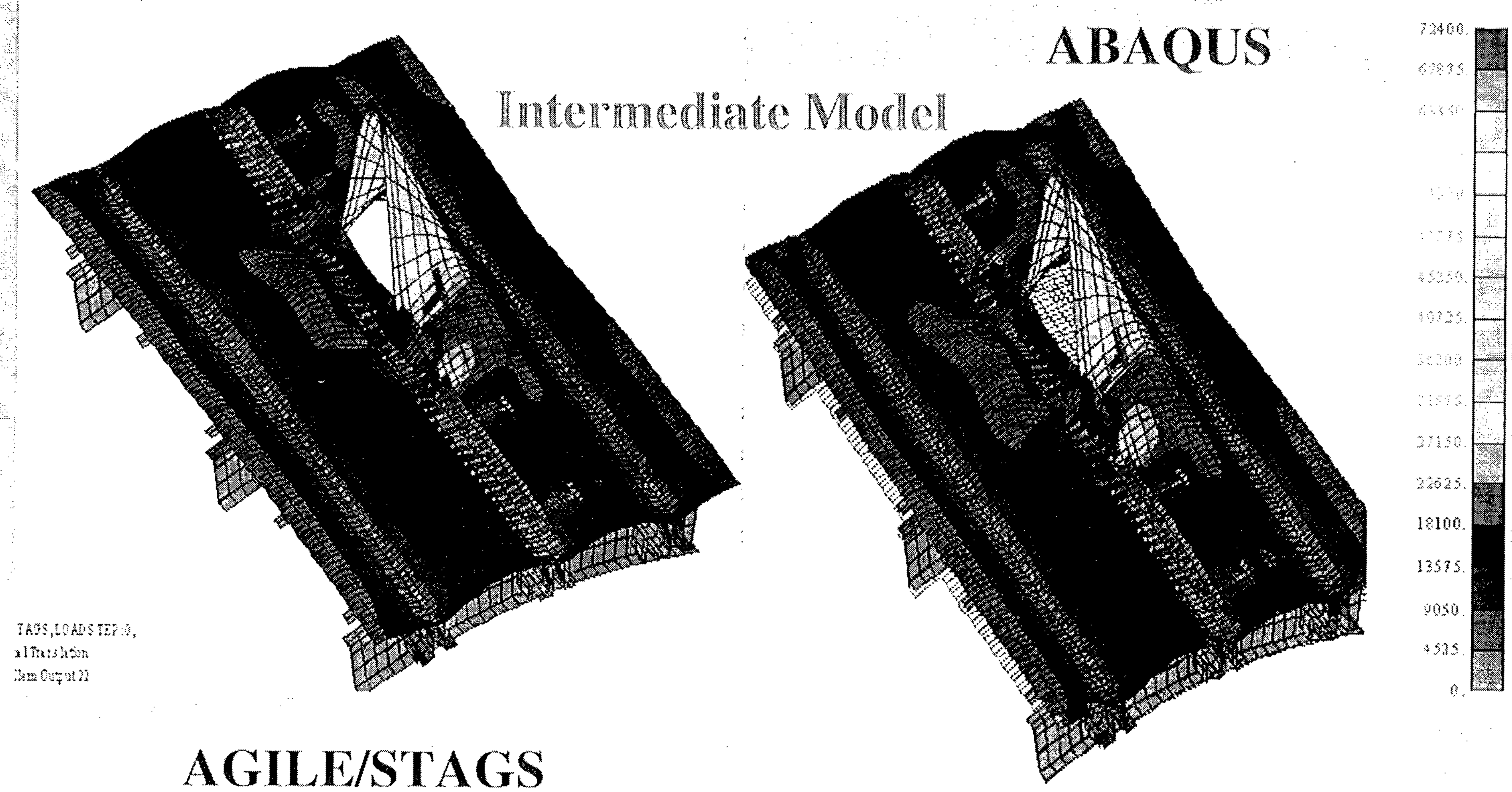

Deterministic Assessment/Validation
Local Model

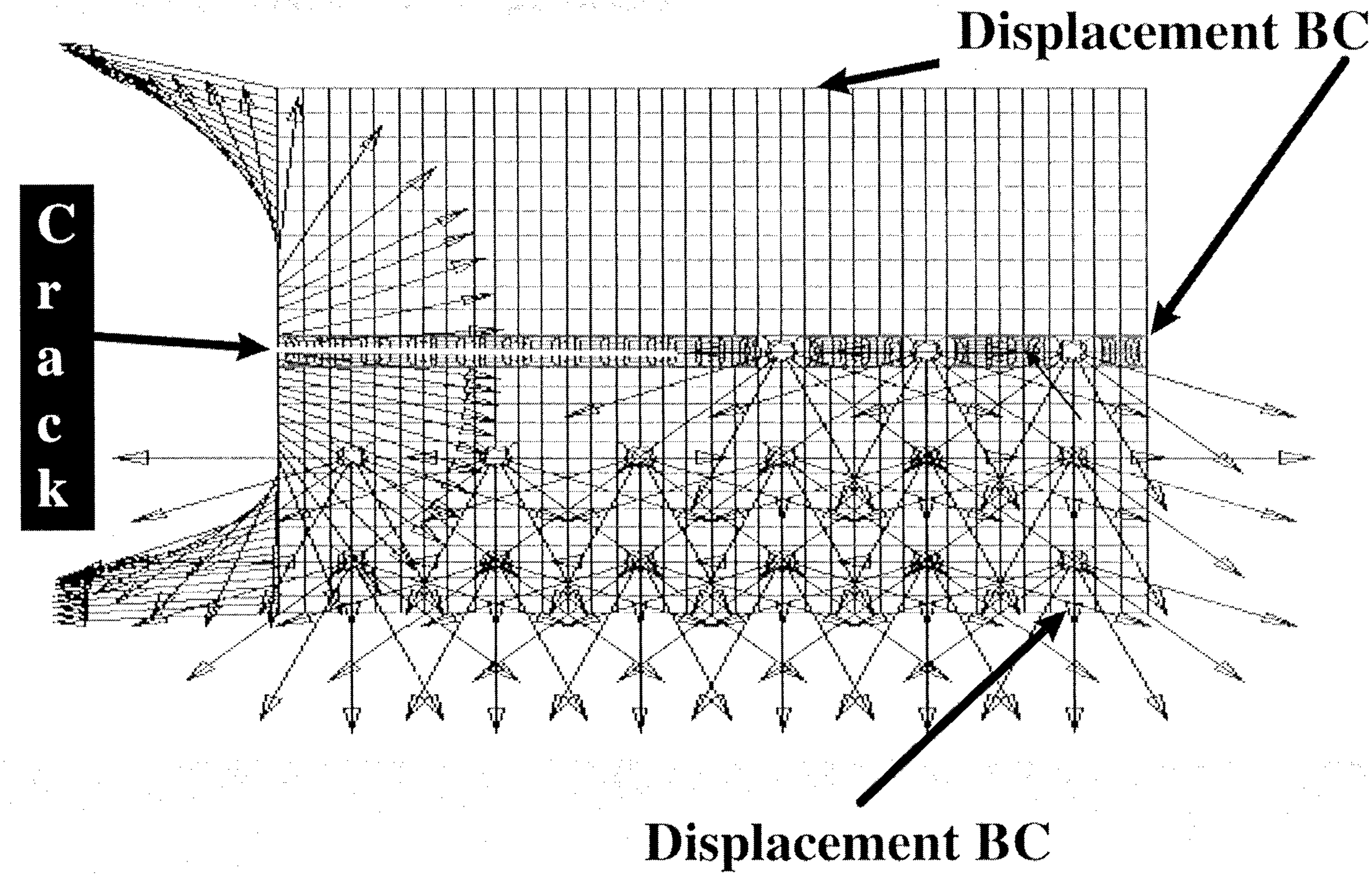

Deterministic Assessment/Validation Local Model - ABAQUS Contour

Y-Normal Stress

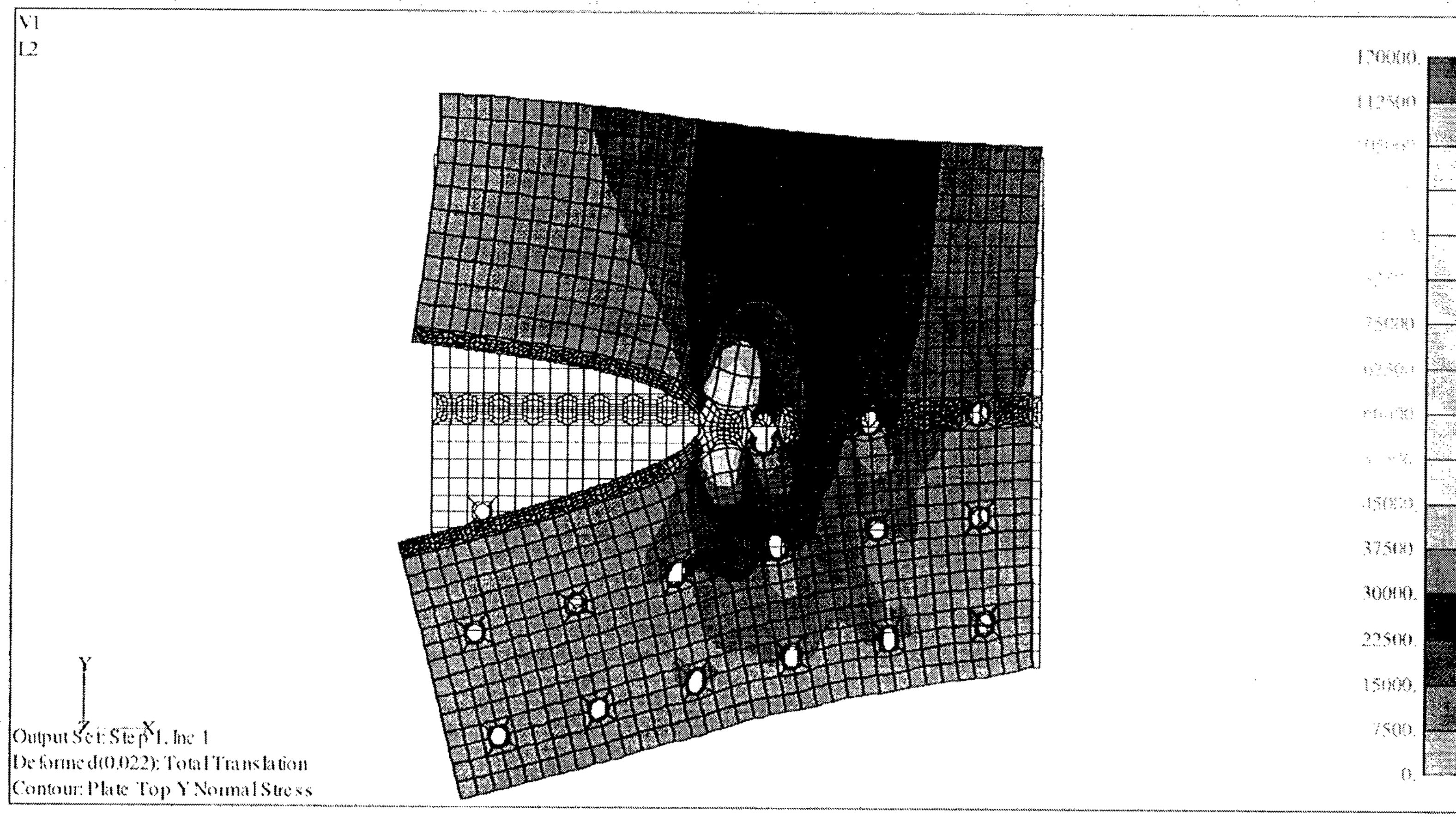

Deterministic Assessment/Validation
Local Model - Y-Stress at Crack Plane

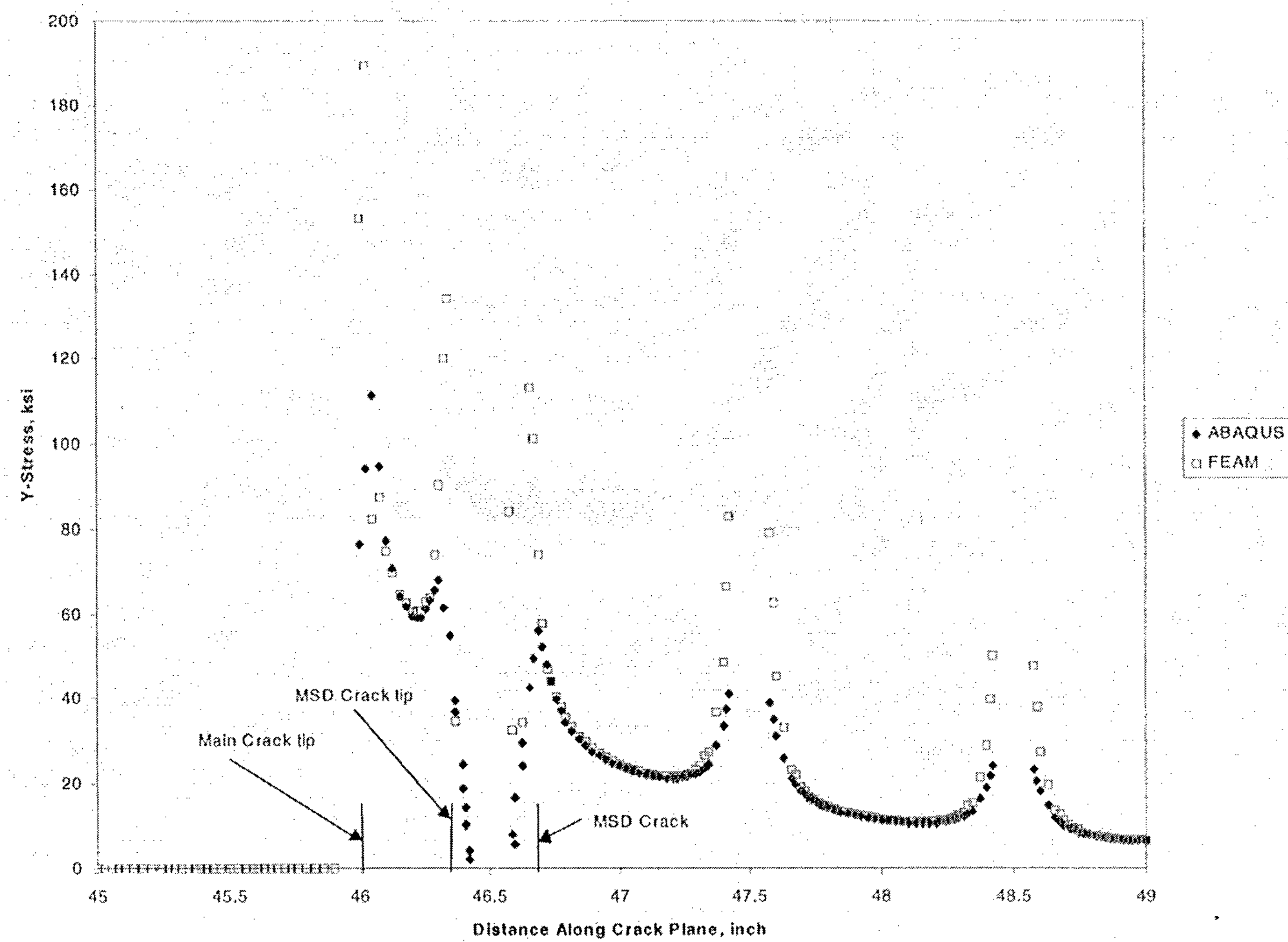

FEAM/ABAQUS K Comparison

	ABAQUS*	FEAM
Crack tip 1 (main)	59.1 ksi-in $^{0.5}$	58.8 ksi-in $^{0.5}$
Crack tip 2 (MSD)	34.8 ksi-in $^{0.5}$	39.5 ksi-in $^{0.5}$
Crack tip 3 (MSD)	33.2 ksi-in $^{0.5}$	33.6 ksi-in $^{0.5}$

* - The calculated J-integral from ABAQUS for the MSD cracks was NOT path independent. The J-integral WAS path independent for the main crack

Fatigue and Fracture: Plans and Goals

Purpose: Review, Choose, and Coordinate the Integration of the (1) Stress Analysis, (2) Fatigue, and (3) Fracture Methods and Codes Which Will Be Part of the PWFD Code.

(1) Stress Analysis

Global → Intermediate → Local

Global: STAGS - Shells, Plates, Beams, Shear Intermediate Fasteners

Elements

Local:

Continuum 2-D, 3-D Solid

Skin MSD - TWC

Frames/Stringers/etc. - SC, TWC

Fatigue and Fracture: Plans and Goals

(2) Fatigue: NASGRO or FLAGRO

(3) Fracture Codes & Parameters: BEM (FLAGRO) FEAM, EPFEAM

Fatigue: K Based (FEAM)

Residual Strength:
- K Based (FEAM)
- Plastic Zone Estimate (FEAM)
- R6 (FAD) FEAM, EPFEAM
  (To Obtain K, J)

(Definition of Limit Load ?)

- J-Integral (EPFEAM)
- T*-Integral
- CTOA (EPFEAM)

Global/Intermediate Model

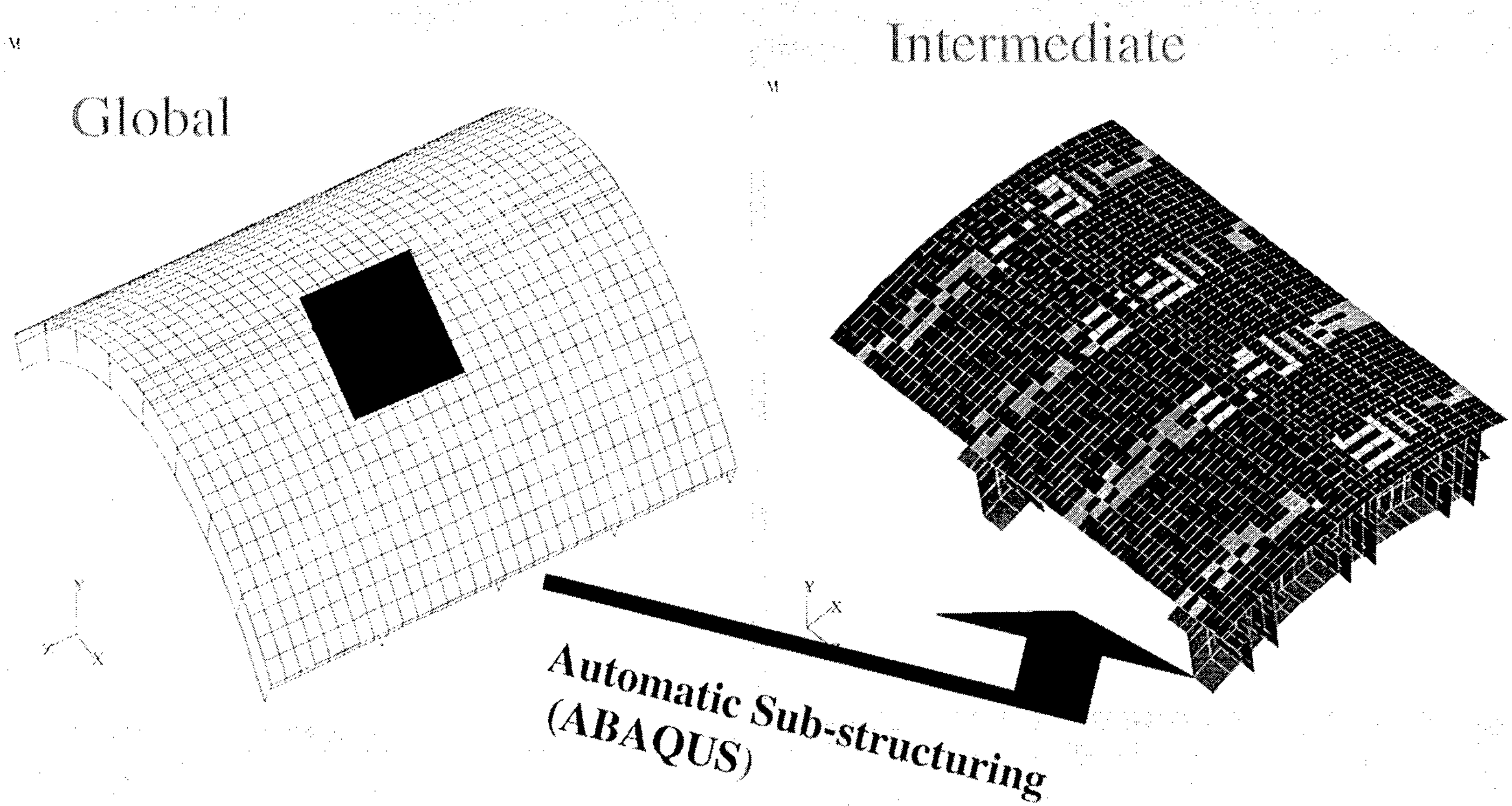

Two Bay Crack Example

AGILE - Global Model

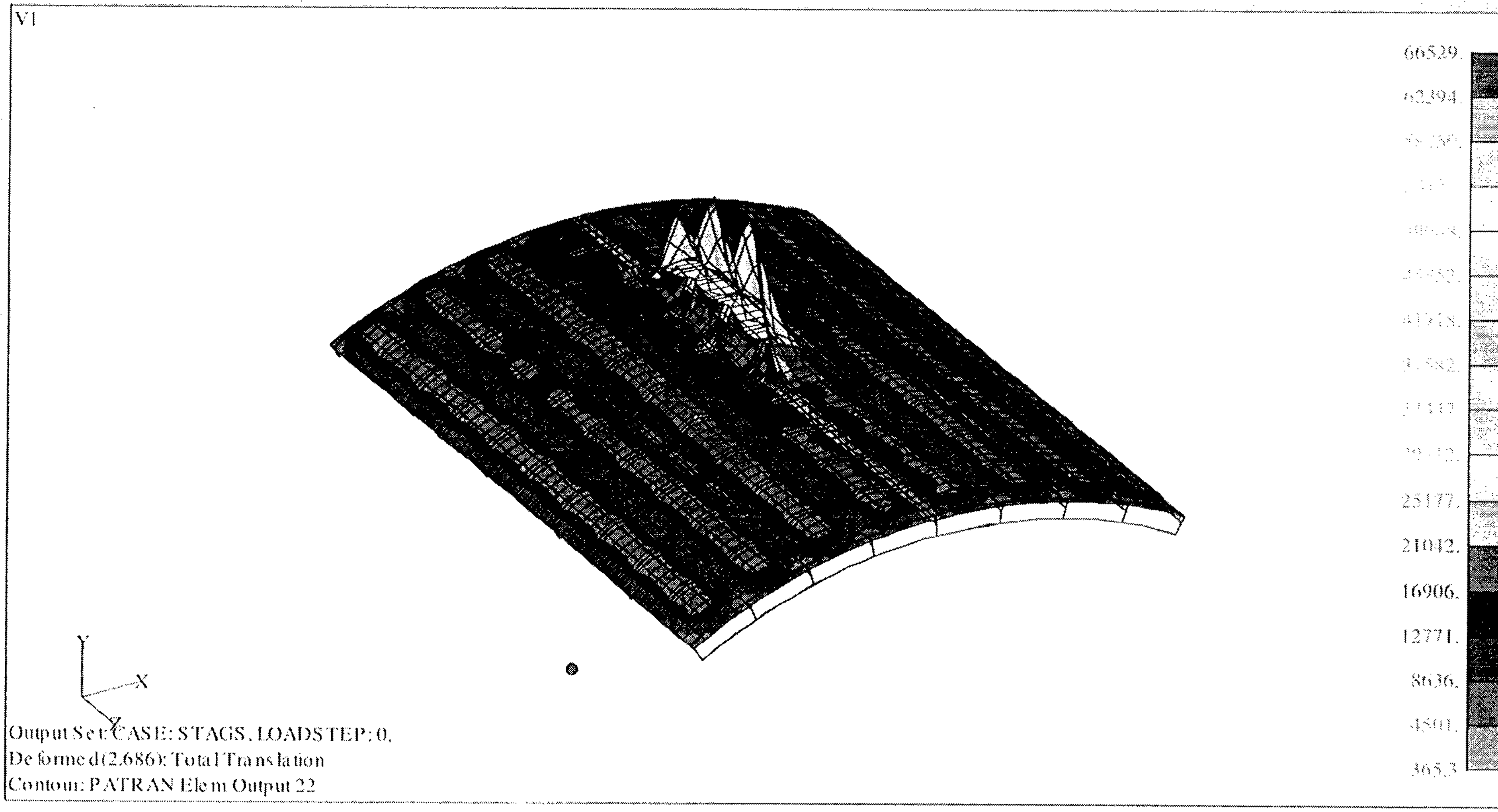

Two Bay Crack Example

AGILE - Intermediate Model

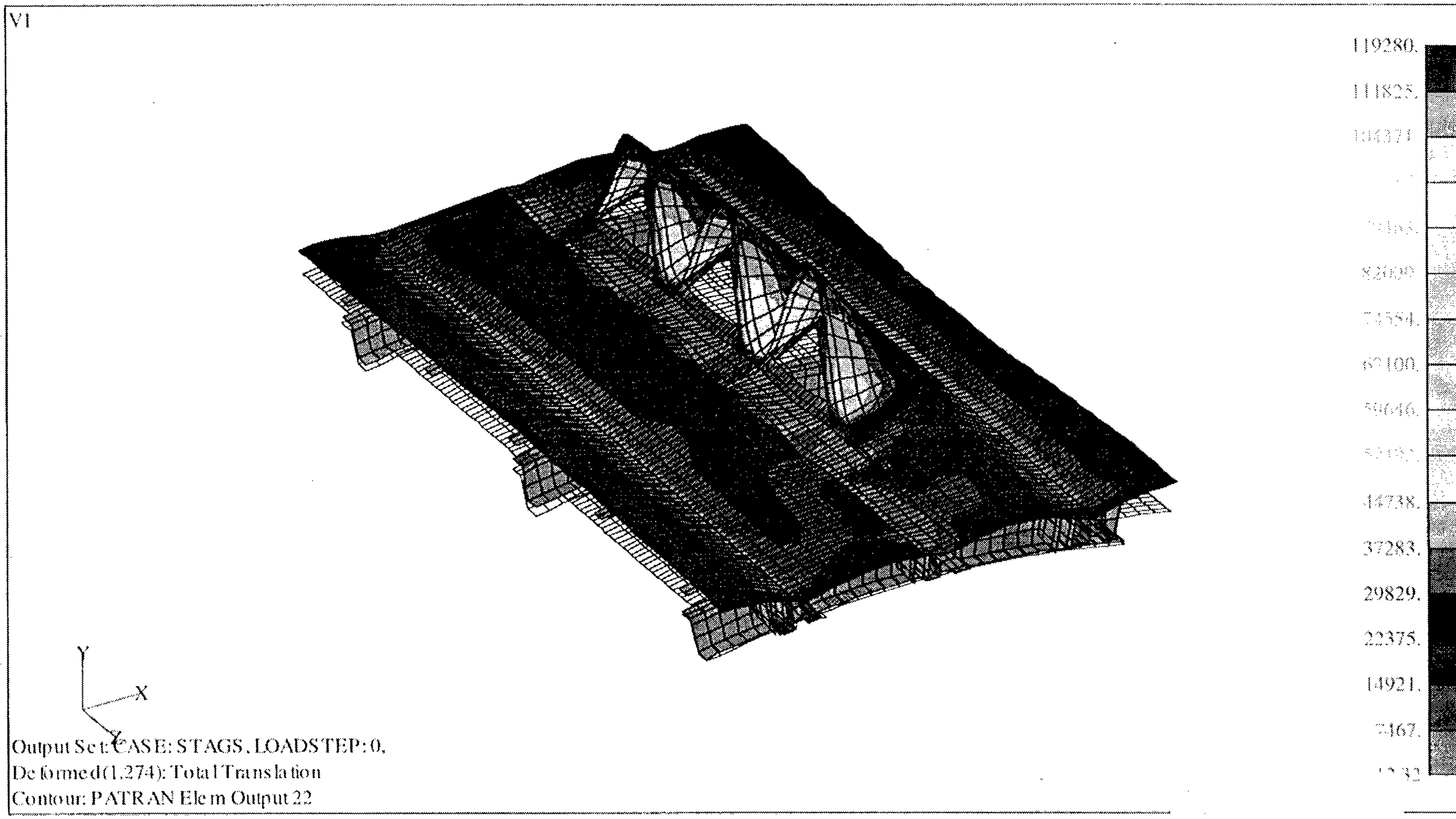

Damage Mechanisms

- Fatigue: AFGRO, NASGRO, Forman
- Corrosion: Local impacts and Patches
  - Fatigue impact
  - Stress impact
  - Repair
- Fracture
  - Link-up
  - Residual strength

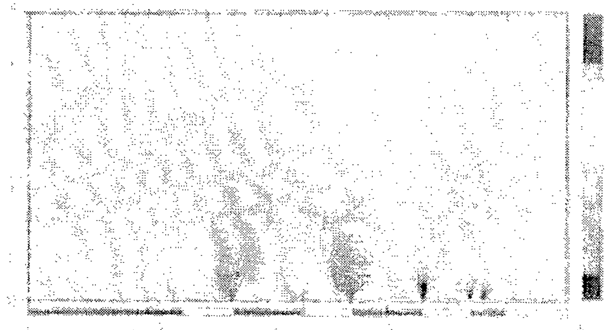

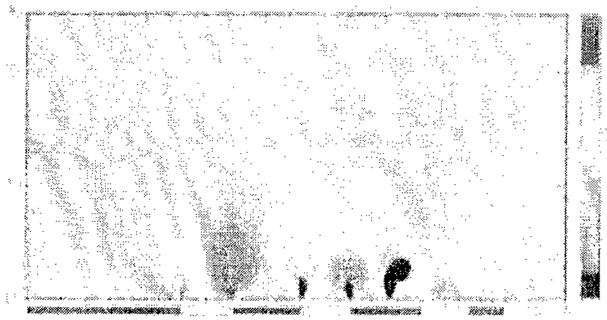

Probabilistic Analysis

- Relative impacts
  - Loadings
  - Material properties
  - Initial damage
  - Corrosion
- Includes uncertainty as design variable
  - Critical to repair
  - Risk management

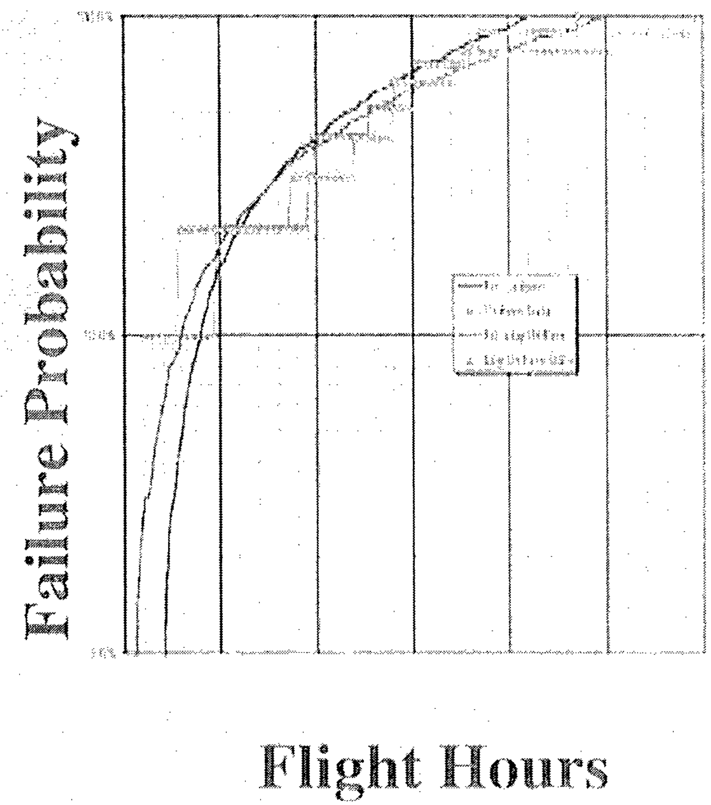

Deterministic Program Status

- AGILE/STAGS - Automatic Mesh Development
  Physical Parameter Input Validation -
  7 Cases to Date (ABAQUS/ANSYS)
-
- FEAM Validated - Elastic/Plastic
  Residual Strength (T*, etc.)
- Enabling Technologies:
  Significant Computer Time Savings
  Significant Manpower Time Savings
- Automation Critical For Probabilistic Analysis

CORROSION AND WIDESPREAD FATIGUE DAMAGE OF CRITICAL AIRCRAFT STRUCTURE

UDRI
UNIVERSITY of DAYTON RESEARCH INSTITUTE

Sponsor: WL/FIBEC
Contractor: UDRI
Contract Number: F09603-95-D-0175
Start: 11 July 1996 *End:* 30 Dec 1997

AIR FORCE RESEARCH LABORATORY

- D. Tritsch, University of Dayton Research Institute, Dayton, OH
- D. Groner, Air Force Research Laboratory, WPAFB, OH

USAF Aircraft Structural Integrity Program Conference
4 December 1997, San Antonio, TX

UDRI
UNIVERSITY of DAYTON RESEARCH INSTITUTE

OVERVIEW

- INTRODUCTION
- APPROACH
- DATA COLLECTED
- DATA REVIEW & QUERIES
- RESULTS
- CONCLUSIONS
- SUMMARY & RECOMMENDATIONS

INTRODUCTION / BACKGROUND

Corrosion and Structural Integrity Program Plan - AFRL/VABE

Consolidate corrosion/fatigue material data into a database

- Crack growth rate (now)
- Crack nucleation (later)

• CINDAS

In-service experimental data database for corrosion/fatigue

• McAir

Identify structural components subjected to corrosion damage

- Damage tolerant
- Fatigue critical
- Geometry
- Loads
- Corrosion description

• UDRI
• ARINC
• Northrop Grumman

Stockpile corroded aircraft material

- KC-135
- P-3

• UDRI

Define preliminary corrosion metrics and transformations for structural components

- Loss of material
  - → Increase in stress
- Pit morphology
  - → ΔK_{th}
- Surface Roughness
  - → EIFS
- Increase in crack growth rate
  - → LEFM
- Other

• McAir

• Dr. Tom Mills
• Dr. James Baldwin

UDRI UNIVERSITY of DAYTON RESEARCH INSTITUTE

INTRODUCTION / BACKGROUND

AIR FORCE RESEARCH LABORATORY

Objective

Establish the extent of corrosion damage and widespread fatigue damage (WFD) which may exist on specified USAF aircraft.

Intent of Project

- Create Database of damage and repair records due to corrosion and fatigue
- Show usefulness of database to ID PSE's with corrosion and fatigue damage
- Setup framework/process for data collection and evaluation

Approach

Gather data from repair orders for C-5A/B Aircraft

Assemble and review the data from C/KC-135, C-130, E-8C (707), & C-5A/B

- Identify damage tolerant critical locations which may be affected
- Identify other effected elements which could contribute to failure

UDRI UNIVERSITY of DAYTON RESEARCH INSTITUTE

INTRODUCTION / BACKGROUND

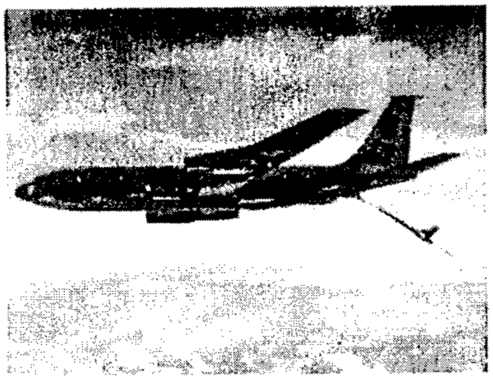

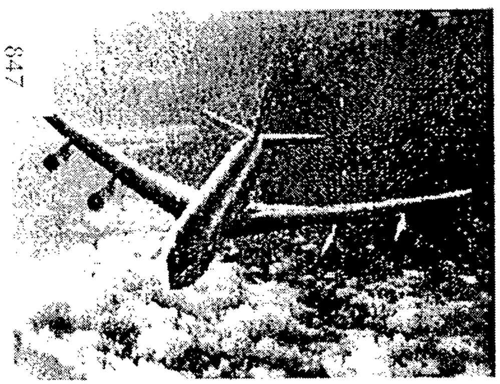

Selected Aircraft:

- C/KC-135 Stratotanker
- E-8C Joint STARS
- C-9A/C Nightingale
- C-130 Hercules
- C-5A/B Galaxy

Aircraft	1990 Total Corrosion $
B-52	$ 80.3 M
C-130	$ 115.7 M
C-135	$ 95.3 M
C-141	$ 57.6 M

Aircraft not selected:
- Fighters
- B-52
- C-141

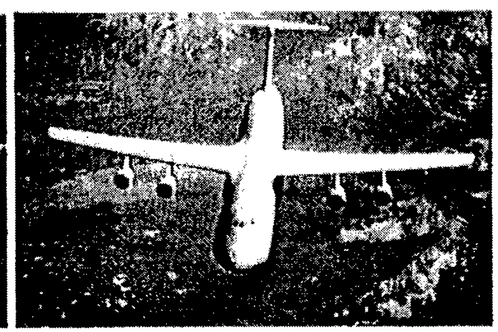

UDRI
UNIVERSITY of DAYTON RESEARCH INSTITUTE

APPROACH

- Collect & review data
  - setup database per aircraft
- Query database to ID relevant details and features
- Query database to ID specific items
  - Damage type, part type, part/damage location
- Cross tab to ID DADTA points and other added info.
- ID similarities and differences between databases
  - Covering 1 fleet and across fleets

UDRI UNIVERSITY of DAYTON RESEARCH INSTITUTE

DATA COLLECTED

C/KC-135 Stratotanker
- OACIS - Over & Above Centralized Information System
- Boeing Reports on EC-135H 61-0291 Disassembly and Hidden Corrosion Program

E-8C Joint STARS
- OACIS - Over & Above Centralized Information System
- Northrop-Grumman Report on Corrosion and Fatigue Study of (2) JSTARS Aircraft

C-9A/C Nightingale
- OACIS - Over & Above Centralized Information System

C-130 Hercules
- AFMC Form 202
- OACIS - Over & Above Centralized Information System
- AIRS - Records from AFTO Form 58, Corrosion and Structural Repair Tracking
- REMIS - Reliability and Maintainability Information System
- ARINC Reports on Extent of Corrosion Damage on Critical Structural Components of C-130 Aircraft

C-5A/B Galaxy
- SA-ALC Engineering disposition records

UDRI UNIVERSITY of DAYTON RESEARCH INSTITUTE

DATA COLLECTED

C/KC-135 Stratotanker

- OACIS - 279 Tail #'s, Oct. 1990 - Jul 1996, 5883 Records
- 291 Disassembly - 1 Tail #, 1992, 3331 records on damage type and location, 1099 records on part and damage description, (Typical of post PDM hidden corrosion)

E-8C Joint STARS

- OACIS - 8 Tail #'s, Jan 1992 - Sep 1996, 33442 records
- Northrop-Grumman O&A - 2 Tail #'s, 1996, 1536 records

C-9A/C Nightingale

- OACIS - 61 Tail #'s, Aug 1990 - Aug 1996, 12950 records

C-130 Hercules

- AFMC202 - 127 Tail #'s, , 1003 records
- OACIS - 101 Tail #'s, , 8065 records
- AIRS - 116 Tail #'s, , 3769 records
- REMIS - 447 Tail #'s, , 2922 records
- ARINC - 875 WUC's, 451 DADTA vs WUC points, 241 component descriptions

C-5A/B Galaxy

- SA-ALC - 124 Tail #'s, 1988 - 1996, 4302 records

DATA COLLECTED

REMIS
- Record number
- MDS
- Geographic Loc.
- A/C Serial Num.
- Work Unit Code
- Corrosion Occ.
- Repair Manhours
- MTBC

OACIS
- Record number
- Work Request Num.
- Date Reported
- Work Unit Code
- How Mal Code
- Action Taken Code
- Discovered Date
- Work Area Code
- Work Zone Code
- Discrepancy Descrip.
- Corrective Action Code
- Tail Number

AFMC202
- Date
- Control Number
- Part Noun
- NSN
- Part Number
- Added Drawings/Notes
- Serial/Tail Number
- Planner
- Deficiency description
- Location description
- Solution
- Damage Classification
- Engineer

C5 SA-ALC
- Record Number
- Date in
- Date
- EAR_NO
- SER_NO
- Description
- Status
- Remarks
- Part_NO
- DWG_TO_NO
- Work_SPEC
- FS
- Area
- Repair instructions
- Engineer

UDRI
UNIVERSITY of DAYTON RESEARCH INSTITUTE

DATA REVIEW

- No Details on corrosion quantity or description
- OACIS and AFMC202 best able to ID corroded or cracked parts
- Not intended to contain the data used in a DADTA evaluation
- Can identify PSE's with corrosion or cracking which need further consideration of their structural integrity and R&M capabilities

UDRI
UNIVERSITY of DAYTON RESEARCH INSTITUTE

DATA QUERIES

Goal: ID part type, damage type, and damage/part location

Familiarity with database
- Part - descriptions, noun, type, number, ...
- Damage - descriptions, Hal Mal Codes, discrepancy, classif., ...
- Location - descriptions, STA/WL/BL, zone, area, ...
- Other relevant data - WUC, DADTA Pts., Tail #, dates, MDS, ...

Query by defect type - corrosion or cracking

Cross-Tab by Part type, Location, WUC, year, Tail #, etc. ...

ID similarities and differences between databases for a fleet

UDRI
UNIVERSITY of DAYTON RESEARCH INSTITUTE

DATA QUERIES

AIR FORCE RESEARCH LABORATORY

C-130 OACIS, Count Records by How Mal Code

Sum 8065

How Mal Code	Description	CountOfRecord
667	Corroded Severe	5109
170	Corroded Mild/Moderate	2035
0		258
799		99
190	Cracked	88
105	Loose, damaged, or missing hardware	80
804		80
710	Bearing failure	51
800		51
553	Does not meet specifications	40

DATA QUERIES

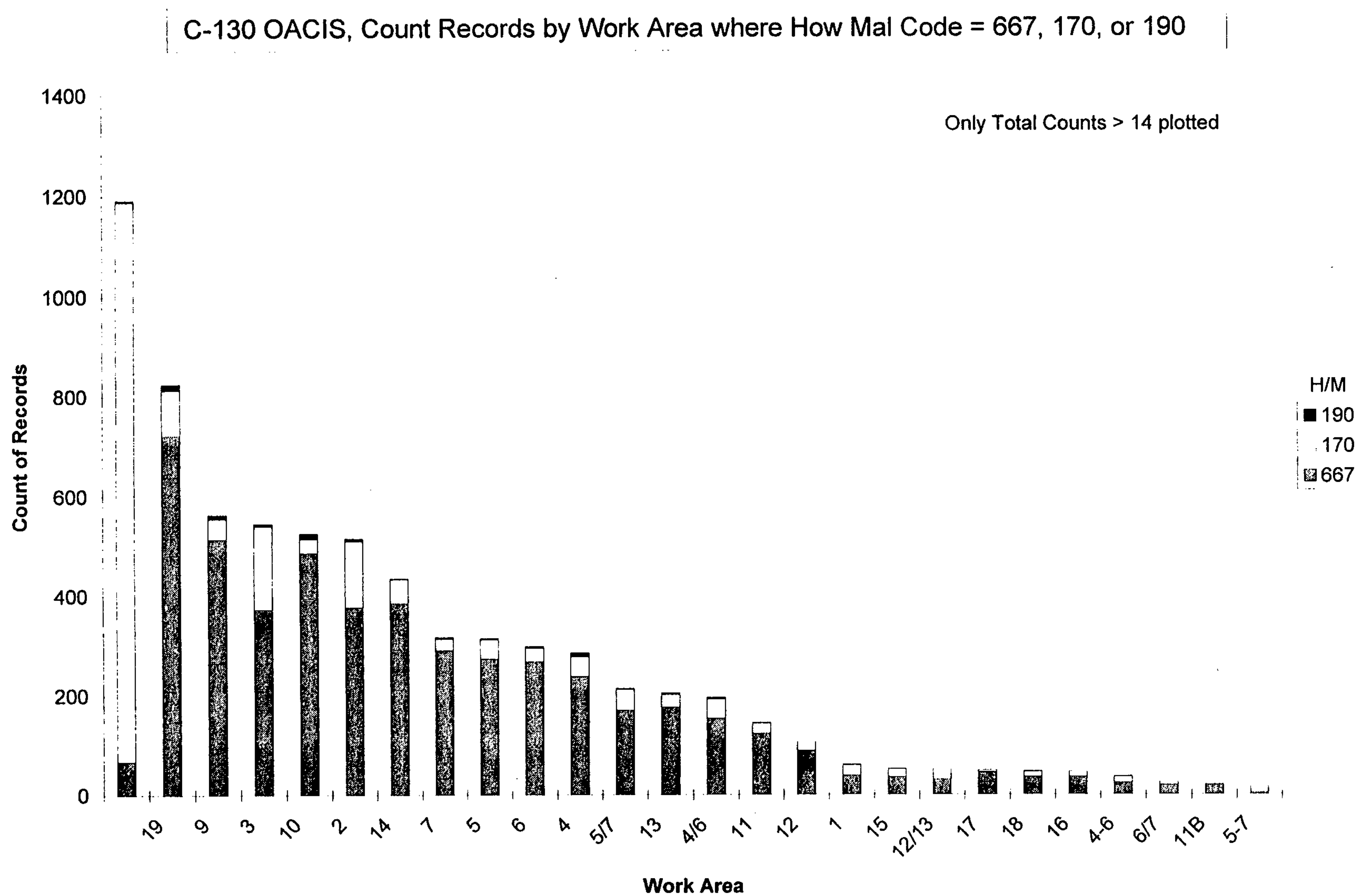

DATA QUERIES

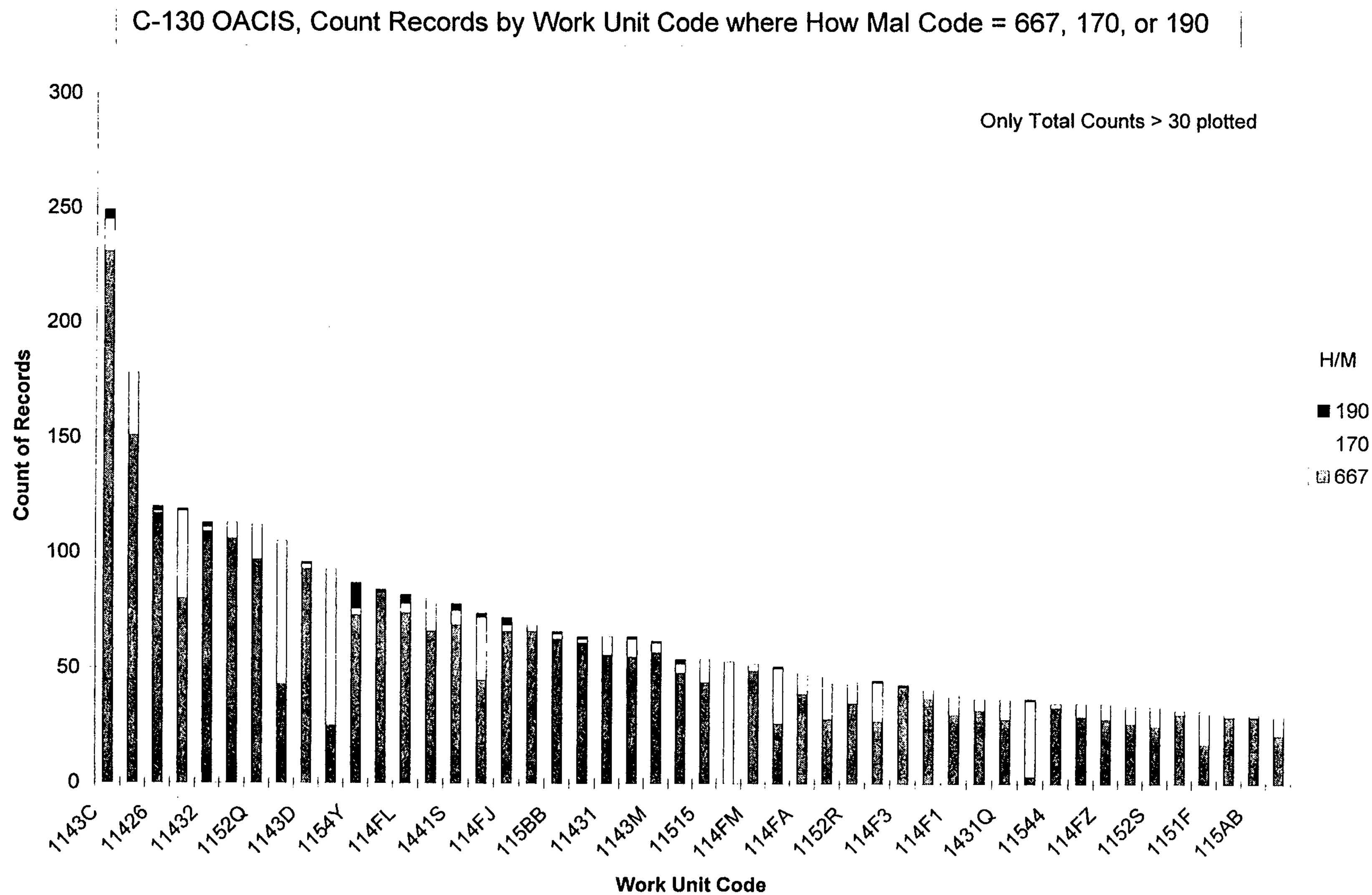

DATA QUERIES

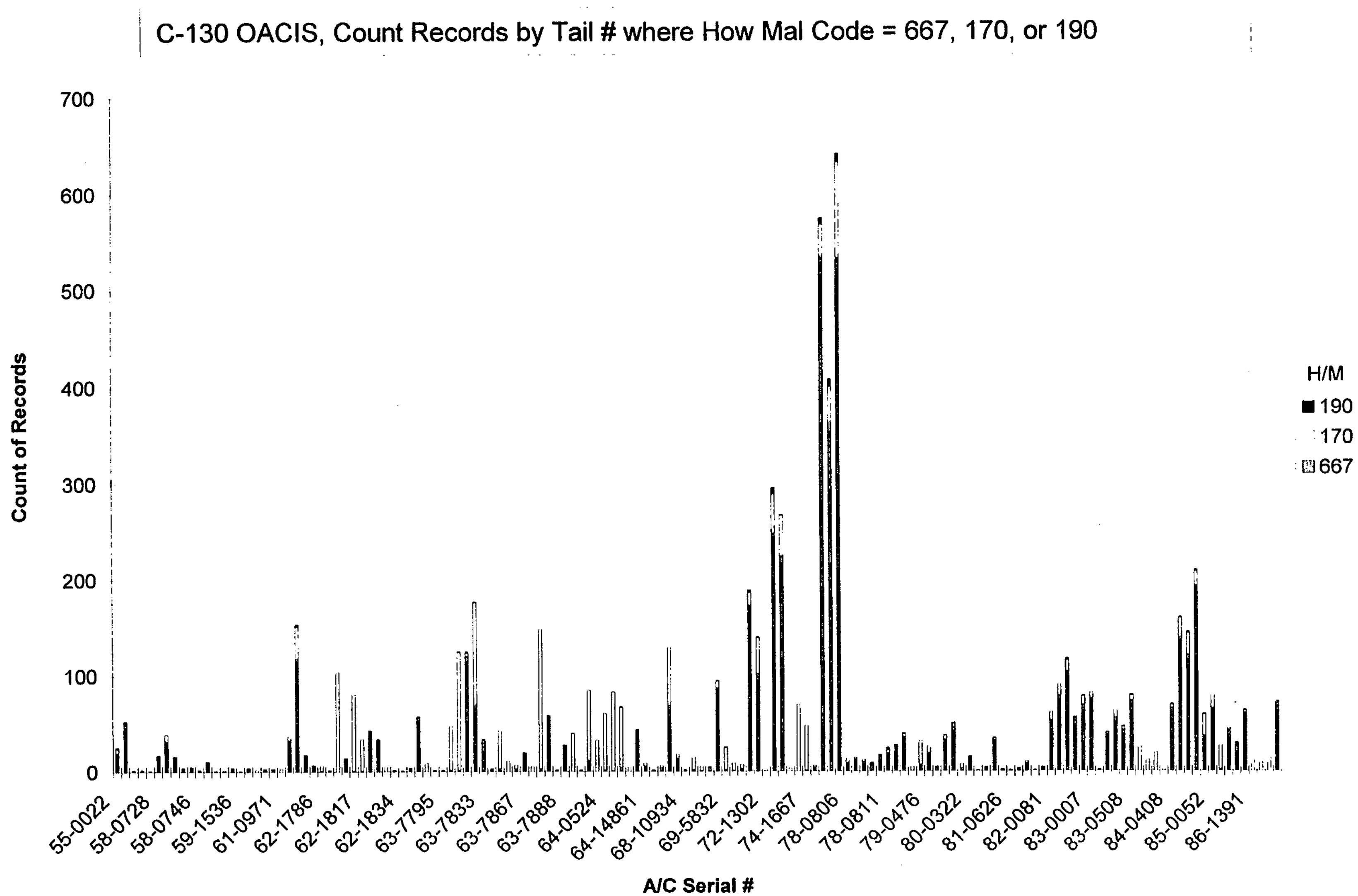

UDRI UNIVERSITY of DAYTON RESEARCH INSTITUTE

DATA QUERIES

C-130 OACIS, Count Records by Tail # where How Mal Code = 667, 170, or 190 and where the Work Unit Code covers a DADTA Component

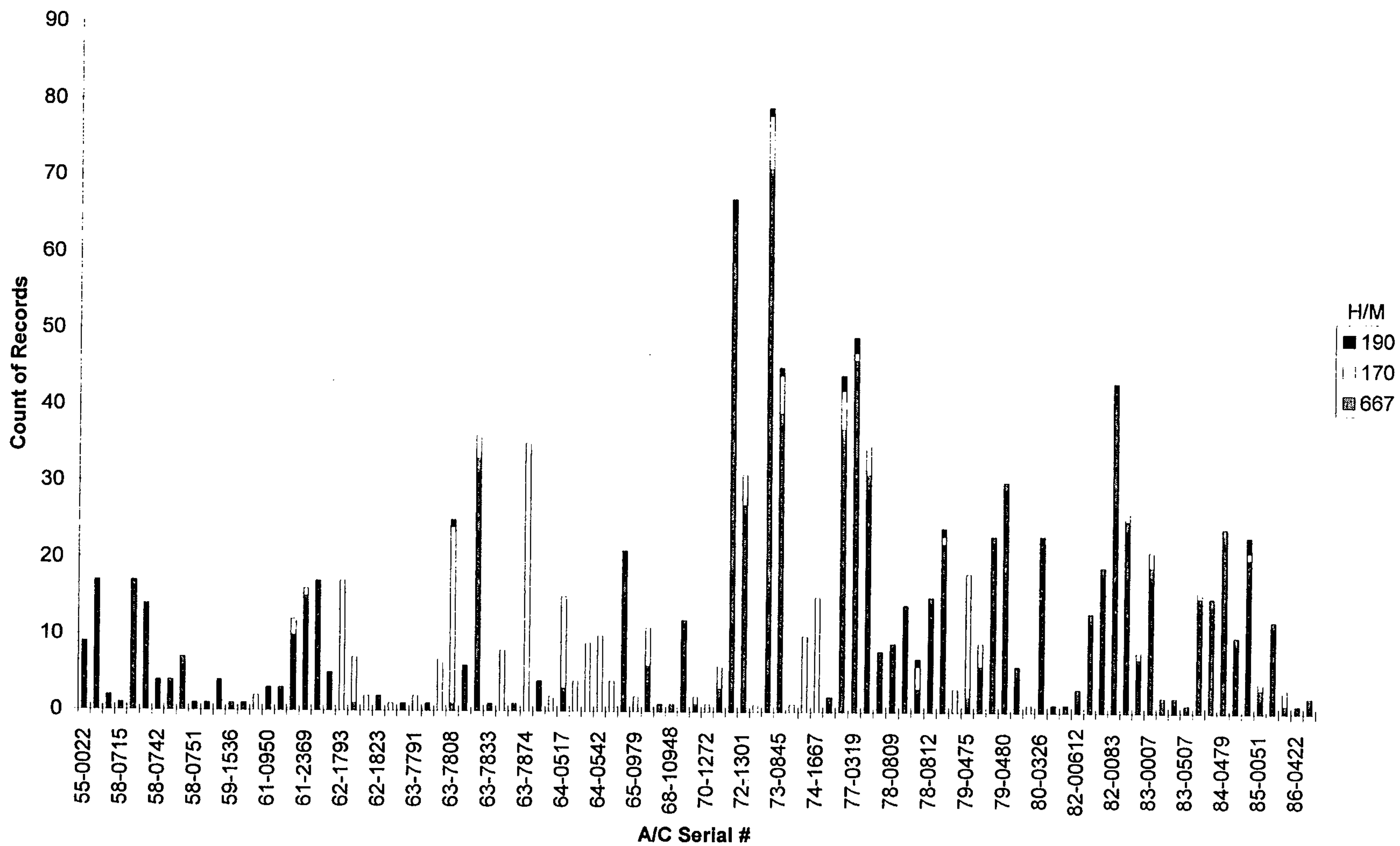

UDRI UNIVERSITY of DAYTON RESEARCH INSTITUTE

DATA QUERIES

C-130 OACIS, Count Records with Discrepancy Text like "?" where How Mal Code = 667, 170, or 190

Discrepancy w/	170	667	190	Sum
Sum	641	1641	31	2313
skin	559	857	14	1430
beam	43	414	13	470
longeron	30	241	3	274
frame	8	106		114
stringer	1	23	1	25

UDRI
UNIVERSITY of DAYTON RESEARCH INSTITUTE

DATA QUERIES

C-130 OACIS, Count Records by Work Area and with Discrepancy Text like "?" where How Mal Code = 667, 170, or 190

Sum	979	417	207	65	24	1692
Work Area	skin	beam	longeron	frame	stringer	Sum
Blank	403					403
9	73	164			5	242
2	129		61	15	1	206
10		169	13		12	194
19	158		13	16	3	190
3	116				3	119
14			88			88
5	100			8		108
11		22		26		48
7		33				33
13			32			32
6		29				29
1				7		7

AIR FORCE RESEARCH LABORATORY

UDRI UNIVERSITY of DAYTON RESEARCH INSTITUTE

DATA QUERIES

C-130 OACIS, Count Records by Work Area and with Discrepancy Text like "?" where How Mal Code = 667, 170, or 190

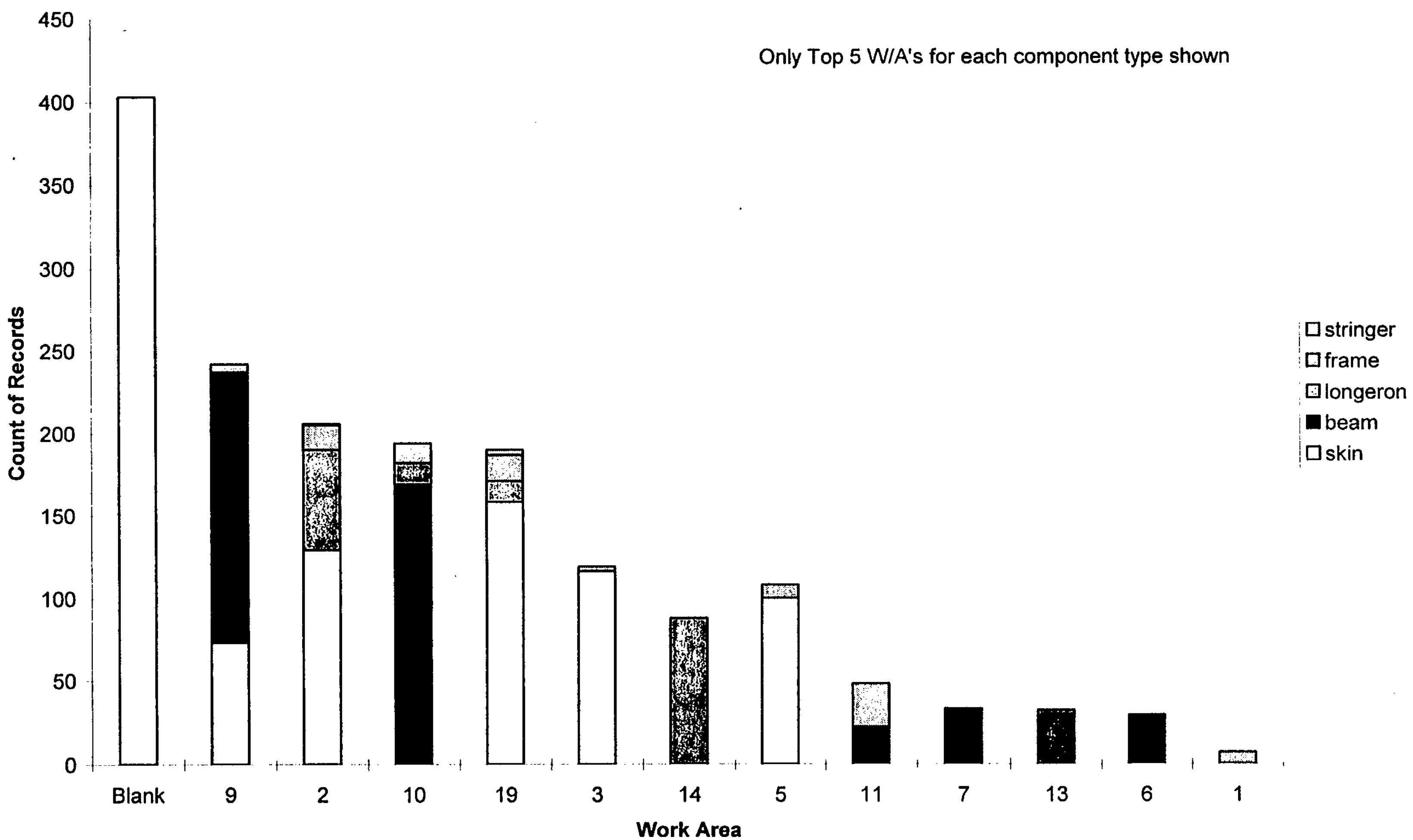

RESULTS

KC-135 OACIS, Count Records by Work Area where How Mal Code = 667, 170, or 190

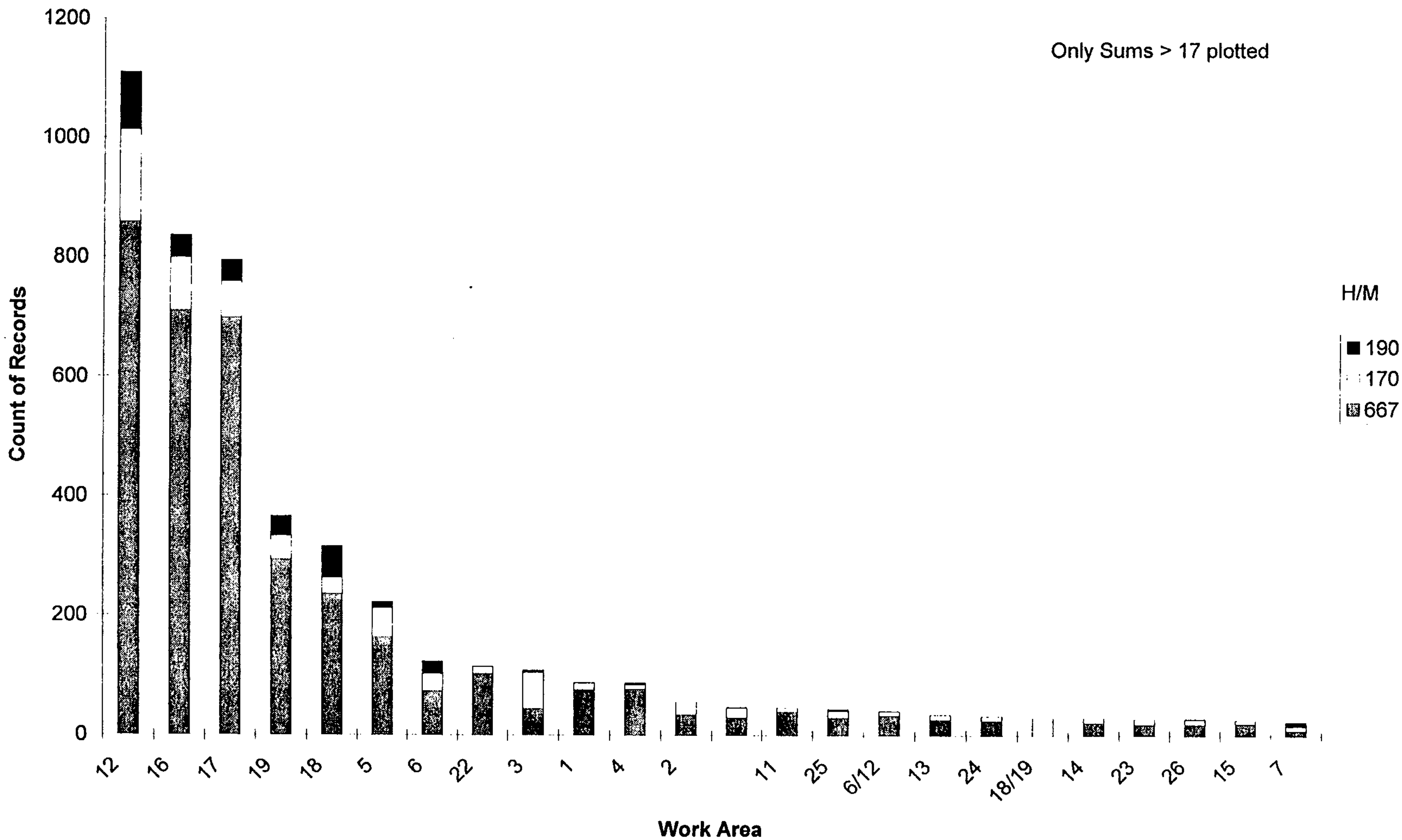

UDRI
UNIVERSITY of DAYTON RESEARCH INSTITUTE

RESULTS

KC-135 OACIS, Count Records by Work Unit Code where How Mal Code = 667, 170, or 190

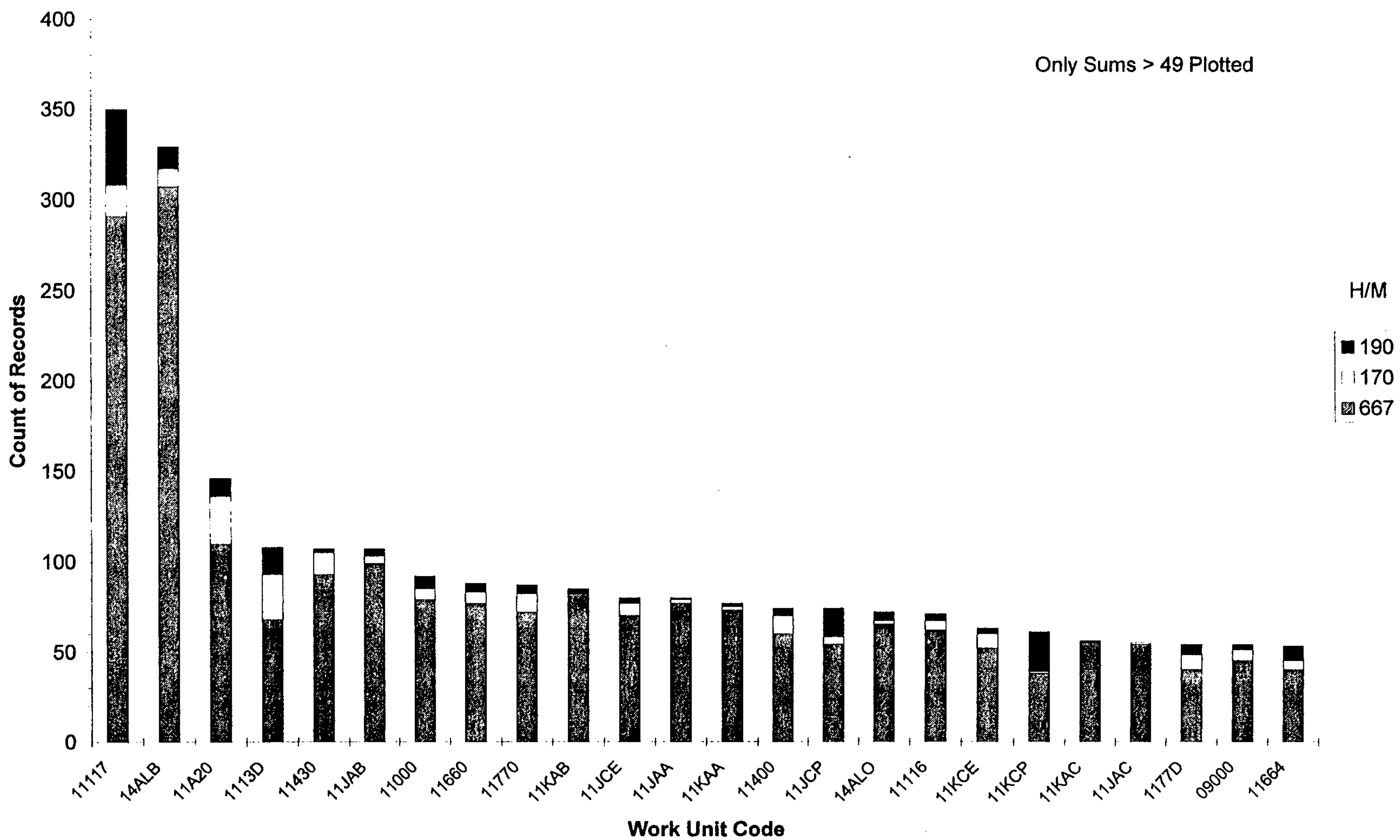

UDRI UNIVERSITY of DAYTON RESEARCH INSTITUTE

RESULTS

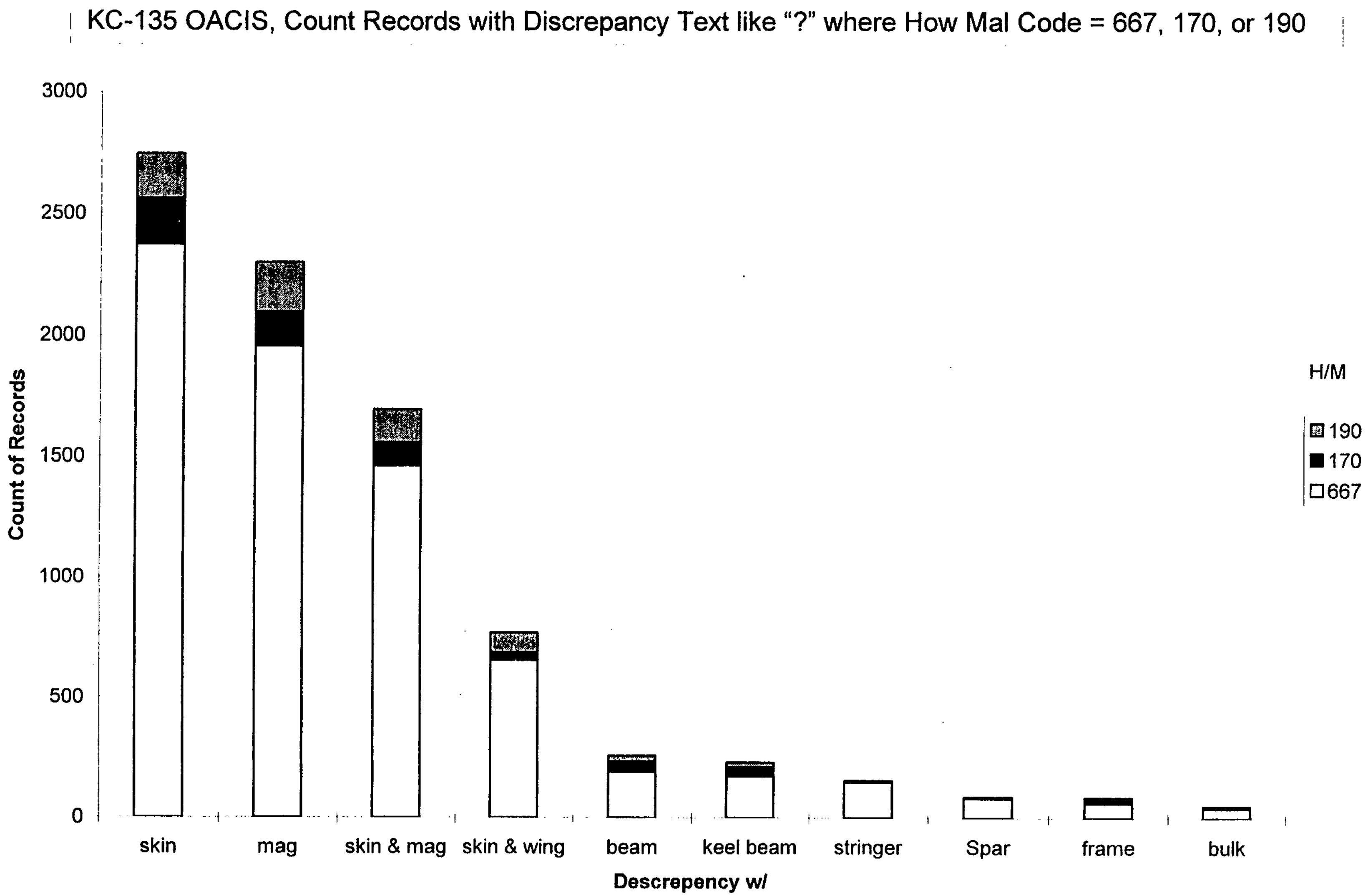

RESULTS

KC-135 OACIS, Count Records with Discrepancy Text like "?" and by Work Area where How Mal Code = 667, 170, or 190

		H/M Count of Records			
Descrepency W/	Work Area	667	170	190	sum
skin	12	584	76	51	711
	16	512	23	26	561
	17	482	7	19	508
	19	236	18	22	276
	18	188	17	44	249
	22	84	8		92
	6	56	14	11	81
	6/12	31	7	1	39

RESULTS

KC-135 OACIS, Count Records by Work Area, Cross Tabbed by Year, where How Mal Code = 667, 170, or 190 and with Discrepancy Text like *mag*

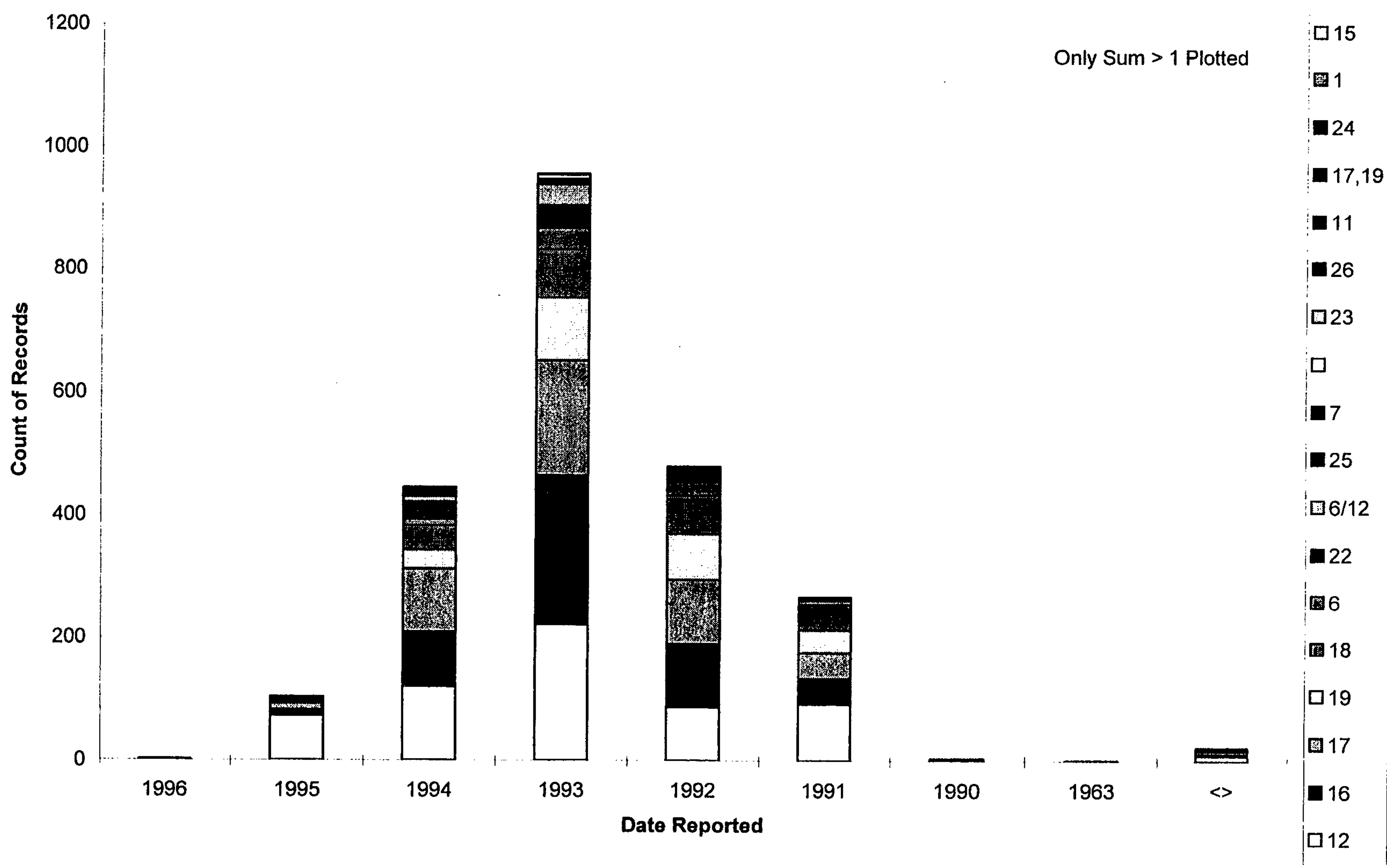

UDRI
UNIVERSITY of DAYTON RESEARCH INSTITUTE

RESULTS

E-8C OACIS, Count Records by Tail #, where How Mal Code = 667, 170, or 190

Tail Number	AIRCRAFT ID	667	170	190	Sum
Sum		7598	21038	557	29193
		How Mal Code Count of Records			
19622	P1	703	8743	56	9502
19295	P2	551	6773	40	7364
19442	P6	1962	1620	120	3702
19293	P5	1255	1153	119	2527
19296	P4	1612	794	103	2509
19294	P3	1343	1013	98	2454
20495		149	904	15	1068
20016		23	38	6	67

E-8C OACIS, Count Records by Work Area, where How Mal Code = 667, 170, or 190

Work Area	667	170	190	Sum
Sum	7598	21038	557	29193
	How Mal Code Count of Records			
8206	2172	9677	167	12016
8202	2546	8249	100	10895
8223	732	1153	15	1900
8221	359	138	157	654
8215	294	256	13	563
8217	309	62	10	381
	142	177	3	322
8241	44	269	6	319

RESULTS

E-8C OACIS, Count Records by Work Zone, where Work Area = 8202
and How Mal Code = 667, 170, or 190

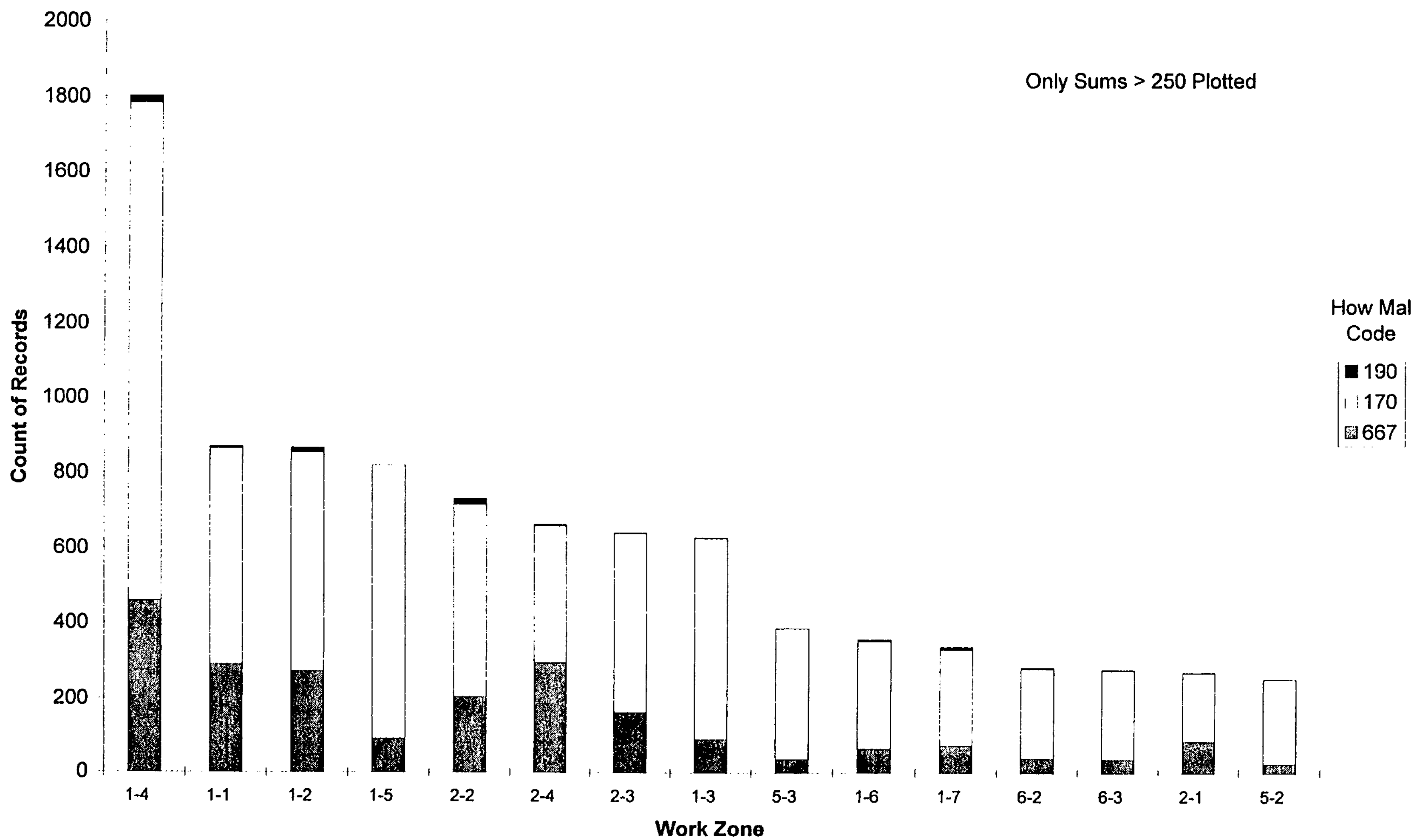

RESULTS

E-8C OACIS, Count Records by Work Zone, where Work Area = 8206 and How Mal Code = 667, 170, or 190

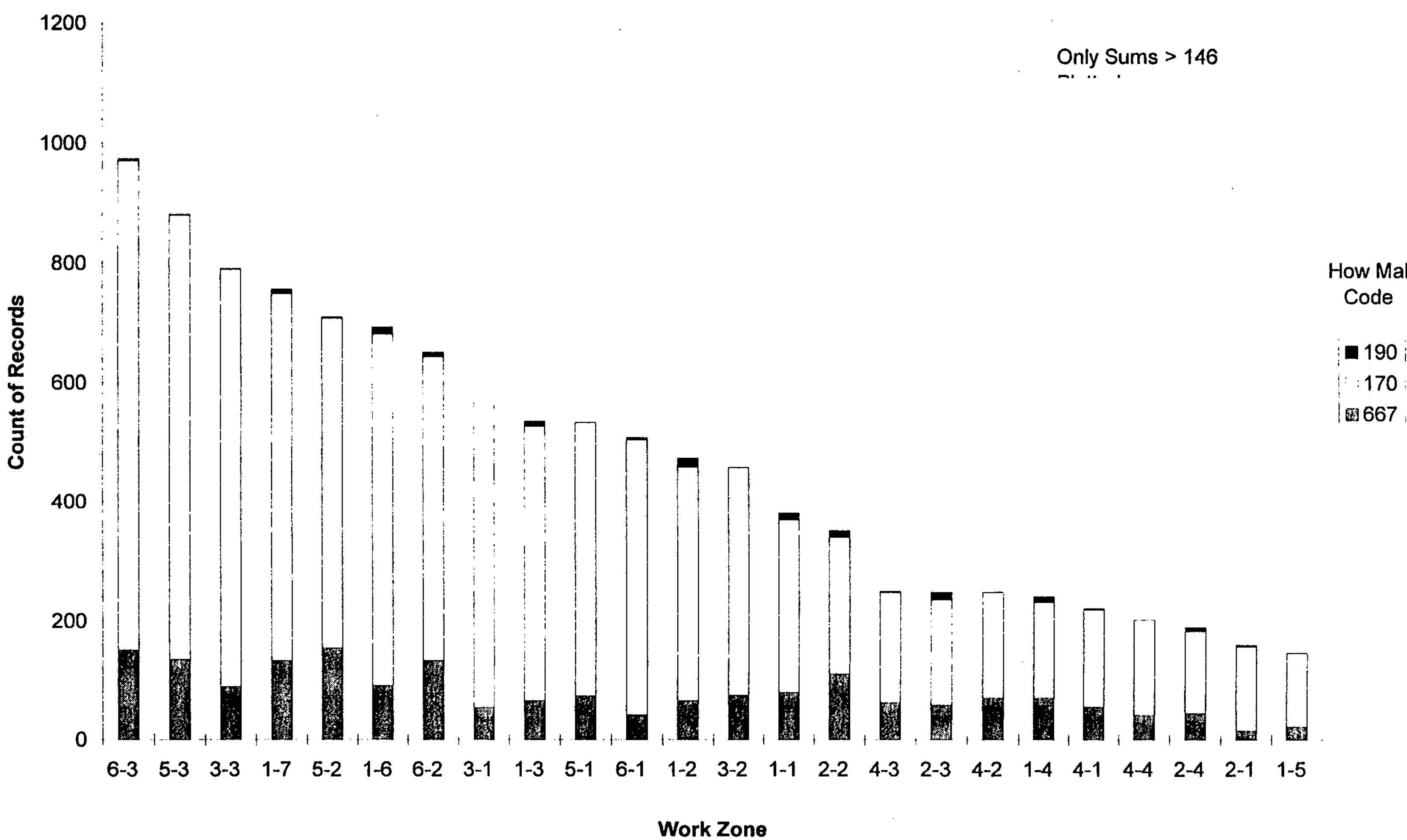

UDRI UNIVERSITY of DAYTON RESEARCH INSTITUTE

RESULTS

E-8C OACIS, Count Records by Work Area, with Discrepancy Text like *skin* and where How Mal Code = 667, 170, or 190

	How Mal Code			
Count of Records				
Work Area	667	170	190	Sum
8206	311	1410	12	1733
8202	215	1495	15	1725
8223	97	151	2	250
8072	3	95		98
8215	17	65		82
8270	4	24		28
Sum	719	3366	33	4118

RESULTS

E-8C OACIS, Count Records with Discrepancy Text like *?* and where How Mal Code = 667, 170, or 190

Sum	3069	6917	154	10140
	How Mal Code			
	Count of Records			
Discrepency w/	667	170	190	Sum
skin	719	3366	33	4118
rib	371	1076	7	1454
frame	524	621	20	1165
beam	309	765	8	1082
stringer	276	760	14	1050
angle	831	116	71	1018
bulk	39	213	1	253

UDRI UNIVERSITY of DAYTON RESEARCH INSTITUTE

RESULTS

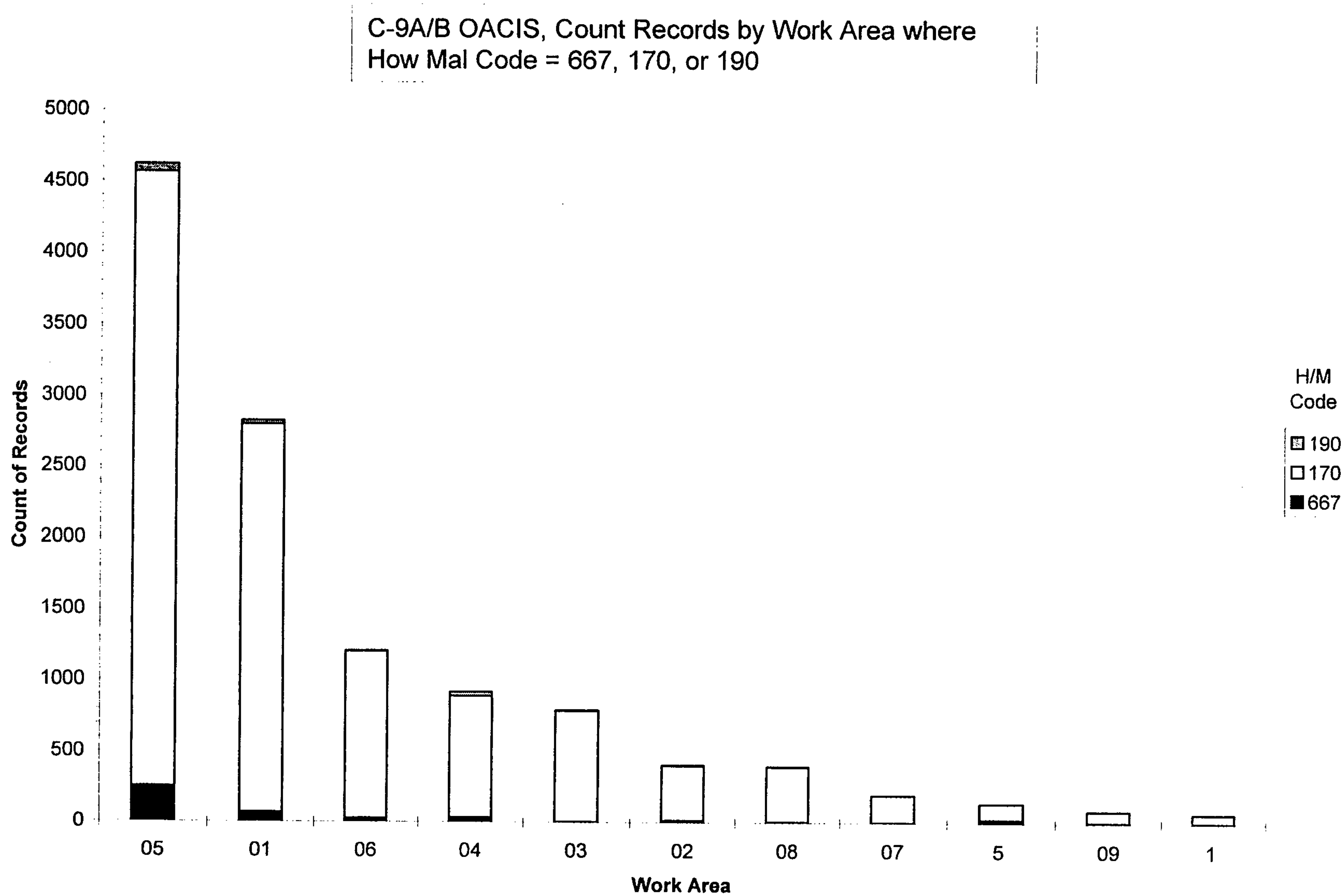

UDRI UNIVERSITY of DAYTON RESEARCH INSTITUTE

RESULTS

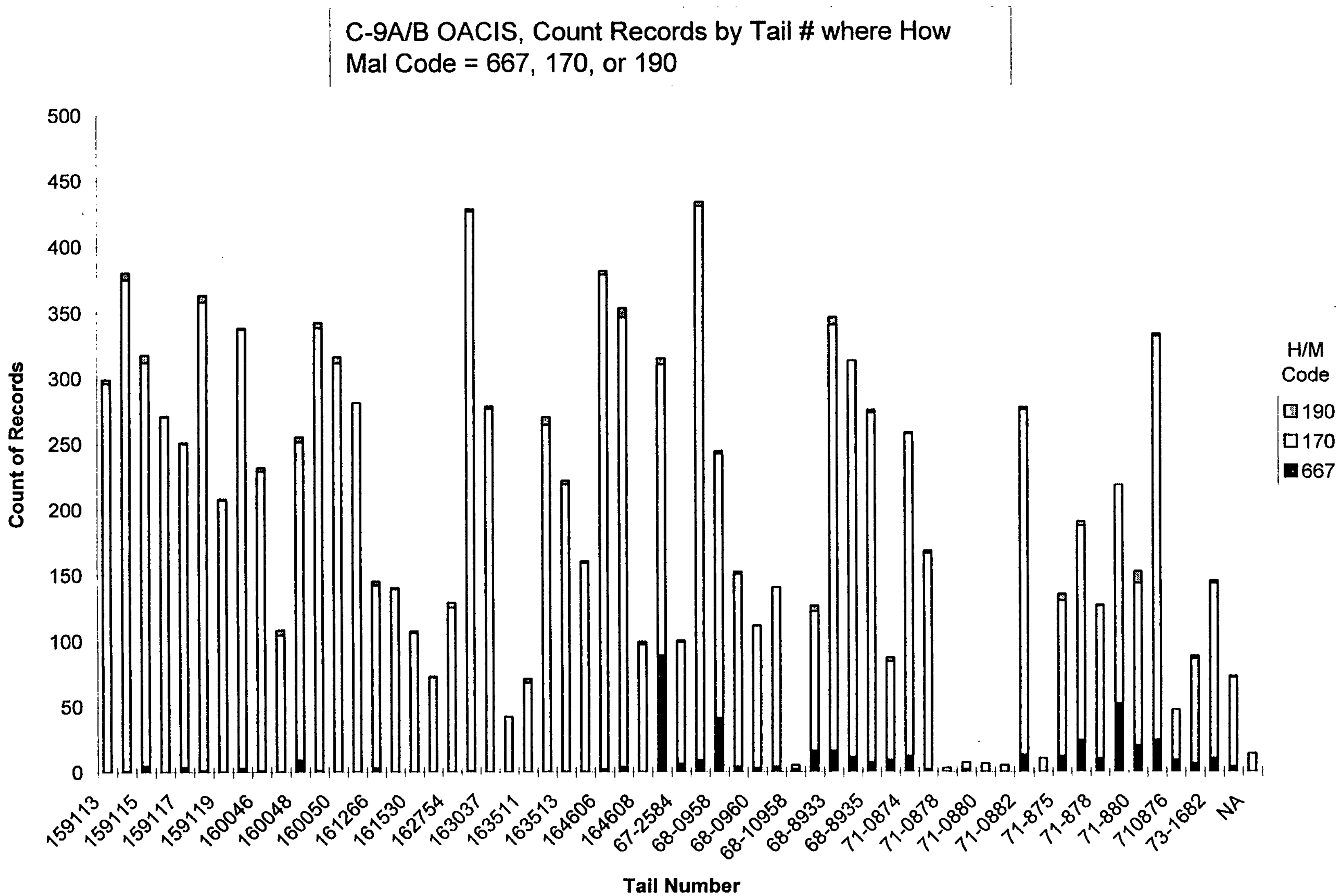

UDRI UNIVERSITY of DAYTON RESEARCH INSTITUTE

RESULTS

C-9A/B OACIS, Count Records with Discrepancy Text Like *skin* and by Work Area where How Mal Code = 667, 170, or 190

	H/M Code Count of Records			
Sum	56	2857	30	2943
Work Area	667	170	190	Sum
01	11	997	9	1017
02	2	147		149
03		246	1	247
04	9	188	3	200
05	16	809	9	834
06	2	222	3	227
07		26		26
08	3	142	2	147
09	2	26	1	29
1	3	20	1	24
11		3		3
2		2		2
3		3		3
4	1	4	1	6
5	6	18		24
6	1	2		3
8		2		2

C-9A/B OACIS, Count Records with Discrepancy Text Like *?* where How Mal Code = 667, 170, or 190

	H/M Code Count of Records			
Sum	161	4303	52	4516
Discrepency w/	667	170	190	Sum
skin	56	2857	30	2943
floor	58	740	15	813
frame	19	384	4	407
beam	22	283	2	307
bulk	4	27	1	32
stringer	2	12		14

UDRI UNIVERSITY of DAYTON RESEARCH INSTITUTE

RESULTS

C-9A/B OACIS, Count Records with Discrepancy Text Like *skin* where Work Area = 05 or 01 and where How Mal Code = 667, 170, or 190

		H/M Code Count of Records			
Sum		3	535	4	542
Work Area	Work Zone	667	170	190	Sum
01	06	1	118	2	121
01	05	1	118		119
05	08	1	65		66
05	07		35		35
05	04		32		32
05	00		31		31
05	01		26		26
05	09		23		23
05	05		21	1	22
05	06		20		20

RESULTS

C-130 OACIS, Count Records with Discrepancy Text Like *?* where How Mal Code = 667, 170, or 190

Discrepancy W/	170	667	190	Sum
Sum	641	1641	31	2313
skin	559	857	14	1430
beam	43	414	13	470
longeron	30	241	3	274
frame	8	106		114
stringer	1	23	1	25

Count of Records

C-130 OACIS, Count Records by Work Area with Discrepancy Text Like *?* where How Mal Code = 667, 170, or 190

Only Top 5 W/A's for each part type shown

Count of Records

Work Area	skin	beam	longeron	frame	stringer	Sum
Sum	979	417	207	65	24	1692
Blank	403					403
9	73	164			5	242
2	129		61	15	1	206
10		169	13		12	194
19	158		13	16	3	190
3	116				3	119
14			88			88
5	100			8		108
11		22		26		48
7		33				33
13			32			32
6		29				29
1				7		7

UDRI
UNIVERSITY of DAYTON RESEARCH INSTITUTE

RESULTS

C-130 OACIS, Count Records by Major Section for Work Unit Codes with DADTA Points and where How Mal Code = 667, 170, or 190

Major Section	667	170	190	Sum
Sum	1143	283	31	1457
	Count of Records			
Center Wing	570	184	9	763
Outer Wing	512	86	21	619
Fuselage	58	9	1	68
Nacelle A	1	2		3
Nacelle D	1	2		3
Nacelle C	1			1

C-130 OACIS, Count Records by Work Unit Codes with DADTA Points where How Mal Code = 667, 170, or 190

Applicable DADTA Point	667	170	190	Sum
Sum	1143	283	31	1457
	Count of Records			
CW-9	131	12	2	145
OW-3	126	5	2	133
CW-10	124	4	2	130
CW-11	124	4	2	130
CW-8	44	8	1	53
OW-52	44	1	2	47
OW-36	42	1	2	45
OW-25	40	4		44
OW-45	40	1		41
CW-12	37		1	38

UDRI UNIVERSITY of DAYTON RESEARCH INSTITUTE

RESULTS

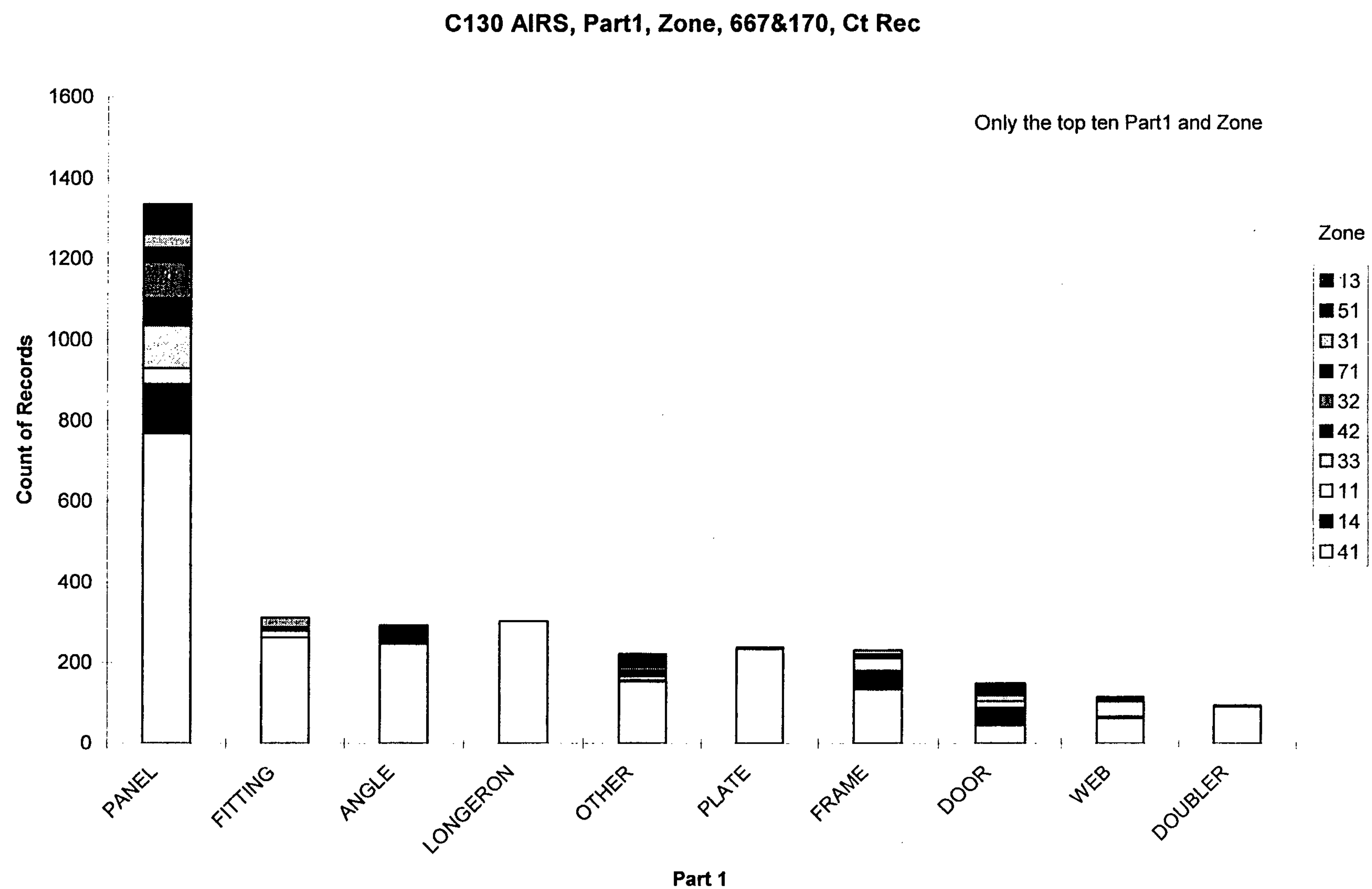

UDRI
UNIVERSITY of DAYTON RESEARCH INSTITUTE

RESULTS

C130 AIRS, Loc, Part1=Panel, 667&170, Ct Rec

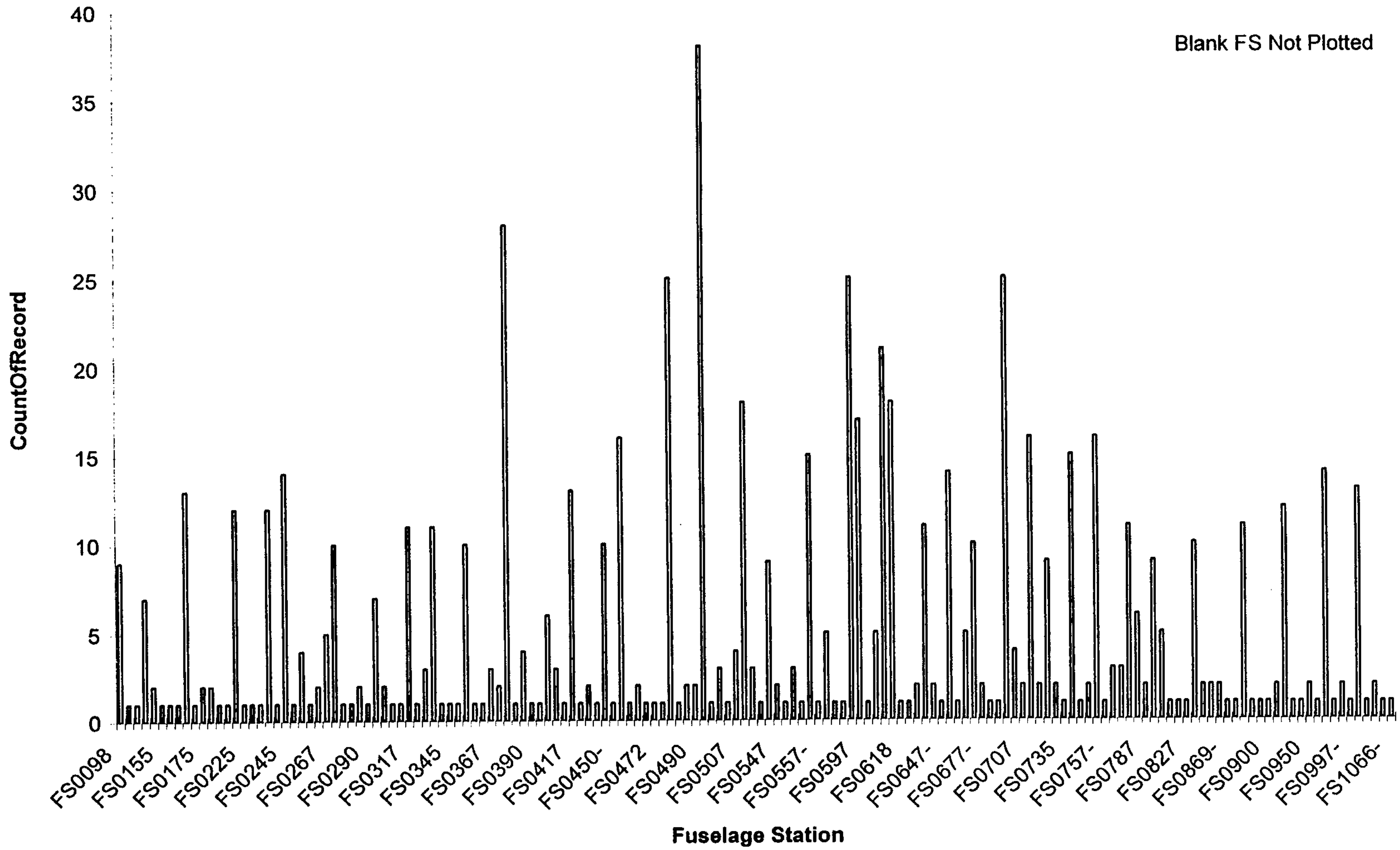

RESULTS

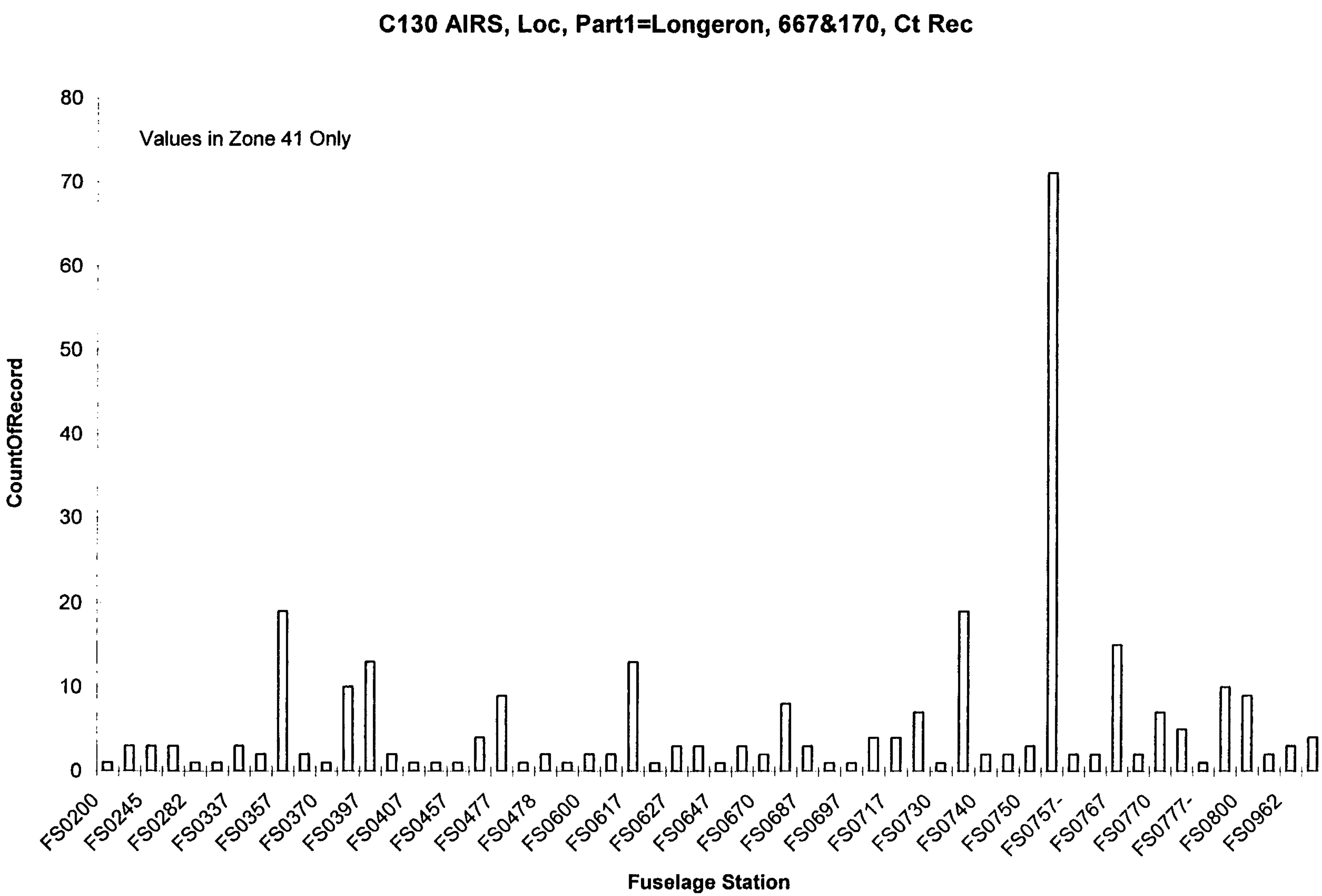

C130 AIRS, Loc, Part1=Longeron, 667&170, Ct Rec
Values in Zone 41 Only
CountOfRecord
0
10
20
30
40
50
60
70
80
FS0200
FS0245
FS0282
FS0337
FS0357
FS0370
FS0397
FS0407
FS0457
FS0477
FS0478
FS0600
FS0617
FS0627
FS0647
FS0670
FS0687
FS0697
FS0717
FS0730
FS0740
FS0750
FS0757-
FS0767
FS0770
FS0777-
FS0800
FS0962
Fuselage Station

RESULTS

C-5 ALC, Count Records by Serial # and Year Repair Action Closed

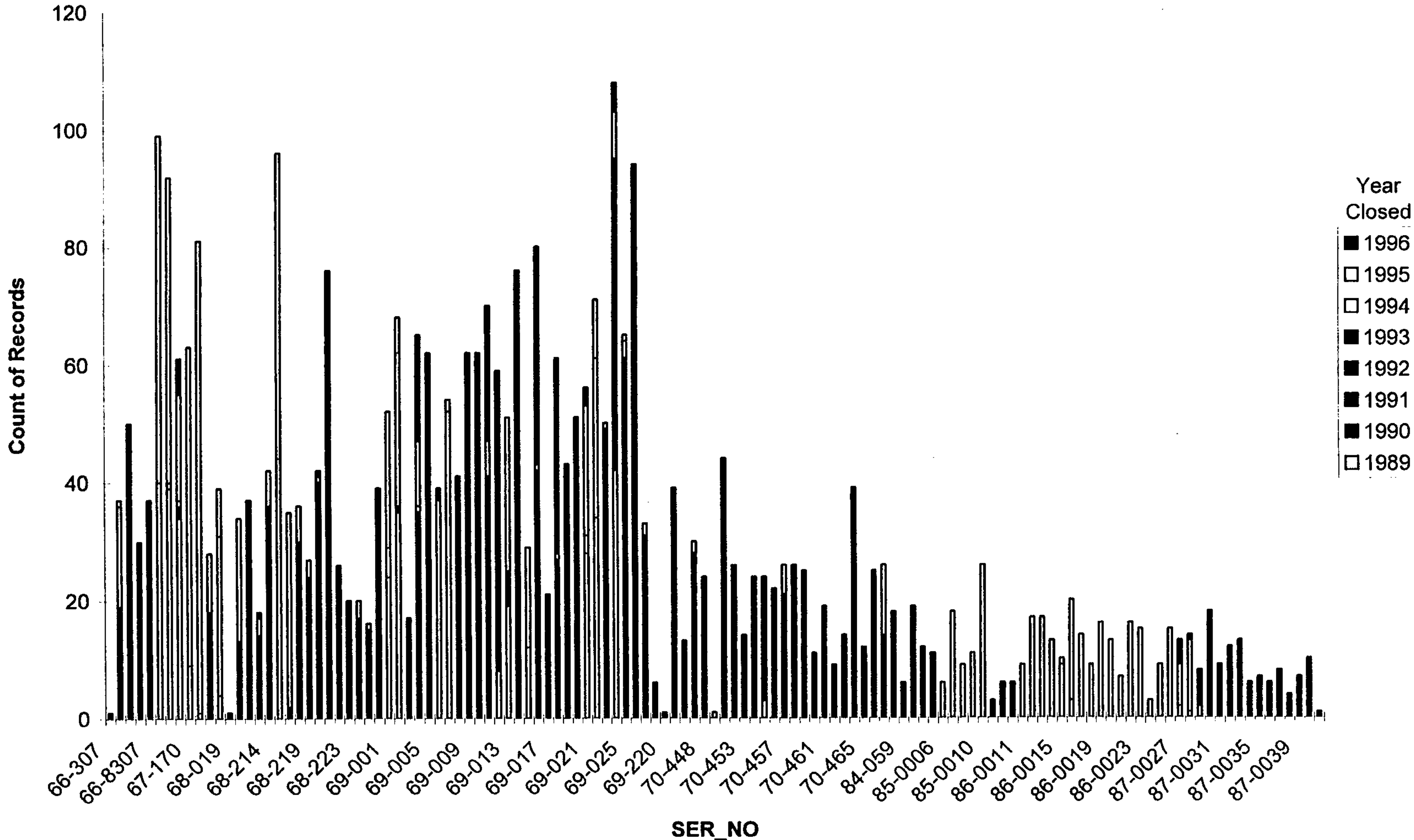

UDRI UNIVERSITY of DAYTON RESEARCH INSTITUTE

RESULTS

C-5 ALC, Count Records by Serial # and Year Repair Action Closed where Defect Code = Corrosion or Crack

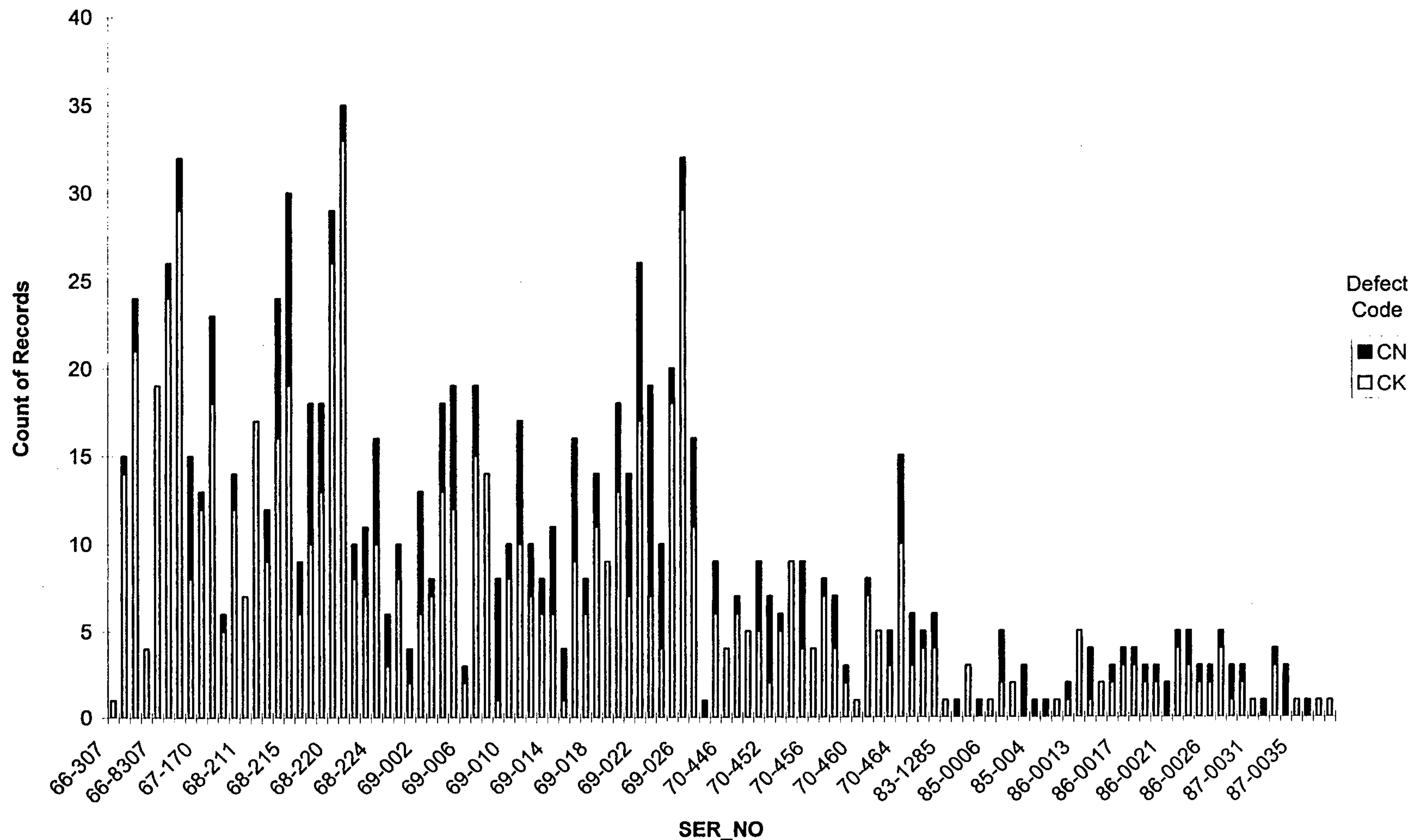

RESULTS

C-5 ALC, Count Records by Work Area Description where
Defect Code = Corrosion or Crack

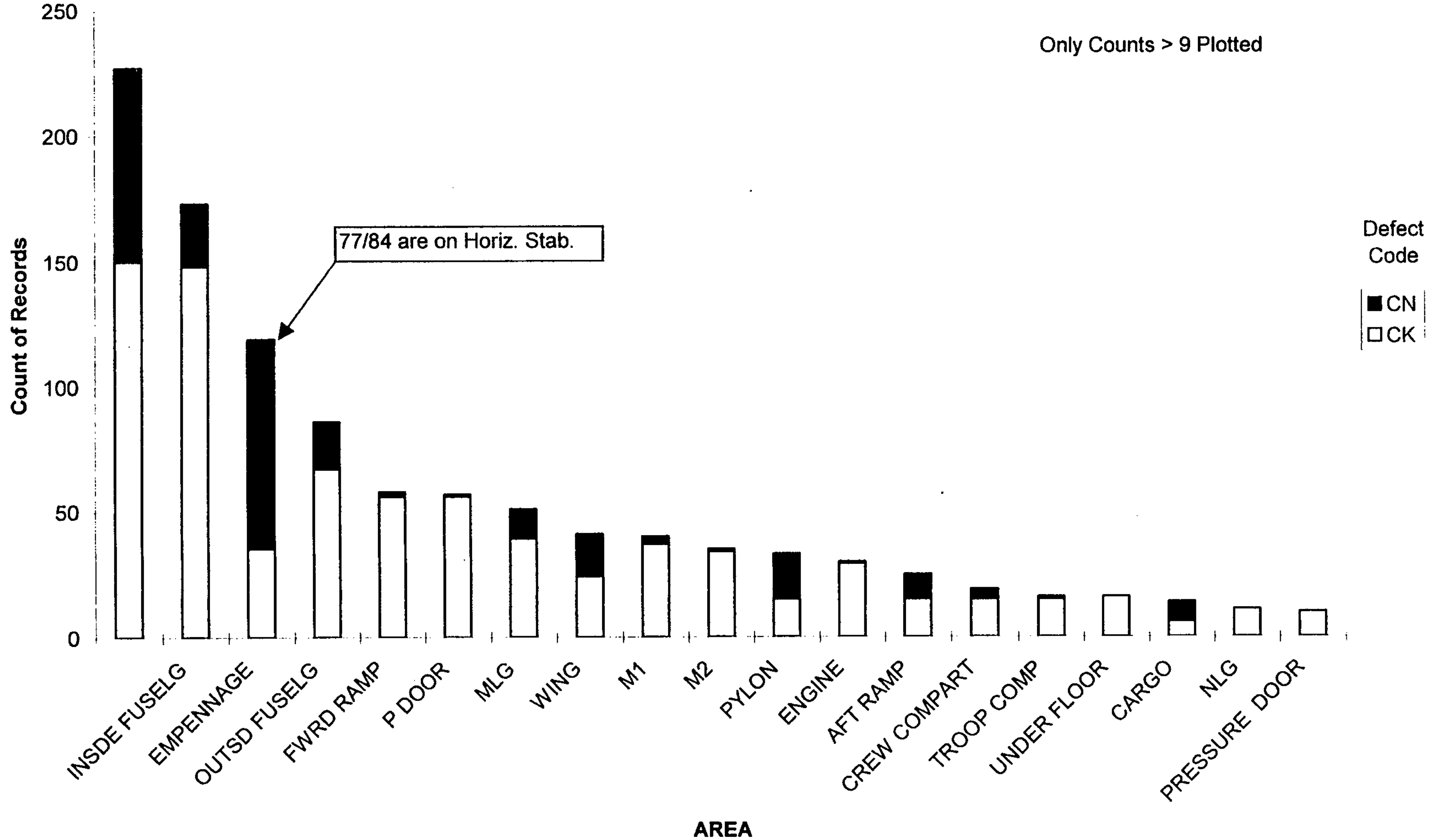

UDRI
UNIVERSITY of DAYTON RESEARCH INSTITUTE

RESULTS

C-5 ALC, Count Records by Discrepancy Text with *?* where Defect Code = Corrosion or Crack

Sum	181	514	695

Damage Code
Count of Records

Descrepency W/	CN	CK	Sum
beam	11	145	156
frame	2	146	148
stab	76	29	105
skin	16	85	101
panel	63	36	99
bulk	3	54	57
string	10	19	29

C-5 ALC, Count Records by Defect Code (CN or CK) and Work Area Description with Discrepancy Text like *Beam*

Descrepency w/	beam
Sum CK	151
Sum CN	5

Code	AREA	CountOfRecord
CK	INSDE FUSELG	54
CK		20
CK	MLG	17
CK	NLG	11
CK	ENGINE	8
CK	PYLON	8
CN	EMPENNAGE	4
CK	FWRD RAMP	4

UDRI UNIVERSITY of DAYTON RESEARCH INSTITUTE

CONCLUSIONS

- Have an assembled database and process to ID PSE's with corrosion and cracking
  - USAF standardized data recording systems are sufficient to ID PSE's with corrosion and fatigue damage
- No details in Std database indicating multiple cracks or WFD
- PSE's can be related to DADTA points with extra data entry
- Data representing the entire fleet provides best trends
- Supplemental data gathering is valuable for further substantiation, insight, and data
  - Northrop-Grumman Evaluation - Corr type and WFD (Y/N)
  - Boeing -0291 disassembly - Corr. Depth and extent of "missed" corr.
- Corrosion & Cracking Record counts for PSE's > those for DADTA's

UDRI UNIVERSITY of DAYTON RESEARCH INSTITUTE

CONCLUSIONS

C/KC-135, E-8C, C-9A/C, and C-130:

- Corrosion Record Counts > Cracking Record Counts
- Corrosion - skins
    - KC-135: skins @ fuselage A/R (Ext.)
    - E-8C: skins on lower fuselage, aft cargo, BS 960 - 1440
    - C-9A/C: wing skins, fuselage below floor
    - C-130: wing skins

C-5A/B:

- Cracking Record Counts > Corrosion Record Counts
- Cracking - Fuselage beams & frames
- Corrosion - Horizontal Stabilizer

Further consideration needed to:

- verify trends
- evaluate the impact to structural integrity

SUMMARY & RECOMMENDATIONS

* Continue to collect and evaluate corrosion and cracking trends
  - ID emerging R&M issues
  - ID emerging safety issues

* Payoff for R&M in identifying and evaluating corroded PSE's
  - ID corroded parts, quantify damage, and evaluate impact to structural integrity

* Adherence to data entry process standards
  - Install smart data entry - Tail #, MDS, WUC, zone, area, damage codes
  - Create standard work zones and areas within a MDS for transports

SESSION X

ANALYTICAL METHODS

Chairman - *F. Bartlett*
U.S. Army

The 1997 USAF Aircraft Structural Integrity Program Conference
San Antonio, Texas, 2-4 December 1997

Modeling Fastened Structural Connections Using Finite Elements

Ricardo L. Actis and Barna A. Szabo
Engineering Software Research and Development, Inc.
7750 Clayton Road, Suite 204
St. Louis, Missouri 63117
phone: 314-645-1423, fax: 314-645-1649
e-mail: ricardo@esrd.esrd.com

Topic Area: Structural Analysis

ABSTRACT

Proper models of fastened structural connections must include all the significant effects that influence their performance. Inherent nonlinear effects make the numerical treatment of these models very cumbersome and far from the reach of non-specialists in finite element analysis. To overcome this difficulty, we have developed a unique capability within our p-version FEA software Stress Check[1] which provides for the computation of the structural and the strength responses of fastened structural connections. The implementation accounts for the following:

- Partial contact between fastener and plate
- Fastener shear stiffness
- Material and geometric nonlinearities
- Interference fitting
- Initial clearance between fastener and plates

It is assumed that the effects of bending are negligible and that there is no friction between the contact surfaces. In other words, all dominant effects in shear connections are accounted for in a single analysis tool.

A unique library feature of Stress Check allows for the creation of handbook-like problem definitions for fastened structural connections parameterized by topological description, material properties and loadings. The output data, such as forces acting on fasteners, stress distributions, estimates of the size of plastic zones, etc. can be produced automatically in tabular or graphical formats. Combined with Stress Check's easy to use handbook framework, this capability provides a unique tool for analyzing structural joints in a reliable and effective way.

Solutions of high quality and reliability can be produced in a reasonably short time by persons who need not have been trained in the use of finite elements. This is because advanced nonlinear finite element analysis procedures are available from the simple handbook-like interface. This feature delivers important benefits: The ability to standardize the analysis of fastened structural connections on the basis of the most advanced FEA procedures available today, while substantially reducing time and costs of design and analysis computations. This feature also allows the computation of stress intensity factors for cracks following repair by fastened doubler plates.

1. Stress Check is a trademark of Engineering Software Research and Development, Inc.

1997 USAF Aircraft Structural Integrity Program
2-4 December 1997 - San Antonio, Texas

Modeling Fastened Structural Connections Using Finite Elements

Ricardo L. Actis and Barna A. Szabo
Engineering Software Research and Development, Inc.
St. Louis, Missouri

esrd

ESRD, Inc.

Overview

- Introduction
- Requirements for an analysis tool
- Fastener modeling in Stress Check
- Example problems:
  - Neat fit and initial clearance fasteners
  - plate doubler
  - cold-working of attachment lug
- Summary and conclusions

ESRD, Inc.

Introduction

- Full analysis of fastened connections requires consideration of:
  - Three-dimensional effects
  - Friction, contact and fastener stiffness
  - Clearance and interference fitting
  - Material and geometric nonlinearities
- Idealizations are required to make the problem tractable by numerical methods

ESRD, Inc.

Requirements for an Analysis Tool

- Easy to use and flexibility in problem definition:
  - topology, materials and boundary conditions
  - neat, interference or clearance fit fasteners
  - crack from fastener holes or broken fasteners
- Account for major nonlinear effects:
  - contact and material nonlinearities
- Provide structural and strength responses:
  - fastener loads and localized stresses

ESRD, Inc.

Fastener Modeling in Stress Check

- Main features of the implementation:
  - p-version FEA with handbook style interface
  - partial contact between fastener and plate
  - accounts for shear stiffness of fasteners
  - geometric and material nonlinearities
  - neat fit, interference fitting or initial clearance
- Restrictive assumptions:
  - The effects of bending are negligible
  - No friction between the contact surfaces

ESRD, Inc.

Fastener Modeling in Stress Check

- *Fastener element*: Distributed spring with a 2 DOF rigid core

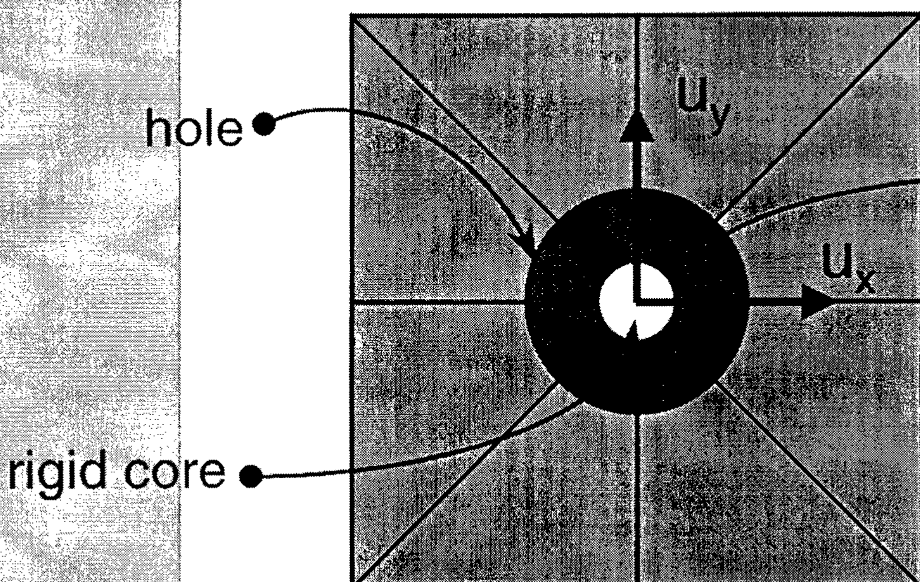

planar body with typical mesh detail

distributed spring

$$K_n = \frac{2E}{D(1+\nu)(1-2\nu)}$$

ESRD, Inc.

Example Problems

- Hole with neat fit fasteners
- Hole with initial clearance fasteners
- Plate doubler with six fasteners
- Cold working of attachment lug

Holes with Neat Fit Fasteners

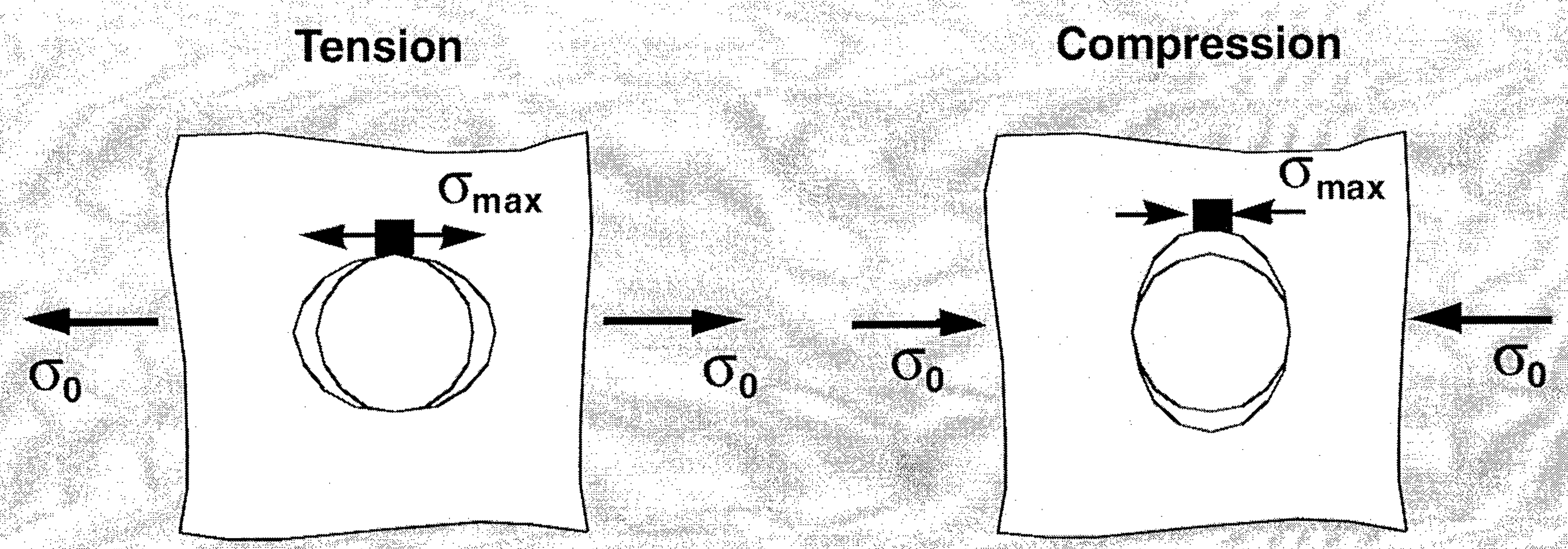

$$K_t = \frac{\sigma_{max}}{\sigma_0}$$

ESRD, Inc.

Hole with Neat Fit Fastener

Fastener	Plate	K_t (tension)		K_t (compression)	
		Ref.*	SC	Ref.*	SC
Steel	Steel	2.595	2.60	1.905	1.75
Steel	Titanium	2.493	2.50	1.716	1.58
Steel	Aluminum	2.425	2.43	1.600	1.52

(*) W. T. Fujimoto, *Tensile and Compressive Stress Concentration Factors for Holes with Clearance Fit Fasteners*, MDA April 1976.

Hole with Clearance Fit Fastener

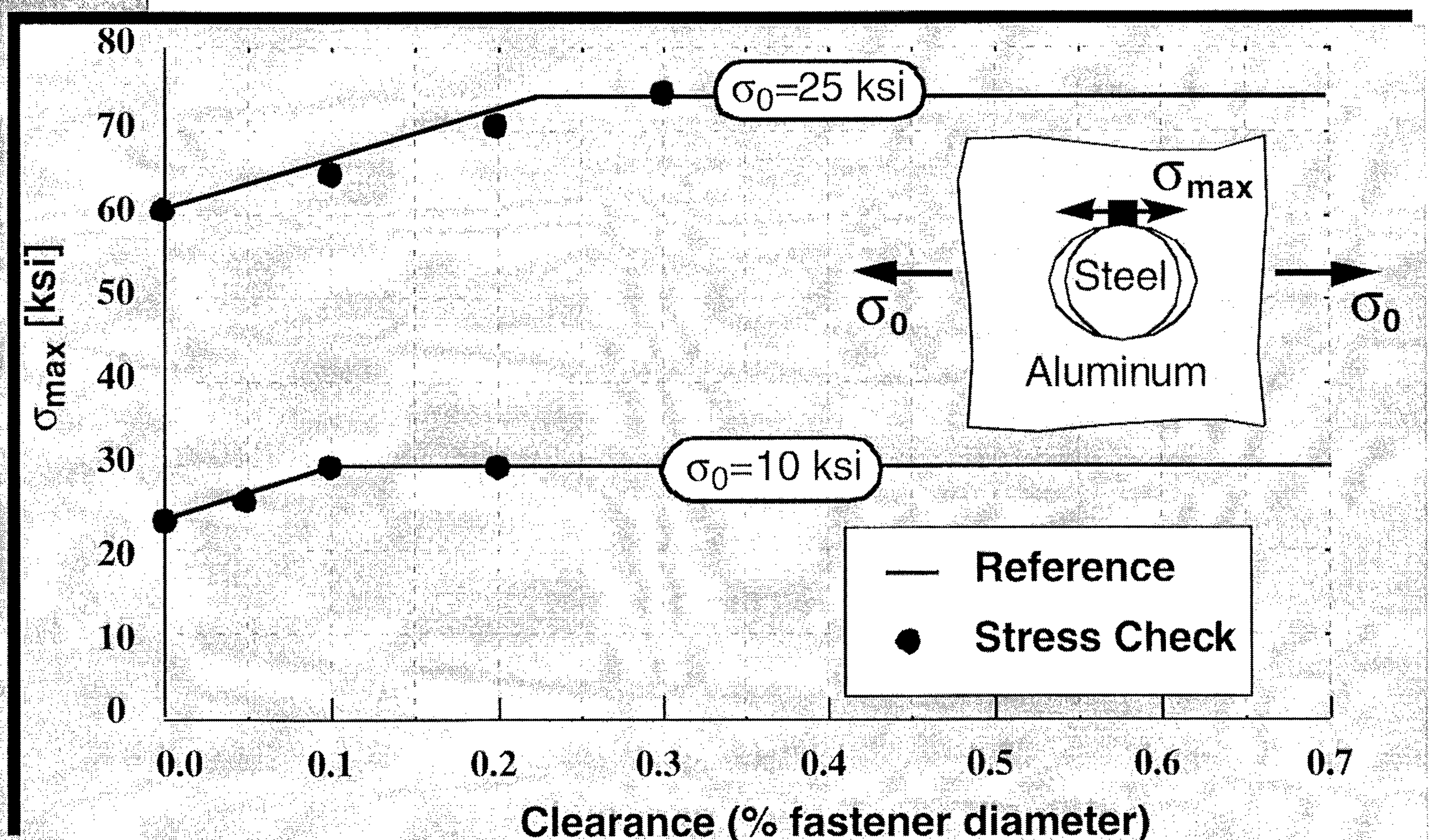

ESRD, Inc.

Results: σ_x and bearing stresses

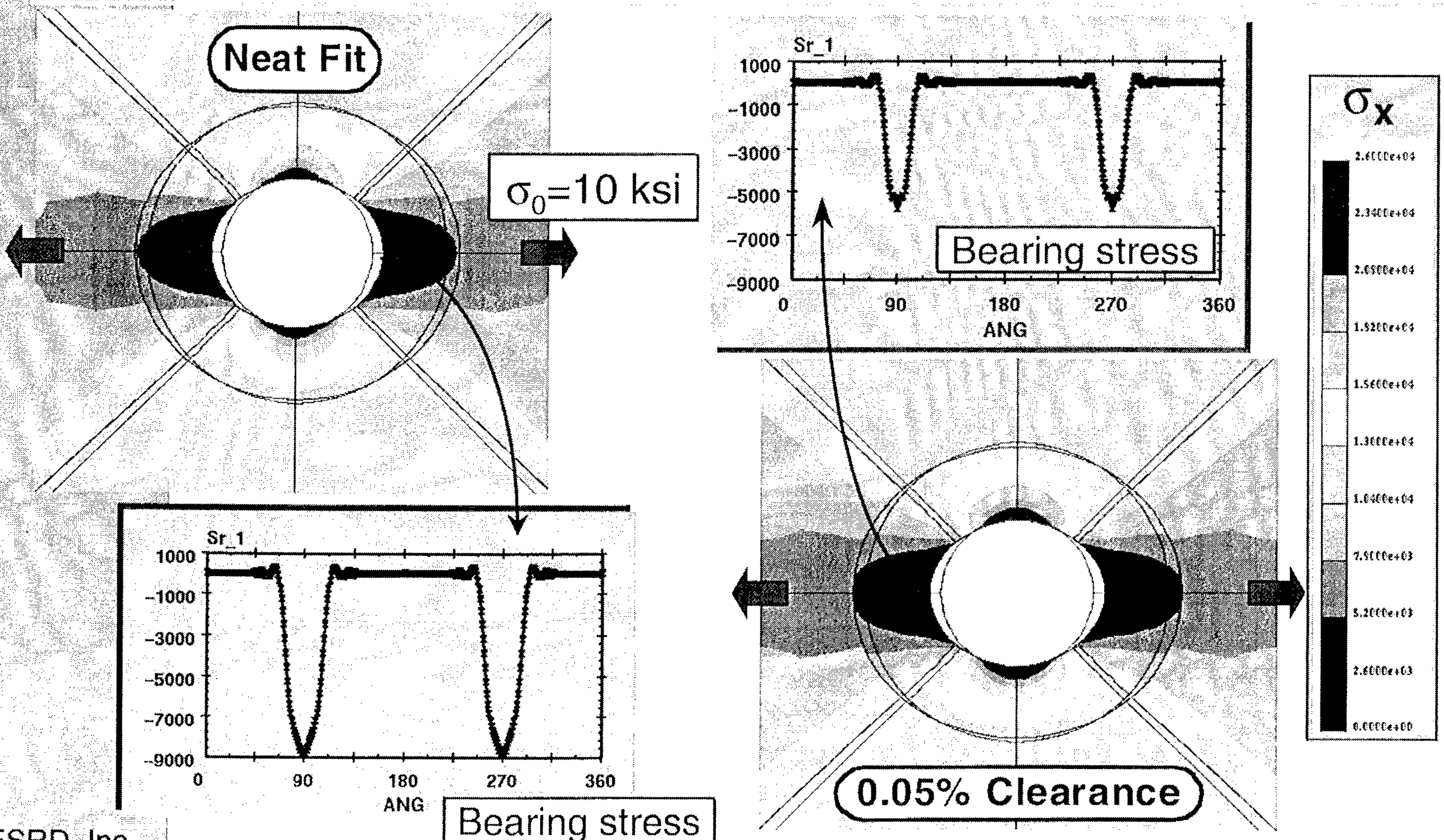

ESRD, Inc.

Plate Doubler

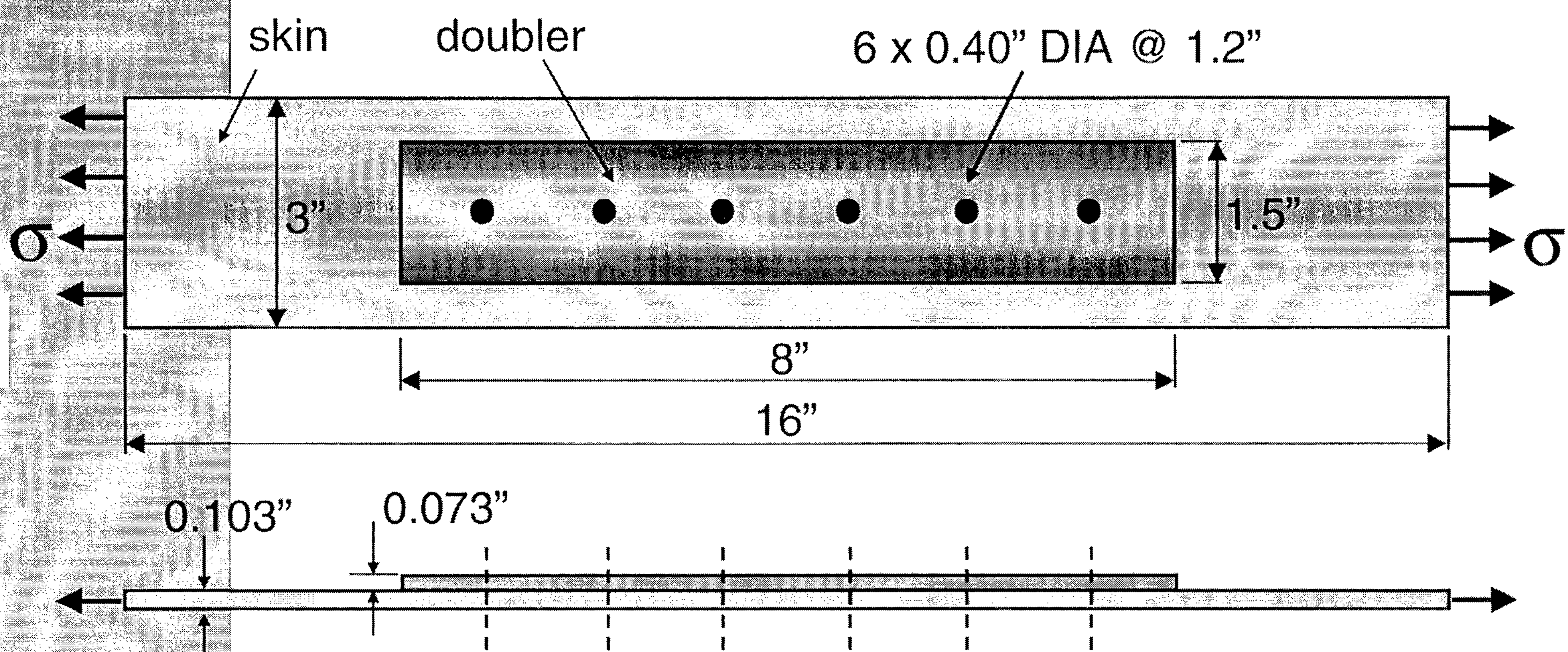

7075-T6 skin & doubler
Steel fasteners

ESRD, Inc.

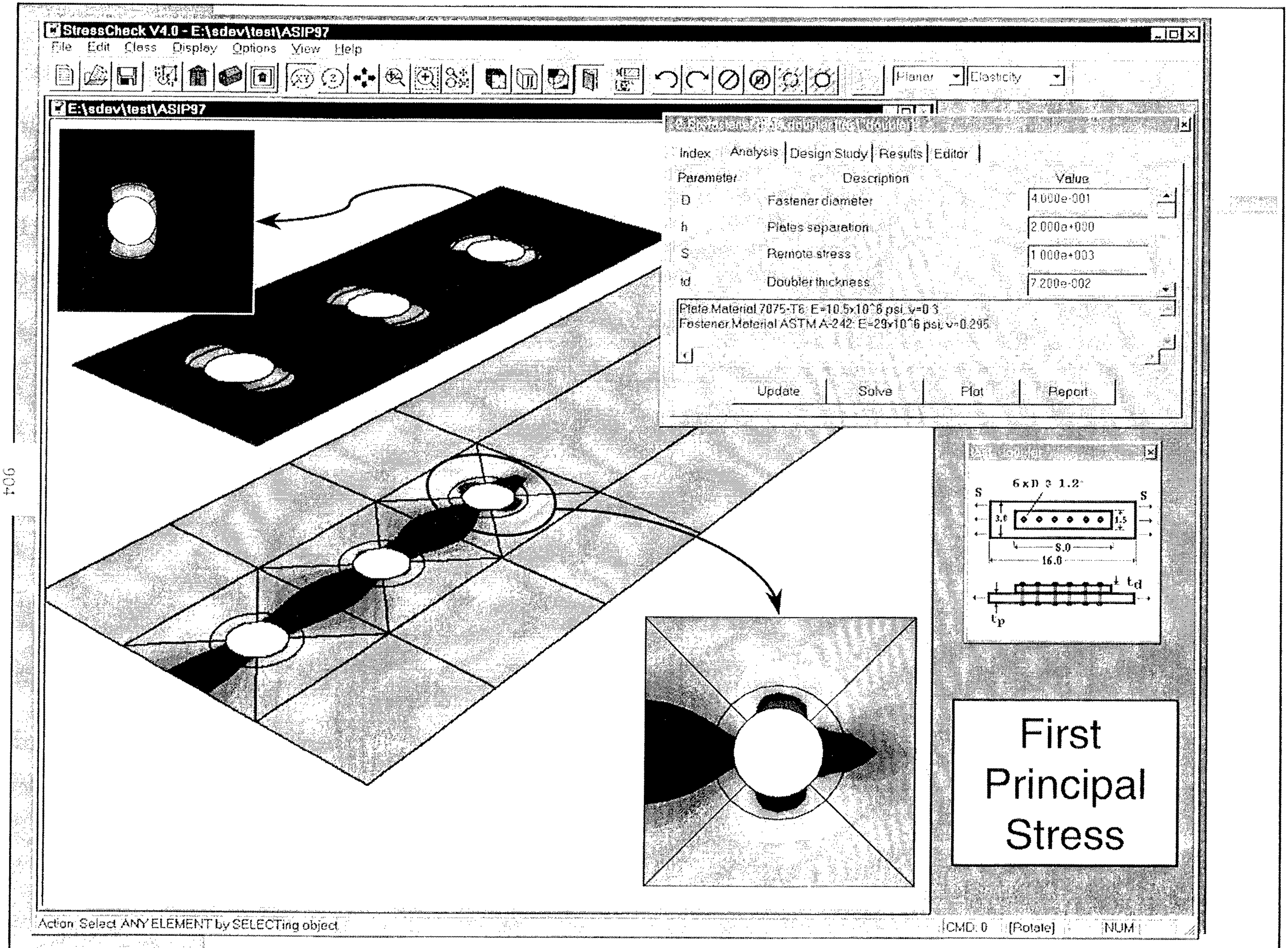
StressCheck V4.0 - E:\sdev\test\ASIP97
File Edit Class Display Options View Help
Planer
Elasticity
E:\sdev\test\ASIP97
Index Analysis Design Study Results Editor
Parameter Description Value
D Fastener diameter 4.000e-001
h Plates separation 2.000e+000
S Remote stress 1.000e+003
td Doubler thickness 7.200e-002
Plate Material 7075-T6: E=10.5x10^6 psi, v=0.3
Fastener Material ASTM A-242: E=29x10^6 psi, v=0.295
Update Solve Plot Report
6 x D @ 1.2
S
S
3.0
1.5
8.0
16.0
td
tp
First Principal Stress
Action: Select ANY ELEMENT by SELECTing object
CMD: 0
[Rotate]
NUM

Bearing Stress data

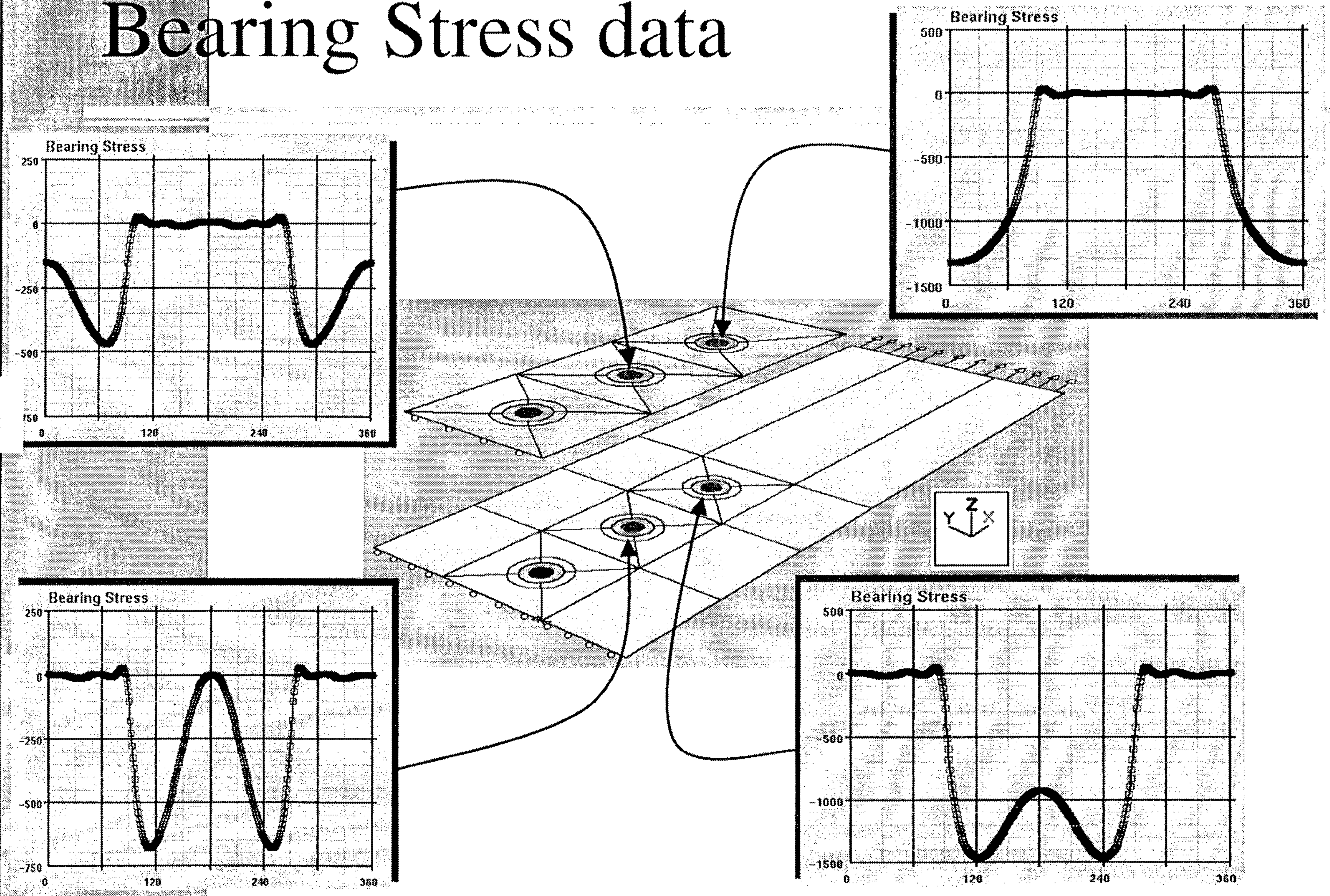

Cold Working of Attachment Lug

- Fastener element simulates mandrel
- Nonlinear analysis using deformation theory of plasticity
- Residual stresses computed by superposition
- Results include residuals, elastic-plastic and combined stresses due to residuals and external loading

ESRD, Inc.

Cold Working of Attachment Lug

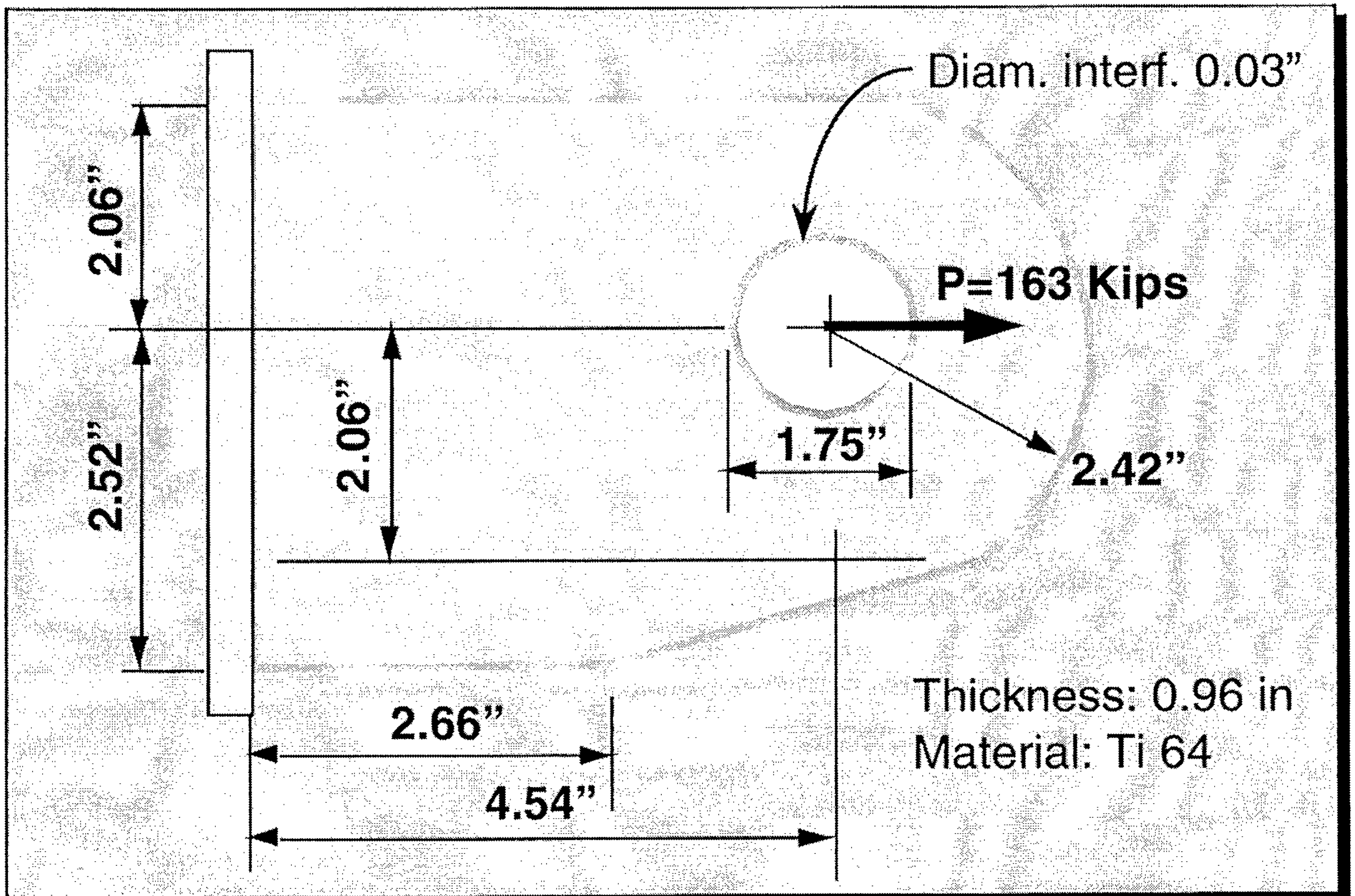

ESRD, Inc.

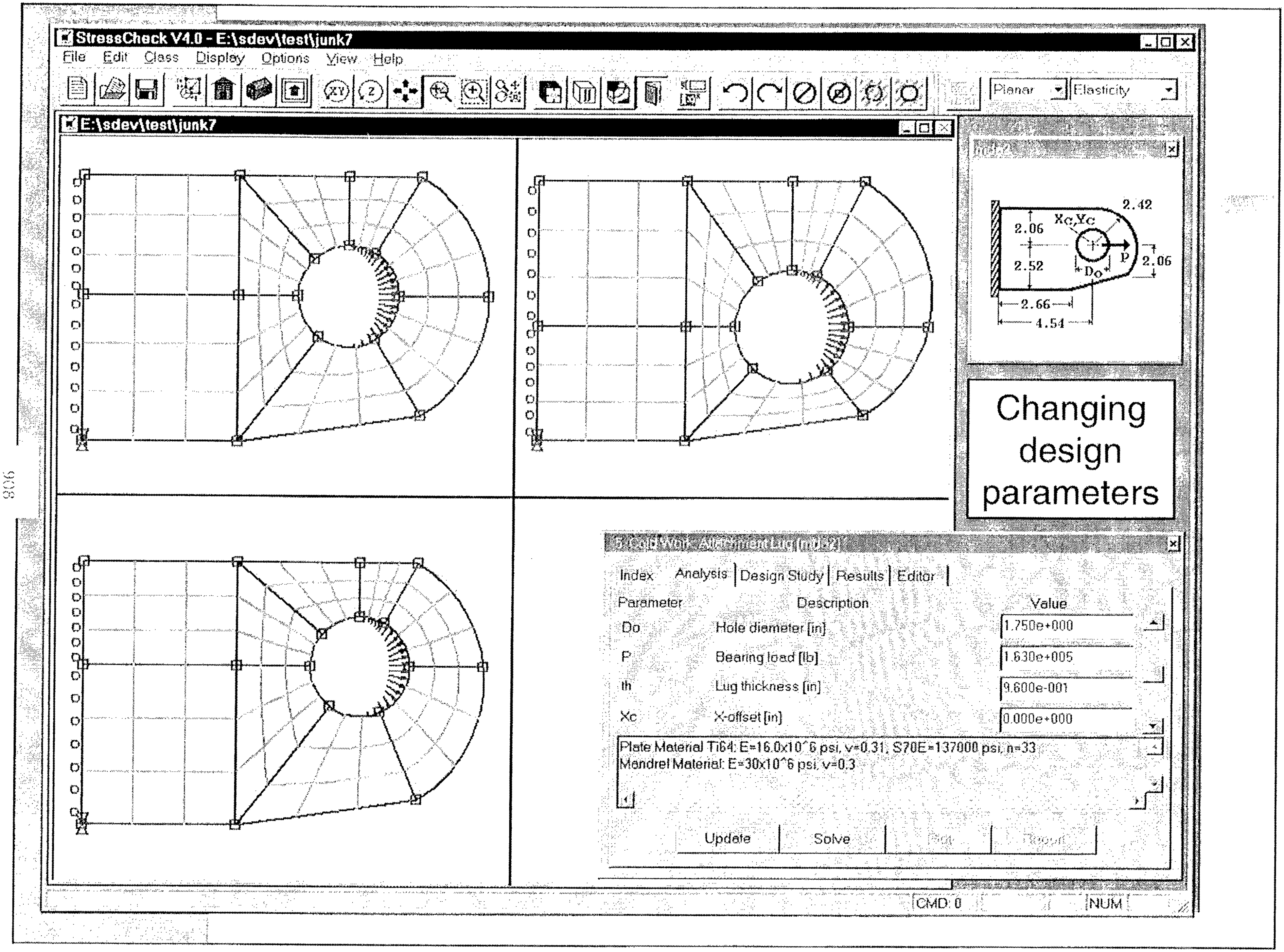
StressCheck V4.0 - E:\sdev\test\junk7
File Edit Class Display Options View Help
Planar
Elasticity
E:\sdev\test\junk7
2.42
2.06
Xc,Yc
2.52
P
2.06
Do
2.66
4.54
Changing design parameters
Index
Analysis
Design Study
Results
Editor
Parameter
Description
Value
Do
Hole diameter [in]
1.750e+000
P
Bearing load [lb]
1.630e+005
th
Lug thickness [in]
9.600e-001
Xc
X-offset [in]
0.000e+000
Plate Material Ti64: E=16.0x10^6 psi, v=0.31, S70E=137000 psi, n=33
Mandrel Material: E=30x10^6 psi, v=0.3
Update
Solve
CMD: 0
NUM

Elastic-Plastic and Residual Stresses

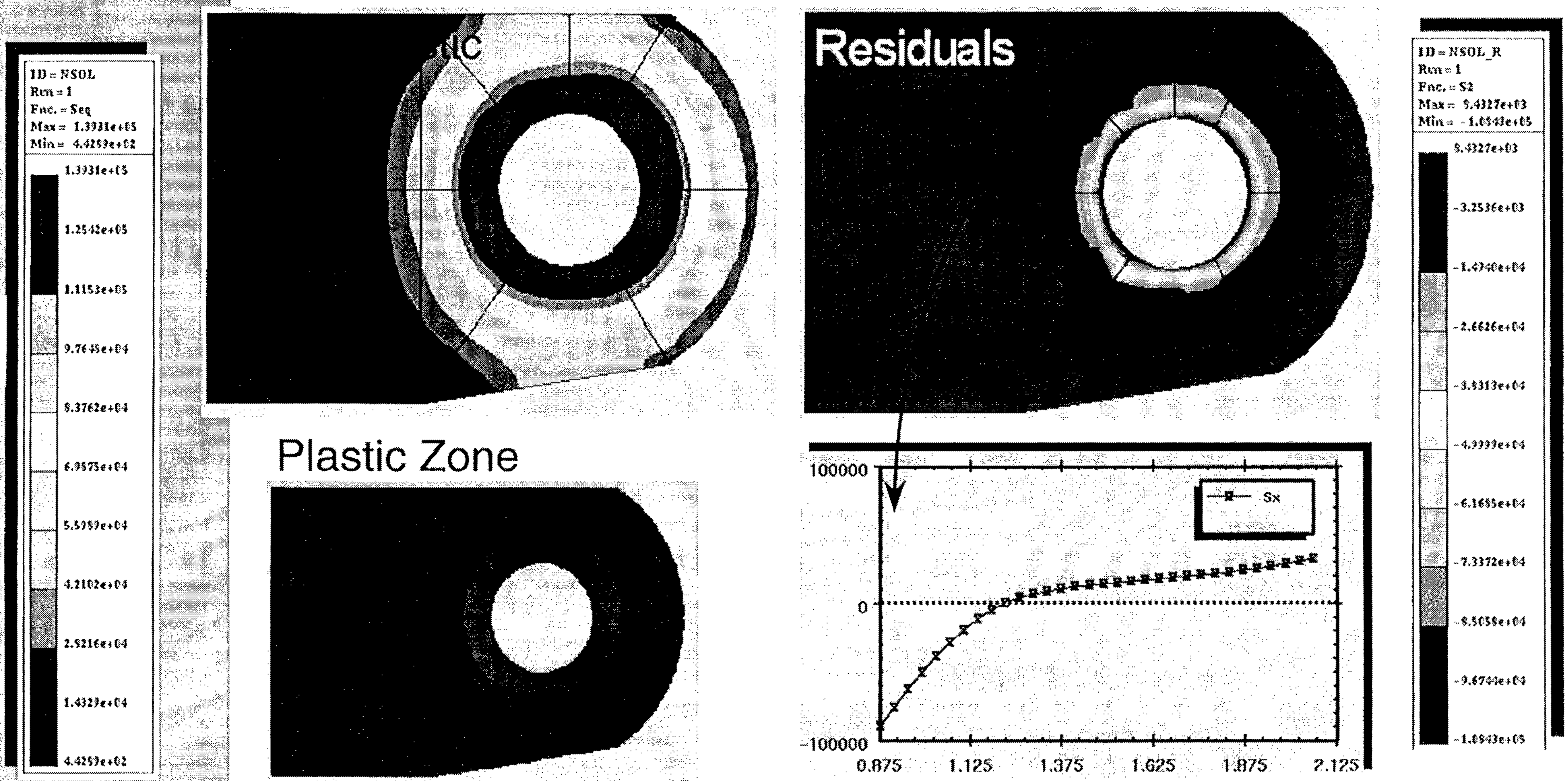

ESRD, Inc.

Stresses Due to the Bearing Load

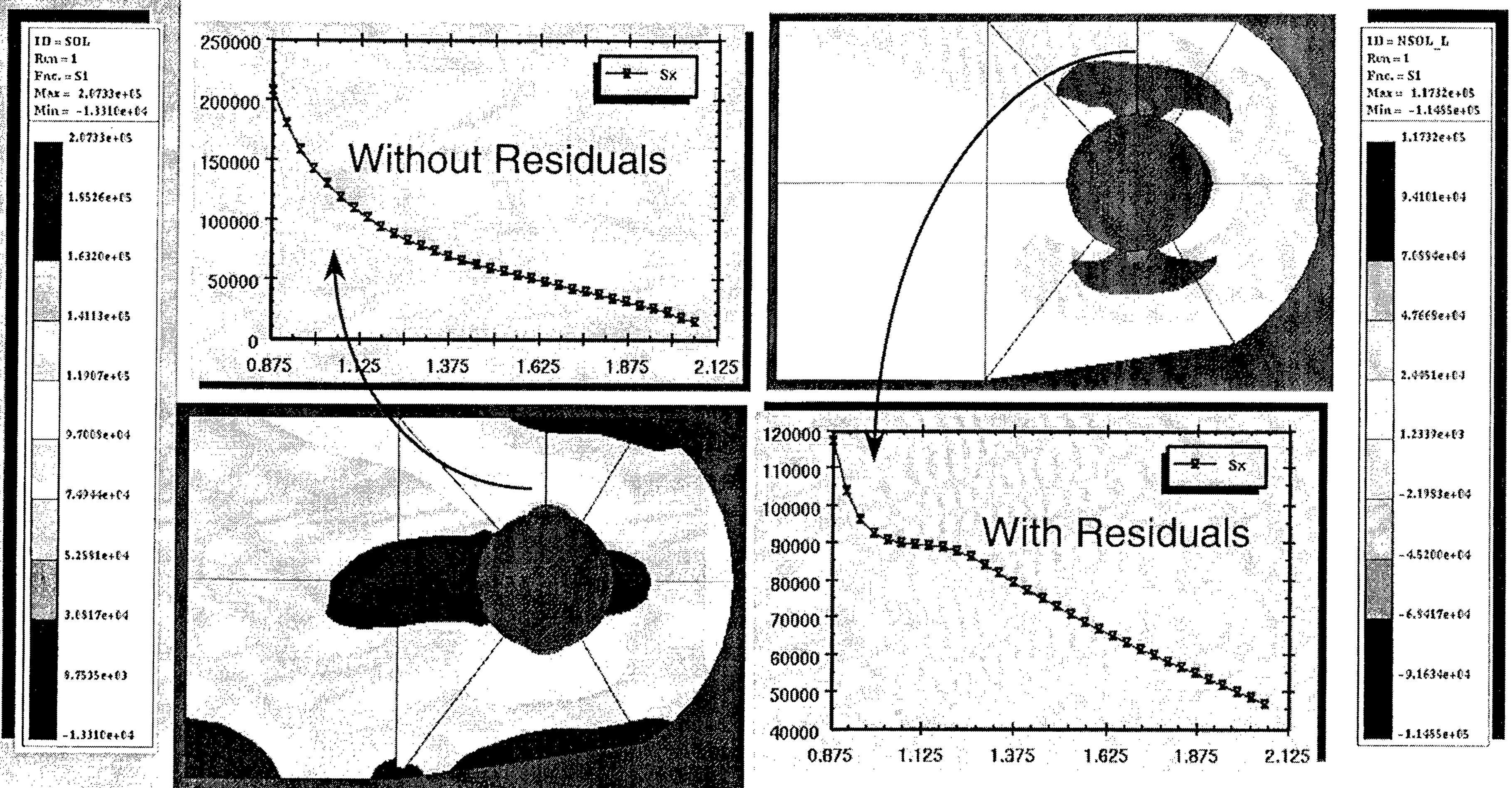

ESRD, Inc.

Summary and Conclusions

- Advanced FEA technology can be made accessible to design engineers through proper implementation
- Structural and strength responses can be obtained with a single model
- Most significant effects in shear connections are accounted for

ESRD, Inc.

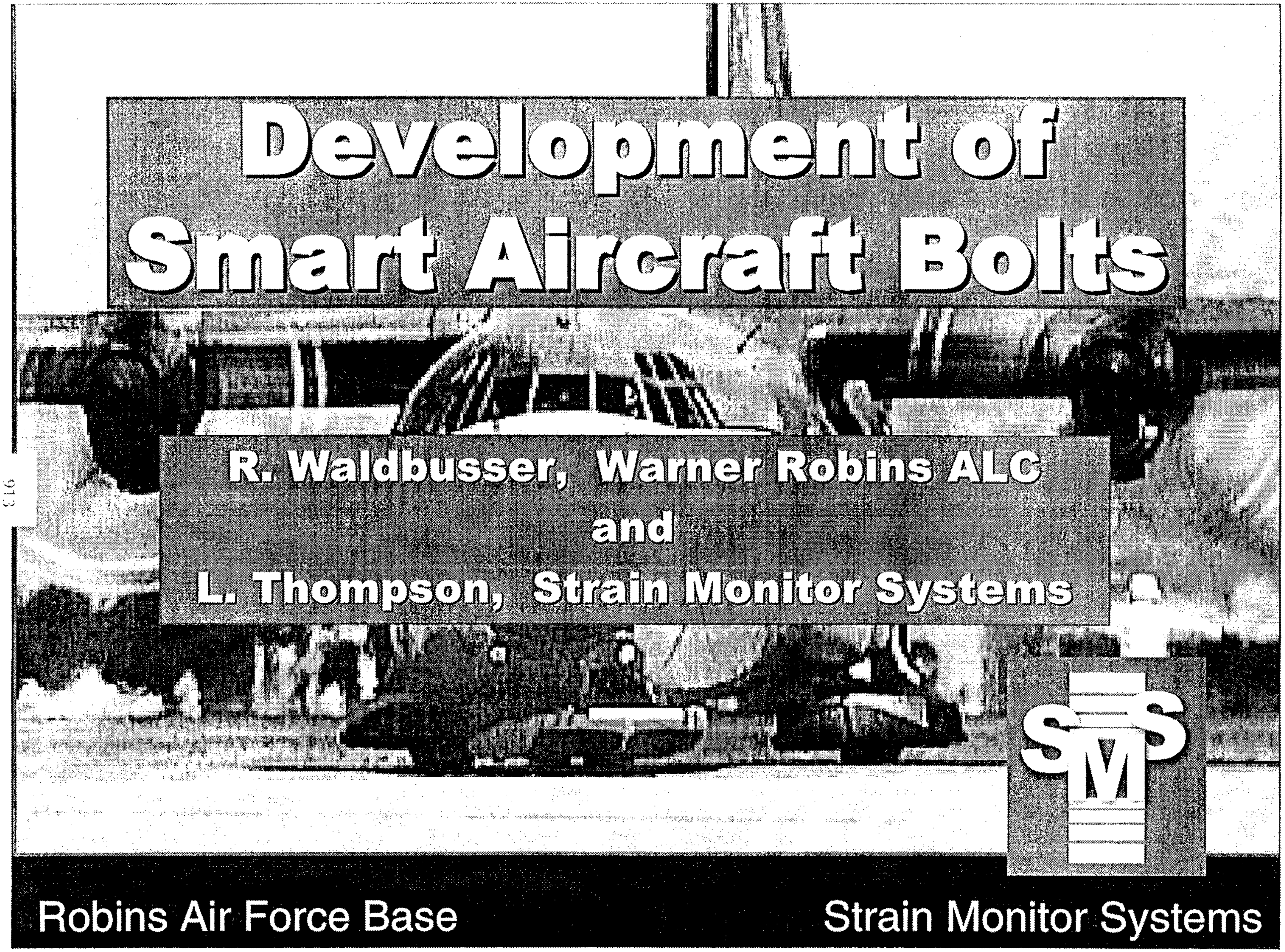
Development of
Smart Aircraft Bolts
R. Waldbusser, Warner Robins ALC
and
L. Thompson, Strain Monitor Systems
Robins Air Force Base
Strain Monitor Systems

Presentation Outline

- Smart Aircraft Bolt: Problem Definition
- TRIP Steels: What and Why?
- SBIR Program Description
- Phase I Results
- Phase II Challenges
- Conclusions and Acknowledgments

Robins Air Force Base

Strain Monitor Systems

Problem

- High-Strength Bolts
  - Require Periodic Inspection
  - Wing, Engine, & Empennage Attachments
- Cause Damage When Removed
  - Scoring of Fittings
  - Fatigue Crack Initiation Points

Solution

- Inspect Bolt While Installed
  - Better Inspection Method
  - Better Bolt
- Develop “Smart” Bolt
  - Detect Damage While Installed
  - Monitor Damage Accumulation During Service
- SBIR Project Initiated
  - Focused on “Smart” Material Approach
  - Passive, Self-Diagnostic Mechanism

Robins Air Force Base — Strain Monitor Systems

TRIP Steels for Aircraft Bolt Applications

- TRansformation Induced Plasticity Steels
- High-Strength and High-Toughness Steels Developed in 1960's at U. C. Berkeley
  - Profs. Earl R. Parker and Victor F. Zackay
  - Goal Was to Compete with High-Strength, Low-Alloy Steels (AISI 4340 and 4140)
  - Strain-Induced Phase Transformation Responsible for Exceptional Mechanical Properties

Robins Air Force Base

Strain Monitor Systems

SBIR Project Goals

- Phase I: Identify Candidate TRIP Steels for MS21250-12 and -14 Applications
  - Three Alloy Compositions Identified
  - Larger Heats Fabricated
- Phase II: Mechanical Testing
  Fabrication Testing
  Design Optimization
  Prototype Field Testing

Robins Air Force Base

Strain Monitor Systems

SBIR Phase I

- Alloy Compositions, wt %
  - RT-1: Fe-8.0Ni-9.0Cr-2.0Mn-0.25C
  - RT-2: Fe-8.0Ni-9.0Cr-2.0Mn-0.30C
  - RT-6: Fe-9.0Ni-13.0Cr-2.0Mn-3.0Mo-0.20C
- Acceptance Based on Strength Characteristics (Yield and Ultimate Tensile Strengths), Ductility, and MS21250 Specified Ultimate Load

Robins Air Force Base   Strain Monitor Systems

Strain-Induced Martensite

- Plastic Straining Triggers a Solid-State Phase Transformation
- Austenite (FCC) to Martensite (BCC or BCT depending on Carbon Content)
- Austenite = Non-Ferromagnetic
- Martensite = Ferromagnetic
- Inherent Damage Monitoring Capacity!

Stress-Assisted Martensite

- Austenite-to-Martensite Phase Transformation Occurs Within Elastic Deformation Regime
- Extent of Transformation Could Be Used as an Indicator of Installation Stresses Below Yield Point
- Useful for Elastic Stress Monitoring
- Passive Detection Mechanism

Robins Air Force Base — Strain Monitor Systems

Typical Smart Bolt Response Characteristics

- Degree of Ferromagnetic Output Increases as Extent of Deformation Increases
- Dislocation Mechanism Independent of Loading Scenario
- Responds Only to Increases in Peak Applied Strain
- Can Detect Elastic, Yielding, and Plastic Deformation
- Ideal for Passive Detection and Monitoring of Damage Accumulation During Service

Robins Air Force Base   Strain Monitor Systems

TRIP Steel Microstructure

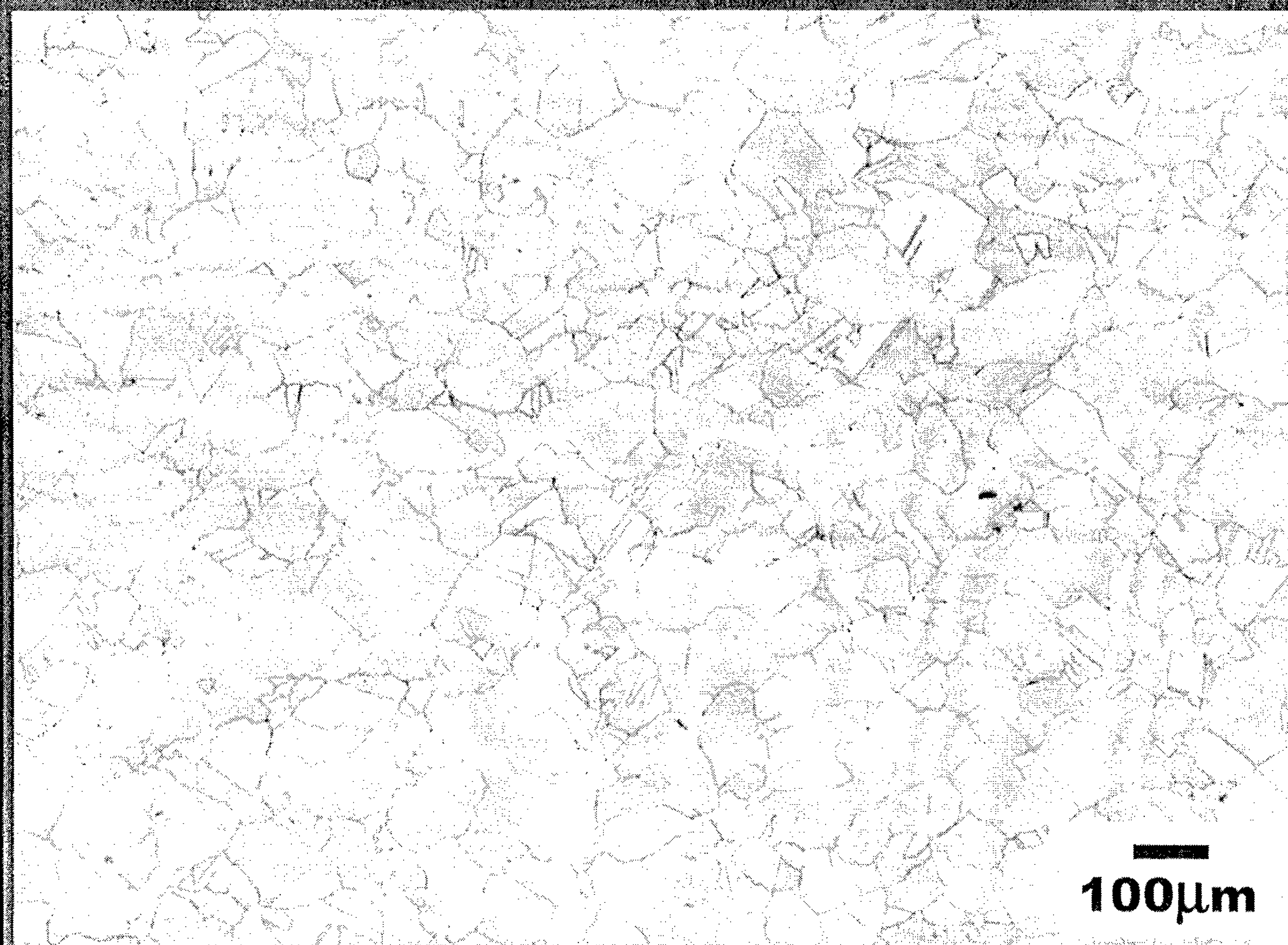

Robins Air Force Base

Strain Monitor Systems

Runaway Grain Growth

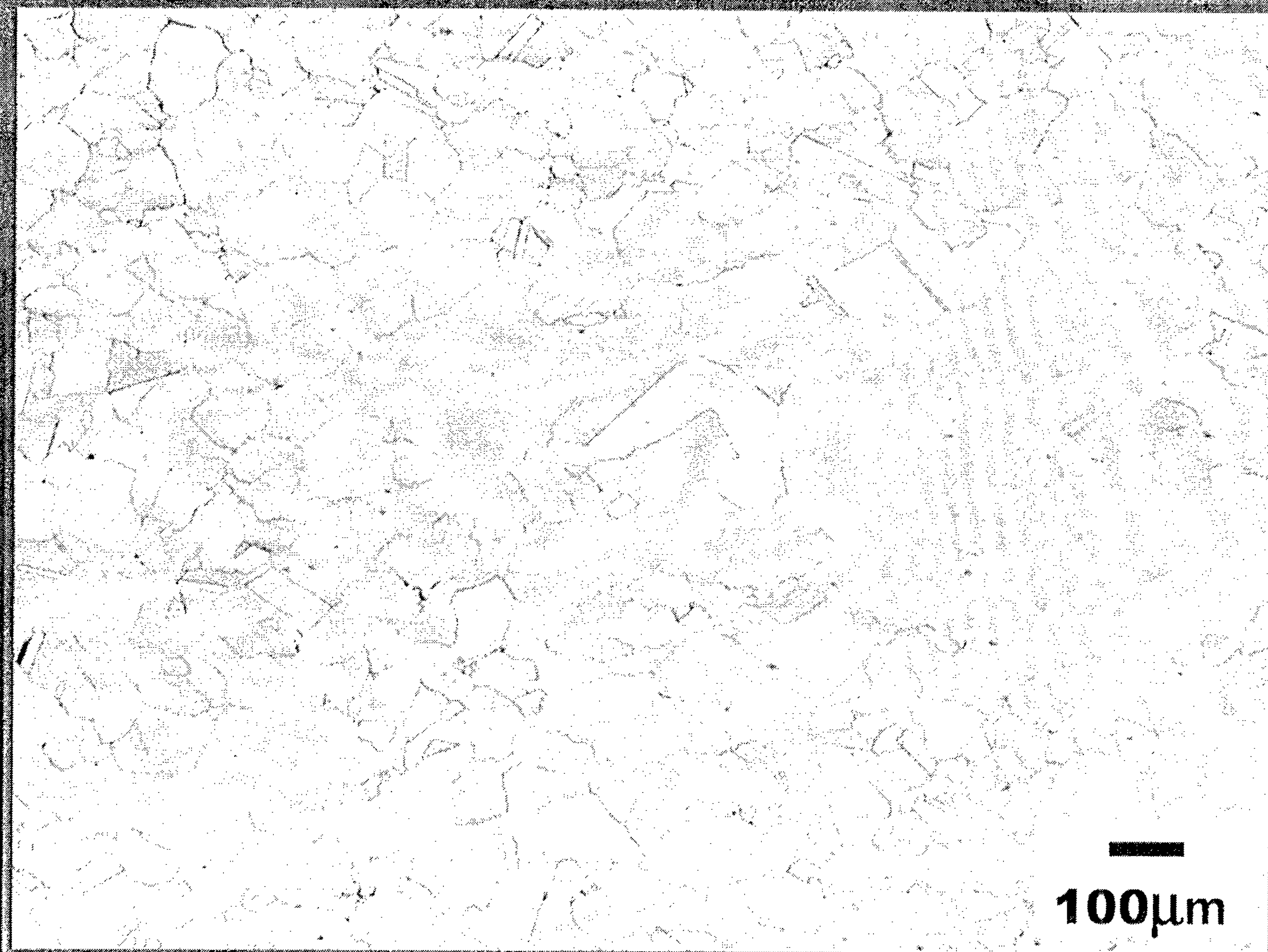

Robins Air Force Base

Strain Monitor Systems

TRIP Steel Mechanical Properties

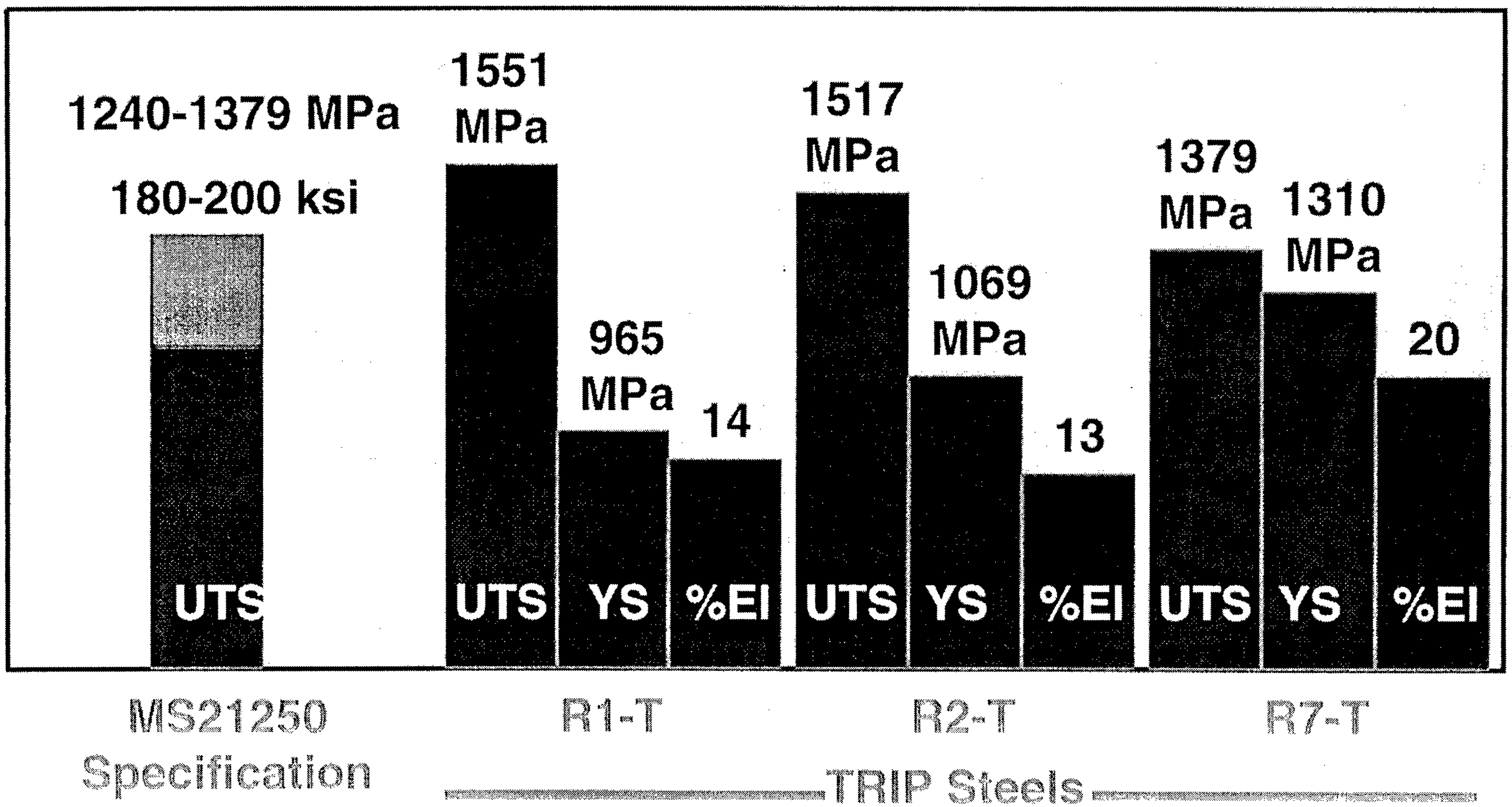

Robins Air Force Base

Strain Monitor Systems

Smart Bolt Design Evaluation Criteria

- Four Smart Bolt Designs Evaluated
- Evaluation Criteria:
  - Fabrication Cost
  - Passive Operation Mode During Service
  - Interrogated During Routine Maintenance Inspections
  - Installation Similar to Conventional Bolts

Robins Air Force Base

Strain Monitor Systems

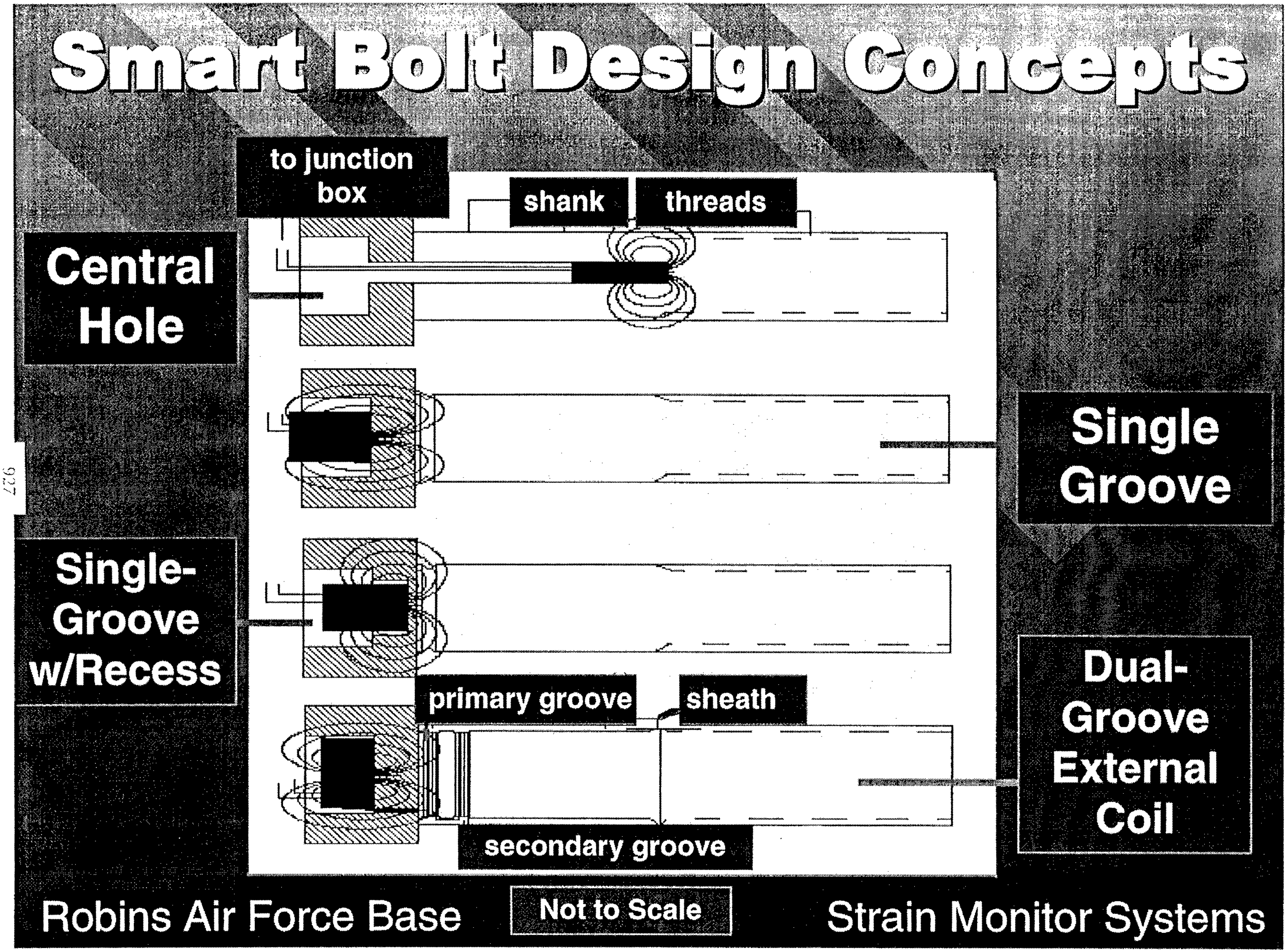
Smart Bolt Design Concepts
to junction box
shank
threads
Central Hole
Single Groove
Single-Groove w/Recess
primary groove
sheath
Dual-Groove External Coil
secondary groove
Robins Air Force Base
Not to Scale
Strain Monitor Systems

Centrally-Drilled Hole Design

- One Extra Fabrication Step
- Ferromagnetic Interference Produced a High Noise Level
- Signal Output Irregular
- Design Abandoned

Robins Air Force Base

Strain Monitor Systems

Dual-Grooved Shank Design

- Externally Wound Detection Coils
- Primary and Secondary Stress-Concentration Grooves in Shank
- Strong Signal Output
- Costly and Cumbersome
- Design Abandoned

Shank-Groove Design

- Single Groove Below Bolt Head
  - Detection Electronics Mounted in Bolt Head Weight-Reduction Cavity
  - Externally Wound Groove Coil
- Groove Formed During Thread Rolling
  - No Extra Fabrication Step
  - Electronics Mount = One Extra Manufacturing Step

Robins Air Force Base

Strain Monitor Systems

Shank-Groove with Bolt Head Recess Design

- Single Shank Stress-Concentration Groove
- Weight Cavity Recess to Move Detection Electronics Closer to Groove Region
- Groove Formed During Thread Rolling
- Cavity Recess Introduced During Head Forging
- Improved Signal Output Strength

Robins Air Force Base — Strain Monitor Systems

Stress Concentration Groove Analysis

h = depth, r = radius, k = stress conc. factor

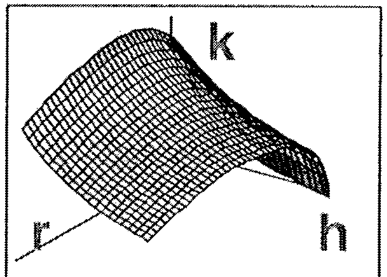

Tension

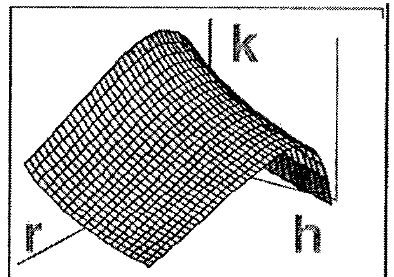

Bending

Tension: 1.36-3.57

Bending: 1.34-3.03

Torsion: 1.33-2.08

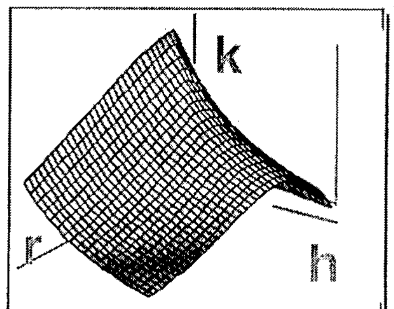

Torsion

Robins Air Force Base

Strain Monitor Systems

External Coil Signal Output: Subscale Bolt Tested in Tension

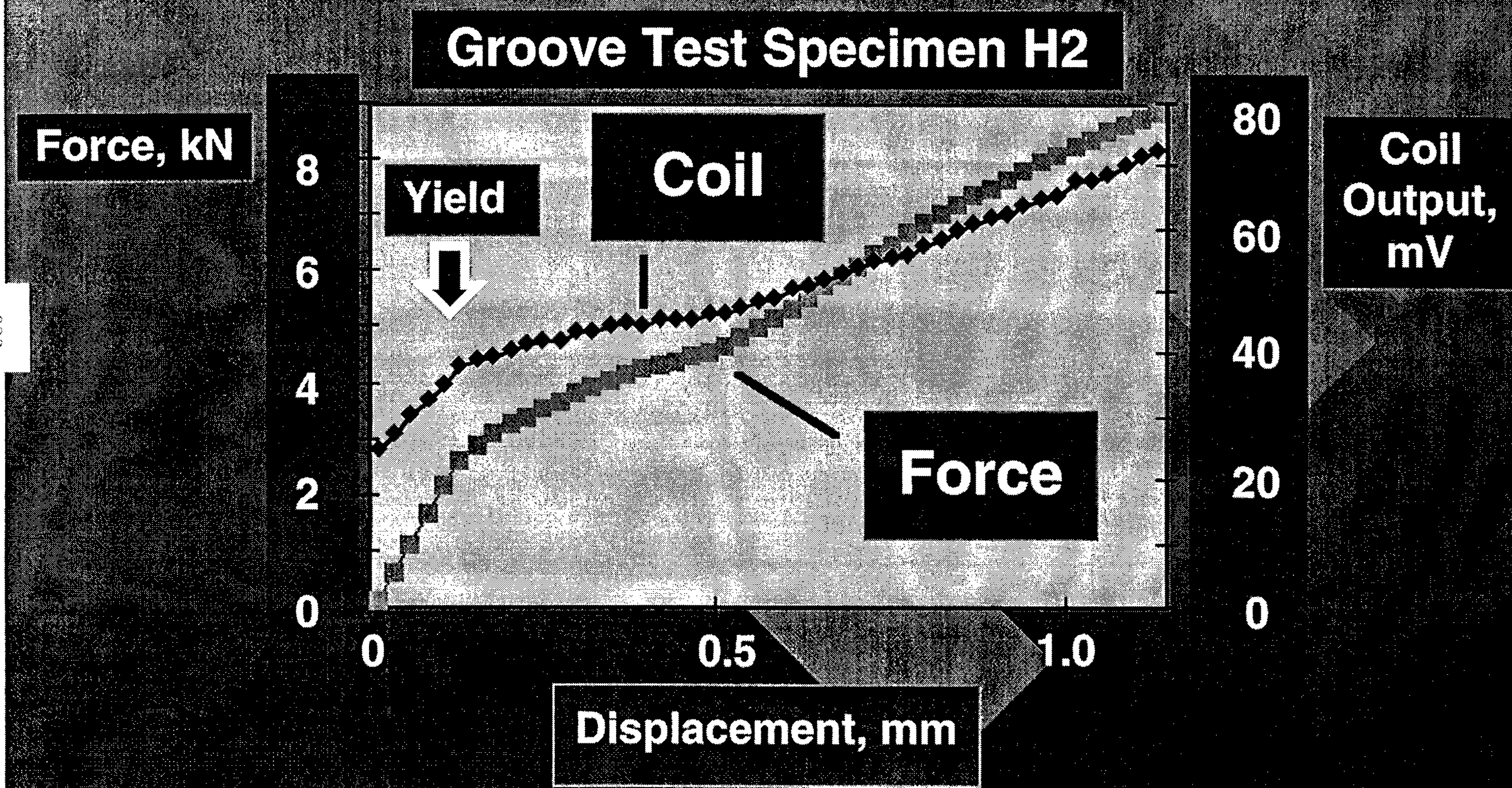

Robins Air Force Base

Strain Monitor Systems

External Coil Signal Output: Tested in Reverse Tension

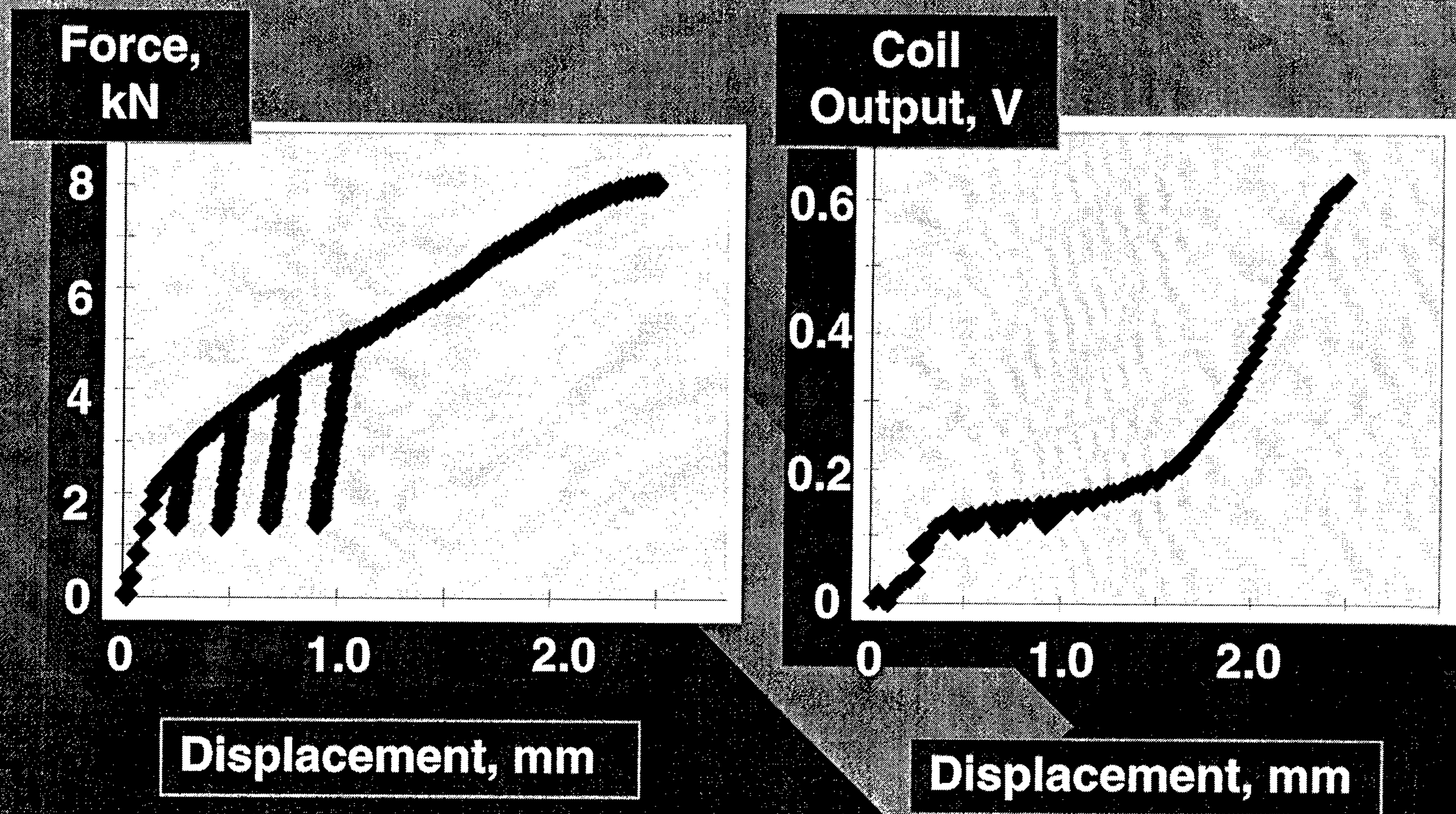

Robins Air Force Base

Strain Monitor Systems

MS21250-12 and -14 Bolt Groove Testing

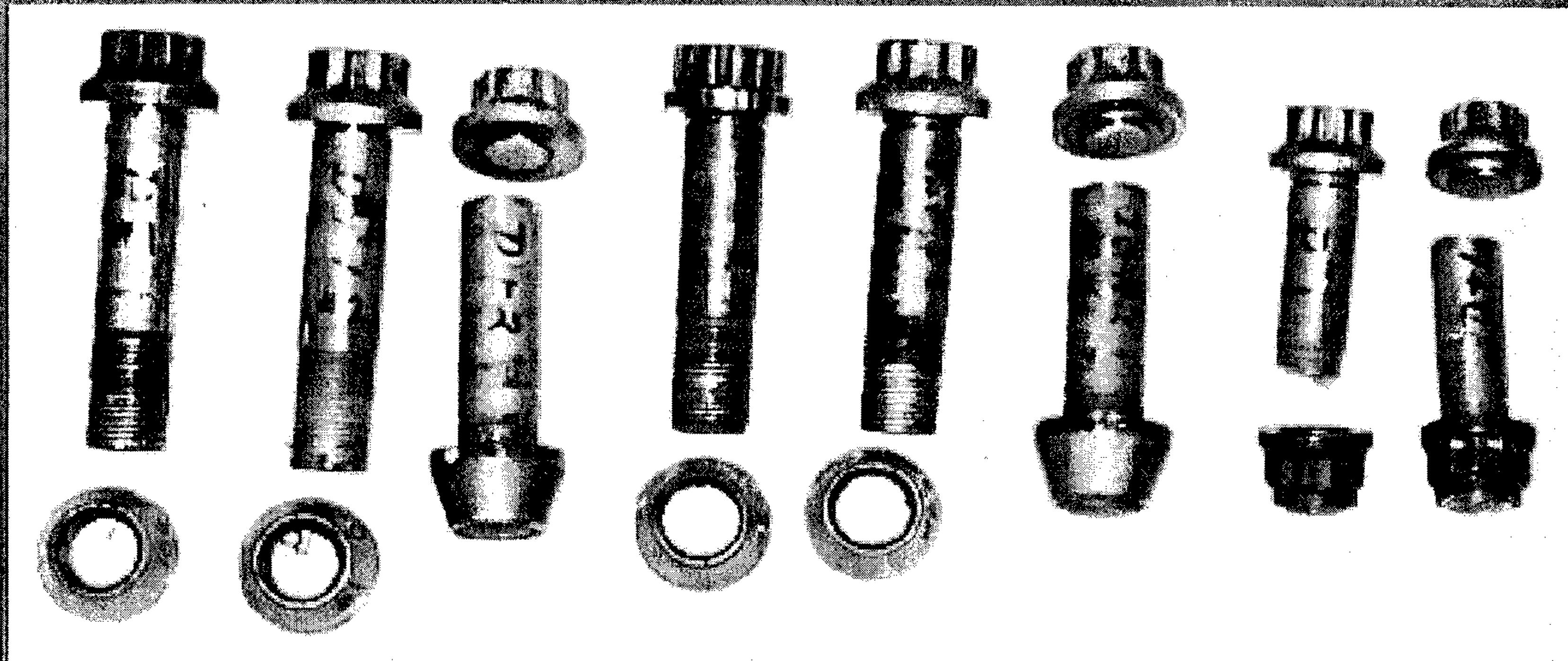

Failure Modes:
1. Thread Fracture
2. Threads Stripped
3. Groove Fracture

Robins Air Force Base

Strain Monitor Systems

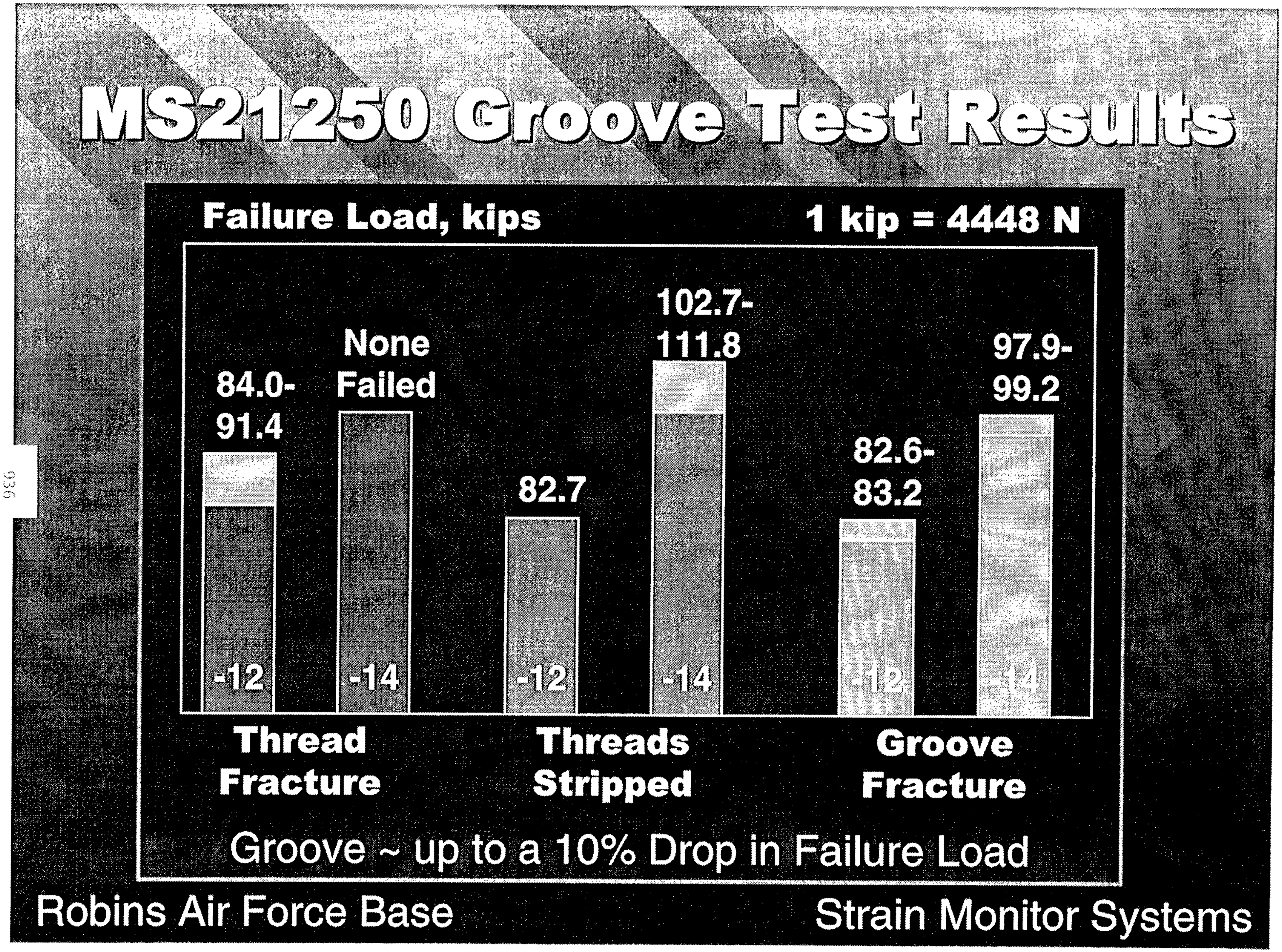
MS21250 Groove Test Results
Failure Load, kips
1 kip = 4448 N
84.0-
91.4
None
Failed
82.7
102.7-
111.8
82.6-
83.2
97.9-
99.2
-12
-14
-12
-14
-12
-14
Thread
Fracture
Threads
Stripped
Groove
Fracture
Groove ~ up to a 10% Drop in Failure Load
Robins Air Force Base
Strain Monitor Systems

Smart Bolt Fabrication Issues

- TRIP Steel Warm Rolling (at 450°C) Required to Meet Yield Strength Specifications
- Head Forging Generally Performed at Higher Temperatures

Robins Air Force Base

Strain Monitor Systems

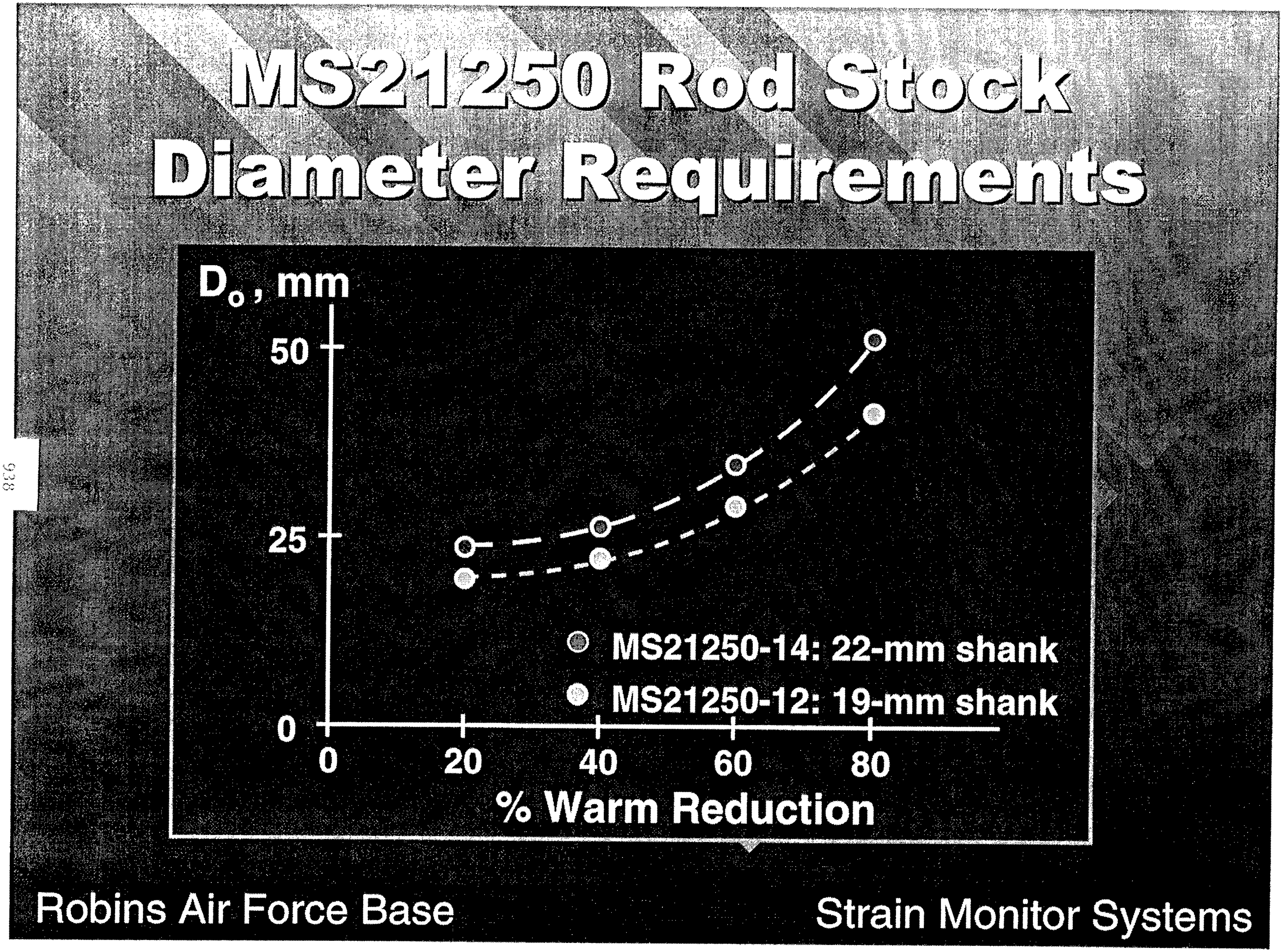

MS21250 Rod Stock
Diameter Requirements
D_o, mm
50
25
0
0
20
40
60
80
% Warm Reduction
MS21250-14: 22-mm shank
MS21250-12: 19-mm shank
Robins Air Force Base
Strain Monitor Systems

Smart Bolt Fabrication Plan

- Forge Alloy to Round Rod Form
- Anneal to Obtain Equiaxed Microstructure
- Warm Rolling to Desired Diameter
  - High Performance Alloys, Inc.
    Tipton, IN 46072-0040
  - Rotary Forging Capability
  - Specialty: Small Lots and High Performance Materials
- Slice to Length for Bolt Manufacturing

Robins Air Force Base

Strain Monitor Systems

Conclusions

- TRIP Steels Offer Potential for Aircraft Fastener Applications
- Passive Monitoring Approach to Save Bolt Inspection Time and Money
- Further Mechanical Testing Required to Identify Optimum Approach
- Cost Target = Widespread Application

Robins Air Force Base   Strain Monitor Systems

Acknowledgments

The authors extend appreciation to the USAF and WPAFB for funding the SBIR Program " Development of a Structural Health Monitoring System" through contract no. F096550-96-C-0382.

We also appreciate the attention given to the program by the USAF Administrative Officer, Lt. Bill Braasch.

Robins Air Force Base — Strain Monitor Systems

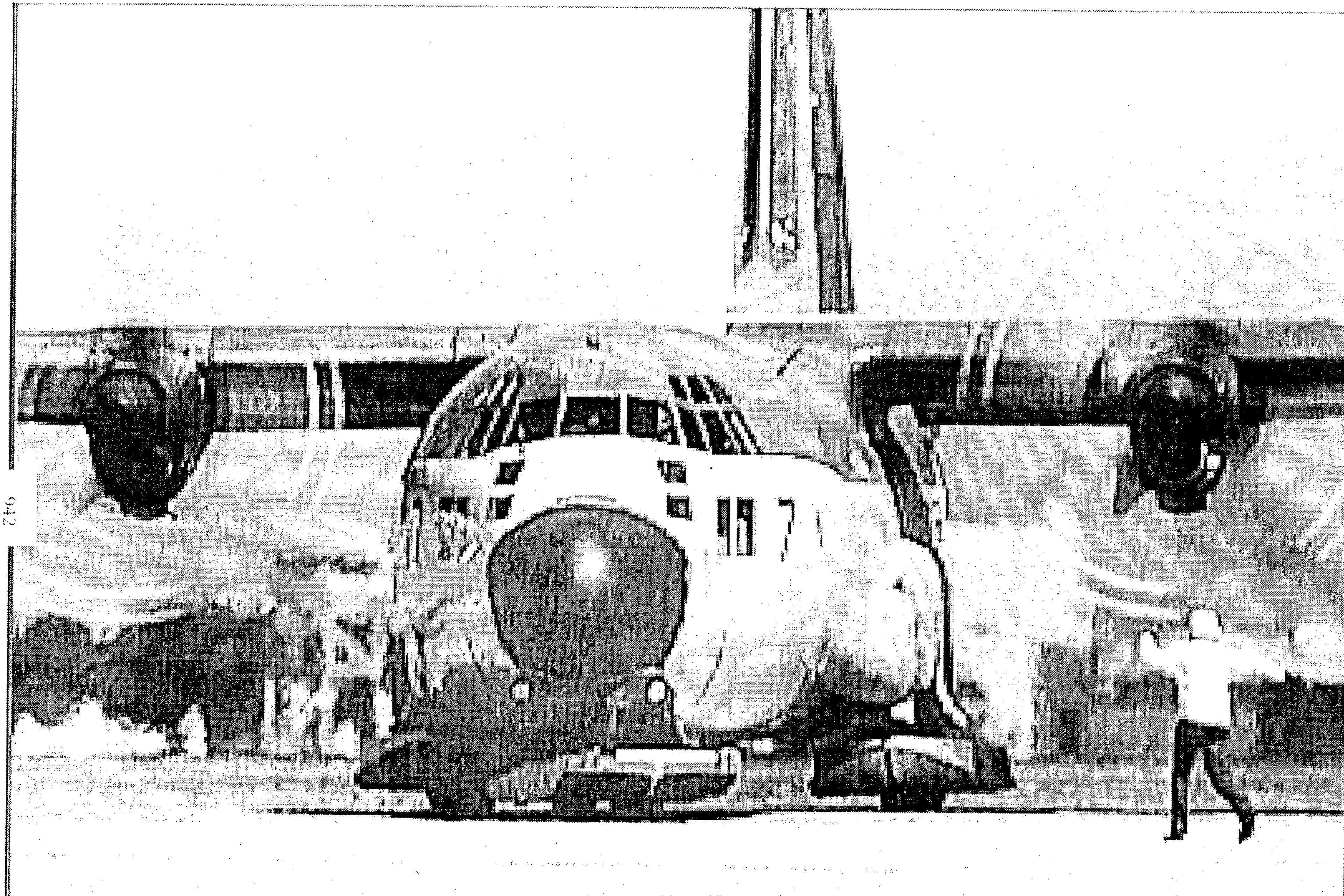

Robins Air Force Base Strain Monitor Systems

Preliminary Design with Damage Tolerance Constraints Using ASTROS

Knowledge Systems, Inc.
D. Pipkins
P. O'Donoghue
H. Kawai

Georgia Tech
S.N. Atluri

Presentation Outline

- ASTROS Introduction
- Integration of a Damage Tolerance Module with ASTROS
- Applications

Structural Optimization

- Minimize an objective function (i.e. weight or cost)
- Enforce constraints (i.e. strength, flutter, displacement, etc.)

ASTROS (**A**utomated **STR**uctural **O**ptimization **S**ystem)

- Supports both preliminary design and design modifications that occur later in the product life cycle
- Combines finite element modeling and optimization techniques to deliver superior aerospace structural designs in significantly reduced times
- Finite element modeling based on NASTRAN

Elements of Design

Conceptual → $\boxed{\textbf{Preliminary}}$ → Detail → Final

Preliminary Design Challenges

- Aerodynamic configuration, materials and design conditions defined
- Determine the structural configuration that provides and optimal structure while satisfying the multiple constraints that multiple engineering disciplines impose

ASTROS v13 Constraints

- Tsai-Wu Stress Criteria
- Von-Mises Stress
- Stiffness (Deflection)
- Natural Frequency
- Flutter
- Laminate Composition
- Panel and Beam Buckling
- Aeroelastic Lift and Control Effectiveness
-

ASTROS Design Variables

- Plate Elements: Thickness
- Beam Elements: Cross-Sectional Area
- Design variable linking keeps optimal design realistic from a manufacturing point of view:
  - element grouping for constant thickness structure
  - shape function for tapered (thickness) structure

Integration of Damage Tolerance Module with ASTROS

ASTROS-DT Model

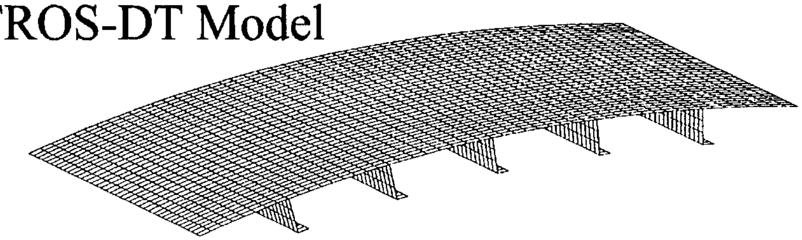

Residual Strength Constraint Evaluations

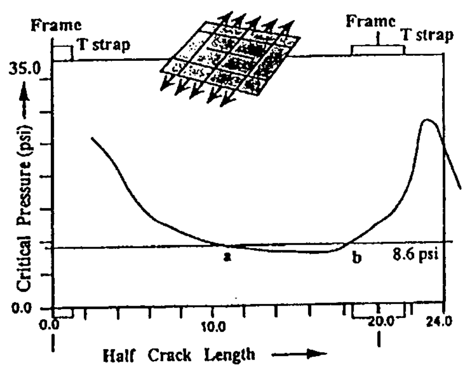

Fatigue Constraint Evaluations

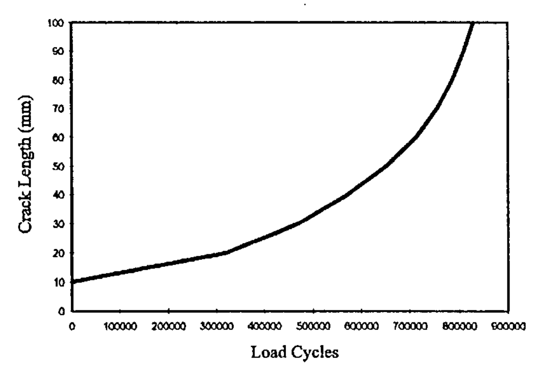

DT Module Capabilities

- The module will consist of local damage models applicable to metallic and composite structure
- Fatigue spectrum generation in terms of ASTROS load cases
- Minimal impact on ASTROS input data file preparation

Local Analysis: Metallic Structure

- Damage in the form of through cracks and surface flaws, including Widespread Fatigue Damage
- Main objective is to calculate a parameter which characterizes the crack-tip fields
  - Linear Elastic Fracture Mechanics: K
- Use parameter to predict residual strength and life

Local Analysis: Composite Structure

- Damage in the form of delamination
- Two objectives:
  - calculate energy release rate
  - calculate buckling load with delamination present
- Predict residual strength

Fatigue Spectrum Generation

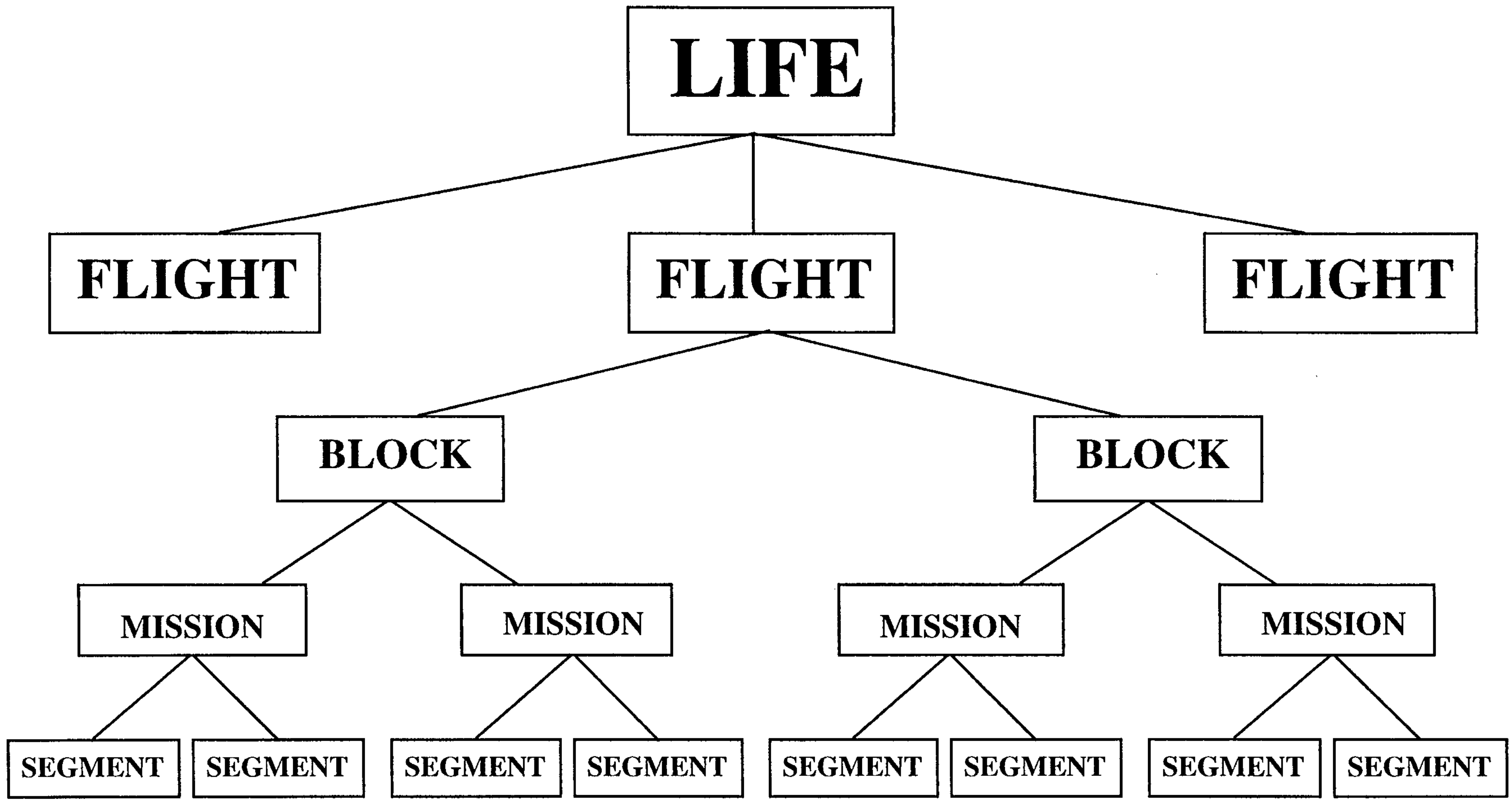

ASTROS Interface

- Approach taken is to use a global-intermediate-local analysis
- The user constructs only the global finite element model, which in preliminary design may be very crude (i.e. smeared stiffener properties, no account of fasteners, etc.)
- Intermediate and local model generation is carried out automatically by an automated geometry modeler and mesh generator

Automated Geometry Modeler and Mesh Generator

- The intermediate and local models are defined by a few additional bulk data cards in the global model bulk data file (ASTROS input is similar to NASTRAN)
- The automated geometry modeler and mesh generator then takes this data and generates intermediate and local meshes sufficient to carry out damage modeling.

Intermediate Model

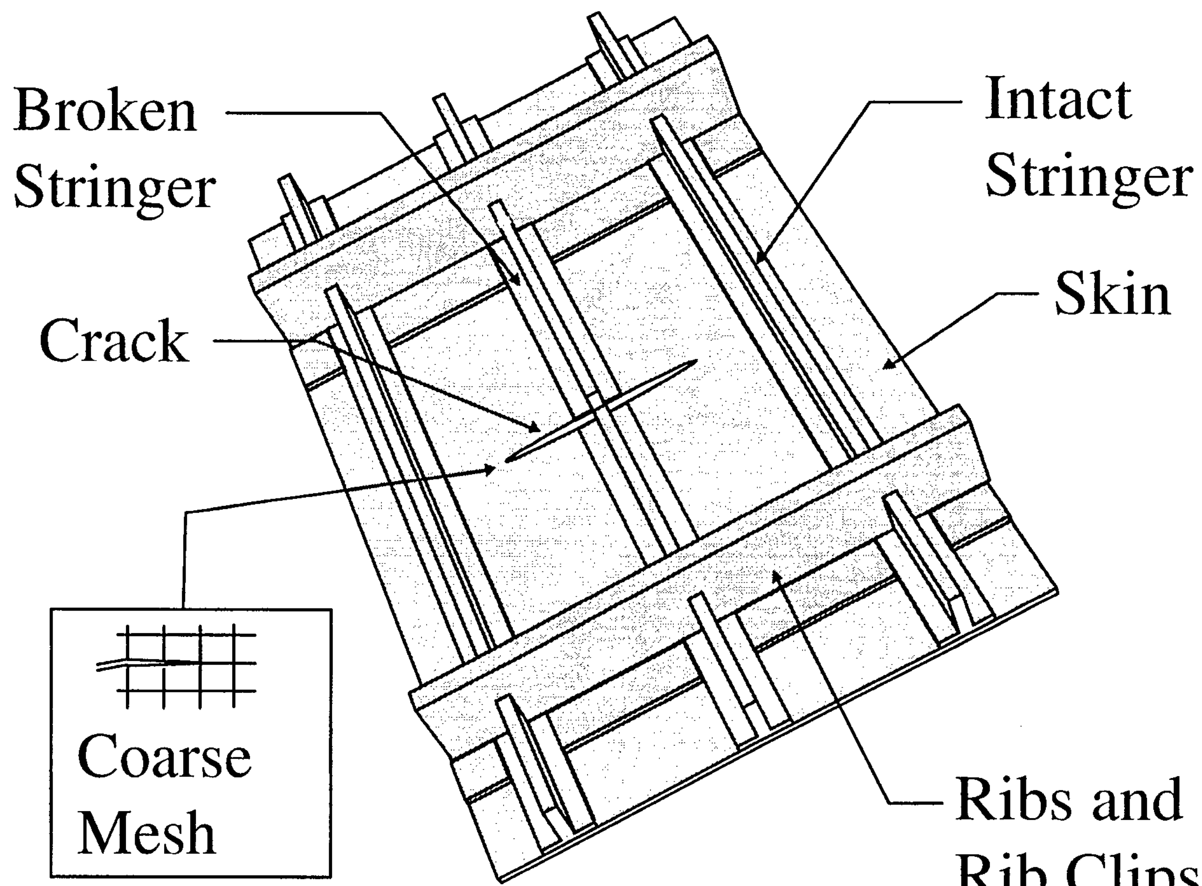

Local Model

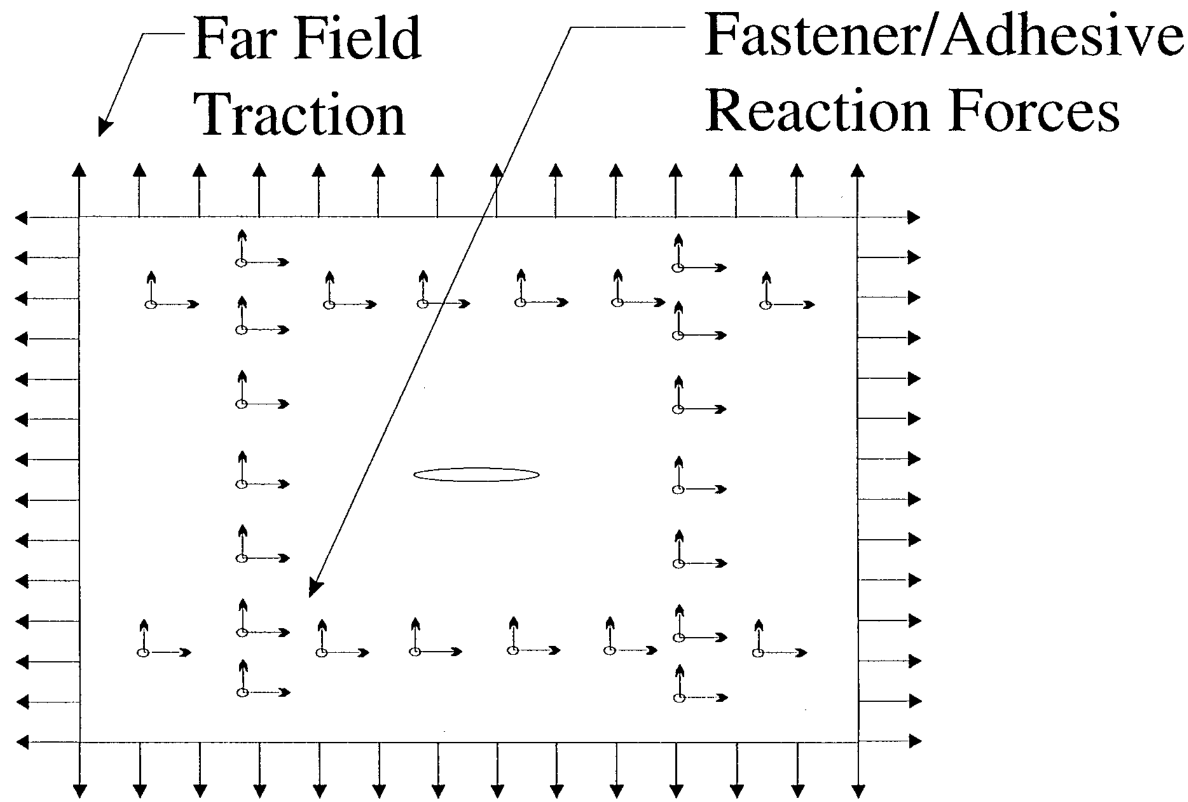

Application to IAS Fuselage

- Study how stress intensity factors of through cracks and surface flaws change with design variables.

Global Model

V1

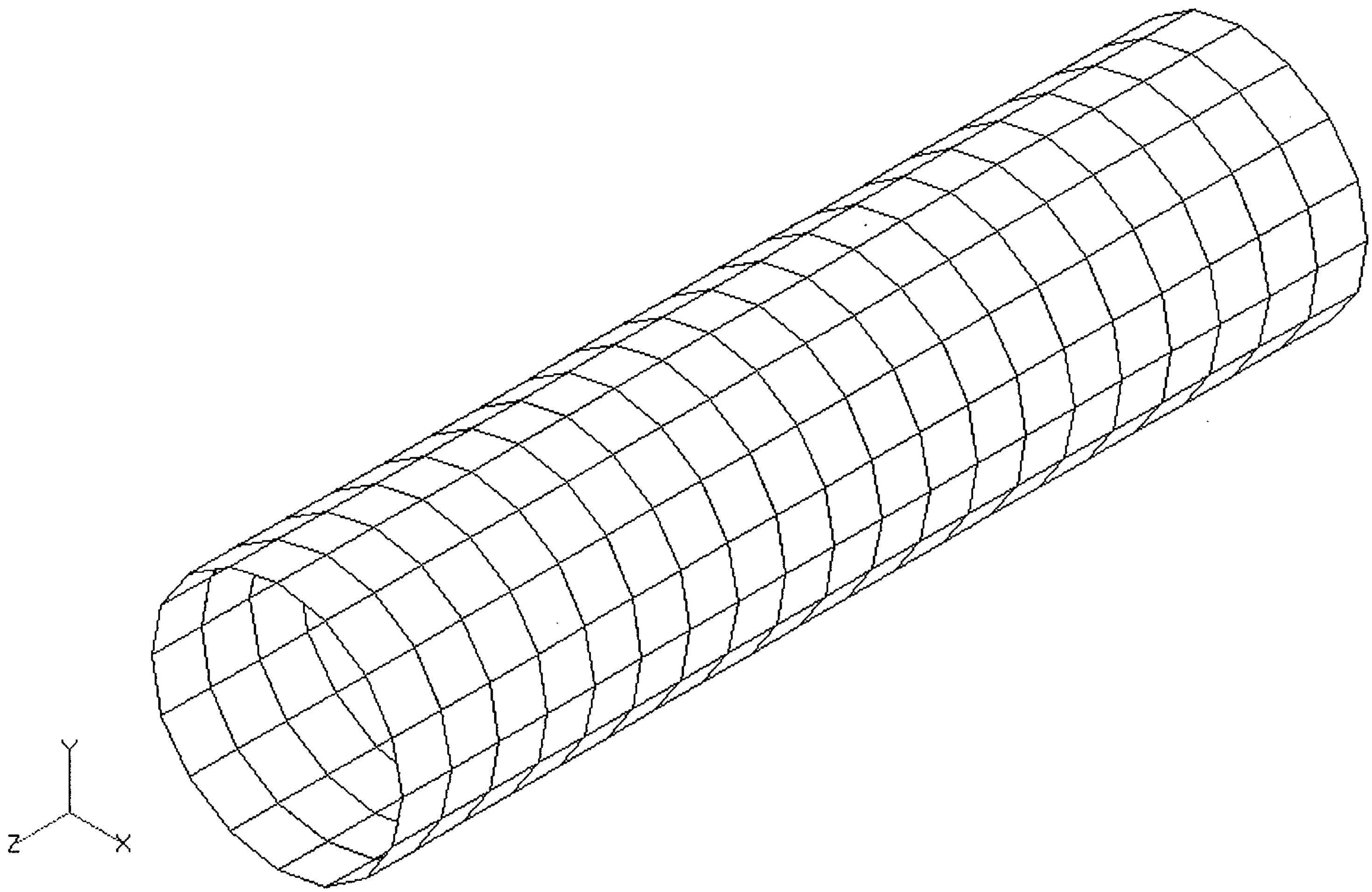

Design Parameter Set

Problem Dependent Key Design Variables of Typical Interest in Preliminary Design

- Topological Parameters (number of frames, stringers)
- Dimensional Parameters (frame, stringer interval, crack length)
- Geometrical Properties (thickness, beam section area)
- Material Properties (Young's modulus)
- Boundary Conditions (displacement, load)
- Body Forces (pressure)

Problem Description

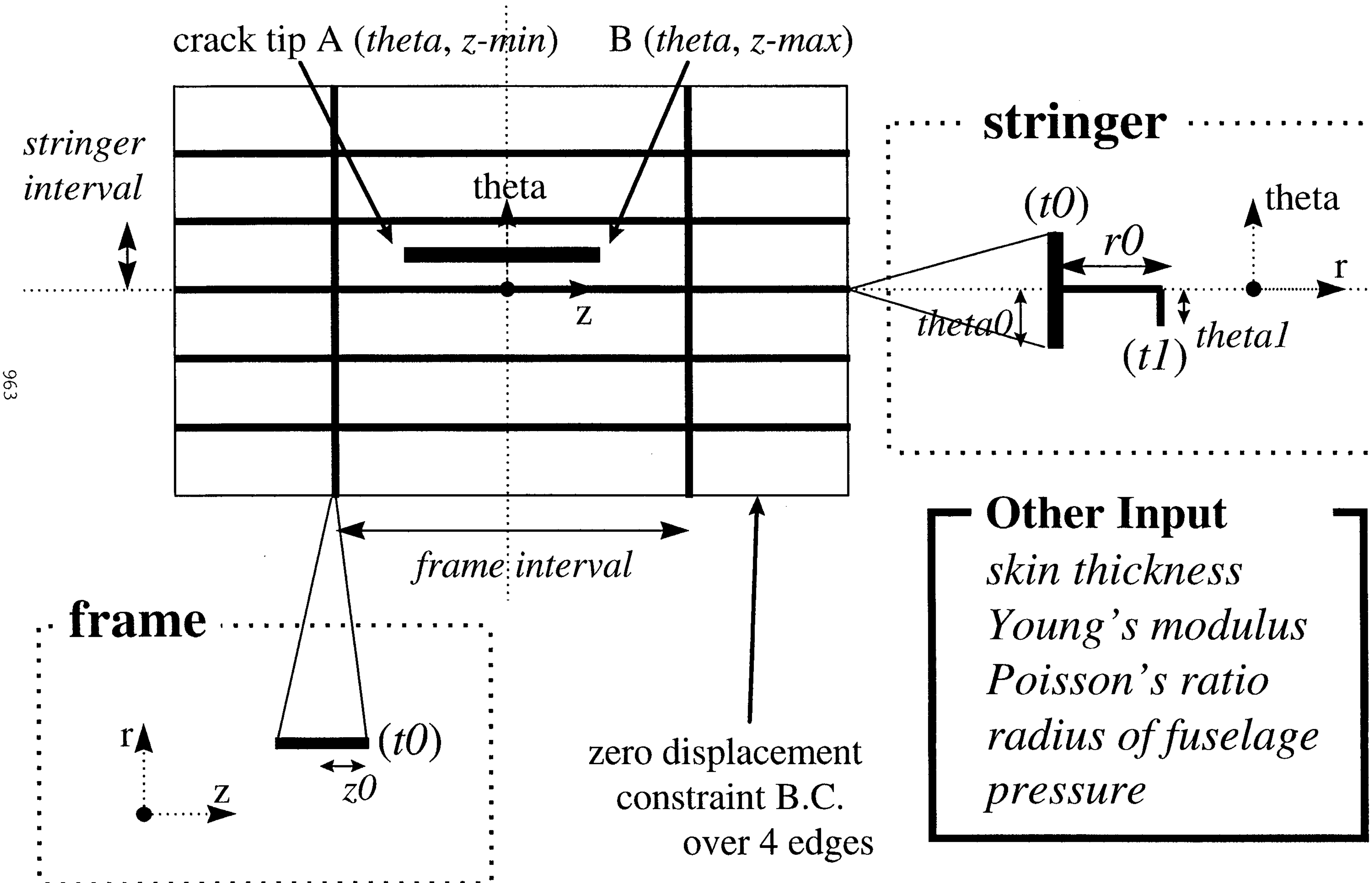

Other Input

skin thickness
Young's modulus
Poisson's ratio
radius of fuselage
pressure

IAS Intermediate Model

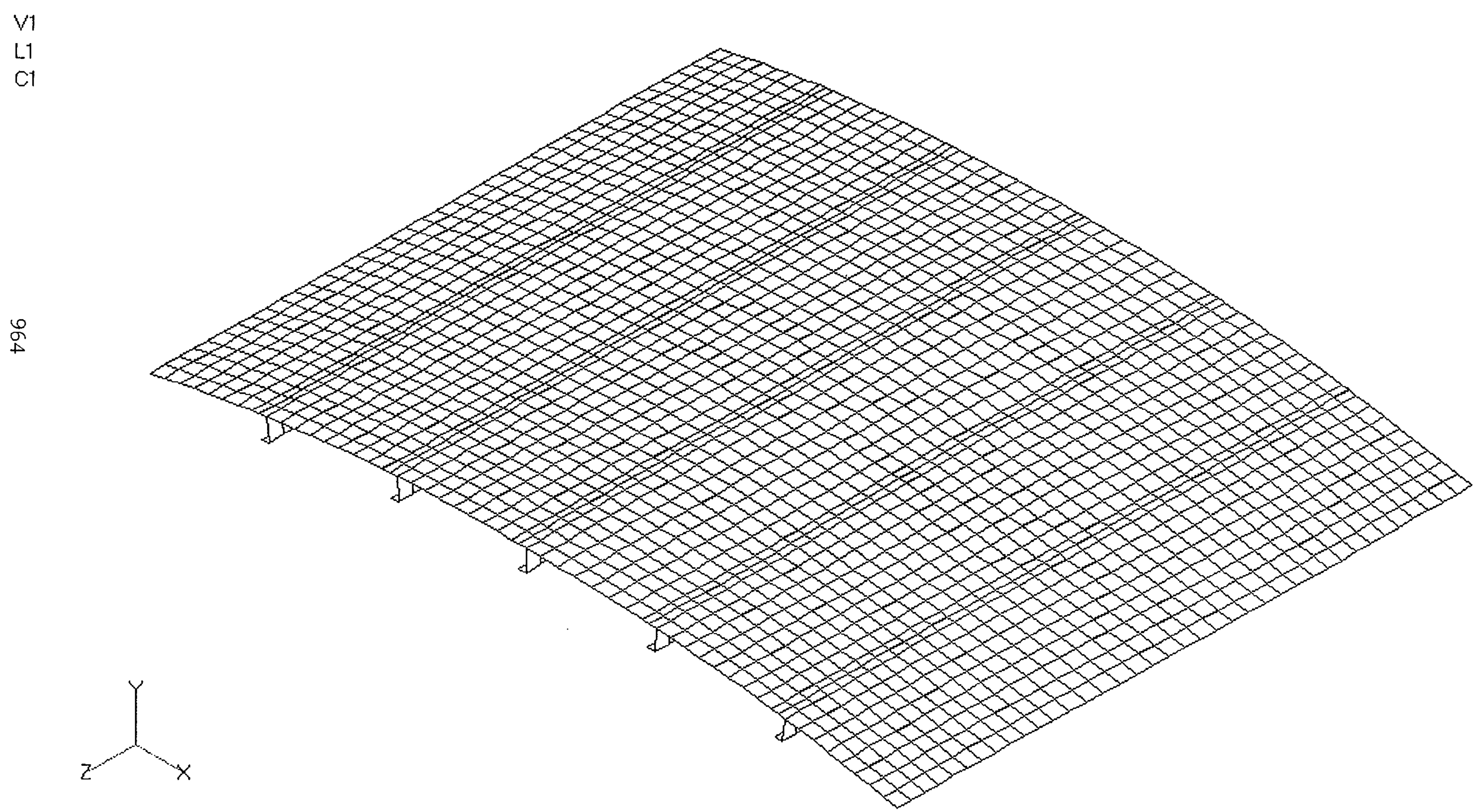

Skin Elements: Thickness Linking

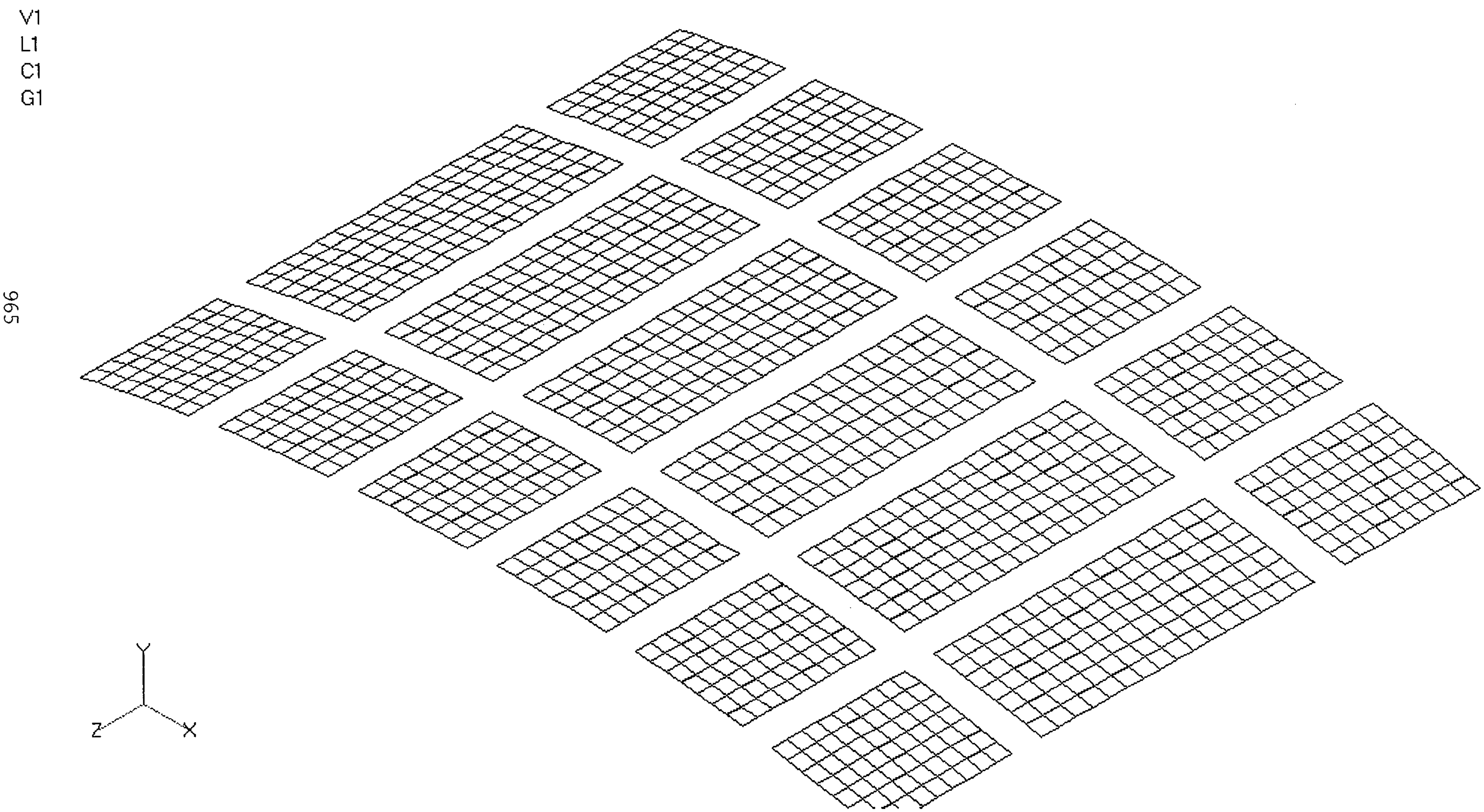

Frame Elements: Thickness Linking

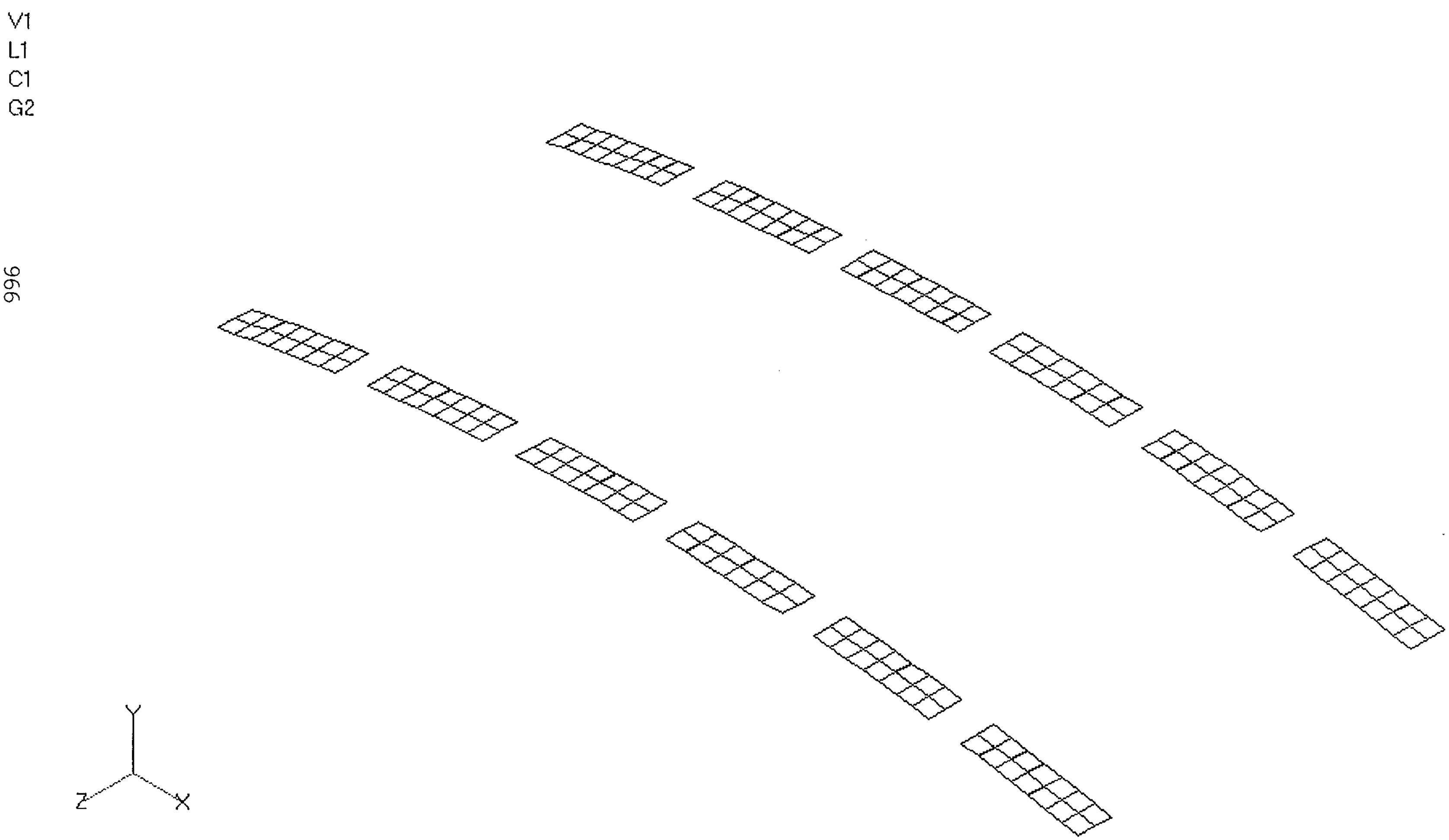

Stringer Elements: Thickness Linking

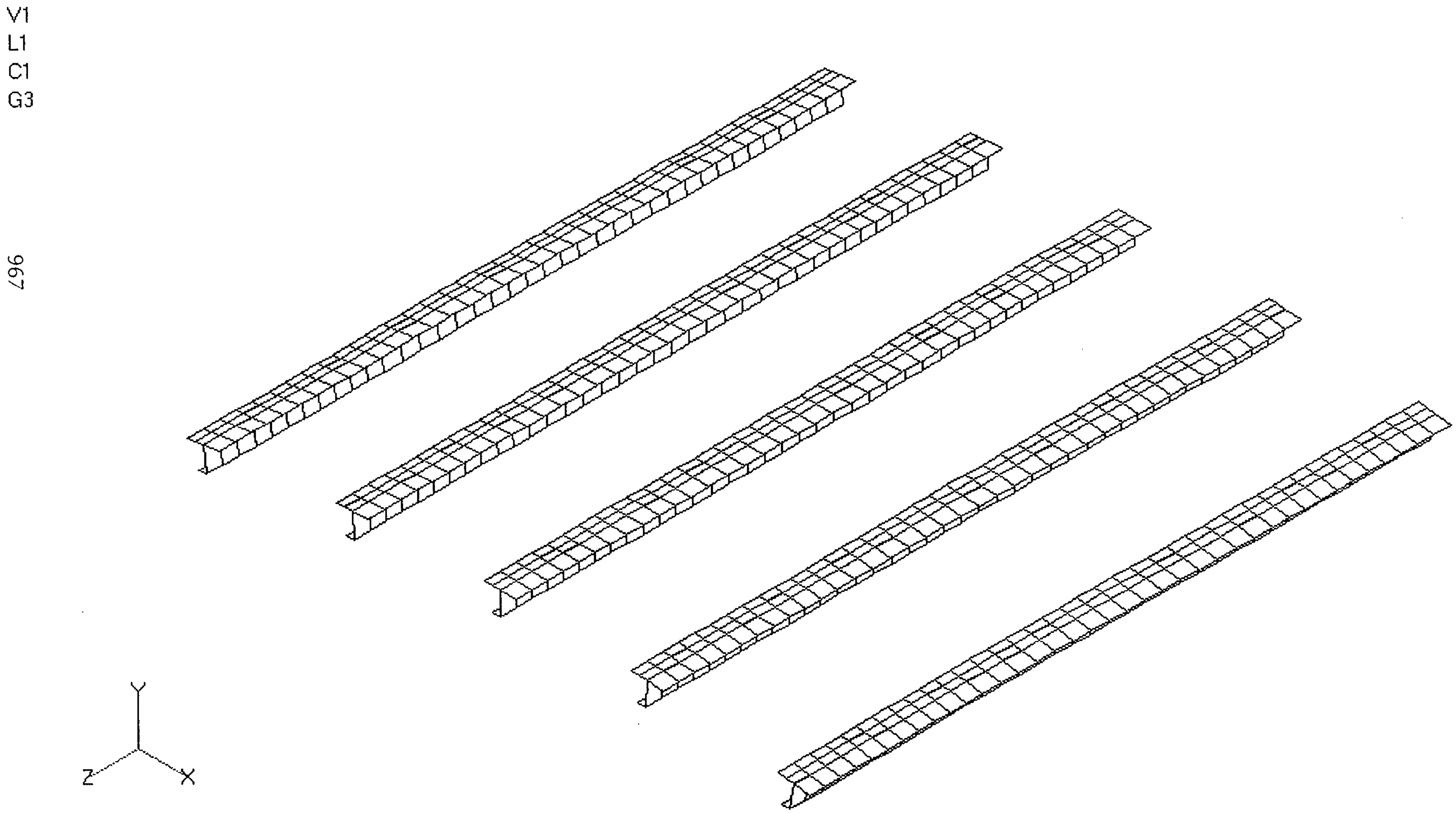

IAS Local Model

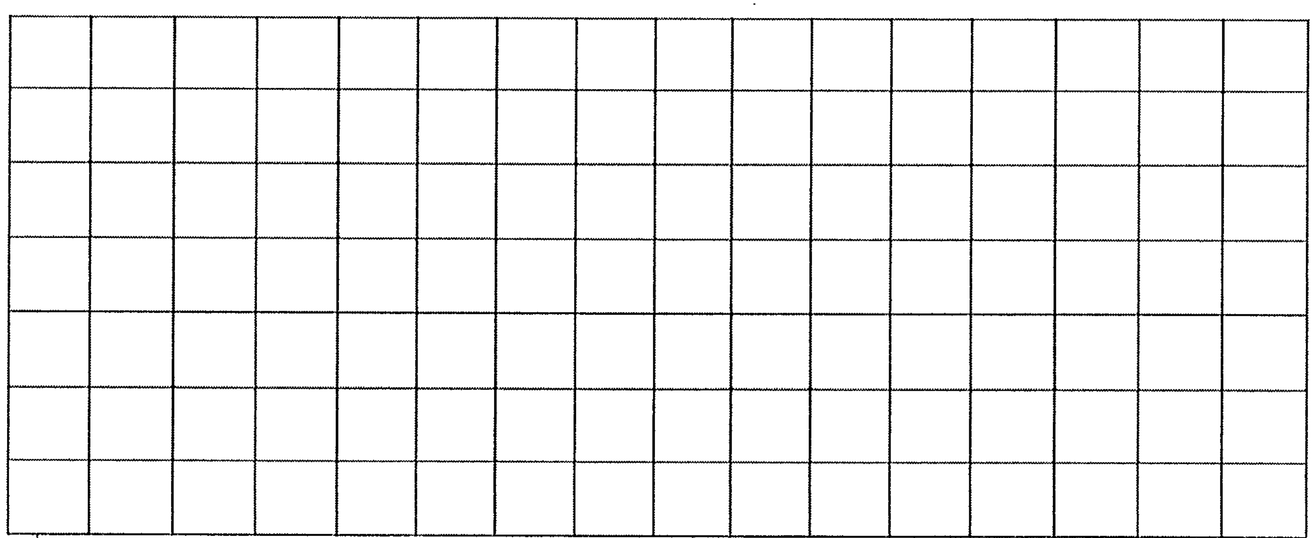

IAS Intermediate Model: Deformed Shape

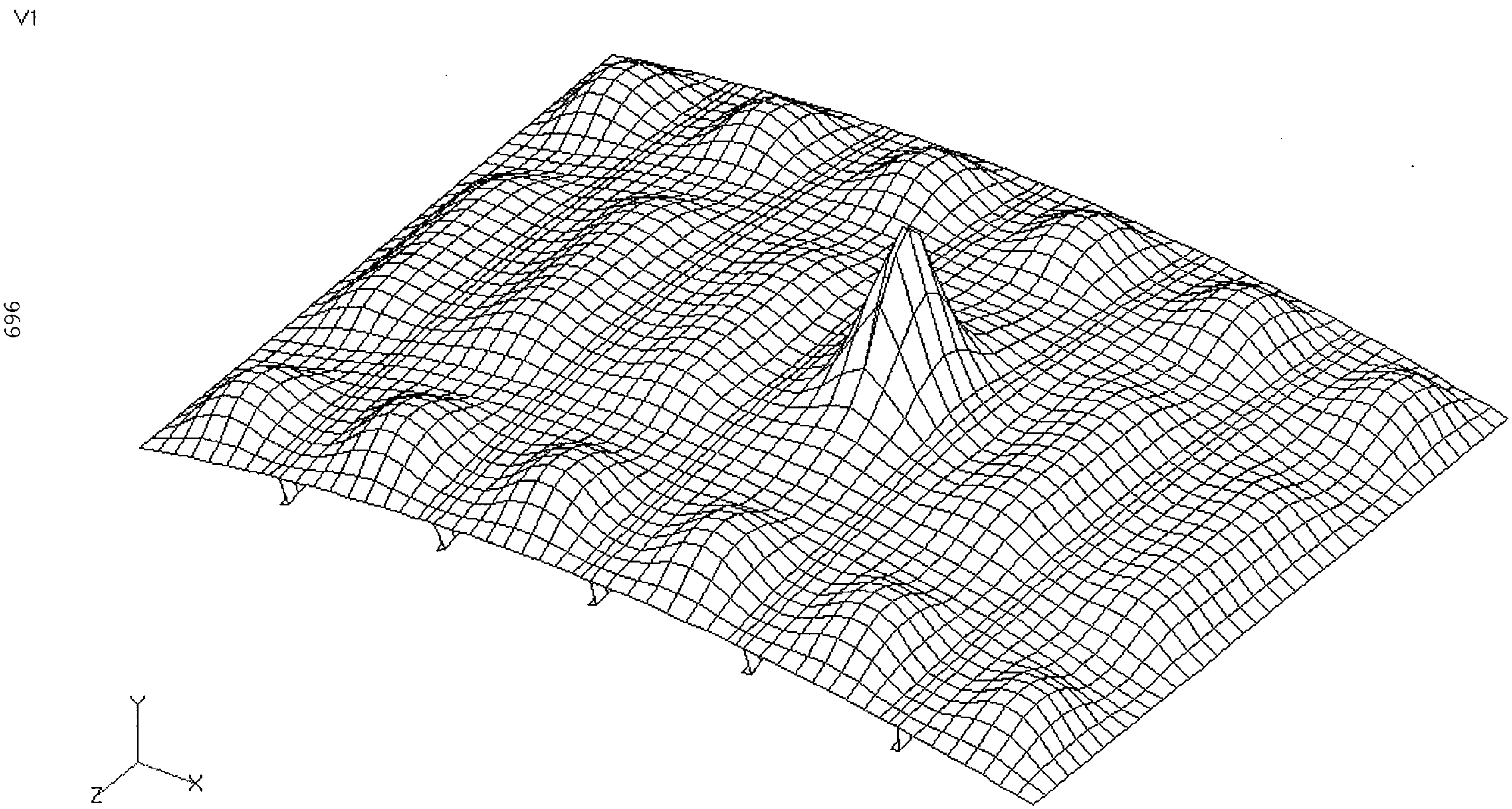

IAS Intermediate Model: Hoop Stress

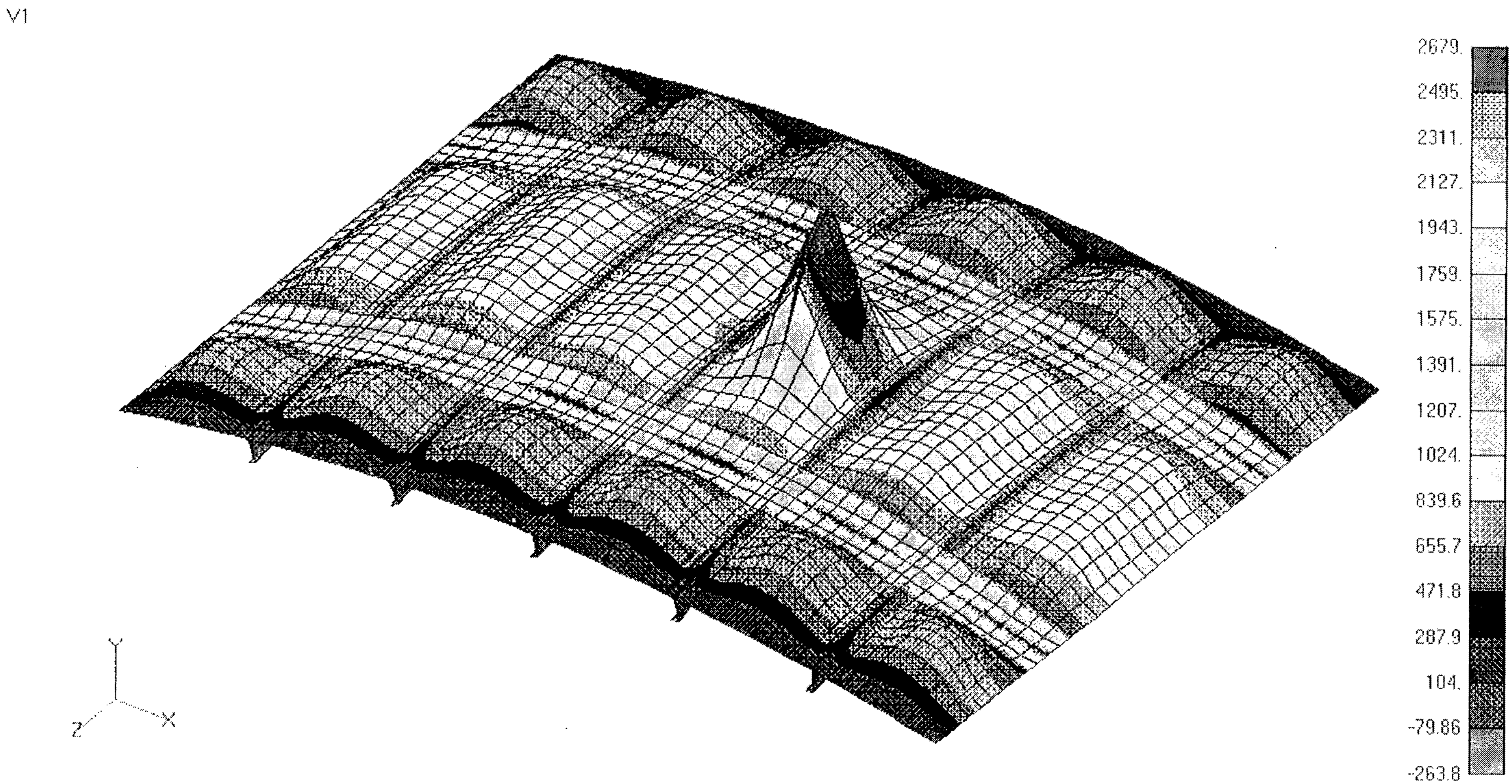

IAS Intermediate Model: Axial Stress

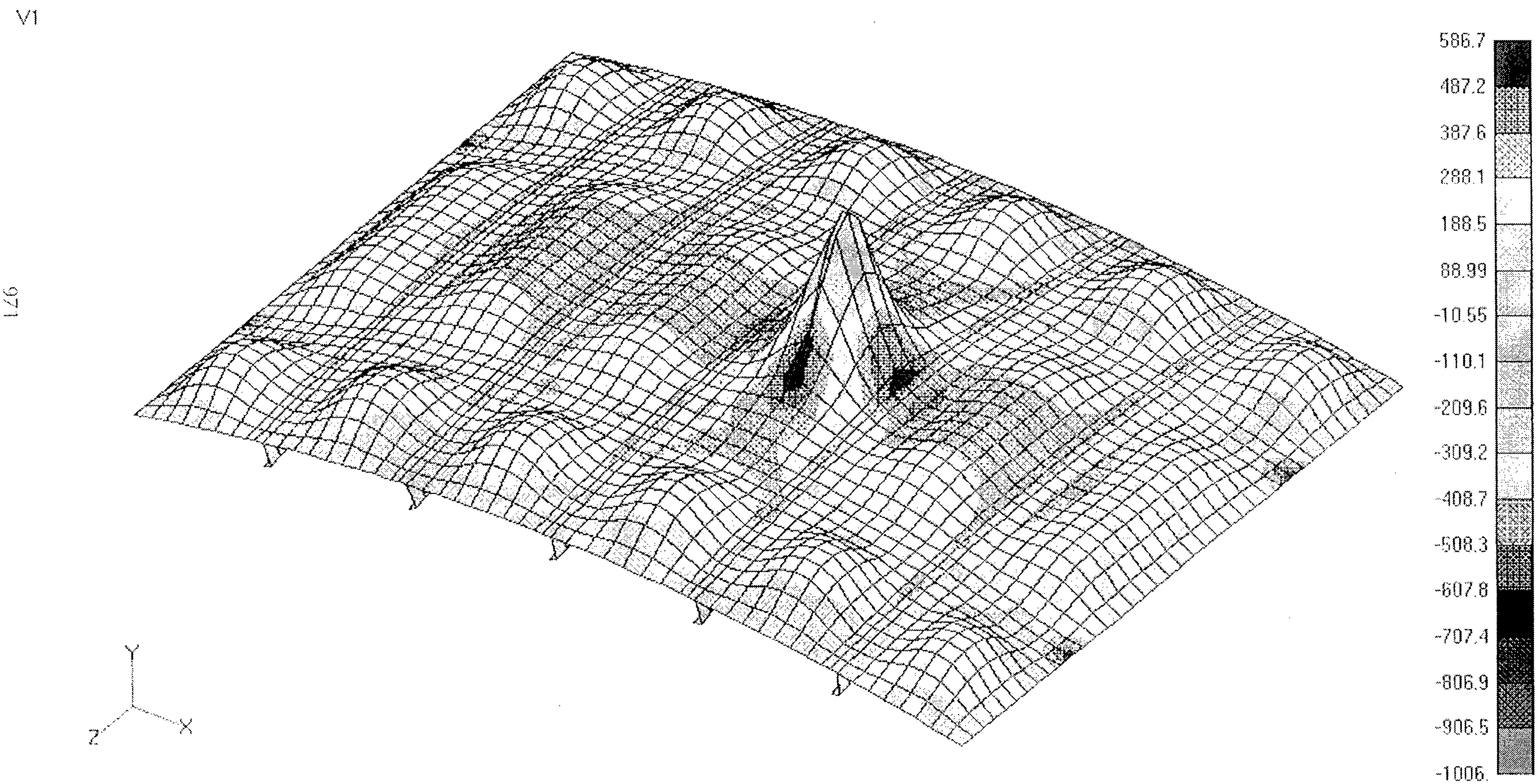

Design Parameter: Skin Thickness (Through Crack)

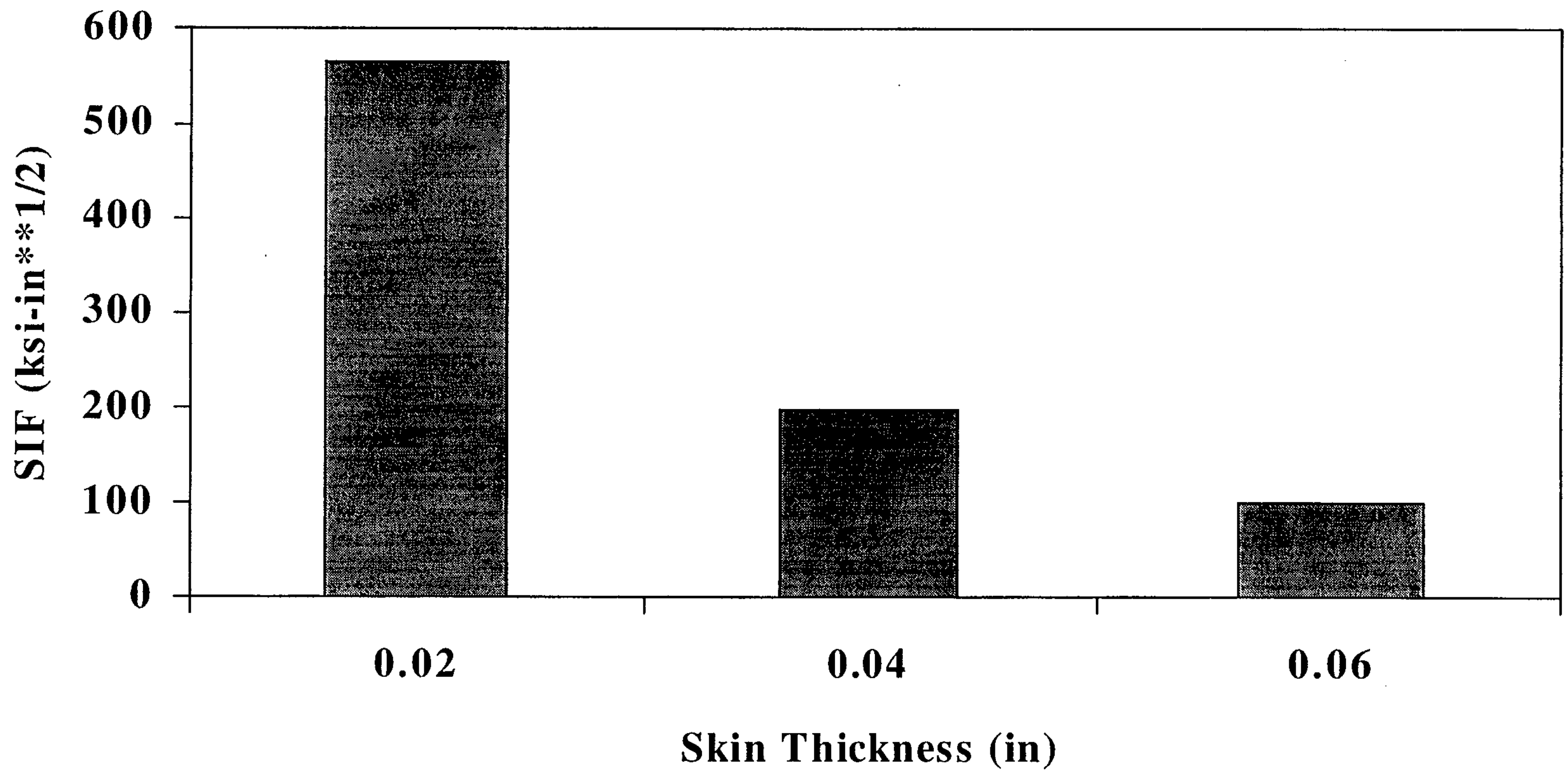

Design Parameter: Skin Thickness (Surface Flaw)

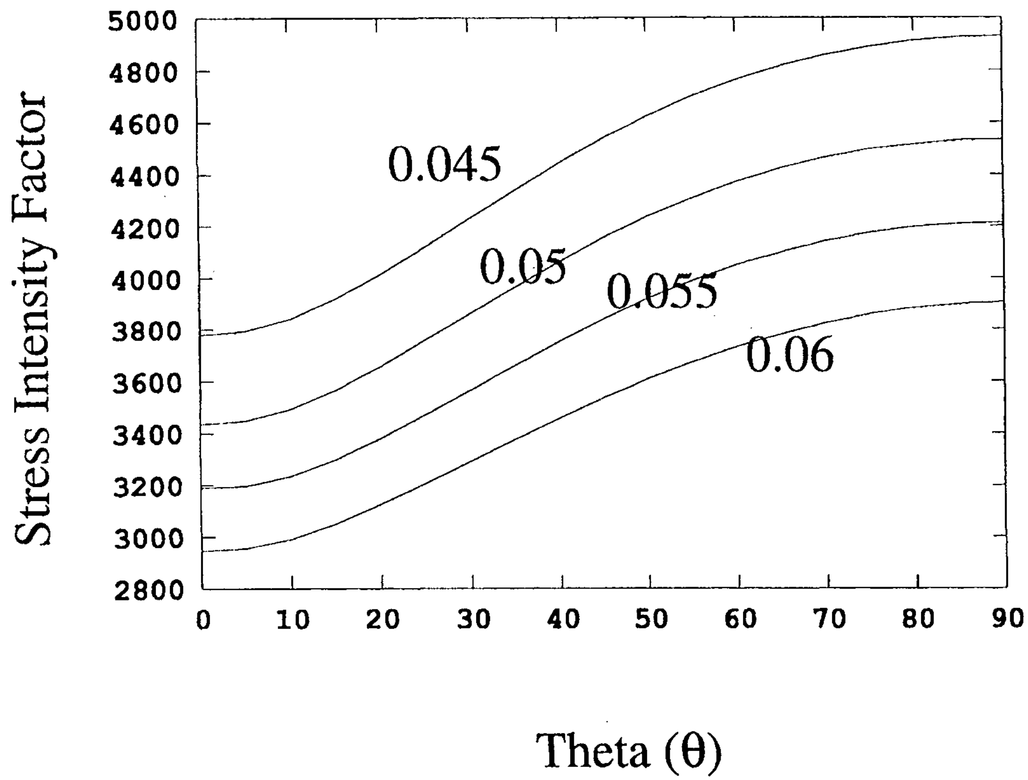

LUNCH PRESENTATION

J. Morgan
Oklahoma City Air Logistics Center

B-1B BOMBER HORIZONTAL STABILIZER SUBSTRUCTURE FAILURES

Prepared By: **John Morgan, Aerospace Engineer**
Structural Engineering Section
B-1B System Support
USAF

INTRODUCTION

In May of 1993, a B-1B aircraft sustained a lightning strike to its left horizontal stabilizer. In an attempt to identify any possible damage, the stabilizer was X-rayed at various locations. Some of these X-rays identified cracks in the substructure that could not be the result of a lightning strike. These cracks later proved to be a part of a larger fleetwide problem with the B-1B aircraft that has only now been fully understood.

In an attempt to understand and control the problem, the US Air Force formed a team of engineering experts from its own ranks and that of the prime contractor, Boeing North American (BNA). This team was responsible for monitoring the status of the fleet's structural integrity, identifying the cause of the problem and developing a structural enhancement to correct the problem. The USAF is currently in the process of implementing the structural enhancement.

The purpose of this paper is to provide an overview of the process that this team used to deal with the horizontal stabilizer problem.

PHYSICAL DESCRIPTION

To fully understand the problem with the B-1B horizontal stabilizers, knowledge of the stabilizer structure is required.

The stabilizers are a symmetric airfoil approximately 20 feet long (see figure 1). The width tapers from 16 feet at the root to 5 feet at the tip. Each stabilizer is mounted on the aircraft via spindles that protrudes from the side of the aircraft. The stabilizers can be rotated symmetrically or asymmetrically about these spindles to control both the pitch and roll of the aircraft.

The stabilizer itself consists of a main structural box, which is the part that is failing and composite fairings which are attached to the leading edge, trailing edge and tip of this box.

As shown in figure 2, the main structural box is composed of relatively thick(0.125 in. to 0.470 in) one piece aluminum upper and lower skins attached to a thin egg crate type substructure. The substructure, as shown in figure 3, is comprised of spars (running in the spanwise direction) and riblines (running in the chordwise direction).

The front and rear spars are machined aluminum I-beams. Integral flanges are machined into the spars for attachment of the riblines. The intermediate spars are titanium I-beam weldments, however, the webs are not flat, but have a sinusoidal shape. These spars are commonly refered to as Sine Wave Beams(SWBs). This configuration provides increased strength at reduced weight when compared to a conventional beam. At three foot intervals the spar web flattens out to provide an attach point for the riblines. The SWB spars are continuous from inboard to outboard and range up to 20 feet in length. Typical thicknesses are 0.012 in. for the web and 0.020 in. for the cap

The riblines are composed of formed aluminum rib segments that are fitted in between the spars. These rib segments are of a two piece design: (1) A rib web with a top, bottom and forward attachment flange, and (2) an aft clip. This design provides only fore and aft adjustment, and would therefore require shimming on installation. Thickness for the ribs varies from 0.040 to 0.125 in.

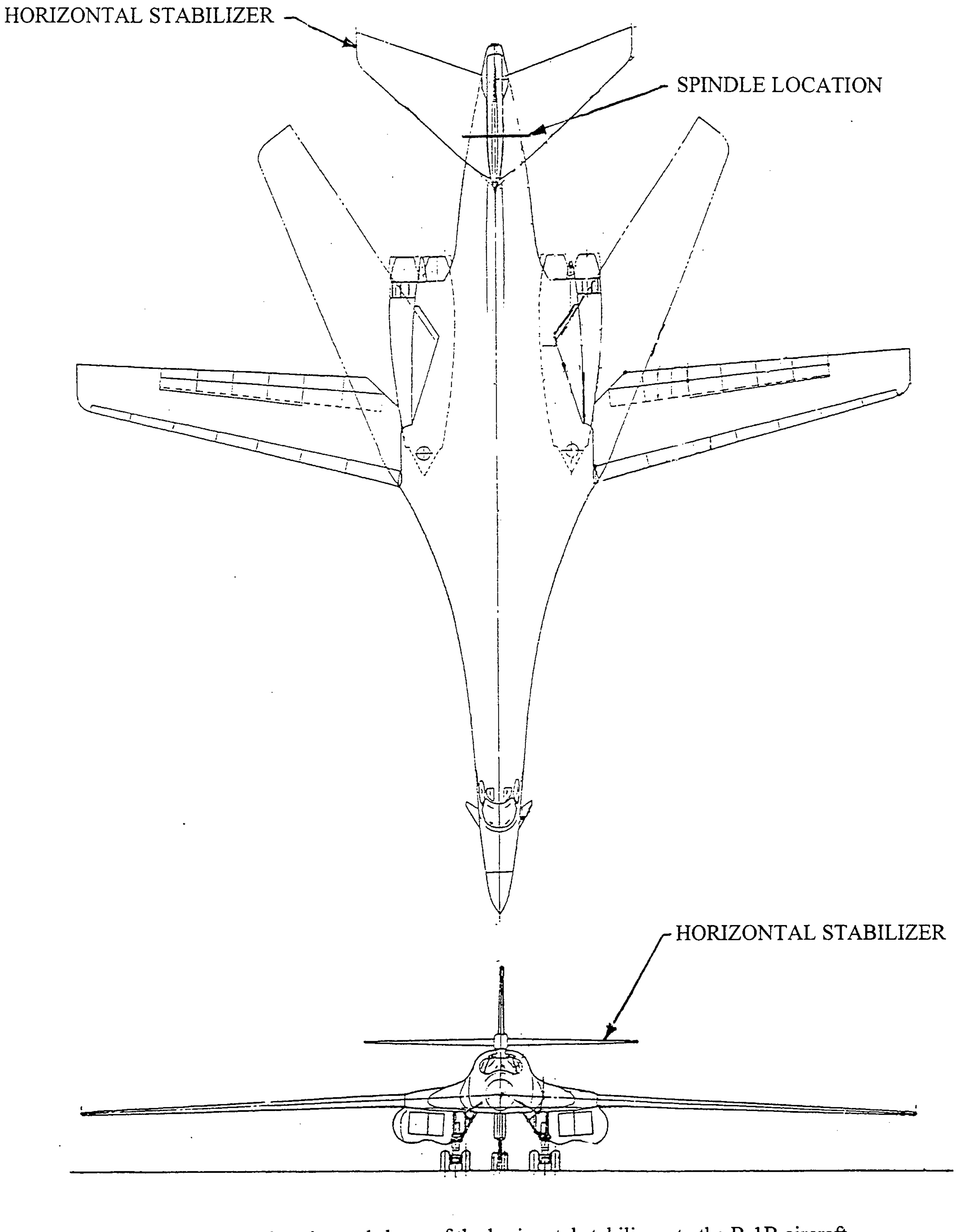

FIGURE 1: Relative size and shape of the horizontal stabilizers to the B-1B aircraft.

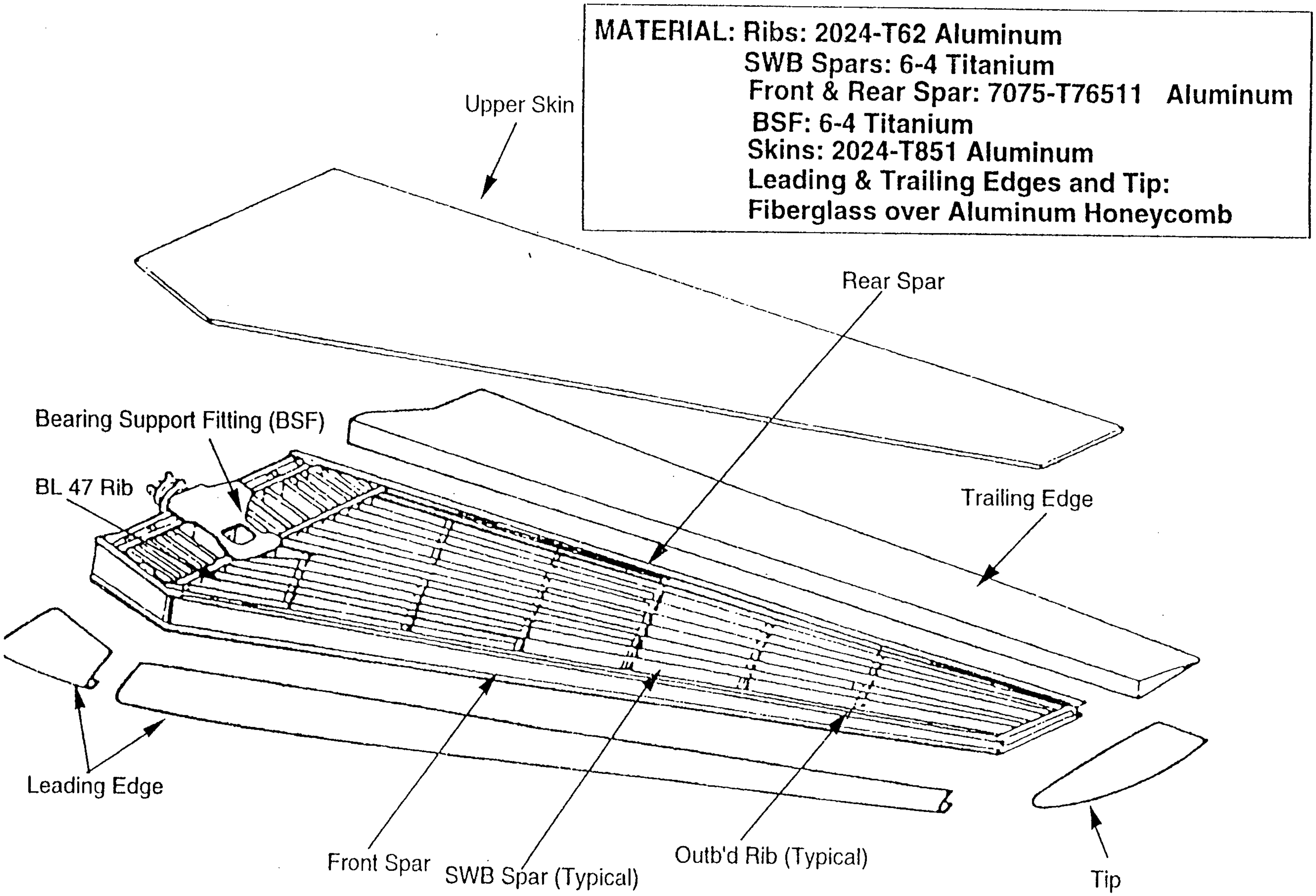

Figure 2. B-1B Horizontal Stabilizer

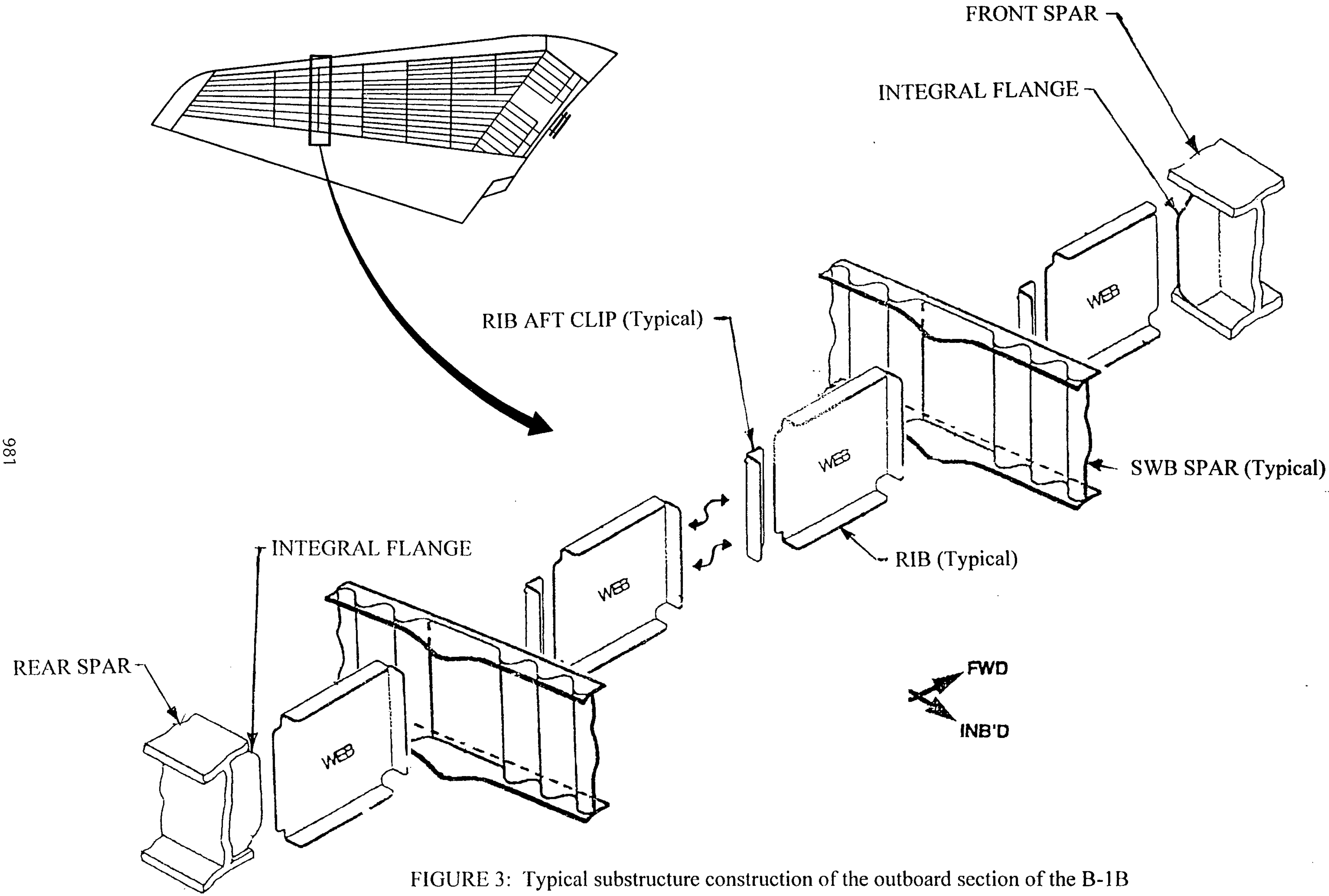

FIGURE 3: Typical substructure construction of the outboard section of the B-1B Horizontal Stabilizer.

In all, the design of the stabilizer provides both a strong and lightweight structure. As stated before, the stabilizers have the strength to pitch or roll a 477,000 lb aircraft, however, they only weighs 1655 pounds each.

FAILURE BACKGROUND

After the initial discovery of the damage in the lightning strike stabilizer, the stabilizer was subjected to a detailed inspection The first finding was that 65 percent of the fasteners attaching the top skin to the substructure were loose or missing in the area where the initial damage was discovered. The stabilizer was partially disassembled by removing the upper skin to further investigate the problem. The subsequent visual inspection identified several interesting anomalies (see figure 4). First, the damage, although widespread was limited to the outboard two thirds (2/3) of the main structural box. The damage itself took several different forms:

- Cracks in rib segments
- Cracks in the SWB spars
- Cracks in the integral flanges on the front and rear spars
- Loose or failed substructure-to-substructure fasteners
- Degraded corrosion coating on aluminum structure

Lastly, the inspection revealed gaps between the skins and the substructure that substantially exceeded the original production drawing tolerances of 0.010 in.. These excessive gaps were caused by three different phenomena

- Lack of shimming to level adjacent parts
- Premature hardening of sealant applied to the weld bead that resulted in standing off the skin
- Severe weld distortion of the SWB caps

As a result of the inspection of this stabilizer, the engineering team turned its attention to determining the extent of the problem in theB-1B fleet.

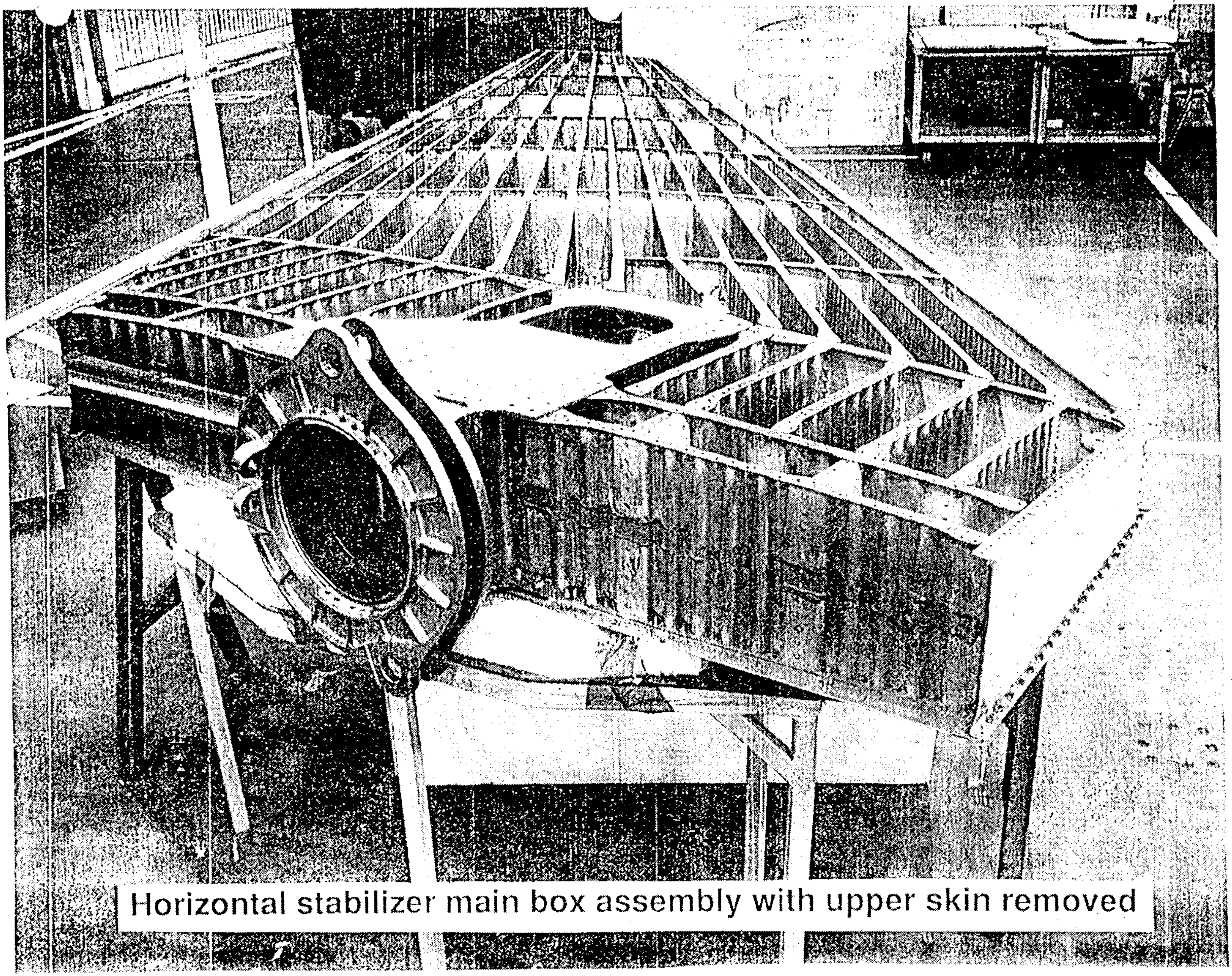

FIGURE 4 (Sheet 1 of 7): Inspection of the 'Lightning Strike' Horizontal Stabilizer.

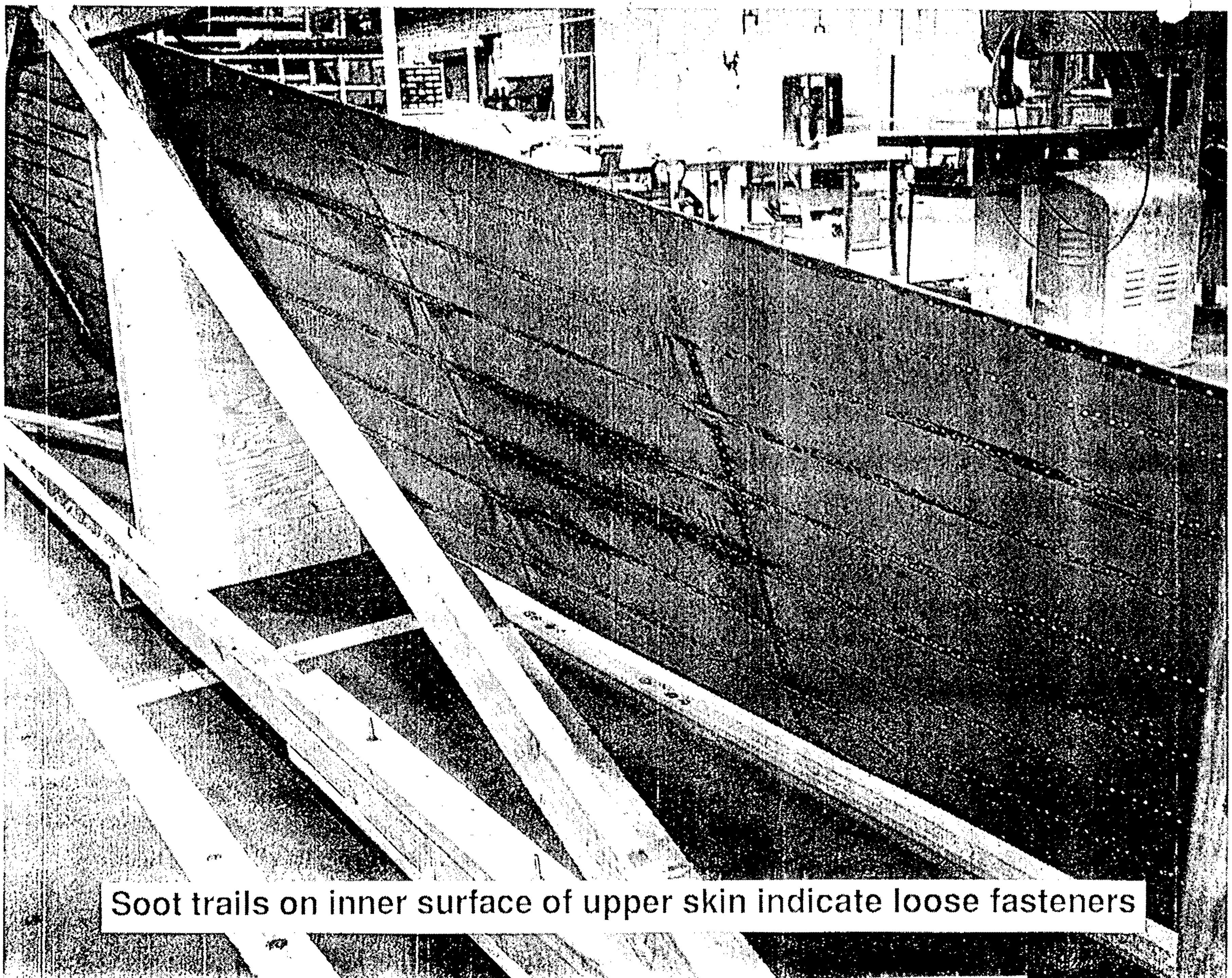

FIGURE 4 (Sheet 2 of 7): Inspection of the 'Lightning Strike' Horizontal Stabilizer.

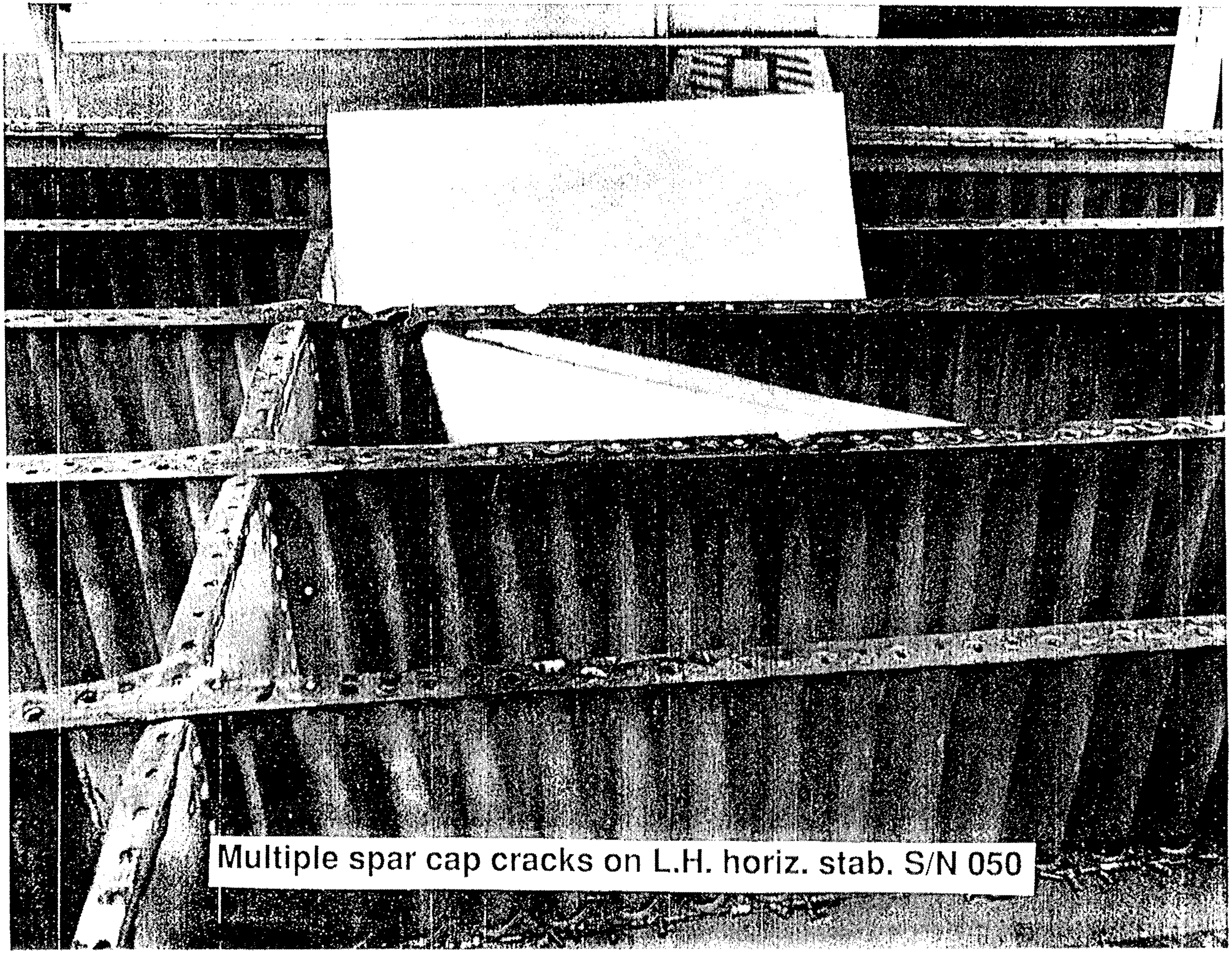

FIGURE 4 (Sheet 3 of 7): Inspection of the 'Lightning Strike' Horizontal Stabilizer.

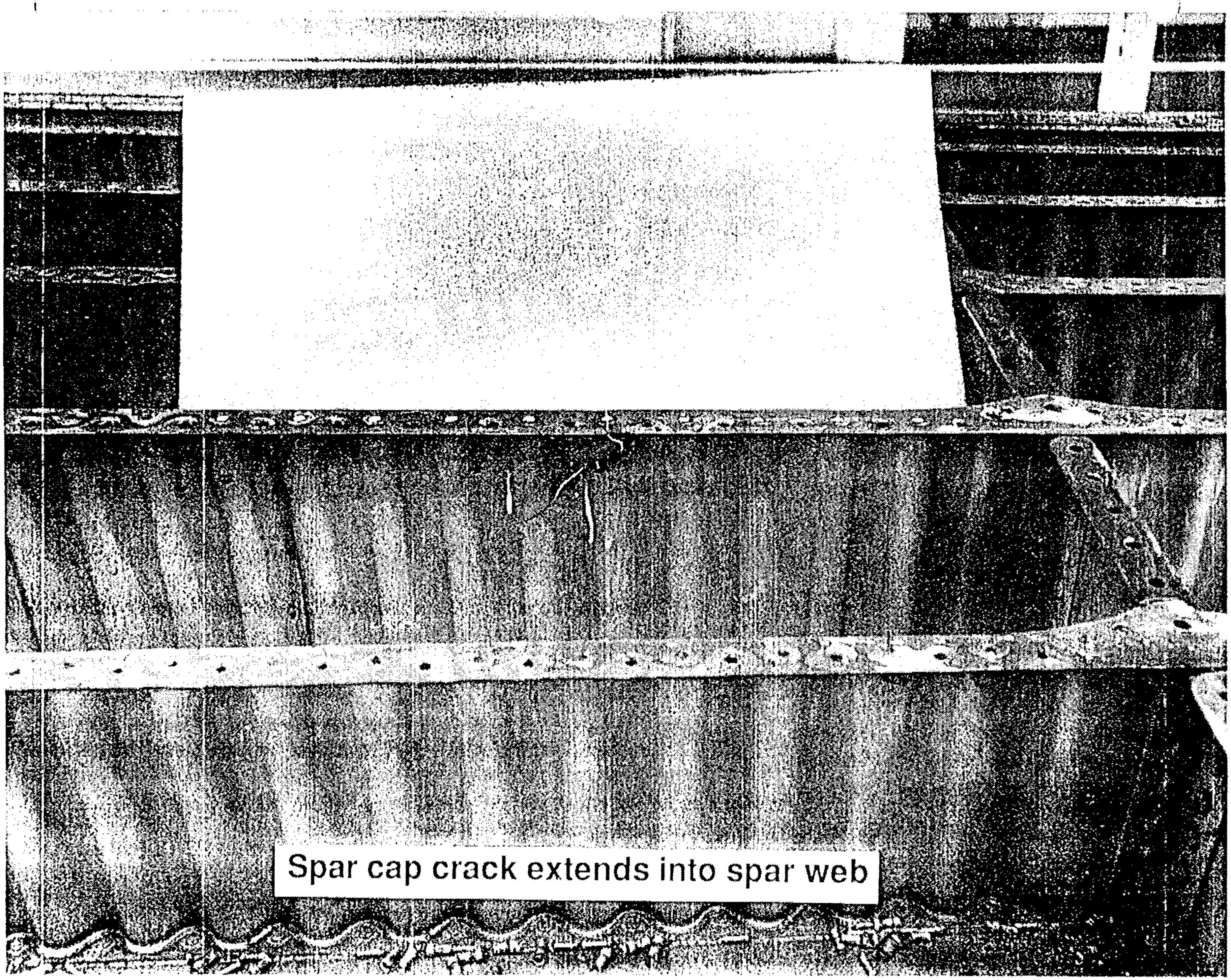

FIGURE 4 (Sheet 4 of 7): Inspection of the 'Lightning Strike' Horizontal Stabilizer.

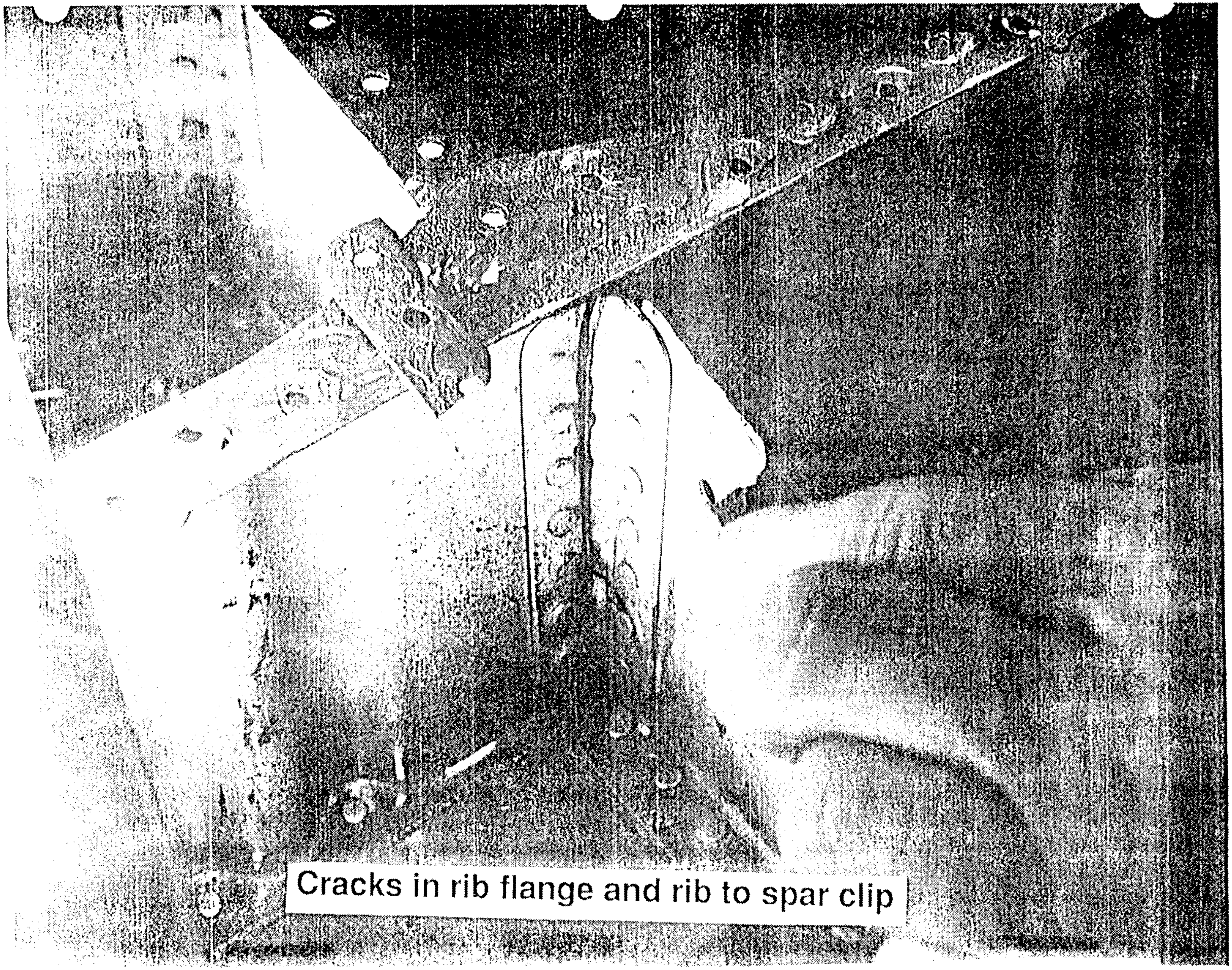

FIGURE 4 (Sheet 5 of 7): Inspection of the 'Lightning Strike' Horizontal Stabilizer.

FIGURE 4 (Sheet 6 of 7): Inspection of the 'Lightning Strike' Horizontal Stabilizer.

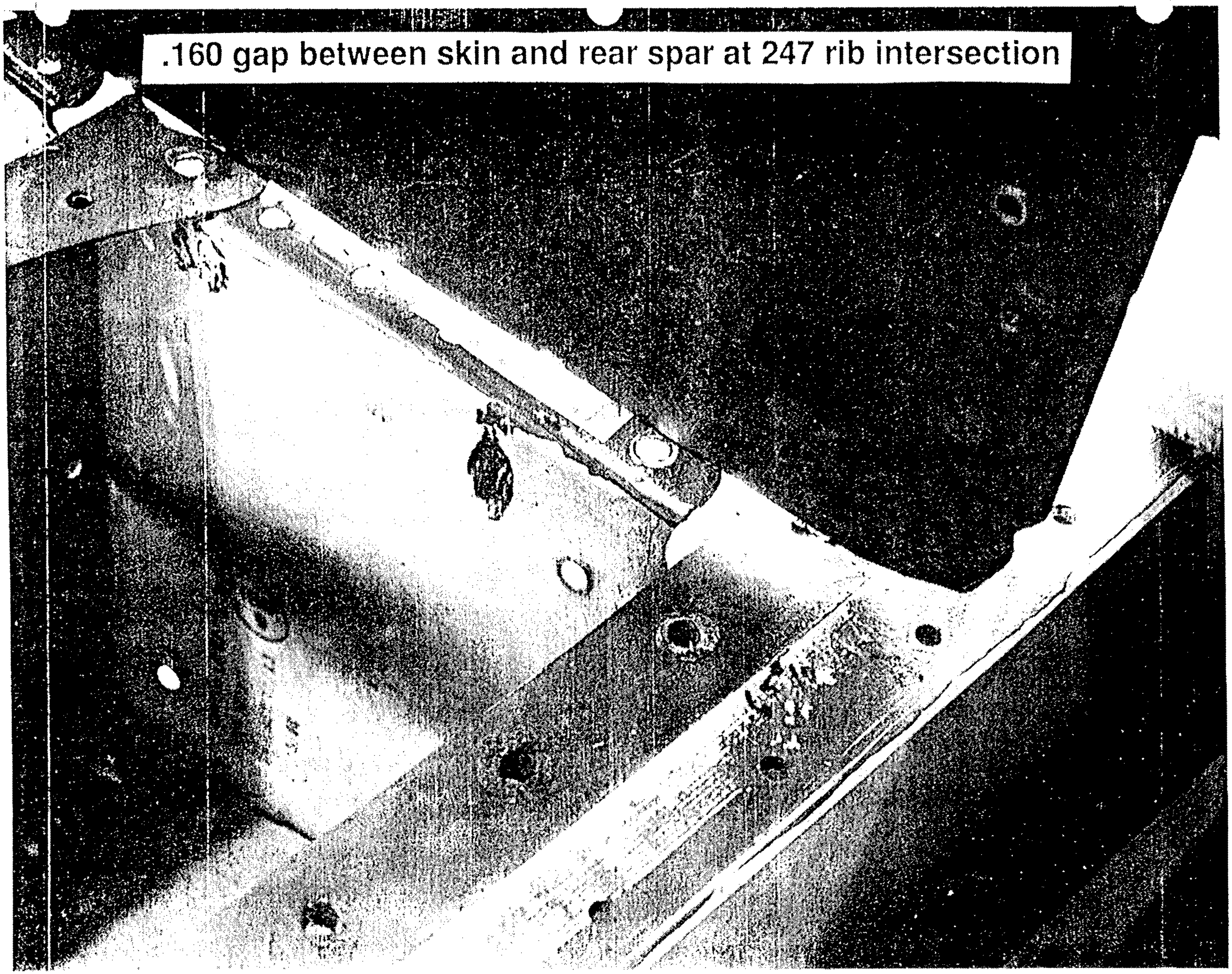

FIGURE 4 (Sheet 7 of 7): Inspection of the 'Lightning Strike' Horizontal Stabilizer.

INSPECTION

The engineering team had three initial goals to achieve with the inspection program. The first was to take care of any fleetwide problem with loose or missing skin fasteners. This was accomplished with a one-time inspection through the fleet for the loose or missing fasteners. Any problems encountered were corrected in conjunction with this inspection.

The second goal was to determine the extent of substructure damage in the fleet. To accomplish this, the team developed a borescope and X-ray inspection procedure to identify the damage in the substructure. Inspection of a sampling of the aircraft soon proved that the problem was fleetwide, therefore, a fleetwide inspection was issued. This inspection showed that practically all stabilizers had some form of substructure damage, and, in a large majority of the cases the damage was substantial (see figure 5).

The third goal was to assess the structural integrity of any stabilizer exhibiting damage and make a recommendation for removal from service or reinspection intervals. This was done by modifying the NASTRAN finite element model to reflect the actual damage, processing for internal loads and routing this data through automated stress analysis programs for the stabilizer structure to determine if acceptable residual strength remained.

The reliability of the substructure inspection has proven to be less than desirable. Visual inspections of some stabilizers disassembled for repair, have shown that less than half of the damage noted during the borescope/X-ray inspections was actually there. In addition, significant damage was found that had not been detected in the borescope/X-ray inspections. Contributing to the low reliability is the size of the inspection: 115 square feet of X-ray film and 200+ borescope locations for each stabilizer. However, the borescope/X-ray inspection remains the only viable technique for inspecting the stabilizer substructure.

B-1B H.S.-Damaged Rib Segment Count

(Based On Inspection Data of The Entire Fleet, With 73 H.S.'s Having More Than 1 Inspection)

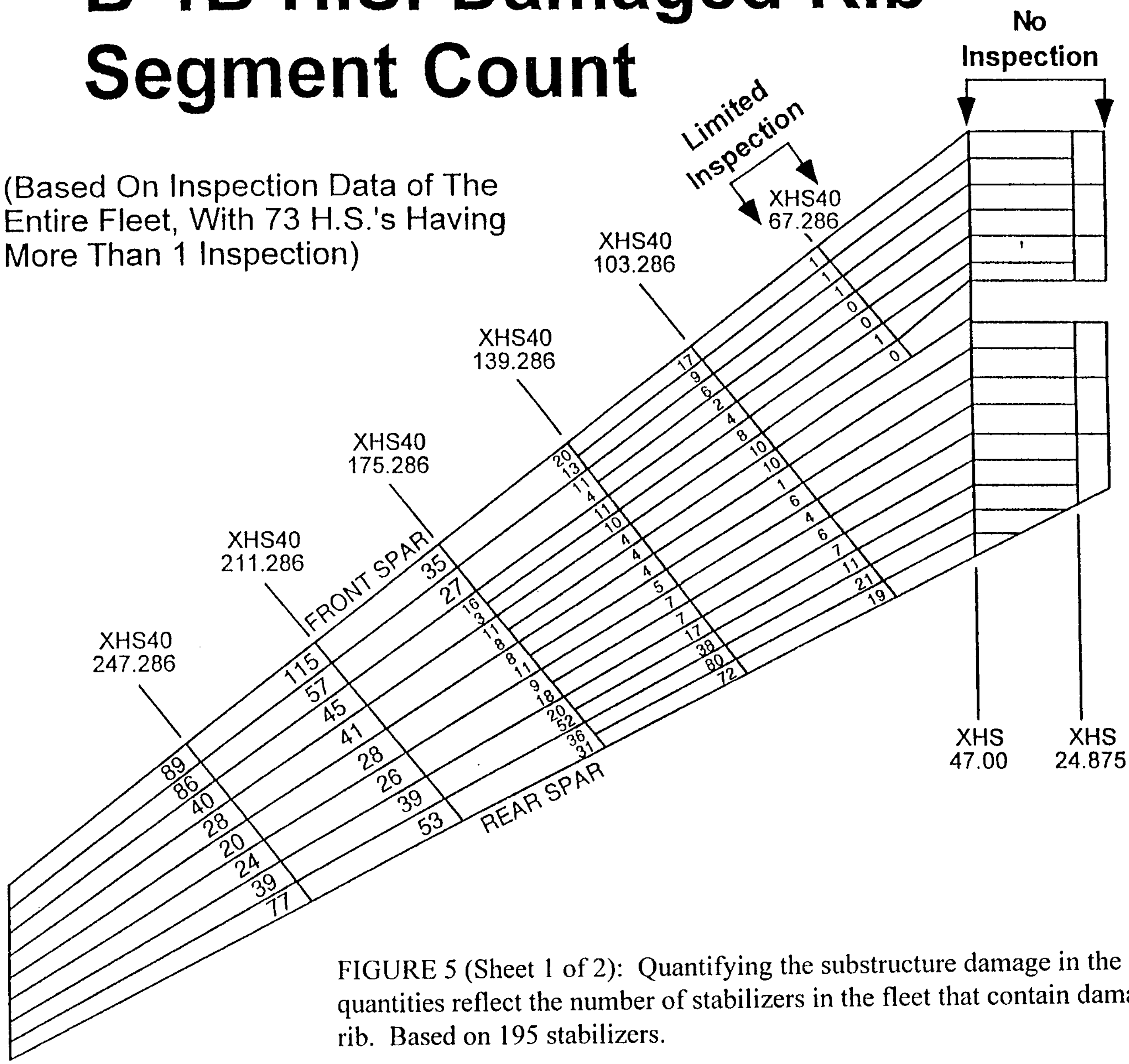

FIGURE 5 (Sheet 1 of 2): Quantifying the substructure damage in the fleet. The quantities reflect the number of stabilizers in the fleet that contain damage in a particular rib. Based on 195 stabilizers.

B-1B H.S.-Damaged Spar Segment Count

(Based On Inspection Data of The Entire Fleet, With 73 H.S.'s Having More Than 1 Inspection)

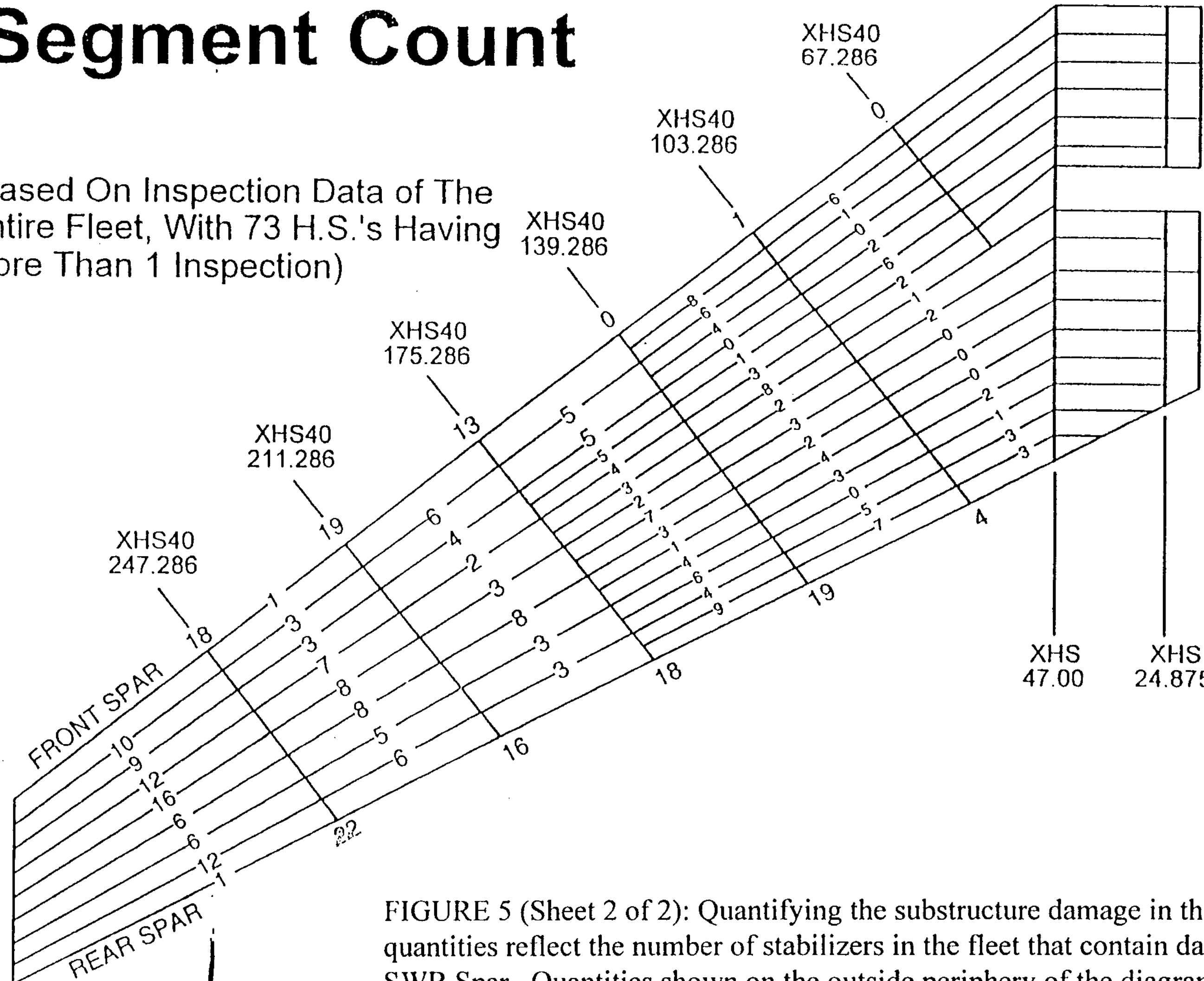

FIGURE 5 (Sheet 2 of 2): Quantifying the substructure damage in the fleet. The quantities reflect the number of stabilizers in the fleet that contain damage in a particular SWB Spar. Quantities shown on the outside periphery of the diagram and centered over the ribline locations reflect damage in integeral flanges. Based on 195 stabilizers.

SAFETY OF FLIGHT ISSUE

An assessment of safety of flight issues regarding an inflight failure of a horizontal stabilizer was aided by a 1992 midair collision between a B-1B and a KC-135 tanker during a midair refueling. The B-1B lost the outboard 2/3 of the left hand horizontal. This damage is consistent with that which would be expected due to failure precipitated by the substructure damage. The B-1B pilot reported no loss in flight control or increase in workload and the aircraft landed safely without further mishap. The B-1B flight simulator was used to evaluate the aircraft/pilot response to an inflight stabilizer failure during critical high workload tasks. These findings confirmed that the aircraft was controllable and the loss of the aircraft was not probable.

FAILURE INVESTIGATION

Metallurgical

The first step the team took in investigating the failures was to evaluate failed samples from the lightning strike stabilizer. The metallurgical results showed the failure mode to be high cycle fatigue with the presence of a high mean stress – cycle counts consistent with a high frequency event.

Review of Original Development and Testing

With the metallurgical results in mind, the team began reviewing the process used in the original design development and testing of the stabilizer.

The stabilizer design strength had been verified by completing a full scale ultimate load static test and a three life, flight by flight fatigue test with no significant failures. A ground and flight test program investigated the actual loads environment of the aircraft

including the engine acoustic loading on the empennage, loads envelope and actual maneuver and gust spectra loads. No surprises were found during this test program.

The review obviously keyed on environmental aspects that could affect the fatigue life. There were no apparent problems found with the process, however, several interesting facts were noted. First , during wind tunnel testing of the aircraft, a vortex was found that originated high on the forward fuselage and passed under the stabilizer. This vortex was determined to be quite powerful and under certain conditions could significantly impact the loading on the stabilizer. Secondly, due to the size of the stabilizers and the high levels of the engine acoustic noise, no full scale test could be performed to verify the acoustic fatigue life of the stabilizer. Since the design process assumed that the primary type of response would be a high frequency panel type response, test boxes were used that attempted to replicate the various "cells" of the stabilizer structure.. Thirdly, some early acoustic test boxes failed prematurely during life cycle testing. The cause was determined to out-of-tolerance assembly gaps similar to those found in the lightning strike stabilizer.

Interim Repair

The on going inspection of stabilizers resulted in a significant number being withdrawn from service due to unacceptable levels of damage. With no spares available, this was having an impact on the readiness of the B-1B fleet. With the information concerning the premature failures in the original acoustic test boxes and the results from the inspections, a preliminary conclusion was reached that at least one cause of the substructure failures were assembly anomalies. Therefore, an interim repair was developed and implemented that would correct the assembly anomalies and replace any damaged substructure. It was recognized that the repair might not be the final solution to the problem, but that it would maintain the serviceability of the fleet, until further investigation and testing could validate this cause.

Verification of the Cause of Failure

With the pressure off to take care of the immediate stabilizer problem, efforts turned to investigating and verifying the causes of failure. The first steps in this process were: (1) verify the response of the stabilizer to input loads, and (2) verify the source and magnitude of cyclic loads on the stabilizer.

Dynamic Response: To verify the response of the stabilizer to dynamic input loads, software tools and hardware capabilities unavailable during the original development of the stabilizers, were used. These tools allowed detailed Finite Element Models (FEMs) to be developed that could determine the dynamic response of the structure to specified inputs.

The first use of these models were used to determine the natural frequencies and associated mode shapes of the stabilizer. The results were surprising because they showed the response of the stabilizer in the neighborhood of 200 Hz(where the engine acoustic spectrum has a peak) consisted of complex mode shapes with the shapes dependent on the overall geometry of the stabilizer acting like a trapazoidal plate with the skins vibrating in unison. As previously stated, the acoustic test box for the stabilizer assumed that individual panel modes (bounded by ribs and spars) would be the primary driver for the stabilizer response.

Ground and Flight Test: The purpose of the ground and flight tests were to investigate any unaccounted for load conditions for the stabilizers and to verify the source, magnitude and response characteristics of the critical cyclic loads on the stabilizer. To accomplish this data was collected from an instrumented stabilizer in all ground and flight regimes that might contribute to the stabilizer loading. No significant unaccounted for load conditions were found during this test program. Although the test verified that the acoustic noise of the engines during full afterburner use during the take-off roll was

the most critical condition, the most interesting result was the verification that the stabilizer responded to the acoustic input as predicted by the dynamic model.

Dynamic Modeling

With the discovery of this new acoustic response mode, emphasis was put into improving the accuracy of the dynamic model. It was felt that this model could be used to quickly and efficiently model both the current configuration and new configurations of the stabilizer. Otherwise, the team would have to resort to slow and expensive laboratory tests.

Improvement of the dynamic model consisted of refinements of the mesh and changes to modern, higher order elements that would more accurately model the complex motion of the stabilizer and the interaction between the various components. Simulation of the acoustic environment and coupling of those loads to the refined NASTRAN model was performed by SDRC who supplies an I-DEAS module for performing vibro-acoustic analysis (see figure 6). A standand NASTRAN frequency analysis was performed with the results being compared with data from ground runup tests. In comparison with test results, the model was able to accurately model the acoustic input from the engines and the response of the stabilizer (see figure 7).

Fatigue Analysis

The dynamic model allowed the team to determine the stress within the substructure during acoustic excitement. With this information, the team could finally perform a fatigue analysis of the substructure. This analysis provided disheartening news to the team. Acoustics alone could not have caused the failures seen in the stabilizer. Therefore, the team was forced to look for other contributing factors.

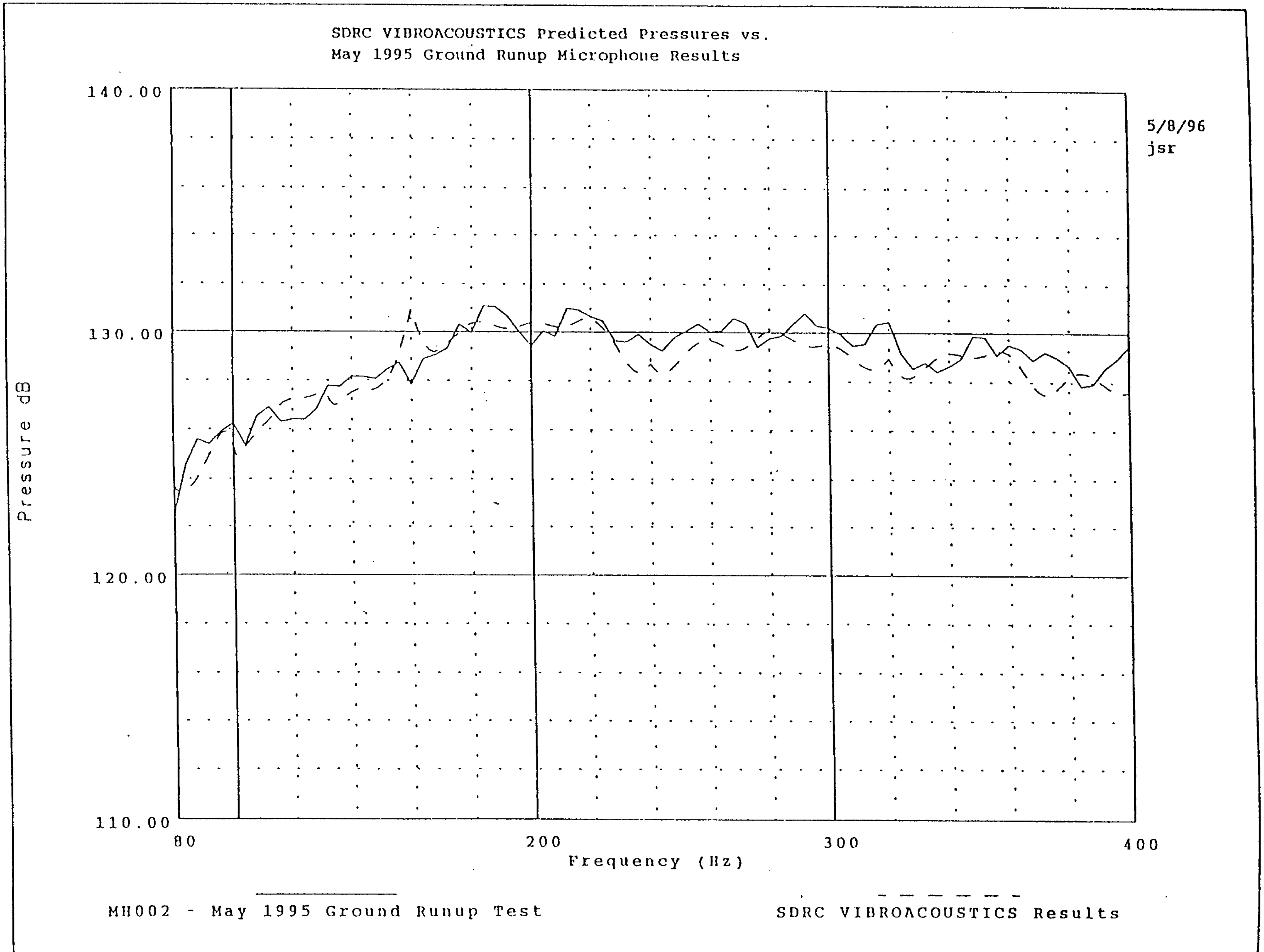

FIGURE 6: Comparison of acoustic environment predicted by SDRC and that measured during a ground test (one location only).

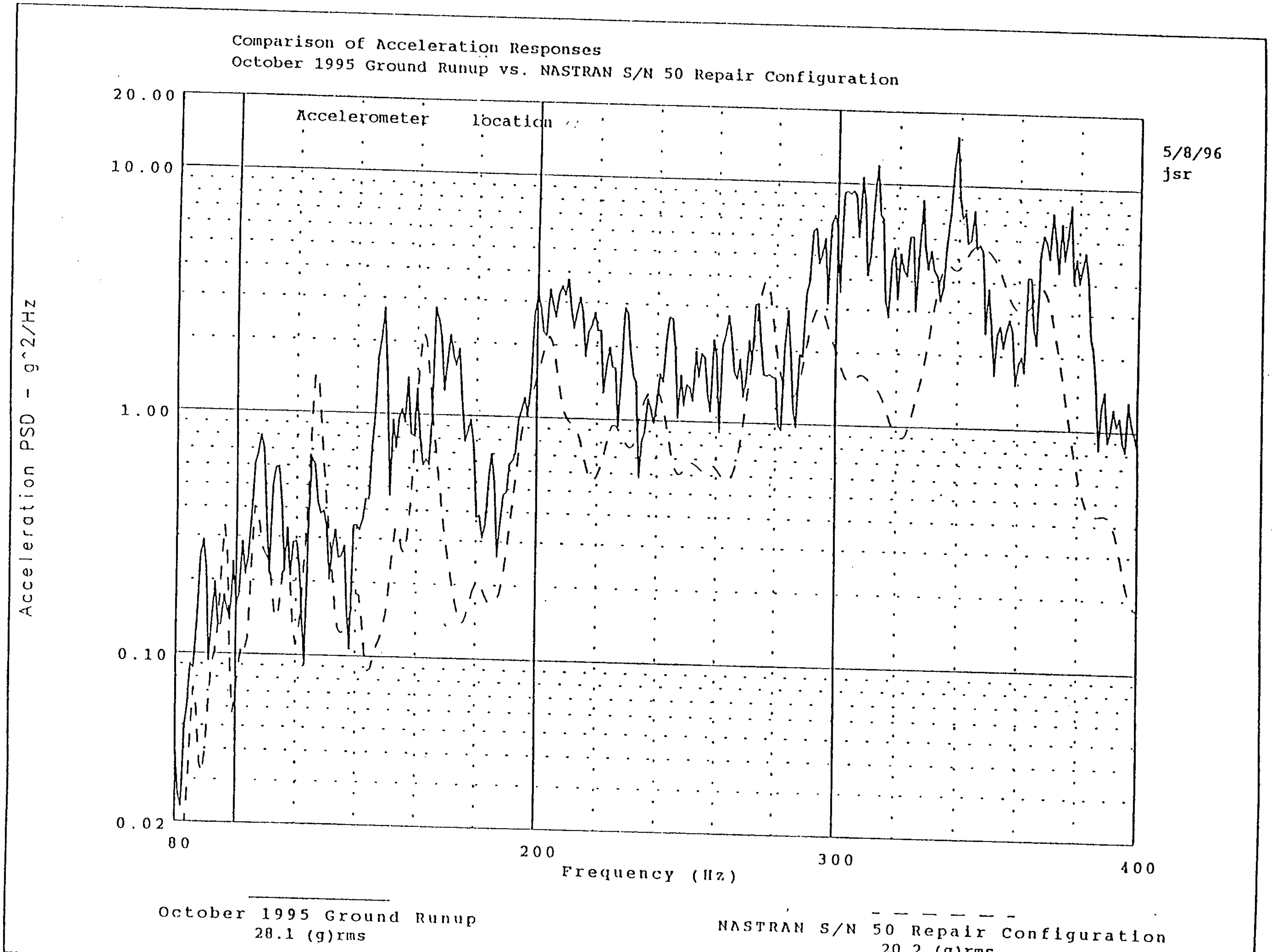

FIGURE 7: Comparison of acceleration response predicted by NASTRAN and that measured during a ground test (one location only).

The team did not have to look far. A high enough residual stress in the substructure, due to attempting to pull out gaps during assembly, could cause fatigue failure when loaded by the acoustic noise (see figure 8). A few analytical models and verification tests, proved that this was the case. In fact, at certain locations pulling out gaps well within the tolerances provided on the engineering drawings would provide sufficient residual stressed to cause a fatigue failure It should be noted that once the contribution of the residual stresses were appreciated, the stabilizer was analyzed for the flight load spectrum and found to have more than adequate life.

Failure Investigation Summary

The final determination of the investigating team was that the vast majority of the damage noted in the substructure was due to a combination of high residual stress and acoustics. The high residual stresses were due to pulling out assembly gaps during fastener installation.

Cure for the Problem

The team had two options for curing the problem of the substructure failures: (1) Lower the residual stress, (2) Lower the cyclic stress. Improvements in design, fabrication of the SWBs and assembly techniques have been shown to significantly reduce substructure gaps, but sufficient residual stresses can be reached by pulling out allowable assembly gaps. The team quickly agreed that reducing this stress was not the sole solution to the problem Therefore, the only option available was to lower the cyclic stress in conjunction with controlling the residual stresses. This could be achieved by stiffening the substructure. The interim repair arbitrarily stiffened the riblines, however, stopped short of changing the spars. The final repair that was developed, included stiffening the sparlines. This repair has been proven analytically to solve the problem. Currently, the team is testing a prototype of the repair to verify the analytical findings. Plans have been enacted to implement the final repair beginning in the year 2000.

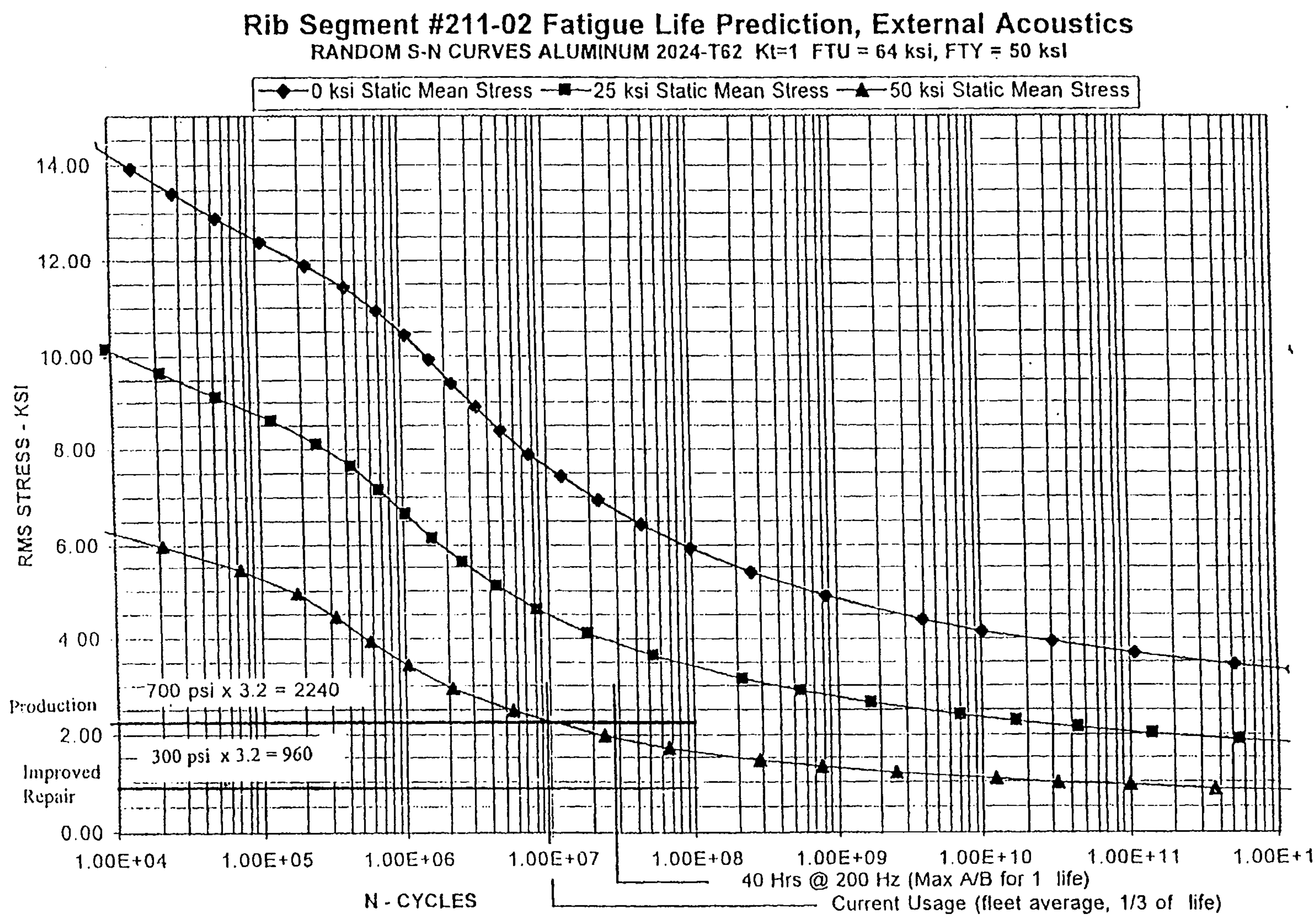

FIGURE 8 (Sheet 1 of 2): Predicted life of one rib segment in the original production stabilizer. The improved repair lowers the cyclic stress in the rib, therefore, provides significant improvement in life.

66

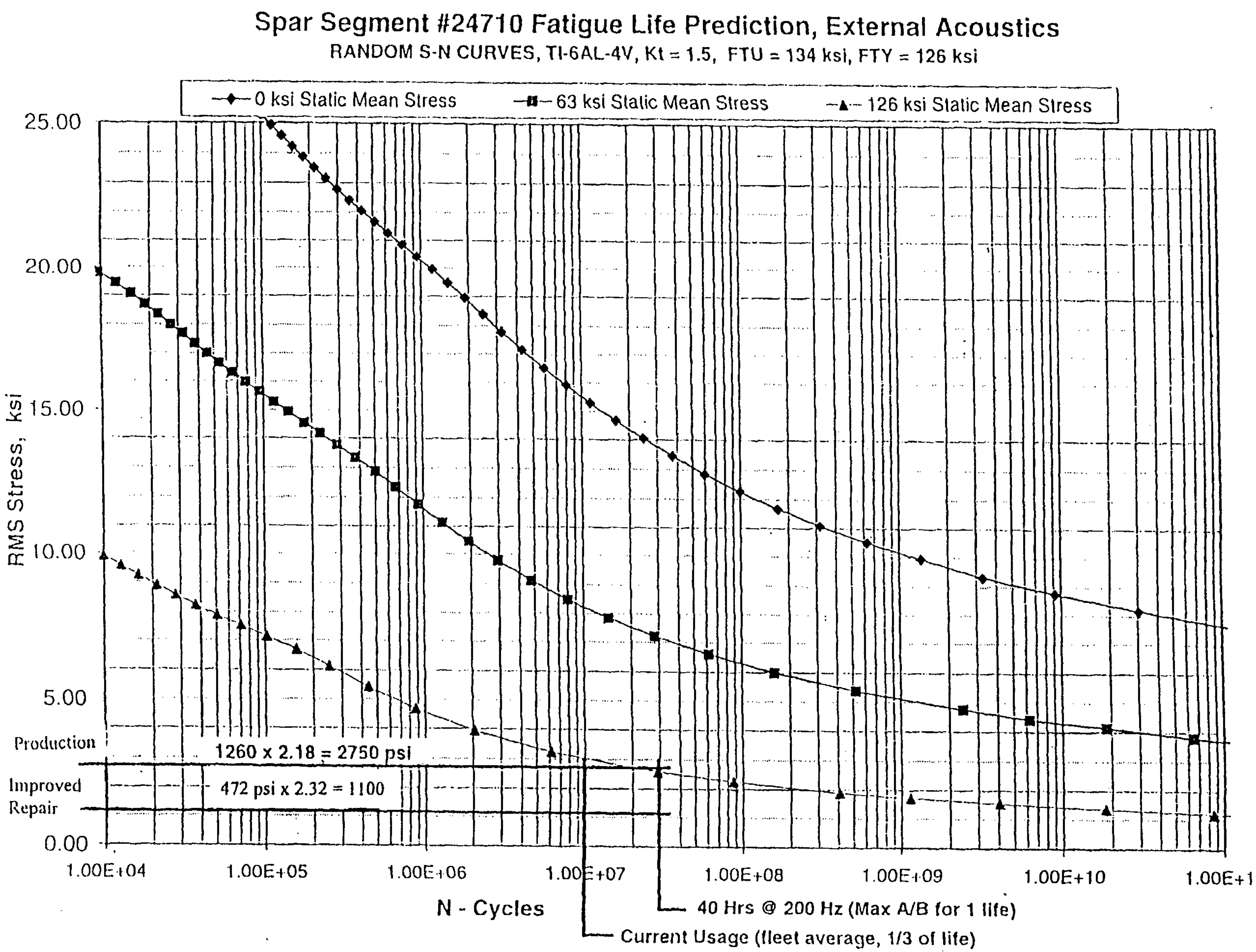

FIGURE 8 (Sheet 2 of 2): Predicted life of one segment of a SWB spar in the original production stabilizer. The improved repair lowers the cyclic stress in the segment, therefore, provides significant improvement in life.

SUMMARY

The substructure failure of the B-1B horizontal stabilizers provided a challenging and interesting problem for the investigating team. In addition, it provided some important lessons learned. For one, the failures showed the possible effect of using such contrasting structure (ie. thin substructure beneath relatively thick skins). Also, the failures show how residual stresses occurring from common assembly processes can cause problems. Therefore, these stresses need to be dealt with during design and the development of the manufacturing/assembly plan Lastly, the use of an important new engineering tool was demonstrated during the failure investigation. This tool is the capability of new software to accurately model acoustic sources and the dynamic responses of complex structure.

SESSION XI

DYNAMICS

Chairman - *M. Basehore*
William J. Hughes Technical Center, FAA

Development of Dynamic Models for the B-1B Horizontal Stabilizer to Predict Responses for Engine Takeoff Noise

Joseph S. Rosenthal
Team Leader B-1B ASIP
Boeing North American
Seal Beach, California 90740-7644

Background/Introduction

- Loose or missing fasteners found early in service life
- Inspection of horizontal hit by lightning (1993)
  - Numerous cracks in substructure
  - Improper fit up during assembly
- Inspection of operational fleet horizontal stabilizers
  - X-ray and boroscope methods
  - Damage was endemic to fleet
  - Cracks were not always in same locations
  - Crack length increased with increasing flight hours
  - Metallographic examination showed high cycle fatigue

Background/Introduction Cont'd

- Horizontal designed for high cycle vibratory stresses
  - Exposed to high engine noise during takeoff
  - Considerable analysis and testing during development
- Full scale development included fatigue (3 lives) and ultimate static load
- Recent effort (March 1994 to July 1996) included additional testing and analysis
  - Testing to indicate if acoustic environment changed during takeoff or if in-flight conditions significant
  - Test responses to correlate with analysis results
  - Analysis objectives
    - » Predict responses close to those measured during test
    - » Identify damage mechanism(s)
    - » Develop analytic acoustic environment independent of structural models

B-1B External Aircraft Configuration

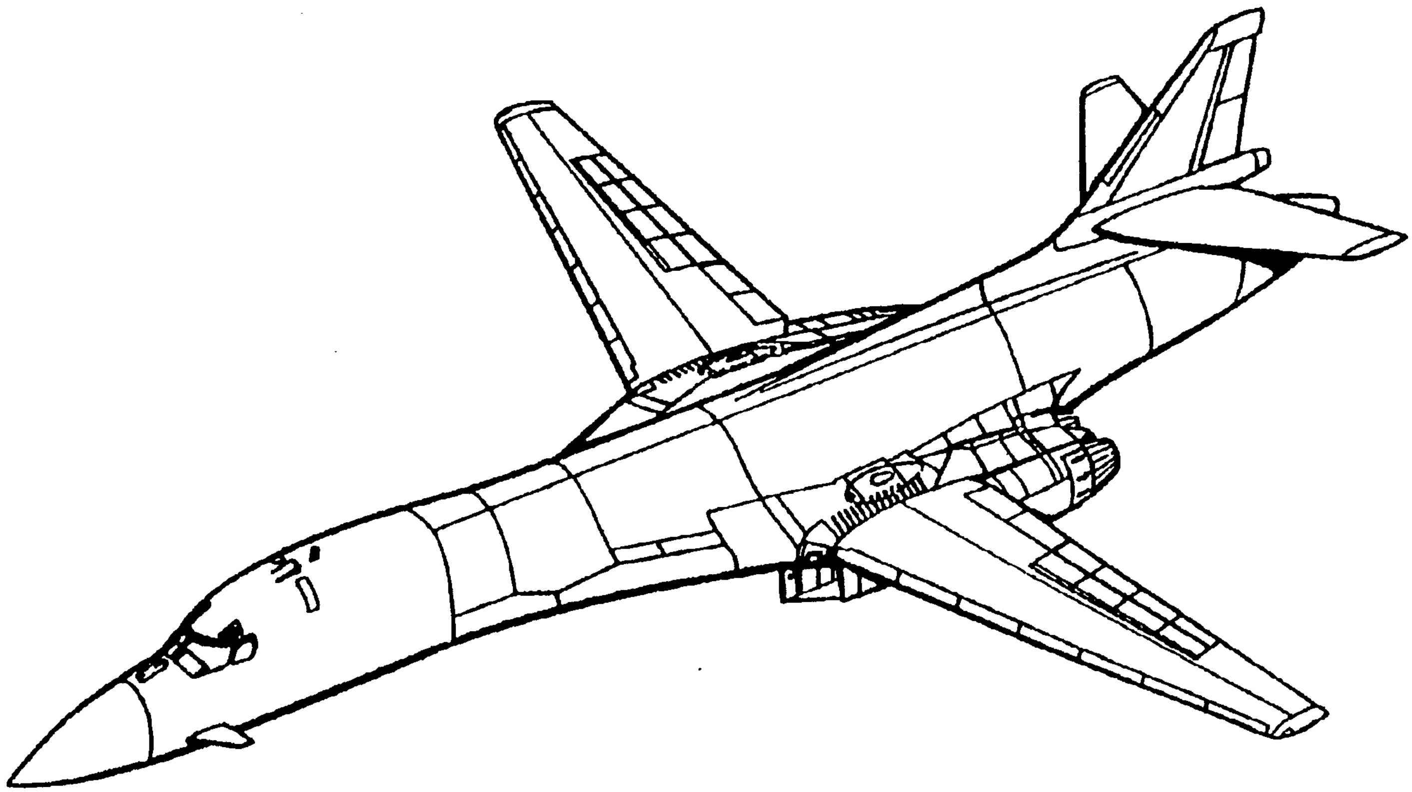

B-1B Horizontal Stabilizer Structural Breakdown

MATERIAL: Ribs: 2024-T62 Aluminum
SWB Spars: 6-4 Titanium
Front & Rear Spars: 7075-T76511 Aluminum
BSF: 6-4 Titanium
Skins: 2024-T851 Aluminum
Leading & Trailing Edges and Tip: Fiberglass over Aluminum Honeycomb

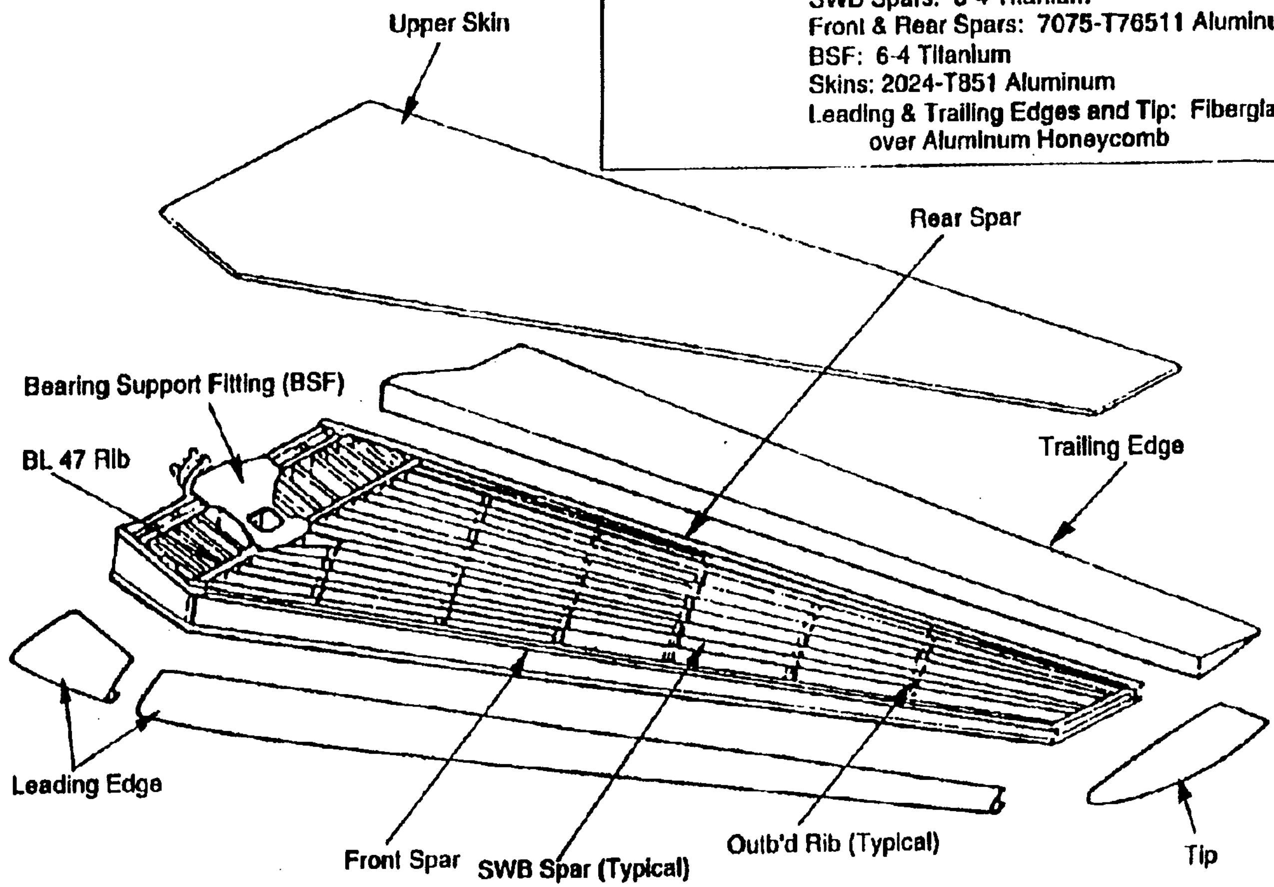

Horizontal Rib Configuration and Representative Damage

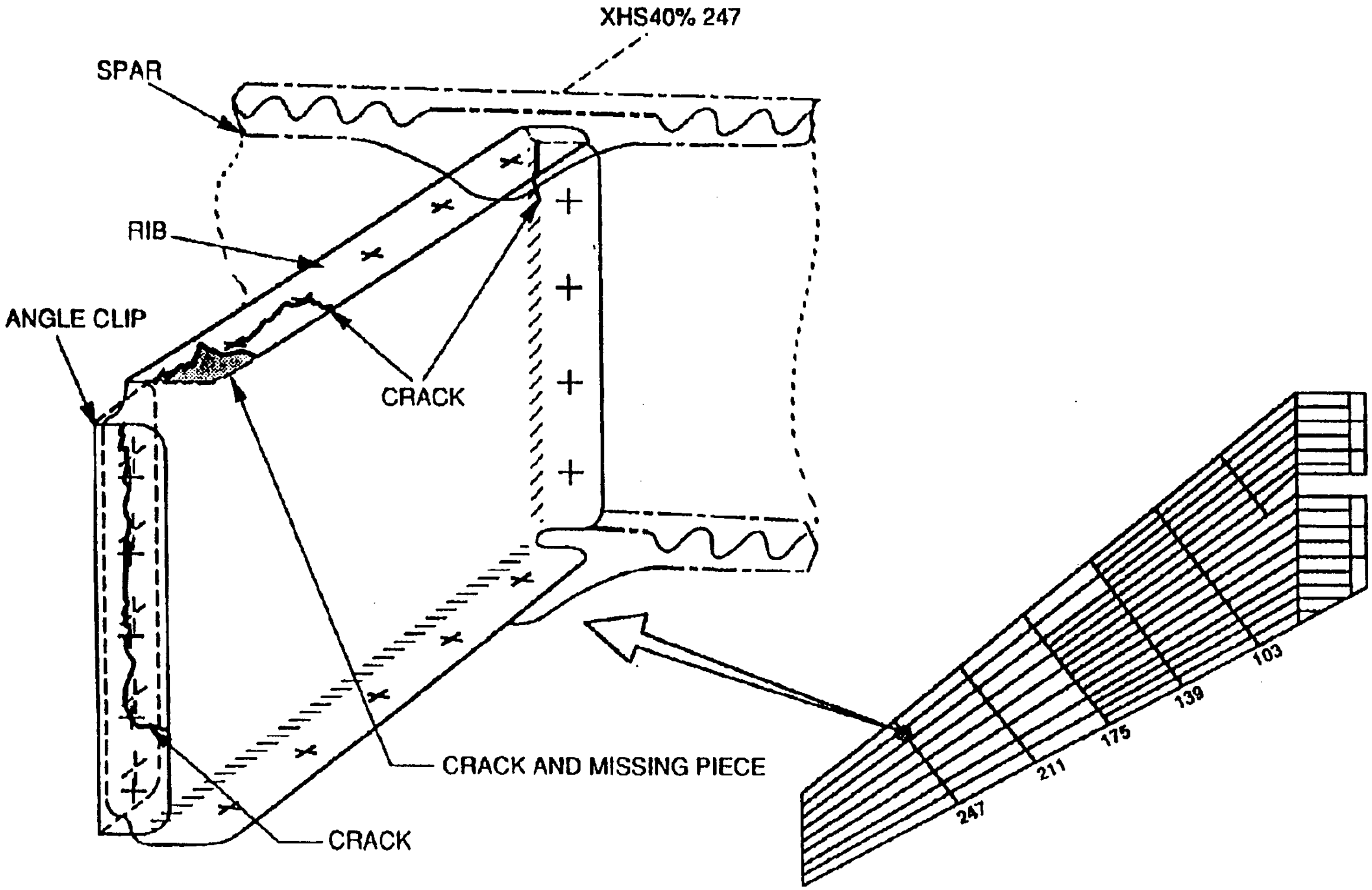

Horizontal Stabilizer Representative Spar Damage

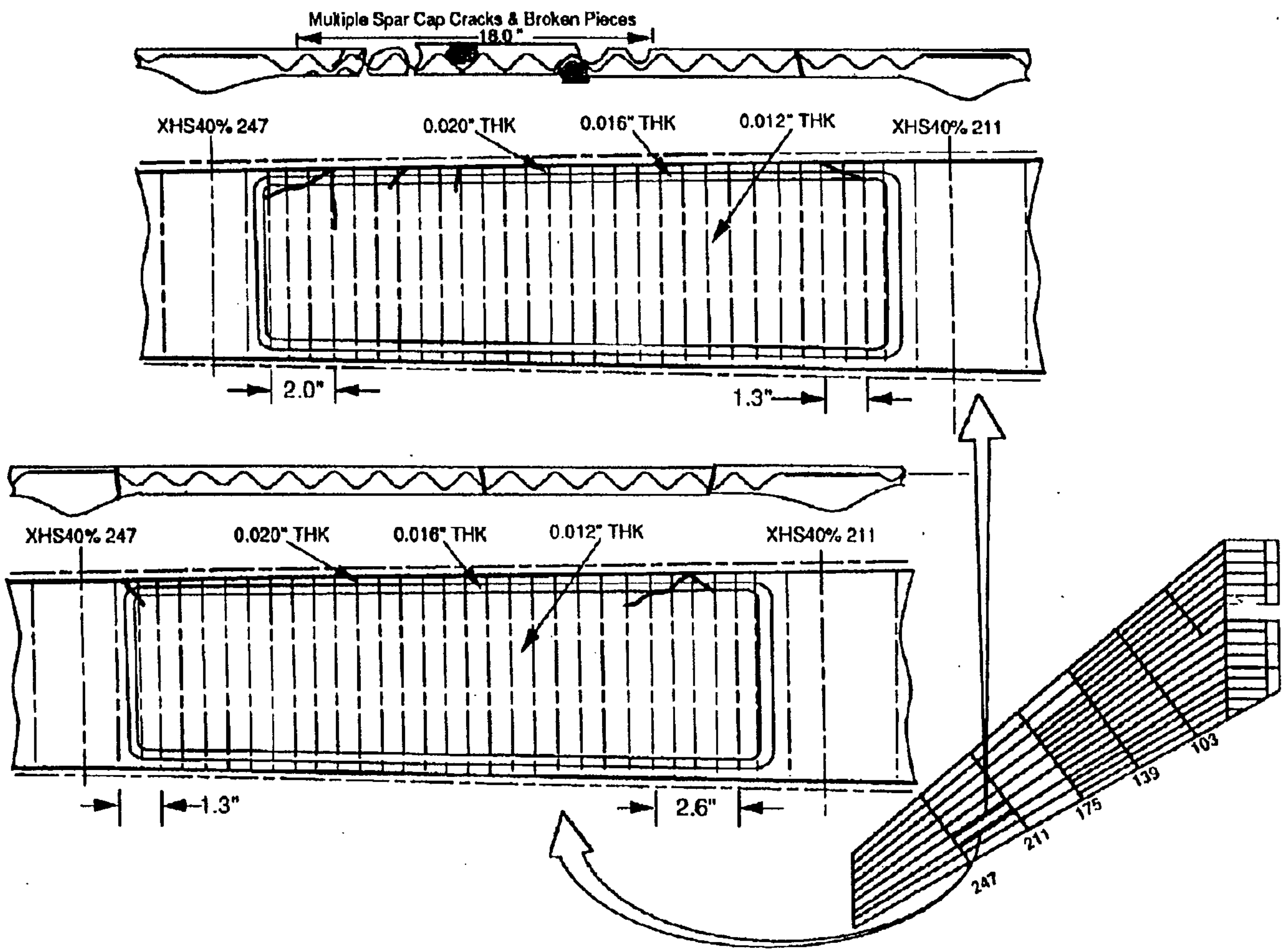

Analysis Overview

- Structural dynamic models
  - NASTRAN
  - MECHANICA, P-element
- Acoustic forcing function response analyses
  - Internal acoustics, stand alone rib and spar models
  - External acoustics, full horizontal stabilizer model
    - » Low frequency - 0 to 80 Hz
    - » High Freqency - 80 to 400 Hz
- Available comparative ground and flight test data
  - Data from two ground runup tests and one flight test
  - External and internal acoustic measurements
  - External accelerometers
  - Limited number of internal strain gages

Significant Results From Test Data

- Highest response in 80 to 400 Hz frequency range
  - Top and bottom surfaces moved together in phase
  - Stabilizer responded like a thick plate rather than as a series of small panels
- In-flight responses below takeoff

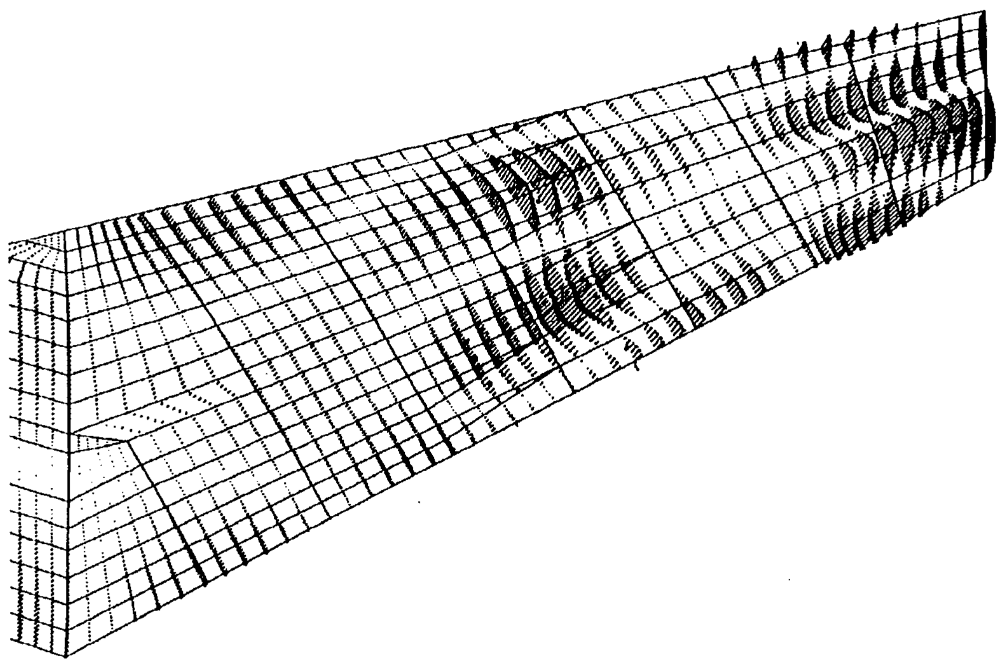

Low Frequency Analysis

- Account for rigid body and fuselage bending and torsion
- Frequency range 0 to 80 Hz
- NASTRAN static FEM was used
- Deflection data determined from flight test data
  - Data from 7 accelerometers recorded in velocity mode
  - Accelerometer data integrated to get displacements
  - Enforced Displacements applied to FEM
  - Resulting stresses compared to static design loads
  - Stress values low compared to design
- Method presented some draw backs
  - Displacements are a function of actual structure
  - Method results in high stresses at enforced points

Internal Acoustic Analyses

- Internal environment results from transmission of external environment mainly through bottom skin
- Detail rib and spar stand alone models generated
- Rib analysis
  - Fundamental frequency is 518 Hz.
  - Maximum stress indicated almost infinite life
  - Shell elements

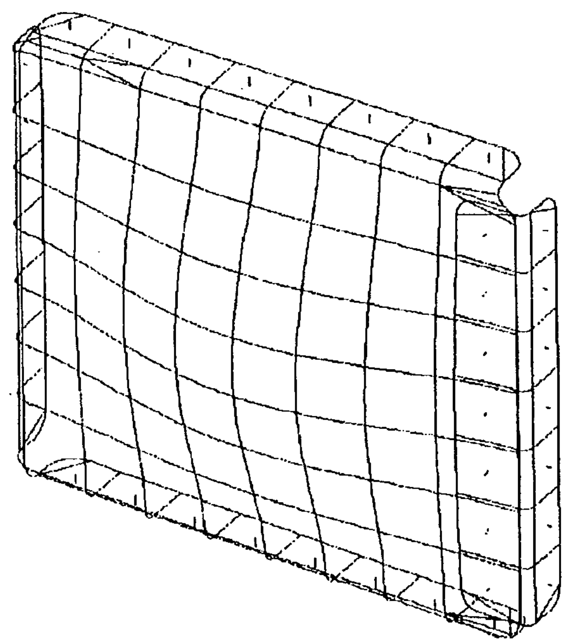

Internal Acoustic Analyses Cont'd

- Spar internal acoustic analysis
  - Shell elements
  - Fundamental frequency 1100 Hz
  - Stresses not large enough to cause cracks

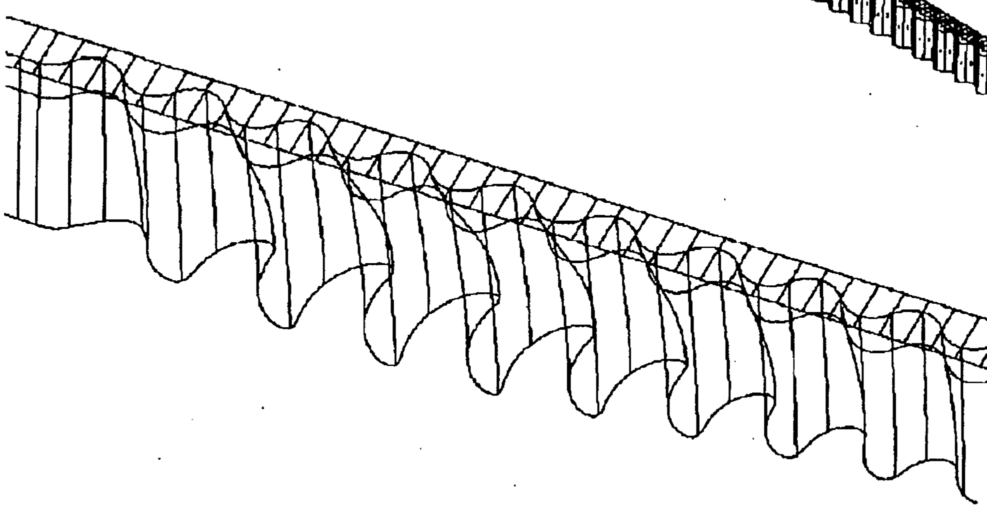

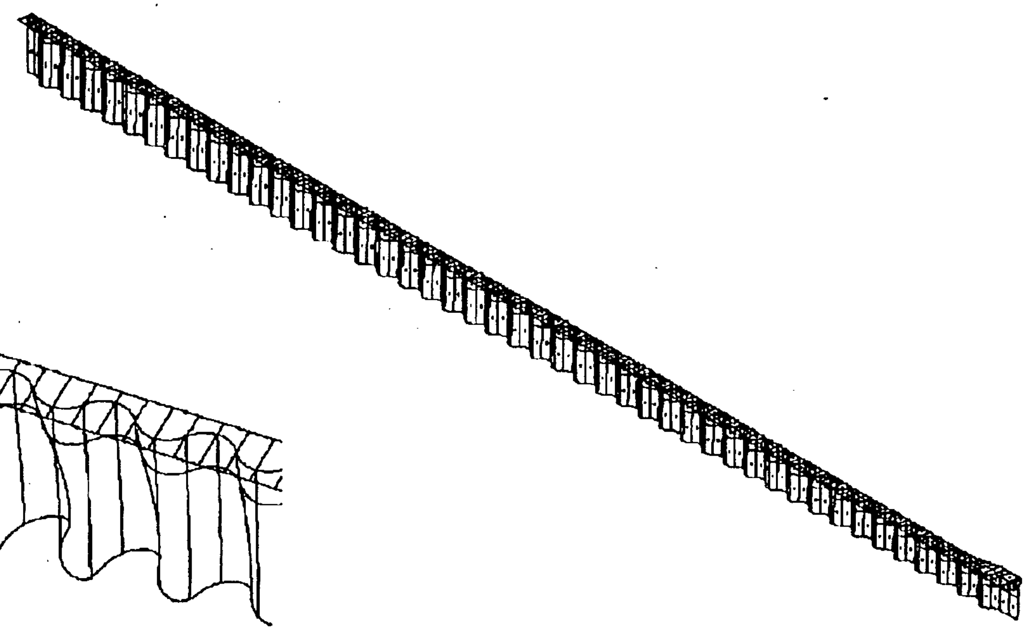

High Frequency Models and Analyses

- Initial NASTRAN FEM (derived from static model)
  - Skins are triangular bending elements
  - Ribs were shear elements only
  - Spars were shear elements with shear modulus reduced 20% to simulate reduced shear stiffness of sine wave beams

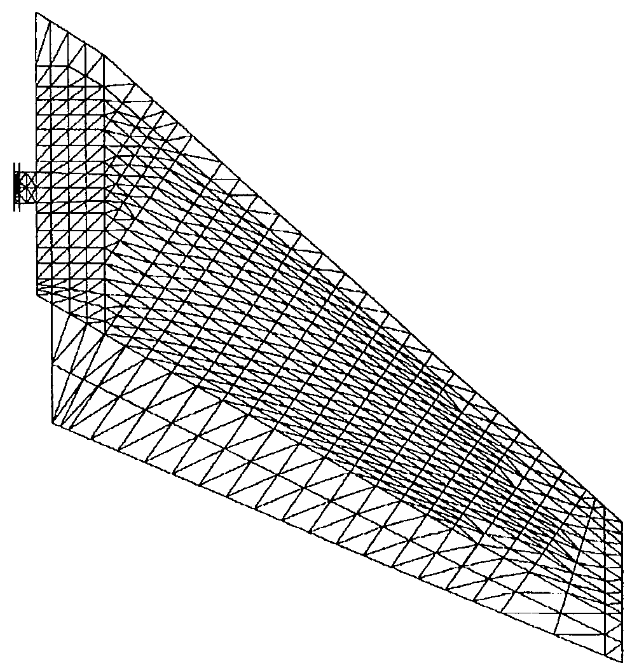

Pressure Time History Analysis

- Used actual pressures from transducers on lower surface
  - Assumed same pressure on area surrounding each transducer
  - Accounts for some phasing and correlation on surface
  - Transient dynamic analysis performed to determine accelerations
  - Accelerations compared to test results
    - » Responses over predicted
    - » Peaks and valleys didn't match

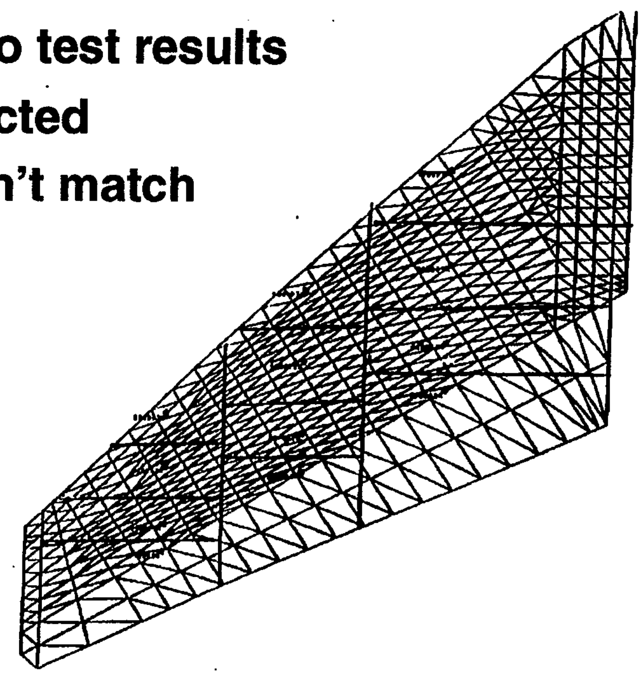

Coupled Acoustic/Structural Model Analysis

- Boeing North American using I-Deas™ software
  - Supplied by Structural Dynamics Research Corporation SDRC of Milford, Ohio
  - Separate module, VIBRO-ACOUSTICS performed coupled analysis
  - Services of SDRC San Diego office obtained
    - » Simulate acoustic environment
    - » Correlate environment with measured
    - » Run coupled analysis to obtain responses
    - » Correlate responses with test data
  - VIBRO-ACOUSTICS module
    - » Developed in France by STRACO
    - » Acoustic field is modeled by boundary element model (BEM)
    - » Determines acoustic and elasto-acoustic modes

Predicted Vs Measured Acoustic Level

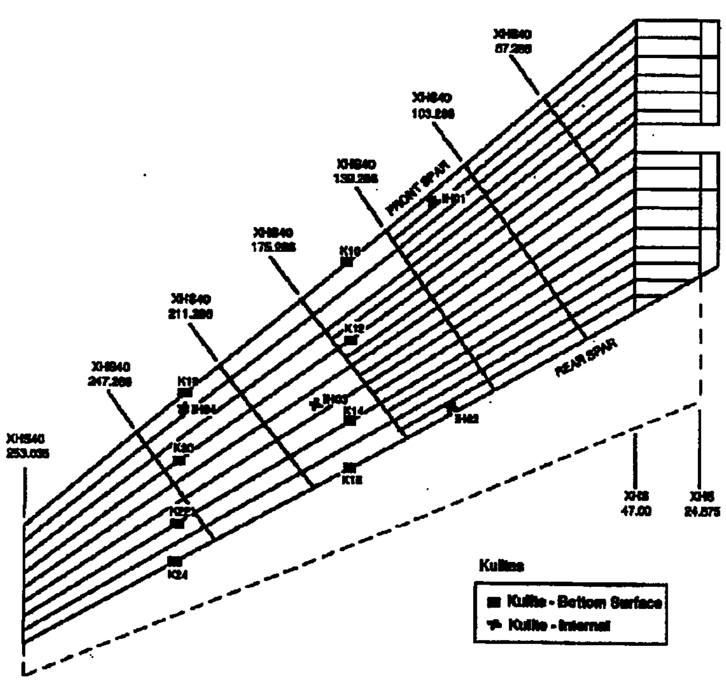

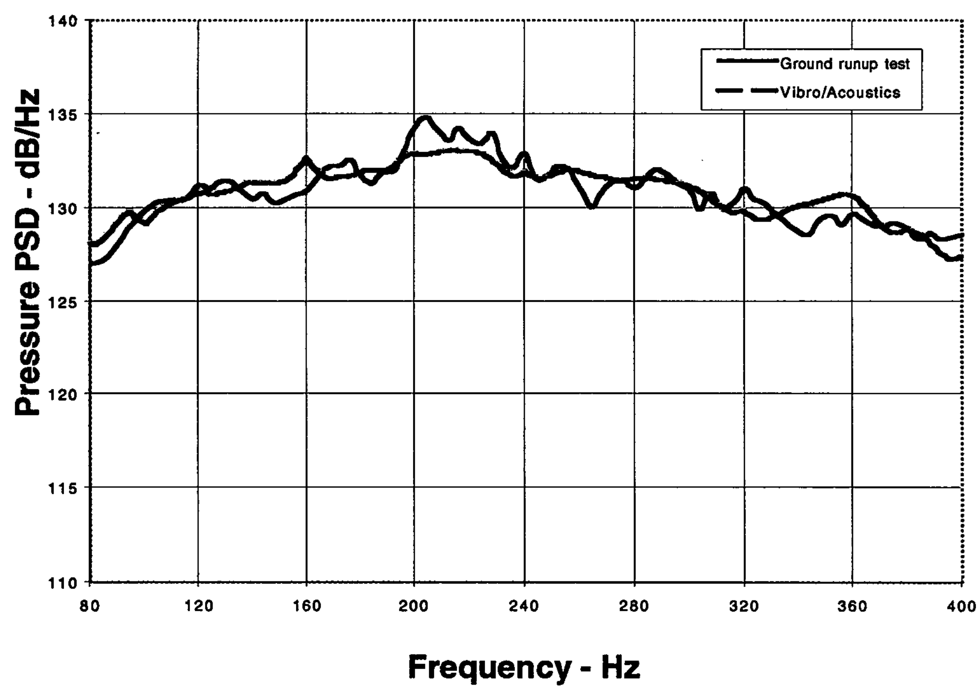

Engine Acoustic Noise Model

- Initially tried to model acoustic field to represent mixing region of exhaust and surrounding air
- Acoustic spectra generated for points where pressure transducers were located during ground tests
- Differences exceeded BNA criteria of $\pm$ 2 dB in the 80 to 400 Hz band
- Finally ten monopole sources were laid out in a grid two meters below stabilizer
- Sources were assumed to be independent & random
- Spectra for bottom surface were within $\pm$ 2 dB
- Spectra for top surface exceeded $\pm$ 2 dB
  - Method not as accurate for diffraction on top surface
  - Measured top surface levels 10 dB below bottom
  - Therefor accurate top surface modeling not required

Predicted vs Measured Acceleration Levels

- **SDRC response analysis results**

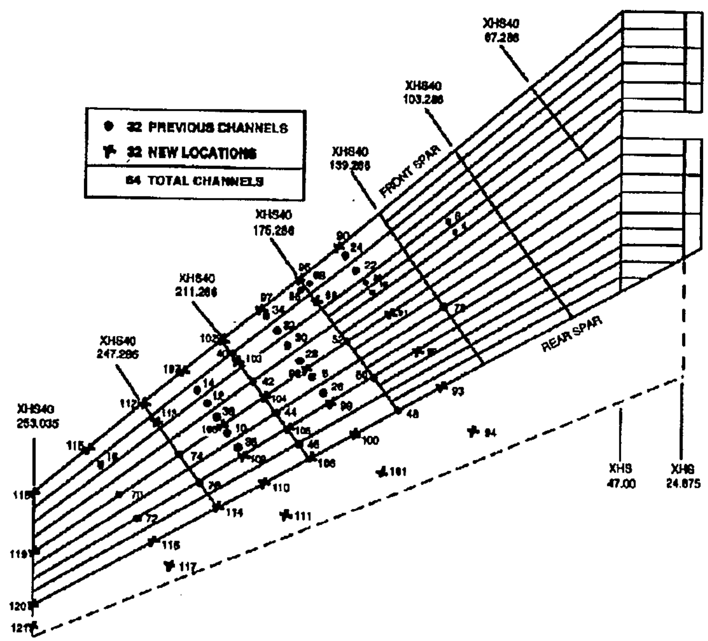

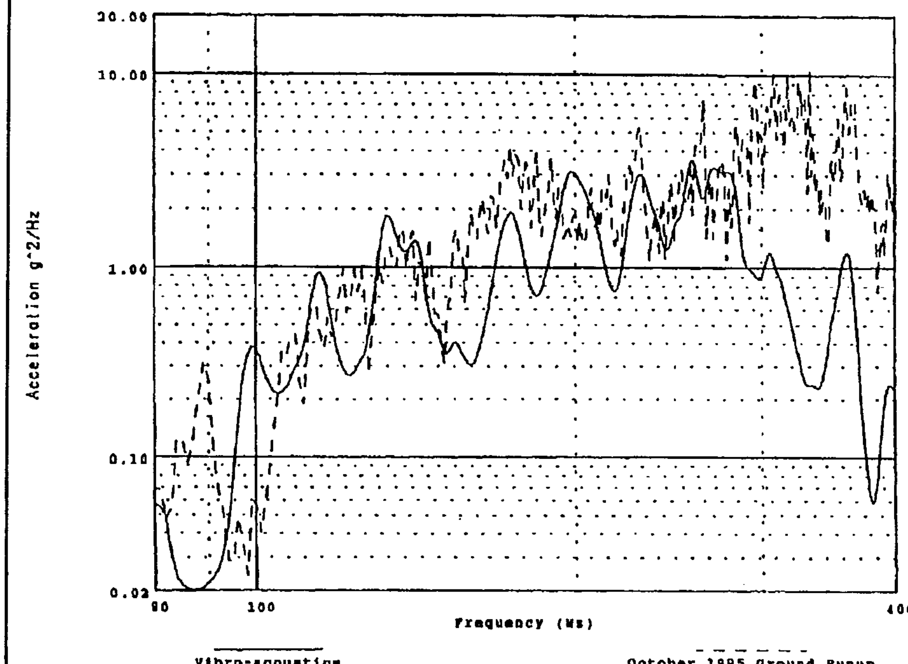

Enhanced NASTRAN Model

- Grids were made 3 times finer in all directions
- Redefined mesh and included fairing structure
- Skins modeled as bending plates
- Membrane elements used for rib sections
- Spars are flat bending elements with reduced shear and bending modulus to simulate SWBs
- Leading, trailing and tip fairings
  - Fiberglass face sheets
  - Core modeled as solid elements with equivalent properties

Enhanced NASTRAN Model Cont'd

- Densities adjusted for wt., cg and moments of inertia
- Support stiffnesses simulated at bearing and actuator attachements

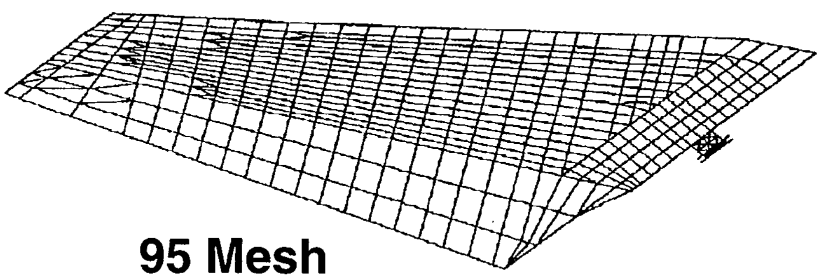

95 Mesh

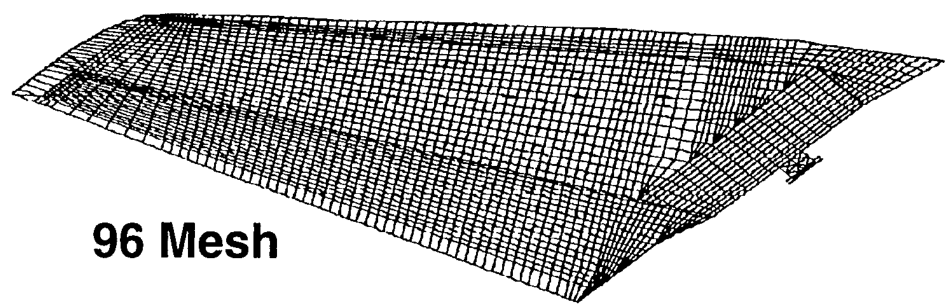

96 Mesh

BNA Response Analysis

- SDRC acoustic pressure data used
- Duplicated SDRC acceleration calculations
- Determined stresses using 96 Mesh enhanced model
- Stresses correlated with limited available ground test data
- Correlation felt to be good
- Methodology used to compare repair concepts with each other and production baseline
- Analytically determined and measured rms stresses were low, < 2 ksi
  - Would not by themselves cause cracking for 10^7 - 10^8 cycles
  - Combined with high fit up stresses, account for damage S/N curves shift down for concurrent static load

Predicted Vs Measured Stress Spectra

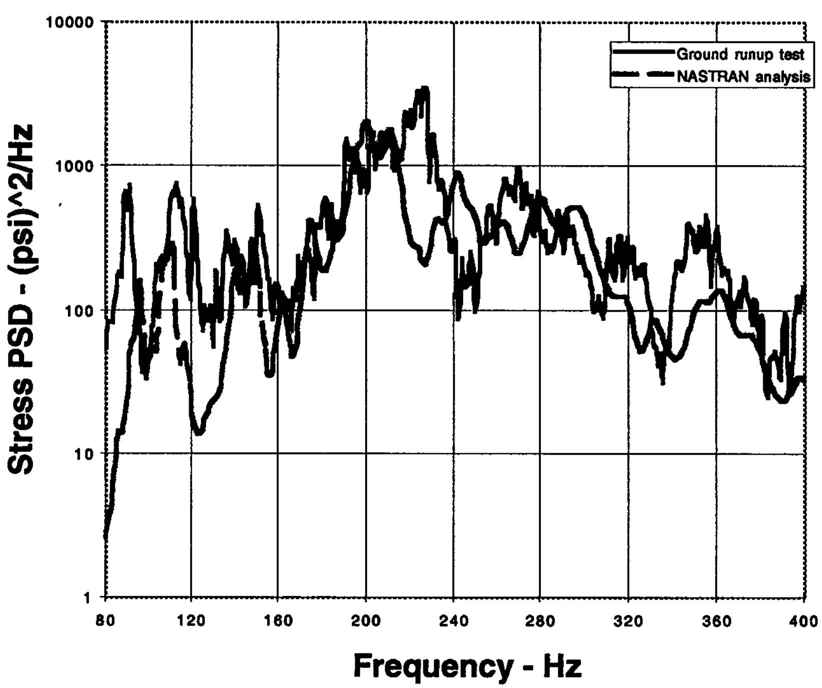

Aft segment 211 rib

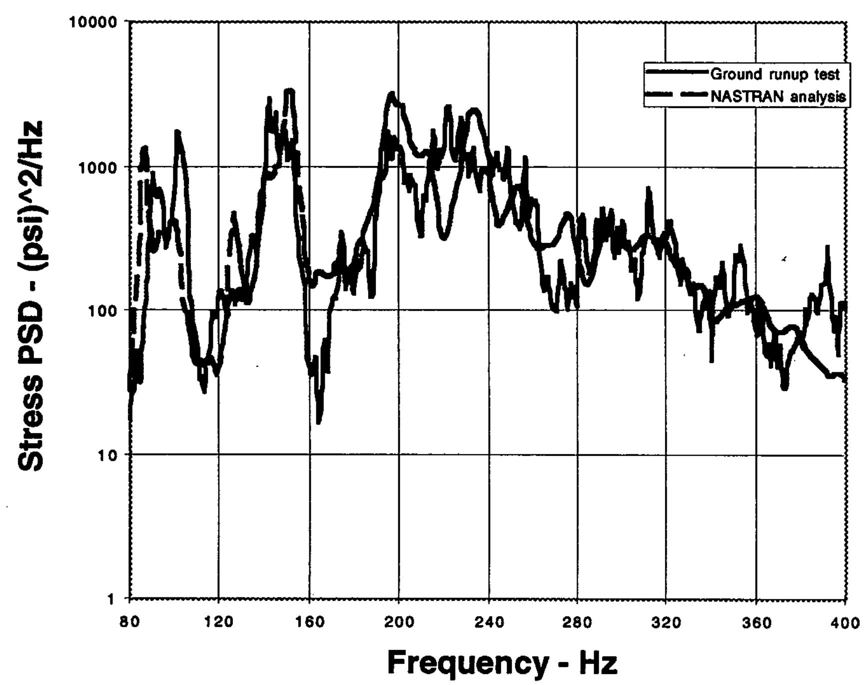

Forward segment 247 rib

Conclusions

- Analysis methods and models were developed which identified the cause of the cracking in B-1B Horizontal Stabilizers
- For this complex problem three different methods were required to investigate the range of possible causes
  - Low frequency region 0 - 80 Hz with full stabilizer model
  - Internal acoustics with stand alone models
  - High frequency, 80 - 400 Hz with full stabilizer model
- Actual ground test data was required to correlate the results
- The complex acoustic field can be modeled as a set of simple sources
- The measured and calculated stresses were not large enough to cause cracking without the presence of high static prestresses
- Reducing both the oscillatory and fit up stresses should allow the repaired horizontal stabilizers to meet their remaining life requirements

Warner Robins ALC

Georgia Tech Research Institute

RECENT TECHNOLOGY ENHANCEMENTS in the HELICOPTER STRUCTURAL INTEGRITY COMPUTER PROGRAM

Structural Integrity Computer Program

AVIATION PROGRESS

- **COMMONLY PROGRESS MEANS FLYING**
  - Faster
  - Farther
  - Higher (or Lower for Helo's)
  - With More Agility
  - Less Detectably
  - With More Payload
  - Seeing / Learning More
  - In Any Weather
- **PROGRESS ALSO MEANS FLYING**
  - Safer
  - Cheaper
  - More Often
  - With Less Maintenance
  - For Many More Years to Come

WR-ALC HSIP GOALS

HELICOPTER STRUCTURAL INTEGRITY PROGRAM

- ENHANCE AIRCRAFT SAFETY
- IMPROVE MAINTENANCE PROCEDURES
- INCREASE MISSION CAPABILITY
- LOWER LIFE CYCLE COST

Note: Enhanced Structural Integrity can be a Force Multiplier

HELO'S ARE DIFFERENT

"Spinning Scrap Metal in Close Formation Flight"

"Flying Fatigue Machines"

- **RAPID FATIGUE CYCLE ACCUMULATION**
  - Power Level Cycles, PLUS
  - 3 to 50 Hz on Airframe, Controls and Dynamic Components
  - Less Importance of Pressure / Gust Cycles
- **INCREASED MANEUVER FREEDOM**
- **HIGH STEADY LOADS / R-RATIOs**
  - Centrifugal Force
- **VARIABLE AMPLITUDE LOADING**
  - Ratio of Steady to Applied Stress Highly Scattered
- **COMPLEX ROTATING COMPONENTS GEOMETRIES**

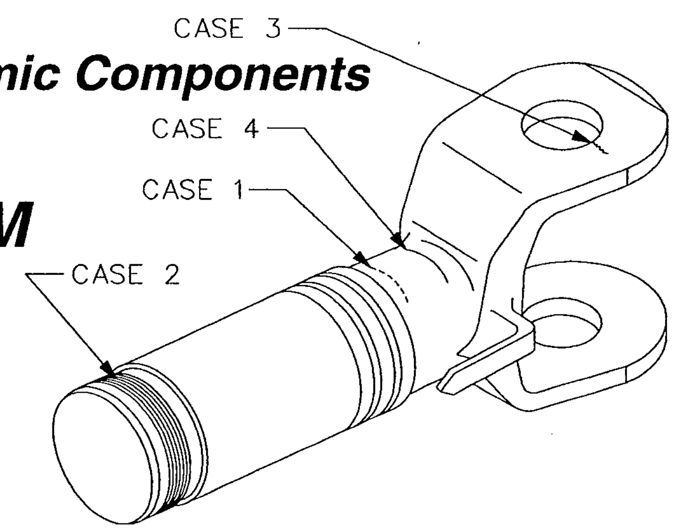

HELICOPTER FORCE MANAGEMENT

- **TRADITIONAL SAFE-LIFE METHODOLOGY**
  - Rotating Sys, Fixed Controls and Engine / Drive Components
- **MANY PARTS NOT MANAGEABLE by DTA**
  - Relatively Rapid Crack Growth
  - Visual Inspection Intervals < 50 hrs Not Viable, Even for Most Accessible Components
- **SMALL CRACK MODELS CRITICAL**
  - Significant Fatigue Crack Growth Occurs Between Initiation and NDI Detectable Crack Size
- **INPUTS ACCURACY CRITICAL**
  - Usage Spectrums
  - Damaging Loads
  - Material Properties / SN Curves

SICP PURPOSE -- FORCE MANAGEMENT

- **DETERMINE**
  - Safe-Life (Empirical S-N Curve) **AND** FCG by DTA
  - Examine Both Facets to Enhance Total Useful Flt Time
- **ALLOW for CHANGES in**
  - Usage, Loads, Initial Crack Size, Geometry, Material
- **STAND ALONE or CONNECTIVITY**
  - Individual Helicopter Tracking Program
  - Logistics Tie-in

SICP PURPOSE -- FORCE MANAGEMENT (Concluded)

- **FLEXIBLE**
  - Core System Usable for Any Helicopter
- **ALLOW MODULE GROWTH**
- **USER FRIENDLY, SHORT COMPUTATIONAL TIME**

INCREASE SAFETY

REDUCE MAINTENANCE

INCREASE AVAILABILITY

Home of the 1996 Olympic Village Georgia Tech Research Institute

SICP CONCEPT

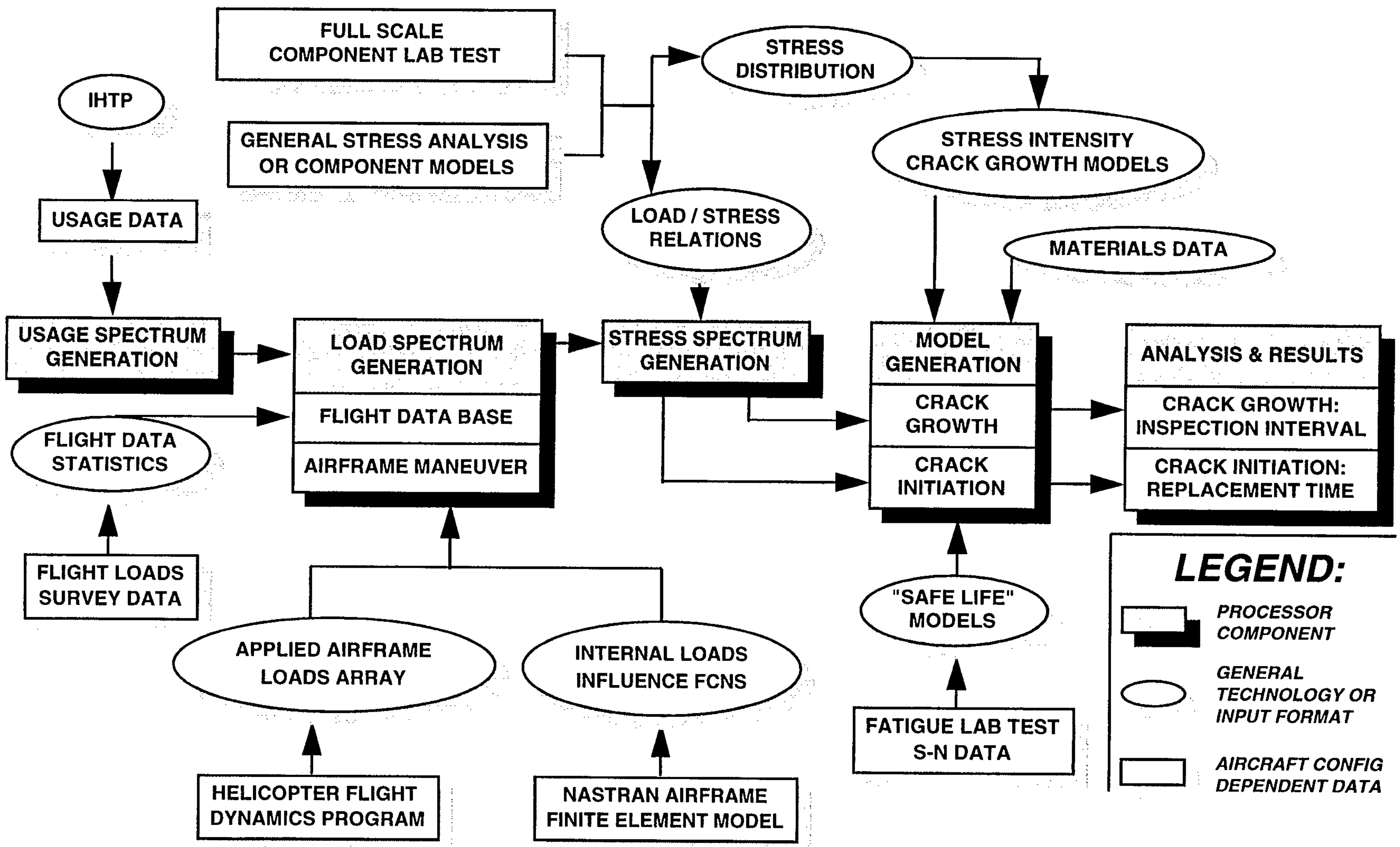

Structural Integrity Computer Program

SICP HERITAGE

- **SIKORSKY DEVELOPED DTA CODE ('84)**
  - Core Routines Completed
- **SIKORSKY DELIVERED DTA CODE ('89)**
  - Rainflow Cycle-Counting Routines Added
  - Geometry Definitions No Longer Hard Wired
- **HELO SIFs MODELS DEVELOPED (1994)**
  - A Joint Sik & GTRI Effort
- **GTRI CODE IMPROVEMENTS (1996)**
  - General Clean-Up / Increase Flexibility / Repair
  - Added Crack Initiation (Empirical S-N Curve) for Dyn Comp
  - 1994 SMFT Strain Survey Data Added

Note: all Above Contract Sponsored by WR-ALC

SICP TODAY

- CODED SPECIFICALLY for MH-53J (SLEP/SBO)
  - Mature Aircraft (1960's Technology)
  - NOT Designed for Damage Tolerance
- EXTENSIVE SMFT LOADS DATA BASE
  - 4 GW's, 2+ CG's, 3 Nr's, 2+ Hd's
  - Approximately 100 Productive Flt Test Hrs
  - High Alt IGE, Slope Landings, & In-flt Refueling
  - Tail Rotor Strain Survey
- COMPONENT GEOMETRIES for KNOWN "HOT SPOTS"

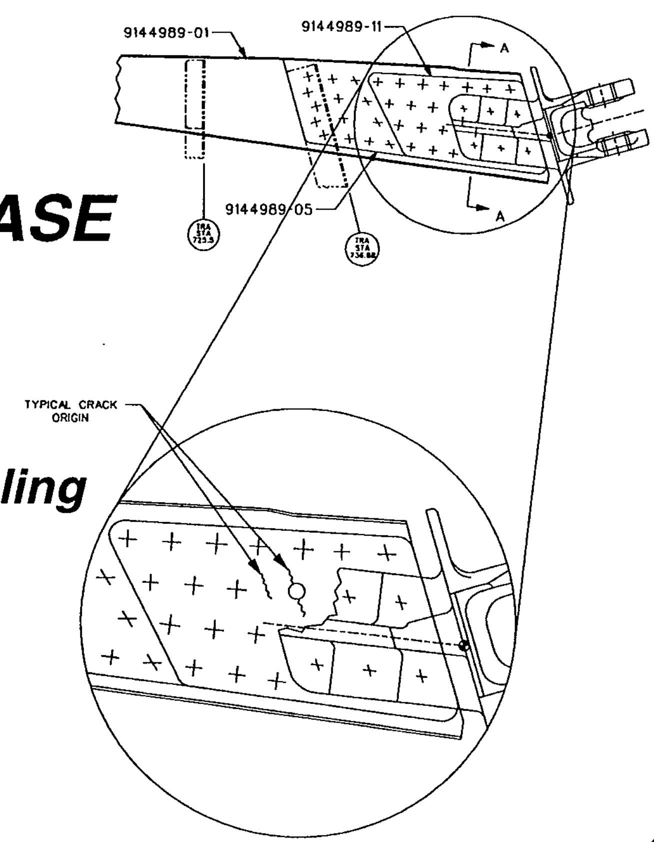

SICP TODAY (Concluded)

- **STRESS INTENSITY FACTOR MODELS**
  - Helicopter-Specific Component Research: Unpressurized, Untorqued Hollow Cylinders
- **FLEXIBLE USAGE SPECTRUM**
  - 80 Regimes, 32 Prorates (GW, CG, Hd, Nr)
- **MULTI-RECORD LOADS AVERAGED**
- **SACGAP CRACK GROWTH CODE**

SICP TOMORROW

- **IMPLEMENT SHORT CRACK MODEL**
  - Necessary for Helicopter (High Cycle) Loading
- **INCORPORATE TOP-OF-SCATTER OPTION**
  - Original Code Not Intended for Empirical S-N Curve Safe-Life
  - Currently Averages All Available Data for Specific Maneuver/Prorate
  - Allow Industry Standard Approach to be used for Crack Initiation
- **MODIFY REGIME SUBSTITUTION ALGORITHM**
  - Intelligent Choice of Replacement Maneuver for Missing Data
- **EXPAND USAGE SPECTRUM GENERATOR**
  - Common Error Trapping (Force Total Usage = 100% ...)
  - Will Allow User to Control Where Adjustments are Made
  - Eliminate Time Allocated to Unachievable Regimes

SICP TOMORROW (Concluded)

- **INTEGRATE NASGRO FCG CODE**
  - Modify SICP Output to Provide NASGRO Input File
- **PROVIDE LOADS PREDICTION**
  - "Comprehensive Analytical Model of Rotorcraft Aerodynamics and Dynamics" -- CAMRAD II
  - Multibody Dynamics, Non-Linear FEs, Structural Dynamics, Rotorcraft Aeromechanics
  - Calculate Performance, Loads, Vibration, Response, Stability
  - Simulate Missing Maneuvers
  - NASTRAN Aircraft and Local, Static and Dynamic Models

Home of the 1996 Olympic Village
Georgia Tech Research Institute

RECOMMENDATIONS

- ENHANCE CRACK GROWTH MODEL VALIDITY thru CRACK PROPAGATION TESTING of COMPLEX HELO CONTROL SYS PARTS
  - After Crack Initiation Measure Propagation as Policy
- CONSIDER NEED for IMPROVED INSPECTION TECHNIQUES at FIELD LEVEL MAINTENANCE
- DUPLICATE SICP for H-60 SERIES
  - Potential Use for Over 1500+ Helo's
- STUDY POTENTIAL of SICP USE with HUMS DATA

SESSION XII

FORCE MANAGEMENT

Chairman - *J. Turner*
San Antonio Air Logistics Center

Detecting High Cycle Fatigue with User Defined Regime Recognition

John A. Cicero, Ph.D.
Senior Software Engineer
Systems & Electronics, Inc.
190 Gordon Street
Elk Grove Village, IL 60007-1120
Tel: (630) 829-6556
FAX: (630) 829-6551
E-mail: jcicero@ben.edu

Introduction

Systems & Electronics, Inc. (SEI) has developed a system that detects high cycle fatigue through user defined regime recognition. The system includes an airborne recorder and a ground-based PC. The airborne recorder records aircraft parameters such as airspeed, altitude, Nz, angular acceleration, etc. This data is compressed and then stored in an electronic (FLASH) memory module. At the end of a flight (or series of flights) the memory module is downloaded into a PC. A decompression algorithm is used to expand the compressed data into time-contiguous data. This time-contiguous data is then processed by a flight condition code processor program. This program is used to identify flight maneuvers that cause fatigue.

Classifying the Maneuvers

What makes this system unique is that the user can classify a specific maneuver by its individual parameter ranges. For example, assume that the user defines an Angle Of Bank 50 Degree Left Turn @ 0.4Vh as one in which:

0.35% <	airspeed (%Vh)	< 0.45%
95% <	rotor RPM	< 115%

20% <	engine torques	< 110%
0.5g <	Nz	< 3g
-60 degrees <	Roll Attitude	< -6 degrees
-45 degrees <	Pitch Attitude	< 45 degrees
20 % <	Latitudinal Stick Position	< 100%
20 % <	Longitudinal Stick Position	< 100%
20 % <	Rudder Stick Position	< 100%
-500 feet/min <	Rate of Climb	< 500 feet/min

Using the flight condition code processor program shown in Figure 1, the user can create a new flight condition code or modify an existing flight condition code. For each input parameter the user selects whether or not the input is used to classify the current flight condition code. If it is selected, the user must determine the lower and upper limits of this input parameter. For any given flight condition code the user can also specify that the following additional flight information be logged:

1) the parameter value at the start of the maneuver,
2) the parameter value at the end of the maneuver,
3) the maximum parameter value during the maneuver, and
4) the minimum parameter value during the maneuver.

The user can also specify discrete event information such as a takeoff and a landing. The flight condition code processor can be configured to first look for a takeoff before it will recognize a landing. After a takeoff occurs, the flight condition code processor can be configured to look for a landing before it will recognize another takeoff.

The Flight Condition Code Processor Output

Once all of the flight condition codes have been entered, the user can select the run option from the flight condition code processor menu. There are essentially two sets of input data to the flight condition recognition program. One set is the decompressed time-contiguous flight data from the flight recorder. The other set is the user specified flight condition codes described above. After the data is run through the flight condition code processor the following output sets will be generated:

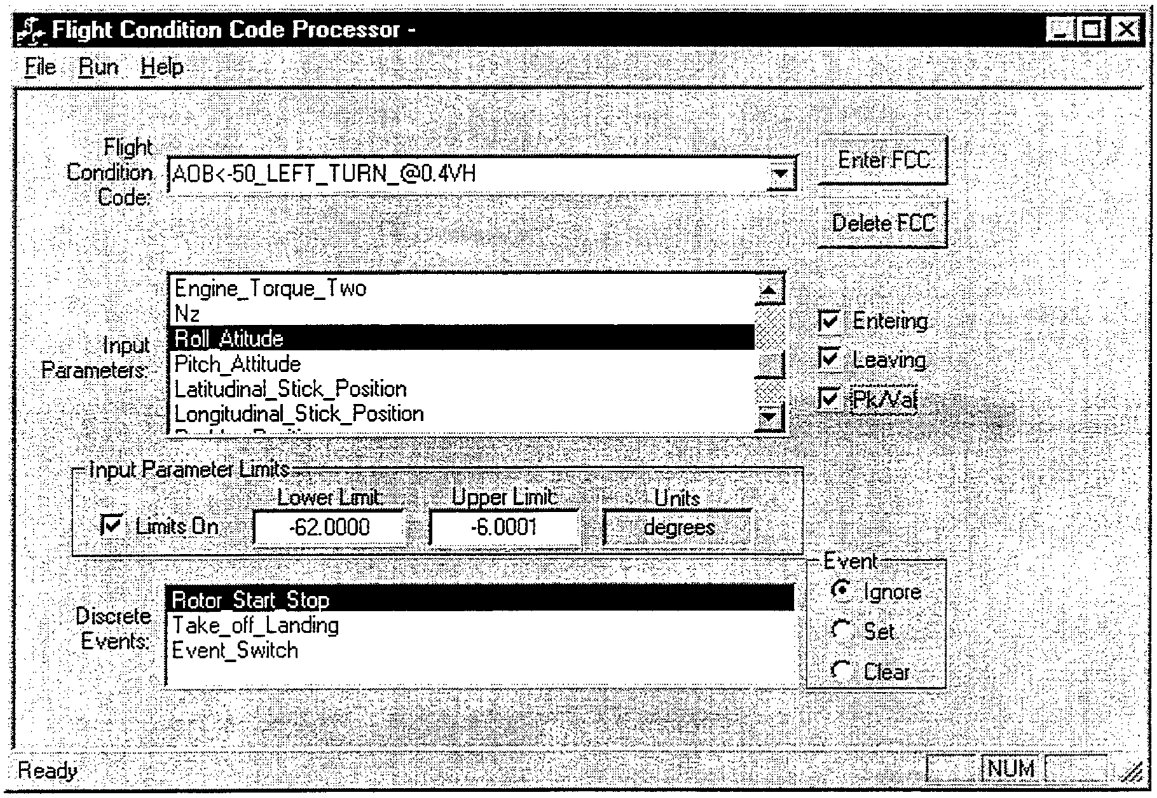

Figure 1. The flight condition code processor.

The first output is a flight profile. When the flight processor encounters recorded data within the parameter limits (that were determined by the user) it will report the following information:

1) a unique flight condition name (i.e., Angle Of Bank 50 Degree Left Turn @ 0.4Vh),
2) the time duration of the flight condition (i.e., 10 seconds),
3) any coincident peak/valley parameter data that occurred during the condition (i.e., If Nz was chosen as a coincident peak/valley parameter, the report might contain the following results: Nz valley = 0.8 g's and Nz peak = 2.6 g's),
4) any coincident parameter data recorded at the start of the flight maneuver, (i.e., If Rate of Climb is chosen as a coincident parameter at the start of the flight maneuver, the report might contain the following results: Rate of Climb Entering = -300 feet/minute), and

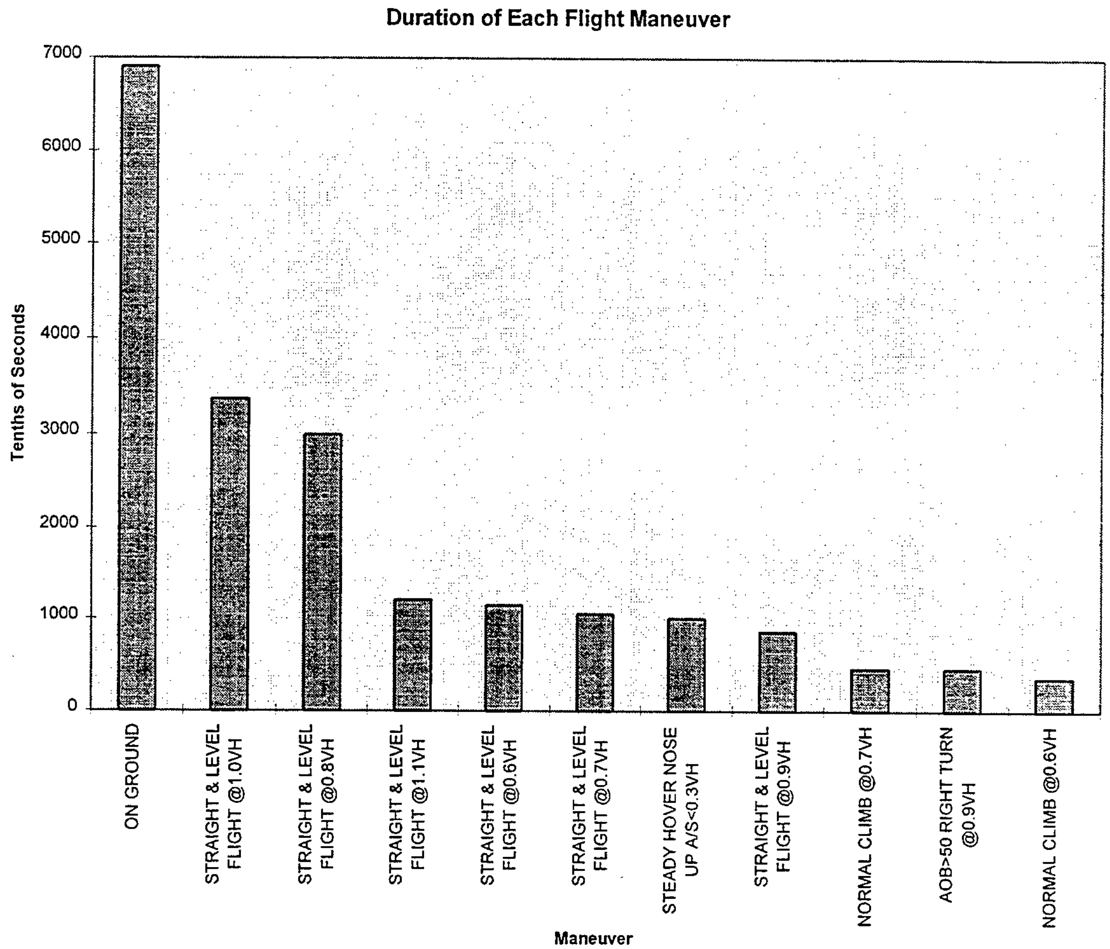

Figure 2. A histogram illustrating the amount of time spent in various maneuvers.

5) any coincident parameter data recorded at the end of the flight maneuver. (i.e., If Rate of Climb is chosen as a coincident parameter at the end of the flight maneuver, the report might contain the following results: Rate of Climb Leaving = -250 feet/minute).

The second output from the flight condition code processor describes the amount of time spent in each maneuver. These results can be placed into a spreadsheet to

generate a histogram of the amount of time spent in the most frequently occurring flight maneuvers. For example, the histogram in Figure 2 shows that the aircraft spent a total of 300 seconds in Straight & Level Flight @ 0.8Vh.If the user is not satisfied with the results from the system, the user can modify the classification of flight conditions, and then rerun the existing data through the flight condition code processor to obtain a new set of results. It is important to note that the aircraft does not have to be flown again to rerun the flight data through the fine-tuned flight condition code processor.

Neural Network Generated Loads

In another version of the system the recorded data is run through neural network algorithms developed by the Navy to obtain predicted loads at various points on the aircraft. This data is also compressed, stored in an electronic memory module, downloaded into a PC, and then expanded for processing. This data is then run through the flight condition recognition algorithms described above. These algorithms can identify load conditions (in addition to flight conditions) that cause fatigue.

The output of the load information is displayed by a viewer. The viewer (Shown in Figure 3.) allows the user to graphically compare flight loads with input parameters at various times during the flight. Each of these graphs are time stamped and flight condition code stamped so that the user can see what type of loads occur during a particular flight.

Conclusion

SEI has developed a set of tools that can detect high cycle fatigue through the following steps:

1.) Display load profiles at various points on the aircraft during an entire maneuver.

2.) Provide Peak/Valley parameter and load values for each maneuver during a flight.

3.) Display the amount of time spent in each maneuver during the entire flight.

4.) Examine the load conditions at various points on the aircraft during the entire flight.

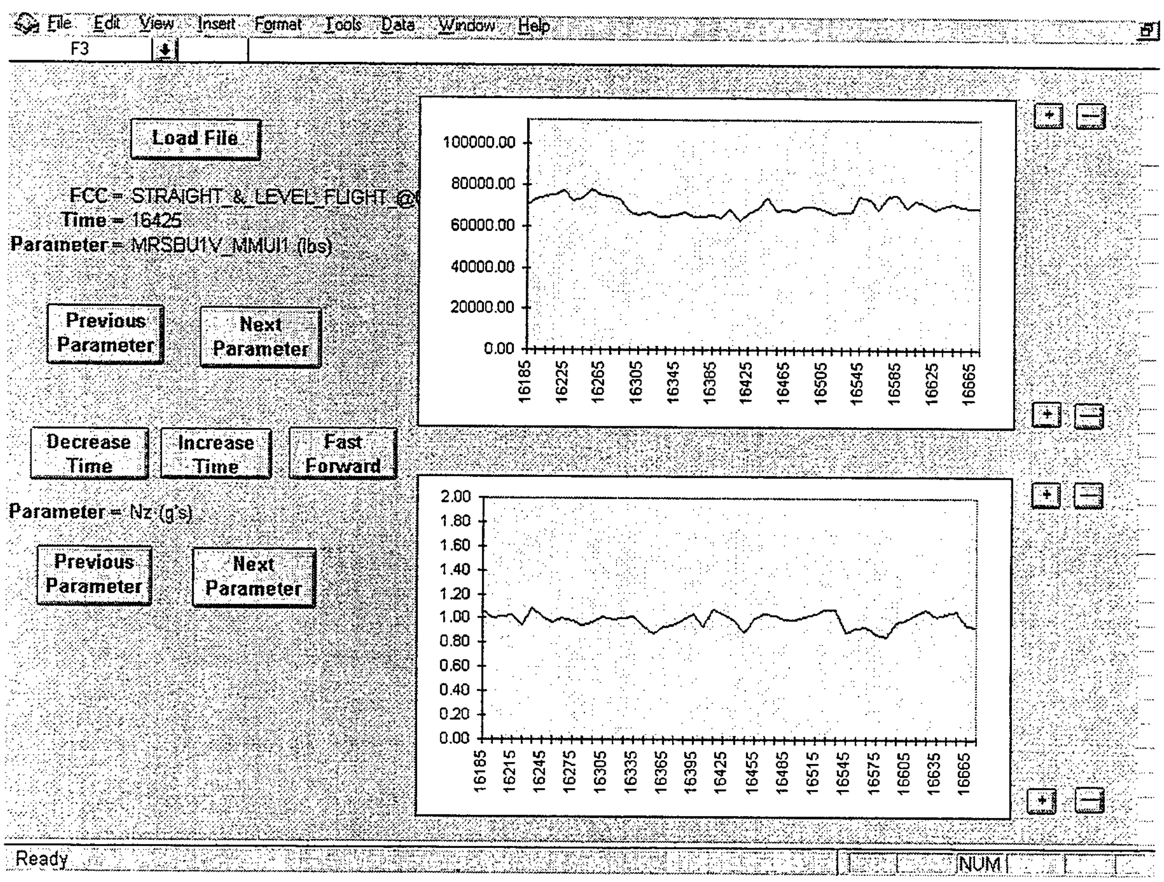

Figure 3. The load viewer tool.

The ABCs of NDE Development and Transition for Aging Aircraft

by Dwight S. Wilson, NDE Manager
and Donald J. Hagemaier, NDE Sr. Technical Fellow
Nondestructive Evaluation Engineering
The BoeingCompany--Long Beach

BOEING®

Things to Cover

- DAC Aging Fleet Statistics -

- Inspections Relating to DAC Fleet -

- New Technology -

But Mostly

- Process Process Process -

BOEING

Introduction

Model	Active	High Time	Produced
DC-3	≈ 1000/1500	90,000 FH 60 Years	10,654
DC-4	≈ 100/200	75,000 FH 50 Years	1,244
DC-6	≈ 200/300	60,000 FH 48 Years	704
DC-7	≈ 25/50	50,000 FH 42 Years	338
Model	**Active**	**High Time**	**Design**
DC-8	300	47,810 LDGS 89,520 FH 37.25 Years	25,000 LDGS 50,000 FH 20 Years
DC-9	864	103,642 LDGS 85,964 FH 30.5 Years	40,000 LDGS 30,000 FH 20 Years
DC-10	415	39,027 LDGS 97,793 FH 25.5 Years	42,000 LDGS 60,000 FH 20 Years

Terminology

- Design Service Life
- Extended Service Life
- Continued Airworthiness
- Economic Service Life

Research vs Application/Transition

- Customer Controlled Budgets
- Compressed Research Time
- A Fleet in Need
- Concentration on Specifics

BOEING

Where the Requirements Come From

- Early Days
- Maintenance Review Board
- Maintenance Significant Item (MSI)
- Structurally Significant Item (SSI)
- FAA AC91-56

BOEING

Typical Wing SSIs

Structurally Significant Items
Typical for Wing
(Left and Right Sides)

Slats

- Slat Assembly -
- Slat Tracks and Link Assembly -
- Slat Track Supports -

Left Outer Wing

- Bulkheads and Ribs -
- Front Spar -
- Inboard Trailing Edge -
- Lower Panel Installation -
- Rear Spar -
- Upper Panel Installation -

Spoilers

- Number One Flight Spoiler -
- Outboard (No. 2 thru No. 5) -

Flaps and Vanes

- Inboard Flap/Vane Assy -
- Outboard Flap/Vane Assy -

Center Wing

- Center Wing Box Bulkhead -
- Center Wing Box Structure -
- Outboard to Center Wing Joint -
- Center Wing Front Spar -
- Underwing Pressure Bulkhead -
- Center Wing Rear Spar -
- Overwing Fuel Tank Structure -

Ailerons

- Inboard Assy -
- Outboard Assy -

Ailerons

- Inboard Assy -
- Outboard Assy -

Slats

- Slat Assembly -
- Slat Tracks and Link Assembly -
- Slat Track Supports -

Right Outer Wing

- Bulkheads and Ribs -
- Front Spar -
- Inboard Trailing Edge -
- Lower Panel Installation -
- Rear Spar -
- Upper Panel Installation -

Spoilers

- Number One Flight Spoiler -
- Outboard (No. 2 thru No. 5) -

Flaps and Vanes

- Inboard Flap/Vane Assy -
- Outboard Flap/Vane Assy -

BOEING®

NDE Methods Used for SID

Primary Method	Location of PSEs by ATA Chapter					Method Totals
	Doors	Fuselage	Pylons	Empennage	Wings	
HFET		83	5	16	64	168
LFET		40		7	61	108
UT		8	14	7	8	37
RT		29	3	4	19	55
MT	5		1	1		7
PT			1			1
VT	1	21	2	1	8	33
Others	1	5	1			7

Alternat Method	Location of PSEs by ATA Chapter					Method Totals
	Doors	Fuselage	Pylons	Empennage	Wings	
HFET		13			108	121
LFET		6			9	15
UT		1	1	3	2	7
RT		15	2	3	2	22
MT						
PT		2			2	4
VT	4	52		6	41	103
Others		1			3	4

Primary Methods as % of Total

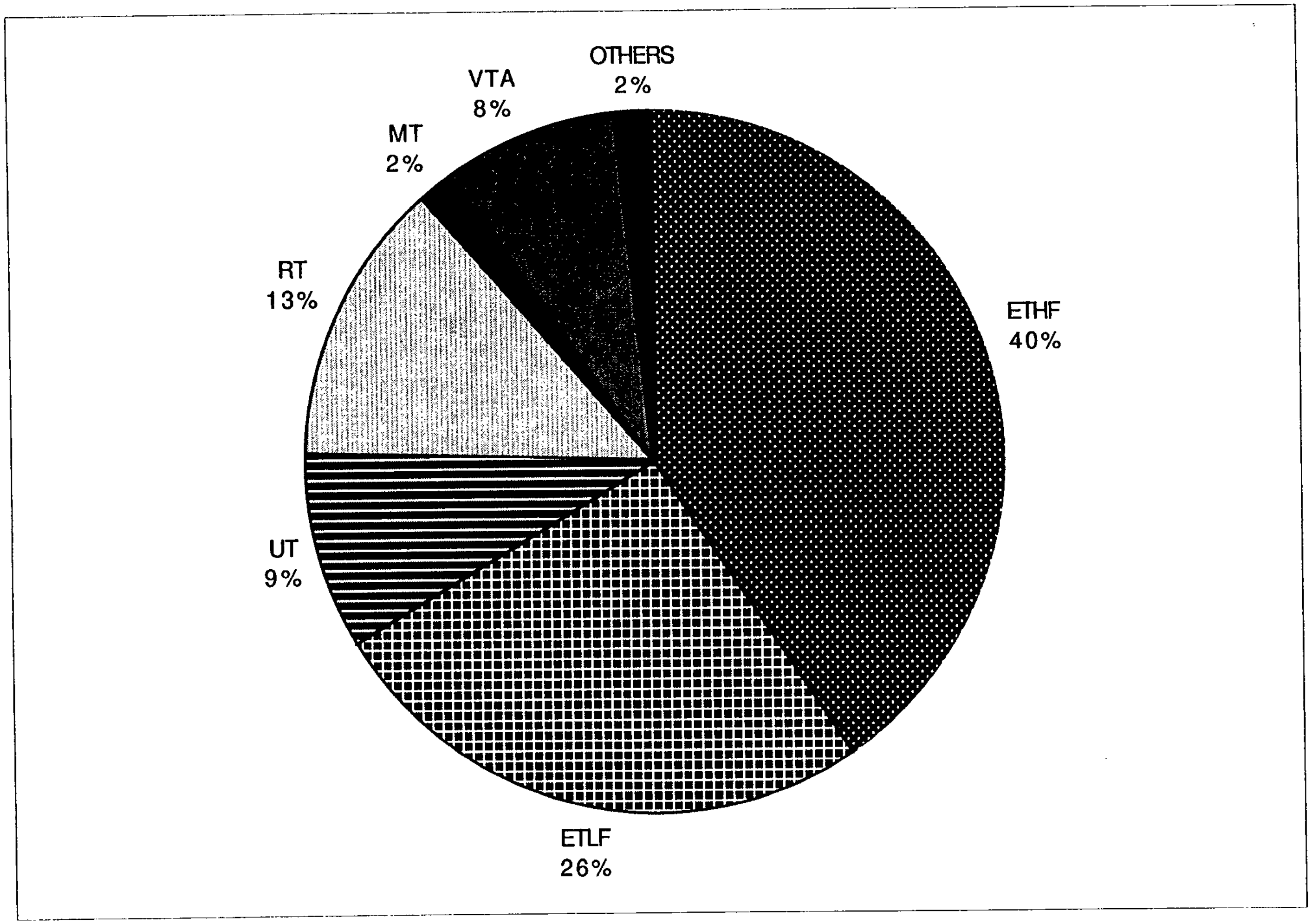

BOEING

Industry Steering Committee (ISC)

- Review and Selection of Candidates
- Review of Operator Maintenance
- Development of Supplemental Program
- Establishment of Fatigue Life Thresholds
- Development of Reporting System

BOEING

Principle Structural Element (PSE)

A PSE is a damage tolerant SSI which is further defined as, “structure whose failure, if it remained undetected, could result in catastrophic failure of the aircraft.”

BOEING®

Damage Tolerance Analysis

Damage-tolerance analysis is performed for each PSE using methodology which included data from sources such as lg stress, limit stress, fail-safe and fatigue margins of safety, full-scale airplane and component fatigue tests, service experience, drawings, inspection documents, and interviews.

NDE Inspection Development Process

- Fatigue and Fracture Package
- Drawing Review
- Reference Standard Design
- Determination of Detectable Flaw Size
- Preliminary Procedure
- On-Aircraft Verification
- Final Documentation and Concurrence

BOEING®

Multiple Load Path Crack Growth Curve

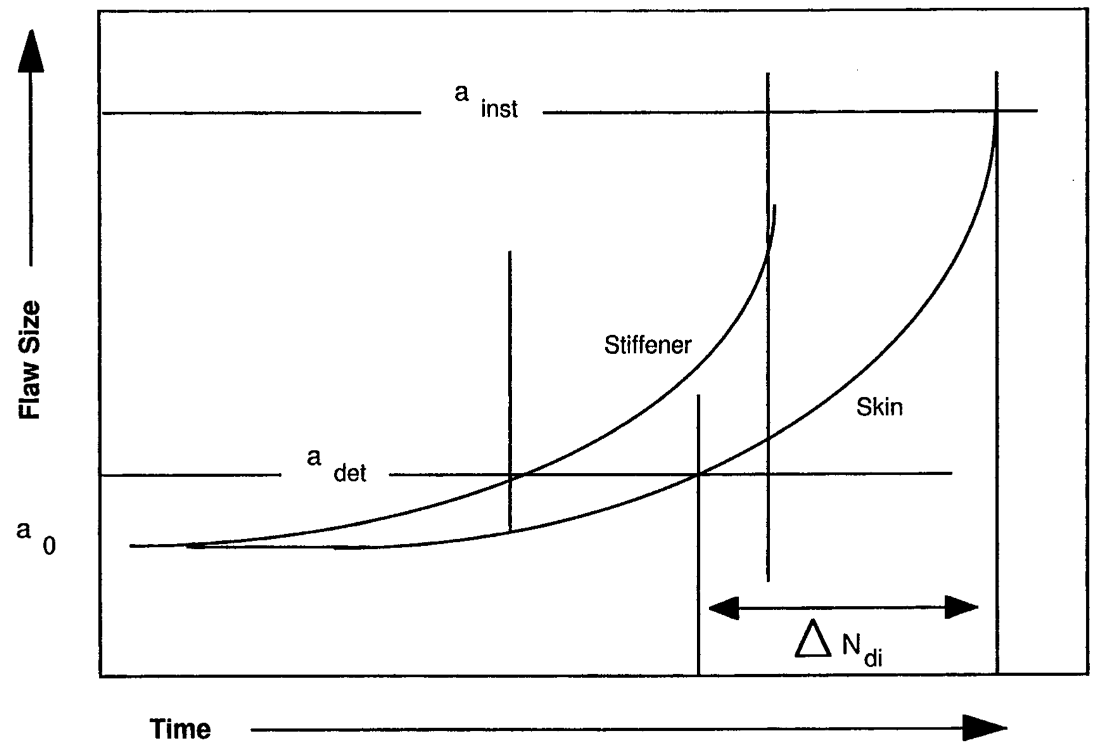

Interaction of Signal/Noise Discrimination and POD

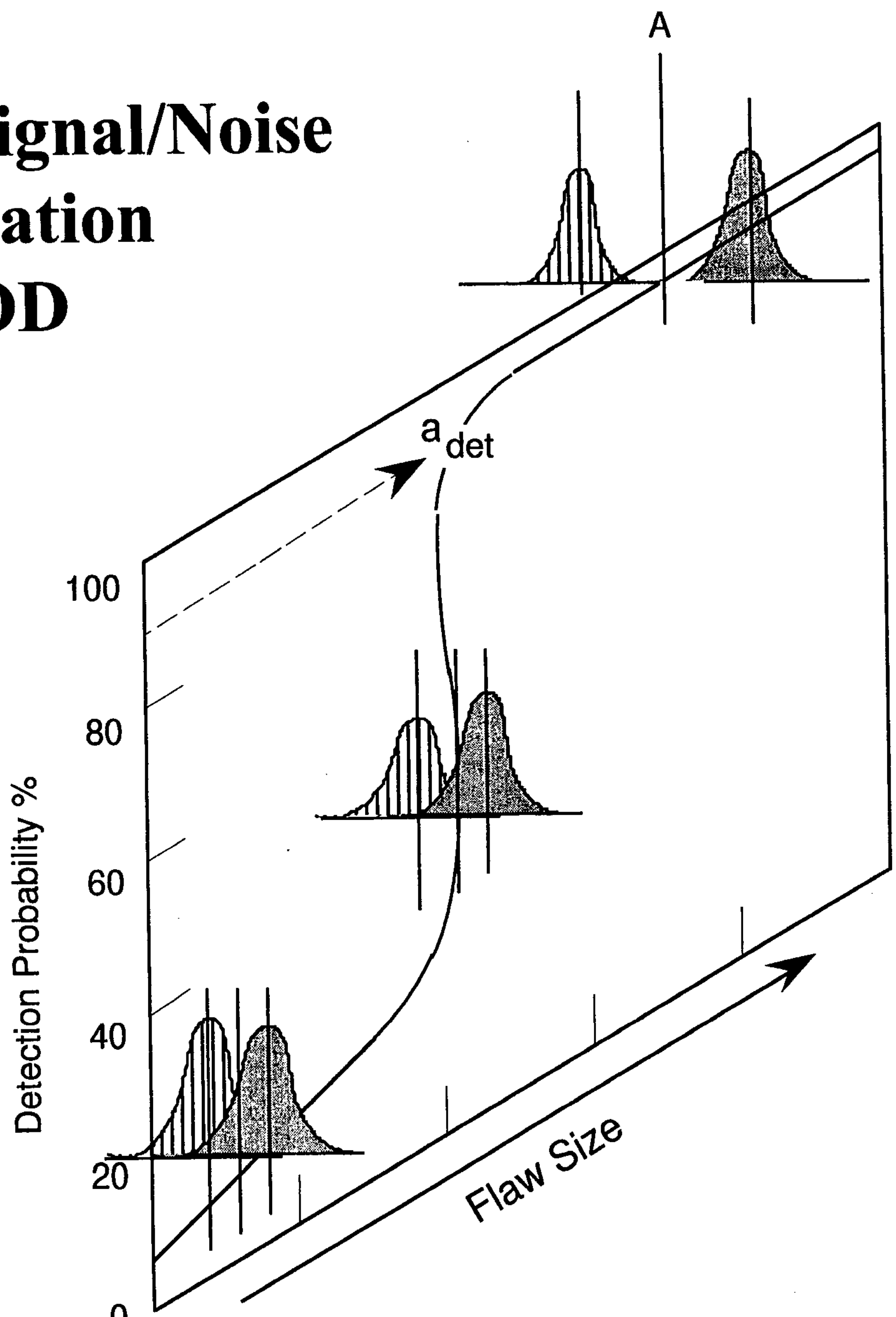

BOEING

Inspection Area

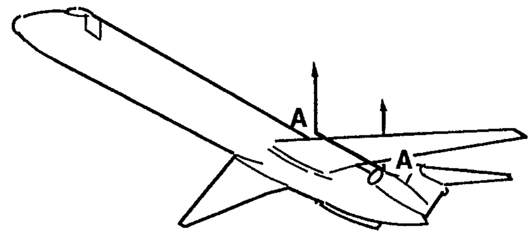

VIEW A-A
Left Wing, Lower Surface
Looking Up At Surface,
Right Side Opposite

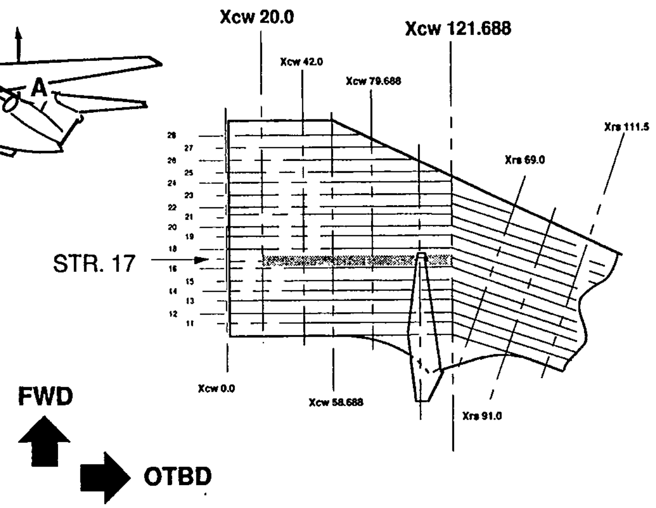

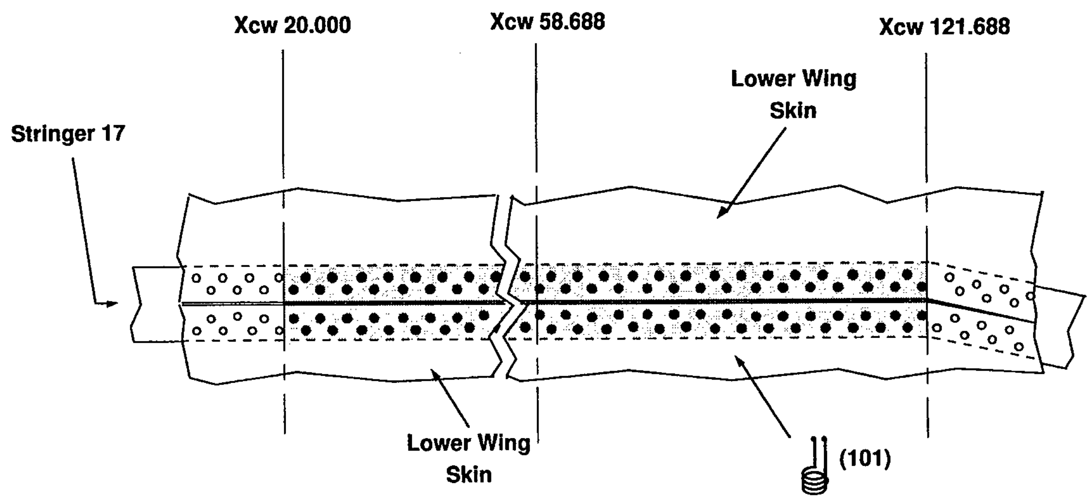

Inspect Forward Lower Wing Skin, Aft Lower Wing Skin, And Stringer 17 At Shaded Fastener Locations

Calibration

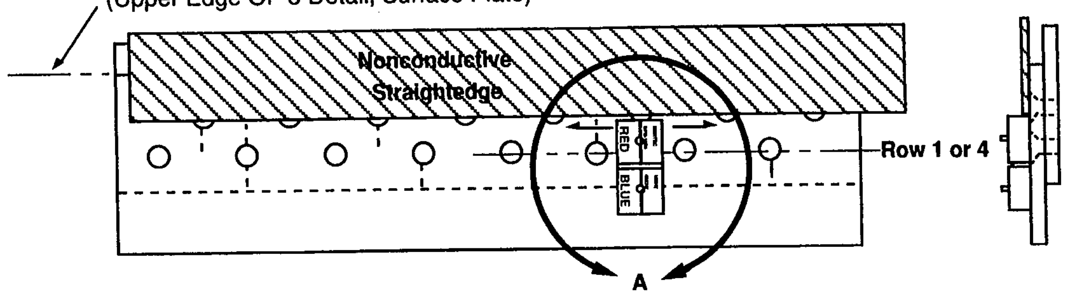

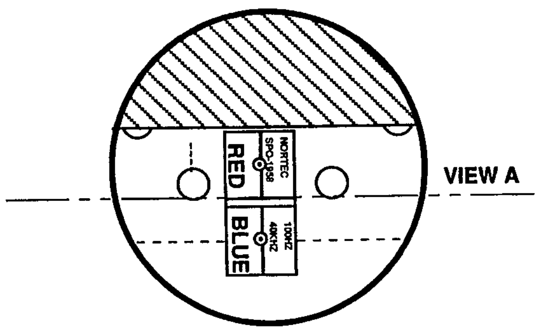

Calibration and Scope Presentation, Inspection for Cracks going away from Stringer C/L in Forward and Aft Fastener Row.

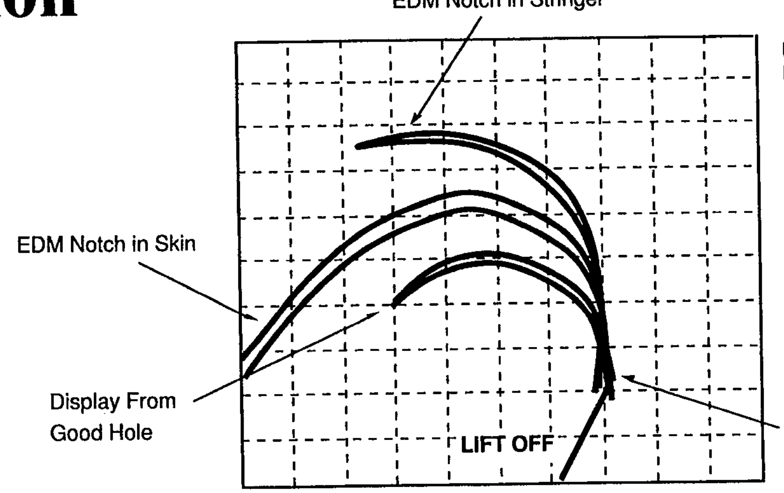

Instrument	**- NDT-19**
Probe	**- SPO 1958 With 5/32 Inch Spacer**
Frequency	**- 400 Hz**
Gain Horiz.	**- 76.5 Db**
Gain Vert.	**- 90.0 Db**
Rotation	**- 209**
Probe Drive	**- Mid**

Note:
Settings Listed Were Used To Develop Procedure. Values May Vary From Instrument To Instrument.

Longitudinal Splice at Longeron 5

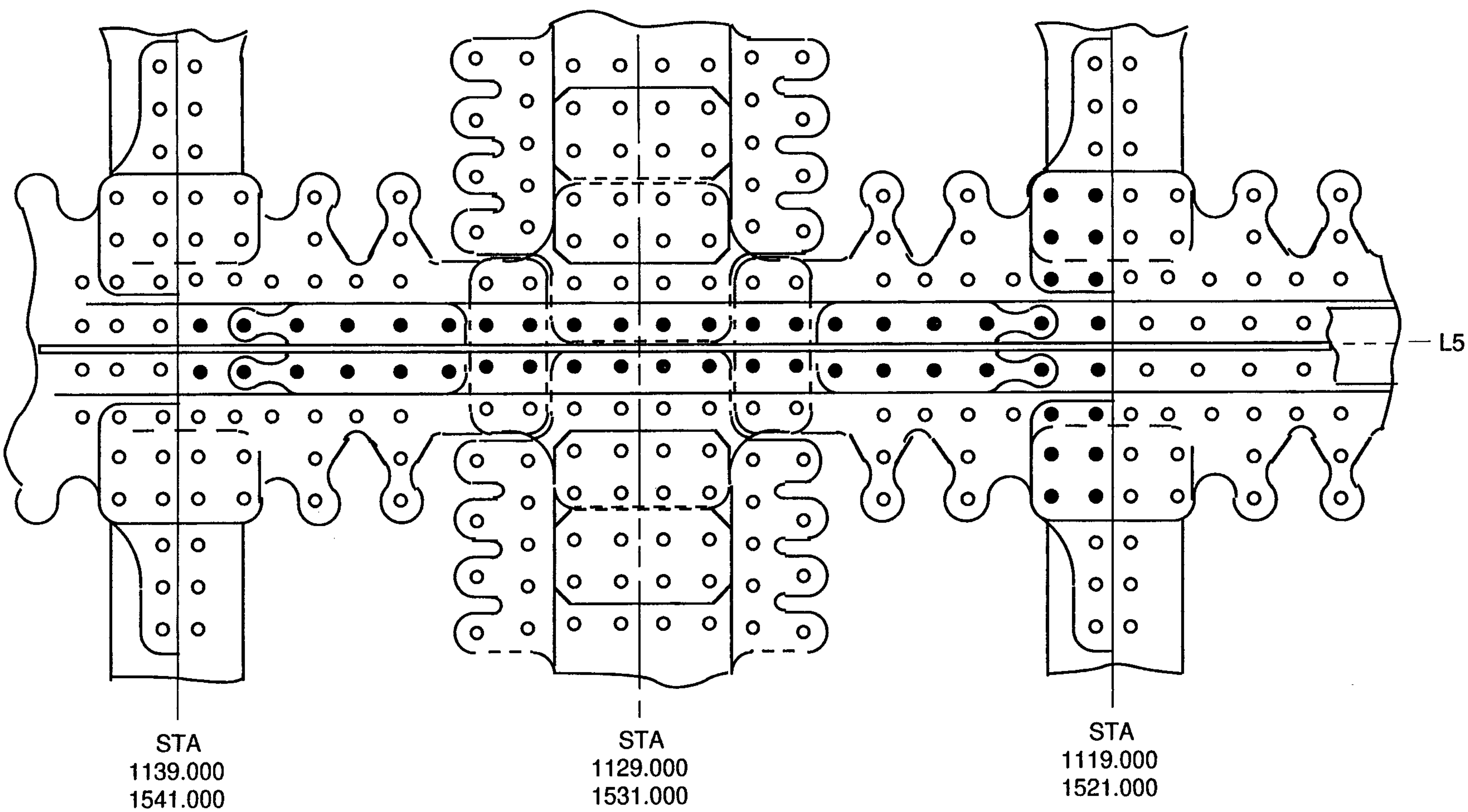

Eddy Current C-Scan Imaging
Longitudinal Splice at Longeron 5

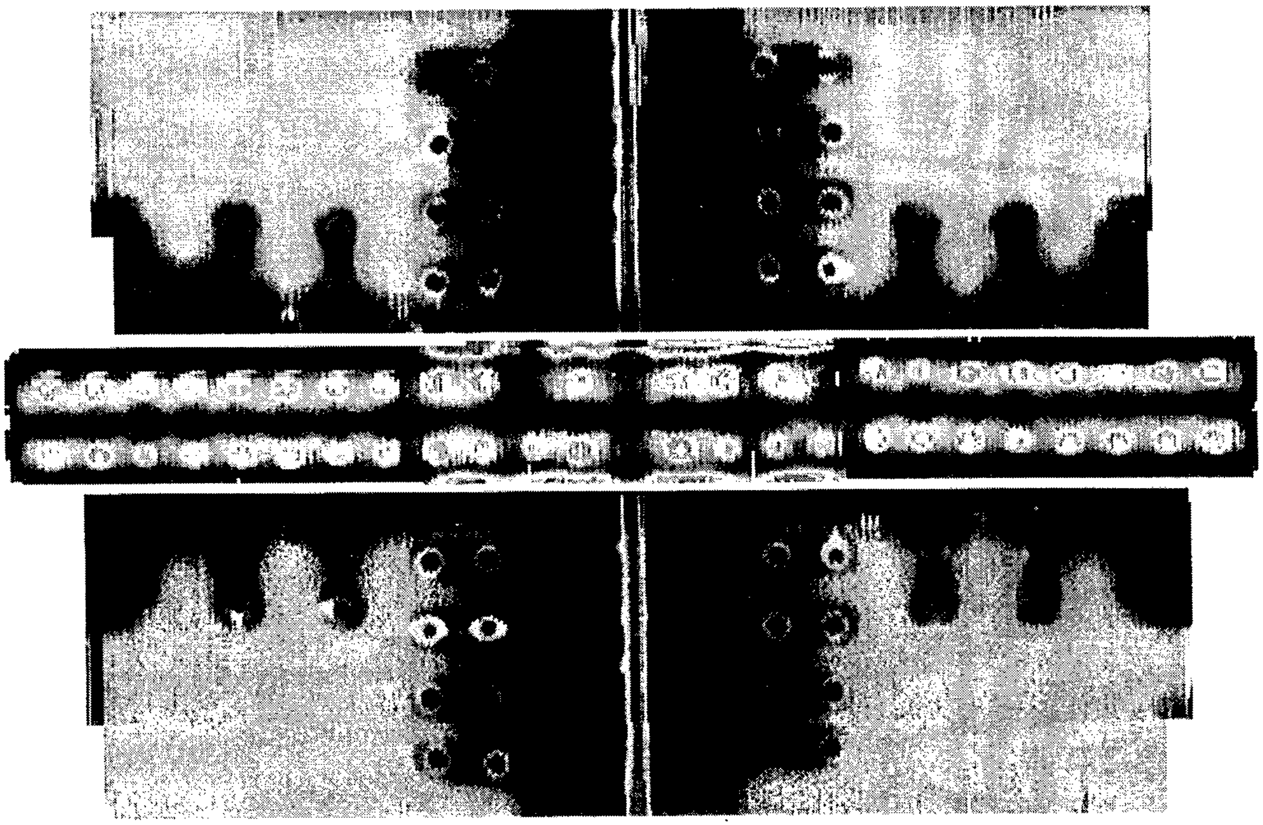

DC-10 Crown Skin Splice

Aging Aircraft

Supplemental Inspection Document (SID)

<u>Complete</u>

DC-3

DC-6

DC-8

DC-9

DC-10

<u>In-Work</u>

MD-80

BOEING

Standardization

1. General
2. X-Ray
3. Gamma Ray
4. Ultrasonic
5. Sonic
6. Eddy Current
7. Magnetic Particle
8. Penetrant
9. Visual/Optical

*10. Physical/Mechanical

*11. Chemical

*12. Leak Testing

*13. Thermal

*14. Laser or Light Energy (Sherography)

*Proposed

BOEING

New Technology

Mobile AUtomated Scanner (MAUS)

- Ultrasonic Pulse-Echo
- Eddy Current
- Ultrasonic Resonance
- Mechanical Impedance Analysis (MIA)
- Pitch/Catch (Sondicator)
- Tap Test

BOEING

Eddy Current Scanning

DC-10 Crown Skin Splices (2)

<u>X-Ray</u> 110 Hours Preparation

100 Hours X-Ray

98 Exposures

2-3 Day Downtime

<u>Eddy Current</u> 6-8 Hours (Overnight)

<u>Savings</u> 95% in Labor Hours

<u>Dollars</u> 10 Aircraft = $1,000,000.00

BOEING

NDE Inspection Development Process

- Fatigue and Fracture Package
- Drawing Review
- Reference Standard Design
- Determination of Detectable Flaw Size
- Preliminary Procedure
- On-Aircraft Verification
- Final Documentation and Concurrence

BOEING®

C-17A INDIVIDUAL AIRCRAFT TRACKING PROGRAM

Rick Selder
C-17 Loads and Dynamics
The Boeing Company
USAF Airlift and Tanker Programs

Ko-Wei Liu
C-17 Durability and Damage Tolerance
The Boeing Company
USAF Airlift and Tanker Programs

1997 USAF Structural Integrity Program Conference, San Antonio, TX, Dec. 2-4

BOEING

The C-17A Individual Aircraft Tracking Program (IATP) is being developed as part of the C-17 full scale engineering development program. IATP computer system programming is nearly complete with full operational capability expected by mid 1998. The IATP system is being developed by the USAF Airlift and Tanker Programs business unit of the Boeing Company in Long Beach, California.

Outline

- Benefit of IATP
- IATP approach
- Improvements over past IATPs
- Data processing flow
- SFDR flight recorded parameters
- Flight data editing
- Stress spectra generation
- Control point selection
- Gap filling missing data
- Future Damage Projection
- Content of output IAT data report
- Computer system characteristics

SLIDE 2

BOEING

Benefit of IATP

• Minimize maintenance:	Inspection of critical areas are defined for each aircraft based on its individual damage assessment.
• Efficient fleet management:	Modifications are scheduled and aircraft base rotations and retirements are based on actual aircraft usage.
• Extended service life:	Appropriate inspections and efficient fleet management will maximize the service life of each aircraft.
• Better field support:	IATP data used to help identify parameters that attribute to problems found in the field.

BOEING

SLIDE 3

Today, the cost of buying and maintaining military aircraft is very high. Therefore, there is a great need to extend the service life of aircraft as long as possible but without jeopardizing safety due to long term structural degradation of the airframe as a result of application of repeated loads. An IATP which gives the ability to track the structural status of individual aircraft is the primary tool to assure a long service life without risk. The main benefits are described as follows:

Minimize maintenance: The structural status of each aircraft is used to define critical areas and inspection intervals for each aircraft based on its individual damage assessment. This will minimize required maintenance without jeopardizing aircraft safety.

Efficient fleet management: Modifications for each aircraft can be scheduled based on its unique structural assessment. Also, decisions on rotating aircraft between bases or retiring aircraft can be based on actual usage statistics.

Extended service life: Performing inspection at appropriate intervals and efficient management of the fleet will maximize the service life of each aircraft.

Better field support: The IATP system gives valuable flight data that can be used to help solve problems found in the field. For example, if a problem was found to be associated with an incident that occurred during a specific flight, IATP flight data can be evaluated to find the circumstances surrounding the incident.

C-17

IATP Approach

- Record aircraft CG Nz cycles and associated flight parameters for each flight of every aircraft.
- Apply analytic methods to recorded data to generate flight-by-flight, cycle-by-cycle stress spectra at selected airframe control points.
- Calculate damage based on cycle-by-cycle crack growth analysis at each control point.
- Compile usage statistics by aircraft, duty base, and fleet.

SLIDE 4

BOEING

The purpose of an IATP system is to calculate damage at selected airframe locations in order to determine differences in aircraft usage and to adjust inspection intervals of critical areas of the airframe. To accomplish this, the approach used for the C-17 starts by recording aircraft vertical acceleration (Nz) cycles and associated flight parameters for each flight of every aircraft. Analytical methods are then applied to calculate flight-by-flight, cycle-by-cycle stress spectra at selected airframe locations (control points). Damage at each control point is then calculated based on cycle-by-cycle crack growth analysis. In addition, usage statistics are compiled for each aircraft, by duty base, and for the C-17 fleet as a whole.

C-17 Improvements Over Past IATPs

- Eliminate dependency on the use of strain gauges.
  - Past experience shows that strain gauges are prone to faults.
  - Production strain gauges expensive to install and maintain.
  - Gives flexibility in choosing or changing control points.
- Damage determined directly from recorded flight profiles rather than assumed to be equivalent to the damage from the closest matching design mission type.
- Reduces flight crew work load: Uses a Standard Flight Data Recorder (SFDR) eliminating the need for flight logs.
- Spectra generation methods are as rigorous and detailed as that used for design analysis of the C-17 airframe.

BOEING

SLIDE 5

The C-17 IATP has many improvements over IATPs used in the past. These improvements are described as follows:

•Control point stress spectra generation does not depend on the use of strain gauges. Production strain gauges are expensive to install and maintain and past experience shows that they are prone to faults. Also, eliminating the need to locate a gauge at each control point location gives greater flexibility in choosing or changing control points.

•Some past IATPs obtain the damage due to a given flight by assuming this damage is equivalent to that given by the closest matching design mission type. The C-17 IATP determines damage due to a given flight directly from its recorded flight profile parameters.

•All flight data needed by the C-17 IATP is recorded by a Standard Flight Data Recorder (SFDR). This eliminates the need to collect flight log data thus reducing the work load of the flight crew.

• The SFDR records 28 separate flight parameters allowing for the generation of flight profiles as detailed as the design mission profiles used for design analysis of the C-17 airframe. This then allows for a rigorous generation of stress spectra.

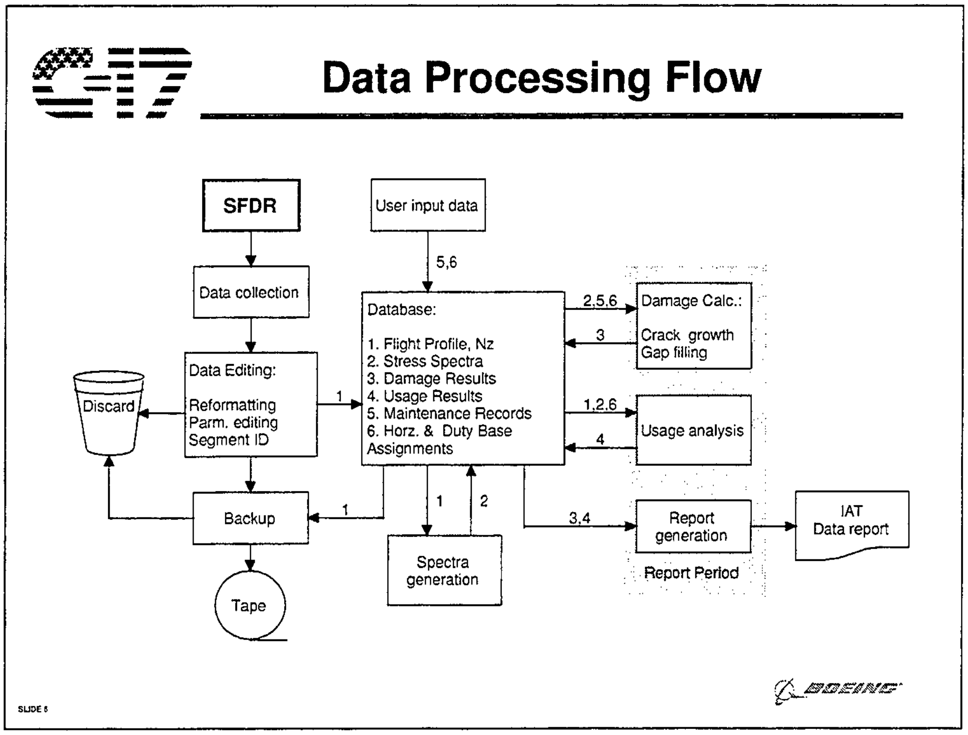

The goal of IATP is to collect and process 100% of operational flight data for every aircraft in the C-17 fleet. Flight data is recorded by use of a digital Standard Flight Data Recorder (SFDR), produced by Smiths Industries, installed on each aircraft.

Data collection starts by downloading compressed flight data from the SFDR onto floppy diskettes by the AMC maintenance crews. The data is then sent to the Oklahoma City Air Logistics Center (OC-ALC) where it is uploaded and archived onto an IBM mainframe computer. Then, before data can be processed by the IATP system, it is decompressed by use of decompression software supplied by Smiths Industry.

The first step of the IATP process is to edit the flight data which includes reformatting data into separate flights, parameter editing, and segment identification. Flights containing erroneous data that cannot be corrected are discarded. Once complete the resulting flight profiles and Nz sequences are stored into a database. In addition to SFDR data, maintenance records and horizontal stabilizer and duty assignments are entered into the database by the user. All valid flights are then processed through a spectra generation program to produce control point stress spectra.

Once all stress spectra have been generated for all fights in a given report period, they are processed through a damage program to calculate damage at each control point. Damage for missing flights is calculated using a gap filling process. In addition, usage statistics are compiled for the report period and accumulated with all previous periods. These usage statistics and damage results are then output as the IAT data report.

The IATP system also provides a backup utility to archive edited flight data and to delete no longer needed data following report generation.

SFDR Parameters

Data Tag

Aircraft Serial Number
Sequential Flight Number
Airframe Time
Mission Type
Date of Flight
Departure Base

Time Tracked

Pressure Altitude
Radar Altitude
Indicated Airspeed
Gross Weight
Fuel Weight
Aircraft CG
Engine Pressure Ratio
Flap Position
Wheel Speed

Event Parameters

Auto-pilot On
Thrust Reverser Deployed
Slats Out
UARRSI Ready
UARRSI Latched
Cargo Door Open
Landing Gear Up
Weight On Wheels
Parking Brake Engaged
Flap Deployed
Speed Brake Deployed
Troop Door Open

Peak/Valley Time History

CG Vertical Acceleration (Nz)

SLIDE 7

Four types of data are recorded by the SFDR. These are data tag, event, time tracked, and peak/valley time history parameters. Data tag parameters give information on the flight as a whole and are recorded once at the beginning of each flight. Event parameters identify a change in aircraft configuration and are recorded when a change in configuration occurs. Time tracked parameters change steadily with time and are recorded whenever their value changes by a predetermined increment (gate value). Peak/valley time history parameters are cyclic in nature and are processed by an onboard algorithm which finds and records peak/valley cycles outside a predetermined threshold.

Flight Data Editing

- Reformatting:
  - Divide data into individual flights.
  - Check continuity of aircraft serial and flight numbers, airframe time, and flight date against previously processed flights.
- Individual Parameter Editing:
  - Check if parameter value is within an acceptable range.
  - Check if rate of change of value is within an acceptable slope.
  - Check if parameter was recorded at predetermined increments (gate value)
  - Check if event parameter (flaps deploy, gear extend, etc.) cycles within an acceptable time span.

BOEING

SLIDE 8

Flight data editing is accomplished in four steps described as follows:

Reformatting:

One download of SFDR data contains several flights. This step divides the data into the separate flights then checks the continuity of aircraft serial and flight numbers, airframe time, and date against the same data for previously processed flights.

Individual parameter editing:

Each parameter is checked to assure that its value is within an acceptable range and its change in value is within an acceptable slope. Also, the parameter value is checked if it was recorded at the predetermined increment (gate value). (example: gross weight is checked to assure it is recorded in 640 lb. increments.) For event parameters, a check is made to assure that the event cycle time is within an acceptable time span. (example: flaps deploy within 30 sec.)

Flight Data Editing

- Parameter Comparison Checks:
  - Compare parameters against each other for conflicts.
- Flight Profile Generation:
  - Divide flight into identifiable segments (ascent, cruise, air-drop, etc.)
  - Check segment sequence for logical flow.
  - Find special event segments. (example: Touch & Go)
  - Categorize flight as one of 35 design mission types. (Provided to give usage information, not used in damage calculation)
- Note: Methods incorporate experience gained as a result of processing over 4,000 flights of actual SFDR data.

BOEING

SLIDE 9

Parameters comparison checks:

Parameters are compared against each other to find any conflicts. (example: Landing gear extended above a placard speed of 250 knots)

Flight profile generation:

The time history of recorded flight parameters is divided into identifiable segments and then the value of each parameter within the time span of the segment is averaged. The exception is peak/valley time history parameters for which all values recorded within a segment are retained. The resulting profile of flight segments is then checked to assure that the segments are sequenced in a logical flow. Also, the profile segments are surveyed to find combinations that make up special event segments. For example, the combination of a landing impact, followed by a landing roll, take-off run, then take-off rotation is identified as a touch and go segment. Once the flight profile is generated it is categorized as one of 35 design mission types by matching its flight characteristics to that of the design mission types.

It should be noted that the above described data editing methods were not developed solely on a preconceived idea of the nature of flight recorded data, but rather incorporate the experience gained and are proven out as a result of processing over 4000 flights of actual SFDR recorded data.

Flight Data Editing

Flight Profile

A/C	FLT	AIFRAME TIME		DATE	BASE	GMT
930603	137	375.250	379.125	950814	KADW	1601 1947

DUR	SEGMENT	PALT	RALT	IAS	GW	FW	CG	EPR	WSPD	FLAP
594.250	FULL STOP	240.	0.	0.	503249.	174481.	36.2	1.0177	0.00	0.00
2.000	TAXI	240.	0.	0.	502080.	173600.	36.3	1.4336	18.00	18.25
29.000	TAKEOFF RUN	240.	0.	0.	502080.	173600.	36.3	1.4336	77.79	18.25
0.000	TAKE OFF ROTATION	240.	0.	148.	502080.	173600.	36.3	1.4336	120.00	18.25
79.000	ASCENT	1031.	826.	187.	502080.	173600.	36.3	1.4336	0.00	18.25
18.000	ASCENT	2028.	1956.	246.	502080.	173600.	36.3	1.4336	0.00	0.00
1632.000	ASCENT	18549.	18531.	299.	493516.	165059.	36.3	1.2363	0.00	0.00
2134.000	CRUISE	27902.	28860.	300.	480627.	152157.	36.3	1.2187	0.00	0.00
358.000	ASCENT	29468.	30557.	297.	472888.	144402.	36.3	1.3029	0.00	0.00
7209.000	CRUISE	30980.	30627.	290.	452072.	123593.	36.3	1.2682	0.00	0.00
1090.000	CRUISE	30992.	26932.	292.	429336.	100828.	36.3	1.2556	0.00	0.00
460.000	DESCENT	21469.	13274.	306.	425857.	97518.	36.3	0.8463	0.00	0.00
301.000	CRUISE	13811.	5545.	270.	424868.	96394.	36.3	1.0199	0.00	0.00
68.000	DESCENT	12602.	5085.	253.	424000.	95400.	36.3	0.9697	0.00	0.00
45.000	DESCENT	10433.	3851.	242.	424000.	95400.	36.3	0.9688	0.00	0.00
17.000	DESCENT	9569.	3269.	212.	424000.	95400.	36.3	0.9688	0.00	18.50
30.000	LANDING APPROACH	8950.	2617.	187.	424000.	95400.	36.3	0.9688	0.00	18.50
140.000	LANDING APPROACH	7547.	1254.	138.	423771.	95177.	36.3	1.1308	0.00	38.25
0.000	LANDING IMPACT	6296.	0.	128.	423360.	94800.	36.5	1.1797	116.00	38.25
21.000	LANDING ROLL OUT	6296.	0.	6.	423360.	94800.	36.5	1.1015	64.18	38.25
4.000	TAXI	6296.	0.	0.	423360.	94800.	36.5	1.0781	14.00	38.25
185.750	FULL STOP	6296.	0.	0.	423360.	94800.	36.5	1.0163	0.00	0.00

SLIDE 10

The above is a generated flight profile for one actual flight. The first record gives information on the flight as a whole with each of the following records describing each segment. Given are the segment duration and type followed by the averaged segment parameters. The peak/valley time history Nz cycles associated with each segment are stored in a separate unformatted file.

Stress Spectra Generation

- Find gust encounters: Separate out gust Nz cycles and time in gust (T_g) by use of the following criteria.
  - Time between successive Nz peaks and valleys less than 1.0 sec.
  - Time between recorded threshold crossings (±0.1g) less than 5.0 sec. Average Nz peak/valleys time difference for gust encounter must remain less than 1.0 sec.
  - Remaining Nz's assumed to be due to symmetric maneuvers.
- Symmetric maneuvers
  - Obtain flight parameter to control point stress transfer coefficients by performance of a regression analysis.
  - Apply transfer coefficients to flight segment parameters to obtain stress versus Nz in terms of slope *(F)* and intercept *(P)*.
  - Convert flight segment maneuver Nz cycles to stress cycles: $\sigma = P + Nz \times F$

BOEING

SLIDE 11

For each flight profile segment control point stress cycles due to loading events occurring within the segment are determined using that segment's parameters and associated Nz cycles. The loading events include symmetric maneuvers, atmospheric turbulence, dynamic taxi, landing impact, and take-off rotation.

During flight segments both symmetric maneuver and atmospheric turbulence (gust encounter) occur. The gust encounters are found by applying the following criteria to the recorded Nz cycles to separate out gust Nz cycles and time in gust (T_g):

1. The gust encounter begins when the time between successive Nz peaks and valleys is less than 1.0 sec.
2. The encounter continues if the above remains true or if the time between recorded threshold crossing is less than 5.0 sec. and the average Nz peak/valley time difference remains less than 1.0 sec.

Note: the 5.0 sec criteria is used to allow for reasonable continuation of a gust encounter despite dropped data values due to the recording threshold of ±0.1g.

All Nz's that do not meet the above criteria are assumed to be due to symmetric maneuvers.

<u>Symmetric maneuvers</u>:

For each maneuver Nz value, control point stress is calculated using the following linear relationship:

$$\sigma = P + Nz \times F$$

Stress Spectra Generation

- Atmospheric turbulence
  - Select one of 60 PSD gust cases by matching on flight segment parameters.
  - Use gust case analytic stress response $(\overline{A}, N_o)$ and segment time in gust (T_g) to generate a random sequence of delta stress $(\Delta\sigma)$ cycles by application of Monte Carlo methods.
  - Add 1.0g stress, calculated using maneuver stress equation, to $\Delta\sigma$ cycles.
  - Future enhancements:
    - Evaluate C.G. Nz to distinguish between non-storm and storm turbulence. (currently an analytic distribution is assumed)
    - Evaluate L/ESS strain gage data to develop a relationship between C.G. Nz/Nx and stress response.

BOEING

SLIDE 12

Symmetric maneuvers (cont.):

The intercept *(P)* and slope *(F)* of this equation were determined by applying stress transfer coefficients, determined by performance of a regression analysis, to the flight segment parameters.

Atmospheric turbulence:

The first step in determining stress cycle for atmospheric turbulence is to select one of 60 PSD gust cases by performing a best match of flight segment to gust case parameters. Then from the chosen gust cases analytic stress response $(\overline{A}, N_o)$ and the flight segments time in gust (T_g) generate a random sequence of delta stress $(\Delta\sigma)$ cycles by application of Monte Carlo methods. To these $\Delta\sigma$ cycles add a 1.0g stress calculated using the maneuver stress equation.

In order to utilize recorded data to determine the gust intensity in addition to the time in gust encounters, enhanced methods will be developed. First, an effort will be made to develop a method to evaluate C.G. Nz to distinguish between storm and non-storm turbulence (currently an analytic distribution is assumed). Following this, when a sufficient database of L/ESS strain gauge data is available, it will be evaluated to develop a C.G. Nz and additional Nx (lateral load factor) to stress relationship.

Stress Spectra Generation

- Dynamic taxi
  - Select one of 25 dynamic taxi cases by matching on taxi segment parameters.
  - Use taxi case analytic stress response *($\overline{A}$, N_0)* and segment duration *(T)* to generate a random sequence of delta stress ($\Delta\sigma$) cycles by application of Monte Carlo methods.
  - Add 1.0g stress, determined by application of regression transfer coefficients to taxi segment parameters, to $\Delta\sigma$ cycles.
  - Future enhancements:
    - Evaluate C.G. Nz to distinguish between prepared and semi prepared airfields. (currently all airfields assumed to be prepared)
    - Evaluate L/ESS strain gage data to development a relationship between C.G. Nz and control point stress response.

SLIDE 13

Dynamic taxi:

The first step in determining stress cycles for dynamic taxi is to select one of 25 dynamic taxi cases by performing a best match of taxi segment to taxi case parameters. Then from the chosen taxi cases analytic stress response *($\overline{A}$, N_0)* and the taxi segments duration *(T)* generate delta stress ($\Delta\sigma$) cycles by application of Monte Carlo methods. To these $\Delta\sigma$ cycles add a 1.0g stress determined by application of stress transfer coefficients, determined by regression analysis, to taxi segment parameters.

In order to utilize recorded data to determine the runway roughness enhanced methods will be developed. First, an effort will be made to develop a method to evaluate C.G. Nz to distinguish between prepared and semi-prepared airfields (currently all airfields are assumed to be prepared). Following this, when a sufficient database of L/ESS strain gauge data is available, it will be evaluated to develop a C.G. Nz to stress relationship.

Stress Spectra Generation

- Landing impact
  - Use the highest Nz occurring during landing impact and along with landing GW analytically convert to aircraft sink speed.
  - Using sink speed and weight (GW, FW, or PW) match to one of 15 landing impact conditions.
  - Ratio landing condition analytic stress sequence to match segment sink speed and weight.
- Take-off rotation
  - Assume the elevator deflection required to rotate the aircraft is the same as used for analysis.
  - Apply regression transfer coefficients to assumed elevator deflection and flight segment parameters to obtain stress during rotation.

SLIDE 14

BOEING

Landing impact:

Control point stress sequences due to landing impact are generated as a function of weight (gross weight, fuel weight, or payload weight) and aircraft sink speed using the following procedure:

1. The highest recorded Nz occurring during the landing impact along with the landing gross weight is converted to aircraft sink speed.
2. One of 15 landing impact conditions is chosen by performing a best match of sink speed and weight. The weight used is dependent on control point location (example: for wing control points, fuel weight is used).
3. The chosen landing conditions stress sequence is ratioed to match the segment sink speed and weight.

Take-off rotation:

Control point stresses that occur during take-off rotation are determined as a function of elevator defection and associated flight segment parameters. The elevator deflection used was assumed to be the same as that used for analysis. Regression stress transfer coefficients were applied to the assumed elevator deflection and flight segment parameters to obtain stress during rotation.

C17

Control Point Selection

Damage Tracking

- Nine control points throughout the airframe were selected to monitor the structural status of each individual aircraft.
- The control points were selected on each major component to track the crack growth life based upon individual aircraft usage.
- Stress intensity solutions for each control point are in tabular form and damage calculation is based on one dimensional (crack length) cycle-by-cycle crack growth analysis to minimize computing time.
- Life at any location on the airplane can be correlated to one of the control points based upon the ratio of the analytical life provided the two locations have the same loading characteristics.

BOEING

SLIDE 15

The continual assessment of the in-service structural integrity of the individual airplanes will be based on damage calculated for each of the control points selected throughout the airframe. Control points were selected on each major component to monitor the change of each damage driving parameter (gust, maneuver, cabin pressure, and etc) and their impact on the life of the component as usage varies. Location of control points selected on each airframe component was based on knowledge gained from the life assessment effort and during full-scale engineering development. Damage accumulation is based on cycle-by-cycle crack growth at each control points. The stress intensity solution for each control point is stored in tabular form and crack growth analyses are performed in the length direction only to minimize the computing time. Structural life at any location on the airplane can be derived from one of the existing control points based upon the ratio of the analytical life of the two locations. This is valid provided the spectra at the two locations have the same loading characteristics for the same mission event.

C-17 Control Point Selection

- AF1 - Aft Fus Canted Bhd Cap
- AF2 - Aft Fus Pressure Bhd
- CF1 - Long #1 at Wing Rear Spar
- HS1 - H.S. Front Spar
- P1 - Inb'd Pylon Stub
- VS1 - V.S. Front Spar
- WF1 - Wing/Fus Trapezoidal Pnl
- W1 - Lwr Wing Skin @ Xw 429
- W2 - Wing Upr Skin @ Xw 165

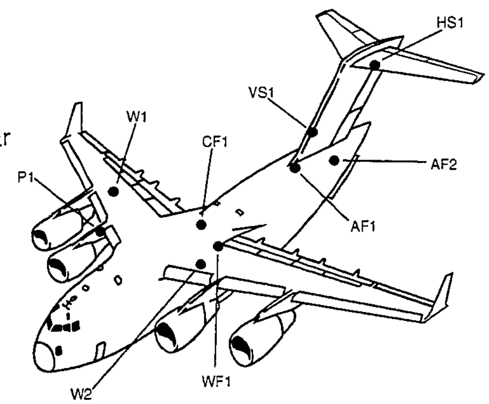

BOEING

SLIDE 16

CPID	LOCATION / DESCRIPTION	DAMAGE DRIVING PARMETERS
AF1	Aft Fuselage, Canted Front Spar, Panel Close to Longeron #3 @ Y_f = 1582.90	Lateral Gust & Maneuver Loads
AF2	Aft Fuselage, Pressure Bulkhead @ (X46.9 and Z304 Aft Cap) Y_f = 1797.55	Pressure
CF1	Center Fuselage; Longeron #1 (intercostal rib) Wing rear Spar @ Y_f 851.60	Gust & Maneuver Loads
HS1	Horizontal Stabilizer; Front spar Upper Cap @ X_{hfs} = 126.87	Gust & Maneuver Loads
P1	Inboard Pylon-Stub, Inboard Upper Cap at Hole 'A19' @ Y_{in} = 263.14	Gust Loads
VS1	Vertical Stabilizer; Front Spar Skin Flange @ Z_{vle} = 613.00	Lateral Gust & Maneuver Loads
WF1	Wing/Fuselage, Rear Trapezoidal Panel Upper Inner Doubler at Edge @ Y_f = 892.00 (X_w = 116.0)	Gust & Maneuver Loads
W1	Lower Wing Basic Structure, Skin @ X_w = 429.00 and Stringer #50	Gust & Maneuver Loads
W2	Upper Wing Basic Structure, Skin @ X_w =165.00 and Stringer #20	Taxi Loads

Gap Filling Missing Data

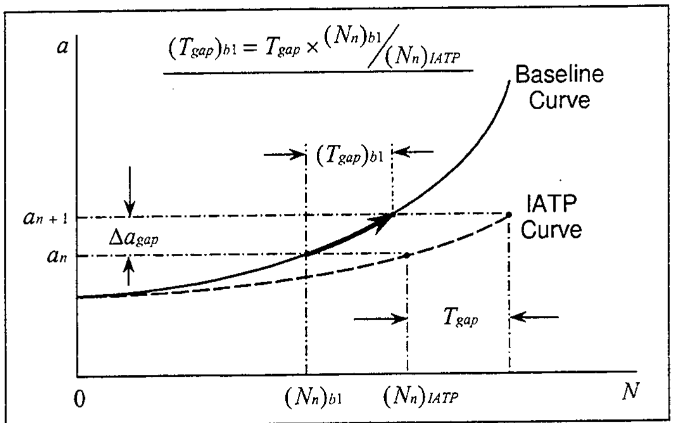

$a_{n+1} = a_n + \Delta a_{gap}$

BOEING

SLIDE 17

A gap in the flight data being processed may be caused by various factors such as: malfunctioning equipment, exceeding memory capacity, bad data rejected during the EDITING process. The amount of crack growth for the gap period is determined by factoring the baseline or analytical crack growth curve based on the design usage for each respective control point by the recent usage or history of the individual airplane. The procedure used is summarized as follows:

1. The edited flight data is assessed by the damage calculation program and the gap in recorded usage is identified in terms of the number of hours unaccounted for. This is T_{gap} . The total flight hours from initial delivery to the end of the last recorded flight is $(N_n)_{IATP}$.

2. From the appropriate baseline curve, determine the time required for the crack to reach the size at the end of the last recorded flight (a_n), from the initial size. This is $(N_n)_{BL}$

3. The equivalent of T_{gap} on the baseline, $(T_{gap})_{BL}$, is determined as follows:

$$(T_{gap})_{BL} = T_{gap} \times \frac{(N_n)_{BL}}{(N_n)_{IATP}}$$

4. The baseline curve is entered at a_n, and is followed for a time interval equal to $(T_{gap})_{BL}$. The increment of growth due to the unlogged hours of usage.

5. The crack size at the end of the unlogged period is given by:

$$a_{n+1} = a_n + \Delta a_{gap}$$

The procedure presented above applies to all control points. By using the ratio of $(N_n)_{BL}$ to $(N_n)_{IATP}$, the difference between the baseline usage and IATP usage is compensated to some extent.

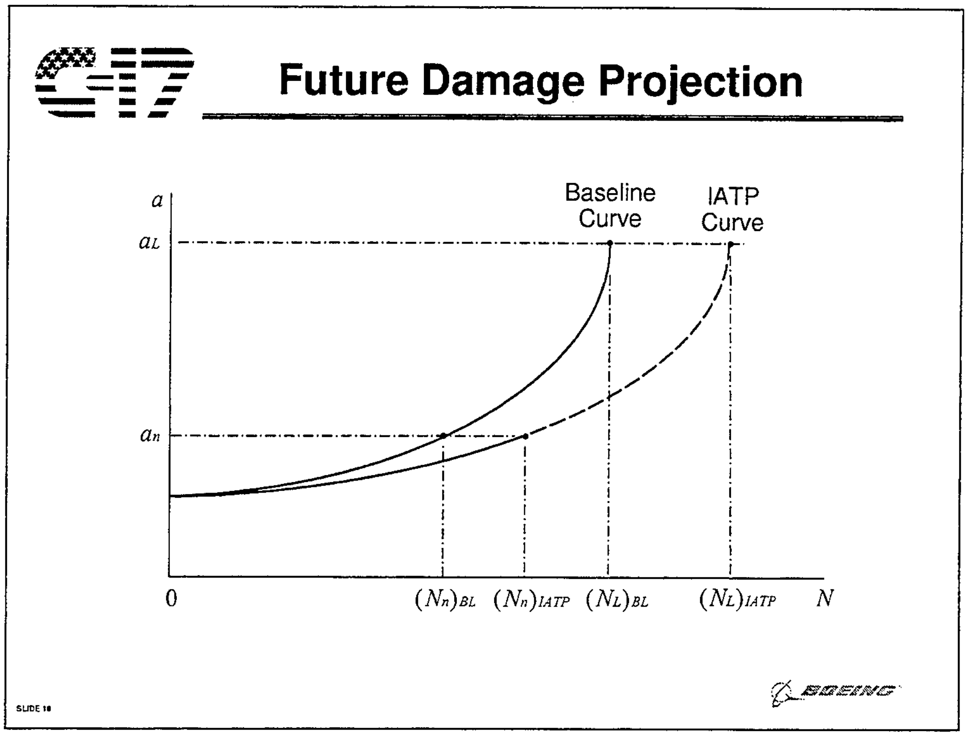

Projection of the time for a crack to reach its limiting size is made for each of the nine control points on each airplane in the force. The procedure is based on the assumption that the relationship between the recorded usage and the design usage crack growth curve, in terms of the ratio between flight hours to reach the same crack size, will remain constant out to limiting crack size, a_L. The procedure to be used to project the time to reach, a_L from a given crack size, a_n and time, $(N_n)_{IATP}$, is as follows:

1. The baseline curve is used to determine the time to reach a_n from the initial crack size based on baseline usage. This is $(N_n)_{BL}$.
2. The baseline curve is used to determine the time to reach the limiting crack size, a_L. This is $(N_L)_{BL}$.
3. The projected time to reach the limiting crack size is found from:

$$(N_L)_{IATP} = (N_L)_{BL} \times \frac{(N_n)_{IATP}}{(N_n)_{BL}}$$

IAT Data Report

- Fleet usage leaders (Airframe time, flights, landings, etc.).
- Usage by aircraft, duty base, and fleet.
- Time spent in segment (ascent, cruise, air-drop, etc.).
- Mission type usage distributions.
- Take-off and landing gross weight, fuel weight, and cargo weight distributions.
- Air drop cargo weight distribution.
- Fleet structural status: Fleet leading current and projected damage tolerance and durability life at the control points .
- Individual aircraft structural status: Current and projected damage tolerance and durability life at the control points for each aircraft.
- Data capture rate
- Duty base and horizontal tail assignment dates.

Note: All data compiled for the current report period and cumulative.

SLIDE 19

The output of IATP is the IAT Data Report which typically is generated on a semi-annual basis. This report contains two types of information: one being usage statistics and the other being aircraft structural status. Usage statistics give information such as airframe time, number of flights and landings, etc. This information is given by aircraft, duty base, fleet, and fleet leaders (aircraft with most flights, landings, etc.). Information is also given in terms of time spent in the different segment types and a distribution of flights over the 35 design mission types. In addition, take-off and landing gross weight, fuel weight, and cargo weight distributions as well as air-drop cargo weight distribution are given.

Aircraft structural status is given as current and projected damage tolerance and durability life at the control points. This information is given for each aircraft and also summarized by the fleet leading aircraft (aircraft with largest damage).

In order to disposition the success of collecting and processing SFDR data capture rates are given in terms of flight hours processed over flight hours flown. Also given are a history for each aircraft of duty base and horizontal stabilizer assignment dates.

The above information is compiled for the current report period and cumulative.

Computer System Characteristics

- Platform: IBM mainframe computer
- Source code written in FORTRAN
- System runs interactively or as a batch process depending on the operations being performed.
- Employs a DB2 relational database for ease of data processing and managing.
- Incorporates utilities to permanently backup processed flight data to tape in order to relieve on-line storage requirements.
- User interface in the form of pull down menus and panels for ease of operation and user data entry.

SLIDE 20

The IATP system resides on an IBM main frame computer and is composed of 12 separate FORTRAN programs that perform the various data processing functions. This system runs interactively for those functions requiring extensive user interaction, or as a batch process for those functions requiring a large amount of data processing time. The system employs a DB2 relational database for storing and retrieving processed flight data and user input data. A relational database allows for efficient data storage and ease of data retrieval and manipulation without extensive coding. The system includes a utility to permanently backup processed flight data to tape in order to relieve on-line storage requirements. The user interface is in the form of pull down menus and panels. This allows for ease of system operations and user data entry without extensive knowledge of mainframe computer operations.

THE C-141 ELECTRONIC FLIGHT USAGE LOG (AFTO 451)

Presented At The 1997 Aircraft Structural Integrity Program (ASIP) Conference, San Antonio, Texas

2-4 December 1997

Heather P. Roland
Lockheed Martin
Marietta, Georgia

TSgt Alfred G. Taus
Altus AFB
Altus, Oklahoma

Background

C-141 Force is in its remaining 20% of service life.

- Inspection & repair activity on the increase.
- Usage reporting (timeliness & accuracy) becoming increasingly important.
- Safety concerns expressed due to lateness of AFTO 451 usage form submittals.

Background

Altus AFB assigned aircraft experience the most severe usage.

- **Quarterly tracking no longer adequate.**
- **Altus aircraft use up remaining service life two times faster than the rest of the force.**
- **Weekly tracking runs required to insure safety.**

Purpose

- The Electronic AFTO 451 Program was developed to streamline the process of tracking aircraft usage and provide near real time usage data.
- This was accomplished by producing a Microsoft Access database to record flight data.

U.S. Air Force C-141B Starlifter

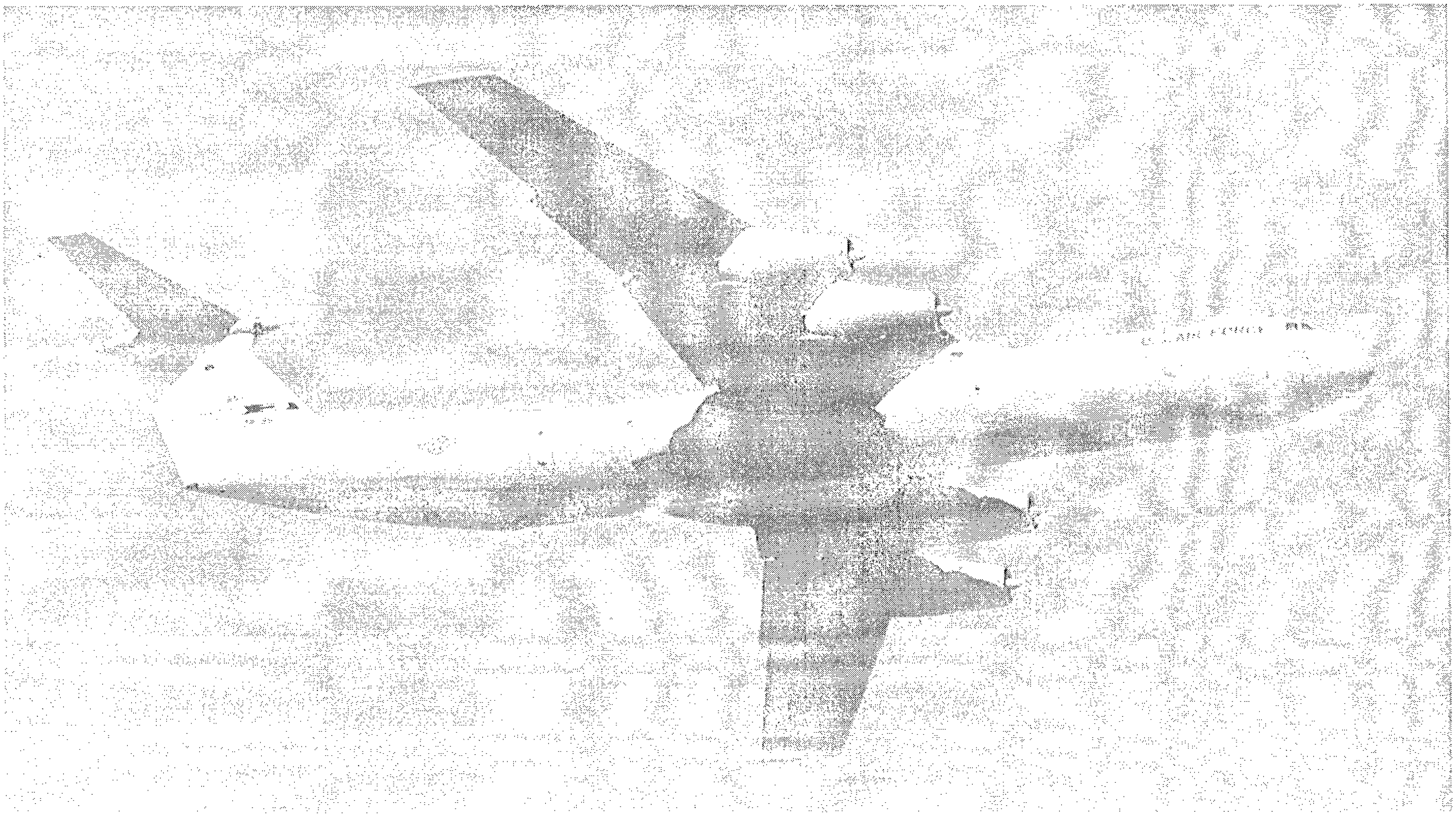

AFTO 451 Forms

Old - Bubble Sheet

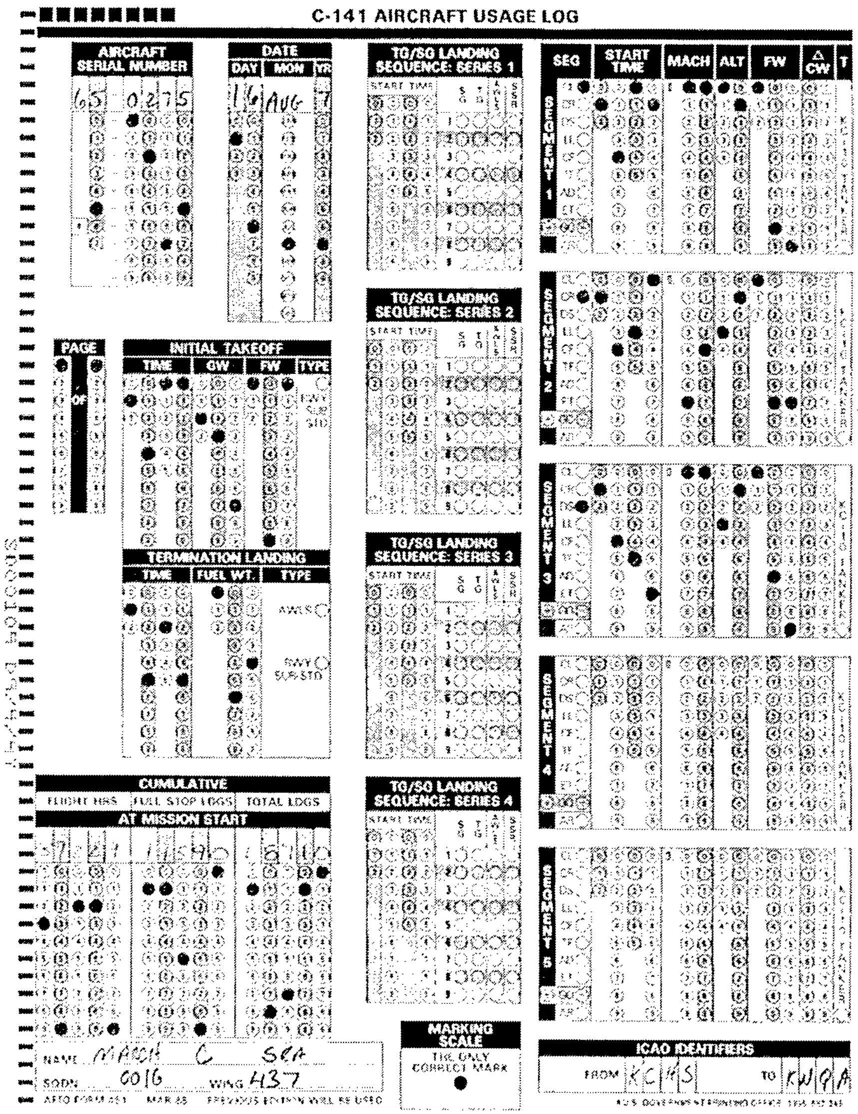

New - Altus Form 1

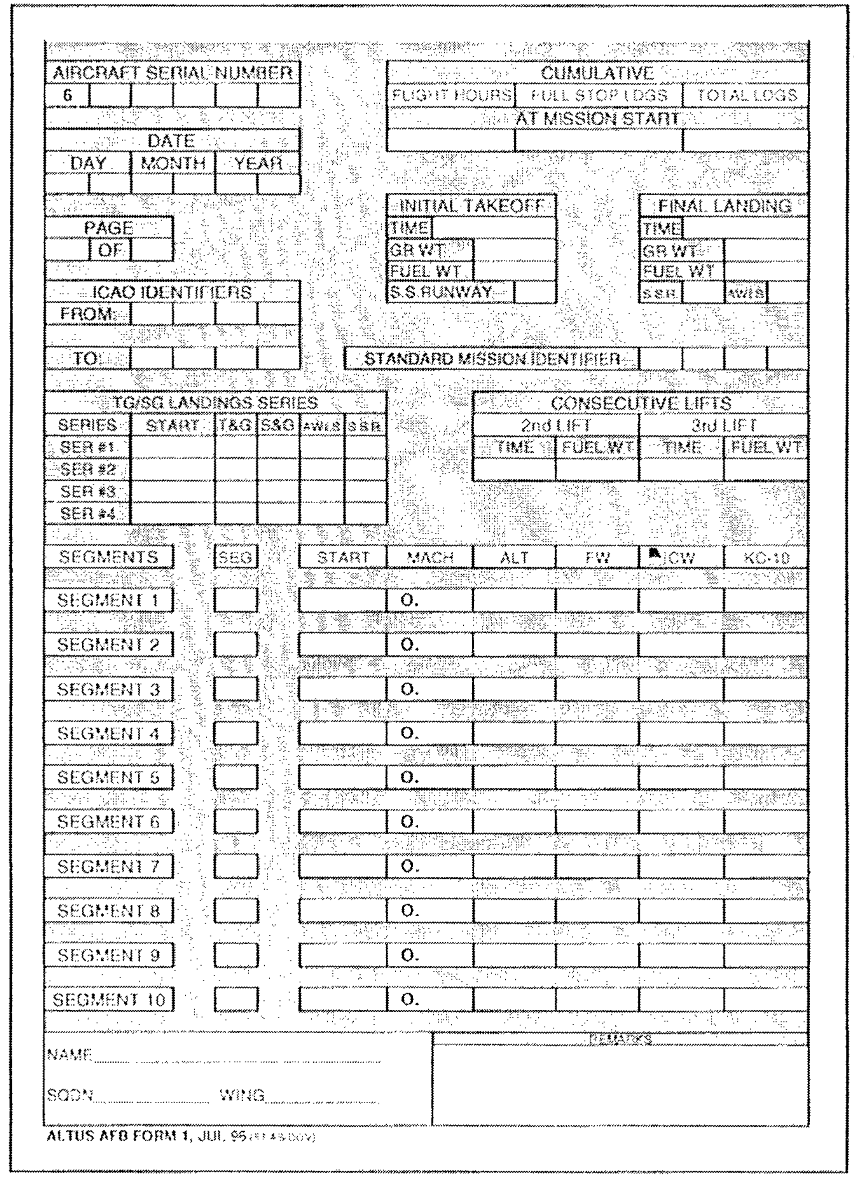

Standard Missions

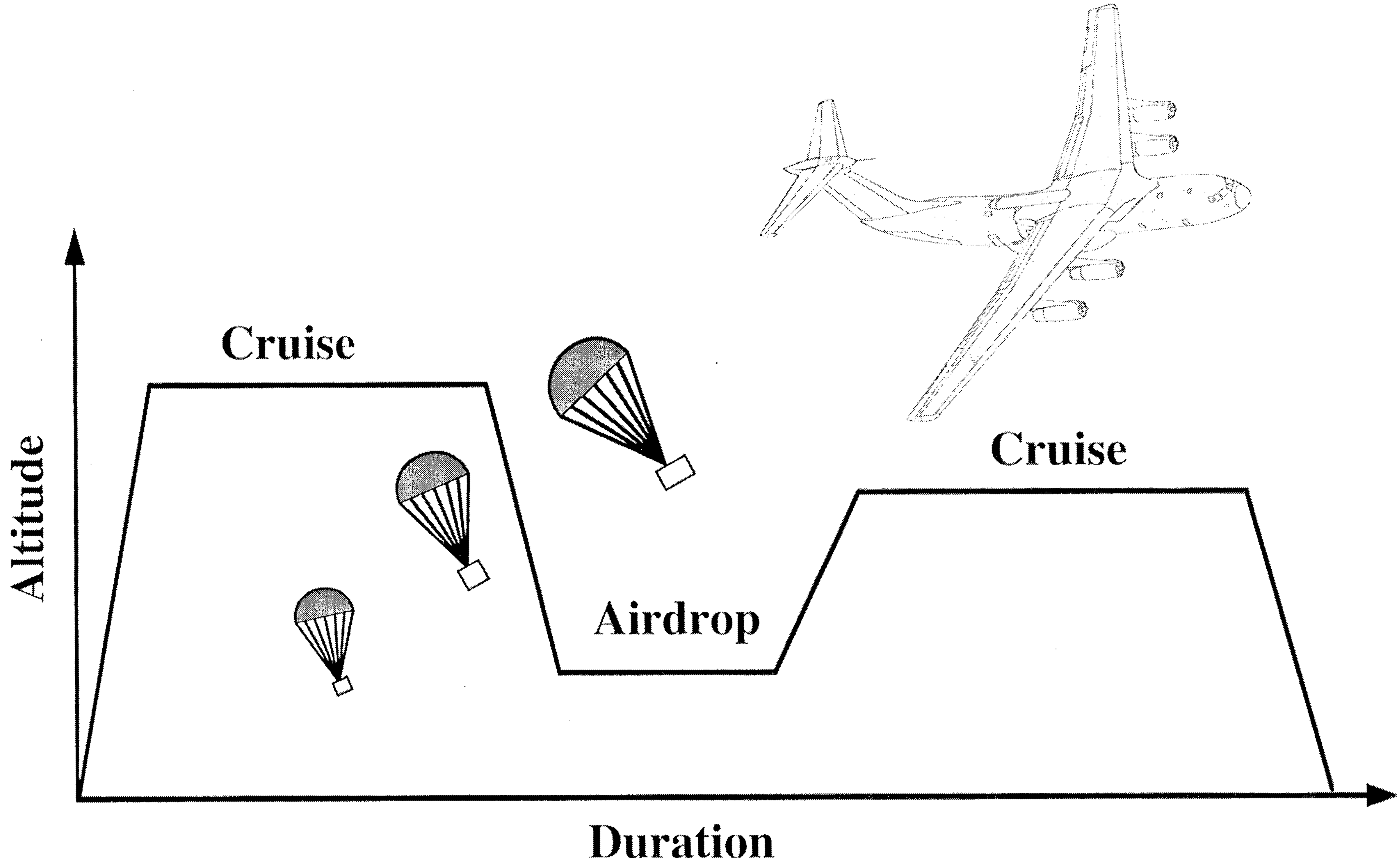

Standard Missions at Altus, AFB

Standard Mission Identifiers (AIRDROP)	Mission Description	
AD1A	VFR:	One Lift
AD2A	SKE:	One Lift
AD3A	SKE/VFR:	One Lift
AD4A	SINGLE SHIP:	One Lift
AD5A	SINGLE SHIP:	One Lift
AD1B	VFR:	Two Lifts
AD2B	SKE:	Two Lifts
AD3B	SKE/VFR:	Two Lifts
AD4B	SINGLE SHIP:	Two Lifts
AD5B	SINGLE SHIP:	Two Lifts
AD1C	VFR:	Three Lifts
AD2C	SKE:	Three Lifts
AD3C	SKE/VFR:	Three Lifts

Advantages of the New Altus Form 1

- Flight engineers no longer have to complete the tedious bubble sheet.
- Standard Mission identifiers greatly reduce the amount of entry time.
- All information from the forms are entered daily into the Electronic AFTO 451 program for quick turnaround.

The Electronic AFTO 451
Main Menu

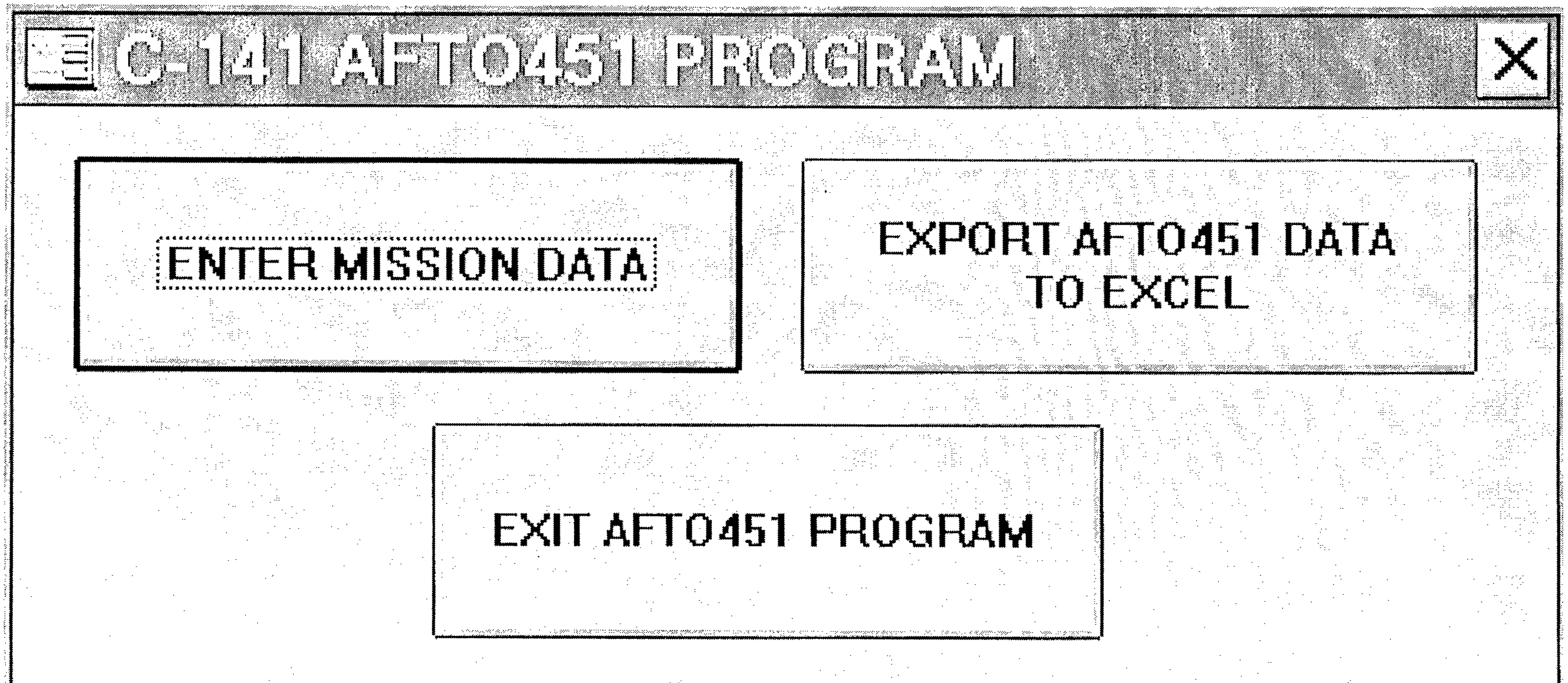

Data Entry Screen

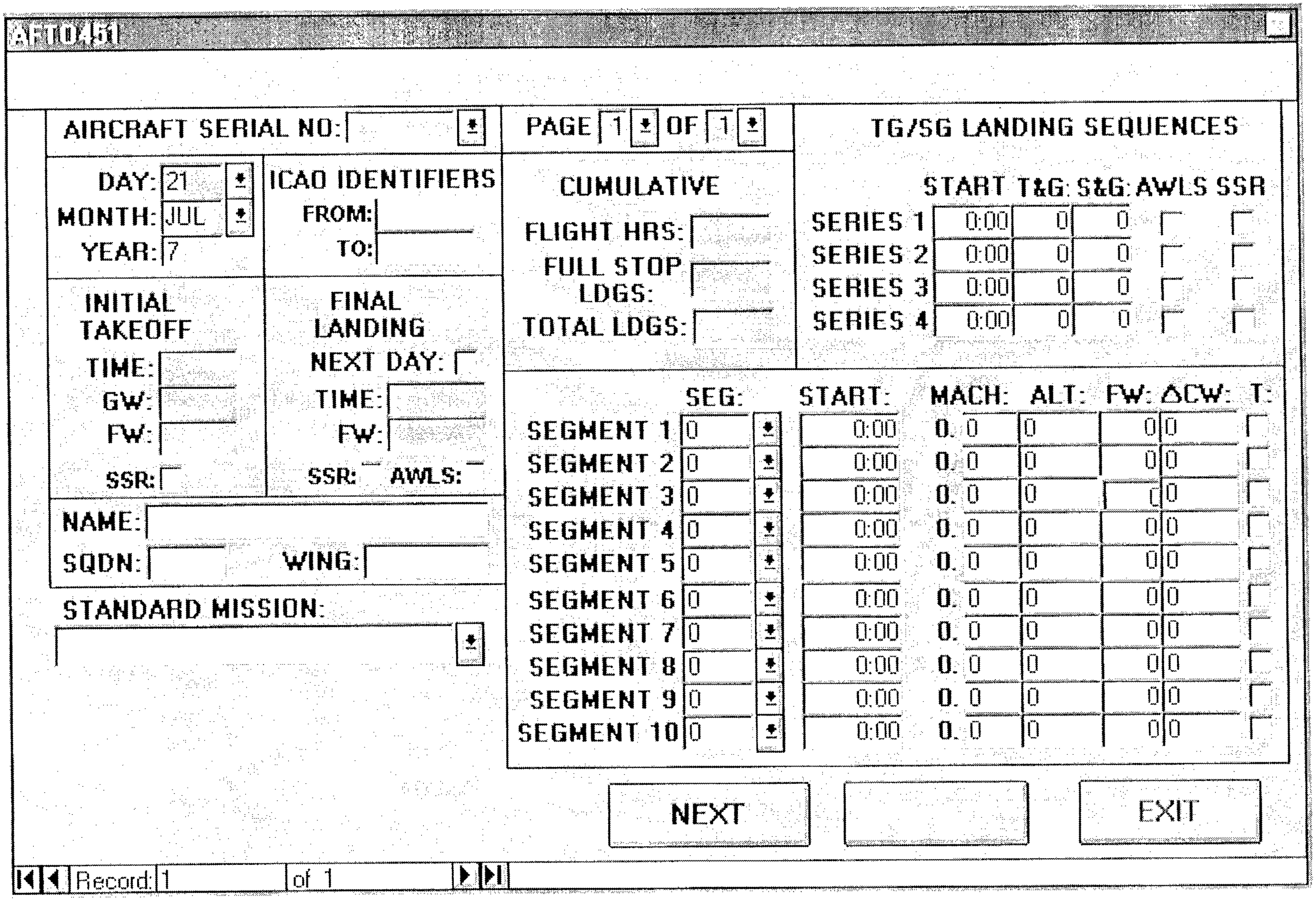

Selecting a Standard Mission

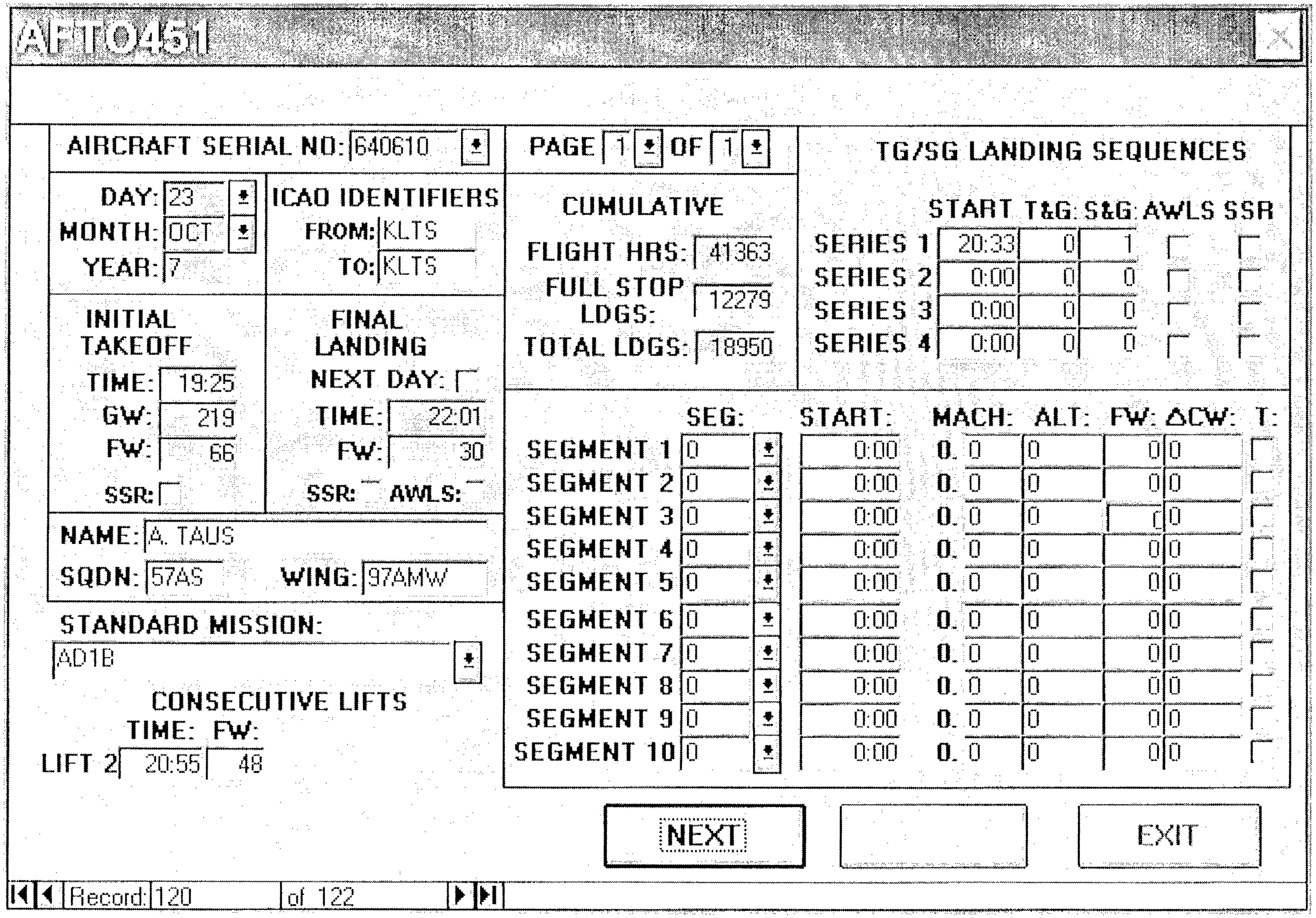

Standard Mission Entry

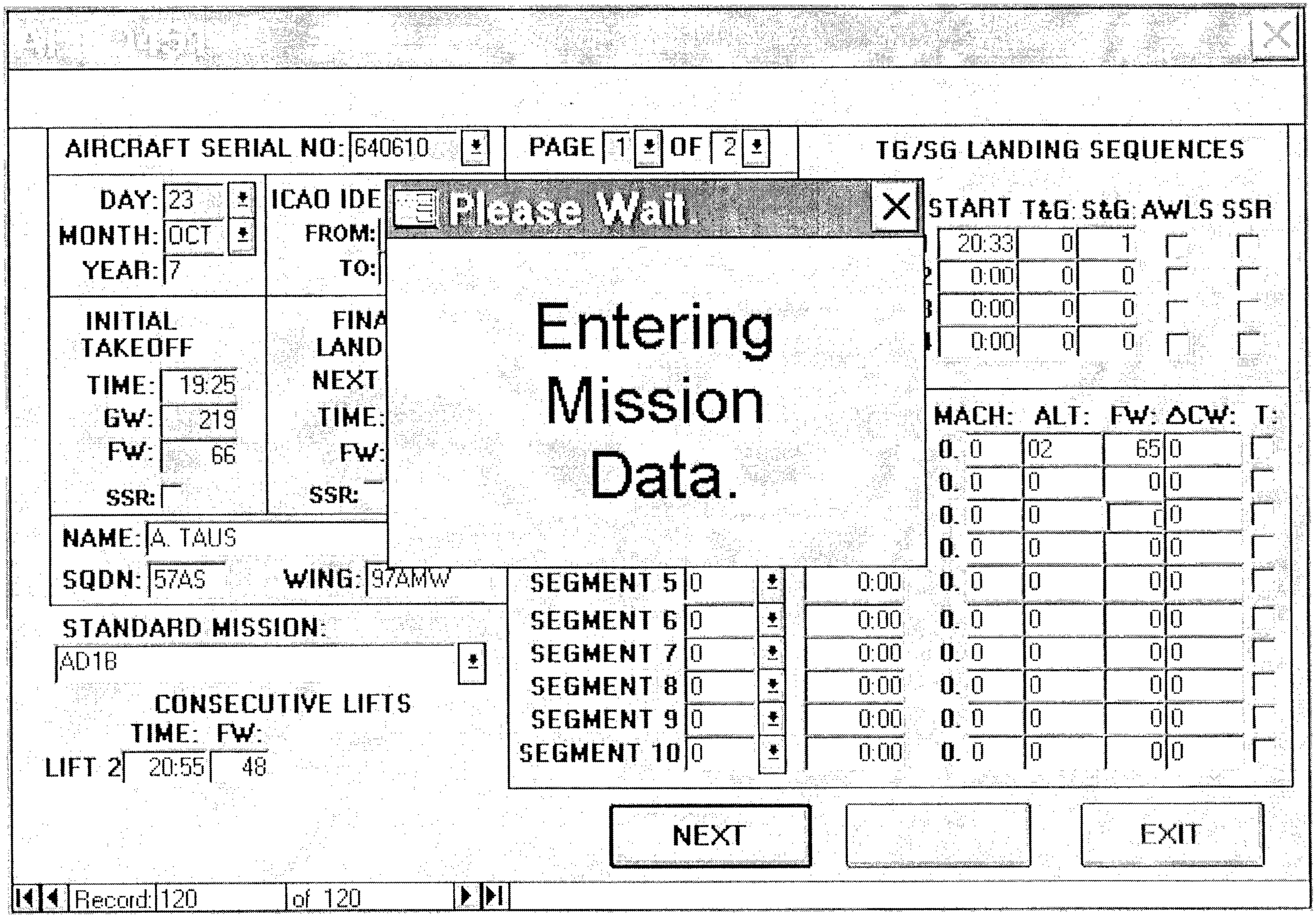

Cargo Drop Weight

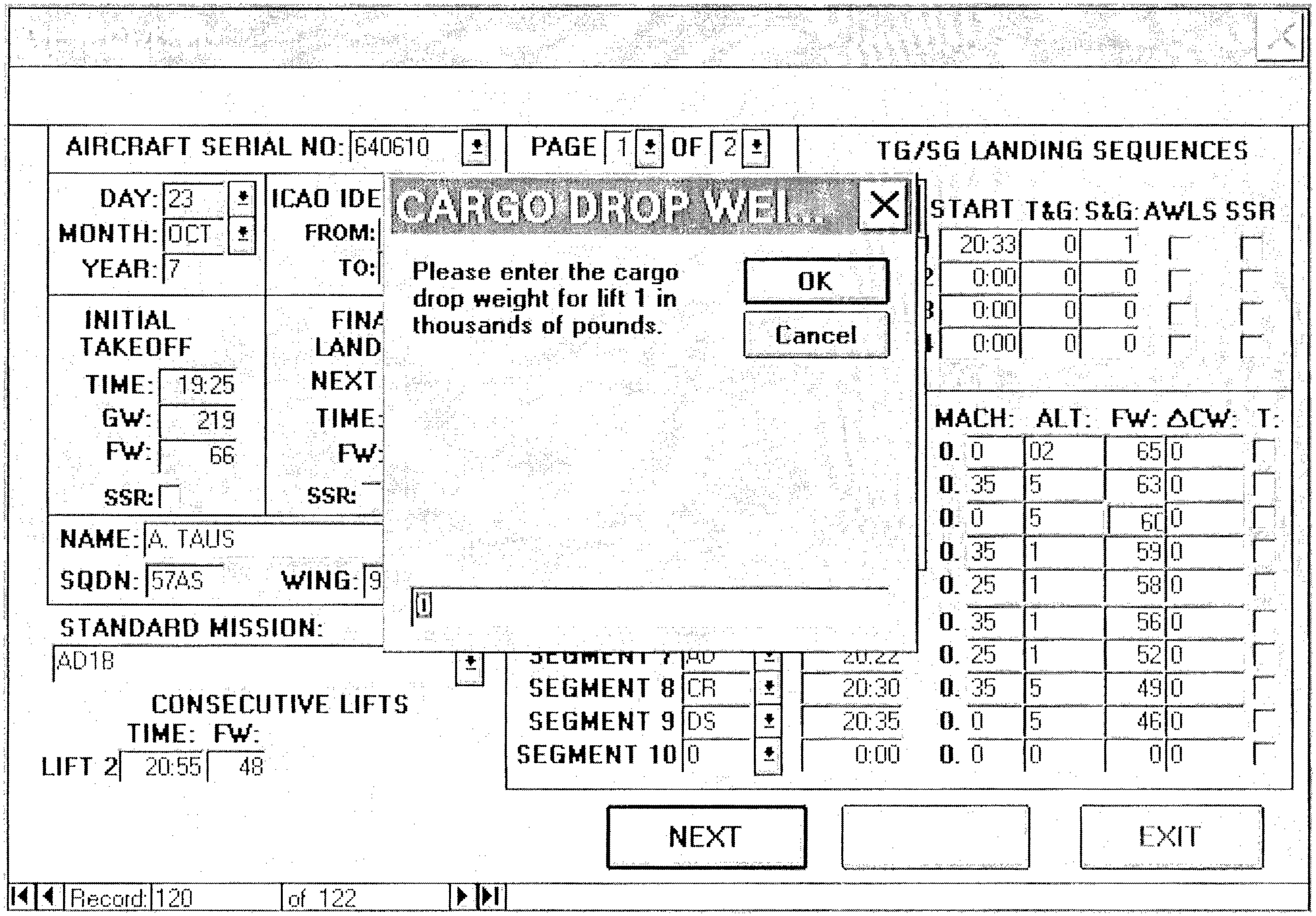

Main Menu

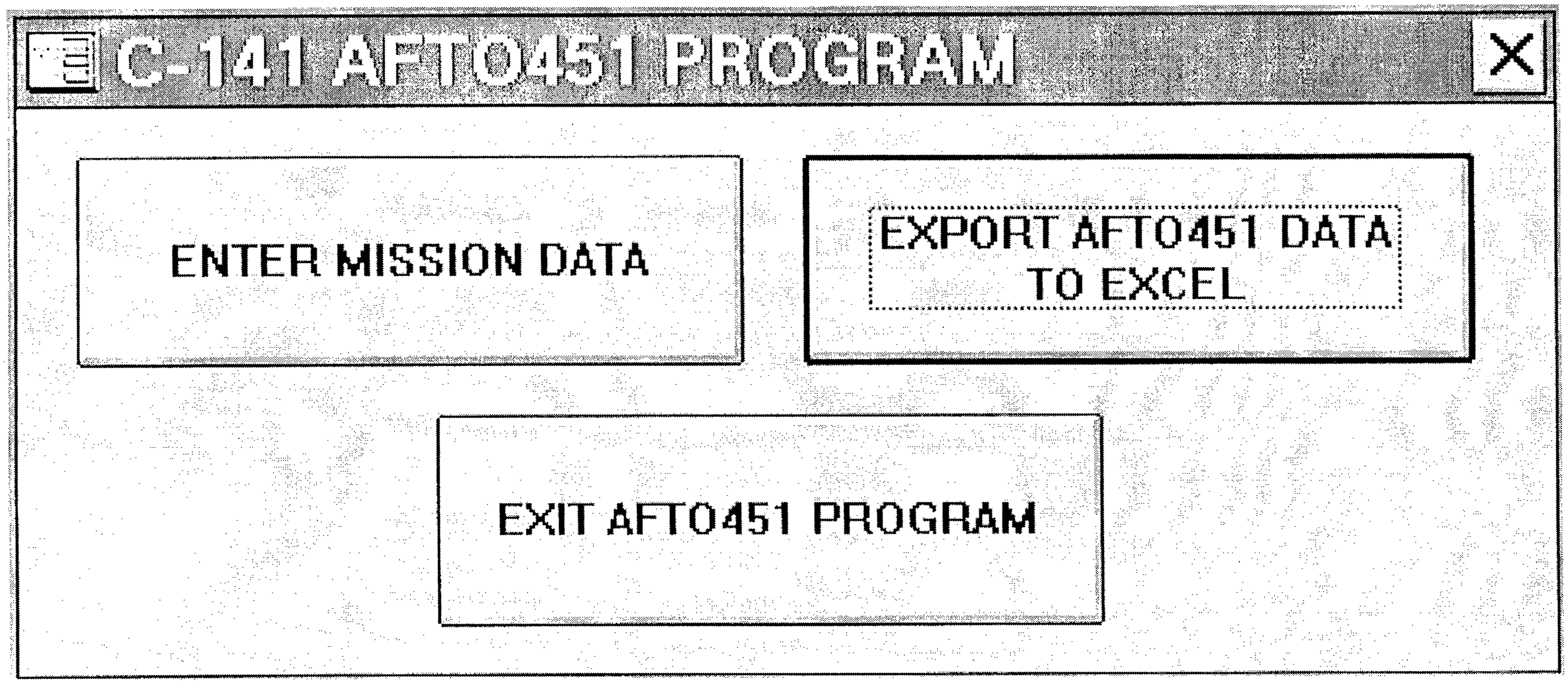
C-141 AFTO451 PROGRAM
ENTER MISSION DATA
EXPORT AFTO451 DATA TO EXCEL
EXIT AFTO451 PROGRAM

Export File

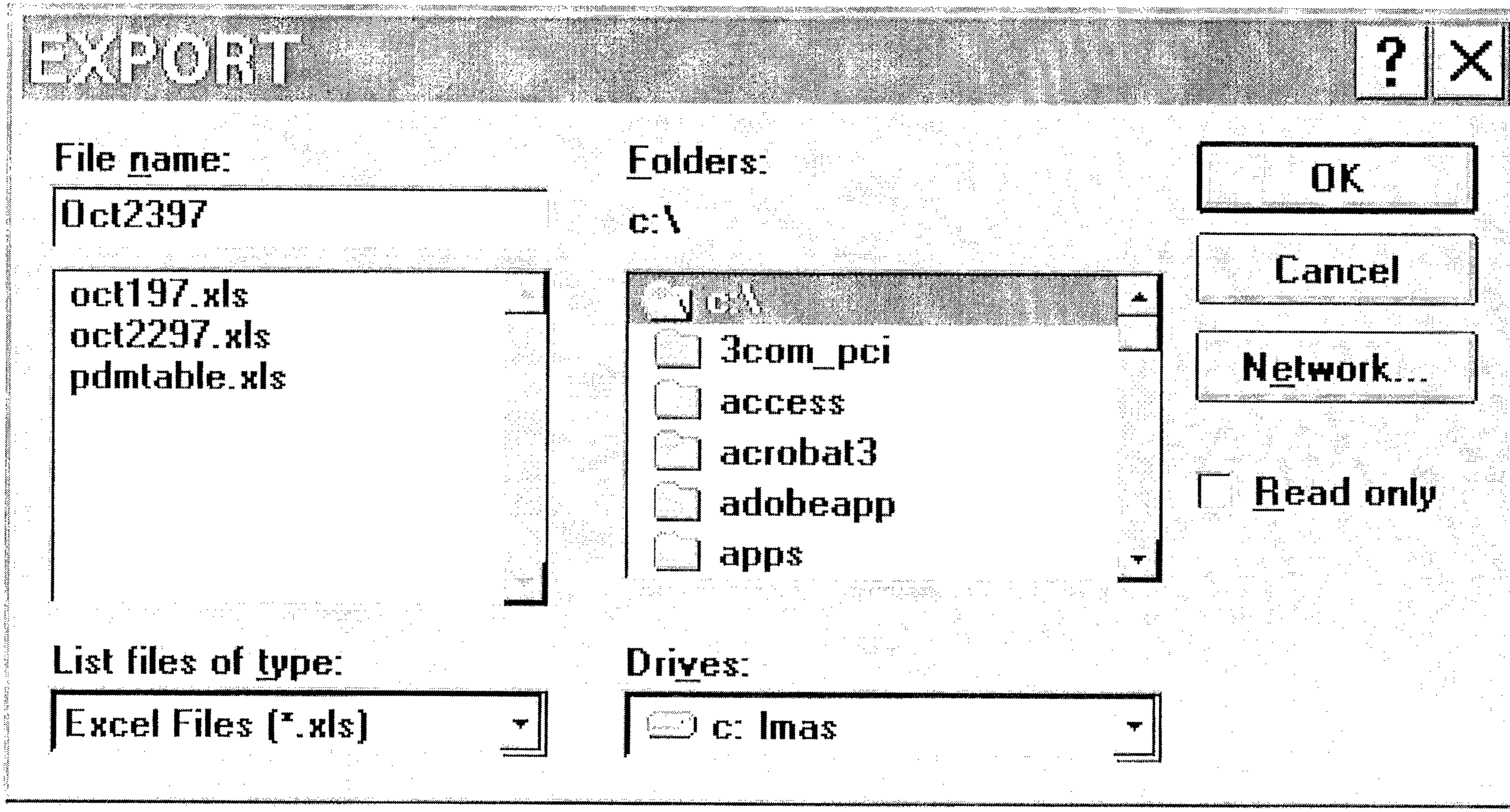
EXPORT
?
File name:
Oct2397
oct197.xls
oct2297.xls
pdmtable.xls
Folders:
c:\
c:\
3com_pci
access
acrobat3
adobeapp
apps
OK
Cancel
Network...
Read only
List files of type:
Excel Files (*.xls)
Drives:
c: lmas

Electronic Data Transfer

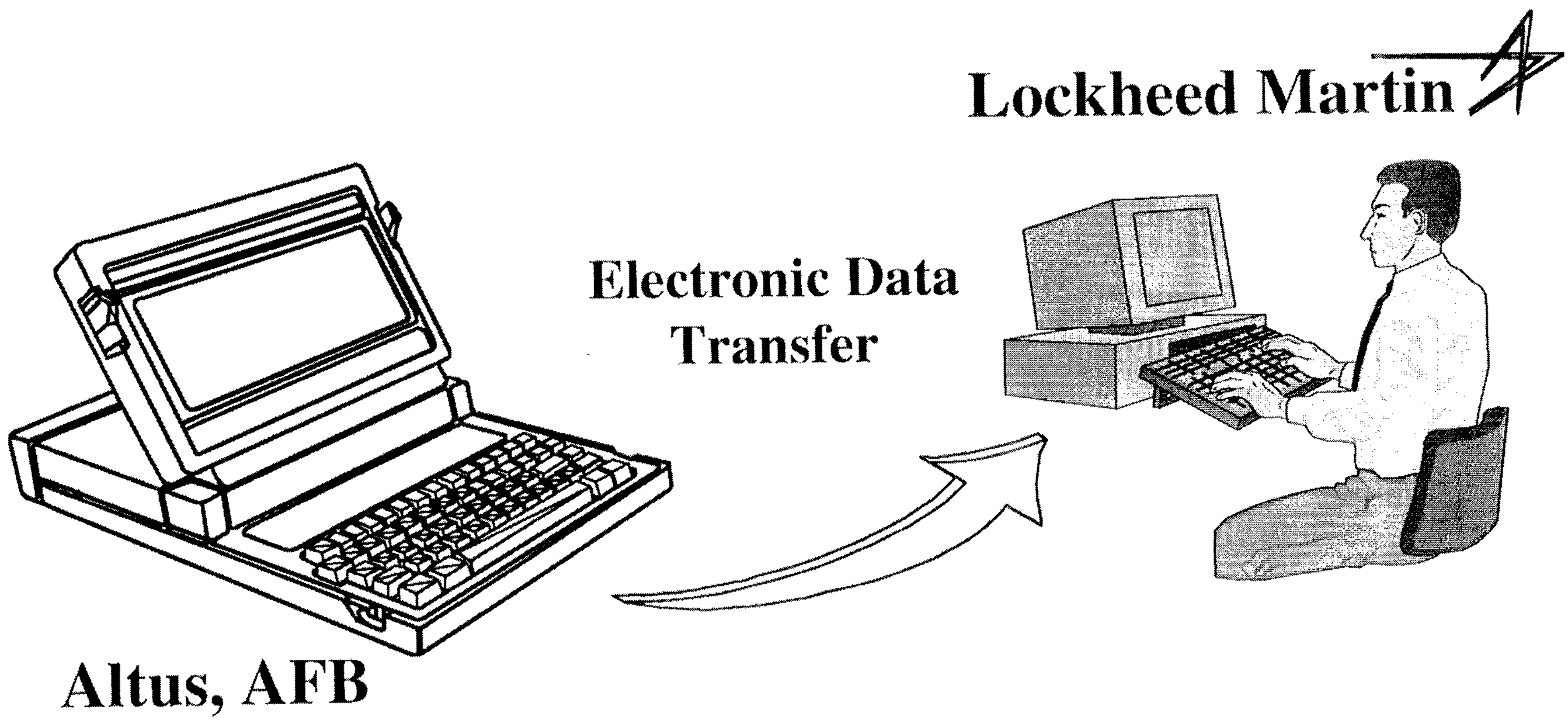

Advantages

- Eliminated problems which resulted from scanning the bubble sheet through an OPSCAN reader.
  - bent up pages
    - stray pencil marks
      - incorrectly marked sheets

- Number of correctly completed forms increased by a factor of 2.5.

- Flight data accounted for in tracking within a week of actual flight date.

Additional Benefits

- Standard Mission Identifiers provide quick and easy data entry.

- Includes checks for obvious mistakes that are otherwise overlooked on the bubble sheet.
  - -invalid aircraft serial numbers
  - -missing information

Future Plans

- Implement the Electronic AFTO 451 at all bases.
- Advance the Electronic AFTO 451 to the World Wide Web.

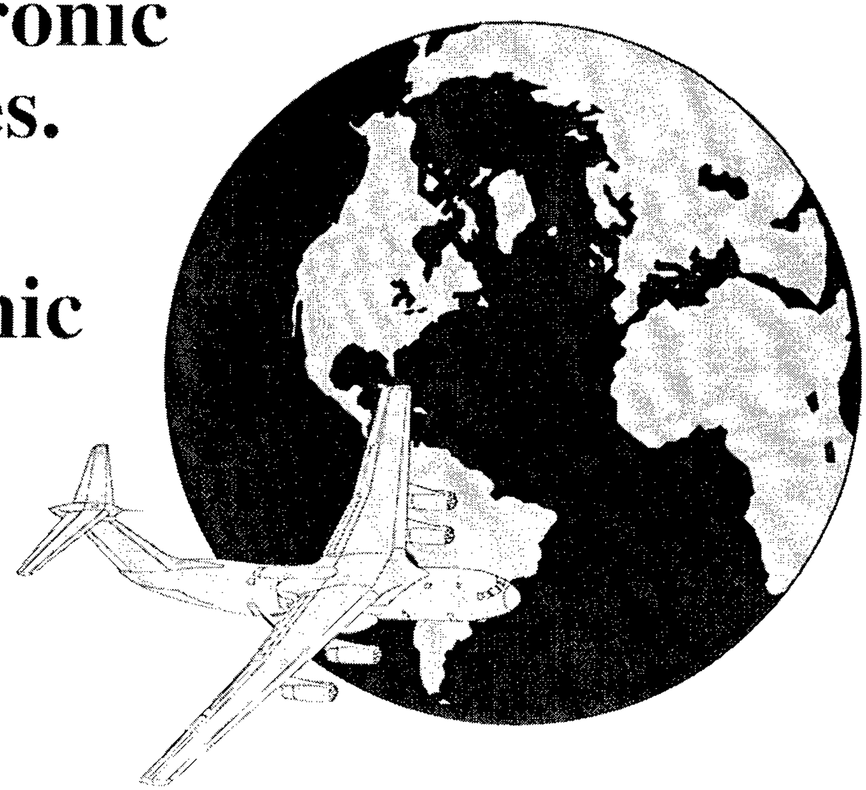

FAA MSR/LSR Flight Inspection Fleet Aircraft Structural Integrity Program

Mr. James M. Marks Jr.
Mr. James J. Abel
Raytheon E-Systems
Greenville Division
P.O. Box 6056 Greenville, Texas 75403-6056

ABSTRACT

Raytheon E-Systems has developed and implemented a comprehensive Aircraft Structural Integrity Program (ASIP) that aims to ensure the long-term structural integrity and continued airworthiness of a broad portion of the Federal Aviation Administration (FAA) Flight Inspection Fleet of aircraft. Specifically, six Learjet Model 60 and three Canadair Challenger CL601-3R aircraft are modified by Raytheon E-Systems to perform the Flight Inspection role for the FAA. Flight Inspection mission profiles are characterized by routine operation below 2000 feet MSL (mean sea level). This low level, structurally harsh environment contrasts significantly with typical corporate jet operational environments. The Flight Inspection usage has a notable impact on the loading spectra experienced by the aircraft structure due to the routine operation in the low-level gust environment, and, as a result, an appreciable impact on the service life of the aircraft.

The ASIP is based on a tailored implementation of the requirements of the U.S. Air Force MIL-STD-1530 approach. The ASIP task elements consist of a Durability and Damage Tolerance Assessment (DADTA), an Individual Aircraft Tracking Program (IATP), a Loads/Environment Spectra Survey (L/ESS), and a Fleet Structural Maintenance Plan (FSMP). The interrelationship, implementation and functional responsibilities of each ASIP task element are identified and distinguished in an ASIP Master Plan. This paper focuses on the development and integration of the IATP as well as the relationship of the IATP with the other ASIP task elements.

INTRODUCTION

The objective of the IATP for the FAA Flight Inspection Fleet is to provide a method for collecting, processing, and analyzing data from various sensors installed onboard each aircraft in order to predict crack growth at potentially critical areas on each airframe. The Durability and Damage Tolerance Analysis (DADTA) for both aircraft types [1] [2] identifies these critical areas as well as the corresponding predicted crack growth expected in service, predicated upon an assumed initial baseline loading spectrum. Crack growth calculations using measured flight data are then compared to the baseline crack growth calculations contained in the DADTA. The results are used to project the scheduling of inspection and/or maintenance activities identified in the Fleet Structural Maintenance Plan (FSMP) for both the Learjet Model 60 and the Canadair Challenger CL601-3R. Prudent fleet management decisions may then be formed based upon actual in-service usage, some of which may include: accelerating or delaying inspections and/or maintenance actions, re-assigning aircraft from one base to another in order to evenly distribute mild and harsh usage environments, and re-evaluation of the DADTA based on the measured flight load spectrum after a significant amount of flight data is collected.

CURRENT AIRCRAFT IN THE IATP

The IATP is designed to track all Learjet Model 60 and Canadair Challenger CL601-3R aircraft in the Flight Inspection Fleet. The Learjet Model 60 performs the Medium Size/ Medium Range (MSR) flight inspection role for the FAA. The Canadair Challenger CL601-3R performs the Large Size/ Long Range (LSR) flight inspection role for the FAA. These aircraft differ in size, manufacturer, fracture analysis methodology, flight recorder parameters, and original certification basis. A depiction of each aircraft is shown in Figures 1 and 2, respectively.

The Learjet Model 60 aircraft has a maximum gross takeoff weight of 23,500 pounds with a maximum operating altitude of 51,000 feet. The Learjet Model 60 is certified to Amendment 23 of FAR Part 25.571 [3] using fatigue and static fail-safe methodologies. Learjet, however, performed a fracture mechanics based damage tolerance analysis of the modified Model 60 MSR Flight Inspection aircraft using assumed baseline load spectra for the planned flight inspection operating environment.

The Canadair Challenger CL601-3R aircraft has a maximum gross takeoff weight of 45,100 pounds with a maximum operating altitude of 41,000 feet. The CL601-3R is certified to Amendment 45 of FAR 25.571 [3] as a "damage

tolerant" aircraft using fracture mechanics based damage tolerance analysis methodologies. In addition, Canadair re-evaluated the structural integrity of the CL601-3R to account for the unique load spectra encountered in the flight inspection environment.

FLIGHT DATA RECORDER

The Flight Data Recorder (FDR) system is installed on each aircraft in the fleet. The FDR system is comprised of eight major line replaceable units (LRUs): a Signal Acquisition Unit (SAU), a Data Transfer Interface Unit (DTIU), a Data Transfer Module (DTM), a Crash Survivable Memory Unit (CSMU), a Flight Data Panel (FDP), an Engine Signal Data Converter (ESDC, LSR aircraft only), a Flight Data Recorder Interface Unit (FDRIU), and a triaxial accelerometer. In addition, eight strain sensors are permanently bonded to each MSR airframe and ten strain sensors are permanently bonded to each LSR airframe. The FDR system diagram is shown in Figure 3. The strain sensor locations for both the MSR and LSR aircraft are shown in Figures 4 and 5, respectively.

The SAU, DTIU, DTM, CSMU, and FDP are supplied by Smiths Industries. The ESDC and FDRIU for the LSR aircraft are supplied by ICE Corporation. The FDRIU for the MSR aircraft is supplied by Learjet. The accelerometer is supplied by Magnetek Transducer Products. The strain sensors are supplied by Columbia Research Labs, Inc.

All aircraft signals monitored by the FDR system interface with the SAU, which processes the data using its internal Operational Flight Program (OFP) and then stores it into the two separate non-volatile memory devices: the CSMU and the DTM. The CSMU is permanently mounted in each aircraft's tail section and is to be retrieved in the event of a mishap. Flight data required by FAR Part 135 Appendix B are stored in the CSMU. The DTM, which is inserted into the face of the DTIU (much like a cassette cartridge) is used to periodically transfer the stored engine and structural data from the aircraft to a ground-based computer system for processing and analysis.

The SAU also receives user input data from the FDP. These data are entered by the crew during preflight and include such parameters as fuel weight, gross weight, center of gravity, date, mission base, etc. The FDP also provides a built-in test (BIT) button and fault annunciators, as well as memory capacity indications that signal DTM memory at 80% (or greater) and 100% full.

The DTIU provides a receptacle for the DTM and transfers the data to the DTM for download. It is also used for uploading the OFP and aircraft specific configuration data from the ground-based sources. The DTIU also contains a display and operator interface used for upload/download commands, as well as for displaying system status messages.

The ESDC unit (LSR aircraft only) converts existing analog engine signals ITT, N1, and N2 (from both engines) into ARINC 429 high speed digital data format. ITT, N1, and N2 engine signals are digitized to ARINC 429 digital data format because these three parameters require the highest accuracy and are the most significant contributors in the engine trend analysis. The Engine Signal Data Converter Unit digitizes, combines, and transmits the ITT, N1, and N2 data to the Flight Data Recorder system on two separate ARINC 429 data bus channels (left engine and right engine data channels). The ESDC incorporates BIT features that allow fault isolation to the LRU level.

The FDRIU is essentially a relay box that converts discrete signals from various parts of the aircraft into a format that is acceptable to the SAU. The SAU accepts mostly open/28VDC type discrete signals and only a few open/ground type discrete signals; whereas, the aircraft provides mainly open/ground type discrete signals. The primary function of the FDRIU, therefore, is to convert a number of discrete signals from open/ground format to open/28VDC format. The FDRIU also provides diode isolation between the monitored aircraft signals and the SAU. The FDRIU incorporates BIT features that allow fault isolation to the LRU level.

The accelerometer provides three-axis acceleration data to the SAU and is used in determining airframe structural loads due to maneuvers, gusts, and ground events. The strain sensors are permanently installed (bonded) at critical locations throughout the airframe for measuring and recording structural strains. The strain sensors provide their signal data to the SAU. These data are used to track and maintain a structural loading history of the airframe.

Stored engine and structural data are periodically downloaded from the aircraft to a ground-based computer system via the DTM for processing and analysis. The computer system is called the Ground Replay and Display Unit (GRDU) and is supplied by Smiths Industries. It consists of an IBM type personal computer (PC) with an internal DTM interface card, and an external Data Transfer Module Receptacle (DTMR). The GRDU contains several software programs used for engine trending and structural analysis, including the Smiths Industries Operational Ground Program (OGP) and various analysis programs. Engine performance trend analysis for the LSR aircraft is accomplished by processing the

downloaded engine data with a General Electric supplied software program named CF34 RJ TREND VERSION 4.0 (RJ stands for Regional Jet; this program is normally used for trend analysis of the CF34 type variant engines on the Regional Jet Challenger aircraft, but is also applicable to the CF34 engines on the CL601-3R). Engine performance trend analysis for the MSR aircraft is accomplished by processing the downloaded engine data with a Pratt & Whitney supplied software program named ECTM IV. Structural Integrity data analysis is performed on a Hewlett Packard workstation using software supplied by Raytheon E-Systems as part of the Individual Aircraft Tracking Program (IATP).

The GRDU can also be used as a Direct Parameter Display (DPD) by connecting it to the FDR system via an aircraft mounted test connector and a test cable. The test connector is called the Ground Replay Equipment (GRE) connector, and it is installed inside the auxiliary equipment rack. The test cable is called the Ground Replay Equipment (GRE) cable. The DPD allows individual parameters to be monitored real time, but the FDR system cannot record data when in DPD mode. In addition, a laptop computer DPD is available to monitor parameters real time in lieu of using the GRDU.

TRACKING ANALYSIS METHODOLOGY

Raw flight recorder data are downloaded periodically (approximately every two weeks or thirty flight hours) from each aircraft in the Flight Inspection Fleet. The data are transmitted via modem to the FAA Flight Inspection Office in Oklahoma City, OK, from the various field bases located throughout the United States and abroad. The data are then forwarded to Raytheon E-Systems in Greenville, TX, via the internet for subsequent processing in the IATP.

The Raytheon E-Systems IATP software reads, stores, and processes raw flight recorder data that have been downloaded and processed on the GRDU using the Smiths Industries supplied Cartridge Ground Program (CGP) software. The processed decompressed data files (ddf) are transferred from the GRDU to a Hewlett Packard (HP) workstation. The Raytheon E-Systems IATP software resides on this HP workstation.

The IATP software reads and stores each ddf in a database. These data form the Loads/Environment Spectra Survey (L/ESS). The L/ESS database contains the structural loading history for all critical areas on each aircraft in the fleet as recorded by each aircraft's individual FDR. The IATP software utilizes these data to perform crack growth analyses at these critical locations.

The IATP reads and interprets the FDR BIT file. The BIT file indicates the fault status of various FDR parameters. The results are displayed on the screen and are also stored in a separate file that may be accessed later by the user. Those parameters critical for crack growth algorithms are highlighted. Also, all FDP entered parameters, strain sensors and accelerations are verified for plausibility by determining if the data exceed certain predetermined maximum and minimum values. Raytheon E-Systems furnishes a monthly report to the FAA customer detailing any BIT faults detected by the IATP. This information is used to investigate and correct potential hardware or software problems associated with the FDR.

The IATP software utilizes an object-oriented architecture with a fully integrated graphical user interface. One significant advantage realized from the object-oriented software architecture is the ability to add new aircraft types, beyond the Learjet Model 60 and Canadair Challenger CL601-3R, with no modification to the essential software code. The graphical user interface enables the software to be user-friendly and dynamic.

IATP FATIGUE CRACK GROWTH

The IATP fatigue crack growth methodologies are based on the Learjet Model 60 MSR Service Life Analysis [1] and the Canadair Challenger CL601-3R LSR DADTA [2]. The theoretical growth of cracks at each control point, from an assumed initial rogue flaw in the aircraft structure, is determined utilizing the applied stress spectrum as collected by each flight data recorder. A cycle-by-cycle analysis approach is utilized such that a full accounting of sequenced peak and valley stress data are incorporated. The IATP utilizes a standard cycle counting method known as Rain Flow Counting. This stress spectrum cycle counting method ensures that the largest delta stress cycles (σ_{max} - σ_{min}) are not neglected in the analysis. Control point locations for both the MSR and LSR aircraft are shown in Figures 6 and 7, respectively.

Stress spectra are determined in two distinct manners. The primary method is to use data from the strain sensors installed onboard each aircraft. The secondary alternative is to calculate the stress spectra based upon other parameters collected by the FDR such as acceleration (g's), aircraft weight, airspeed and altitude. The IATP will use the secondary method only when the necessary strain sensor data are not available on a control point-by-control point, decompressed data file-by-decompressed data file basis. Transfer functions are established that define specific relationships between strain sensor values and/or various combinations of other parameters collected by the FDR in order to determine the appropriate values of

stress at each control point location. In addition, if the FDR data are completely or partially unusable, a gap-filling technique is employed by the IATP. This is accomplished by copying portions of decompressed data files from previously flown missions in an attempt to create data that are representative in terms of flight hours, landings, and pressure cycles.

The fatigue crack growth analysis involves the modeling of various structural control points on the Learjet Model 60 and Canadair Challenger CL601-3R. Each control point model consists of a crack growth system with one-dimensional and two-dimensional crack growth combined to achieve a multi-phase crack growth capability. Each crack growth model includes the relevant material properties, stress intensity solution, and crack growth retardation model. Crack growth involves an incremental growth (Δa) per stress cycle (ΔN). Material properties are included in the form of da/dN data. These data are a function of applied stress spectrum (σ_{max} and σ_{min}) and environment. Control point geometry effects are included through the use of a factor, β, such that the stress intensity, K, is given by:

$$K = \beta \sigma \sqrt{\pi a} \qquad \text{(Eqn. 1)}$$

Crack growth is retarded when an enlarged plastic zone is developed at the crack tip due to an overload. The crack growth retardation model incorporated in the IATP is the industry-accepted Generalized Willenborg Retardation Model.

INSPECTION INTERVALS

Inspection intervals for each control point are based upon a linear function of time with respect to structural failure of the control point. Initial as well as recurring inspection intervals are determined by each aircraft manufacturer. The IATP includes a comparison of calculated crack growth based on actual usage versus predicted crack growth in terms of crack length versus flight time. Criteria are implemented in the IATP to adjust inspection intervals when crack growth based on actual usage deviates from predicted crack growth.

Figure 8 depicts the initial inspection interval adjustment criterion. Let t_{ip} be the time corresponding to the predicted initial inspection. Let t_a be the time corresponding to the current crack length based on actual usage. Let t_p be the time at which the predicted crack growth curve would yield the same crack length corresponding to the crack growth curve based on actual usage. Therefore, the adjusted initial inspection time (t_{ia}) as a function of predicted initial inspection time is:

$$t_{ia} = (t_a/t_p) * t_{ip} \qquad \text{(Eqn. 2)}$$

The delta time to next inspection, Δt_i, is therefore defined as:

$$\Delta t_i = t_{ia} - t_a \qquad \text{(Eqn. 3)}$$

Figure 9 depicts the recurring inspection interval adjustment criterion. This criterion is identical to the initial inspection adjustment criterion except that the times t_a, t_p, t_{ia}, and t_{ip} are referred to the time of last inspection rather than time zero.

When actual crack growth deviates sufficiently, a significant change in usage is reported by the IATP. This occurs when there is a 10% reduction in the predicted inspection time interval ($t_{ia}/t_{ip} < 0.90$).

The IATP also has the ability to adjust the actual usage crack growth curve to account for inspection and maintenance results. This is depicted in Figure 9. The crack length is adjusted to the maximum non-detected length if no crack is found during inspection. Theoretically, the crack length could also be set to the length discovered during inspection; however, in practice, all cracks found during inspection will likely be repaired.

INSPECTION/MAINTENANCE SCHEDULING

Semi-annually the IATP data are compiled and reported to the FAA customer along with appropriate discussion and recommendations. Each semi-annual report relates the structural integrity status of the Flight Inspection Fleet. For example, the following information, at a minimum, is included in each semi-annual report: crack growth curve and stress exceedance curve for each control point for each aircraft for the current reporting period as well as accumulated totals, remaining hours to inspection or maintenance for each control point for each aircraft, a listing of the inspections and maintenance actions required during the following two calendar years for each aircraft; flight hours, landings, and pressure cycles grouped by individual aircraft and by aircraft type (MSR or LSR) for the current reporting period as well as accumulated totals, and a stress exceedance curve for each control point grouped by aircraft type (MSR or LSR).

Detailed inspections and maintenance procedures are included in the FSMP or maintenance manuals for each aircraft type. The inspection intervals are based upon the DADTA performed by each aircraft manufacturer using assumed initial baseline load spectra. The IATP semi-annual reports will convey any applicable

recommendations relative to inspection interval adjustment due to actual usage. This is of particular importance to safety in that each aircraft may experience a more severe loading in service than originally anticipated.

A link among the FAA customer, the FAA maintenance infrastructure, and Raytheon E-Systems is vital in order to ensure that inspection/maintenance results are incorporated into the IATP. This link ensures that inspection/maintenance information flows freely among the three entities. Each entity performs a function that affects the overall execution of the ASIP for the Flight Inspection Fleet.

Inspection/maintenance actions are dependent upon the projected usage of the fleet considering design mission profiles and the stress spectra that result from these missions. These baseline stress histories will either be validated by the IATP or indicate that an update is required. If the latter is found to be true, the DADTA will be re-evaluated with more accurate stress spectra from the L/ESS. This may then result in changes to the inspection intervals found in the FSMP for each control point.

CONCLUSION

As the FAA Flight Inspection MSR and LSR aircraft accumulate flight hours in a structurally harsh low-level environment, the IATP system will provide detailed inspection and maintenance recommendations to the FAA operator. Concurrently, the L/ESS data contained in the IATP will further define the loading spectrum unique to the operation of the MSR and LSR aircraft in the flight inspection environment. The careful application of results from the IATP will no doubt increase aircraft safety and reduce overall maintenance costs.

ACKNOWLEDGMENTS

The author is indebted to the FAA Structural Advisory Group (SAG) that was formed specifically for the FAA Flight Inspection Fleet ASIP. The FAA SAG is comprised of nationally recognized experts in the field of damage tolerance/fracture mechanics. Several key members of the FAA SAG include: Mr. Charles Tiffany, Dr. John Lincoln, Mr. Thomas Swift, and Mr. Leonard Wright. The FAA SAG provided valuable technical advice and guidance to Raytheon E-Systems, Learjet, and Canadair in the development and implementation of the FAA Flight Inspection Fleet ASIP.

The author also acknowledges the technical accomplishments of both Learjet and Canadair. Each was instrumental in the development of the FAA Flight

Inspection Fleet ASIP. The author is also indebted to several key Raytheon E-Systems personnel including: Mr. Richard Sayler, Mr. Robert Bishop, and Mr. Timothy Kelley. Finally, the author recognizes the efforts of the FAA personnel associated with the FAA Flight Inspection Program at the FAA Aircraft Maintenance and Engineering Division in Oklahoma City, OK.

REFERENCES

[1] Bombardier Learjet Report No. 50 SN85-6, Rev. B, Model 60 FIAS Service Life Analysis, December, 1996.

[2] Bombardier Canadair Report No. RAS 601-916, Rev. A, DADT Analysis for Inspection Aircraft, October, 1995.

[3] Federal Aviation Regulations Part 25, Airworthiness Standards: Transport Category Airplanes, February, 1965, as amended by Amendments 25-1 through 25-73.

DEFINITIONS, ACRONYMS, ABBREVIATIONS

ARINC	Aeronautical Radio Incorporated
ASIP	Aircraft Structural Integrity Program
BIT	Built-in Test
CGP	Cartridge Ground Program
CSMU	Crash Survivable Memory Unit
DADTA	Durability and Damage Tolerance Analysis
DDF	Decompressed Data File
DPD	Direct Parameter Display
DTIU	Data Transfer Interface Unit
DTM	Data Transfer Module
DTMR	Data Transfer Module Receptacle
ESDC	Engine Signal Data Converter
FAA	Federal Aviation Administration
FDP	Flight Data Panel
FDR	Flight Data Recorder
FDRIU	Flight Data Recorder Interface Unit
FSMP	Fleet Structural Maintenance Plan
GRDU	Ground Replay and Display Unit
GRE	Ground Replay Equipment
HP	Hewlett Packard
IATP	Individual Aircraft Tracking Program
ITT	Interturbine Temperature
L/ESS	Loads/ Environment Spectra Survey
LSR	Large Size/ Long Range (Canadair CL601-3R)
LRU	Line Replaceable Unit
MSL	Mean Sea Level
MSR	Medium Size/ Medium Range (Lear Model 60)
N1	Engine Fan Speed
N2	Engine Core Speed
OFP	Operational Flight Program
OGP	Operational Ground Program
PC	Personal Computer
SAG	Structural Advisory Group
SAU	Signal Acquisition Unit

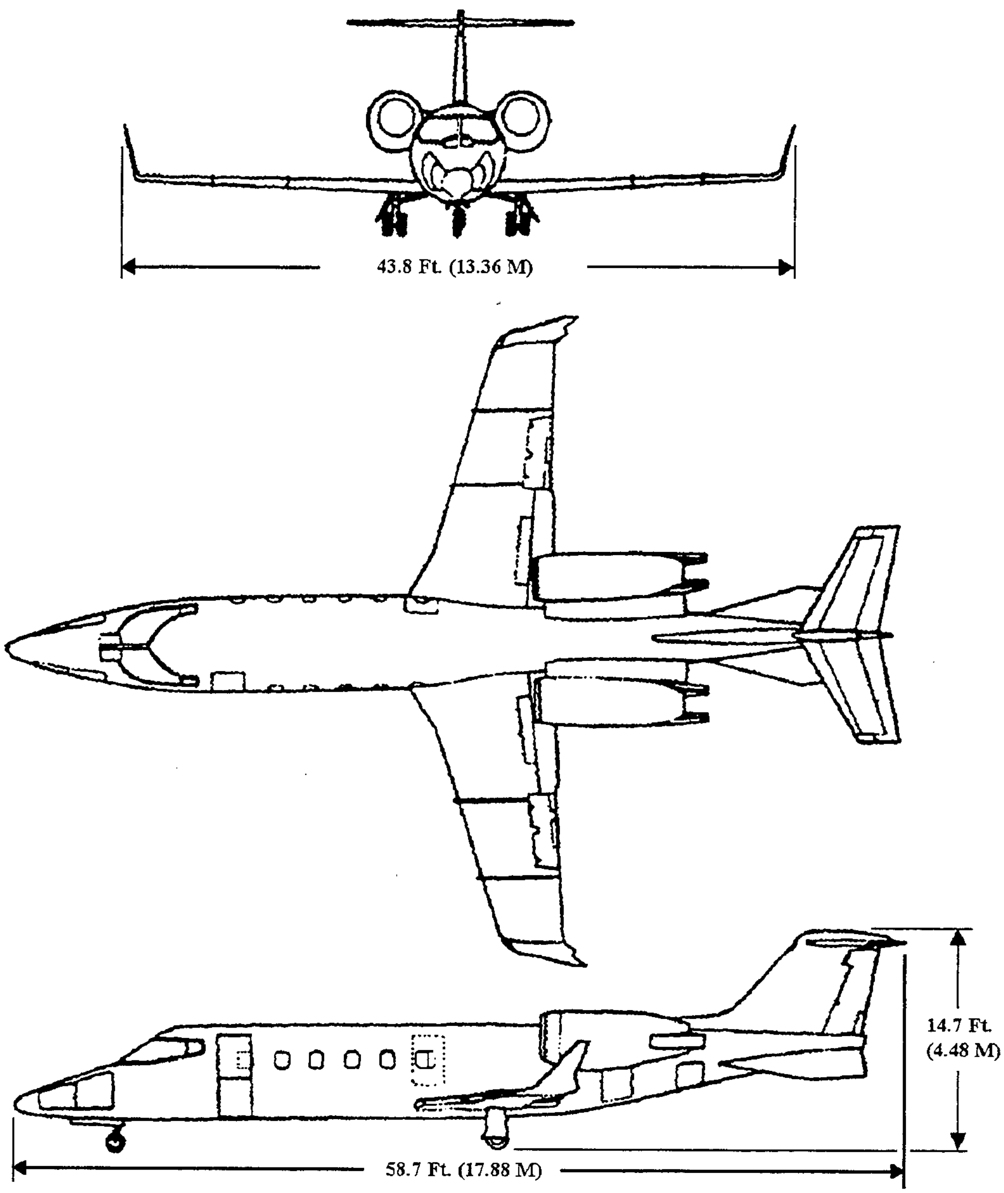

Figure 1

Learjet Model 60 MSR Flight Inspection Aircraft

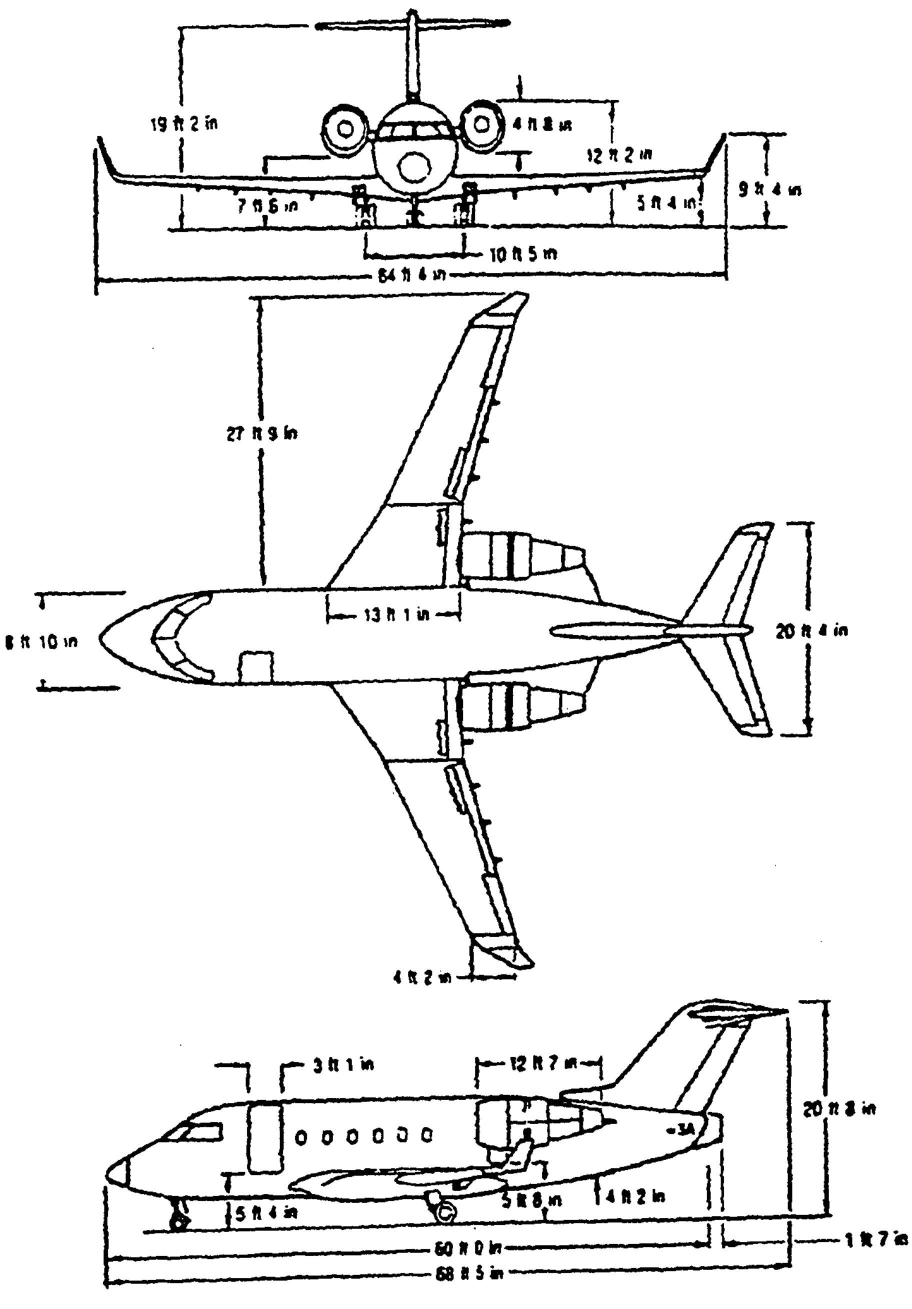

Figure 2

Canadair Challenger CL601-3R LSR Flight Inspection Aircraft

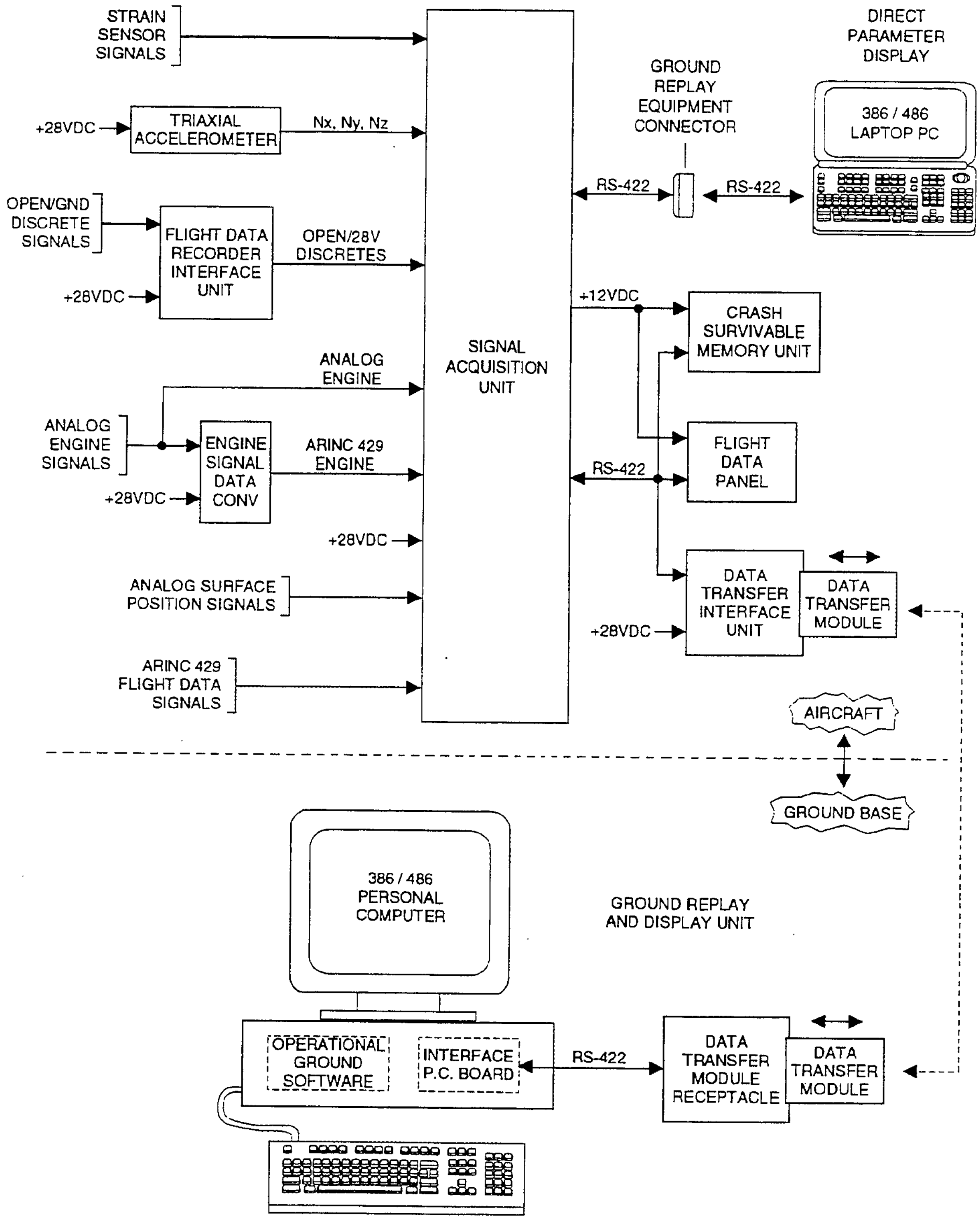

Figure 3

Flight Data Recorder System Diagram

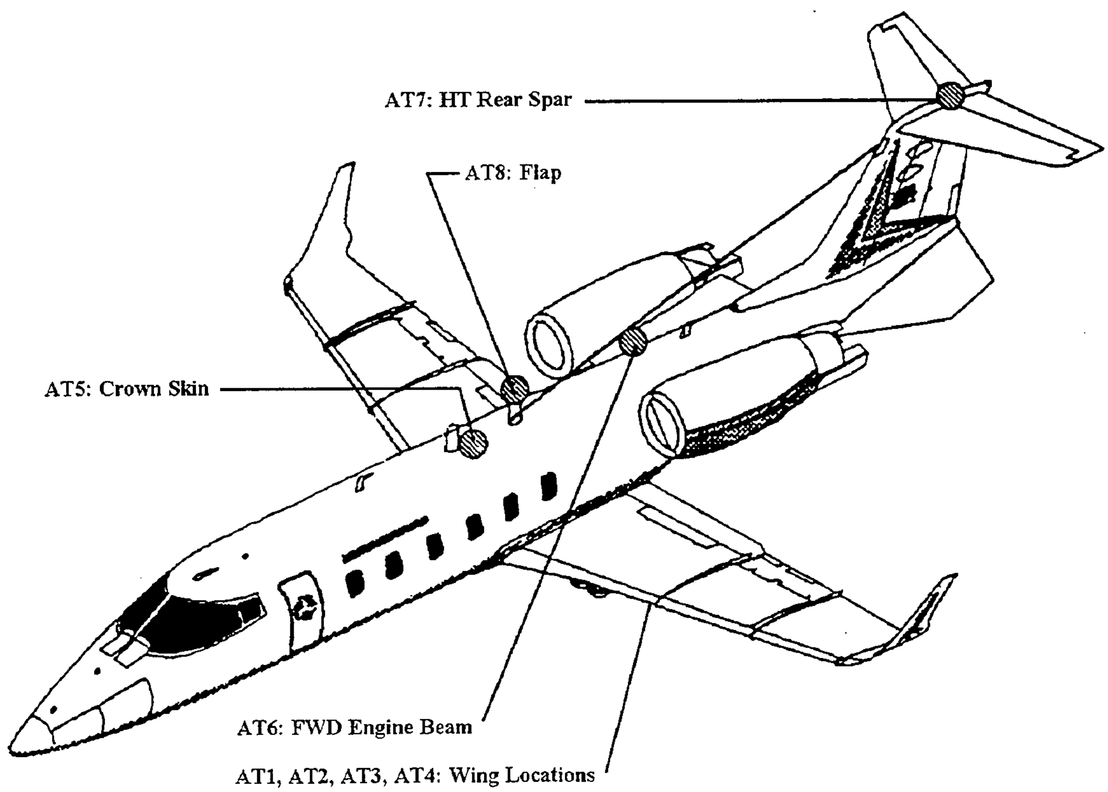

Figure 4

FAA Flight Inspection (MSR) Learjet Model 60

Flight Data Recorder Strain Sensor Locations

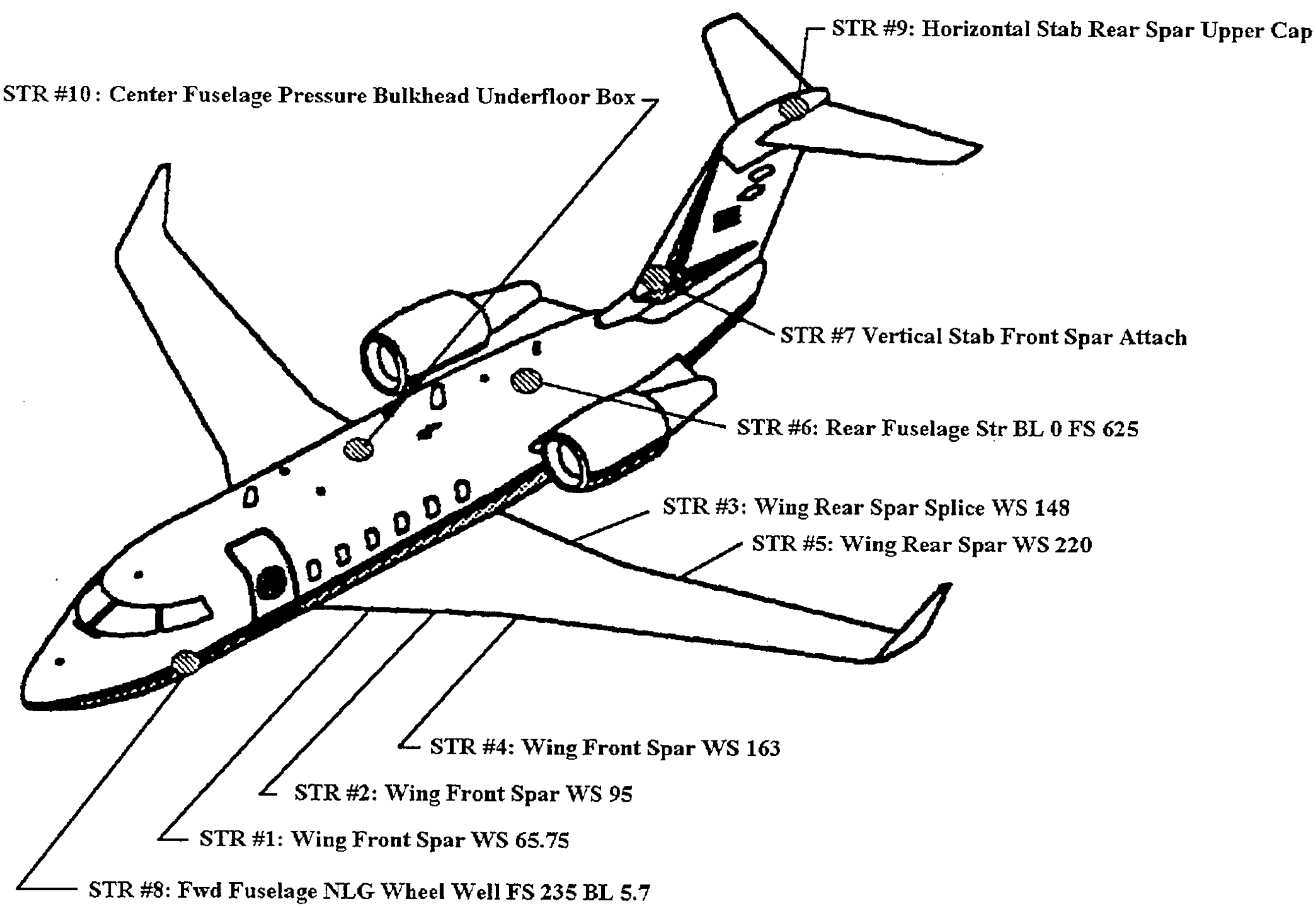

Figure 5

FAA Flight Inspection (LSR) Challenger CL601-3R

Flight Data Recorder Strain Sensor Locations

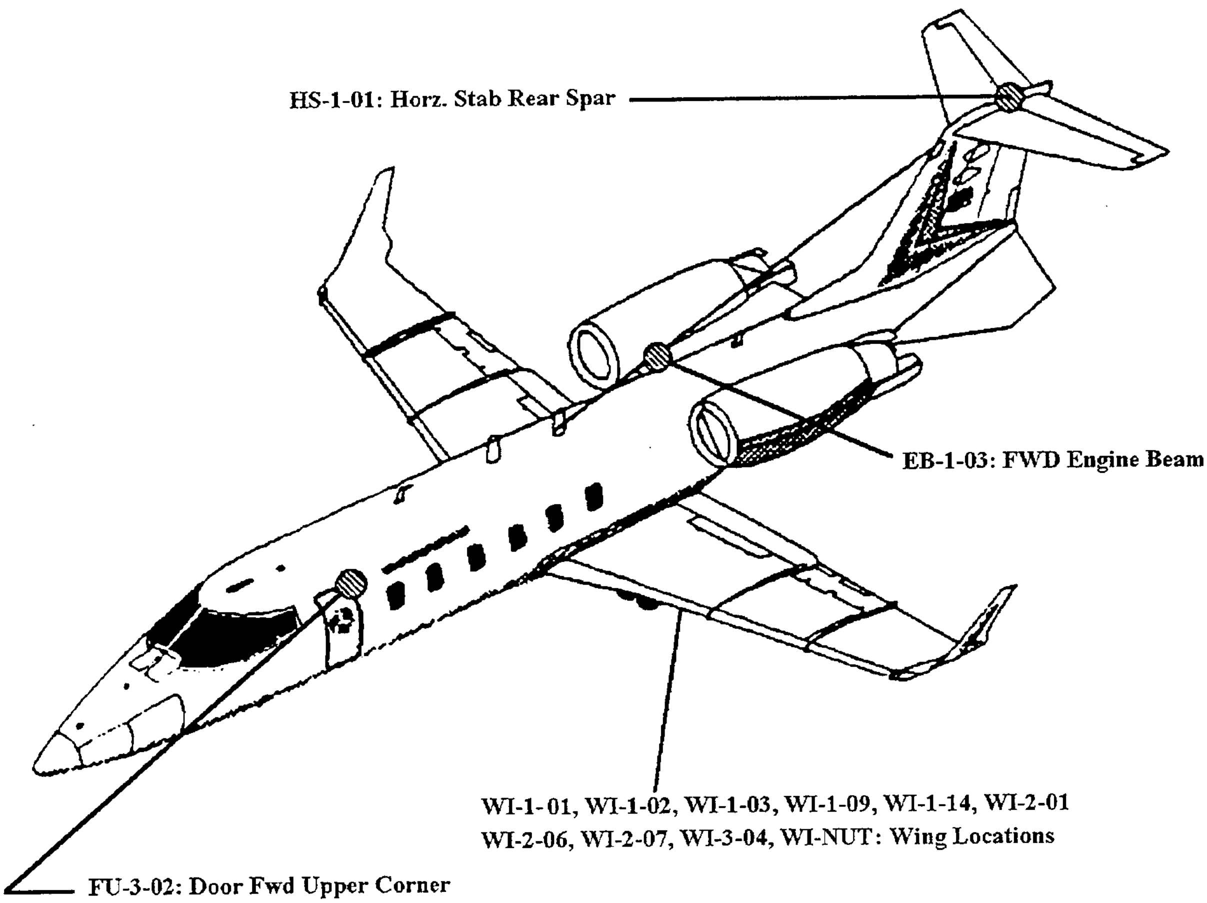

Figure 6

FAA Flight Inspection (MSR) Learjet Model 60

DADTA Control Point Locations

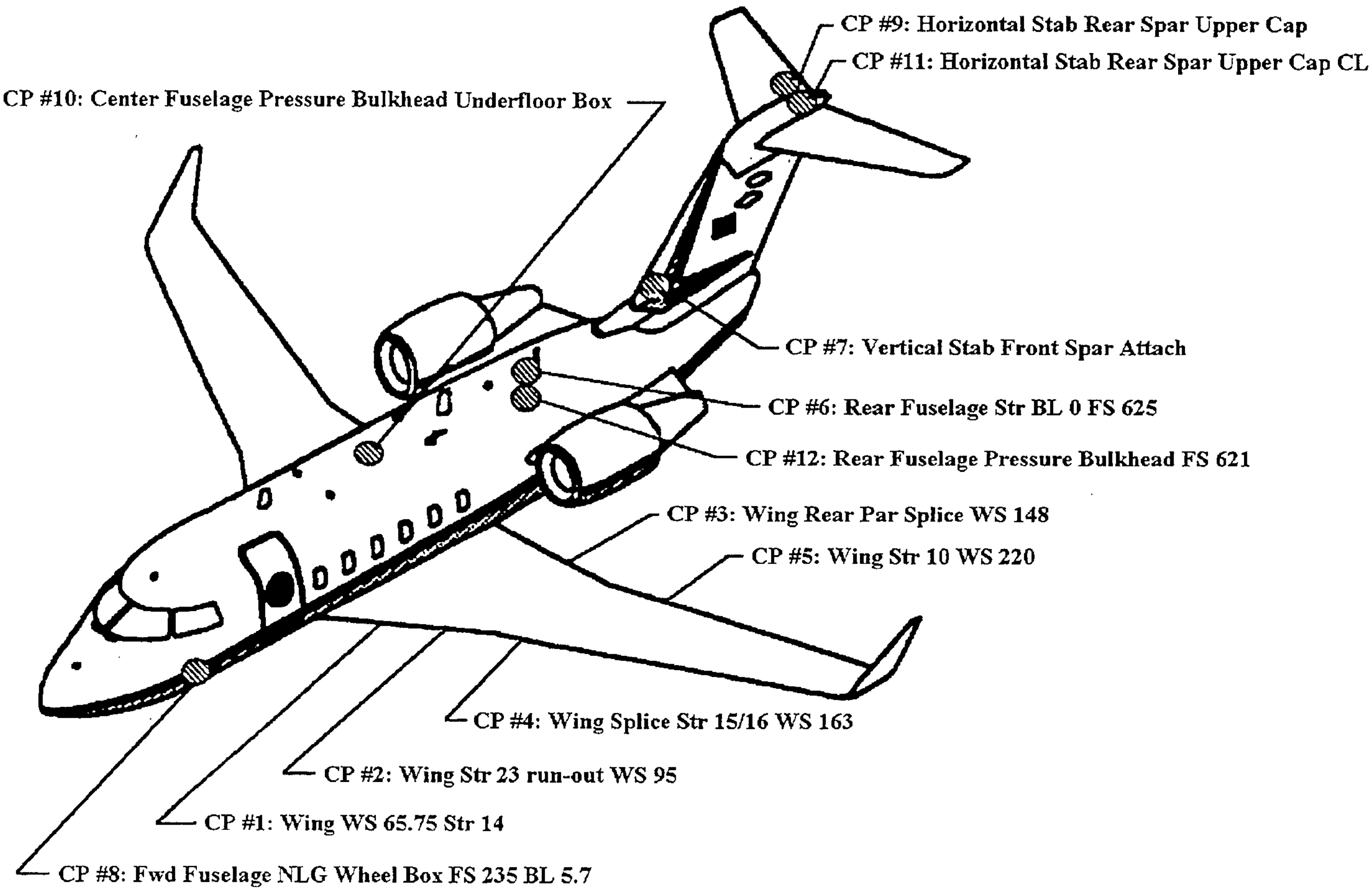

Figure 7

FAA Flight Inspection (LSR) Challenger CL601-3R

DADTA Control Point Locations

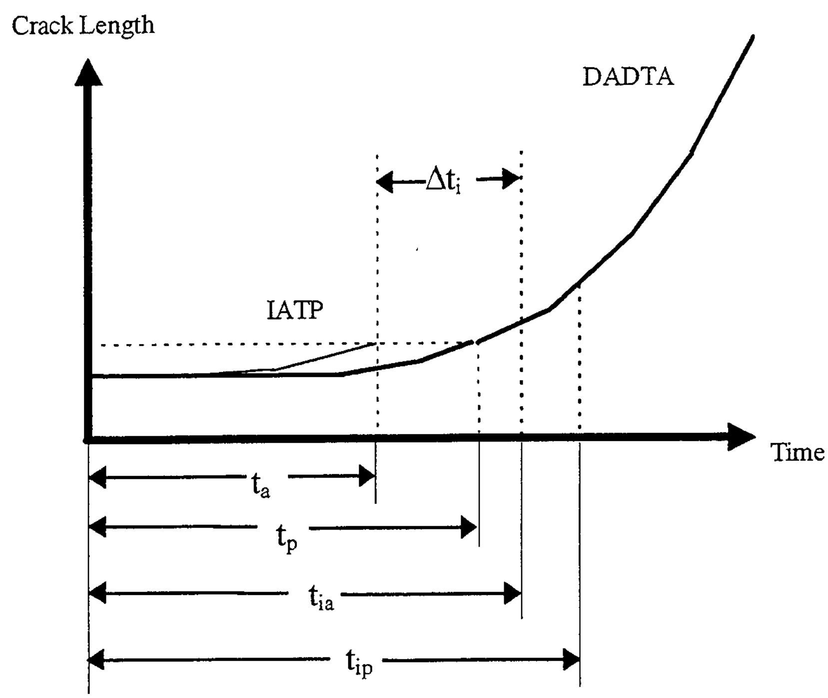

Figure 8

Initial Inspection Adjustment Criterion

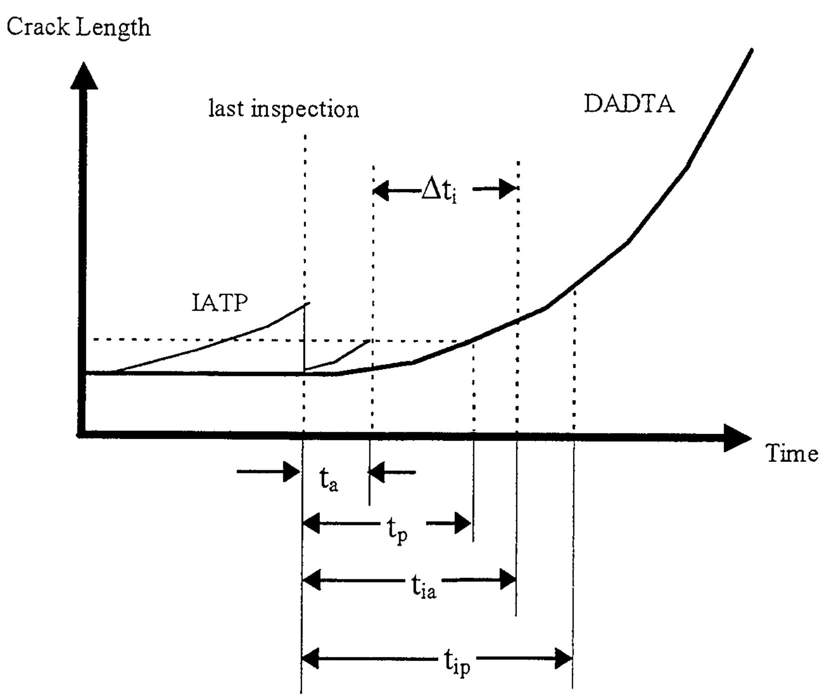

Figure 9

Recurring Inspection Adjustment Criterion

ATTENDANCE LIST

Mr RICHARD ABBOTT
RAYTHEON AIRCRAFT CO
MS 90B7
PO BOX 85
WICHITA KA 67201-0001
PH:(316)-676-7840 Fax:(316)-676-4126

MR JAMES ABEL
RAYTHEON E-SYST INC
FM1570 MAJORS FIELD
M/S CBN 192
GREENVILLE TX 75403-6056
PH:(903)-457-7708 Fax:(903)-457-4888

MR H NORMAN ABRAMSON
SOUTHWEST RES INST
6220 CULEBRA RD
PO DRAWER 28510
SAN ANTONIO TX 78228-0510
PH:(210)-522-2207 Fax:(210)-522-5122

MR JOHN ACH
USAF AFRL/VA
2790 D ST RM 504
BLDG 65
WRIGHT-PATTERSON AFB OH 45433-7402
PH:(937)-255-6104 Fax:(937)-656-4999

DR RICARDO ACTIS
ESRD INC
7750 CLAYTON RD
STE 204
ST LOUIS MO 63117-1342
PH:(314)-645-1423 Fax:(314)-645-1649

DR ROBERT ADDISON
ROCKWELL INTL CORP
1049 CAMINO DOS RIOS
PO BOX 1085
THOUSAND OAKS CA 91360-0001
PH:(805)-373-4251 Fax:(805)-373-4810

MS DONG AHN
DAEWOO HEAVY IND LTD
24 SEONGJU-DONG
CHANGWOON
KYUNSANGNOM-DO KOREA 00000-0001

MAJOR YUZI AIHARA
AIR STATT OFF/JASDF
9-7-45 AKASAKA
MINATO-KU
TOKYO JAPAN 184-0001

MR RUSSELL ALFORD
USAF WR-ALC/LJLEA
270 OCMULGEE CT
ROBINS AFB GA 31098-1646
PH:(912)-926-9146 Fax:(912)-926-9142

MR ROBERT ALLEN
LOCKHEED AERO SYS CO
M/S 0484 DEPT 73-51
86 S COBB DR
MARIETTA GA 30063-0484
PH:(770)-494-3972 Fax:(770)-494-2028

MR PHU AN
NAVAIRSYSCOM
BLDG 2187 STE 2320-B4
AIR 4.3.3.4
PATUXENT RIVER MD 20670-1547
PH:(301)-429-3261 Fax:(301)-342-9404

MR BRETT ANDERSON
BOEING COMMERCIAL AIRPLANE GRP
PO BOX 7730
M/S K31-19
WICHITA KS 67277-0001
PH:(316)-526-8725

MR MICHAEL ANDERSON
BOEING CO
00000-0001
PH:(206)-662-3062

MR CHARLES ANNIS
PRATT & WHITNEY
M/S 707-22
PO BOX 109600
W PALM BEACH FL 33410-9600
PH:(561)-796-6565 Fax:(561)-796-7454

MR ALBERT ARRICATA
TINKER AFB
4750 STAFF DR
TINKER AFB OK 73145-3317
PH:(405)-736-5008 Fax:(405)-738-3992

MR ADAR AZANCOT
ELECTRONIC INDUSTRIES LTD
PO BOX 2059
HERZLIYA B 46120-0001

MR ROBERT BADER
CONSULTANT
1613 KINGSWAY DR
XENIA OH 45385-9589
PH:(937)-255-0193 Fax:(937)-255-3740

MS DEBORAH BAILEY
USAF
2145 MONAHAN WAY
WPAFB OH 45433-7017
PH:(937)-255-6053 Fax:(937)-656-4410

DR ALAN BAKER
DEFENSE SCIENCE & TECH ORG
506 CORIMER ST
PO BOX 4331
MELBOURNE VICTORIA AUSTRALIA-3001

DR JOHN BAKUCKAS
FAA DEPT OF TRANS
MC AAR 433 BLDG 210
WILL J HUGHES TECH CTR
ATLANTIC CITY NJ 08405-0001
PH:(609)-485-4784 Fax:(609)-485-4569

MR DALE BALL
LOCKHEED FT WORTH CO
M/S 2275
LOCKHED BLVD
FT WORTH TX 76108-0001
PH:(817)-777-3760 Fax:(817)-777-2115

MR FELTON BARTLETT
US ARMY
LANGLEY RES CNTR
M/S 266
HAMPTON VA 23681-0001
PH:(757)-864-3956 Fax:(757)-864-7796

DR MIKE BASEHORE
FAA-W J HUGHES TECH CNTR
ATLANTIC CITY INT'L AIRPORT
ATLANTIC CITY NJ 08405-0001
PH:(609)-485-6342 Fax:(609)-485-4101

LTC GREGORY BAUGHMAN
USAF
6236 COURTSIDE DR
NORCROSS GA 30092-0001
PH:(770)-368-0233

MR SCOTT BAYS
BOEING
3801 S OLIVER
MS K84-40
WICHITA KS 67277-0001
PH:(316)-523-1311 Fax:(316)-526-4214

MR YVES BEAUVAIS
BOMBARDIER INC
MONTREAL INTL AIRPORT
CARGO RD A-4
MIRABEL QUEBEC CANADA J7N-1C7
PH:(514)-476-4414 Fax:(514)-476-4451

MR WILLIAM BECKER
MTS SYSTS CORP
26500 W AGOURA RD
M/S 202
CALABASAS CA 91302-5000
PH:(818)-878-9512 Fax:(818)-878-9515

DR THEODOR BEIER
BOEING PHANTOM WORKS
DEPT 341N M/S S102-2147
PO BOX 516
ST LOUIS MO 63166-0516
PH:(314)-232-0634 Fax:(314)-234-8915

MR ROBERT BELL
LOCKHEED MARTIN AERO SYS
DEPT 73-22 ZONE 0160
86 S COBB DR
MARIETTA GA 30063-0160
PH:(770)-494-5600 Fax:(770)-494-9610

DR ALAN BERENS
UNIV OF DAYTON RES INST
300 COLLEGE PARK AVE
DAYTON OH 45469-0120
PH:(937)-229-4475 Fax:(937)-229-3712

MR GUNNAR BERG
USAF
3001 STAFF DR
STE 1AG110
TINKER AFB OK 73145-3018
PH:(405)-736-3853 Fax:(405)-736-4188

MR ROBERT BERNSTEIN
MAT TECH INC
11661 SAN VICENTE BLVD
STE 707
LOS ANGELES CA 90049-0001
PH:(310)-208-5589 Fax:(310)-473-5177

MR HENRY BERRY
BERRY ENGINEERING INC
11712 C JEFFERSON AVE
NEWPORT NEWS VA 23606-0001
PH:(757)-596-4146 Fax:(757)-596-4146

MR REMMER BERTRAM
GERMAN AIR FORCE
HEIDERSTR 245
M/S PF 903500
COLOGNE, GERMANY 51140-0001

FIT LT STEPHEN BEVERLEY
ROYAL AIR FORCE
RAF ST ATHAN
SOUTH GLAMORGAN UK CF62 4WA-0001

DR CATHERINE BIGELOW
FEDERAL AVIATION ADMIN
WILLIAM J HUGHES TECH CNTR
AAR-430 BLDG 210
ATLANTIC CITY INTL NJ 08405-0001
PH:(609)-485-6662 Fax:(609)-485-4569

MR RONALD BIRDSEYE
LOCKHEED MARTIN AERO SYSTS
8B S COBB DR
M/S 0160
MARIETTA GA 30063-0001
PH:(770)-494-3100 Fax:(770)-494-9610

MR EDWARD BITTEL
ROYAL AIR FORCE
ROOM W114 SWALES PAVILION
M/S RAF WYTON
HUNTINGDON UK PE172DL-0001

MR NEIL BLAYLOCK
SOUTHWEST RES INST
BLDG 53 DIV 06
PO DRAWER 28510
SAN ANTONIO TX 78228-0510
PH:(210)-522-3238 Fax:(210)-522-5606

DR ANDERS BLOM
AERONAUTICAL RESEARCH INST OF SWEDE
PO BOX 11021
BROMMA SWEDEN S-161 11-0001

MR KEVIN BOYD
US AIR FORCE
2790 D ST RM 504
WPAFB OH 45433-7402
PH:(937)-255-0434 Fax:(937)-476-7379

MR ART BRAUN
MTS SYSTEMS CORP
AERO STRUCT & MATLS GRP
14000 TECH DR MS/231
EDEN PRAIRIE MN 55344-0001
PH:(612)-937-4045 Fax:(612)-937-4515

MR HENRY BRODMAN
GULFSTREAM AEROSPACE
M/S D-04
132 DUTCH ISLAND DR
SAVANNAH GA 31406-0001
PH:(912)-965-4897 Fax:(912)-965-4812

MR CRAIG BROOKS
APES INC
3542 OXFORD AVE
ST LOUIS MO 63143-0001
PH:(314)-644-6040 Fax:(314)-644-0229

MR ABRAHAM BROT
ISRAEL AIRCRAFT INDUSTRIES
DEPT 4441
BEN-GURION INTL AIRPORT
ISRAEL

MR ALBERT BRUETSCH
USAF
5020 DUDLEY BLVD
MCCLELLAN AFB CA 95652-1391
PH:(916)-643-5300 Fax:(916)-643-1405

DR FREDERICK BRUST
BATTELLE
505 KING AVE
COLUMBUS OH 43201-2693
PH:(614)-424-5034 Fax:(614)-424-3457

DR ROBERT BUCCI
ALCOA TECH CTR
100 TECHNICAL DR
ALCOA CTR PA 15069-0001
PH:(412)-337-2671 Fax:(412)-337-5436

MR WILLIAM BUCKEY
US AIR FORCE
2100 MONAHAN WAY
FLIGHT TRAINING SPO
WRIGHT-PATTERSON AFB OH 45433-7014
PH:(937)-255-7076 Fax:(937)-255-8516

MR STEVEN BULLOCK
LOCKHEED MARTIN SKUNK WORKS
BLDG 611-2 DEPT 72-16
1011 LOCKHEED WAY
PALMDALE CA 93599-7216
PH:(805)-572-7808 Fax:(805)-572-7515

MR JEFFREY BUNCH
NORTHROP GRUMMAN CORP
8900 E WASHINGTON BLVD
M/S 6J80/UB
PICO RIVERA CA 90660-0001
PH:(562)-948-8685

DR O HAL BURNSIDE
SOUTHWEST RES INST
6220 CULEBRA RD
SAN ANTONIO TX 78238-5166
PH:(210)-522-2332 Fax:(210)-522-3042

MR BERND BURZYNSKI
GERMAN AIR FORCE
HEIDESTR 245
M/S PF 902500
COLOGNE, GERMANY 51140-0001

DR LAWRENCE BUTKUS
USAF ASC/EN
2530 LOOP RD WEST
WRIGHT-PATTERSON AFB OH 45431-7101
PH:(937)-255-7138 Fax:(937)-656-4546

MR STEPHEN CALLARY
CELERIS AEROSPACE CANADA INC
255 CENTRUM BLVD
ORLEANS ONTARIO
CANADA K1E 3V8-0001
PH:(613)-837-1161 Fax:(613)-834-6420

DR JOHN CAMMETT
NAVAL AVIATION DEPOT
PSC BOX 8021
CHERRY POINT NC 28533-0021
PH:(919)-464-7168 Fax:(919)-464-8108

MR DAVID CAMPBELL
LOCKHEED MARTIN AERO SYSTS
86 S COBB DR
M/S 0580
MARIETTA GA 30063-0001
PH:(770)-494-1128 Fax:(720)-494-8478

MR JOSEPH CARDINAL
SOUTHWEST RES INST
6220 CULEBRA RD
SAN ANTONIO TX 78238-5166
PH:(210)-522-3323 Fax:(210)-522-3042

MR JOSEPH CARLOS
SIKORSKY AIRCRAFT
6900 MAIN ST, MS S313A2
STRATFORD CT 06497-0001
PH:(203)-386-5214 Fax:(203)-386-7496

MR ANDERS CARLSSON
SAAB AB
LINKOPING SWEDEN SE-58188-0001

MR DOUGLAS CARMODY
NORTHROP GRUMMAN
2000 NASA BLVD
M/S H11-223
MELBOURNE FL 32902-0001
PH:(407)-726-7821 Fax:(407)-951-6115

DR CHRISTOS CHAMIS
NASA LEWIS RES CTR
21000 BROOKPARK RD
M/S 49-7
CLEVELAND OH 44135-3191
PH:(216)-433-3252 Fax:(216)-433-5802

MR PAUL CHAPMAN
LEARJET
ONE LEARJET WAY
M/S 29
WICHITA KS 67277-7707
PH:(316)-946-6367 Fax:(316)-946-2990

MR JEAN CHAREST
BOMBARDIER INC
10000 CARGO A-4 STREET
MONTREAL INTNATL AIRPORT
MIRABEL QUEBEC CANAD J7N 1H3-0001
PH:(514)-476-4168 Fax:(514)-476-4451

MR CHUN CHEN
MCDONNELL DOUGLAS AEROSPACE W
M/S C071-0034
2401 E WARDLOS RD
LONG BEACH CA 90807-0001
PH:(562)-593-2385 Fax:(562)-982-7367

MR FRED CHILD
LOCKHEED MARTIN AERO SYS
M/S D59-10 ZONE 0050
86 S COBB DR
MARIETTA GA 30063-0617
PH:(770)-494-5430 Fax:(770)-494-5104

DR JAYCEE CHUNG
RAYTHEON E-SYSTEMS
CBN 204 MAJORS FIELD/FM1570
PO BOX 6056
GREENVILLE TX 75403-6056
PH:(903)-457-5096 Fax:(903)-408-8793

MR JOHN CICERO
SYS & ELECTRONICS INC
190 GORDON ST
ELK GROVE VILLAGE IL 60007-0001

MR AL CLARK
OC-ALC/LHR
3001 STAFF DR
STE 2AH191
TINKER AFB OK 73145-3021
PH:(405)-736-5643 Fax:(405)-736-2717

DR ALLAN CLAUER
LSP TECHNOLOGIES
6145 B SCHERERS PL
DUBLIN OH 43016-1272
PH:(614)-718-3000 Fax:(614)-718-3007

MR JOSEPH COCHRAN
LOCKHEED AERO SYS CO
DEPT 73-25 ZONE 0160
86 S COBB DR
MARIETTA GA 30063-0160
PH:(770)-494-2166 Fax:(770)-494-9610

MR ELIAS COLLAS
US AIR FORCE
SA-ALC/LADD BLDG 823
514 SHOP LN STE 2
KELLY AFB TX 78241-6434
PH:(210)-925-4525 Fax:(210)-925-1416

MR DALE COLTER
USAF
2543 HOLLEY CT
NAVARRE FL 32566-0001
PH:(904)-939-5379 Fax:(904)-884-4983

MR THOMAS COOPER
UNIVERSAL TECHNOLOGY CORP
1270 N FAIRFIELD RD
DAYTON OH 45432-2600
PH:(937)-426-8530 Fax:(937)-426-8755

MR DALE COPE
BOEING DEF & SPACE GRP
PO BOX 7730
M/S K8681
WICHITA KS 67277-7730
PH:(316)-526-9873 Fax:(316)-523-3130

MR DOUGLAS CORNOG
USAF ASC/EN
2530 LOOP RD WEST
WRIGHT-PATTERSON AFB OH 45433-7101
PH:(937)-255-8375 Fax:(937)-476-4546

MR LAWRENCE CORNWELL
US COAST GUARD
265 OCMULGEE CT
M/S LBCG
ROBINS AFB GA 31098-1647
PH:(912)-926-2018 Fax:(912)-752-8209

MR WILLIAM CORWIN
OAK RIDGE NATL LAB
PO BOX 2008
MS 6161
OAK RIDGE TN 37831-6161
PH:(423)-574-4648 Fax:(423)-574-4066

MR SCOTT COTE
NAVAL AIR WARFARE CTR
22195 ELMER RD
UNIT 4
PATUXENT RIVER MD 20670-0001
PH:(301)-757-0514

MR THOMAS COURBE
FRENCH MINISTRY OF DEFENCE
DEPT STPA
26 BLVD VICTOR
PARIS FRANCE 00460 ARMEES-0001

MR BRITT COVINGTON
AIR FORCE SAFETY CTR
9700 G AVE SE
STE 250C
KIRTLAND AFB NM 87117-5670
PH:(505)-846-0990 Fax:(505)-846-6826

MR WILLIAM COWIE
GE AIRCRAFT ENGINES
M/D Q105
ONE NEUMANN WAY
EVENDALE OH 45215-6301
PH:(513)-243-1133

MR BRADFORD COWLES
PRATT & WHITNEY
MS 707-22
PO BOX 109600
WEST PALM BEACH FL 33410-9600
PH:(561)-796-6554 Fax:(561)-796-6443

DR JOE COX
ARTI/DYNCORP
ONE RIDGMAR CENTRE
6500 WEST FREEWAY
FORT WORTH TX 76116-2187
PH:(817)-732-4481 Fax:(817)-737-1605

DR MATTHEW CREAGER
STRUCTURAL INTEGRITY ENGRG
STE 200
9560 TOPANGA CANYON BLVD
CHATSWORTH CA 91311-0001
PH:(818)-718-2195 Fax:(818)-718-2212

MR JAMES CRONKHITE
BELL HELLICOPTER TEXTRON INC
600 E HURST BLVD
HURST TX 76052-0001
PH:(817)-280-5597 Fax:(817)-280-4933

MR WIEDE CUTSHALL
ADSI
351 E RAMSEY
SAN ANTONIO TX 78216-0001
PH:(210)-979-7698 Fax:(210)-979-7698

MR JAMES DALY
METAL IMPROVEMENT CO
10 FOREST AVE
PARAMUS NJ 07652-0001
PH:(201)-843-7800 Fax:(201)-843-3460

MR FRANK DANIELS
BOEING NORTH AMERICAN
MAIL CODE AD60
12214 LAKEWOOD BLVD
DOWNEY CA 90242-2693
PH:(562)-922-5126 Fax:(562)-922-1292

MR EDWARD DAVIDSON
USAF ASC/ENFS
2530 LOOP RD WEST
WRIGHT PATTERSON AFB OH 45433-0001
PH:(937)-255-8596

MR JOHN DAVIES
BOMBARDIER INC
MONTREAL INTL AIRPORT
10000 CARGO ST A-4
MIRABEL QUEBEC CANADA J7N-1H3
PH:(514)-476-4352 Fax:(514)-476-4207

DR GUY DAVIS
DACCO SCI INC
10260 OLD COLUMBIA RD
COLUMBIA MD 21046-0001
PH:(410)-381-9475 Fax:(410)-381-9643

DR DAVID DAWICKE
NASA LANGLEY RES CTR
M/S 188E
HAMPTON VA 23681-0091
PH:(757)-864-3477 Fax:(757)-864-8911

MR TIM DEMPSEY
MTS SYST CORP
250 S STEMMONS
LEWISVILLE TX 75067-0001
PH:(972)-221-2713 Fax:(972)-221-4315

MR CLAUDE DESROCHERS
MARTEC LIMITED
STE 400
1888 BRUNSWICK ST
HALIFAX NOVA SCOTIA CANADA B3J-3J8
PH:(902)-425-5101 Fax:(902)-421-1923

MR JOSE DIAZ ALONSO
SPANISH AIR FORCE
AV AVIACION SIN
MADRID SPAIN 28044-0001

2LT NATHANIEL DIEDRICH
USAF AFRL/MLLP
BLDG 655
2230 TENTH ST STE 1
WRIGHT-PATTERSON AFB OH 45433-7817
PH:(937)-255-9796 Fax:(937)-255-9804

DR B BORO DJORDJEVIC
THE JOHNS HOPKINS UNIV
CNDE/MARYLAND HALL 102
3400 N CHARLES ST
BALTIMORE MD 21218-0001
PH:(410)-516-5215 Fax:(410)-516-5293

MR ALAN DOBYNS
SIKORSKY AIRCRAFT
M/S S314A
STRATFORD CT 06497-0001
PH:(203)-386-3818 Fax:(203)-386-3717

DR PAUL DOMAS
GE AIRCRAFT ENGINES
PO BOX 156301
ONE NEUMANN WAY M/S K105
CINCINNATI OH 45215-6301
PH:(513)-243-4894 Fax:(513)-243-4888

MR MIKE DUBBERLY
FATIGUE TECH INC
6250 TERRAPIN DR
MANASSAS VA 22111-3807
PH:(703)-791-3634 Fax:(703)-791-5467

MR JONATHAN DUBKE
US AIR FORCE
SA-ALC/LADD
404 GREIG ST BLDG 179
KELLY AFB TX 78241-5944
PH:(210)-925-4525 Fax:(210)-925-1416

DR VERONIQUE DUBOIS
SWISS AIRCRAFT & SYS CO
SYS MGMT & FATIGUE ENGRG
PO BOX 301
EMMEN SWITZERLAND 6032-0001

MR ROBERT EASTIN
FAA
3960 PARAMOUNT ST
LAKEWOOD CA 90712-4137
PH:(562)-627-5205 Fax:(562)-627-5210

MR RANDAL EDWARDS
ROCKWELL INTL-NAAD
PO BOX 3644/MS SL 15
2600 WESTMINSTER BLVD
SEAL BEACH CA 90740-7644
PH:(310)-797-2842 Fax:(310)-797-3756

DR CHARLES ELLIOTT
UNIV OF UTAH / QIDEC
50 S CENTRAL CAMPUS DR
RM 2202
SALT LAKE CITY UT 84112-9208
PH:(801)-581-8981 Fax:(801)-585-9826

MR MICHAEL ELLIOTT
USAF
5022 BAILEY LOOP
MCCLELLAN AFB CA 95652-1369
PH:(916)-643-0372 Fax:(916)-643-0361

MR WILLIAM ELLIOTT
USAF WR-ALC/TIED
420 SECOND ST STE 122
ROBINS AFB GA 31098-1637
PH:(912)-926-9835 Fax:(912)-926-1743

MR GERALD ELMERS
US AIR FORCE WL/MLMA
BLDG 22B STE 2
2500 P STREET
WRIGHT-PATTERSON AFB OH 45433-7405
PH:(937)-255-2456 Fax:(937)-255-1268

MS ANN EMBREY
FEDERAL AVIATION ADMIN
M/S AVN-347
6500 S MCARTHUR
OKLAHOMA CITY OK 73125-4932
PH:(405)-954-8713 Fax:(405)-954-9532

MS HELEN ENG
USAF ASC/ENFS
2530 LOOP ROAD WEST
WRIGHT-PATTERSON AFB OH 45433-7101
PH:(937)-255-6464 Fax:(937)-656-4546

MR TERRY ERCOLANI
CESSNA AIRCRAFT CO
1 CESSNA BLVD
M/S W7-6
WICHITA KS 67277-7704
PH:(316)-941-8421 Fax:(316)-941-7395

MR CENAP ERENBEN
DE HAVILLAND INC
123 GARRATT BLVD
DOWNSVIEW ONTARIO
M3K 1Y5 CANADA 00000-0001
PH:(416)-373-5196 Fax:(416)-375-4539

MR GAVIN EVANS
USAF
3001 STAFF DR
STE 2AB 85A
TINKER AFB OK 73145-0001
PH:(405)-736-7264 Fax:(405)-736-5598

MR RICHARD EVERETT
US ARMY VEHICLE STRUCTURES DIR
M/S 188E
2 W REID ST
HAMPTON VA 23681-0001
PH:(804)-864-3459 Fax:(804)-864-8911

MR TIMOTHY FALLON
NAVAIR
48110 SHAW RD
BLDG 2187 STE 2320A
PATUXENT RIVER MD 20670-1906
PH:(301)-342-9325 Fax:(301)-342-9402

MR MICHAEL FALUGI
USAF
2130 EIGHTH ST STE 1
WRIGHT-PATTERSON AFB OH 45433-7542
PH:(937)-255-6639 Fax:(937)-255-7723

MR PHILLIP FARLEY
US AIR FORCE
SA-ALC/LFESCG
485 QUENNTIN ROOSEVELT RD
SAN ANTONIO TX 78241-6425
PH:(210)-925-4284 Fax:(210)-925-0097

CAPT SCOTT FAWAZ
US AIR FORCE
2790 D ST
BLDG 65 RM 504
WPAFB OH 45433-7402
PH:(937)-255-6104 Fax:(937)-656-4999

MR JAY FIEBIG
WR ALL/TIEDO
420 SECOND ST
STE 100
ROBINS AFB GA 31098-1640
PH:(912)-926-4228 Fax:(912)-926-1640

MR SCOTT FIELDS
BOEING CO
M/S 1022147
PO BOX 516
ST LOUIS MO 63166-0001
PH:(314)-234-0032 Fax:(314)-234-8915

MR RONAN FINLEY
BOEING
PO BOX 3707
SEATTLE WA 98124-2207
PH:(253)-657-0470 Fax:(253)-657-3736

MR JAY FISHER
SOUTHWEST RES INST
6220 CULEBRA RD
PO DRAWER 28510
SAN ANTONIO TX 78238-5166
PH:(210)-522-2028 Fax:(210)-684-4822

MR JOHN FLOOD
BOEING
PO BOX 516
M/SS111-1221
ST LOUIS MO 63166-0001
PH:(314)-232-7623 Fax:(314)-232-1394

MS LEONA FLORES
ABDA INC
3040 PRESIDENTIAL DR
STE 201
FAIRBORN OH 45324-0001
PH:(937)-427-2229 Fax:(937)-427-1937

DR THOMAS FLOURNOY
FAA
FAR TECHNICAL CTR
ATLANTIC CITY NJ 08405-0001
PH:(609)-485-5327 Fax:(609)-485-4569

MR TIMOTHY FOLAND
NORTHRUP GRUMMAN
PO BOX 9650
M/S H11-223
MELBOURNE FL 32902-9650
PH:(407)-951-6893 Fax:(407)-951-6048

MR JAMES FOLCK
USAF
BLDG 652 STE 1
2179 TWELTH ST
WRIGHT-PATTERSON AFB OH 45433-7718
PH:(937)-255-7484 Fax:(937)-476-4419

MR GEORGE FOO
SINGAPORE AEROSPACE
540 AIRPORT RD
PAXA LEBAR
SINGAPORE 539938-0001

MR SYLVAIN FORGUES
BOMBARDIER INC
10000 CARGO A-4 ST
MONTREAL INTL AIRPORT
MIRABEL QUEBEC CANADA J7N-1H3
PH:(514)-476-4201 Fax:(514)-476-4207

MR ROYCE FORMAN
NASA JOHNSON SPACE CTR
2101 NASA RD ONE
M/S AH3
HOUSTON TX 77058-0001
PH:(281)-483-8926 Fax:(281)-244-2319

MR DONALD FORNEY
UNIVERSAL TECH CORP
1270 N FAIRFIELD RD
DAYTON OH 45432-2600
PH:(937)-426-8530 Fax:(937)-426-7753

MR SCOTT FORTH
UNITED TECH RES CTR
411 SILVER LANE
M/S 129-73
EAST HARTFORD CT 06108-0001
PH:(860)-610-7883 Fax:(860)-610-7526

MS ANDREA FOTIAS
SMITHS INDUSTRIES
4141 EASTERN AVE
M/S 119
GRAND RAPIDS MI 49518-0001
PH:(616)-241-8678 Fax:(616)-241-7965

MS CHERYL FRANCIS
NAVAL AVIATION DEPOT
CODE 342
PSC BOX 8021
CHERRY POINT NC 28533-0021

MR RONALD FRANCIS
NAVAL AIR SYSTS COMD
STE 5
6255 LAKE GRAY BLVD
JACKSONVILLE FL 32244-0001
PH:(904)-779-3544 Fax:(904)-779-3507

MR JOBST FRANK
GERMAN MOD
AMC PO BOX 33668
WRIGHT-PATTERSON AFB OH 45433-0668
PH:(937)-255-6660 Fax:(937)-255-7260

MAJ ROBERT FREDELL
HQ USAFA/DFEM
STE 6H2
2354 FAIRCHILD DR
US AIR FORCE ACADEMY CO 80840-6240
PH:(719)-333-4393 Fax:(719)-333-2944

MR CARL FRENCH
BOEING DEF & SPC GRP
2601 LIBERTY PKWY
RM-00
MIDWEST CITY OK 73110-0001
PH:(405)-739-1410 Fax:(405)-739-1416

MR DOUGLAS FRIEND
GEORGIA TECH RES INST
7220 RICHARDSON RD
BLDG 2-150
SMYRNA GA 30080-0001
PH:(770)-528-7924 Fax:(770)-528-3271

DR JOSEPH GALLAGHER
USAF AFRL/XPZ
2130 EIGHTH ST
WPAFB OH 45433-7542
PH:(937)-255-4269 Fax:(937)-656-4646

MR HAROLD GAY
NAVAL AVIATION DEPOT
PSC 8021
MCAS CHERRY POINT
CHERRY POINT NC 28533-0021
PH:(919)-466-8517 Fax:(919)-466-8517

MR WILLIAM GEESE
USAF
1912 MONAHAN WAY
WRIGHT-PATTERSON AFB OH 45433-7205
PH:(937)-656-5652 Fax:(937)-656-4896

MR MICHAEL GEORGE
LOCKHEED MARTIN AERO
103 CHESAPEAKE PARK PLAZA
M/S 40
BALTIMORE MD 21220-0001
PH:(410)-682-2144 Fax:(410)-682-0531

MR ROBERT GERAMI
USAF ASC/ENFS
2530 LOOP RD WEST
WRIGHT-PATTERSON AFB OH 45433-7101
PH:(937)-255-3330 Fax:(937)-656-4546

MR FRANCIS GERBER
DAYTON T BROWN INC
DEPT 17
555 CHURCH ST
BOHEMIA NY 11716-0001
PH:(516)-589-6300 Fax:(516)-567-9045

SQNLDR ALEXANDER GIBBS
ROYAL AUSTRALIAN AF
WR-ALC/FM-AT
480 SECOND ST STE 200
ROBINS AFB GA 31098-1640
PH:(912)-926-2580 Fax:(912)-328-3502

MR ROBERT GIESE
USAF OO-ALC/LACM
7278 4TH ST
HILL AFB UT 84056-5205
PH:(801)-777-4970 Fax:(801)-777-9482

DR NEIL GOLDFINE
JENTEK SENSORS INC
200 DEXTER AVE
WATERTOWN MA 02172-0001
PH:(617)-926-8422 Fax:(617)-926-8744

DR MATTHEW GOLIS
ADVANCED QUALITY CONCEPTS
PO BOX 141388
COLUMBUS OH 43214-0001
PH:(614)-268-0518 Fax:(614)-267-6288

MR ALLEN GONSISKA
USAF ASC/EN
2530 LOOP RD WEST
WRIGHT-PATTERSON AFB OH 45433-7101
PH:(937)-255-5485 Fax:(937)-656-4546

MAJ RAFAEL GONZALEZ
SPANISH AIR FORCE
AV AVIACION S/N
MADRID SPAIN 28046-0001

MR MARKUS GOTTIER
MCDONNELL DOUGLAS CORP
M/S S2704396
5775 CAMPUS PKWY
ST LOUIS MO 63042-0516
PH:(314)-232-4932 Fax:(314)-232-1672

MR PETER GOULD
RAYTHEON ACFT CO
9709 E CENTRAL
M/S B90
WICHITA KS 67037-0001
PH:(316)-676-7898 Fax:(316)-676-6787

MR STEPHEN GOULD
US AIR FORCE
SA-ALC/LADD
514 SHOP LN/STE 2
KELLY AFB TX 78241-6434
PH:(210)-925-4525 Fax:(210)-925-9940

MR BOHDAN GOYANIUK
TRANSPORT CANADA
AARDD-S
200 KENT ST 7TH FLOOR
OTTAWA ONTARIO CANADA K1A-ON8
PH:(613)-952-4410 Fax:(613)-996-9178

DR ALTEN GRANDT
PURDUE UNIV
AERO & ASTRO
1282 GRISSOM HALL
W LAFAYETTE IN 47907-1282
PH:(765)-494-5141 Fax:(765)-494-0307

MR JONATHAN GREENE
F&S INC
2801 COMMERCE ST
BLACKSBURG VA 24060-0001
PH:(540)-953-4269 Fax:(540)-951-0760

MR LOUIS GRENIER
BOMBARDIER AEROSPACE
400 COTE UERTU QUEST
MONTREAL QUEBEC CANADA-0001
PH:(514)-855-7548 Fax:(514)-855-7202

MR STEPHEN GRESLEY
SMITHS INDUSTRIES
M/S 231
4141 EASTERN SE
GRAND RAPIDS MI 49505-8727
PH:(616)-241-8643 Fax:(616)-241-7318

MR FRANK GRIMSLEY
US AIR FORCE
ASC/YC
WRIGHT-PATTERSON AFB OH 45440-0001
PH:(937)-255-1024 Fax:(000)-000-0001

CAPT DAN GRONER
USAF
2145 MONAHAN WAY
WPAFB OH 45433-7017
PH:(937)-255-5664 Fax:(937)-656-7723

MR CORNELIS GUIJT
HQ USAFA/DFEN
STE 6H2
2354 FAIRCHILD DR
US AIR FORCE ACADEMY CO 80840-6240
PH:(719)-333-3043 Fax:(719)-333-2944

MR ALAN GUNDERSON
UNIVERSAL TECH CORP
1270 N FAIRFIELD RD
DAYTON OH 45432-2600
PH:(937)-426-8530 Fax:(937)-426-7753

MR GEORG GUNTHER
DAIMLER-BENZ AERO AG
PO 801160
MUNICH GERMANY 81663-0001

MR ANDERS GUSTAVSSON
SWEDISH DEF MATL ADMIN
S-115 88 STOCKHOLM SWEDEN-0001

MR FRED HAAKE
PRATT & WHITNEY
M/S 707-22
PO BOX 109600
WEST PALM BEACH FL 33410-9600
PH:(561)-796-6579 Fax:(561)-796-6443

MR LLOYD HACKEL
LAWRENCE LIVERMORE NATL LAB
PO BOX 5508
MS L-446
LIVERMORE CA 94550-0001
PH:(510)-422-9009 Fax:(510)-422-9554

MR RICHARD HADCOCK
RNH ASSOCIATES INC
6 SUE CIRCLE
HUNTINGTON NY 11743-1979
PH:(516)-271-7037 Fax:(516)-271-7137

MR DONALD HAGEMAIER
BOEING
MS C071-0013
2401 E WARDLOW RD
LONG BEACH CA 90807-0001
PH:(562)-593-7304 Fax:(562)-593-8092

MR DENNIS HAGER
USAF
2179 TWELFTH ST
WRIGHT-PATTERSON AFB OH 45433-7718
PH:(937)-255-3370 Fax:(937)-476-7844

MAJ ROTEM HALEVI
ISRAELI AIR FORCE
ADIR STREET #22
RASH HAAIN ISRAEL-0001

MR STEPHEN HALL
CELERIS AERO CANADA INC
255 CENTRUM BLVD
STE 300
ORLEANS ONTARIO CANADA K1E-3V8
PH:(613)-837-1161 Fax:(613)-834-6420

MR JOHN HAMM
NORTHROP GRUMMAN
9314 W JEFFERSON ST
M/S 94-01
DALLAS TX 75211-0001
PH:(972)-266-2046 Fax:(972)-266-4404

MR WILLIAM HAMMOND
BOEING DEF & SPACE GRP
M/S K86-81
PO BOX 7730
WICHITA KS 67277-7730
PH:(316)-526-3297 Fax:(316)-523-2972

MR DAVID HARPER
US AIR FORCE HQ AFSC/SEF
9700 AVE G SE
KIRTLAND AFB NM 87185-5670
PH:(505)-846-0996 Fax:(505)-846-6826

MR JAMES HARPER
USAF WR-ALC/LBRA
265 OCMULGEE CT
ROBINS AFB GA 31098-1647
PH:(912)-926-7980 Fax:(912)-926-2211

DR CHARLES HARRIS
NASA LANGLEY RES CTR
M/S 188M
HAMPTON VA 23681-0001
PH:(757)-864-3447 Fax:(757)-864-7729

MR JAMES HARRISON
METAL IMPROVEMENT CO INC
1618 S IDA
WICHITA KS 67211-0001
PH:(316)-267-8201 Fax:(316)-267-5735

MAJ KARL HART
USAF HQ AMC/LGXR
402 SCOTT DR UNIT 2A2
SCOTT AFB IL 62225-5308
PH:(618)-256-6698 Fax:(618)-256-2009

MR JAMES HARTER
USAF WL/FIBEC
BLDG 45
2790 D STREET RM 504
WRIGHT-PATTERSON AFB OH 45433-7402
PH:(937)-255-6104 Fax:(937)-656-4999

MR ROBERT HARTLEY
US AIR FORCE
OC/ALC
7851 SECOND ST STE 128
OKLAHOMA CITY OK 73145-9145
PH:(405)-736-3236 Fax:(405)-736-3086

MR BRETT HAUBER
USAF
BLDG 125
2335 SEVENTH ST STE 6
WRIGHT-PATTERSON AFB OH 45433-7809
PH:(937)-255-5059 Fax:(937)-255-6210

DR D ROBERT HAY
TEKTREND INTL INC
2113A ST REGIS BLVD
DOLLARD-DES-ORMEAUX
QUEBEC H9B 2M9-0001
PH:(514)-421-1417 Fax:(514)-421-1487

MR RICHARD HAZARD
BOEING
16172 CHIPPER LANE
HUNTINGTON BEACH CA 92649-0001
PH:(562)-982-6320 Fax:(562)-496-6480

MR MARO HEIMERDINGER
NORTHROP GRUMMAN
DEPT 9B70/W8
ONE HORNET WAY
EL SEGUNDO CA 90245-2804
PH:(310)-332-0543 Fax:(310)-332-9160

MR MICHAEL HEINER
US AIR FORCE OO-ALC/LFIT
6089 WARDLEIGH RD
HILL AFB UT 84056-5838
PH:(801)-777-9318 Fax:(801)-773-9782

DR MARKUS HEINIMANN
CESSNA AIRCRAFT CO
PO BOX 7704
WICHITA KS 67277-7704
PH:(316)-941-7157 Fax:(316)-941-5985

MR JAMES HELBLING
NORTHROP GRUMMAN
M/S 9870/89
ONE NORTHROP AVE
EL SEGUNDO CA 90245-2804
PH:(310)-332-6004 Fax:(310)-331-6648

MR KURT HELLBOM
SAAB A8
LINKOPING SWEDEN SE-581 88-0001

MR DAVID HEMPE
FAA HEADQUARTERS
WASHINGTON DC 00000-0001
PH:(202)-267-8807 Fax:(202)-267-5340

MR MICHAEL HENGST
GERMAN AIR FORCE
HEIDESTR 246
M/S PF 902500
COLOGNE, GERMANY 51140-0001

DR DAVID HOEPPNER
UNIV OF UTAH
50 S CENTRAL CAMPUS DR
RM 2202
SALT LAKE CITY UT 84112-0001
PH:(801)-581-3851 Fax:(801)-585-5889

MR H J TEN HOEVE
NLR
PO BOX 153
EMMELOORD
NETHERLANDS 8300 AD-0001

DR PAUL HOFFMAN
NAVAIRSYSCOM
BLDG 2187 STE 2340 UNIT 5
48110 SHAW RD
PATUXENT RIVER MD 20670-1906
PH:(301)-342-9361 Fax:(301)-342-9404

MR GEORGE HOLDERBY
US AIR FORCE WL/FIB
2130 EIGHTH ST STE 1
WRIGHT-PATTERSON AFB OH 45433-7542
PH:(937)-255-5006 Fax:(937)-255-3740

MR JOSEPH HOLTON
LOCKHEED MARTIN AERONAUTICAL SYS CO
M/S 30063-0199
86 S COBB DR
MARIETTA GA 30063-0199
PH:(770)-494-2885 Fax:(770)-494-9617

MR YOSHIYUKI HOTEI
MITSUBISHI HEAVY IND LTD
1 TOYOBA TOYOYOMA-CHO
NISHIKASUGAI-GUN
AICHI-KEN 480-02 JAPAN-0001

DR PETER HOVEY
USAF
BLDG 65
2790 D ST RM 504
WRIGHT-PATTERSON AFB OH 45433-7402
PH:(937)-255-6104 Fax:(937)-656-4999

DANIELE HOVINGTON
BOMBARDIER INC
MONTREAL INTL ARPT
10000 CARGO A-4 ST
MIRABEL QUEBEC CANADA J7N-1H3
PH:(514)-476-4620 Fax:(514)-476-4451

MRT MICHAEL HOWARD
ARINC
2551 RIVA RD
M/S 1-203
ANNAPOLIS MD 21401-0001
PH:(410)-266-4725 Fax:(410)-572-3171

MR DAVID HOWELL
OAK RIDGE NATL LAB
PO BOX 2009
M/S 8050
OAK RIDGE TN 37831-8050
PH:(423)-576-8283 Fax:(423)-574-0740

MR ROGER HOWELL
USAF
6064 DOGWOOD AVE
HILL AFB UT 84056-0001
PH:(801)-777-0535 Fax:(801)-777-9482

MR JACOB HUFFMAN
USCG
USCG ARSC BLDG 78
ELIZABETH CITY NC 27909-0001
PH:(919)-335-6123 Fax:(919)-335-6463

MR TROY HULLANDER
NAVAL AVIATION DEPOT
48110 SHAW RD UNIT 5
BLDG 2187 STE 2350
PATUXENT RIVER MD 20670-1906
PH:(301)-342-9370 Fax:(301)-342-9412

MR LEX HUTCHESON
SVERDRUP TECH INC
4538 CENTERVIEW DR
SUITE 130
SAN ANTONIO TX 78228-0001
PH:(210)-733-3383 Fax:(210)-733-3389

MR JOHN INGRAM
LOCKHEED MARTIN
86 S COBB DR
M/S 0648
MARIETTA GA 30063-0001
PH:(770)-494-8172 Fax:(770)-494-8345

MR WILLIAM IRBY
LOCKHEED MARTIN AERO SYS
M/S 0303 DEPT 73-71
86 S COBB DR
MARIETTA GA 30063-0303
PH:(770)-494-2873 Fax:(770)-494-7738

MR RANDY JANSEN
US AIR FORCE
WR-ALC/TIEDD
420 2ND ST/STE 100
ROBINS AFB GA 31098-1640
PH:(912)-926-4228 Fax:(912)-926-1743

DR DAVID JEONG
US DEPT OF TRANS
M/S DTS-76
KENDALL SQ
CAMBRIDGE MA 02142-1093
PH:(617)-494-3654 Fax:(617)-494-3066

MR RONALD JOHNSON
RAYTHEON E-SYSTS
FM 1570 MAJORS FIELD
M/S CBN 176
GREENVILLE TX 75403-0001
PH:(903)-457-5690 Fax:(903)-457-4119

DR CRAIG JONES
SANDIA NATL LABS
PO BOX 5800
M/S 0615
ALBUQUERQUE NM 87185-0615
PH:(505)-843-8722 Fax:(505)-843-8760

LTCOL JOHN JOOSTEN
ROYAL NETHERLANDS AF
BINCKHORSTLAAN 135
PO BOX 20703
THE HAGUE HOLLAND 2500ES-0001

MR VICTOR JUAREZ
DAMAGE TOLERANT STRUCTURES ENGRS
PO BOX 460873
SAN ANTONIO TX 78246-0001
PH:(210)-863-8347 Fax:(210)-490-6726

MR KIM JUHALA
FINNISH AF DEPOT
PO BOX 210
TAMPERE FINLAND 33101-0001

MR MASAMI KAGEYAMA
JAPAN DEFENSE AGY
3RD RESEARCH CTR
1-2-10 SAKAE-CHO
TACHIKANA TOKYO JAPAN-190

MR HARUHIRO KANEKO
MITSUBISHI HEAVY IND LTD
10 OYE-CHO MINATO-KU
NAGOYA JAPAN 455-0001

MR TAKERO KAWAMURA
IHI
3-5-1 MUKODAI-CHO
TANASHI-SHI TOKOYO 188-0001

MR DAVE KELLY
US AIR FORCE
SA-ALC/LADD
514 SHOP LN/STE 2
KELLY AFB TX 78241-6420
PH:(210)-925-4525 Fax:(210)-925-9940

MR ALAN KERR
ARTI
1 RIDGMAR CENTRE
6500 W FREEWAY
FT WORTH TX 76116-2187
PH:(817)-737-1656 Fax:(817)-737-1605

DR JINSEONG KIM
LYNNTECH, INC
7610 EASTMARK DR STE 105
COLLEGE STATION TX 77840-0001
PH:(409)-693-0017 Fax:(409)-764-7479

MIN-SUNG KIM
508 SUMMIT WALK CIRCLE
MARIETTA GA 30067-0001
PH:(770)-494-4878 Fax:(770)-494-8174

MR RICHARD KINZIE
USAF
325 2ND ST
ROBINS AFB GA 31098-1640
PH:(912)-926-3284 Fax:(912)-926-6619

MR PHILLIP KLOOS
MTS SYSTEMS CORP
M/S 231
14000 TECHNOLOGY DR
EDEN PRARIE MN 55344-2290
PH:(612)-937-4854 Fax:(612)-937-4515

MR KAZUO KOEDA
MITSUBISHI HVY IND LTD
10 OYE-CHO MINATO-KU
NAGOYA JAPAN 455-0001

MR STEPHEN KOKKINS
FOREST-MILLER INC
350 SECOND AVE
WALTHAM MA 02154-1196
PH:(781)-684-4265 Fax:(781)-890-3489

MS INGRID KONGSHAVN
SWISS ACFT & SYST CO
PO BOX 301
EMMEN CH-6032-0001

MS JULIE KRAMER
NASA JOHNSON SPACE CTR
MC ES23
2101 NASA RD
HOUSTON TX 77058-0001
PH:(281)-483-8866 Fax:(281)-483-3789

MR KOSTAS KRIATSIOTIS
HELLENIC AEROSPACE INDUSTRY S.A.
PO BOX 23
TANAGRA
SCHIMATARI-VIOTIAS GREECE 32-009

DR ROBERT KURTH
BATTELLE
505 KING AVE
COLUMBUS OH 43201-2693
PH:(614)-424-7151 Fax:(614)-424-3457

MR JOSEPH KUZNIAR
US AIR FORCE WL/XP
BLDG 45
2230 TENTH ST STE 1
WRIGHT-PATTERSON AFB OH 45433-7817
PH:(937)-255-4843 Fax:(937)-255-1522

COL HANK LAAKMAN
BOEING DEFENSE & SPACE GRP
2601 LIBERTY PKWY
MS RM-00
MIDWEST CITY OK 73130-0001
PH:(405)-739-1407 Fax:(405)-739-1416

MAJ MARCEL LAMBRICHS
ROYAL NETHERLANDS AF
BINCHORSTLAAN 135
M/S 1500 ES
THE HAGUE NETHERLAND 2500ESA-0001

MR MARKUS LANG
AIR FORCE RES LAB
10TH STREET
BLDG 655 RM 032
WPAFB OH 45433-7817
PH:(937)-255-5007 Fax:(937)-656-4840

CAPT JEAN-FRANCOIS LECLERC
CANADIAN ARMED FORCES
MGEN GEORGE R PEARKES BLDG
OTTAWA
ONTARIO CANADA K1A 0K2-0001
PH:(613)-991-9541 Fax:(613)-998-6922

LT COL ENRIQUE LEGORBURU
SPANISH AIR FORCE
MAESTRANZA AEREA DE MADRID
AVDA.AVIACION S/N
28044 MADRID SPAIN-0001

MR TOMAS LEIJON
FMV
S-11588
STOCKHOLM SWEDEN 00000-0001

MR KALMEN LEIKACH
NAVAIRSYSCOM
BLDG 2187 STE 2340A
48110 SHAW RD UNIT 5
PATUXENT RIVER MD 20670-1906
PH:(301)-342-9362 Fax:(301)-342-9402

DR CHARLIE LIAO
BOEING CO
3855 LAKEWOOD BLVD
M/S D801-45
LONG BEACH CA 90846-0001
PH:(562)-497-6587 Fax:(562)-982-7955

DR DAVID LIGHT
BRITISH AEROSPACE
NEWFILTON HOUSE
BRISTOL BS997AR-0001

DR JOHN LINCOLN
USAF ASC/EN
BLDG 560
2530 LOOP RD W
WRIGHT-PATTERSON AFB OH 45433-7101
PH:(937)-255-5312 Fax:(937)-656-4546

LT JASON LINDSEY
USAF ESC/JSIP
75 VANDENBERG DR
HANSCOM AFB MA 01731-0001
PH:(617)-377-9683 Fax:(617)-377-4292

MILA LITTLE
CANADIAN NATL DEFENSE
MAJOR-GENERAL GEORGE R PEARKES BLDG
OTTOWA
ONTARIO CANADA K1A OK2-0001
PH:(613)-993-5566 Fax:(613)-998-6922

MR KO-WEI LIU
THE BOEING COMPANY
M/S C052/0660
2401 E WARDLOW ROAD
LONG BEACH CA 90807-5309
PH:(310)-982-5422 Fax:(310)-982-5164

MAJ RICHARD LOCKWOOD
US AIR FORCE
1725 JEFFERSON DAVIS HWY
M/S STE 1003
ARLINGTON VA 22202-4102
PH:(703)-607-3509 Fax:(403)-602-5387

MR AUDGEIR LUNDE
ROYAL NORWEGIAN AF MATL CMD
M/S DFIS
PO BOX 10
N2007 KJELLER NORWAY 00000-0001

MR JOSEPH LUZAR
BOEING PROD SUPPORT DIV
M/S K86-81
PO BOX 7730
WICHITA KS 67277-7730
PH:(316)-523-5408 Fax:(316)-523-3130

MR JAMES MALINAK
BOEING DEF & SPC GRP
STE 400
2600 PARAMOUNT PL
FAIRBORN OH 45324-6765
PH:(937)-427-1767 Fax:(937)-427-5255

MR CHRIS MANDERS
RAYTHEON E-SYSTEMS
M/S 1134
7500 MAEHR RD
WACO TX 76705-0001
PH:(254)-867-4051 Fax:(254)-867-2115

MR SCOTT MANGRUM
USAF WR-ALC/LREA
750 3RD ST
ROBINS AFB GA 31098-0001
PH:(912)-926-3466 Fax:(912)-929-5320

DR S MANNAVA
GENERAL ELECTRIC CO
10270 ST RITA LN
M/S Q20
EVENDALE OH 45215-0001
PH:(513)-552-2191

MS STACY MANOLAKAS
BOEING
M/S 4X-53
4062 172ND PL SE
BELLEVUE WA 98008-0001
PH:(425)-393-0804

MR STEPHEN MARINSHAW
DYNCORP
6500 WEST FREEWAY
FT WORTH TX 76116-2187
PH:(817)-737-1584 Fax:(817)-737-1605

MR JAMES MARKS
RAYTHEON E-SYSTS
PO BOX 6056
M/S 151
GREENVILLE TX 75403-0001
PH:(903)-457-6529 Fax:(903)-457-5611

MR PERRY MARTIN
NTS
PO BOX 857
NORTH HIGHLANDS CA 95660-0001
PH:(916)-779-3110 Fax:(916)-779-3115

MR MICHAEL MATTHEWS
DELTA AIRLINES
PO BOX 20706
DEPT 578
ATLANTA GA 30320-6001
PH:(404)-714-1460 Fax:(404)-714-1168

DR GEORGE MATZKANIN
NTIAC TRI
415 CRYSTAL CREEK DR
AUSTIN TX 78746-4725
PH:(512)-263-2106 Fax:(512)-263-3530

CAPT V SCOTT MAY
USAF
2130 EIGHTH ST STE 1
WRIGHT-PATTERSON AFB OH 45433-7542
PH:(937)-255-5664 Fax:(937)-656-7723

MR JAMES MAZZA
USAF
2179 TWELFTH ST STE 1
WRIGHT-PATTERSON AFB OH 45433-7718
PH:(937)-255-7778 Fax:(937)-656-4419

DR R CRAIG MCCLUNG
SOUTHWEST RES INST
MATLL & STRUCTS DIV
PO DRAWER 28510
SAN ANTONIO TX 78228-0510
PH:(210)-522-2422 Fax:(210)-522-5122

MR CHARLES MCDONALD
USAF CCM
100 TURNBERRY COVE N
NICEVILLE FL 32587-0001
PH:(904)-897-7051 Fax:(904)-897-7051

MR PETE MCKEIGHAN
SOUTHWEST RES INST
6220 CULEBRA RD
SAN ANTONIO TX 78228-0001
PH:(210)-522-3617 Fax:(210)-522-5122

MR FRASER MCMASTER
SOUTHWEST RES INST
6220 CULEBRA RD
SAN ANTONIO TX 78238-5166
PH:(210)-522-2576 Fax:(210)-522-5122

CAPT GREGORY MCNEW
JOINT STARS PRGM OFF
75 VANDENBERG DR
HANSCOM AFB MA 01731-2119
PH:(781)-377-6838 Fax:(781)-277-2119

MR ROBERT MELLYN
ELECTRODYNAMICS INC
1200 HICKS RD
ROLLING MEADOWS IL 60008-0001
PH:(847)-259-0740 Fax:(847)-255-3827

LCDR JOSEPH MIHELIC
US COAST GUARD
ARSC ENGINEERING
USCG/ARSC/ENGDIV/BLDG 78
ELIZABETH CITY NC 27909-0001
PH:(919)-335-6837 Fax:(919)-335-6463

DR JENNIFER MILLER
NAVAIRSYSCOM
48110 SHAW ROAD
M/S 5
PATUXENT RIVER MD 20670-1906
PH:(301)-342-8099 Fax:(301)-342-9402

DR THOMAS MILLS
USAF WL/FIBE
2790 D ST
BLDG 65 RM 504
WRIGHT-PATTERSON AFB OH 45433-7402
PH:(937)-255-6104 Fax:(937)-656-4999

MR GERALD MINTZ
BOEING NORTH AMERICAN
M/S AD46 DEPT 270
12214 LAKEWOOD BLVD
DOWNEY CA 90242-2693
PH:(562)-922-3358 Fax:(562)-922-2523

MR EFRAIN MIRON
SPANISH AIR FORCE
MAESTRANZA AEREA DE MADRID
AVDA. AVIACION S/N
28044 MADRID SPAIN-0001

MR GEOFFREY MITCHELL
ARINC RES CORP
6205 S SOONER RD
OKLAHOMA CITY OK 73135-0001
PH:(405)-739-0939 Fax:(405)-739-0003

MR W CRAIG MITCHELL
USAF
6089 WARDLEIGH RD
HILL AFB UT 84056-5838
PH:(801)-777-9859 Fax:(801)-773-7620

MR LORIS MOLENT
DEF SCI & TECH ORG
506 LORIMER ST
M/S AED AMRL FISHERMANS BEND
VICTORIA AUSTRALIA-3207

MR ROBERT MOORE
USAF ASC/ENFS
2530 LOOP ROAD WEST
WRIGHT-PATTERSON AFB OH 45433-7101
PH:(937)-255-8515 Fax:(937)-656-4546

MR JOHN MORGAN
US AIR FORCE
OC-ALC/LABEF STE 2AB85A
3001 STAFF DR
TINKER AFB OK 73145-3006
PH:(405)-736-7264 Fax:(405)-736-5598

MR JOSEPH MOSHER
USAF ASC/SMA
2145 MONAHAN WAY
WRIGHT-PATTERSON AFB OH 45433-7017
PH:(937)-255-6053 Fax:(937)-255-7757

DR RICHARD MULLER
HQ USAFA/DFEM
STE 6H2
2354 FAIRCHILD DR
US AIR FORCE ACADEMY CO 80840-6241
PH:(719)-333-2531 Fax:(719)-333-2944

LT COL MASATO NAKAO
ASD/JASDF
9-7-45 AKASAKA
MINATO-KLI
TOKYO JAPAN 184-0001

MR GEORGE NEAT
US DOT/VOLPE CTR
KENDALL SQUARE
M/S DTS-74
CAMBRIDGE MA 02142-1093
PH:(617)-494-2679 Fax:(617)-494-3096

MR DAVID NEFF
RAYTHEON E-SYSTS
7500 MAEHR RD
M/S 1134
WACO TX 76715-4580
PH:(254)-867-4070 Fax:(254)-867-2115

MR ROGER NESJE
ROYAL NORWEGIAN AF
MATERIAL COMMAND
PO BOX 10
KJELLER NORWAY N2007-0001

MS CATHY NGUYEN-QUOC
CANADAIR/BOMBARDIER
DEPT 771
400 COTE VERTE WEST
DORVAL QUEBEC CANADA H4S-1Y9
PH:(514)-855-7548 Fax:(514)-855-8201

MR ED NICHOLS
NORTHROP GRUMMAN
M/S 49L-66
9314 W JEFFERSON
DALLAS TX 75211-0001
PH:(972)-266-3612 Fax:(972)-266-2407

MR DANIEL O'NEILL
BOEING CO
PO BOX 3707
M/S 4X-56
SEATTLE WA 98124-2207
PH:(425)-393-2133 Fax:(425)-393-7044

MR ROBERT ODIAN
STRUCTURAL INTEGRITY ENGRG
9560 TOPANGA CYN
M/S 200
CHATSWORTH CA 91311-0001
PH:(818)-718-2195 Fax:(818)-718-2212

MR MITSUGI OHKI
MITSUBISHI HEAVY IND LTD
NISHIKASUGAI-GUN
AICHI-KEN 480-02
JAPAN 00000-0001

MR TORU OHTA
JAPAN AIR SELF DEF FORCE
NAKA-KANYUCHI
KAKAMIYAHARA-CITY
GIFU PREF JAPAN 504-0001

MR MATS-OLOF OLSSON
FMV
S-111588
STOCKHOLM SWEDEN 00000-0001

MR THOMAS OOLE
USAF ASC/ENFS
2530 LOOP ROAD WEST
WRIGHT-PATTERSON AFB OH 45433-7101
PH:(937)-255-6609 Fax:(937)-656-4546

MR DONALD OPLINGER
FAA W.J. HUGHES TECH CNTR
AAR-431
ATLANTIC CITY AIRPORT
ATLANTIC CITY NJ 08405-0001
PH:(609)-485-4914 Fax:(609)-485-4004

MR TAKASHI OTA
JAPAN DEFENSE AGENCY
4100 INTERNATIONAL PLAZA #302
FORT WORTH TX 76109-0001
PH:(817)-762-2665 Fax:(817)-763-8398

CAPT YASUO OTANI
JAPAN DEFENSE AGY
NAKA-KANYUCHICTR
KAKAMIGAHARA CITY
GIFU-PREF JAPAN 504-0001

DR ARUN PASRICHA
NORTHROP GRUMMAN CORP
MILITARY AIR SYS DIV
ONE HORNET WAY
EL SEGUNDO CA 90245-0001
PH:(310)-332-2122 Fax:(310)-332-9160

MR HEIMO PATYNEN
FINAVITEC OY
35600 HALLI FINLAND 00000-0001

MR MICHAEL PAULK
AF NDI PROGRAM OFFICE
485 QUENTIN ROOSEVELD RD
STE 7
KELLY AFB TX 78241-5442
PH:(210)-925-6408 Fax:(210)-925-2726

DR RIGO PEREZ
BOEING CO
PO BOX 516
M/S S102 2147
ST LOUIS MO 63166-0001
PH:(314)-234-0656 Fax:(314)-234-8915

MR MARTIN PETERS
USAF OO-ALC/LFSS
6080 GUM LANE
HILL AFB UT 84056-5825
PH:(801)-775-4318 Fax:(801)-777-3928

MR DONALD PETTIT
LOCKHEED MARTIN AERO SYS
73-51 TEST LAB M/S 0484
86 S COBB DR
MARIETTA GA 30063-0484
PH:(770)-494-5313 Fax:(770)-494-2028

MR PAUL PIPER
USAF SA-ALC/LFES
485 QUENTIN ROOSEVELT RD
BLDG 1712
SAN ANTONIO TX 78241-6425
PH:(210)-925-4284 Fax:(210)-925-3129

DR DANIEL PIPKINS
KNOWLEDGE SYS INC
81 EAST MAIN ST
FORSYTH GA 31029-0001
PH:(912)-994-4051 Fax:(912)-994-8800

WNG COMM MICHAEL POBOG-JAWOROWSKI
NEW ZEALAND EMBASSY
37 OBSERVATORY CIRCLE NW
WASHINGTON DC 20008-0001
PH:(202)-328-4806 Fax:(202)-265-9238

MR PETER POOLE
DEFENSE RESEARCH AGENCY
DRA X34 BD
GUI4 6TD
FARNBOROUGH HANTS UK GU14OLX-0001

MR JONATHAN POPE
NAVAIR
23220 BENT TREE LANE
CALIFORNIA MD 20619-0001
PH:(301)-342-9328 Fax:(301)-342-9404

MR BRAD PREVALLET
LOCKHEED MARTIN/FT WORTH
PO BOX 738
M/S 2846
FT WORTH TX 76101-0001
PH:(817)-763-2517 Fax:(817)-777-2115

MR ADARSH PUN
NORTHROP GRUMMAN
M/S 9B70/W8
ONE NORNET WAY
EL SEGUNDO CA 90505-0001
PH:(310)-332-4200 Fax:(310)-332-4160

MR KURT RABIDEAU
USAF SA-ALC/LADD
404 GREIG ST
BLDG 179
KELLY AFB TX 78241-5944

CHANTAL RAJOTTE
BOMBARDIER INC.
MONTREAL INTL ARPT
10000 CARGO A-4 ST
MIRABEL QUEBEC CANADA J7N-1H3
PH:(514)-476-4395 Fax:(514)-476-4451

CAPT THOMAS RAMSEY
US AIR FORCE
OC ALC/LACRA STE ZAC489
3001 STAFF DR
TINKER AFB OK 73071-0001
PH:(405)-736-3832 Fax:(405)-736-5604

MR JEFFREY REGISTER
NORTHWEST AIRLINES
MPLS/ST PAUL INTL AIRPORT
M/S C8840 5101 NORTHWEST DR
ST PAUL MN 55111-0001
PH:(612)-726-7274 Fax:(612)-726-6714

MR LEONARD REID
FATIGUE TECH INC
100 ANDOVER PARK W
SEATTLE WA 98188-2868
PH:(206)-246-2010 Fax:(206)-244-9886

MR MICHAEL REID
GULFSTREAM AEROSPACE
M/S D-04
PO BOX 2206
SAVANNAH GA 31402-2206
PH:(912)-965-4268 Fax:(912)-965-4812

MR WALTER REIMANN
8220 WELLINGTON NECK
FRANKTOWN VA 23354-0001
PH:(757)-442-6377 Fax:(757)-442-6377

MR JEREMY REMACHA
LOGISTICS DIRECTORATE
HQ NZ DEFENCE FORCE
PRIVATE BAG
WELLINGTON NEW ZEALAND-0001

MR ROBERT RENNELL
ARINC INC
6205 S SOONER RD
OKLAHOMA CITY OK 73135-0001
PH:(405)-739-0939 Fax:(405)-739-0003

MR JUDE RESTIS
FATIGUE TECHNOLOGY INC
100 ANDOVER PARK WEST
SEATTLE WA 98188-0001
PH:(206)-246-2010 Fax:(206)-244-9886

MR ROBERT REYNOLDS
LOCKHEED MARTIN AERO SYST
86 S COBB DR
MARIETTA GA 30063-0303
PH:(770)-494-5951 Fax:(770)-494-1738

MR RICHARD RICE
BATTELLE
505 KING AVE
COLUMBUS OH 43201-2963
PH:(614)-424-4133 Fax:(614)-424-7618

MR LUC RICHARDSON
BOMBARDIER INC
MONTREAL INTL ARPT
10000 CARGO A-4
MIRABEL QUEBEC CANADA J7N-1H3
PH:(514)-476-4590 Fax:(514)-476-4451

MAJ DAVE ROBERTSON
US AIR FORCE
325 2ND ST
ROBINS AFB GA 31098-0001
PH:(912)-926-3284 Fax:(912)-926-6617

MR ERIC ROBESON
AATD
FT EUSTIS VA 23604-0001
PH:(757)-878-2925 Fax:(757)-878-2053

MS HEATHER ROLAND
LOCKHEED MARTIN
86 SOUTH COBB DR
M/S 0160
MARIETTA GA 30063-0001
PH:(770)-494-0287 Fax:(770)-494-9610

MR DENNIS ROMANO
NAVAL AVIATION DEPOT
302 DIABLO CREEK CT
M/S 4.3.3
CLAYTON CA 94517-0001
PH:(619)-545-0626 Fax:(619)-545-0763

MR CHRISTOPHER ROOT
NAVAL AVIATION DEPOT
CODE 41102
PO BOX 357058
SAN DIEGO CA 92135-7058
PH:(619)-595-3935 Fax:(619)-545-4765

MR JOSEPH ROSENTHAL
BOEING CO
2600 WESTMINSTER BLVD
M/S SL15
SEAL BEACH CA 90740-7644
PH:(562)-797-1891 Fax:(562)-797-3756

MR JAMES RUDD
USAF WL/FIB
2130 EIGHTH ST/STE 1
BLDG 45 RM 203A
WRIGHT-PATTERSON AFB OH 45433-6553
PH:(937)-255-3031 Fax:(937)-255-3740

MR STEVEN RUEDY
USAF
STE 2AH1 100B
3001 STAFF DR
TINKER AFB OK 73145-3022
PH:(405)-736-4323 Fax:(405)-736-5412

MR WARD RUMMEL
D & W ENTERPRISES LTD
8776 W MOUNTAIN VIEW LN
LITTLETON CO 80125-9406
PH:(303)-791-1940 Fax:(303)-977-1145

MR STEPHAN RUSS
USAF
BLDG 655 STE 1
2230 TENTH ST
WPAFB OH 45433-7817
PH:(937)-255-1356 Fax:(937)-656-4840

MR JOHN RUSTENBURG
UNIV OF DAYTON RES INST
500 COLLEGE PARK
DAYTON OH 45469-0120
PH:(937)-229-4485 Fax:(937)-229-4485

LT JAMES RYAN
USAF WL/FIBE
2790 D ST
RM504
WRIGHT-PATTERSON AFB OH 45433-0001
PH:(937)-255-6104 Fax:(937)-656-4999

MS ROBYN RYAN
RAYTHEON ACFT
PO BOX 85
M/S 934 B-6
WICHITA KS 67201-0085
PH:(316)-676-7127 Fax:(316)-676-8381

DR SAM SAMPATH
FAA
WPAFB OH 45433-0001
PH:(937)-255-6793

MR SUBHASIS SARKAR
GEORGIA TECH
COMP MODELING CTR
M/S 30332-0356
ATLANTA GA 30332-0001
PH:(404)-894-9334 Fax:(404)-894-2299

MS MARY SCHLEIDER
MERCER ENGR RES CTR
ENGR ANALYSIS & DESIGN
1861 WATSON BLVD
WARNER ROBINS GA 31093-0001
PH:(912)-929-6400 Fax:(912)-929-6479

MR GEORGE SCHNEIDER
SIKORSKY AIRCRAFT
M/S 5314A2
6900 MAIN ST
STRATFORD CT 06497-0001
PH:(203)-386-3784 Fax:(203)-386-3717

MR KURT SCHRADER
SOUTHWEST RES INST
6220 CULEBRA RD
SAN ANTONIO TX 78228-5166
PH:(210)-522-3322 Fax:(210)-522-4826

DR JOEL SCHUBBE
USAF AFRL/VASS
2145 FIFTH ST STE 2 BLDG 24C
WRIGHT-PATTERSON AFB OH 45433-7006
PH:(937)-255-5200 Fax:(937)-255-6684

CAPT TIMOTHY SCHULTEIS
USAF
KELLY AFB TX 00000-0001
PH:(210)-925-4525

MR WILLIAM SCHWEINBERG
US AIR FORCE
420 SECOND ST WR-ALC
ALC/TIEDD
ROBINS AFB GA 31098-0001
PH:(912)-926-4228 Fax:(912)-926-1743

MR JASON SCOTT
CAE AVIATION LTD
PO BOX 9864
EDMONTON INT'L APT
EDMONTON AB CANADA TGE 4R3-0001
PH:(403)-890-6616 Fax:(403)-890-6543

MR PAUL SCREEN
ROYAL AIR FORCE
RAF WADDINGTON
ENGLAND LN5 9NB--

MR IAN SEARLE
BOEING ISDS
M/S 82-97
20403 68TH S 18-28 BLDG
KENT WA 98032-0001
PH:(253)-773-3894 Fax:(253)-773-4946

MR RICK SELDER
THE BOEING COMPANY
2401 E WARDLOW RD
M/S C052-0660
LONG BEACH CA 90207-4418
PH:(562)-982-5392 Fax:(562)-982-5164

MR JEFFERY SERMERSHEIM
BOEING CO
MC 51063511
PO BOX 516
ST LOUIS MO 63166-0516
PH:(314)-234-4641 Fax:(314)-777-1045

LT DARREN SEXTON
ROYAL AUSTRALIAN AIR FORCE
1195 CAMDEN COURT
WARNER ROBINS GA 31088-0001
PH:(912)-926-4226 Fax:(912)-926-1743

MR WILLIAM SHEPPARD
NORTHROP GRUMMAN CORP
ONE HORNET WAYE
M/S 9B71/63
EL SEGUNDO CA 90250-0001
PH:(310)-332-9635 Fax:(310)-332-0583

DR DONALD SHOCKEY
SRI INTL
M/S AA277
333 RAVENSWOOD AVE
MENLO PARK CA 94025-3493
PH:(650)-859-2587 Fax:(650)-859-2260

MR MICHAEL SHOCKEY
USAF
2145 MONAHAN WAY
WRIGHT-PATTERSON AFB OH 45433-7017
PH:(937)-255-6053 Fax:(937)-656-4410

MR DAVID SHOWERS
FEDERAL AVIATION ADMINISTRATION
601 E 12TH ST
M/S ACE-111
KANSAS CITY MO 64106-0001
PH:(816)-426-6941 Fax:(816)-426-2169

MR DAVID SIMPSON
NATL RES COUNCIL OF CANADA
INST FOR AERO RES
MONTREAL RD
OTTAWA ONTARIO CANADA K1A-0R6
PH:(613)-993-0899 Fax:(613)-952-7136

DR PAVEL SINDELAR
FFA AERO RES INST OF SWEDEN
BOX 11021
S-161-11
BROMMA SWEDEN

MR JODI SIRMANS
LOCKHEED AERO SYS CO
86 SOUTH COBB DR
M/S D7371 20303
MARIETTA GA 30063-0303
PH:(770)-494-7697 Fax:(770)-494-7738

DR THANGAVEL SIVAM
RAYTEON E SYST WACORN SYS
PO BOX 4500
7500 MAEHR RD MS 1143
WACO TX 76715-0001
PH:(254)-867-4282 Fax:(254)-867-4106

MR JOHN SLYE
US AIR FORCE
ASC/YTJ
BLDG 56 2100 MONAHAN WAY
WRIGHT-PATTERSON AFB OH 45433-7014
PH:(937)-255-9306 Fax:(937)-255-8516

MR TIMOTHY SORENSEN
USAF OO-ALC/LFSS
6080 GUM LANE
HILL AFB UT 84056-5825
PH:(801)-777-9601 Fax:(801)-777-3928

MR WILLIAM SPARKS
31220 POST OAK TRAIL
FAIR OAKS RANCH TX 78015-0510
PH:(830)-981-8725

MR CHRISTOPHER SPENCER
BEL HELICOPTER TEXTRON
PO BOX 482
FT WORTH TX 76101-0001
PH:(817)-280-5732 Fax:(817)-280-6320

MR DIRK-JAN SPIEKHOUT
NATL AEROSPACE LAB
VOORSTERWEG
M/S 31
MARKNESSE NETHERLAND 8316PR-0001

MR CHRISTOPH STAHN
GERMAN AIR FORCE
HEIDESTR 245
M/S PF 902500
COLOGNE, GERMANY 51140-0001

MR HUGO STEIN
USAF SA-ALC/LFE
485 QUENTIN ROOSEVELT RD
KELLY AFB TX 78241-6425
PH:(210)-925-6311 Fax:(210)-925-0097

MR BRIAN STELLY
RAYTHEON E-SYST INC
FM 1570 MAJORS FIELD
MS CBN 192
GREENVILLE TX 75403-0001
PH:(903)-457-7345 Fax:(903)-457-5605

MR JAMES SULLIVAN
LOCKHEED MARTIN
PO BOX 748
M/S 4272
FT WORTH TX 76101-0001
PH:(817)-763-3528 Fax:(817)-777-7722

DR REDA TADROS
BMW ROLLS RR
ESCHWENWEG 11
M/S ED-3
DAHLEWITZ GERMANY D-15827-0001

MR LARRY TARRANT
US AIR FORCE
OC-ALC/TILOF
7851 2ND ST/RM 107
TINKER AFB OK 73145-9145
PH:(405)-736-5424 Fax:(405)-736-3086

MR ROBERT TASHIRO
NORTHROP GRUMMAN CORP
8900 E WASHINGTON BLVD
M/S 6J80/UB
PICO RIVERA CA 90660-0001
PH:(562)-942-5287 Fax:(562)-948-8146

DR RACHAEL TAY
SINGAPORT TECH AERO
540 AIRPORT RD
PAYA LEBAR
SINGAPORE 539938-0001

MS AMY TAYLOR
TEXSEM LABS INC
3545 E APOLLO DR
SALT LAKE CITY UT 84124-0001
PH:(801)-495-2750 Fax:(801)-495-2758

MR ROBERT TEMUCIN
NAVAL AVIATION DEPOT
PSC BOX 8021
CODE 4.3.3
CHERRY POINT NC 28533-0001
PH:(919)-464-7332 Fax:(919)-464-8326

MR DAVE THOMAS
ROYAL AIR FORCE
RAF ST ATHAN
SOUTH GLAMORGAN UK CE62 4WA-0001

MR GIBBY THOMAS
FEDERAL EXPRESS
3131 DEMOCRAT ROAD
M/S 5413
MEMPHIS TN 38118-0001
PH:(901)-224-4807 Fax:(901)-224-4819

MR LARRY THOMPSON
STRAIN MONITOR SYSTEMS
1425 RUSS BLVD
STE T-112C
SAN DIEGO CA 92101-0001
PH:(619)-702-7002 Fax:(619)-702-3122

MR CHARLES TIFFANY
4160 VIA DEL CUCULIN
TUCSON AZ 85718-3321

MR PAUL TOIVONEN
BOEING
S111-1221
PO BOX 516
ST LOUIS MO 63166-0516
PH:(314)-234-4912 Fax:(314)-232-1394

DR DUNG DUC TRAN
TRANSPORT CANADA
300 SPARKS PLACE
TOWER C 2ND FLR AARDG
OTTAWA ONTARIO CANADA K1A-ON5
PH:(613)-952-4325 Fax:(613)-996-9178

MR DOUGLAS TRITSCH
UNIV DAYTON RES INST
STRUCTURAL INTEGRITY
300 COLLEGE PK
DAYTON OH 45469-0120
PH:(937)-229-4417 Fax:(937)-229-3712

MR BILLY TRUSSEL
WR-ALC/LFEFS
296 COCHRAN ST
ROBINS AFB GA 31098-1622
PH:(912)-926-5482 Fax:(912)-926-5463

DR ERIC TUEGEL
APES INC
3542 OXFORD AVE
ST LOUIS MO 63143-0001
PH:(341)-644-6040 Fax:(314)-649-0229

MR JIMMY TURNER
US AIR FORCE
SA-ALC/LADD
404 GREIG ST
KELLY AFB TX 78241-0001
PH:(210)-925-4525 Fax:(210)-925-1416

MR MICHAEL TYSON
LOCKHEED-MARTIN AERO
D/73-76 ZONE 0160
86 S COBB DR
MARIETTA GA 30063-0001
PH:(770)-494-1869 Fax:(770)-494-9610

MR DIMITRIOS TZIMIS
HELLEXIC AEROSPACE INDUSTRY S.A.
PO BOX 23
TANAGRA
SCHIMATARI-VIOTIAS GREECE 32-009

MR MICHAEL URBAN
SIKORSKY AIRCRAFT
6900 MAIN ST
M/S $328A7
STRATFORD CT 06494-9129
PH:(203)-386-7159 Fax:(203)-386-6708

MR JOHN VAN DOREN
SIGNATURE CTRL SYSTS
4071 S ELIOT ST
ENGLEWOOD CA 80110-0001
PH:(303)-783-0500 Fax:(303)-783-0800

MR DOUGLAS VAN OTTERLOO
LOCKHEED MARTIN AERO SYS
DEPT 73-51 ZONE 0484
86 S COBB DR
MARIETTA GA 30063-2028
PH:(770)-494-3232 Fax:(770)-494-2028

MR WILLIAM VAN SICKLE
BOEING DEF & SP GROUP/PSD
M/S K84-40
PO BOX 7730
WICHITA KS 67277-7730
PH:(316)-523-1326 Fax:(316)-526-4214

MR DANA VANA
BOEING
EAST MARGINAL WAY
M/S 41-14
SEATTLE WA 98124-0001
PH:(206)-655-6475 Fax:(206)-655-0315

MR SCOTT VANDERSALL
USAF
C-130 TCG
265 OCMULGEZ CT
RAFB GA 31098-1647
PH:(912)-926-9881 Fax:(912)-328-1647

DR A VASUDEVAN
OFF OF NAVAL RES
CODE 332
800 N QUINCY ST
ARLINGTON VA 22217-5560
PH:(703)-696-8181 Fax:(703)-696-0934

MR MAKOTO VEMURA
JAPAN DEFENCE AGENCY
1-2-10 SAKAE-CHO
TACHIKAWA-CITY
TOKYO JAPAN 190 00000-0001

DR CHANDRASEKARAN VENKATESAN
UNIVERSITY OF UTAH
50 S CENTRAL CAMPUS DR
RM 2202, MEB
SALT LAKE CITY UT 84112-0001
PH:(801)-581-4025

MR STEPHAN VERHOEVEN
USAFA
2354 FAIRCHILD DR
RM 2J2A
USAFA CO 80840-0001
PH:(819)-333-3043 Fax:(819)-333-2944

MR CHRIS VICKERS
USAF ASC/YC (AV/AF)
2590 LOOP RD WEST
WRIGHT-PATTERSON AFB OH 45433-7142
PH:(937)-255-1034 Fax:(937)-255-3207

MR JOHN VIEGER
SINO SWEARINGEN AIR CO SYS INC
1770 SKYPLACE
SAN ANTONIO TX 78216-0001
PH:(210)-258-8658 Fax:(210)-258-3953

DR AD VLOT
UT DELFT
PO BOX 5058
2600 GB DELFT
NETHERLANDS

LT COL MARINUS VOS
ROYAL NETHERLANDS AIR FORCE
OO-ALC/LFA-NE
6061 GUM LN
HILL AFB UT 84056-0001
PH:(801)-777-7741 Fax:(801)-773-7250

MR MICHAEL WADDELL
USAF WL/MTPN
2977 P STREET
BLDG 653 STE 6
WRIGHT-PATTERSON AFB OH 45433-7739
PH:(937)-255-7277 Fax:(937)-656-4420

MR THOMAS WADE
US COAST GUARD HQ
2100 2ND ST SW
M/S G-SEA-12
WASHINGTON DC 20593-0001
PH:(202)-267-2816 Fax:(202)-267-4135

MR GARY WAGGONER
USAF
BLDG 652 STE 1
2179 TWELFTH ST
WRIGHT-PATTERSON AFB OH 45433-7718
PH:(937)-255-4651 Fax:(937)-476-4419

MR RAYMOND WALDBUSSER
US AIR FORCE
WR-ALC/LBRA
265 OCMULGEE CT
ROBINS AFB GA 31098-1647
PH:(912)-926-9602 Fax:(912)-926-2211

MR KEVIN WALKER
DEF SCI & TECH ORG
506 LORIMER ST
M/S AED AMRLEND FISHERMANS BEND
VICTORIA AUSTRALIA-3207
PH: Fax:( )- -

MS SHEILA WALL
USAF ASC/ENFS
2530 LOOP ROAD WEST
WRIGHT-PATTERSON AFB OH 45433-7101
PH:(937)-255-7304 Fax:(937)-656-4546

MR DOUG WALLING
NADEP
AV-8B IN SERVICE SUPPORT TEAM
PSC 8021
MCAS CHERRY POINT NC 28533-0021
PH:(919)-466-8517 Fax:(919)-466-8502

MR CHARLES WARREN
ALCOA
101 TECHNICAL DR
M/S A-DE
ALCOA CTR PA 15069-0001
PH:(412)-337-5417 Fax:(412)-337-4075

MR GREGORY WATTIS
SOUTHWEST RES INST
6220 CULEBRA RD
M/S DIV 04
SAN ANTONIO TX 78228-0510
PH:(210)-522-2333 Fax:(210)-522-4506

MR RON WEEDON
ROYAL AIR FORCE
RAF ST ATHAN
SOUTH GLAMORGAN UK CF52 4WA-0001

MR GREG WEITZ
LOCKHEED MARTIN
M/S D/73-25 Z0160
86 S COBB DR
MARIETTA GA 30063-0001
PH:(770)-494-6990 Fax:(770)-494-8478

MR TOMMY WHITE
US NAVY
NORTH ISLAND
PO BOX 357058
SAN DIEGO CA 92135-7058
PH:(619)-545-3922 Fax:(619)-545-4765

DR WILLIAM WHITE
USAF WR-ALC/TIE
420 2ND ST ST 100
ROBINS AFB GA 31098-1640
PH:(912)-926-0540 Fax:(912)-926-7420

MR ROBERT WILKINS
BOEING
12214 LAAKEWOOD BLVD
M/S AC04
DOWNEY CA 90241-7009
PH:(562)-922-3609 Fax:(562)-922-3728

MR RICHARD WOLF
BOEING PROD SUPPORT DIV
M/S K86-92
PO BOX 7730
WICHITA KS 67277-7730
PH:(316)-526-8220 Fax:(316)-523-2972

MR ARCHIE WOODS
USAF ASC/ENFS
BLDG 206
2530 LOOP RD W
WRIGHT-PATTERSON AFB OH 45433-7101
PH:(937)-255-6583 Fax:(937)-656-4546

DR HSING YEH
USAF ASC/ENFS
BLDG 125
2530 LOOP RD W
WRIGHT-PATTERSON AFB OH 45433-7101
PH:(937)-255-8547 Fax:(937)-656-4546

MR GREGORY YOUNG
ROYAL AUSTRALIAN AIR FORCE
NATL RES COUNCIL
BLDG M-14 MONTREAL RD
OTTAWA ONTARIO CANADA K1M-1G7
PH:(613)-990-5019 Fax:(613)-952-7136

MR JESS YOUNG
OGDEN ALC/LACM
7278 4TH ST
HILL AFB UT 84056-5205
PH:(801)-777-5262 Fax:(801)-777-9482

DR MASOOD ZAIDI
BOEING
2401 E WARDLOW RD
MS C071-0013
LONG BEACH CA 90807-4418
PH:(562)-593-9569 Fax:(562)-593-8092

MR DAVID ZAVITZ
BOMBARDIER INC CANADAIR
796 - F/A-18 ENGR
10000 CARGO RD A-4
MIRABEL QUEBEC CANADA J7N-1H3
PH:(514)-476-4597 Fax:(514)-476-4416

MR MICHAEL ZEIGLER
USAF WL/VASE
BLDG 45
2790 D ST RM 504
WRIGHT-PATTERSON AFB OH 45433-7402
PH:(937)-255-6104 Fax:(937)-656-4999

MR MIRKO ZGELA
MARTEC LTD
221 FREEMAN RD
STE 150
HULL QUEBEC CANADA J8Z 2A8-0001
PH:(819)-595-3526 Fax:(819)-595-1739

MR BOB ZIMMERMAN
BOEING
2401 E WARDLOW (C078-0209)
LONG BEACH CA 90807-0001
PH:(562)-593-1124 Fax:(562)-982-7367

MR ERIC ZIMMERMAN
NAVAIR
48110 SHAW RD
M/S 5
PATUXENT RIVER MD 20670-1906
PH:(301)-342-9324 Fax:(301)-342-9402